UNCLASSIFIED

AD NUMBER

AD804723

NEW LIMITATION CHANGE

TO

Approved for public release, distribution unlimited

FROM

Distribution authorized to U.S. Gov't. agencies and their contractors; Administrative/Operational Use; 06 SEP 1966. Other requests shall be referred to Federal Aviation Agency, Office of Supersonic Tramsport Development Program, Washington, DC.

AUTHORITY

FAA notice, 3 Jul 1973

THIS PAGE IS UNCLASSIFIED

804723

# PHASE III PROPOSAL

SUPERSONIC TRANSPORT DIVISION

SEPTEMBER 6, 1966

(6) Supersonic Transport Development Program

Phase III Proposal

**BOEING MODEL 2707**

Volume II-a.

# AERODYNAMIC DESIGN REPORT

(14) V2-B2707-3

September 6, 1966

DDC
RECEIVED
JAN 13 1967
B

(11) 6 Sep 66

(12) 371 p.

PREPARED BY Clarence S. Howell, Jr. APPROVED BY

(10) Clarence S. Howell, Jr. (15) FA-SS-66-5

*Prepared for*

**FEDERAL AVIATION AGENCY**

*Office of Supersonic Transport Development Program*

"THIS DOCUMENT CONTAINS SENSITIVE, COMPETITIVE, AND PROPRIETARY DATA, AND IS NOT TO BE REPRODUCED OR RELEASED OUTSIDE OF YOUR ORGANIZATION OR USED FOR ANY PURPOSE OTHER THAN SUPERSONIC TRANSPORT EVALUATION WITHOUT THE WRITTEN PERMISSION OF EITHER THE FEDERAL AVIATION AGENCY, OFFICE OF SUPERSONIC TRANSPORT DEVELOPMENT, ATTENTION: SS-30, OR THE BOEING COMPANY, SUPERSONIC TRANSPORT DIVISION, ATTENTION: CONTRACT ADMINISTRATION"

402 77

THE BOEING COMPANY
SUPERSONIC TRANSPORT DIVISION

FAA

ISSUE NO 1 99

PAGES _____

ARE

MISSING

IN

ORIGINAL

DOCUMENT

## FOREWORD

### ENGINE AND AIRPLANE PERFORMANCE DATA

The engine and airplane performance provided in the main body of this document is based on engine performance data received prior to 15 July 1966.

The RFP provides for firm technical engine data to be submitted on 8 August 1966. The predicted effect of these data is of interest to the readers of this document. Accordingly, an addendum summarizing the effect of the 8 August 1966 engine performance on the B-2707 SST has been inserted into the following documents:

| | |
|---|---|
| V2-B2707-3 | Aerodynamic Design Report |
| V2-B2707-12 | Propulsion Report - Part A |
| V4-B2707-1 | Operational Suitability Report |
| V4-B2707-4 | Airport and Community Noise Program |

The performance information contained in the Summary document, the Model Specification, and the Statement of Work is based upon the 8 August 1966 firm technical data.

CONTENTS:


| | | Page |
|---|---|---|
| 1.0 | SUMMARY | 1 |
| 1.1 | CONFIGURATION DESCRIPTION | 1 |
| 1.2 | AIRPLANE PERFORMANCE | 2 |
| 1.3 | LIFT-TO-DRAG RATIO | 11 |
| 1.4 | STABILITY AND CONTROL | 11 |
| 1.5 | AEROELASTICITY | 11 |
| 1.6 | GROWTH | 11 |
| 2.0 | PERFORMANCE | 17 |
| 2.1 | MISSIONS | 19 |
| 2.2 | TAKEOFF PERFORMANCE | 19 |
| 2.3 | APPROACH AND LANDING PERFORMANCE | 31 |
| 2.4 | OFF-DESIGN AND EMERGENCY RANGE PAYLOAD PERFORMANCE | 36 |
| 2.5 | PERFORMANCE CALCULATION METHODS | 40 |
| 3.0 | PERFORMANCE SUBSTANTIATION | 47 |
| 3.1 | CRUISE CONFIGURATION | 47 |
| 3.2 | TAKEOFF AND LANDING CONFIGURATIONS | 105 |
| 3.3 | AEROELASTIC ANALYSIS METHODS | 131 |
| 3.4 | AERODYNAMIC DEVELOPMENT PROGRAM | 137 |
| 4.0 | STABILITY AND CONTROL | 145 |
| 4.1 | CONTROL AND TRIM | 145 |
| 4.2 | STATIC STABILITY | 179 |
| 4.3 | DYNAMIC STABILITY | 210 |
| 4.4 | CROSS-COUPLING CHARACTERISTICS | 230 |
| 4.5 | EMERGENCY OPERATIONS | 231 |
| 5.0 | FLIGHT CONTROLS AND STABILITY AUGMENTATION SYSTEM | |
| 5.1 | PRIMARY FLIGHT CONTROL SYSTEM | 245 |
| 5.2 | SECONDARY FLIGHT CONTROL SYSTEM | 254 |
| 5.3 | STABILITY AUGMENTATION SYSTEM | 254 |
| SYMBOLS | | 275 |
| REFERENCES | | 280 |
| APPENDIX A | CONFIGURATION DESCRIPTION | 283 |
| APPENDIX B | ADDENDUM: SUMMARY REPORT — 8 AUGUST 1966<br>ENGINE PERFORMANCE DATA | |

# B-2707 PHASE III PROPOSAL DOCUMENTATION INDEX

## VOLUME I

SUMMARY V1-B2707


Phase III Proposal Summary -1

Boeing Model 2707 Warranties Program -2


## VOLUME II

AIRPLANE TECHNICAL REPORT V2-B2707


System Engineering Report -1

Mockup Plan -2

Aerodynamic Design Report -3

Airplane Performance (GE) -4

Airplane Performance (P&W) -5

Airframe Design Report- -6-1
Part A Weight & Balance

Airframe Design Report- -6-2
Part B Component Design

Airframe Design Report- -7
Part C
Design Criteria
Loads
Aerodynamic Heating
Flutter

Airframe Design Report- -8
Part D
Materials and Processes

Airframe Design Report- -9
Part E
Structural Tests

Systems Report-Part A 10
Environmental Control
Electric
Navigation and Communications

Systems Report-Part B -11
Hydraulics
Landing Gear
Auxiliary Systems

Propulsion Report-Part A -12
Engine, Inlet, & Controls

Propulsion Report-Part B -13
Engine Installation
Fuel System
Exhaust System

Propulsion Report-Part C -14
Engine Evaluation


## VOLUME III

ENGINE CONTRACTORS ONLY

## VOLUME IV

SYSTEM INTEGRATION V4-B2707


Operational Suitability -1

Sonic Boom Program -3

Airport & Community Noise Program -4

Internal Noise Program -5

System Safety Plan -6

Training & Training Equipment Program -7

Human Engineering Program -8

Test Integration & Management -10

Integrated Test Program -11

Simulation Program -12

Flight Simulation Program -13

Flight Test Program -14

Maintainability Program -15

Reliability Program -16

Quality Control Program -17

Value Engineering Program -18

Standardization Program -19

Product Support Program -20

Quality Assurance Program -21


## VOLUME V

MANAGEMENT MANUFACTURING V5-B2707


Configuration Management Plan -1

Data Management Plan -2

Master Program Plan -3

Detail Work Plan -4

Procurement Program -5

Cost & Schedules Control Program -6

Facilities Program -7

Program Management -8

Manufacturing Program -9


## VOLUME VI

COST V6-B2707


Cost Baseline Report Summary Data -1

Cost Baseline Report Cost Support Data -2


## VOLUME VII

ECONOMICS V7-B2707


Economic Summary -1

Economic Summary - For Government Use Only -2

# 1.0 SUMMARY


| | | |
|---|---|---|
| 1.1 | CONFIGURATION DESCRIPTION | 1 |
| 1.2 | AIRPLANE PERFORMANCE | 2 |
| 1.3 | LIFT-TO-DRAG RATIO | 11 |
| 1.4 | STABILITY AND CONTROL | 11 |
| 1.5 | AEROELASTICITY | 11 |
| 1.6 | GROWTH | 11 |

# 1.0 SUMMARY

Aerodynamic analysis of the B-2707 configuration is reported in three documents: Aerodynamic Design Report, V2-B2707-3, Airplane Performance (General Electric), V2-B2707-4, and Airplane Performance (Pratt & Whitney), V2-B2707-5. The documents are part of a series under Volume II, Airplane Technical Report, called for by the FAA Request for Proposal for Phase III of the Supersonic Transport Development Program.

The B-2707 configuration meets the FAA design objectives while providing a large increase in payload over previous supersonic transport configurations submitted by The Boeing Company. This improvement has been achieved without loss of aerodynamic efficiency and offers increased economy in airline operation as indicated by the payload-range curves shown in Fig. 1-1. The performance data shown in this figure and on the following pages are based on characteristics established for the production version of the airplane which is estimated to have a cruise lift-to-drag ratio of 8.2. Refinement of the B-2707 is expected to yield characteristics that are better than those quoted because only a modest 5 percent lift-to-drag improvement is assumed relative to the current status; this is considerably less than would be indicated by past Boeing history for a comparable time span (Fig. 1-2).

Aerodynamic characteristics of the B-2707 airplane are based on wind tunnel test data corrected for scale effects and geometric differences between the full-scale and wind tunnel model configurations; they are adjusted for the expected improvement resulting from the design refinements of the planned programs. These programs include additional detailed studies of body shape, wing and horizontal tail camber and planform, the use of direct-lift control, and local boundary layer control. These programs are described in Secs. 3.0 and 4.0. Approximately 11,000 hours of wind tunnel testing have been devoted to aerodynamic research during Phase II; of these more than 2,000 hours have been used specifically for development of the B-2707 configuration.

## 1.1 CONFIGURATION DESCRIPTION

A three-view drawing of the B-2707 configuration is shown in Fig. 1-3. The design consists of a six-abreast body with a variable sweep wing and

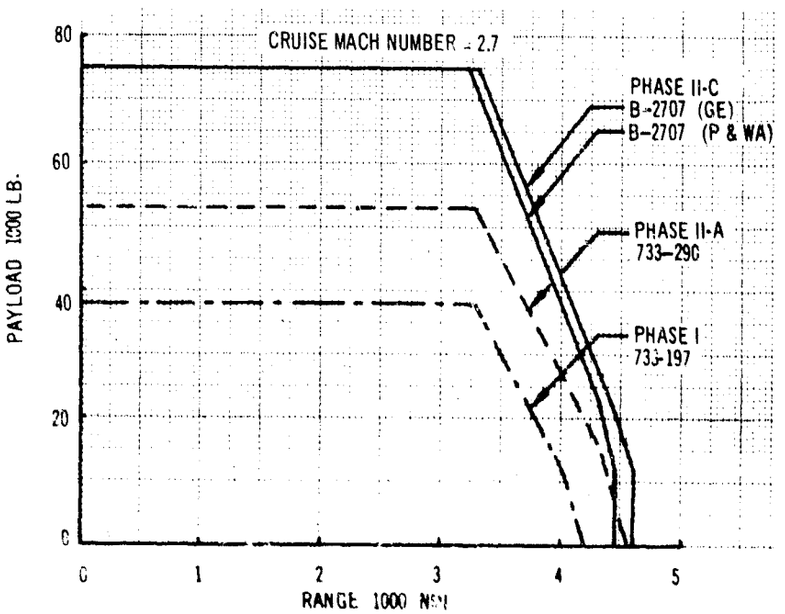


*Figure 1-1. Payload Range Improvements*

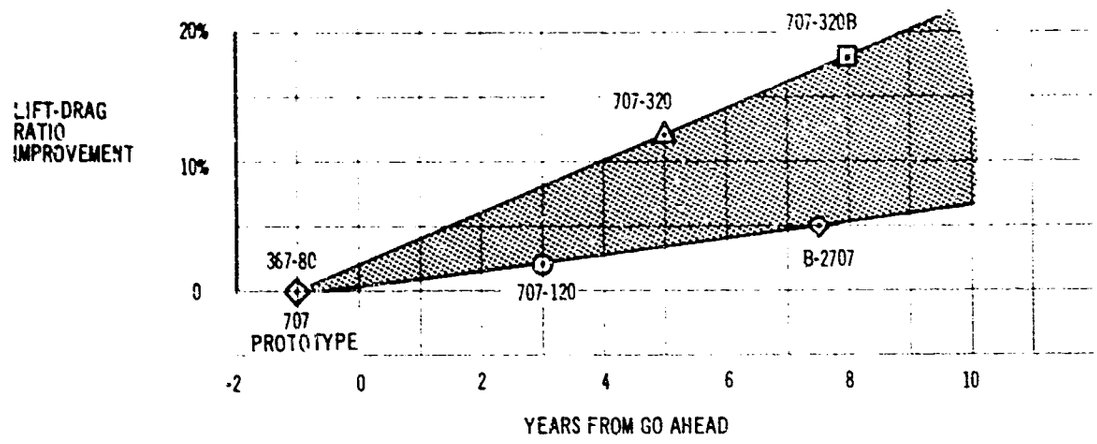


*Figure 1-2. Aerodynamic Efficiency Improvements*

four augmented engines (either General Electric GE4/J5P or Pratt and Whitney JTF17A-21B) located under the horizontal tail. The engines are mounted in individual nacelles near the trailing edge to provide favorable aerodynamic interference effects and an unobstructed area for the engine exhaust. Inlet foreign object ingestion is minimized by locating wing trailing edge flaps between the landing gear and the inlets. A vertical tail and ventral fin are incorporated in the design to achieve adequate directional stability.

A wing sweep of 30 degrees is used for takeoff and landing. During subsonic climb, acceleration, and cruise, the wing sweep is 42 degrees. At transonic and supersonic speeds the wing sweep is 72 degrees; the wing is joined to the horizontal tail in this position. The variable-sweep feature provides a high degree of operational flexibility. Principal dimensions, areas, and weights are given in Fig. 1-3, and a detailed description of the airplane geometry is given in Appendix A.

## 1.2 AIRPLANE PERFORMANCE

Payload range performance for the intercontinental version of the production airplane is shown in Figs. 1-4 and 1-5. The airplane is capable of carrying the following payloads:

| | B-2707 (GE) | B-2707 (P&WA) |
|---|---|---|
| FAA Mission (4,000 Statute Miles) | 66,000 lb | 63,000 lb |
| New York - Paris | 75,000 lb | 74,000 lb |
| New York - Rome | 55,000 lb | 51,500 lb |

The domestic airplane can carry a payload of 63,000 lb (B-2707 GE) or 62,500 lb (B-2707 P&WA) from New York to Los Angeles.

# DATA MODEL B-2707

| | G.E. | P&WA |
|---|---|---|
| POWER PLANTS (4) | G.E. 4/J5P | JTF 17A-21B |
| TOTAL ENGINE AIRFLOW | 2480 LBS/SEC | 2748 LBS/SEC |
| MAX. DESIGN TAXI WEIGHT | 675,000 LBS | 675,000 LBS |
| NOMINAL PAYLOAD | 50,000 LBS | 50,000 LBS |
| OPERATIONAL EMPTY WEIGHT | 287,500 LBS | 285,000 LBS |
| FUEL | 374,700 LBS | 374,700 LBS |

| | |
|---|---|
| MAIN GEAR | 16 - 45 x 19.2 TIRES TYPE VIII |
| NOSE GEAR | 2 - 34 x 16 TIRES TYPE VIII |
| MAX. DESIGN TAXI WEIGHT C.G. - LIMITS, GEAR DOWN | |
| MOST FORWARD C.G. | 59.5 % REF. LENGTH - WINGS FWD |
| MOST AFT C.G. | 64.0 % REF. LENGTH - WINGS AFT |

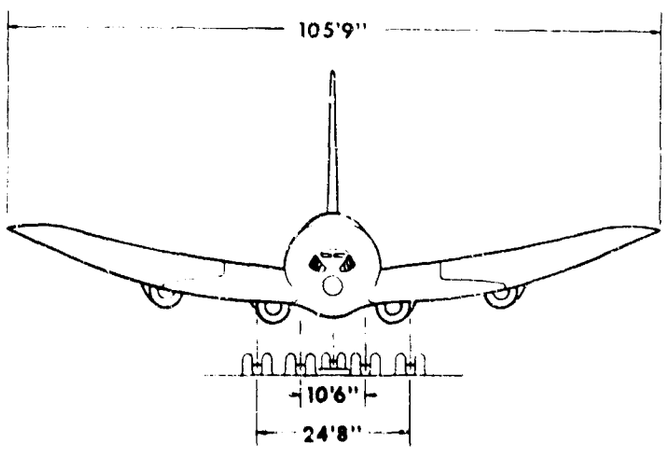


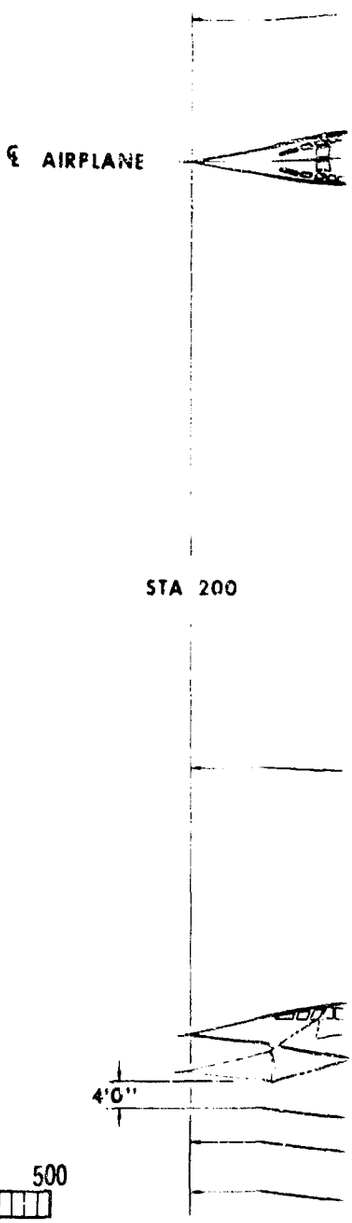


0 250 500

SCALE (INCHES)

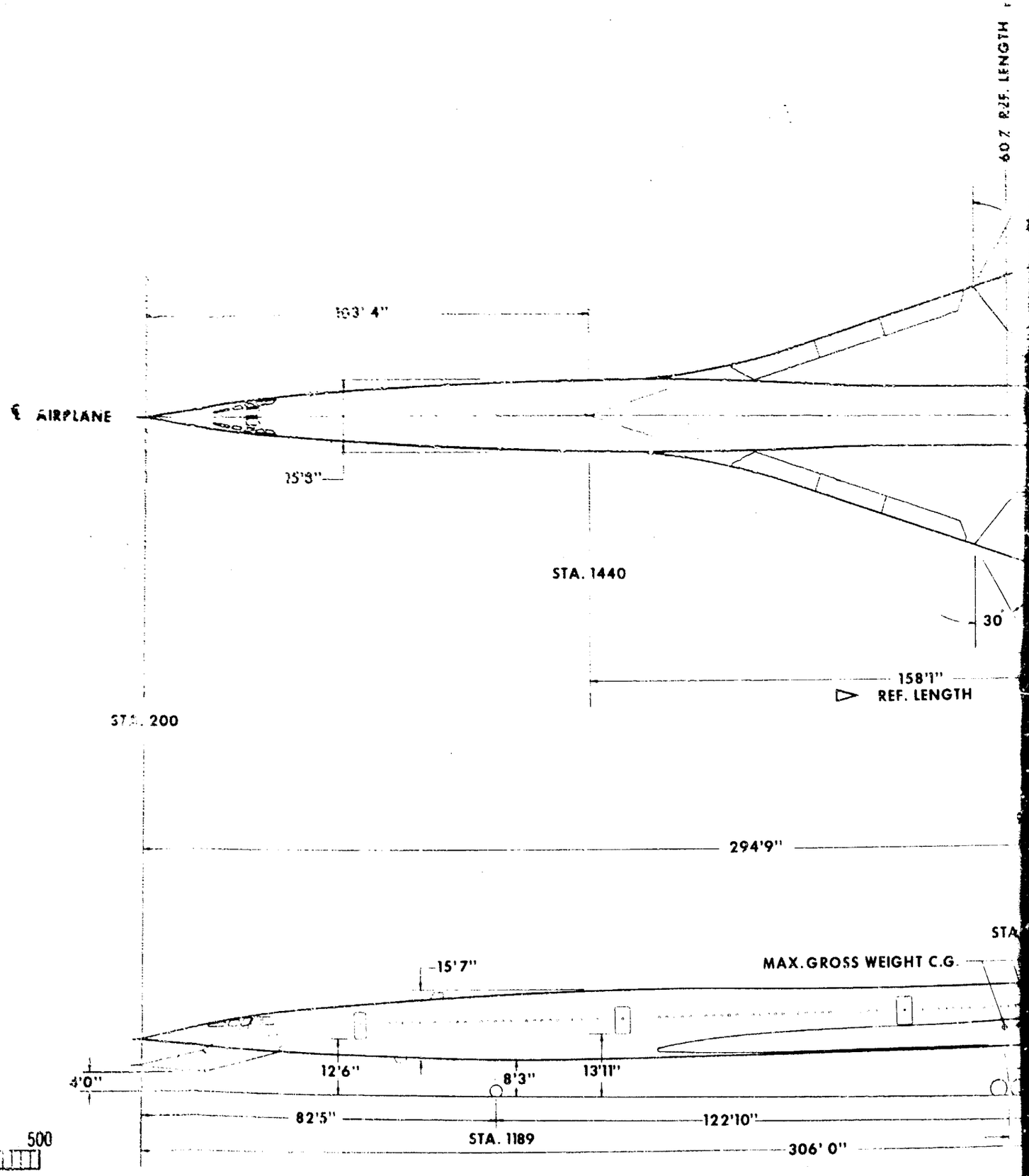
60% REF. LENGTH
℄ AIRPLANE
193' 4"
35'3"
STA. 1440
30°
158'1"
REF. LENGTH
STA. 200
294'9"
MAX. GROSS WEIGHT C.G.
15'7"
12'6"
8'3"
13'11"
4'0"
82'5"
122'10"
STA. 1189
306' 0"
500

B

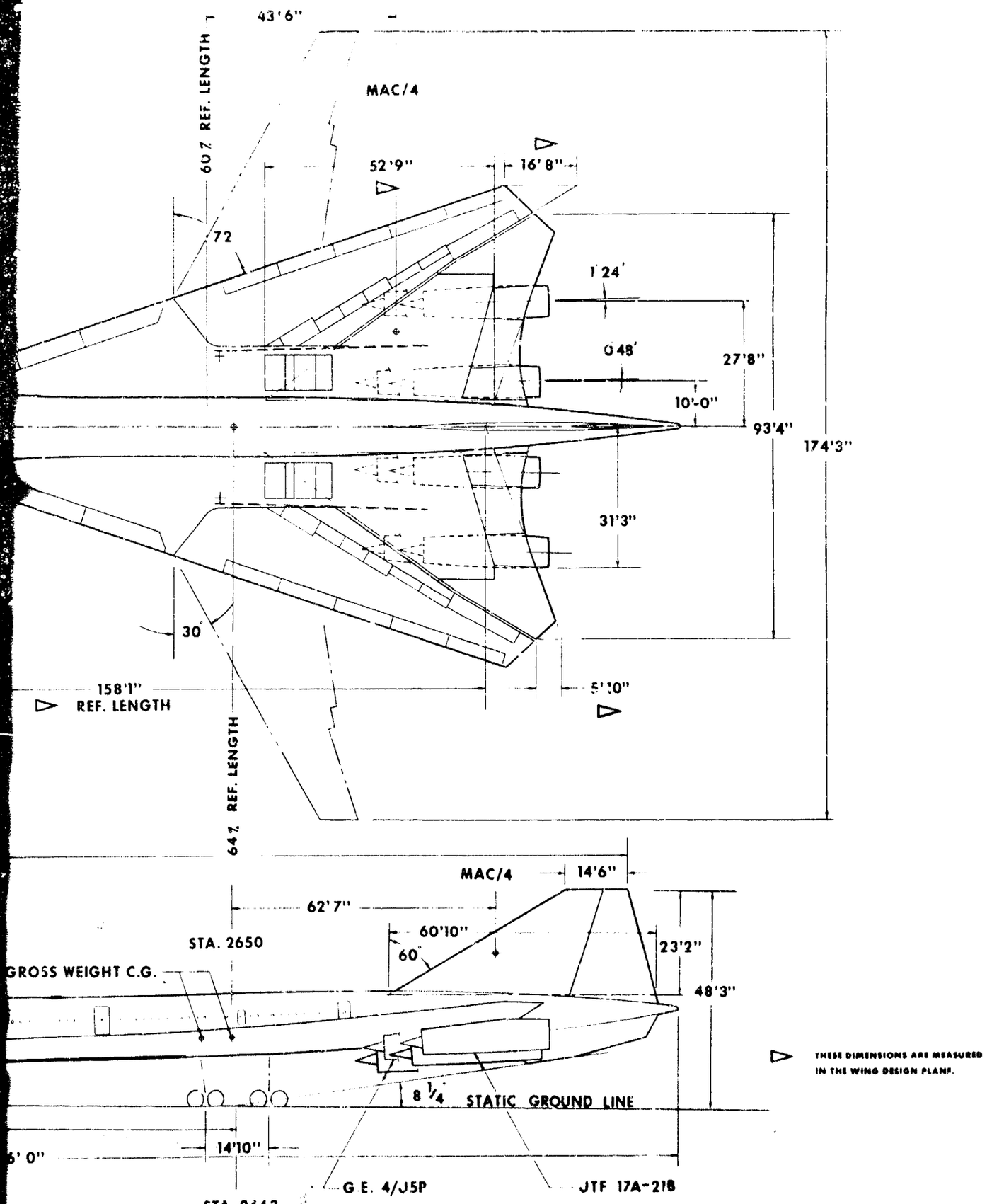


*Figure 1-3. General Arrangement Model B2707*

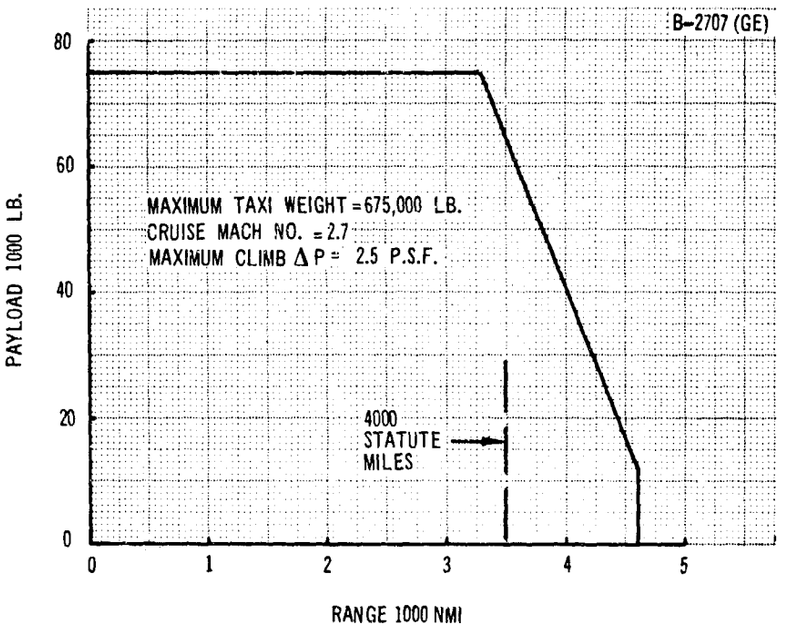


*Figure 1-4. Payload Range Performance (GE)*

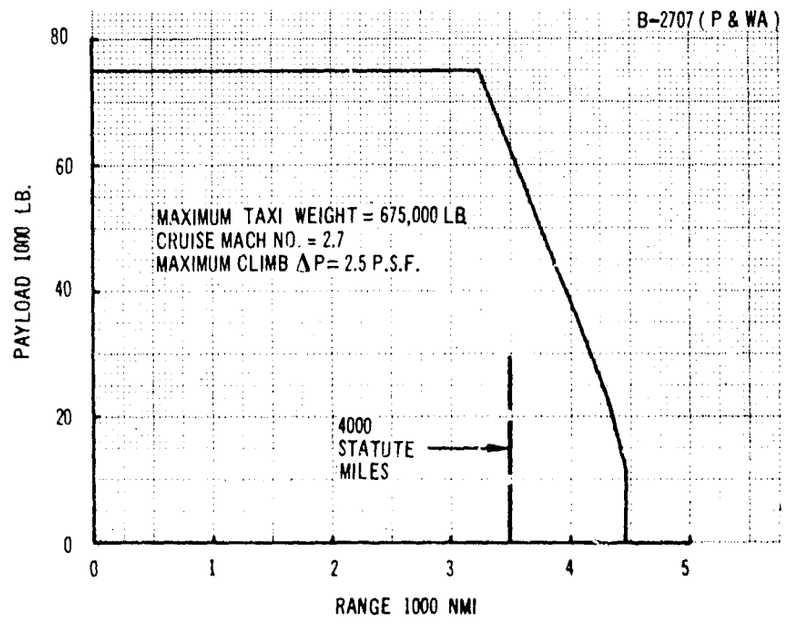


*Figure 1-5. Payload Range Performance (P&WA)*

The FAR takeoff field lengths, liftoff speeds, and community noise levels as a function of takeoff weight are shown in Figs. 1-6 and 1-7. The B-2707 has the following takeoff performance at the maximum design taxi weight of 675,000 lb and maximum augmented thrust:

| | B-2707 (GE) | | B-2707 (P&WA) | |
|---|---|---|---|---|
| Center of gravity location | 0.595$C_R$ Forward | 0.615$C_R$ Normal | 0.595$C_R$ Forward | 0.615$C_R$ Normal |
| FAR takeoff field length (ft) | 7,000 | 6,300 | 7,300 | 6,600 |
| Liftoff speed, kn EAS | 169 | 162 | 169 | 162 |
| Airport noise, PNdb | 121 | 121 | 117 | 117 |
| Community noise, PNdb | 100 | 99 | 105 | 104 |

The noise levels quoted above are those for the B-2707 with only the engine exhaust noise suppression systems provided by the engine manufacturer, and with a sonic throat in the inlet. Exhaust noise suppression systems under development by The Boeing Company offer even greater reductions in airport noise levels. With the Boeing suppressors, airport noise levels are reduced 9 PNdb for the GE engines and 4 PNdb for the P&WA engines; community noise levels are reduced 1 to 2 PNdb for both engines.

Approach speeds, FAR landing field lengths, and approach noise levels as a function of landing weight are shown in Figs. 1-8 and 1-9. At maximum landing weight and with maximum flap deflection, the airplane has the following landing performance:

| | B-2707 (GE) | | B-2707 (P&WA) | |
|---|---|---|---|---|
| Maximum landing weight (lb) | 430,000 | | 420,000 | |
| Center of gravity location | 0.595$C_R$ Forward | 0.615$C_R$ Normal | 0.595$C_R$ Forward | 0.615$C_R$ Normal |
| Approach speed, kn EAS | 153 | 145 | 151 | 143 |
| FAR landing field length (ft) | 7,500 | 7,000 | 7,400 | 6,900 |
| Constant velocity approach noise level, PNdb | 112 | 111 | 115 | 114 |

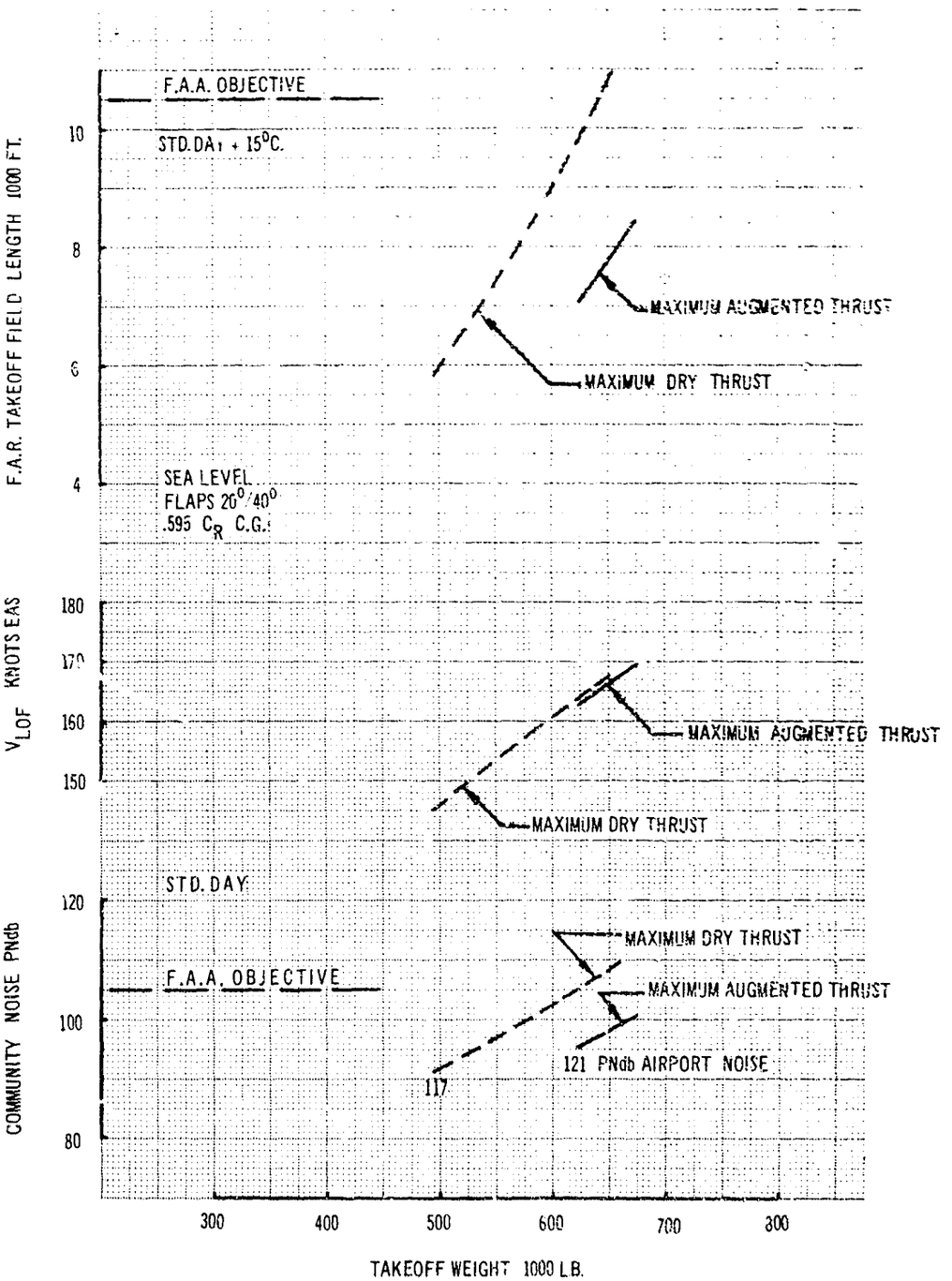


*Figure 1-6. Takeoff Performance (GE)*

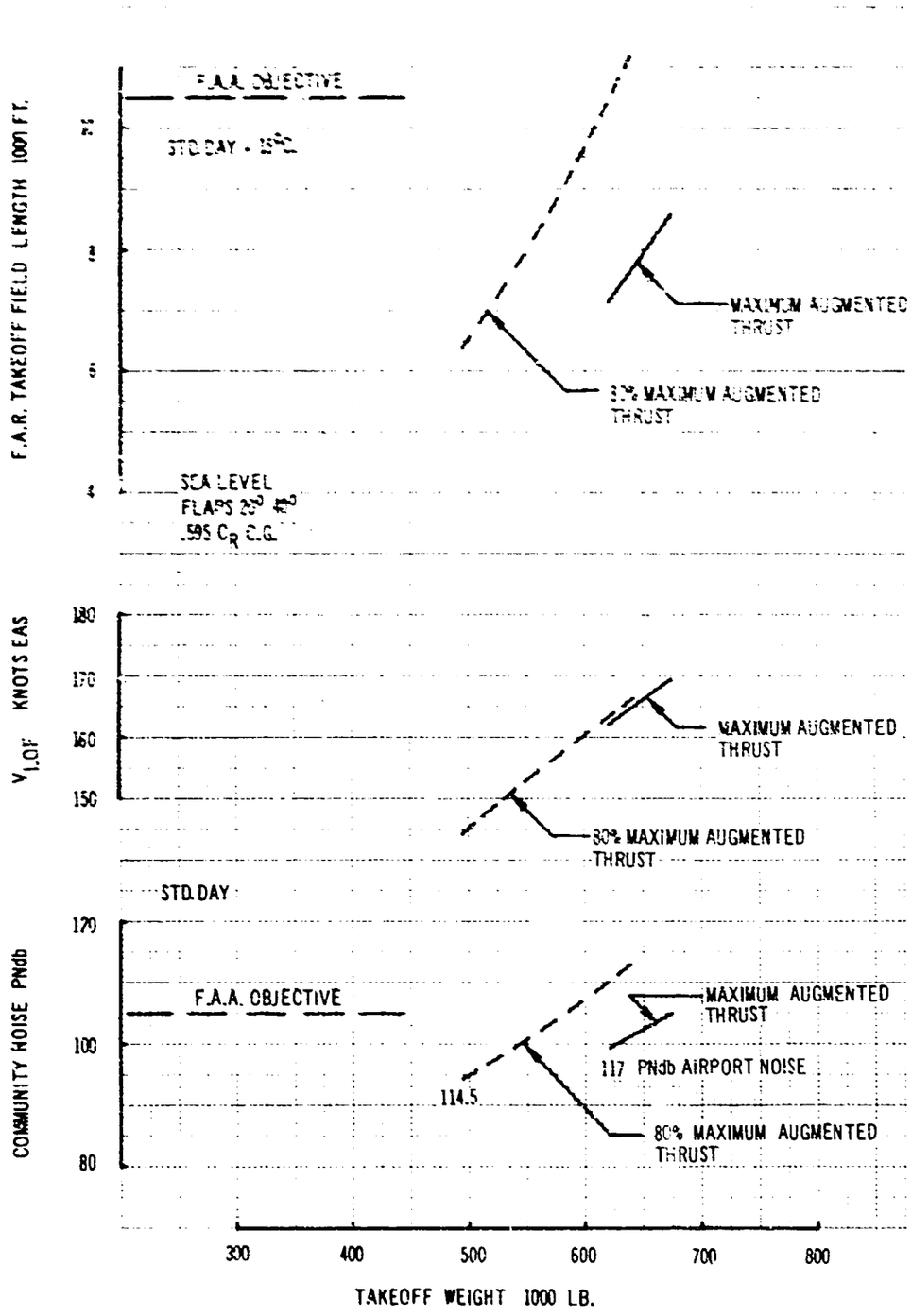


*Figure 1-7. Takeoff Performance (P&WA)*

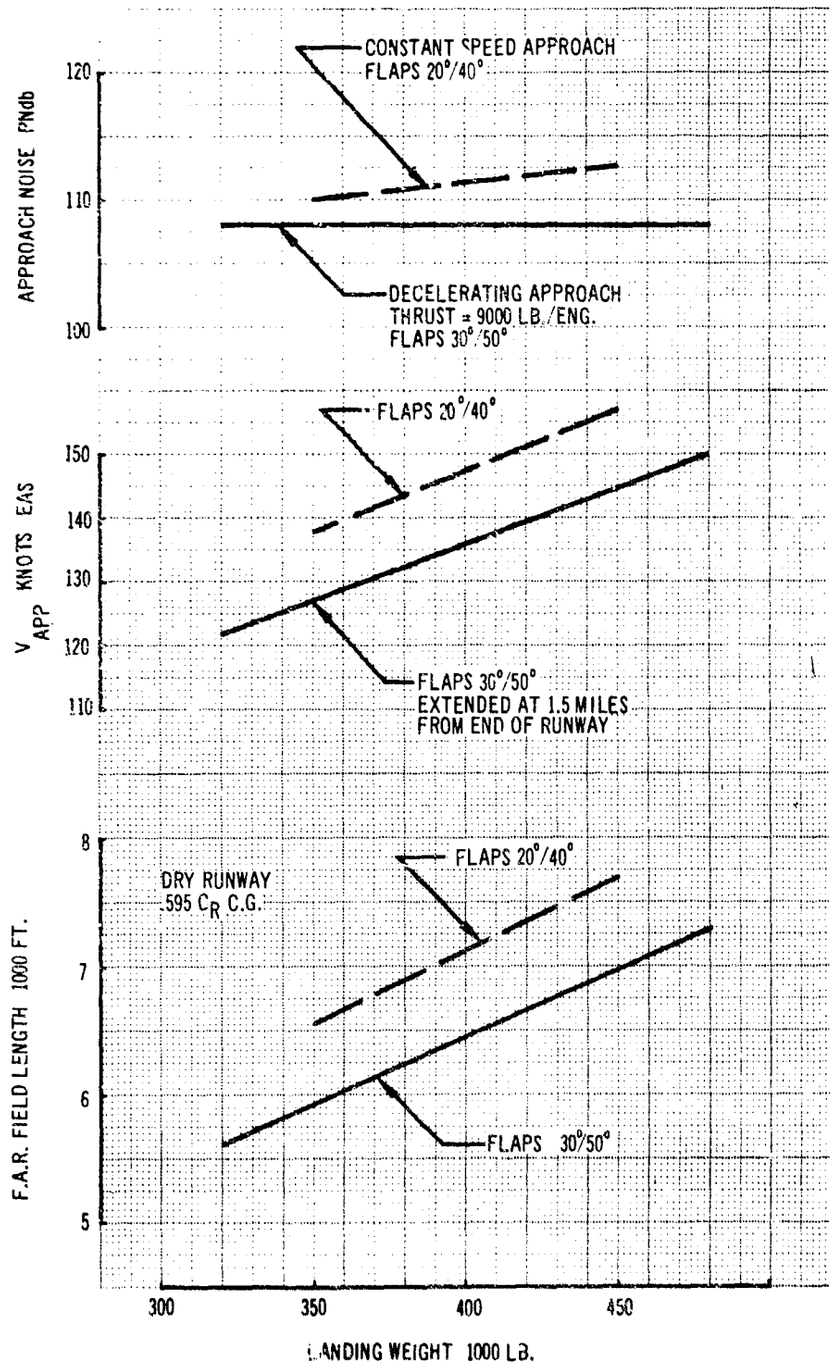


*Figure 1-8. Landing Performance (GE)*

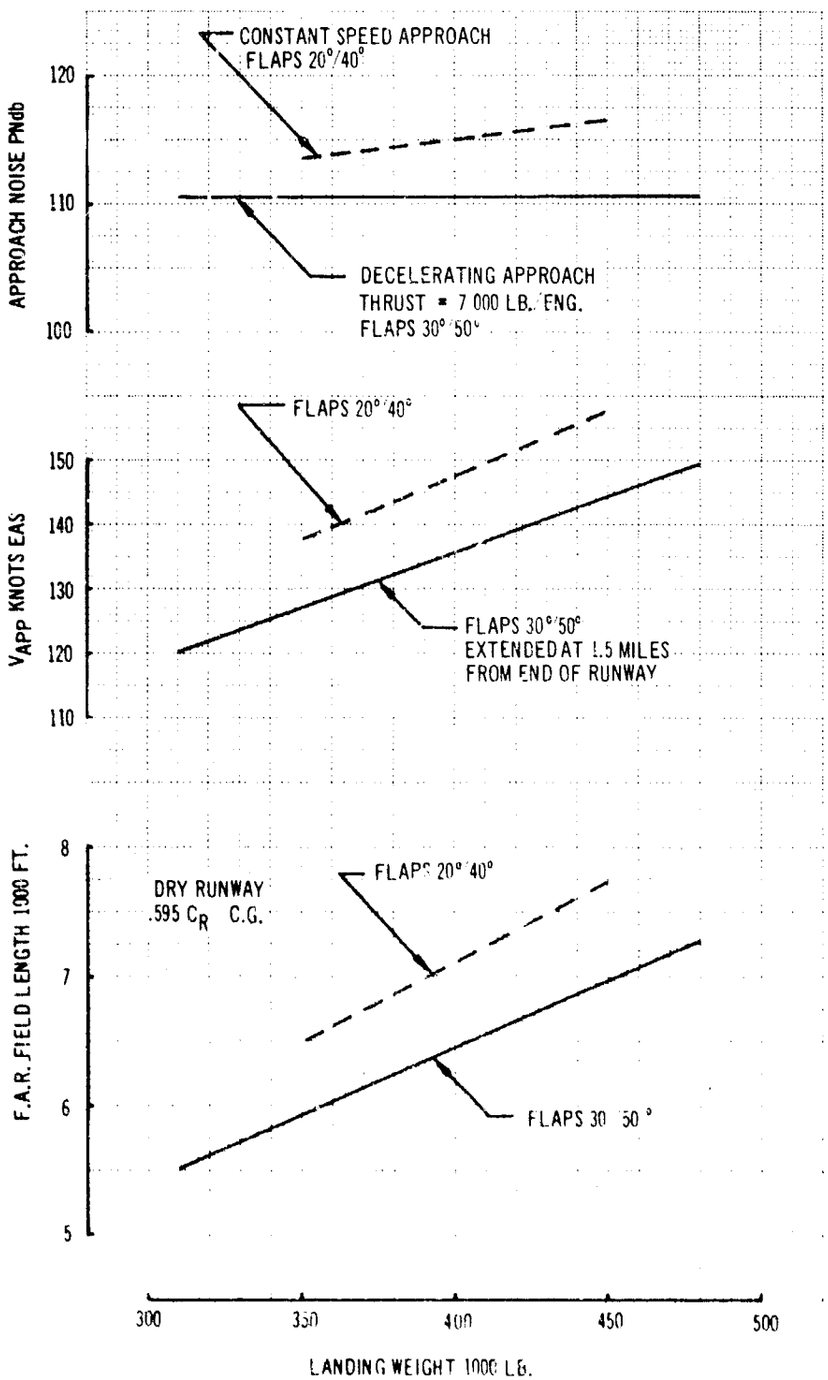


*Figure 1-9. Landing Performance (P&WA)*

## 1.3 LIFT-TO-DRAG RATIO

Current wind tunnel data indicate a Mach 2.7 maximum lift-to-drag ratio of 7.8 for the B-2707 configuration. Although achieved with a six-abreast body, this value is higher than that achieved with the previous five-abreast configuration. Refinements in the wing, body shape, cab design, and nacelle installation for the B-2707 have contributed to this high level of aerodynamic efficiency. The development of low drag nacelles having inlets aligned with the local flow, exit nozzles aligned for optimum thrust effects, and shape tailored to house the engine and accessories has been a major effort during the past two years. The wide variety of nacelle shapes which have been wind tunnel tested and have lead to the present design are shown in Fig. 1-10. All wind tunnel force and moment tests of complete configurations have been made with flow-type nacelles which properly duplicate the complete interference effects. Exploration of configuration refinements is continuing in order to ensure the best possible production airplane characteristics. This work is discussed in Sec. 3.0.

## 1.4 STABILITY AND CONTROL

A unique combination of stability and control surfaces is incorporated in the B-2707 design. The variable-sweep wing, in the forward position, permits longitudinal and lateral control of the airplane to be provided by separate and independent systems. This is a particularly desirable feature during gusty crosswind landings. Longitudinal control is provided by trailing edge elevators and tip elevons on the horizontal tail. Conventional ailerons near the wing tips and wing spoilers provide lateral control that is comparable to that on present jet transports. With the wings swept aft, longitudinal control is provided by the elevators and elevons with the elevons also providing lateral control. The four inboard segments of the wing spoilers also provide lateral control during high speed flight. Wind tunnel tests and theoretical analyses indicate that these systems, with normal development, provide the good handling qualities and the high levels of safety necessary for commercial transport operation.

## 1.5 AEROELASTICITY

The development of accurate methods for predicting the effects of aeroelasticity on airplane aerodynamic characteristics has been a continuing program at Boeing for nearly 20 years. During the past eight years a number of analysis methods have been developed for determining airplane aeroelastic effects at subsonic, transonic, and supersonic speeds, and the results have been correlated with wind tunnel and flight test data. Typical correlations for a flexible wing model at Mach 2.7 are shown in Fig. 1-11 where initial lift curve slope, aerodynamic center location, and zero-lift pitching moment coefficient are shown for a range of dynamic pressures. Theoretical and experimental results for both a rigid and a scaled stiffness model are shown. The scaled stiffness model simulated the structural and geometric characteristics of the movable portion of a variable sweep configuration. Tests of a more sophisticated scaled stiffness model of the B-2707 configuration are scheduled for September, 1966. This model will provide the capability for testing both flexible and rigid wings, tails, and forward body sections.

## 1.6 GROWTH

Takeoff performance of the B-2707 configuration at gross weights greater than 675,000 lb is shown in Figs. 1-12 and 1-13. The gross weight of the basic configuration can be increased to 750,000 lb and at the same time meet the FAA objective of a 10,500-ft FAR takeoff field length, and the FAR second-segment climb gradient requirement on a hot day. Additional fuel volume can be provided by slight changes to the airplane's external contours, which will allow the space-limited payload of 75,000 lb to be carried a distance of 3,830 nmi (B-2707 GE) or 3,760 nmi (B-2707 P&WA) as shown in Figs. 1-14 and 1-15.

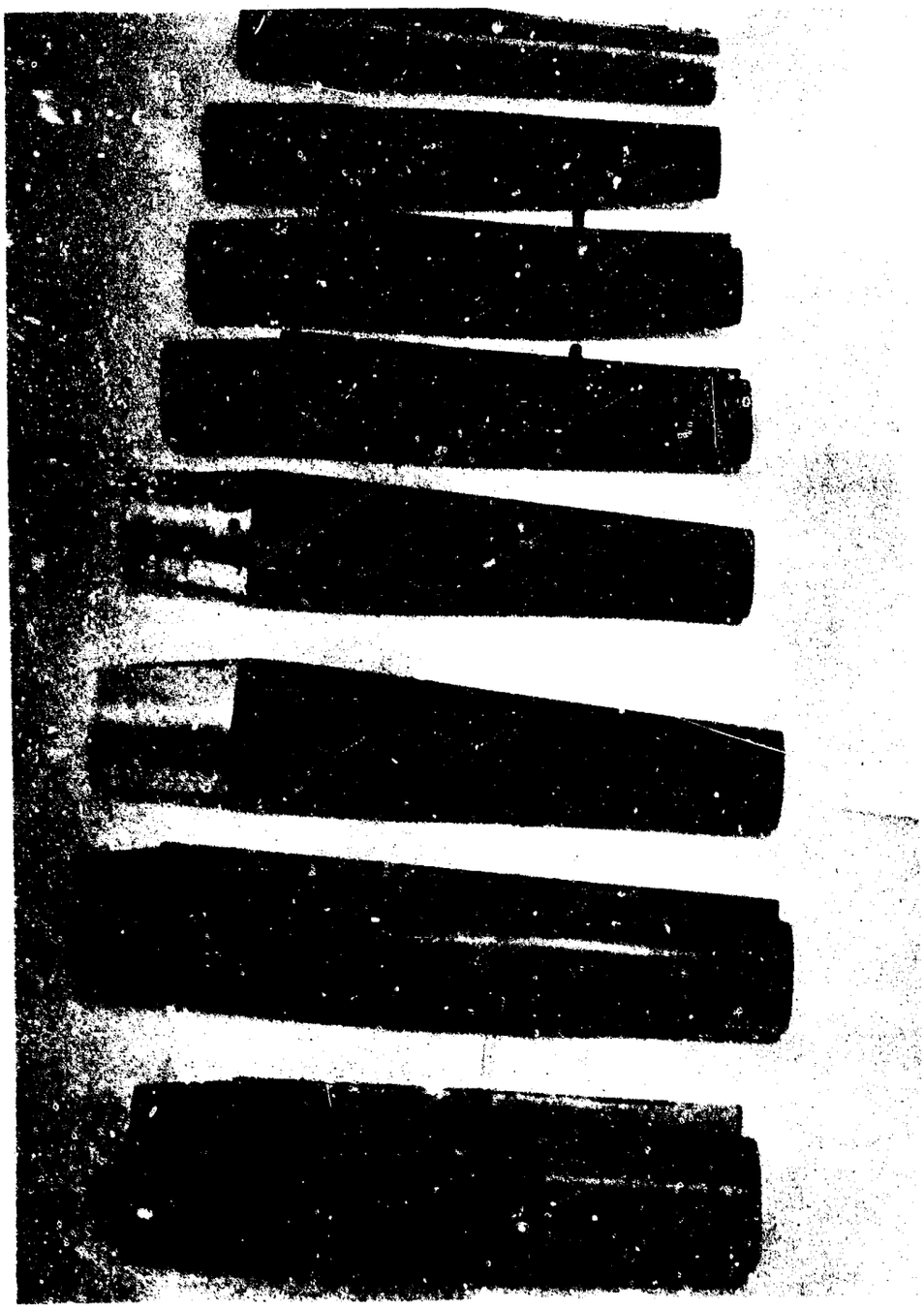

*Figure 1-10. Flow Nacelle Development*

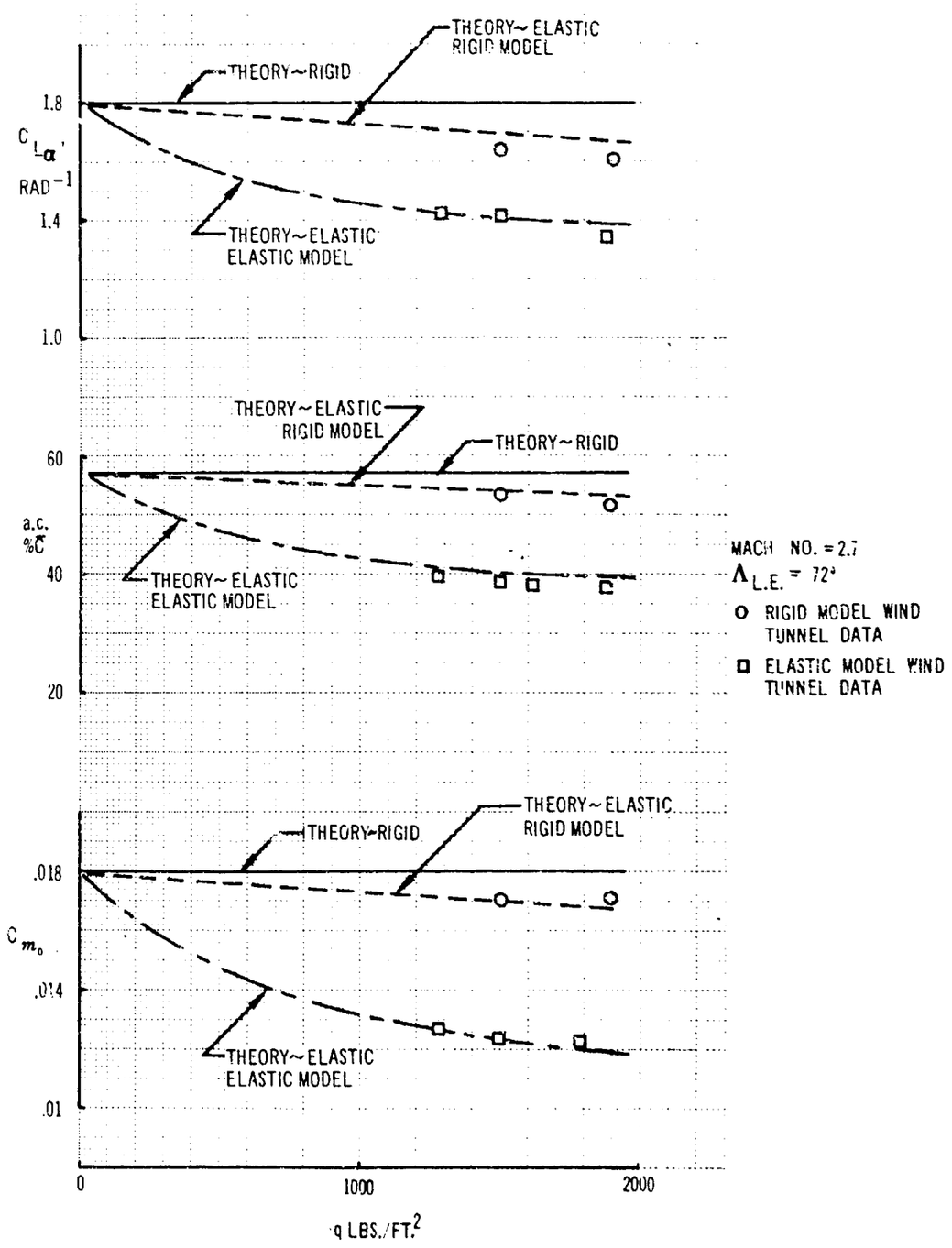


*Figure 1 – 11. Effects of Aeroelasticity on Aerodynamic Characteristics*

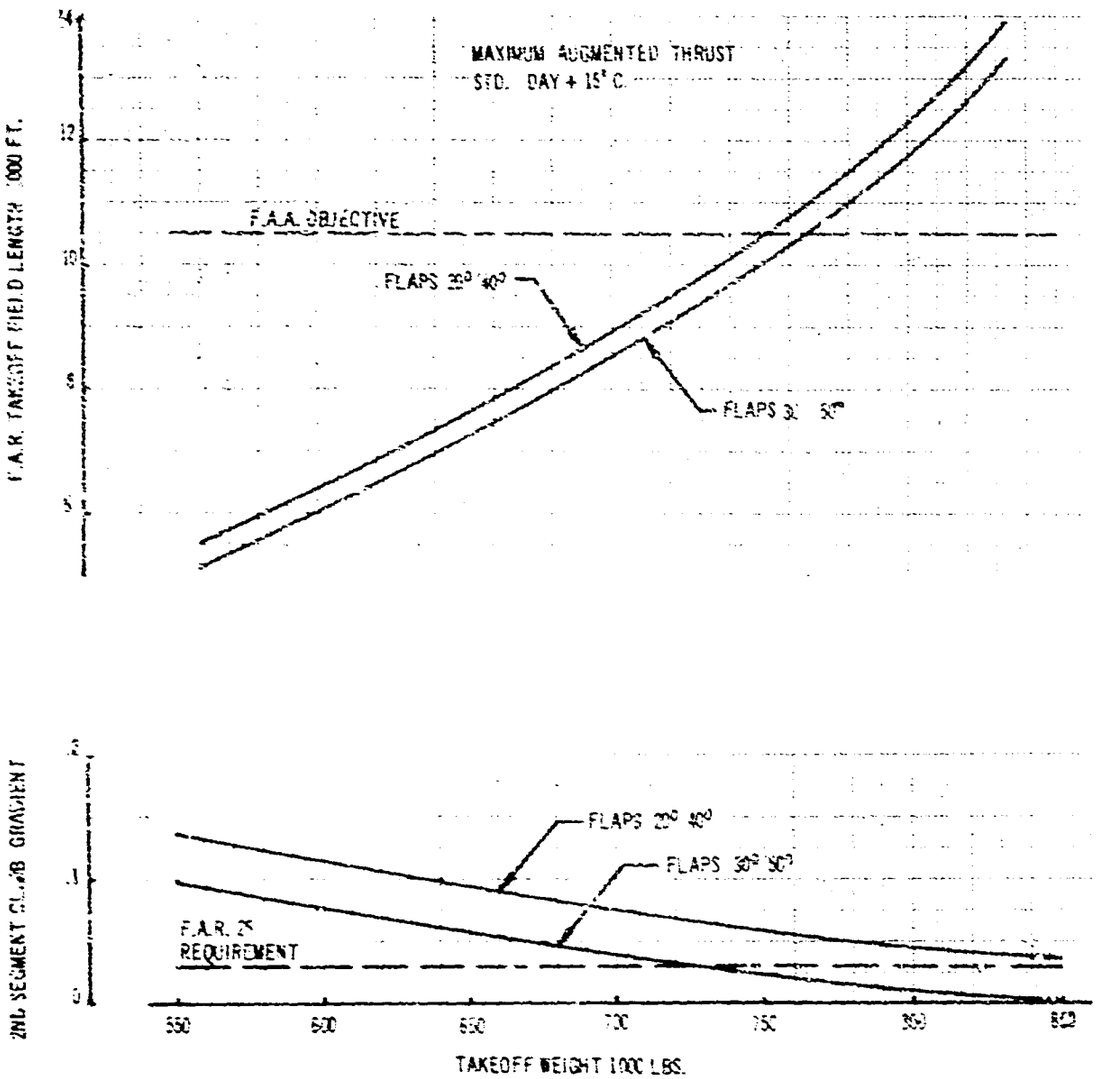


*Figure 1-12. Growth Takeoff Performance (GE)*

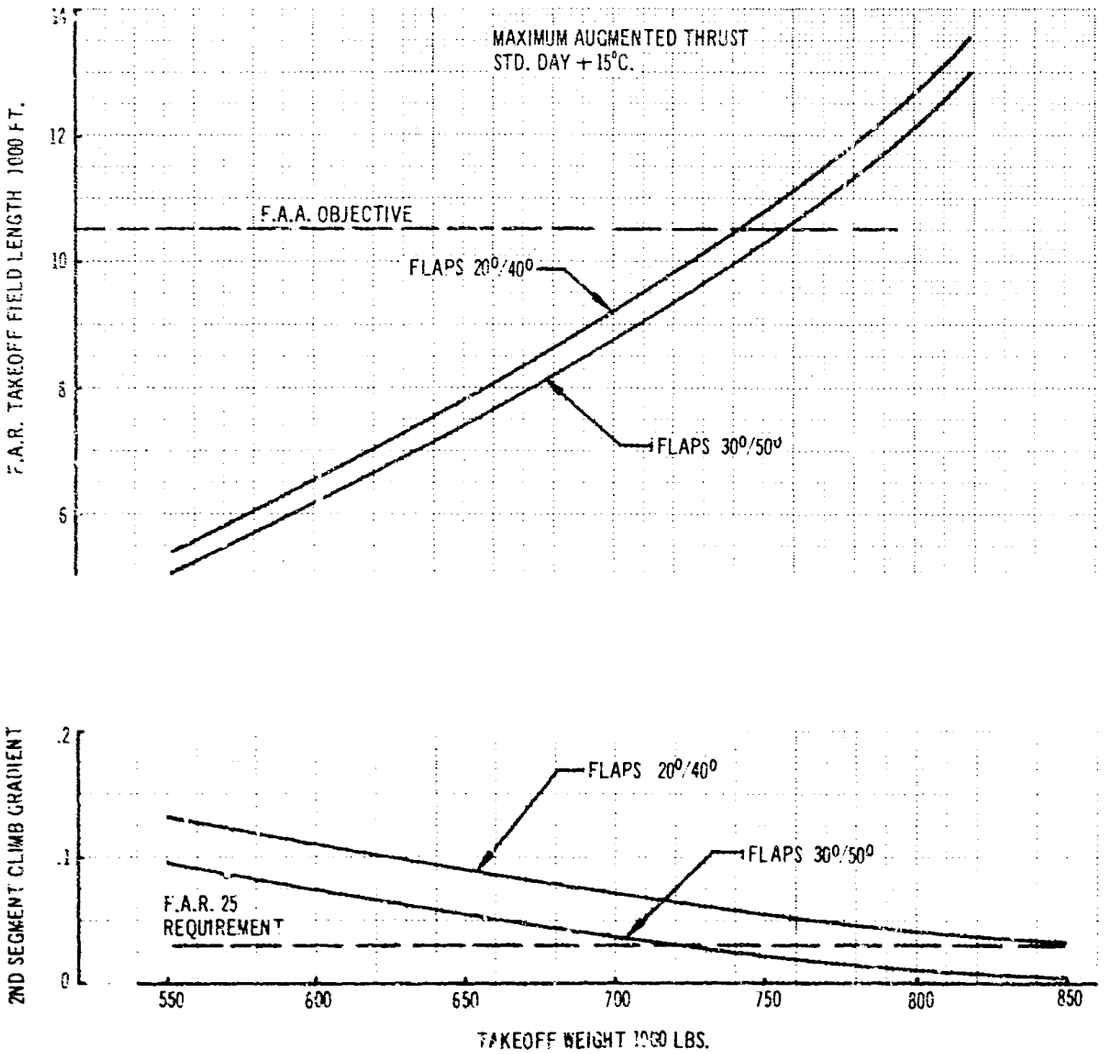


*Figure 1-13. Growth Takeoff Performance (P&WA)*

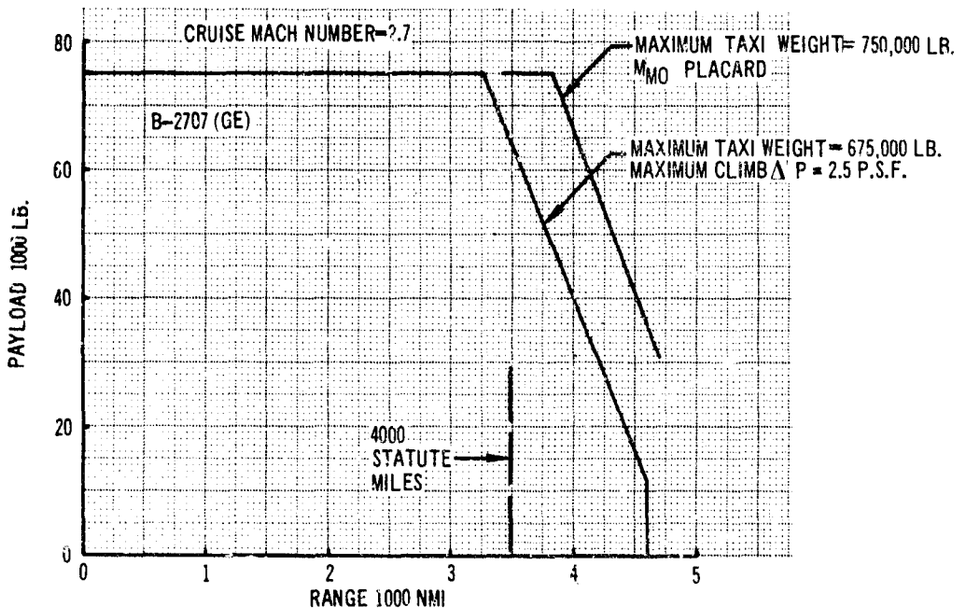


*Figure 1-14. Growth Payload Range Performance (GE)*

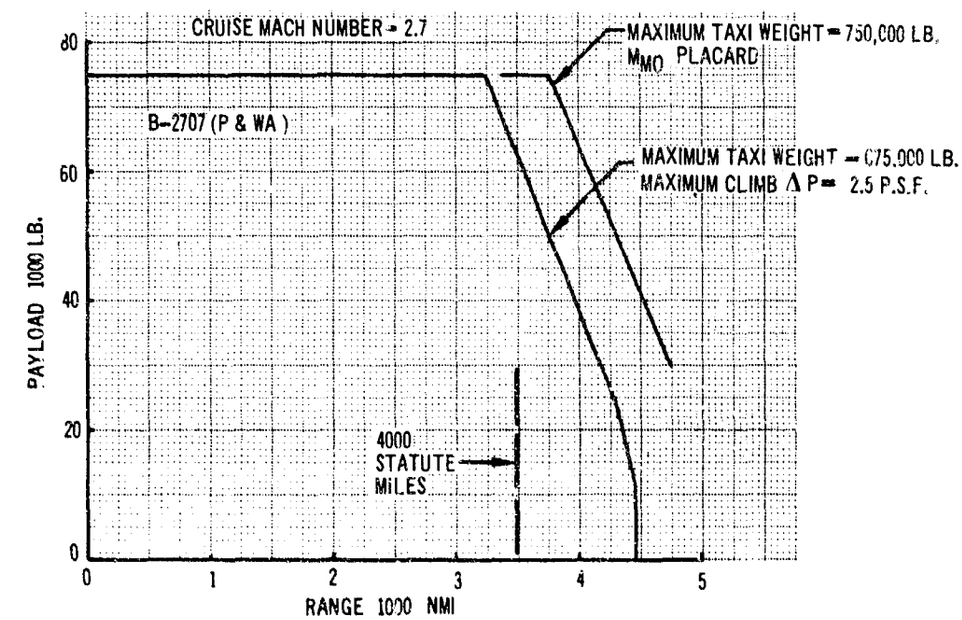


*Figure 1-15. Growth Payload Range Performance (P&WA)*

## 2.0 PERFORMANCE


| | | Page |
|---|---|---|
| 2.1 | MISSIONS | 19 |
| 2.2 | TAKEOFF PERFORMANCE | 19 |
| 2.3 | APPROACH AND LANDING PERFORMANCE | 31 |
| 2.4 | OFF-DESIGN AND EMERGENCY RANGE PAYLOAD PERFORMANCE | 36 |
| 2.5 | PERFORMANCE CALCULATION METHODS | 40 |

## 2.0 PERFORMANCE

This section presents a summary of the major performance capabilities of the Boeing Model 2707, powered with either General Electric or Pratt and Whitney engines. More detailed performance data, such as that required for airline route analyses and expansion upon all topics discussed here, are presented in Airplane Performance (General Electric Engines), V2-B2707-4, and Airplane Performance (Pratt and Whitney Engines), V2-B2707-5.

Evolution of the B-2707 has brought improved payload range capability, substantially greater than the Phase III objectives, while retaining good low speed performance and low community noise levels. The B-2707 has been designed in response to the airlines desire for long range, high payload capacity with six-abreast passenger seating accommodations. Up to 314 passengers can be carried using an international tourist seating arrangement. In addition, use of the variable-sweep design results in exceptional operational versatility, for example, where mixed subsonic-supersonic missions are required.

The performance of the B-2707 airplane on international routes is summarized in Table 2-A. Comparative performance data on the B-2707 with four 620-lb/sec General Electric GE4/J5P engines and with four 687-lb/sec Pratt and Whitney JTF17A-21B engines are shown based upon engine data received before July 16, 1966. (See the foreword and Appendix B to this document for changes in performance caused by engine changes after July 15, 1966.) Especially noteworthy are: The excellent payload range capability with either engine—over 4,300 statute miles with 50,000 lb of payload; the low community noise values on landing approach—only 108 PNdb for the B-2707 (GE) and 111 PNdb for B-2707 (P&WA); and the excellent landing performance on dry or wet runways because of the high lift capabilities of the variable-sweep wing. Without the use of reverse thrust and including the 1.15 factor specified by the FAR, the wet-runway FAR landing field length is only 7,500 ft. Use of two engines with reverse thrust reduces the FAR wet-landing field length to only 6,200 ft.

The noise suppression characteristics used in the performance calculations are those offered by the engine manufacturers in their augmentation and exhaust nozzle systems plus the application of a sonic throat in the propulsion air inlet. Comparative performance and noise contour data are shown with a Boeing suppressor under development in noise research programs. The Boeing jet suppressor reduces the airport noise from 121 to 112 PNdb for the GE engine and from 117 to 113 PNdb for the P&WA engine. The engine data used in the performance calculations are given in Propulsion Report (V2-B2707-13). The engine noise data used are contained in Airport and Community Noise Program report (V4-B2707-4).

Landing approach noise has been calculated for a constant speed procedure and for a decelerating approach. Using the decelerating approach method reduces the community noise 4 PNdb. The decelerating approach only requires that the pilot extend the flaps to a higher angle setting as the community is approached. Trim and attitude changes are negligible. In the decelerating approach, the community noise is 108 PNdb for the B-2707 (GE) and 111 for the B-2707 (P&WA).

Sonic boom overpressures for the airplane performance are based upon the far-field calculation method. The method used is consistent with that established by the FAA and the NASA for Phases I, II-A, and II-C and is described in Ref. 1. To account for the effect of the atmosphere, the approximate correction factor $\sqrt{P_g/P_a}$ was used. Sonic boom overpressures using the near-field theory have also been calculated for the B-2707 and are shown in this section. Details are given in Sonic Boom Program, V4-B2707-3.

All performance data are based upon the U.S. Standard Atmosphere, 1962, at 45 degrees latitude, geometric altitude. Hot day performance has been computed for a modified standard atmosphere wherein the temperatures given by the U.S. Standard Atmosphere are increased +10 degrees C at all altitudes. The basis for computing performance during all phases of flight and the definition

Table 2-A. Performance Summary, International

| Item | Configuration | *General Electric GE4/J5P | *Pratt & Whitney JTF17A-21B | FAA Phase III objectives |
|---|---|---|---|---|
| Weights | Maximum design taxi weight (lb) | 675,000 | 675,000 | |
| | Operational empty weight (lb) | 287,500 | 285,000 | |
| | Maximum allowable payload (lb) | 75,000 | 75,000 | |
| | Nominal payload (lb) | 50,000 | 50,000 | |
| | Maximum landing weight (lb) | 430,000 | 420,000 | |
| Range | Range, M = 2.7, statute miles | 4,380 | 4,300 | |
| Std day | Maximum ΔP (PSF) of: | | | |
| | climb/cruise/descent | 2.50 | 2.50 | 2.5 |
| | | 1.88 | 1.87 | 1.7 |
| | | 1.66 | 1.65 | 1.5 |
| P.L.= 50,000 lb | Range, M=0.85, statute miles | 3,780 | 4,455 | |
| Std day +10 deg C | Range, M = 2.6, statute miles | 3,995 | 3,995 | |
| | Maximum Δ P (PSF) of: | | | |
| | climb/cruise/descent | 2.50 | 2.50 | |
| | | 1.85 | 1.83 | |
| | | 1.64 | 1.63 | |
| Takeoff | Thrust setting | Max. Aug. | Max. Aug. | |
| Max. design taxi wt. S.L. Std. day | FAR Field Length (ft) | 7,000 | 7,300 | |
| | $V_{LOF}$ Kn (equivalent air speed) | 169 | 169 | ------ |
| | Airport noise (PNdb) | 121 | 117 | 116 |
| | Community noise (PNdb) | 100 | 105 | 105 |
| S.L. Std day +15° C | FAR Field Length (ft) | 8,300 | 8,500 | 10,500 |
| Landing | FAR Field Length (ft) (dry) | 7,500 | 7,400 | ------ |
| | FAR Field Length (ft) (wet) | 7,600 | 7,500 | 8,000 |
| Max. ldg wt. S.L. Std day | Community noise (using one Kn/sec decelerating approach) (PNdb) | 108 | 111 | 109 |
| | Community noise (using constant velocity approach) (PNdb) | 112 | 115 | |

*Based upon engine data received before July 16, 1966. See Appendix B to this volume for effects of subsequent changes in engine data. The data shown are without the Boeing jet noise suppressor.

of the nonstandard day atmosphere models used are described in Par. 2.5.

## 2.1 MISSIONS

### 2.1.1 Payload Range Capability

Figure 2-1 shows the payload-range capability of the B-2707, calculated using the FAA Supersonic Transport Economic Model Ground Rules (SST 66-3, dated June 30, 1966) for international missions. The special effects included in the payload range performance are those listed and calculated according to the instructions given in the Request for Proposal. The incremental range payload effects are given in Par. 2.5. Using these rules, the B-2707 has an international mixed seating capacity of 277 passengers. With this passenger payload, the M = 2.7 mission range is 3,720 nmi for the B-2707 (GE) and 3,640 nmi for the B-2707 (P&WA) when a climb schedule for a sonic boom overpressure of 2.5 psf is followed. Range payload capability is also shown for a climb procedure which follows $M_{MO}$, the maximum operating Mach number schedule. Climb at $M_{MO}$ results in a maximum sonic boom overpressure of about 3.3 psf during climb and a range increase of 130 nmi for the B-2707 (GE) and 120 nmi for the B-2707 (P&WA). This climb procedure may be acceptable for overocean flights. For subsonic missions, the cruise Mach number is 0.85 and the wing leading edge sweep is 42 degrees. The all-subsonic mission range is 3,200 nmi for the B-2707 (GE) and 3,750 nmi for the B-2707 (P&WA). The detailed breakdown of time, fuel, and distance for these missions are presented in Airplane Performance (GE) V2-B2707-4 and Airplane Performance (P&WA) V2-B2707-5.

Figure 2-2 shows the payload range capability for standard day temperatures ±10°C. The maximum sonic boom overpressure during climb is 2.5 psf. Stagnation temperature is limited to 500°F which results in a slight cruise Mach number reduction on hot days. A 50,000-lb payload can be carried 4,000 statute miles by the B-2707 with either engine installation on a standard +10°C day. A payload of 72,000 lb can be carried by the B-2707 (GE) and 75,000 lb by the B-2707 (P&WA) on a standard -10°C day.

A domestic airplane with a maximum taxi weight of 575,000 lb has been derived from the international version. It is identical in all respects with the 675,000-lb airplane except that the operational empty weight (OEW) has been reduced 12,000 lb.

Payload range data are shown in Fig. 2-3 for domestic missions in which the climb and cruise overpressure objectives of 2.0 and 1.5 psf are met. The domestic mixed seating arrangement of the economic model ground rules results in a 261-passenger payload. At 575,000 lb maximum taxi weight and with this passenger payload, the domestic B-2707 (GE) has a range of 2,400 nmi; and the domestic B-2707 (P&WA) has a range of 2,380 nmi. Also shown are the trades of range payload capability if the sonic boom overpressures are allowed to increase slightly. The range is increased 380 nmi for the domestic B-2707 (GE), and 340 nmi for the domestic B-2707 (P&WA) for a 10 percent increase in climb overpressure.

### 2.1.2 Flight Profiles

A typical flight profile for the B-2707 for an international mission is shown in Fig. 2-4. Variations of far-field sonic boom overpressures under the flight path are shown. The far-field sonic boom overpressure calculation method is used for this proposal (Ref. 1). In descent the maximum overpressure reaches 1.65 psf. Descent schedules which meet the 1.5-psf objective are included in documents V2-B2707-4 and -5. The 1.5-psf descent schedule results in no range change but increases the descent time by approximately 3 minutes.

Figure 2-5 shows the effect of using the near-field theory for calculation of the sonic boom overpressures in climb. The overpressure values are up to 15 percent less during climb using the near-field method. Using near-field theory to calculate the $\Delta P = 2.5$ psf climb schedule gives a lower altitude Mach number schedule as compared to the far-field method. A range increase of 80 nmi for the B-2707 (GE) would result if near-field theory were used. A 100-nmi increase would occur for the B-2707 (P&WA).

## 2.2 TAKEOFF PERFORMANCE

The B-2707 has good takeoff performance using maximum augmented thrust for the maximum taxi weight of 675,000 lb. Equally good performance and reduced airport noise are possible for weights of 600,000 lb or less using maximum dry engine thrust for the B-2707 (GE) and 80-percent maximum augmented thrust for the B-2707 (P&WA).

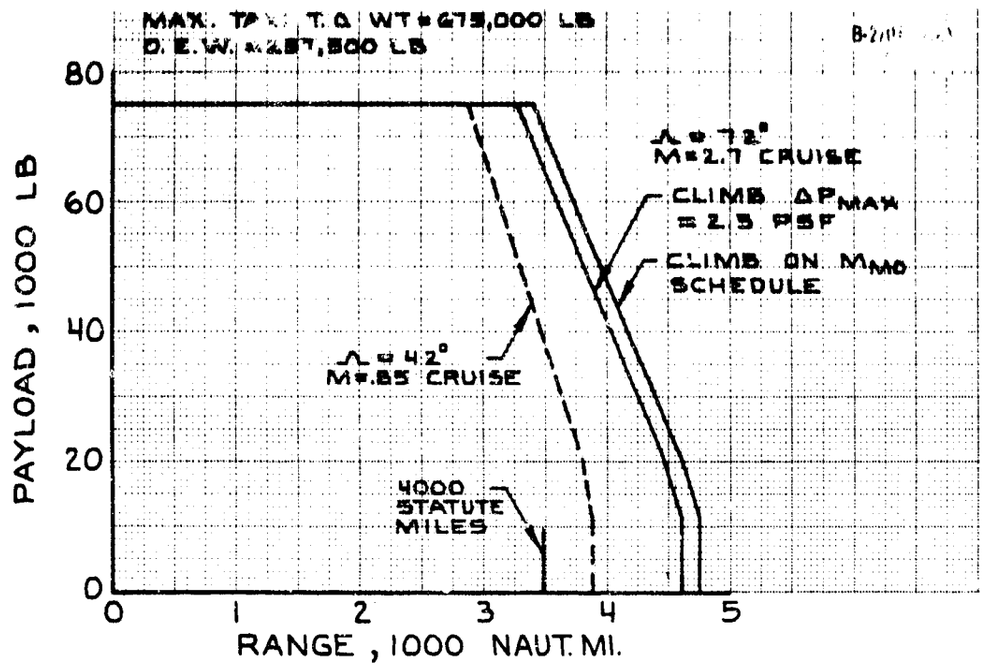


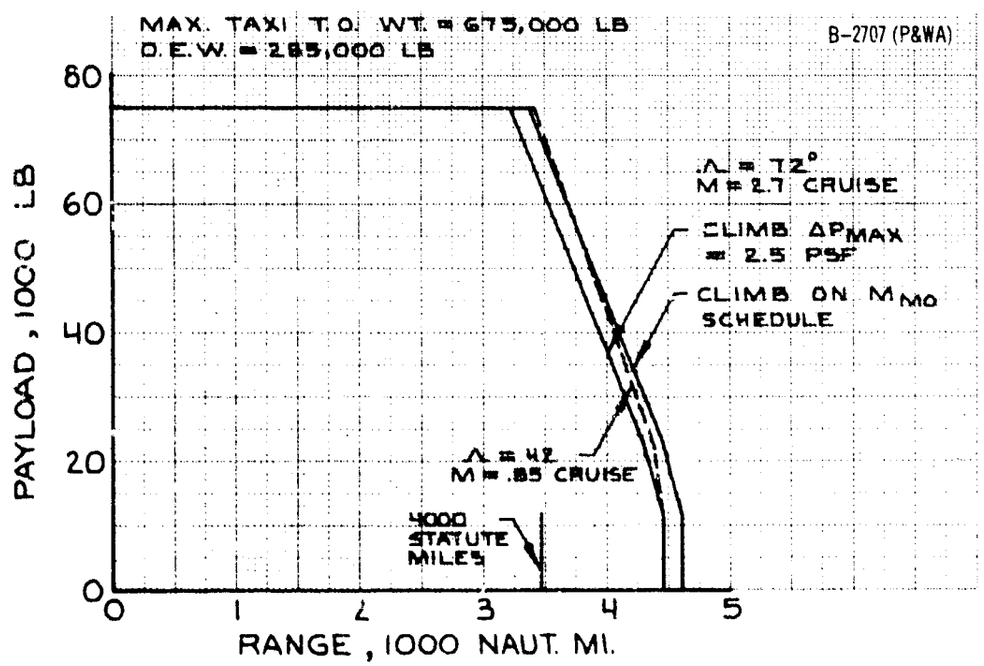


*Figure 2-1. Payload Range, International Mission, Standard Day*

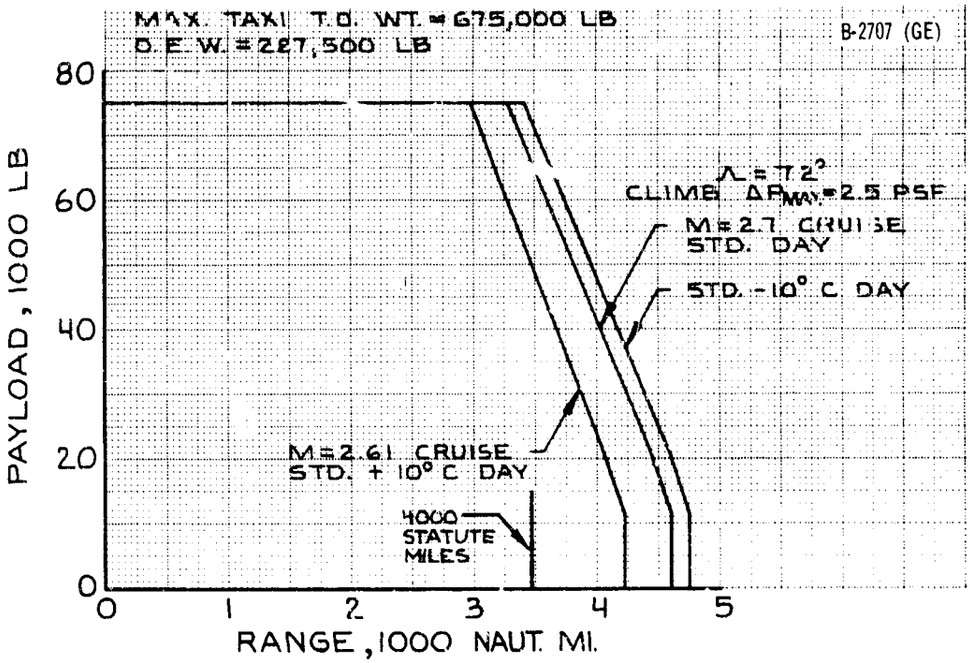


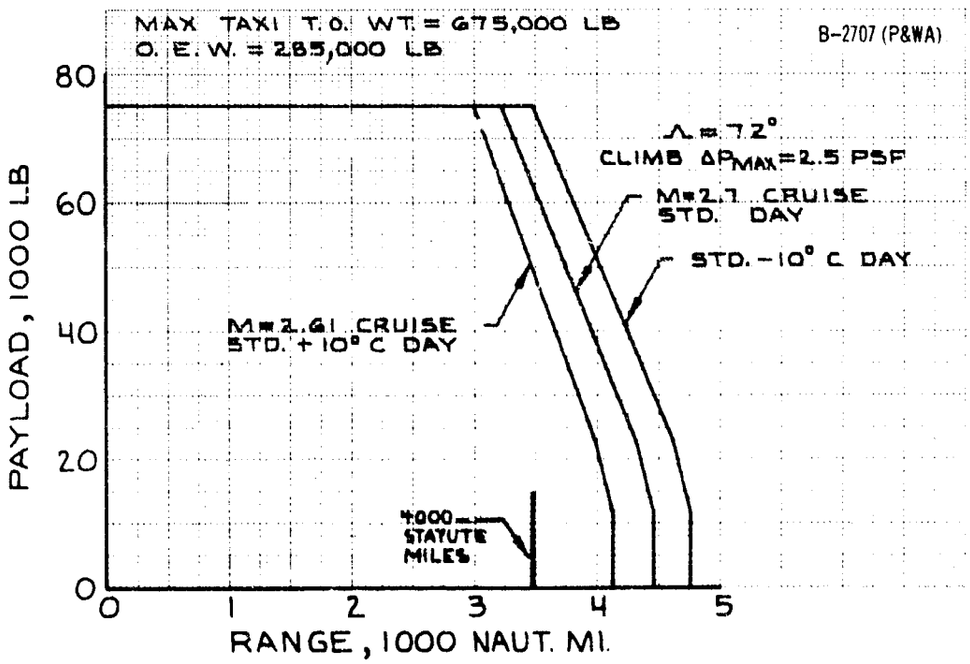


*Figure 2-2. Payload Range, International Mission, Non Standard Day*

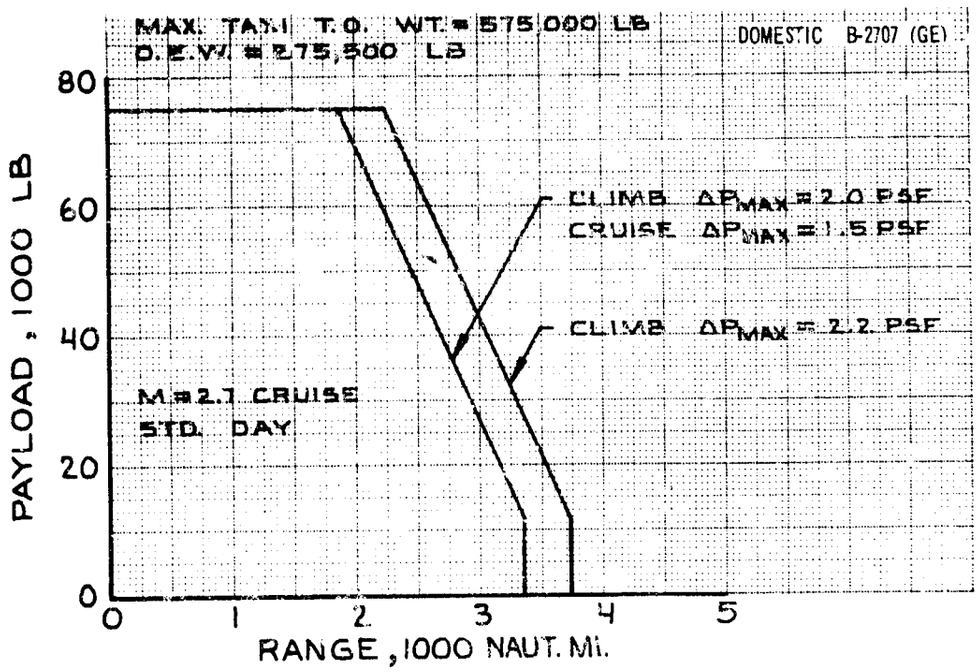


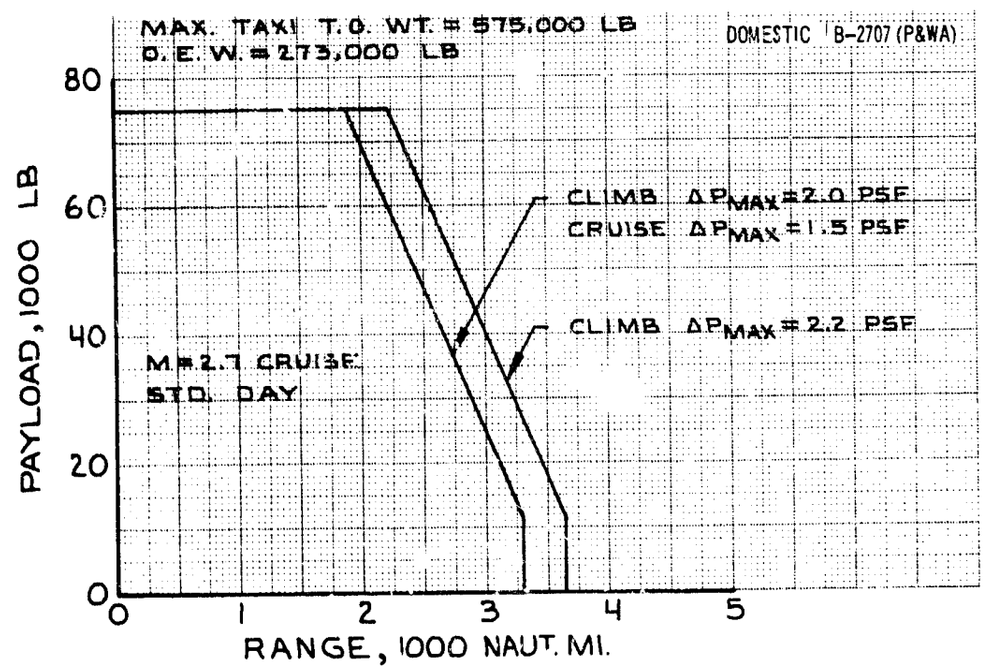


*Figure 2-3. Payload Range, Domestic B-2707*

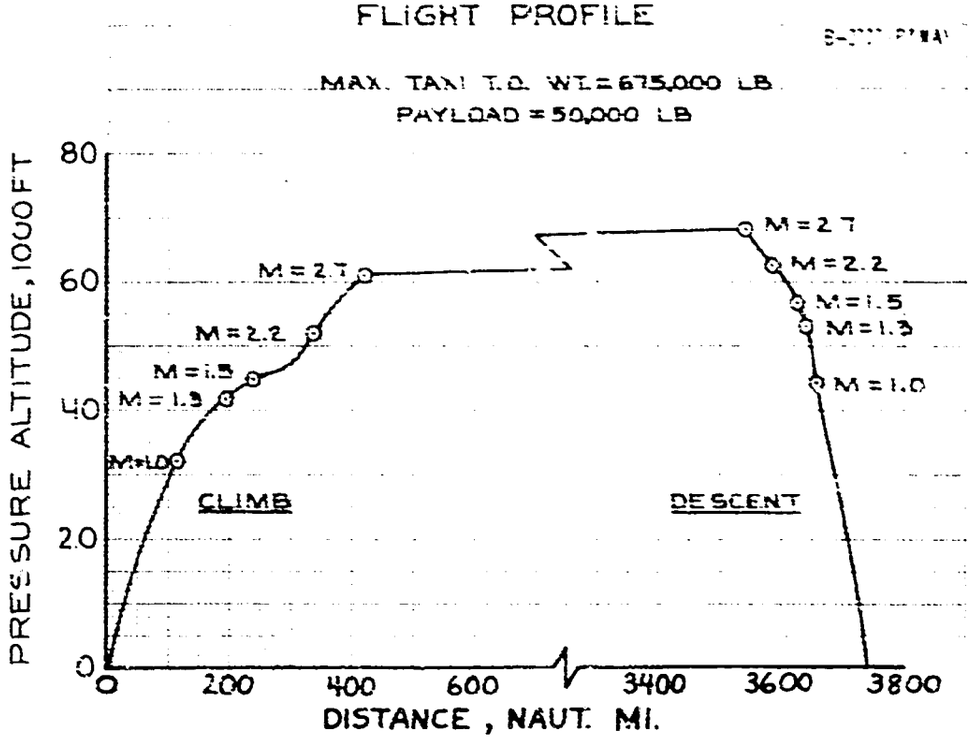


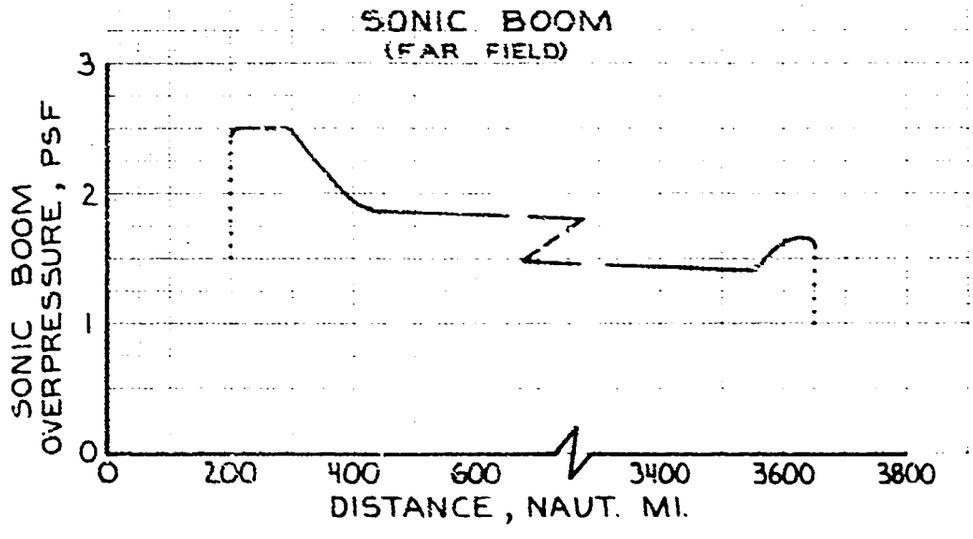


*Figure 2-4. Far Field Sonic Boom Overpressures*

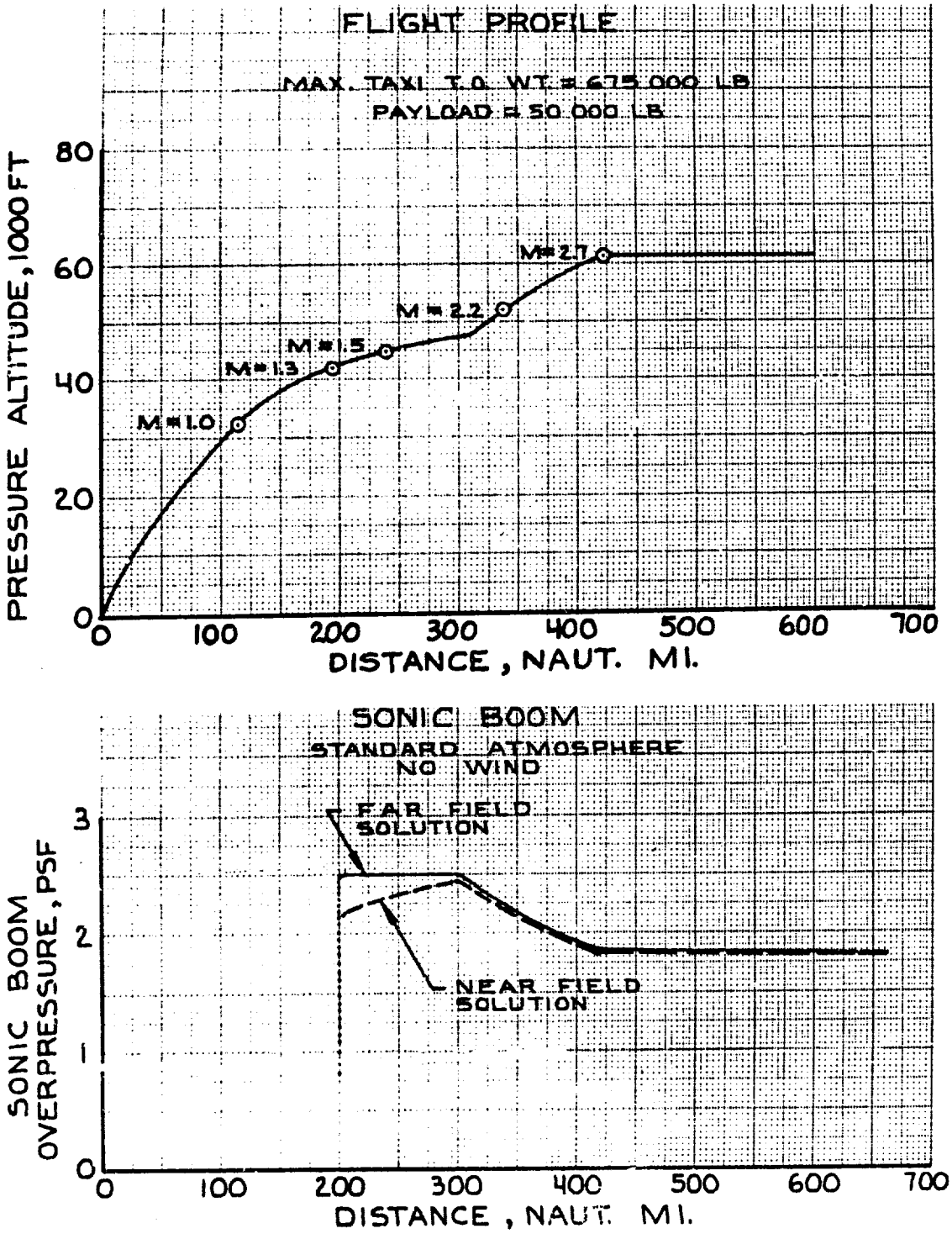


*Figure 2-5. Sonic Boom Under Flight Track*

A flap setting of 20/40 degrees was selected as the basic takeoff flap for the performance shown in the following paragraphs. This choice provides moderate liftoff speeds ($V_{LO}$ = 169 kn at 675,000 lb) while meeting the FAA community noise objective of 105 PNdb. At the maximum taxi weight, liftoff speeds as low as 159 kn are possible using a 30/50-degree flap setting.

All takeoff performance shown is based on a forward cg location of 0.595 $C_R$. Most normal takeoffs will be accomplished at a cg location of 0.615 $C_R$ which results in improved takeoff lift coefficient and improved climb out lift to drag ratio. At a gross weight of 675,000 lb on a standard day, the field length is reduced from 7,000 ft to 6,300 ft, the takeoff speed from 169 kn to 162 kn, and the community noise from 100 PNdb to 99 PNdb for the B-2707 (GE). The corresponding improvements for the B-2707 (P&WA) are: The field length is reduced from 7,300 to 6,600 ft, the takeoff speed from 169 kn to 162 kn, and the community noise from 105 PNdb to 104 PNdb.

2.2.1 Takeoff Field Lengths and Community Noise

FAR takeoff lengths are shown in Fig. 2-6 for a sea level standard +15°C day. At a weight of 675,000 lb, the FAR takeoff field length is 8,300 ft for the B-2707 (GE) and 8,600 ft for the B-2707 (P&WA). On a standard day the field lengths will be reduced to 7,000 ft for the GE and 7,150 for the P&WA engines. Data for maximum augmented thrust for both engines, dry thrust for the GE, and reduced augmentation for the P&WA are presented. Rotation, liftoff, and flare to climb altitude follow conventional practices as outlined in Federal Aviation Regulations Part 25. The FAR takeoff field length is determined by the all-engines-operating case. Comparisons with the balanced field lengths are given in documents V2-B2707-4 and -5.

Liftoff occurs at 169 kn after a ground roll of 4,800 ft. The flaps are retracted to 5/5-degree setting at an altitude of 400 ft. Noise abatement over the community is achieved with thrust reduction to the minimum consistent with a 500-ft-per-minute rate of climb. The takeoff speeds shown in Fig. 2-6 are based upon a body attitude of 10 degrees at liftoff. The liftoff speeds are 10 percent greater than the nongeometry limited minimum unstick speeds in the current FAR. Airplane geometry prevents demonstration of minimum unstick speed in ground effect; however, the liftoff speeds are always at least 5 percent above the geometry-limited minimum speed.

All takeoff climb gradient requirements outlined in FAR 25.121 are easily met by the B-2707 with the critical engine inoperative. At sea level on a standard +15°C day, both the FAR requirement of 0.03 second segment gradient and the takeoff field length objective can be met at weights of 750,000 lb for the B-2707 (GE) and 740,000 lb for the B-2707 (P&WA) with a 20/40-degree flap setting.

2.2.2 Takeoff Noise

Community noise levels are shown in Fig. 2-7 corresponding to the takeoff performance shown in Fig. 2-6. Takeoff noise levels around the airport and community are presented in Fig. 2-8 for takeoff with maximum augmented thrust and taxi weight of 675,000 lb. The B-2707 (GE) is 1,750 ft over the community. The B-2707 (P&WA) is at 1,450 ft altitude. The noise characteristics shown reflect the jet noise levels of the two offered engines together with inlet noise suppression.

In addition to noise suppression studies using the nozzle ejector combinations offered by the engine manufacturers, Boeing has also conducted an intensive noise suppression research and development program to find methods of further improving the noise characteristics. This work is detailed in Propulsion Report, V2-B2707-12. The use of the Boeing jet noise suppressor, based on this research work, results in significant reductions in airport noise levels with only a slight increase in takeoff field lengths as shown in Table 2-B.

A comparison of the noise contours with the Boeing jet noise suppressor and inherent suppression is given in Fig. 2-9. The lateral spread of the 110-PNdb contours is reduced from more than 5,000 to less than 3,000 ft on the airport for the B-2707 (GE). Use of the Boeing jet noise suppressor results in essentially the same noise contours with either engine.

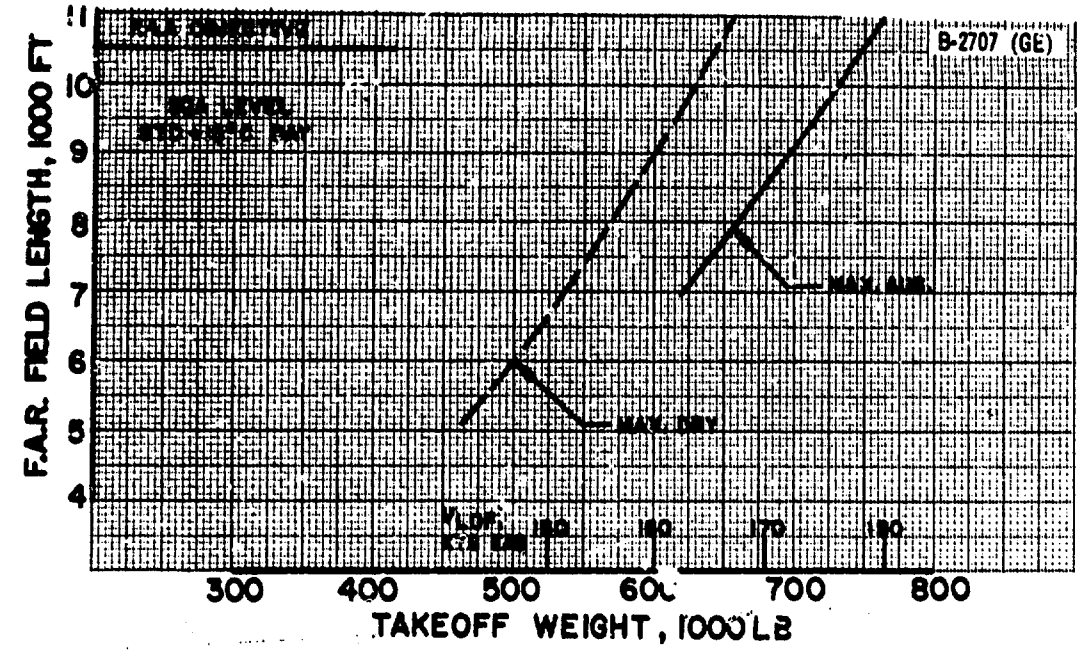


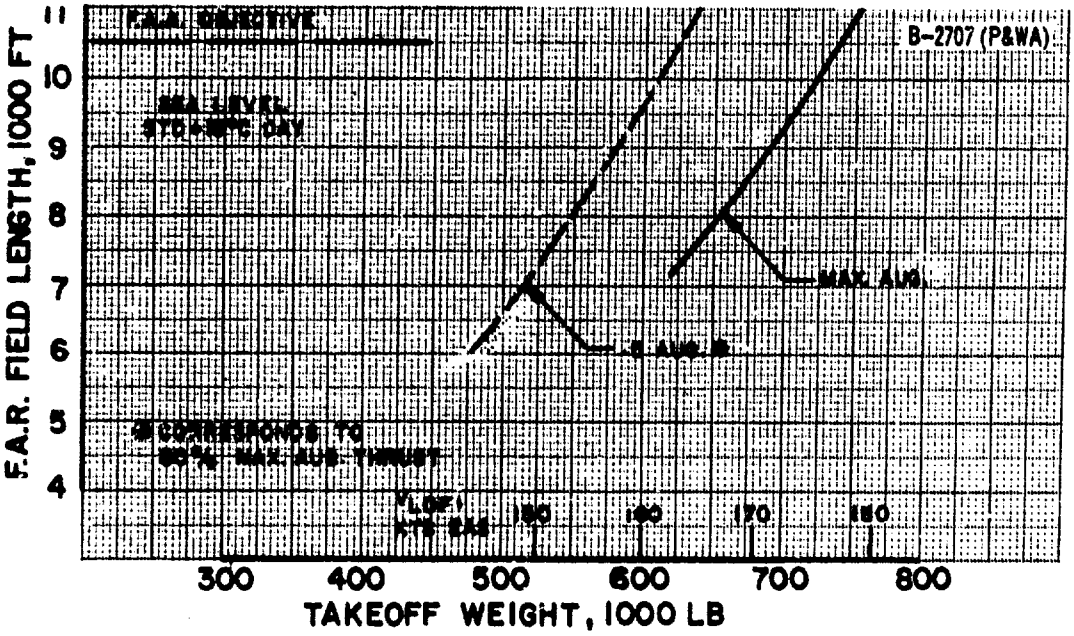


*Figure 2-6. Takeoff Field Lengths and Speeds*

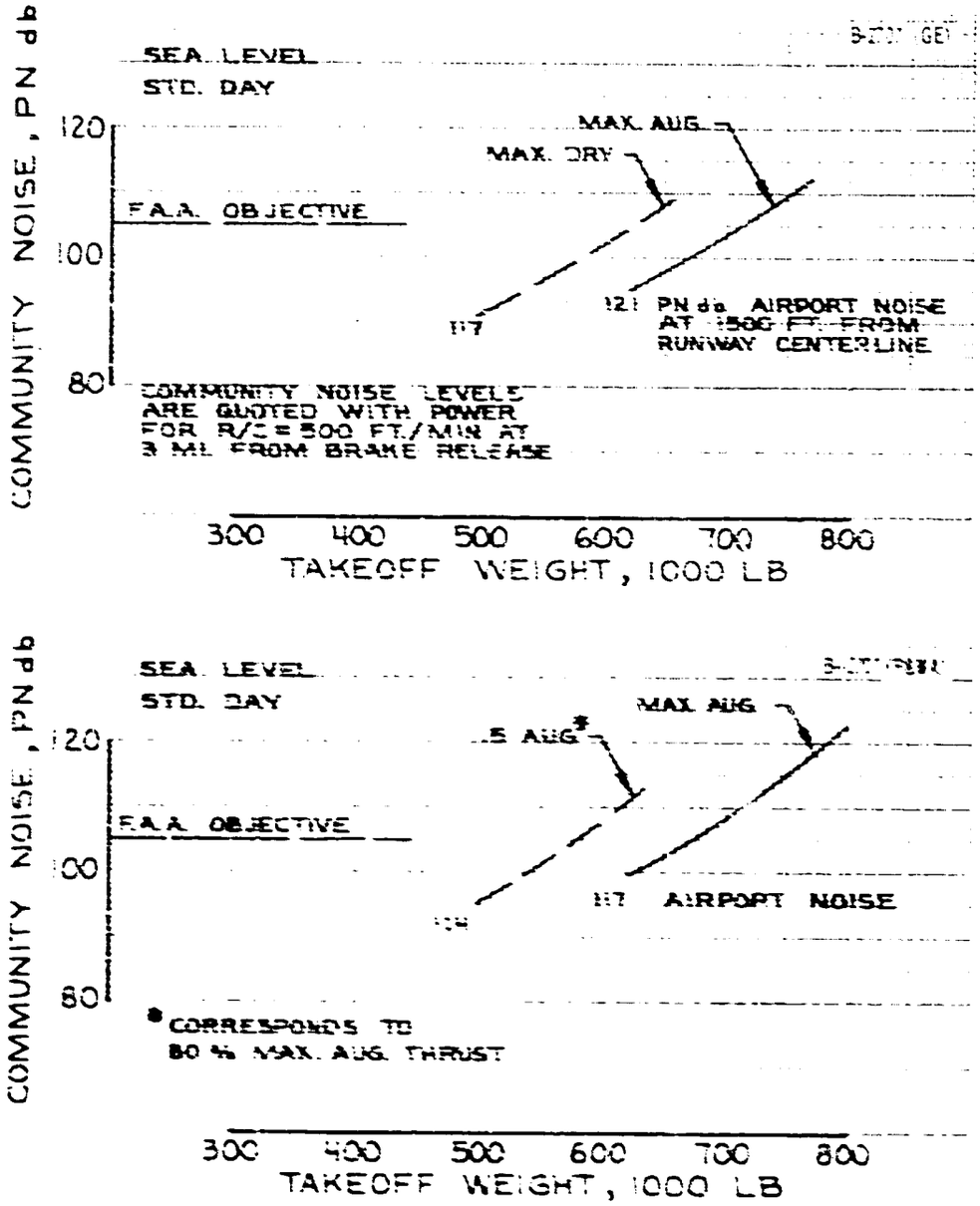


Figure 2-2. Takeoff Community Noise

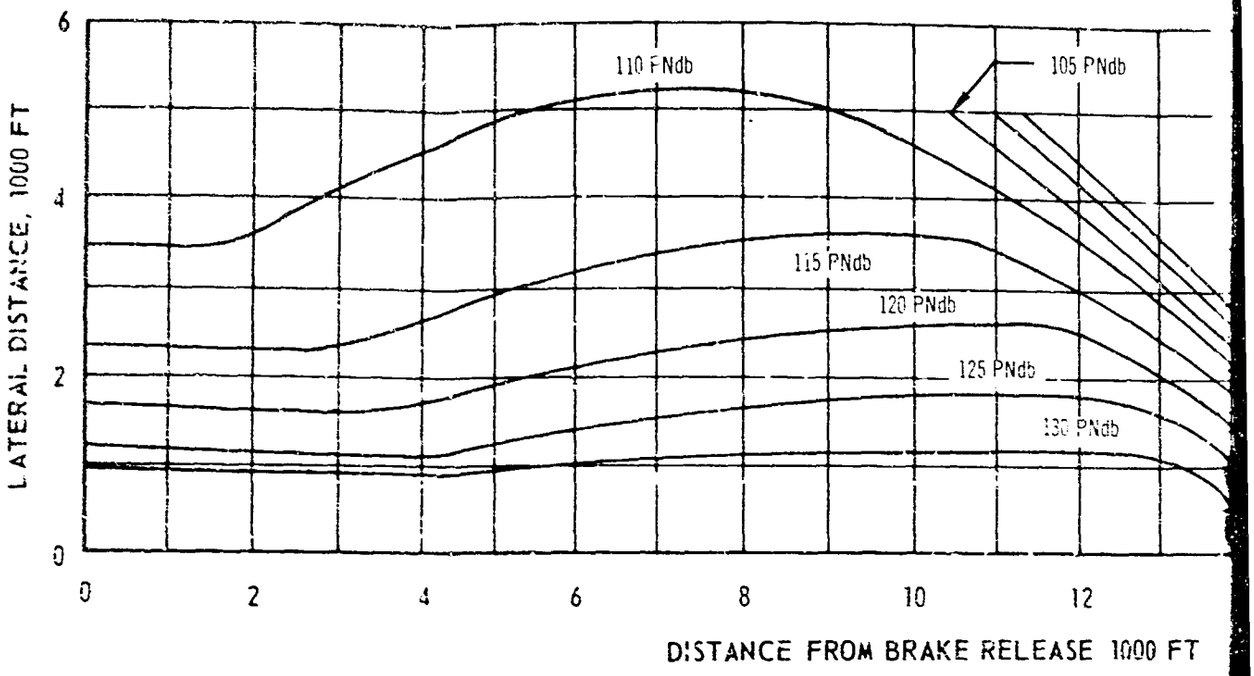


MAXIMUM TAXI WEIGHT 675,000 LB
MAXIMUM AUGMENTED TAKEOFF THRUST
STANDARD DAY

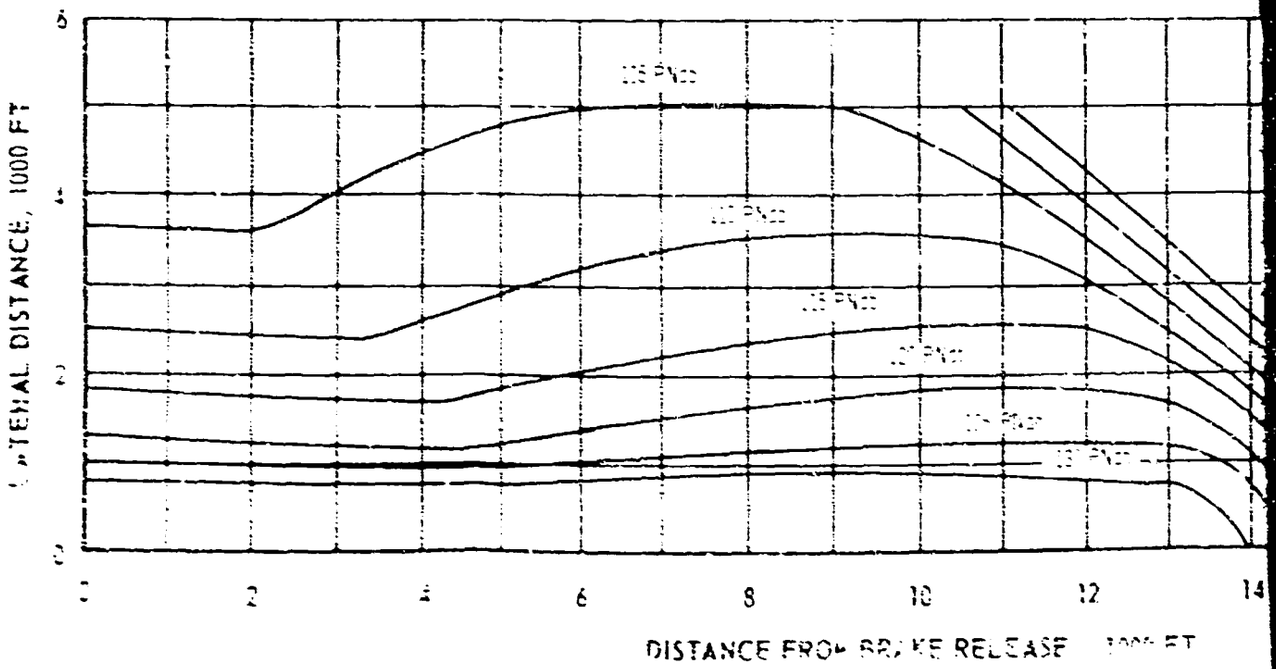

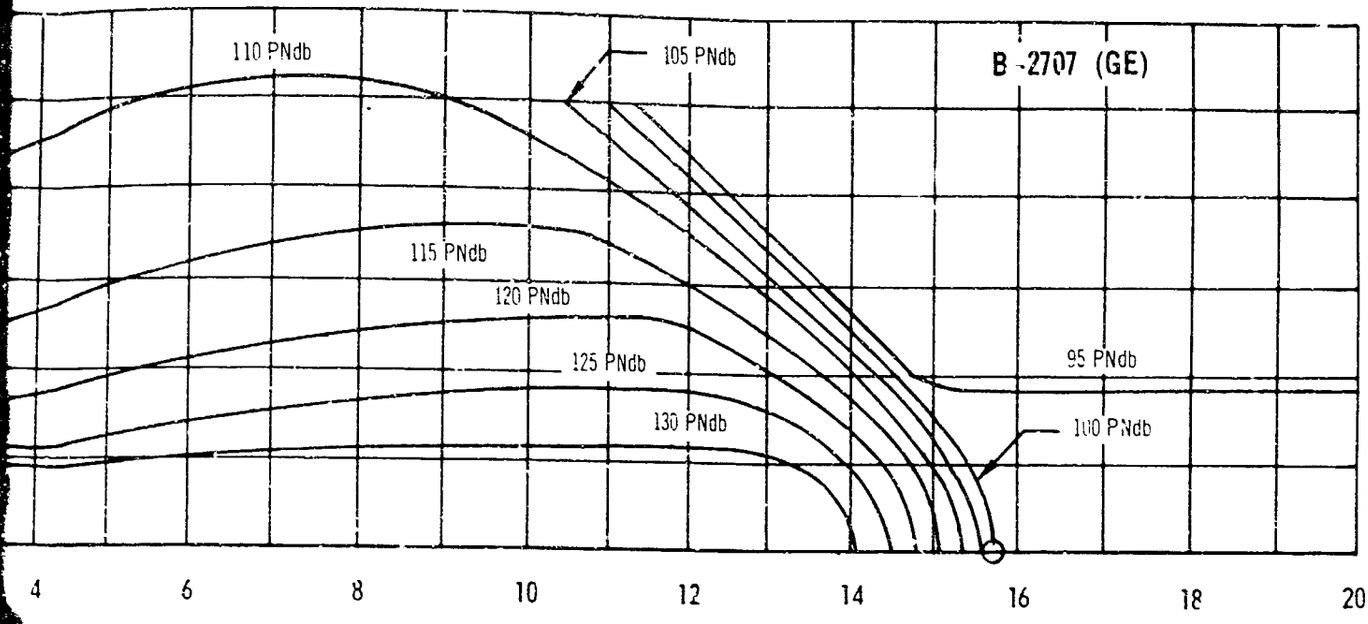


DISTANCE FROM BRAKE RELEASE 1000 FT

MAXIMUM TAXI WEIGHT 675,000 LB
MAXIMUM AUGMENTED TAKEOFF THRUST
STANDARD DAY

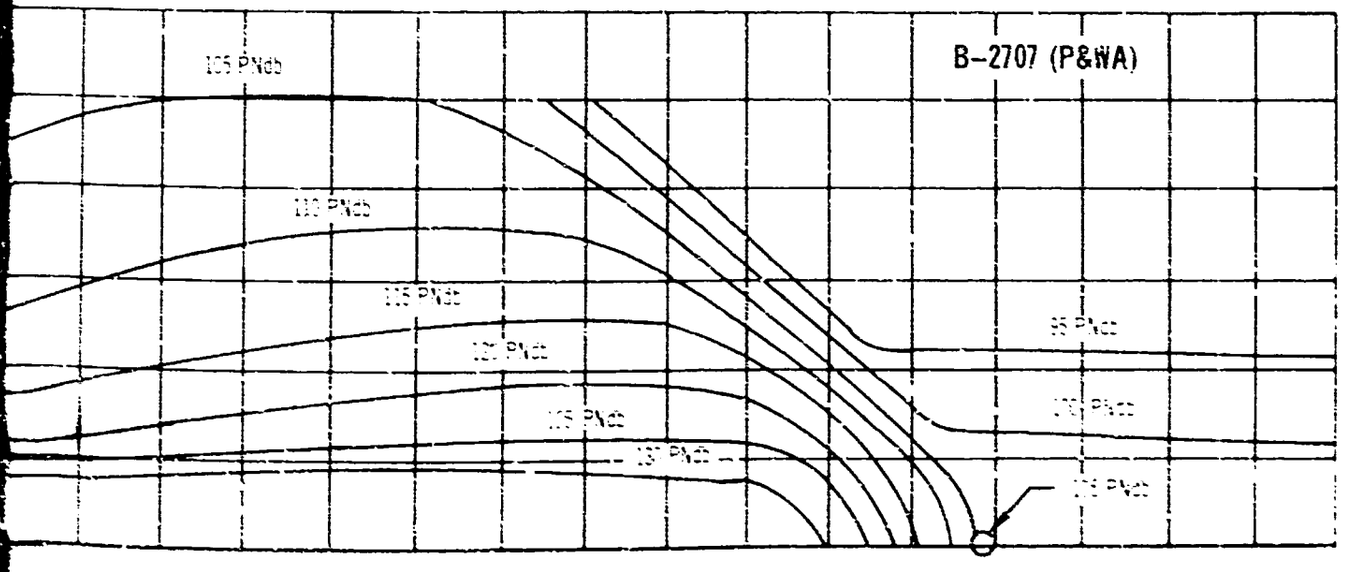


DISTANCE FROM BRAKE RELEASE 1000 FT

B

Figure 2-8. Takeoff Noise Contours

Table 2-B. Noise Comparison With Boeing Jet Noise Suppressor

| Item | GE 4/J5P Engine | P&WA JTF17A-21B Engine |
|---|---|---|
| Airport noise, (PNdb) | | |
| Inherent suppression | 121 | 117 |
| Boeing jet suppressor | 112 | 113 |
| Community noise (PNdb) | | |
| Inherent suppression | 100 | 105 |
| Boeing jet suppressor | 98 | 104 |
| FAR takeoff field length (ft) on a standard day +15° C | | |
| Inherent suppression | 8,300 | 8,500 |
| Boeing suppression | 8,800 | 9,000 |

2.3 APPROACH AND LANDING PERFORMANCE Landing field lengths, speeds, and approach noise levels are presented in this paragraph. The performance shown is based upon use of the 20/40-degree flap setting. This setting was selected as a compromise of attitude, approach noise, speed, and field length, giving an approach speed in excess of that required under present FAR 25.

Performance and noise trades for other flap settings are presented in documents V2-B2704-4 and -5.

2.3.1 FAR Landing Field Lengths and Speeds Figure 2-10 shows the FAR landing field lengths for a range of landing weights under wet and dry runway conditions. A 3-degree glide slope has been used to compute performance. Field lengths have been computed using brakes and spoilers only. The wet-runway field lengths have been computed using the alternate method of compliance according to FAA Advisory Circular 121.195 d-1 effective November 19, 1965. The wet runway FAR landing field lengths at maximum landing weight are 7,600 ft for the B-2707 (GE) and 7,500 ft for the B-2707 (P&WA). The use of a 30/50-degree flap setting would reduce the wet-runway FAR landing field length 500 ft. The use of two engines with reverse thrust and the 30/50-degree flap setting would result in a further reduction in FAR field length to 6,000 ft. Dry runway FAR landing field lengths are also shown in Fig. 2-10.

All landing approaches are made on the stable side of the thrust required curve. At maximum landing weights and using 20/40-degree flaps, the approach speed of the B-2707 (GE) is 153 kn while the B-2707 (P&WA) approaches at 151 kn. If lower approach speeds are desired, 30/50-degree flaps may be used resulting in approach speeds of 141 kn for the B-2707 (GE) and 140 kn for the B-2707 (P&WA). These speeds are only slightly above these of current subsonic jets. For example, a 707-300C airplane at a maximum landing weight of 258,000 lb approaches at 137 kn.

All landing performance is based on a forward cg location of 0.595 $C_R$ corresponding to the maximum payload capacity. At smaller payloads, the cg's are more aft, resulting in improved approach lift-to-drag ratio and improved landing lift coefficients. With 50,000-lb payload at 0.615 $C_R$ and a maximum landing weight of 430,000 lb, the FAR field length for a dry runway is reduced from 7,500 to 7,000 ft, the approach speed from 153 to 145 kn, and the community noise from 112 to 111 PNdb for the B-2707 (GE).

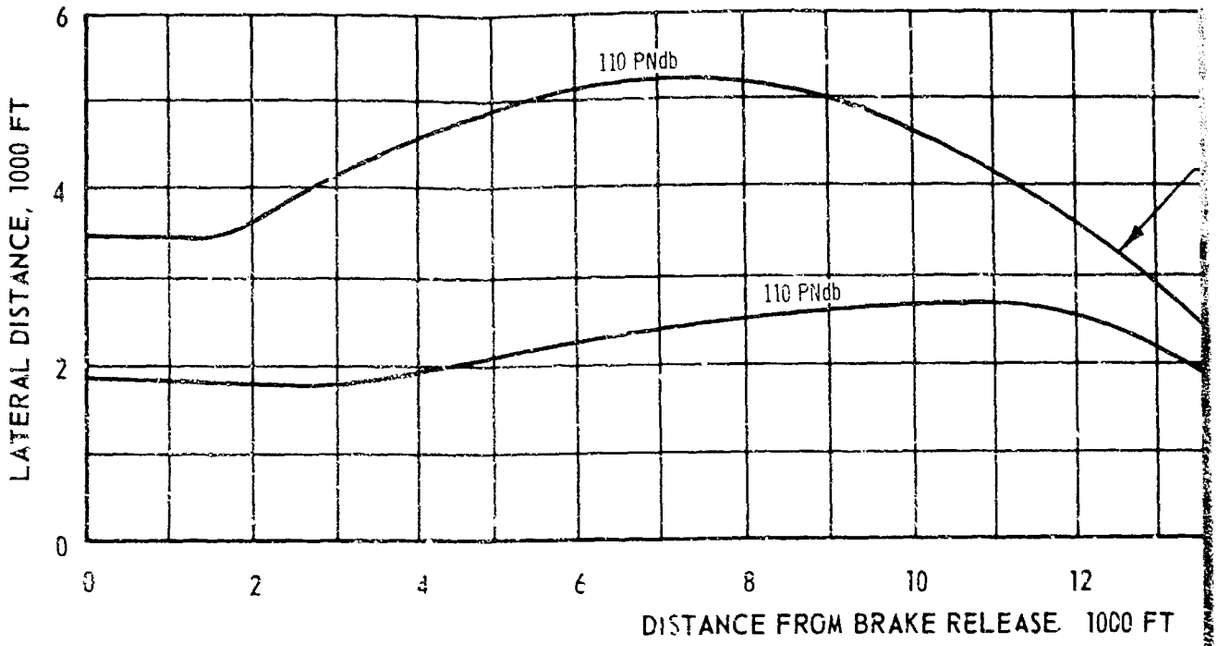


MAXIMUM TAXI WEIGHT 675,000 LB
MAXIMUM AUGMENTED TAKEOFF THRUST
STANDARD DAY

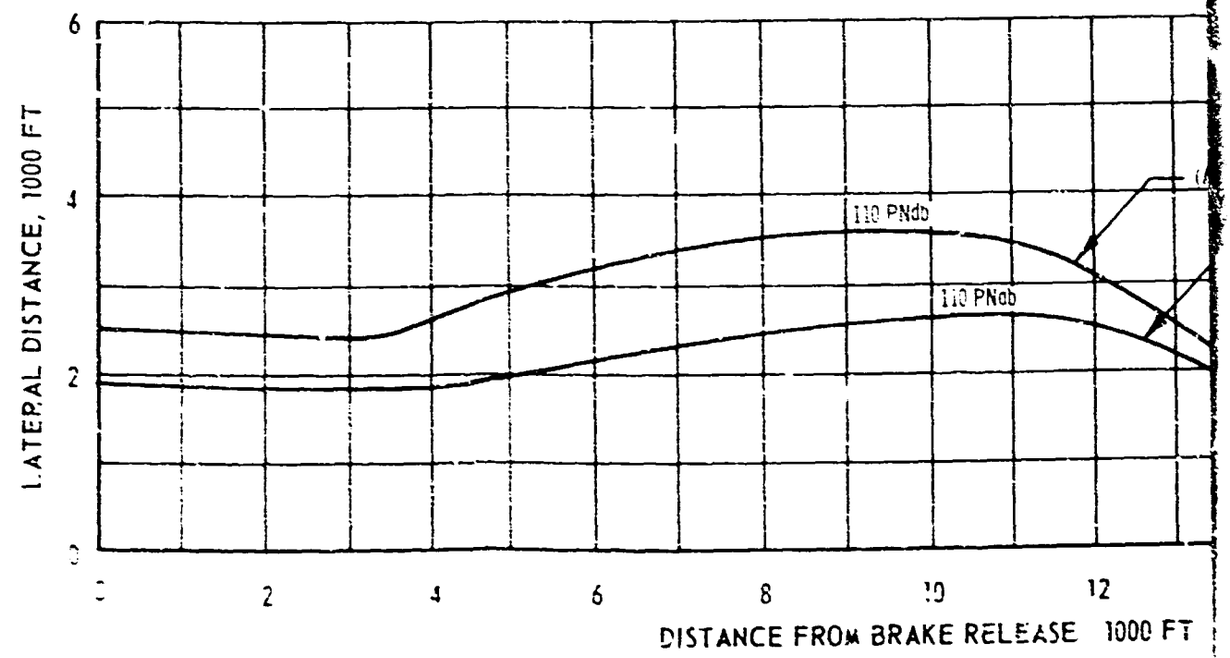

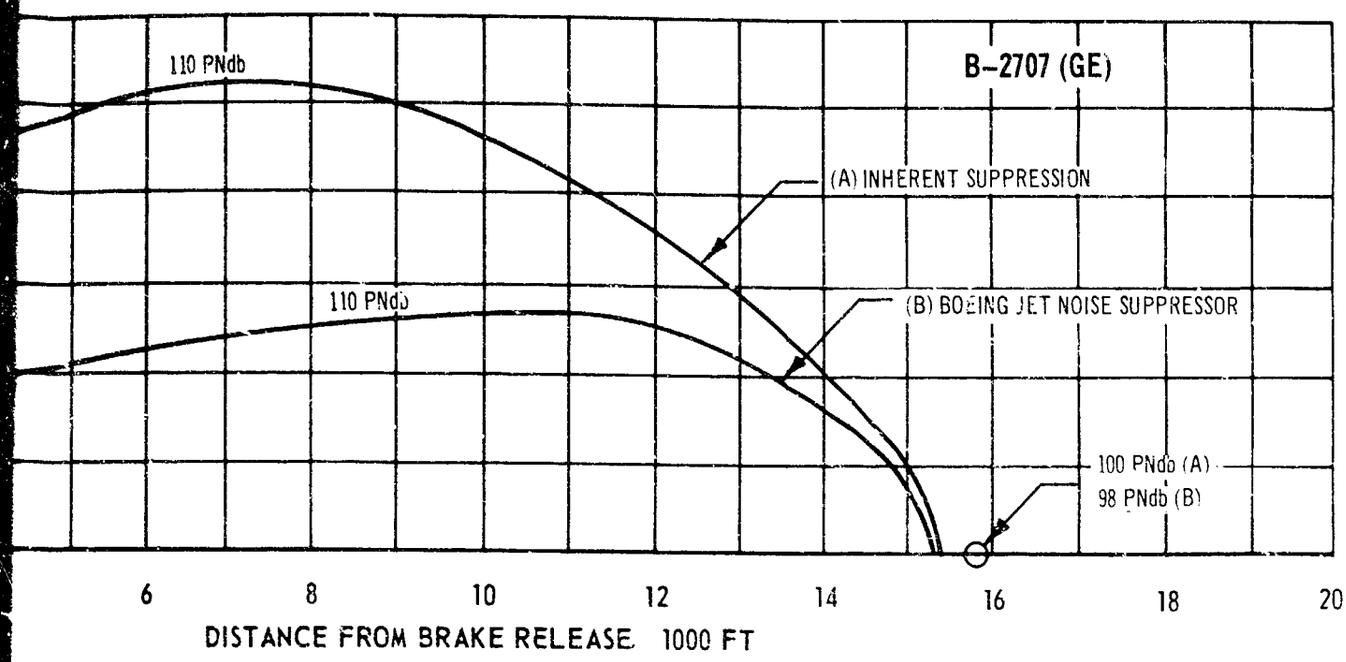


MAXIMUM TAXI WEIGHT 675,000 LB
MAXIMUM AUGMENTED TAKEOFF THRUST
STANDARD DAY

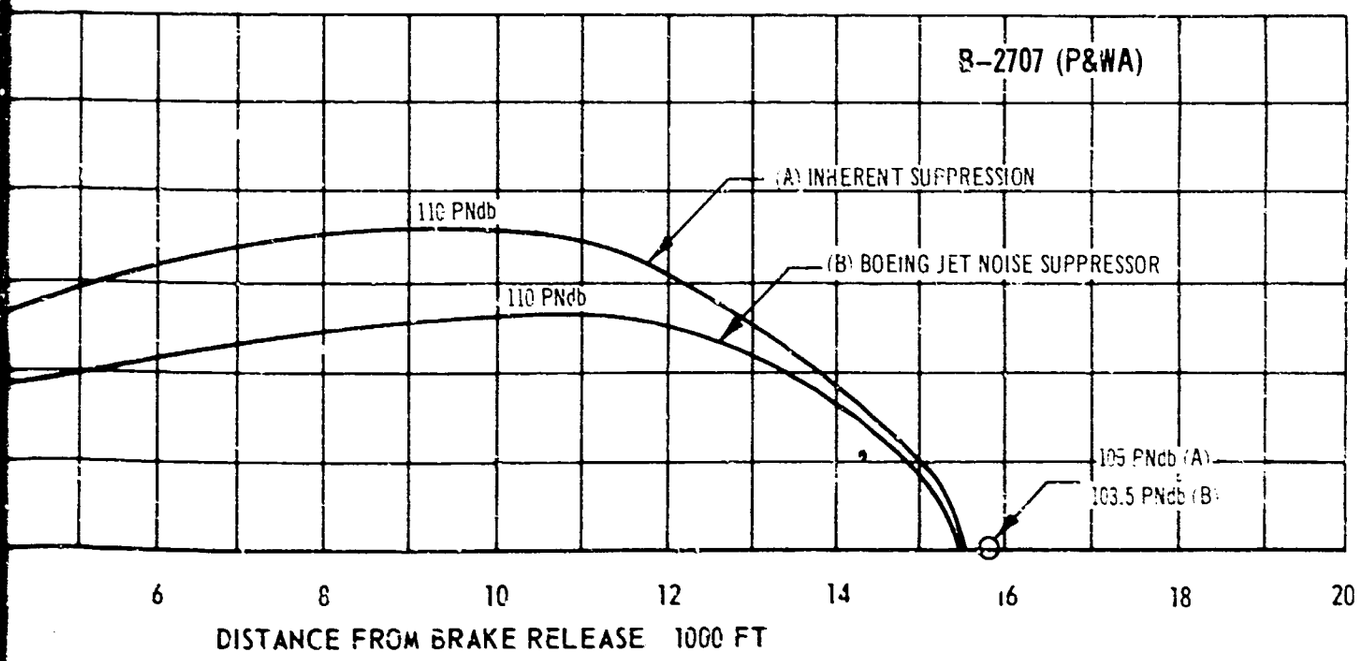


*Figure 2-9. Boeing Jet Suppressor, Effect on Takeoff Noise*

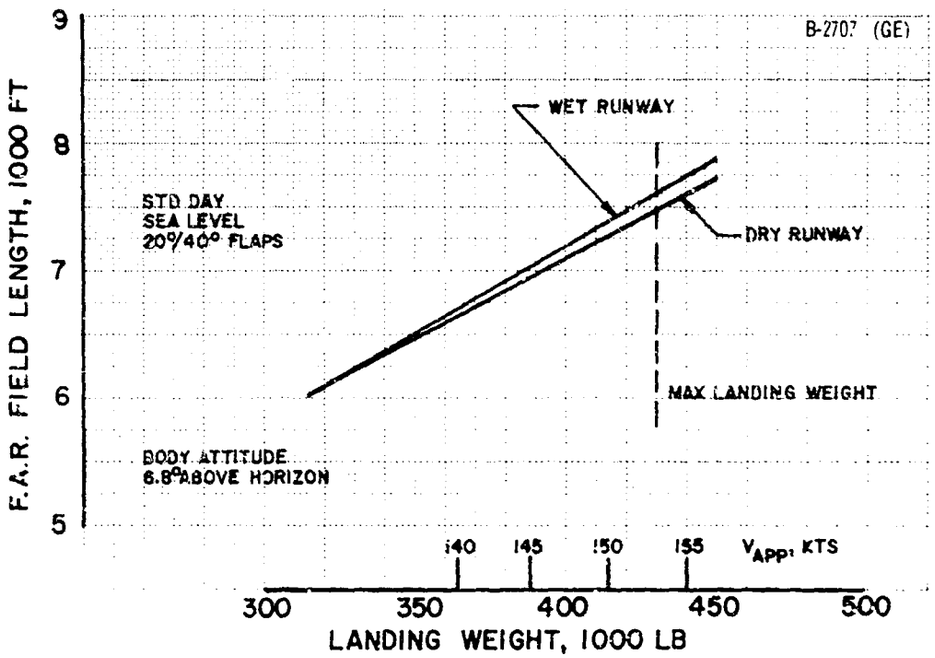


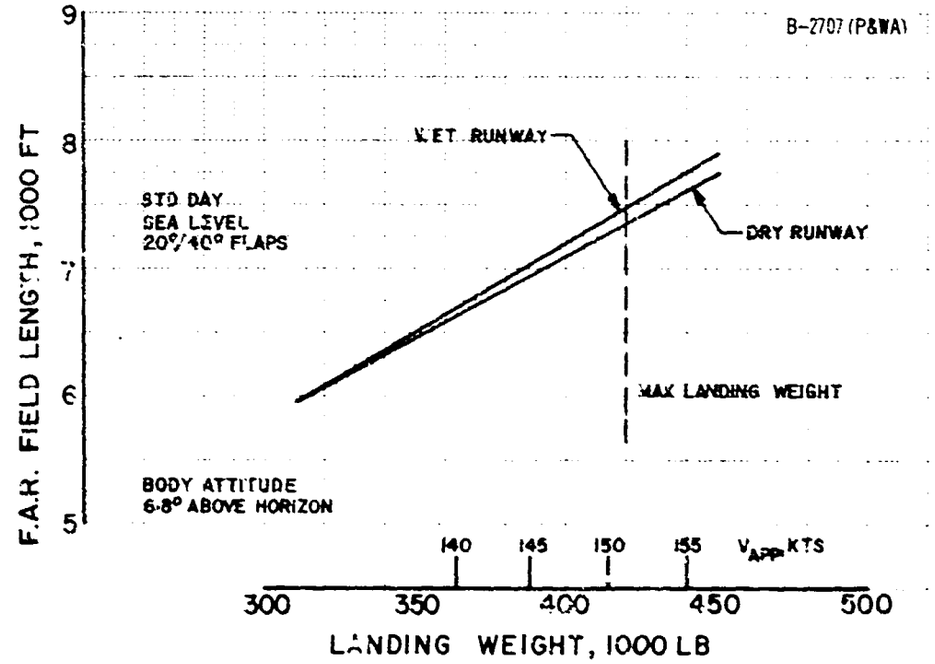


*Figure 2-10. Landing Field Lengths and Speeds*

The corresponding improvements for the B-2707 (P&WA) and a maximum landing weight of 420,000 lb are: The field length is reduced from 7,400 ft to 6,900 ft; the approach speed is reduced from 151 to 143 kn; and approach noise is reduced from 115 to 114 PNdb.

In the event of a go-around, 95 percent of maximum dry thrust is available in approximately 2.5 sec from the time the throttle is advanced. All landing and approach climb gradient requirements of FAR 25.119 and FAR 25.121 are easily met.

### 2.3.2 Approach Noise

Figure 2-11 shows the community noise levels 1 mi from the end of the landing runway, based on a constant speed and decelerating approach. For the constant speed approach, 20/40-degree flaps are used. A decelerating approach can be used to achieve lower noise levels than are possible with a normal constant speed approach. With this procedure the pilot extends the flaps to 30/50 degrees and reduces the engine thrust at 1.5 mi from the runway threshold. The pilot increases the thrust to maintain reference approach speed after passing over the community. During this maneuver the body attitude remains essentially constant and no trim change is required. The procedure is described in more detail in Operational Suitability (V4-B2707-1, Sec. 2.0).

The approach noise levels are based upon engine operation with a choked inlet which suppresses inlet noise and an open nozzle which provides low jet noise at low power settings. This is discussed in detail in Propulsion Report (V2-B2707-13) and Airport and Community Noise Program (V4-B2707-4).

### 2.3.3 Landing Field Length With Wing Sweep of 72 Degrees, Wet Runway

With a payload of 50,000 lb and fuel for a balked approach, the wings aft wet runway actual landing distance from a 50-ft obstacle is only 6,900 ft using four-engine reverse thrust at a weight of 350,000 lb for the B-2707 (GE). The wet runway landing distance is 7,400 ft for corresponding conditions using four-engine reverse thrust for the B-2707 (P&WA). The approach speed is 205 kn with a body attitude of 9 degrees.

## 2.4 OFF-DESIGN AND EMERGENCY RANGE PAYLOAD PERFORMANCE

### 2.4.1 Subsonic Cruise

Supersonic flight may possibly be prohibited over certain areas; in this event, subsonic cruise at the beginning or ending of a mission would be required. Figure 2-12 shows the capabilities of the B-2707 for such cases. The wing sweep is 42 degrees and the cruise Mach number is 0.85 for the subsonic cruise. For the B-2707 (GE) and for a 400-nmi subsonic cruise requirement, the total range would be reduced about 80 nmi; for a subsonic leg flown at the end of the mission, the total range would be reduced about 120 nmi. For the B-2707 (P&WA), there is no range reduction for a 400-nmi subsonic leg flown at the beginning of the mission; for a subsonic leg flown at the end of the mission, the total range would be reduced only 40 nmi.

### 2.4.2 Range With Engines Inoperative

The effects on the cruise performance and on the destination reserves of one and two engines being inoperative are shown in Fig. 2-13. The reserves remaining for a planned mission range of 4,000 statute miles (3,470 nmi) for a standard +10° C day is shown for supersonic cruise with one engine inoperative, subsonic cruise with one engine inoperative, and subsonic cruise with two engines inoperative. For the very severe condition of continuing subsonic cruise with two engines inoperative, only 1,500 lb of payload would have to be off loaded for the B-2707 (GE). For cruise with a single engine inoperative for either the subsonic or supersonic cases, about three times the FAR reserve requirements would be remaining after reaching the planned destination.

It is necessary to off load 5,000 lb of payload for the B-2707 (P&WA) to permit the airplane to continue a 4,000-statute-mile mission subsonically with two engines inoperative on a standard +10° C day. For the single-engine-inoperative subsonic or supersonic cases, the planned destination of 4,000 statute miles could be reached with a minimum of three times the FAR reserve requirements remaining.

The effect of enroute engine failures for the domestic B-2707 has been studied for standard and standard +10° C day conditions. The destination reserve remaining following a two-engine failure at the midpoint and then continuing cruise at M = 0.80 is about twice the minimum 15-minute holding allowance on a hot day. In the case of an engine failure prior to reaching

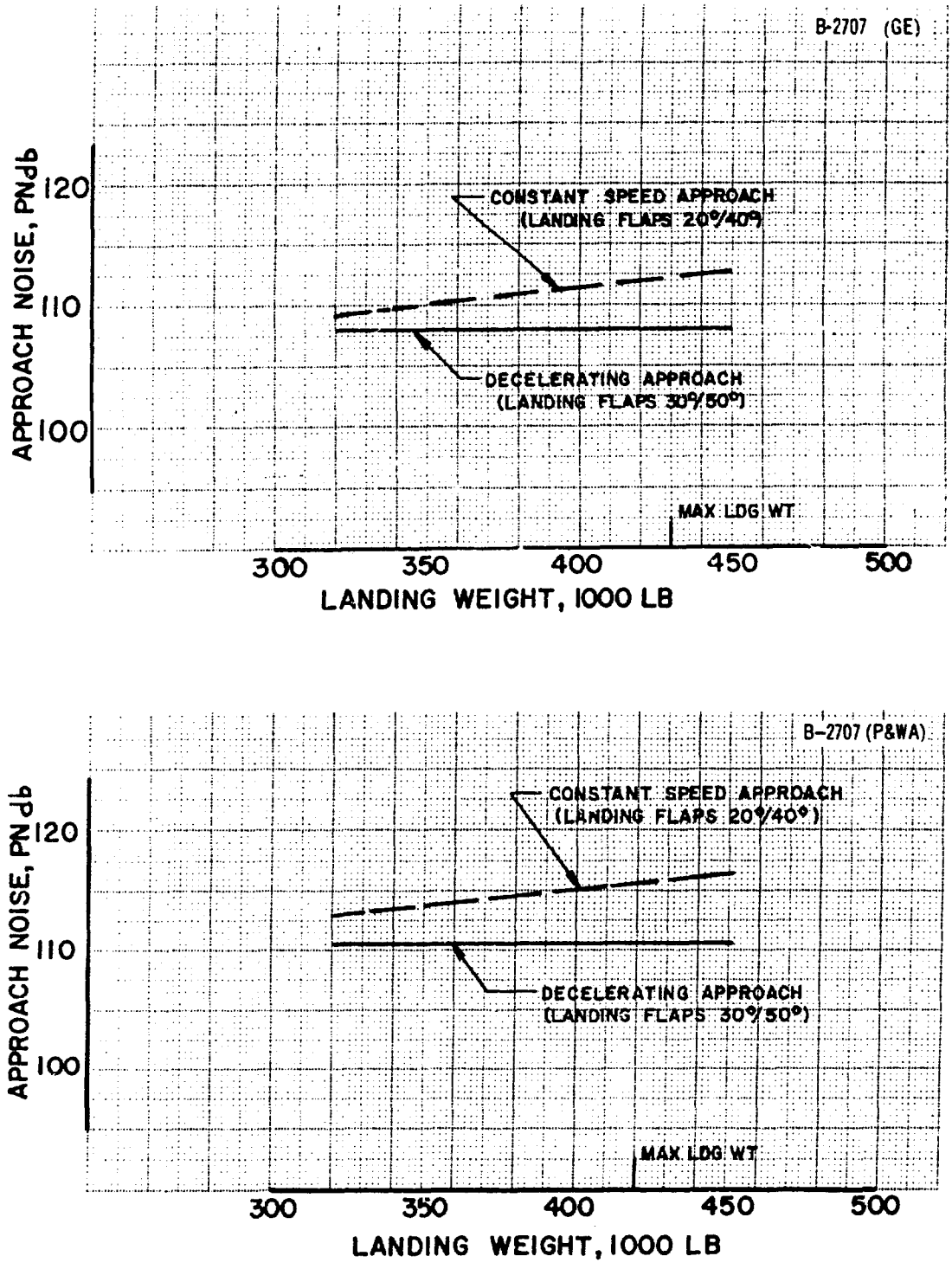


*Figure 2-11. Landing Approach Noise*

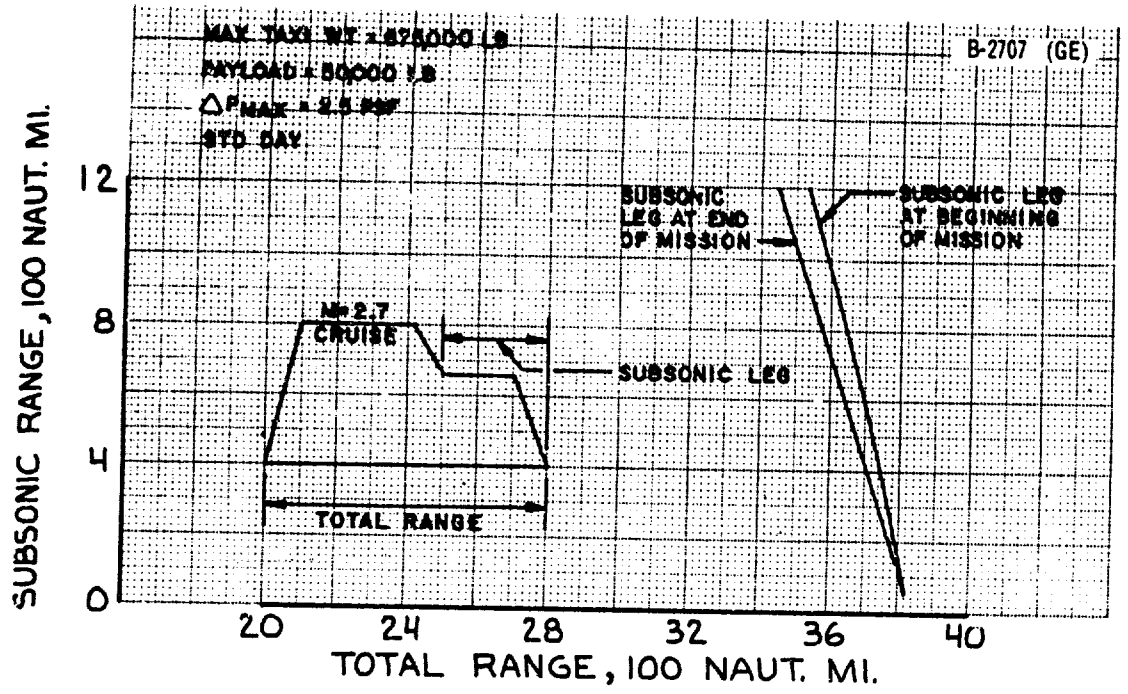


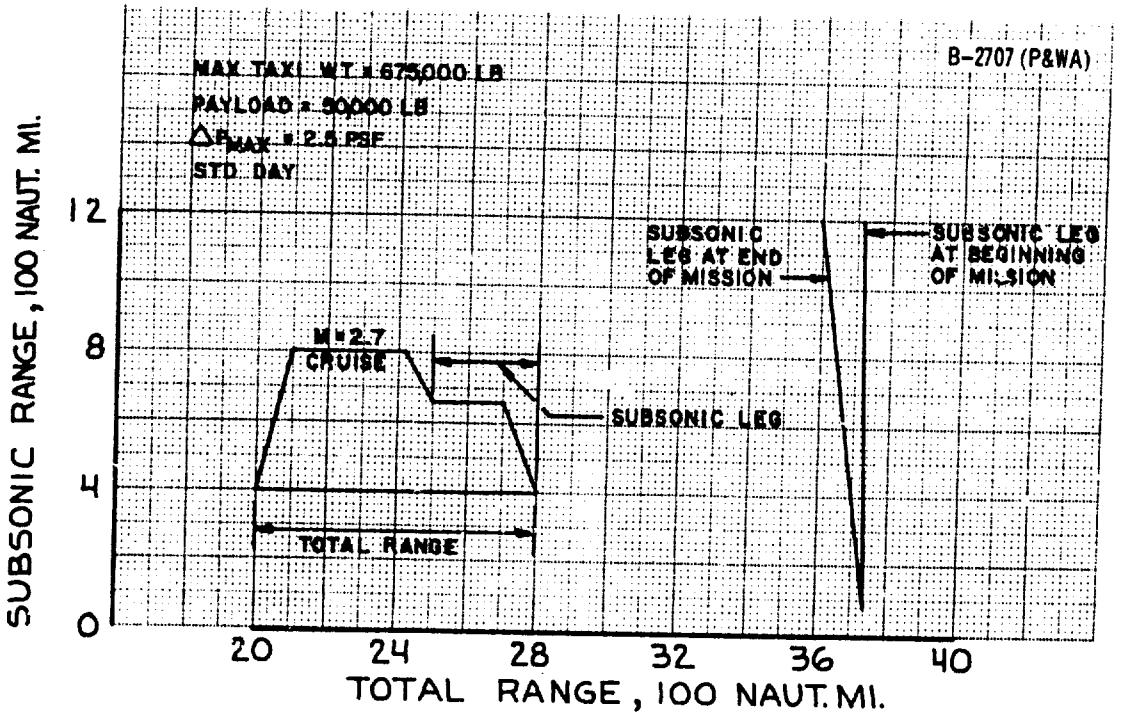


*Figure 2-12. Operational Versatility, Subsonic Legs*

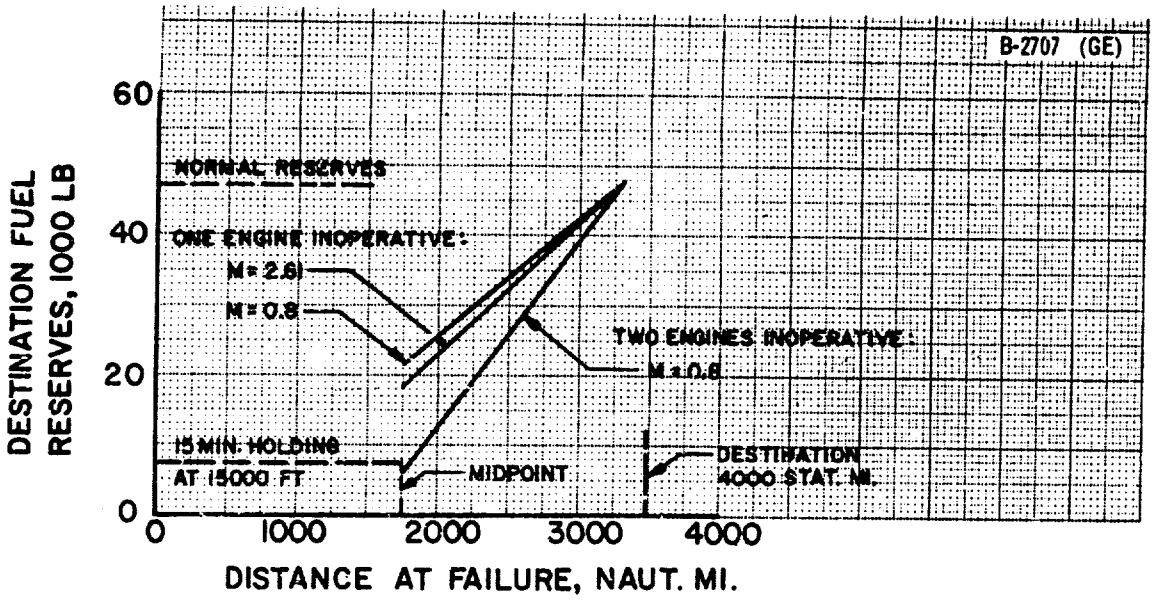


MAX TAXI WT = 675,000 LB
RANGE = 3470 NAUT. MI.
PAYLOAD = 50000 LB
STD+10°C DAY
MAX CLIMB ΔP = 2.5 PSF

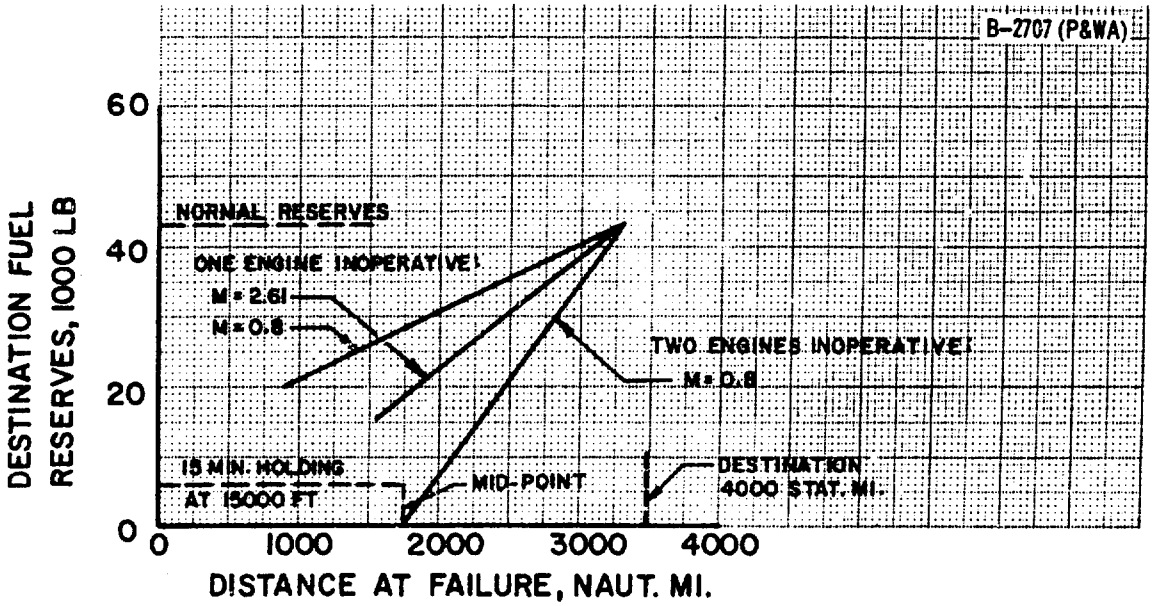


*Figure 2-13. Operational Reliability and Safety, International, STD+10° C Day*

transonic acceleration altitude, missions involving supersonic cruise would be cancelled.

2.4.3 Range With Augmentors Inoperative
Range payload performance has been studied for 1, 2, 3, or 4 augmentors inoperative. Figure 2-14 shows the destination fuel reserves remaining for augmentor failures as a function of distance to failure for a M = 2.7 international mission on a standard day. For the worst case, i.e. four augmentors inoperative at midpoint, the B-2707 (GE) would cruise at M = 0.85, wing sweep 42 degrees, and could complete the mission with destination fuel reserves of 21,700 lb. Sufficient cruise thrust would be available to continue cruise at M = 2.7 at ranges beyond 2,300 nmi. The destination reserves would be 43,000 lb.

The planned destination would be reached with 32,000 lb of fuel reserves remaining if 4 augmentors failed at the midpoint on the B-2707 (P&WA).

2.5 PERFORMANCE CALCULATION METHODS
The FAA Supersonic Transport Economic Model Ground Rules for Phase III (SST 66-3, dated June 30, 1966) were used in calculating the mission performance.

All performance data are based upon the U.S. Standard Atmosphere, 1962, at 45 degrees latitude, geometric altitude. Hot day performance has been computed for a modified standard atmosphere wherein the temperature is increased 10° C at all altitudes. A similar procedure was used in defining the atmosphere for the cold day performance. The characteristics for the nonstandard atmospheres are shown in Fig. 2-15. Cruise speed with a stagnation temperature limit of 500° F is shown in Fig. 2-16.

The following special effects are included in the mission performance and have been computed according to the instructions given in the Request for Proposal:

a. Centrifugal force, computed for non-rotating earth

b. Gravitational change with altitude

c. Thrust inclination effect on lift and drag

d. Increase in range required because of arc length at altitude

e. Cabin air weight

f. Effect of increased thrust required because of climbing cruise procedure.

Table 2-C shows the detailed effect of these items on the basic international mission for the B-2707 (GE) and B-2707 (P&WA) in the form requested by the RFP.

2.5.1 Mission Calculations
The methods used in calculating the basic performance are the same as those used in Phase I, Volume A-V, Aerodynamics (D6-2400-11, B.3.9). Breakdowns of the time, fuel, and distances for typical missions are given in documents V2-B-2707-4 and -5, Figs. 1-5 and 1-6. A 4-minute air maneuver allowance following takeoff and a 5-minute allowance before landing are made with no distance credit. The reserve fuel consists of 5 percent of the block fuel plus fuel for a missed approach, then climb to 1,500 ft above sea level, then a climb, cruise, and descent to sea level at an alternate airport 300 statute miles away; and finally a 20-minute hold at 15,000 ft over the alternate airport. The alternate cruise altitude and Mach number are selected to minimize the total fuel required for the 300-statute-mile distance.

2.5.1.1 The engine thrust settings used are as follows:

a. Takeoff, maximum dry or maximum augmented

b. Climb, maximum dry from $V_2$ to Mach 0.85, maximum augmented Mach 1.0 to 2.7 for GE maximum dry, $V_2$ to Mach 0.8, maximum augmented, Mach 1.0 to 2.7 for P&WA

c. Cruise, optimum

d. Descent, flight idle, Mach 2.7 to Mach 0.3 at 1,500 ft

e. Reserves, throttled from maximum dry as required by airplane weight, altitude and speed.

2.5.1.2 The wing sweep schedules used in the mission are as follows:

a. Takeoff, leading edge sweep = 30 degrees

b. Departure air maneuver, leading edge sweep = 42 degrees

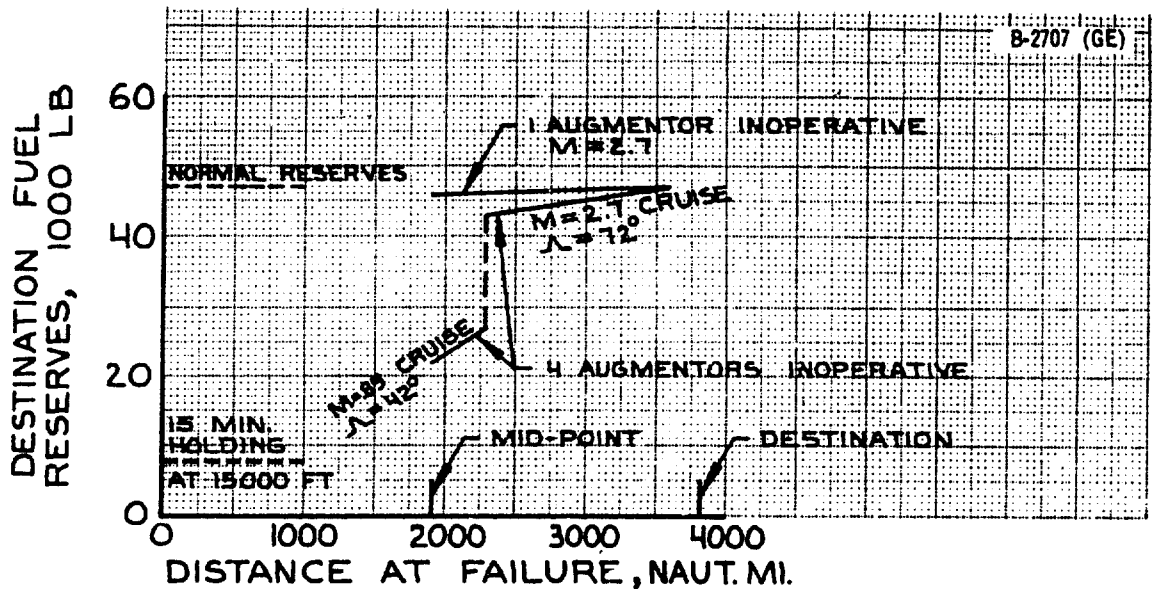


MAX. TAXI WT. = 675,000 LB
PAYLOAD = 50,000 LB
STD. DAY
MAX CLIMB ΔP = 2.5 PSF

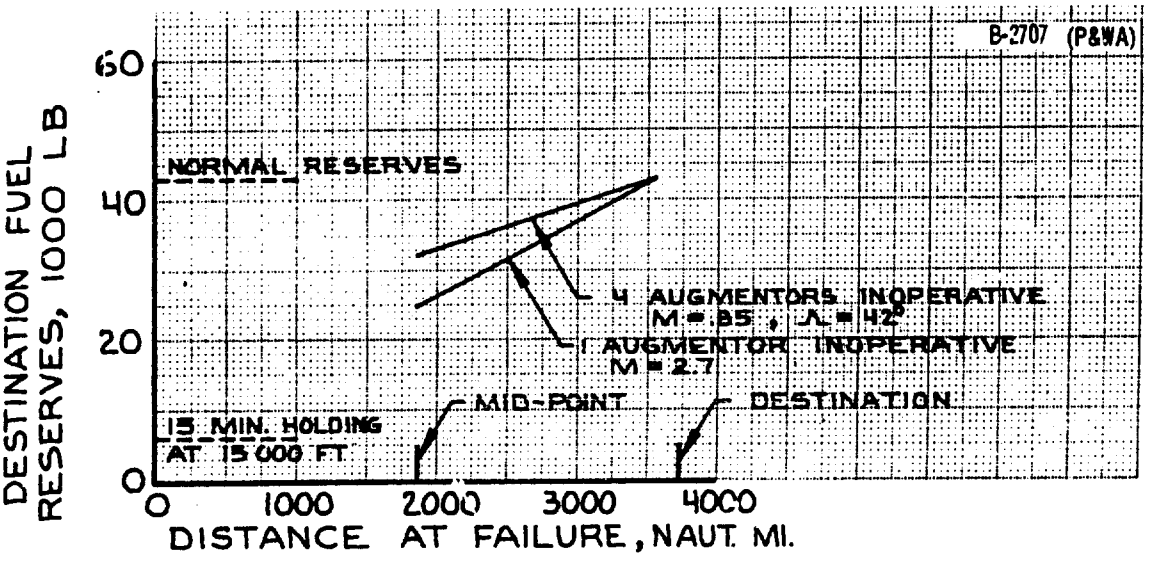


*Figure 2-14. Range Capability With Augmentor Failure, Standard Day*

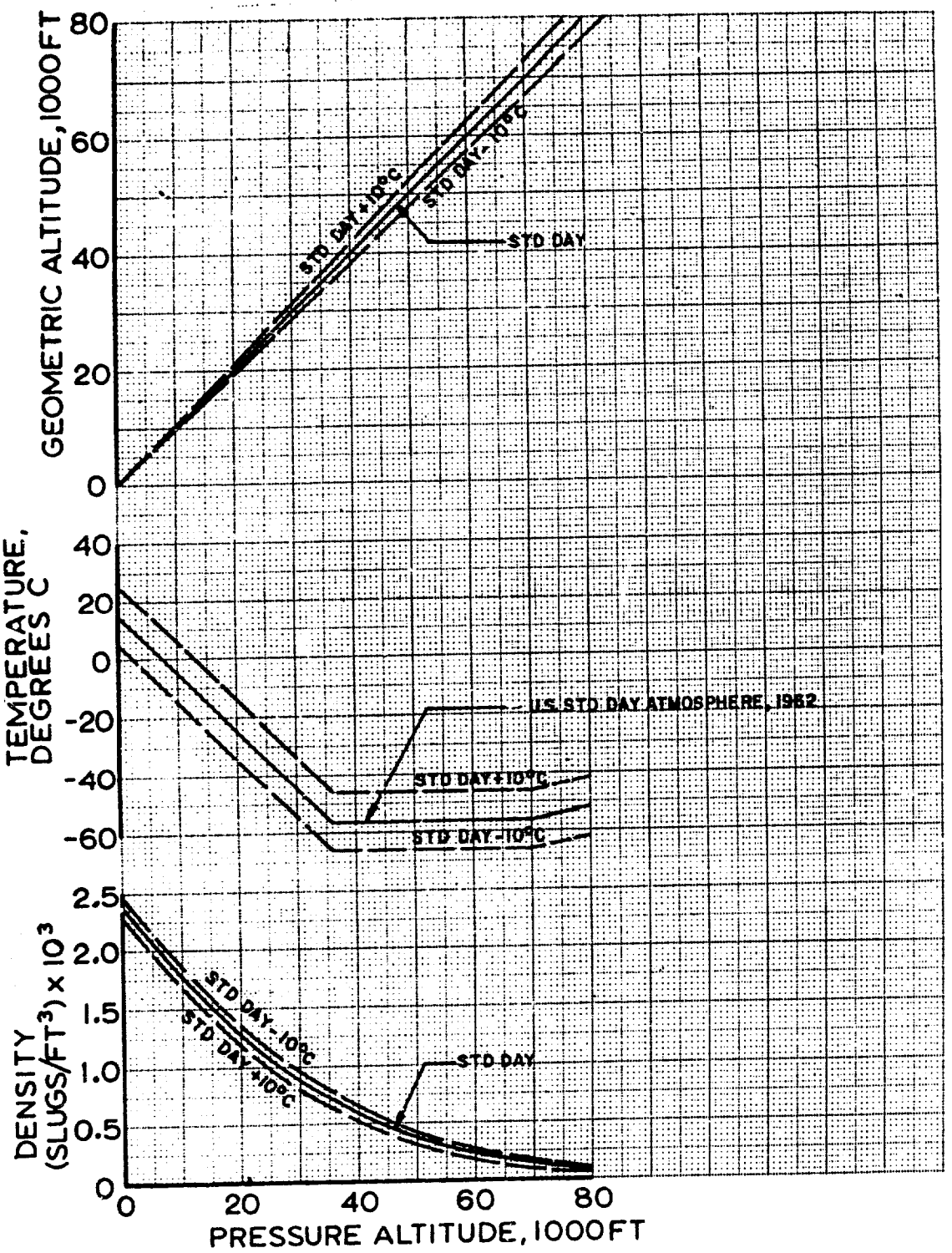


*Figure 2–15. Nonstandard Day Atmosphere Definitions*

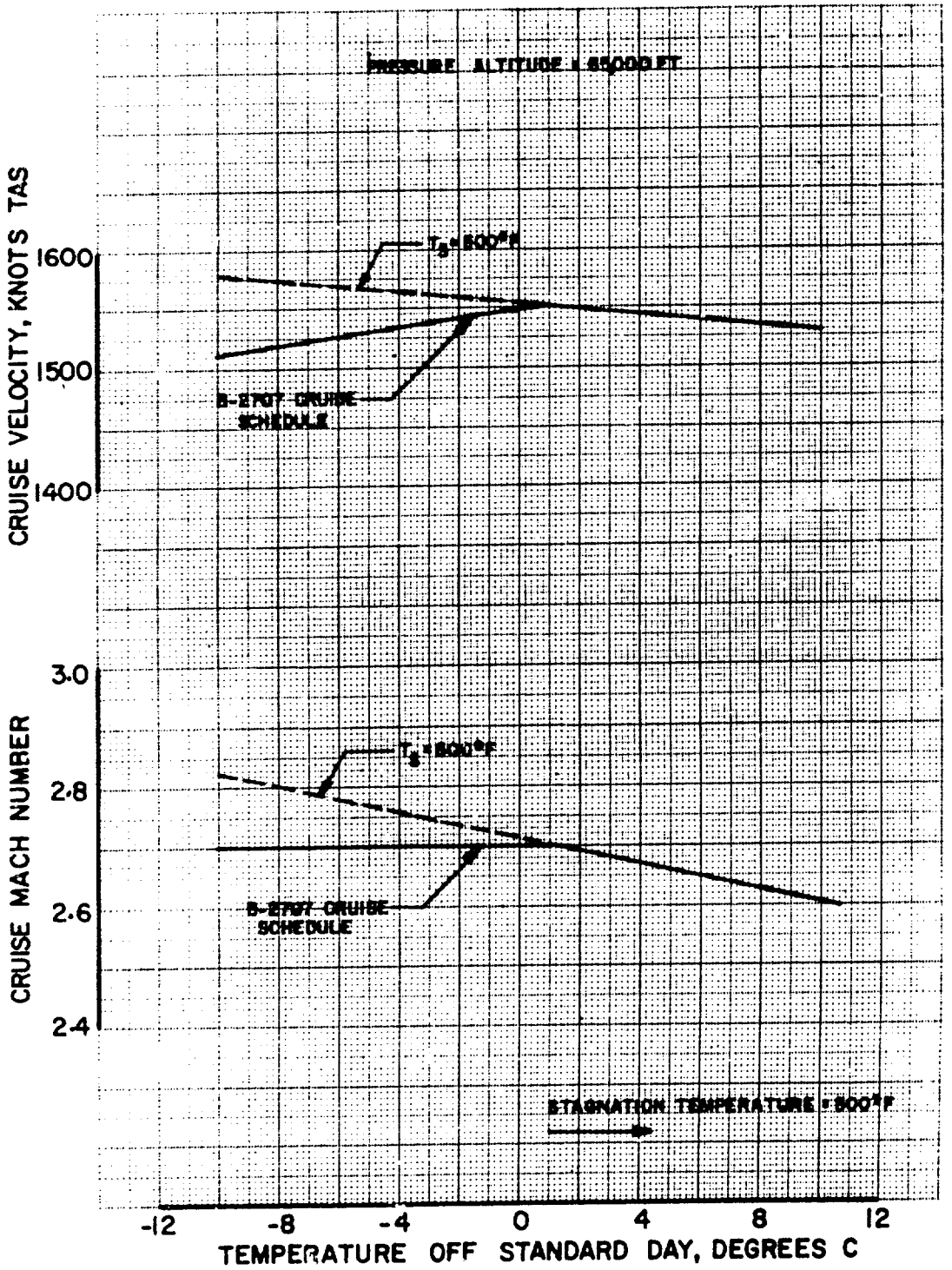


*Figure 2-16. B-2707 Cruise Speed and Mach Number*

*Table 2-C. Special Effects on Mission Performance*

| Item | Range, (nmi) (For a fixed payload of 50,000 lb) | | Payload (lb) (For a fixed range of 4,000 statute miles) | |
|---|---|---|---|---|
| | General Electric GE4/J5P | Pratt & Whitney JTF17A-21B | General Electric GE4/J5P | Pratt & Whitney JTF17A-21B |
| Basic mission (excluding all special effects) | 3,751 | 3,670 | 62,872 | 59,750 |
| Effect of | | | | |
| Centrifugal force only | 36 | 36 | 1,656 | 1,721 |
| $g/g_o$ only | 13 | 18 | 828 | 860 |
| Thrust effects on lift and drag, only "T sin $\alpha$" | 50 | 45 | 2,300 | 2,151 |
| Arc length at altitude only | -10 | -10 | -460 | -478 |
| Cabin air weight only | -11 | - 9 | -506 | -430 |
| Cruise climb only | -15 | -12 | -690 | -574 |
| Basic Mission (including all special effects) | 3,819 | 3,738 | 66,000 | 63,000 |

c. Climb, Fig. 4-24, V2-B-2707-4, -5

d. Cruise, leading edge sweep = 72 degrees

e. Descent, Fig. 6-1, V2-B2707-4, -5

f. Destination air maneuver, leading edge sweep = 30 degrees

2.5.1.3 Spoilers are used during the normal and high-speed descents to prevent the cabin rate of descent from exceeding 300 fpm. The normal descent uses full spoilers (45 degrees) below 10,000 ft altitude. The high-speed descent and landing uses full spoilers below 40,000 ft altitude for the B-2707 (GE) and 34,500 ft altitude for the B-2707 (P&WA). Full spoilers are used throughout the emergency descent. The spoiler drags used are as follows:

M = 0.32 to M = 0.85, wing sweep = 42 degrees, $\Delta C_D$ = 0.0150

Below M = 1.0, wing sweep = 72 degrees, $\Delta C_D$ = 0.0020

M = 1.1 to 2.7, wing sweep = 72 degrees, $\Delta C_D$ = 0.0077 to 0.0028 (linear variation with Mach number)

2.5.2 Takeoff and Landing Distance
Takeoff and landing field lengths have been calculated by the flight manual performance methods used for the certification of present Boeing jet transports, as described in Phase I (Volume A-V, Aerodynamics) with the exception of flare time. The method for computing takeoff flare is the same as that used in the Phase II-A and II-C studies. Rotation capability was based on a maximum angular velocity of 2.5 degrees per second and an angular acceleration of 2 degrees per second per second. The load factor increment applied during the air distance from liftoff was limited to 0.2 g. Angle of attack was reduced above the 35-ft altitude level when necessary to maintain this load factor limit. Airspeed increases from the speed at 35 ft to the steady state climb speed which is held until power cutback 1 statute mile beyond the end of the runway.

A load factor of 1.15 was used for the landing flare calculations. Speed at brake application is approximately 0.90 Vapp. The time delays and thrust decay factors used during landing and refused takeoff are shown in Table 2-D.

*Table 2-D. Time Delays and Thrust Settings, Takeoff and Landing*

| Item | Time delay (sec) | Engine thrust |
|---|---|---|
| Refused takeoff | | |
| Engine failure recognition and start of throttles back to brakes on | 0.4 | 95 percent takeoff power |
| Brakes on to throttles back | 1.4 | 80 percent takeoff power |
| Throttles back to spoilers up | 2.0 | 10 percent takeoff power |
| Start of throttles back to start of reverse thrust windup | 2.4 | |
| Start of reverse thrust windup to full-reverse thrust | | |
| a. GE engine | 3.0 | Maximum dry power |
| b. P&W engine | 3.5 | 80 percent maximum dry power |
| Landing | | |
| Nose gear touchdown to brakes on | .4 | Idle |
| From the beginning of engine windup to reverse thrust power setting | | |
| a. GE engine | 6.0 | Maximum dry power |
| b. P&W engine | 6.0 | 80 percent maximum dry power |
| Full reverse thrust to 60 kn | --- | Full percent maximum reverse thrust |
| 60 kn to full stop | --- | Full reverse thrust to idle reverse thrust |

## 3.0 PERFORMANCE SUBSTANTIATION


| | | Page |
|---|---|---|
| 3.1 | CRUISE CONFIGURATION | 47 |
| 3.2 | TAKEOFF AND LANDING CONFIGURATIONS | 105 |
| 3.3 | AEROELASTIC ANALYSIS METHODS | 131 |
| 3.4 | AERODYNAMIC DEVELOPMENT PROGRAM | 137 |

## 3.0 PERFORMANCE SUBSTANTIATION

The aerodynamic characteristics of the B-2707 are substantiated in this section. The substantiation is based on wind tunnel results, corrected to full-scale flight conditions, and on well-proved analytical methods. There are two parts to this section, Pars. 3.1 and 3.2, where the characteristics of the cruise configuration and the takeoff and landing characteristics are discussed respectively. Supersonic airplanes are particularly sensitive to aeroelastic effects; in Par. 3.3 aeroelastic studies are discussed comprehensively. The aerodynamic development program is presented in Par. 3.4.

### 3.1 CRUISE CONFIGURATION

The aerodynamic data for the calculation of airplane performance have been prepared taking into account refinement and improvements that will be made to the design in the following phases. Improvements in aerodynamic efficiency that were obtained during the 707 jet transport development are presented in Fig. 3-1. Continuous design refinement has led to significant improvements. Accordingly, a performance level has been selected for the production Model B-2707 which includes a modest 5 percent improvement in maximum lift-to-drag ratio.

To ensure that the development of the airplane will benefit from continuous advances in the state of the art, an aerodynamic development program has been prepared; all possibilities of drag improvement will be examined during refinement of the design to determine worth and cost of each.

As a part of that program, well-defined targets have been set for the components of drag, such as wave drag, friction drag, etc. In order to be sure that the targets were achievable, an aerodynamic development model was designed. It retained the general B-2707 geometric features, volumes, surface thicknesses, and arrangements but incorporated a large number of individual configuration variations; many or all could be reflected in the production airplane configuration without compromising the benefits of the prototype program. The variations incorporated were based on NASA and Boeing research activities. The limited extent of the variations can be seen by comparing Figs. 3-2 and 3-3 for the B-2707 and the aerodynamic development model respectively.

All of the features exhibited by the aerodynamic development model will be examined for incorporation into the B-2707 refinement work. High-speed wind tunnel tests of this configuration have just been completed. Photographs of this model and a model of the B-2707 are shown in Fig. 3-4. Based on the results of the first series of tests, a full-scale maximum lift drag ratio in excess of 8.7 has been obtained at Mach 2.7. The comparable current lift drag ratio for the B-2707 is 7.8 and the basis of performance has been set at 8.2; a conservative estimate for the production airplane in light of the extensive prototype and production development programs. In Fig. 3-5 the corresponding drag polars based on a continuing series of wind tunnel tests are compared with the lift drag characteristics that have been defined for performance calculations.

Aerodynamic characteristics that have been defined for performance calculations are tabulated for various flight conditions in Par. 3.1.1. Drag characteristics for installations of both GE and P&WA engines have been examined. Although differences in wetted area and in engine bleed characteristics have a perceptible effect on incremental drag, the drag difference is well inside the accuracy of drag determination. Tabulated drag characteristics have been prepared for airplanes with GE and P&WA engines so that performance calculations will reflect the small drag difference. For purposes of substantiation however, the two installations are considered to be equivalent in drag and only one set of data, applicable to both installations, is considered. Test data obtained with wind tunnel models for both installations are presented and discussed in Par. 3.1.3.5.

Detailed discussion of performance substantiation for the cruise configuration is presented in the following paragraphs:

- Lift drag characteristics of the B-2707
- Theoretical drag analysis
- Wind tunnel test results

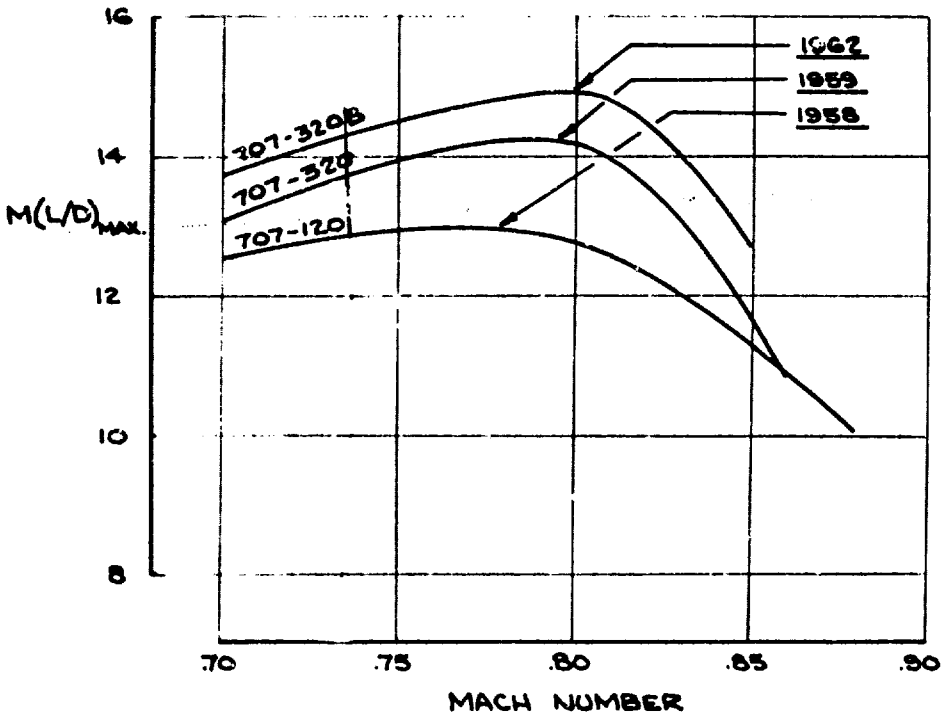


*Figure 3–1. Boeing Jet Transport Efficiency Improvement*

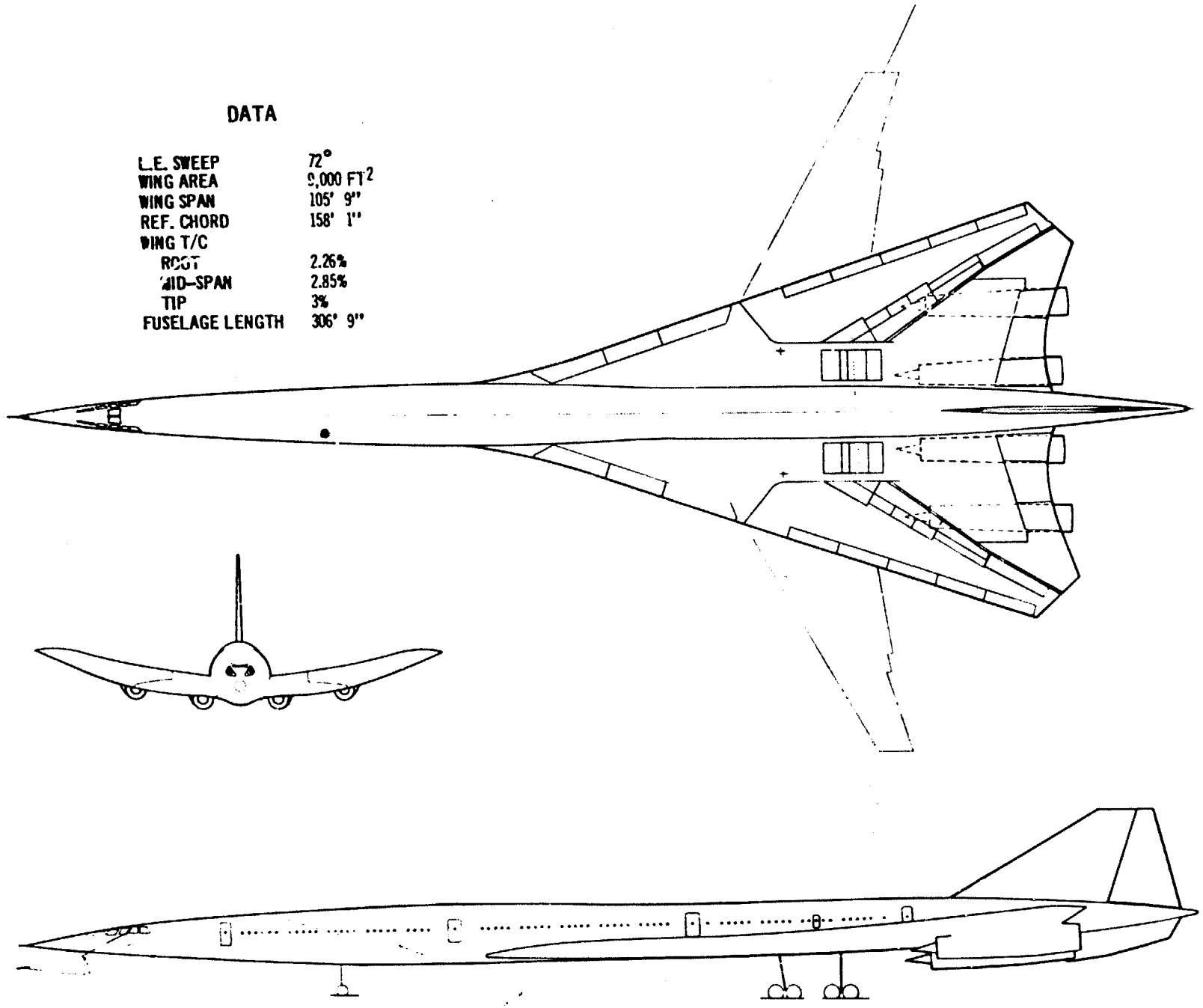


*Figure 3-2. B-2707 General Arrangement*

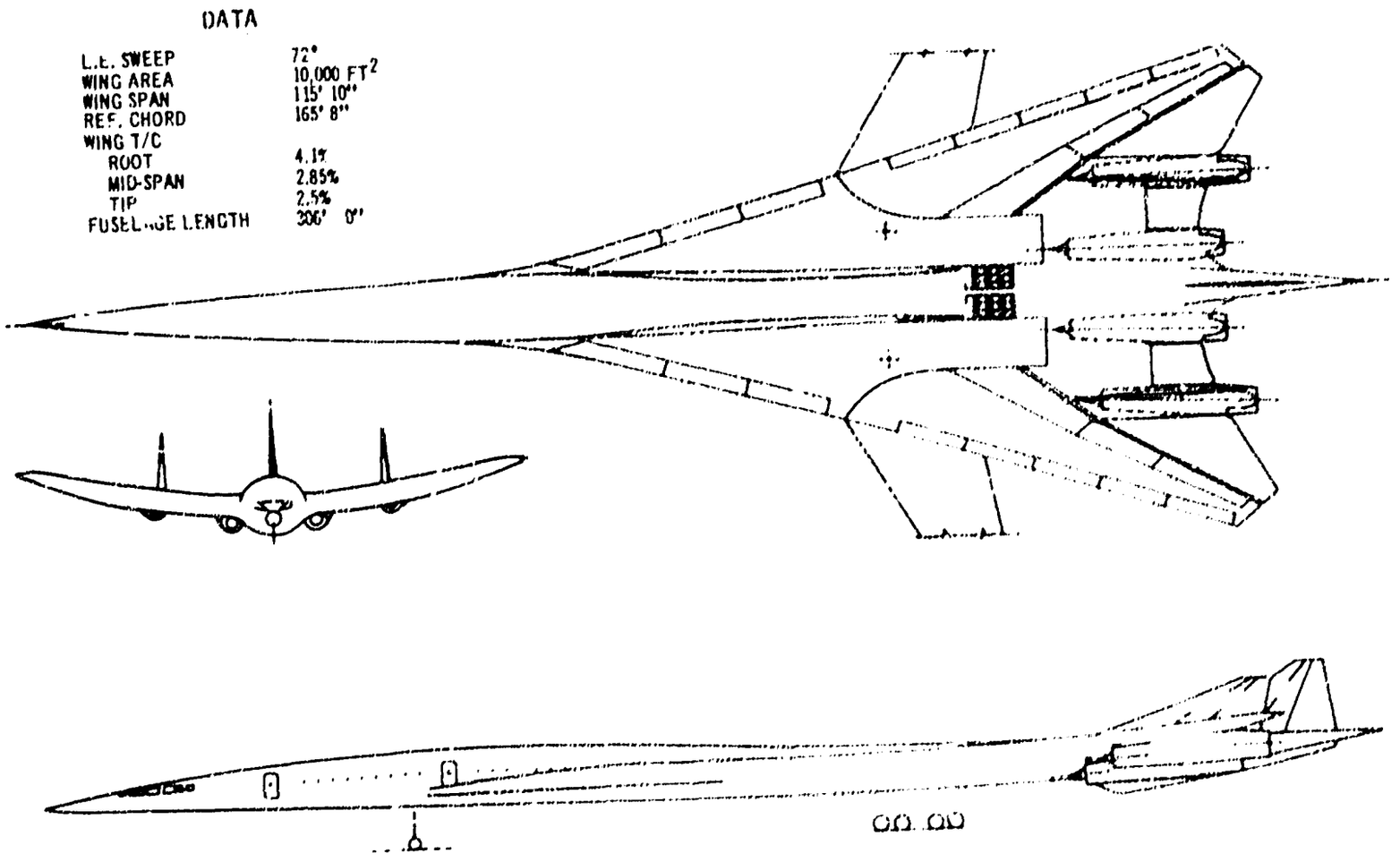


*Figure 3-3. Aerodynamic Development Model*

(a) Model SA 966 B-2707

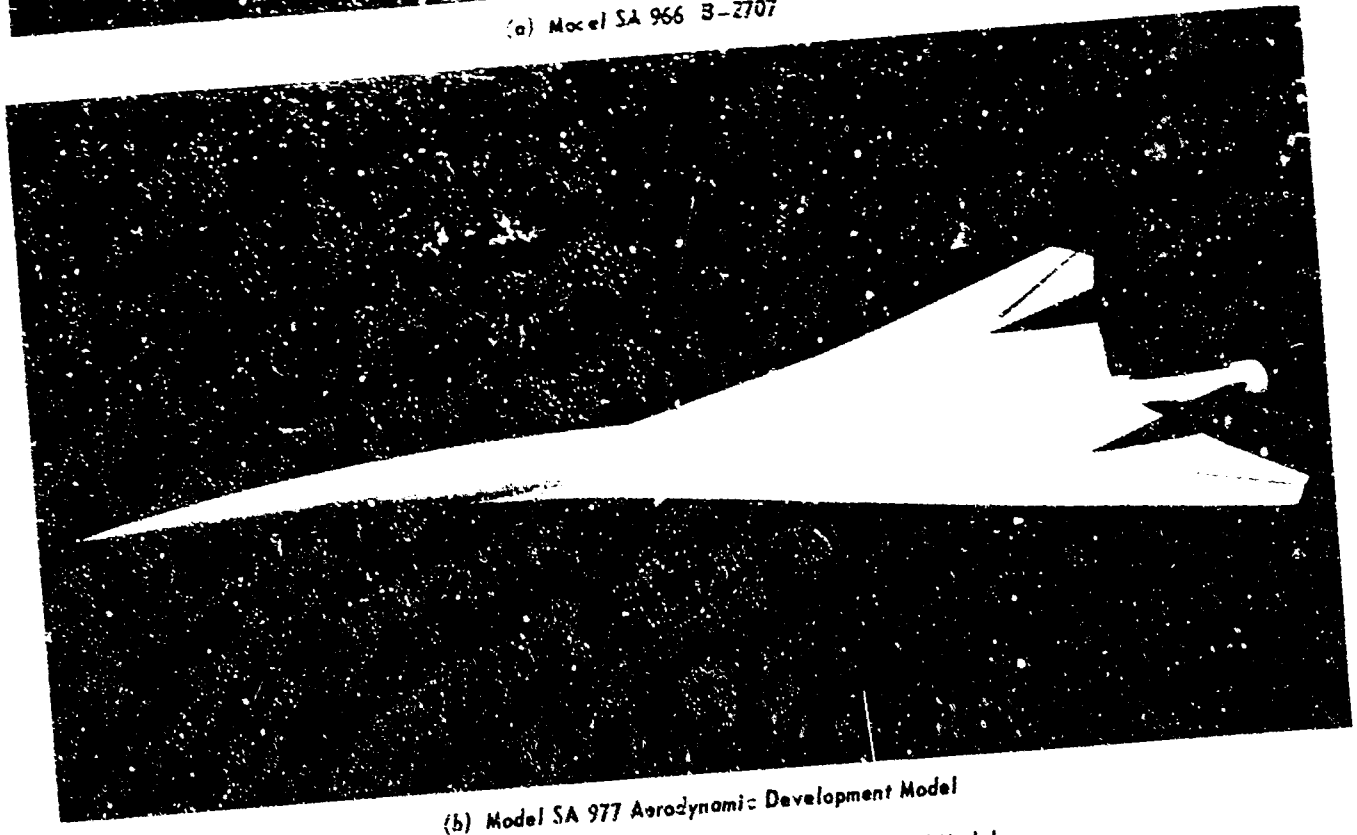

(b) Model SA 977 Aerodynamic Development Model

Figure 3-4. Photographs of Supersonic Wind Tunnel Models

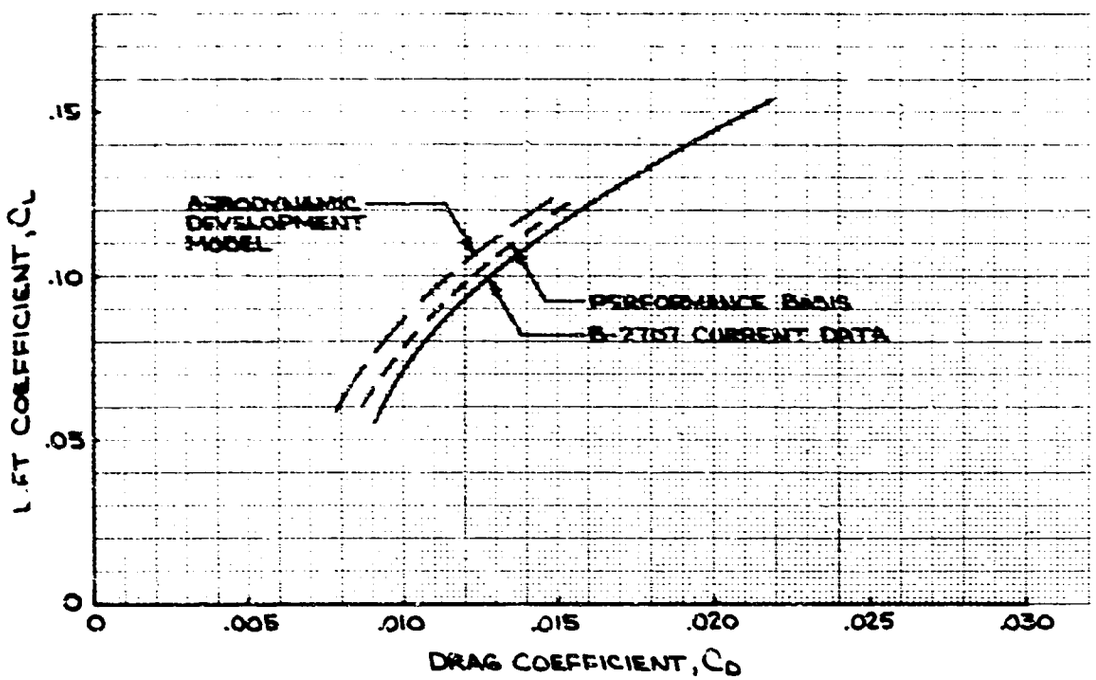


*Figure 3-5. (a) B-2707 Lift Drag Characteristics – Mach 2.7*

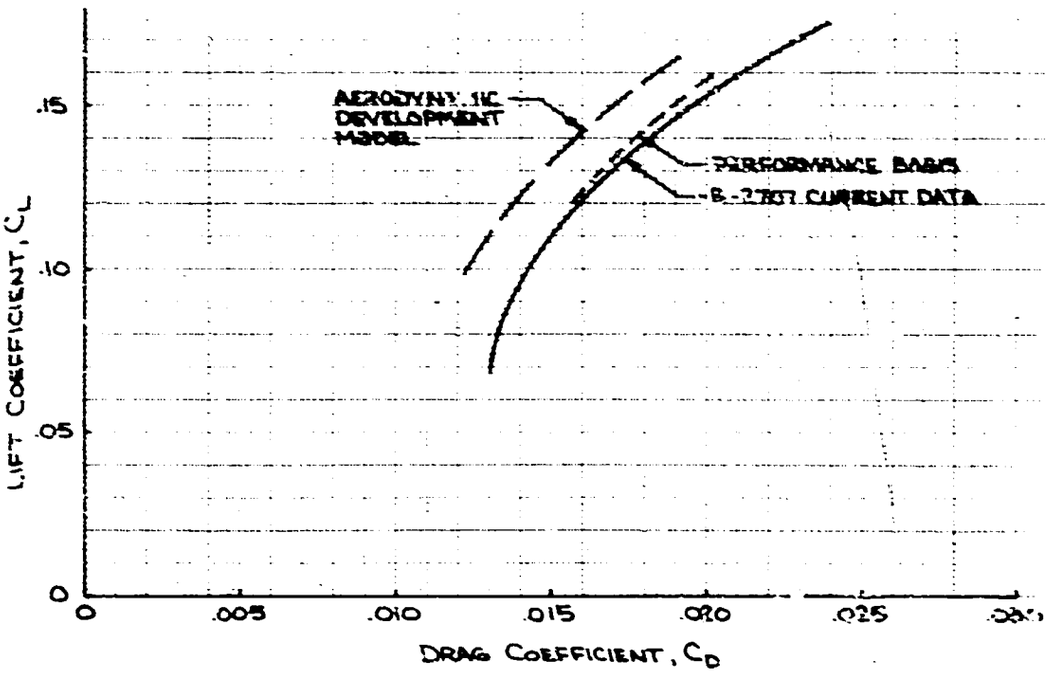


*Figure 3-5 (b) B-2707 Lift Drag Characteristics – Mach 1.5*

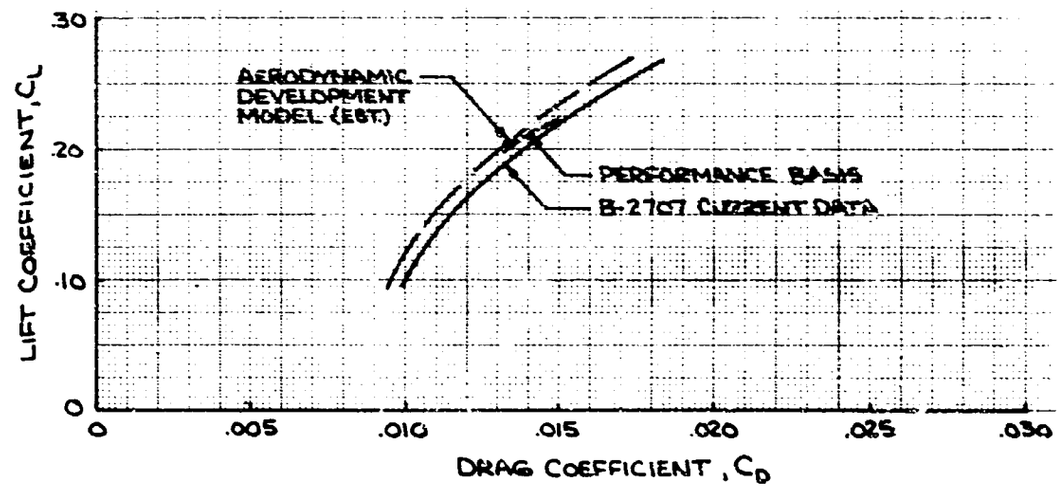


*Figure 3-5 (c) B-2707 Lift Drag Characteristics – Mach 0.85*

3.1.1 Lift Drag Characteristics of the B-2707
For performance calculations, the variation of airplane drag, $C_D$, with lift, $C_L$, is described by the following expression:

$$C_D = C_{D_{min}} + K(C_L - C_{L_O})^2$$

where:

$C_{D_{min}}$ - Minimum drag coefficient

K - An asymmetric drag due to lift factor

$C_{L_O}$ - Lift coefficient corresponding to $C_{D_{min}}$

The terms of this equation are tabulated as a function of altitude (H), and Mach number in Tables 3-A to 3-H. In addition, the lift slope $C_{L_\alpha}$, the lift coefficient at zero body reference angle of attack $C_{L_{\alpha_O}}$, and the rate of change of skin friction drag with altitude $\frac{\Delta C_{D_F}}{\Delta H}$ are shown. The data are tabulated separately for airplanes powered by GE and P&WA engines. The tabulations are for the nominal mission profile as well as at ±10,000 ft except where operating criteria, such as limiting angle of attack or maximum operating Mach number ($M_{MO}$), limit the operation.

The tabulations differentiate between the following cases: climb cruise, takeoff and landing air maneuvers, holding, and cruise to alternate. The climb cruise flight schedules are shown in Fig. 3-6 and the angles of leading edge sweep for all flight conditions are shown in Fig. 3-7.

3.1.2 Theoretical Drag Analysis
Theoretical analyses have been carried out to:

a. Determine incremental drag items such as wave drag, friction drag, etc.

b. Define increments to be applied to the wind tunnel model drag level in order to extrapolate this drag to the airplane flight conditions.

c. Evaluate the performance of the wind tunnel models, using the theoretical drag level as a yardstick, to determine that the design objectives of the wind tunnel models have been achieved.

3.1.2.1 Skin Friction Drag
At supersonic Mach numbers the skin friction drag has been calculated assuming fully turbulent, equivalent flat plate conditions. At subsonic Mach numbers an increment of form drag is added to the flat plate friction drag. The procedure used to calculate the equivalent flat plate turbulent skin friction drag is an application of the reference temperature method of Sommer and Short and the Karman-Schoenherr incompressible formula. Each component of the airplane is considered separately and the wing is further subdivided into chordwise strips. The calculations have been carried out with a digital computer program.

The effect of heat transfer on skin friction has been considered but found to be negligible. A skin emissivity of 0.2 and a solar absorptivity of 0.7 were used in the calculations. The effects of thermal conduction into the airplane, radiation heat input and output, and convective heat transfer by Reynolds analogy were considered. The skin friction drag along the flight schedule indicated in Fig. 3-6, is shown in Fig. 3-8. The wetted area breakdown of the B-2707 is tabulated in Tables 3-I and 3-J. A second wetted area breakdown of the aerodynamic development model is given in Tables 3-K and 3-L. Increments in skin friction drag for flight profiles that are slightly different from the one shown in Fig. 3-6 are shown in Table 3-M.

*Table 3-A. B-2707 (G.E.) Performance Inputs (Reference Altitude)*

| MACH | $H_{REF}$ (ft) | $C_{D_{MIN}}$ x10$^{4}$ | K | $C_{L_o}$ | $C_{L_\alpha}$ | $C_{L_{\alpha=o}}$ | $\Delta C_{D_{F/A}}$ H x10$^{8}$ |
|---|---|---|---|---|---|---|---|
| .26 | 35 | 631.3 | .142 | 0.20 | .0460 | .1170 | 2.50 |
| .40 | 1,501 | 81.7 | .202 | 0.035 | .0502 | -.1060 | 2.29 |
| .60 | 7,500 | 78.7 | .189 | 0.035 | .0537 | -.1205 | 2.40 |
| .80 | 23,000 | 84.3 | .190 | 0.035 | .0572 | -.1315 | 2.55 |
| .85 | 26,000 | 86.3 | .190 | 0.035 | .0580 | -.1340 | 2.74 |
| .90 | 28,200 | 96.9 | .350 | 0.0 | .0345 | -.1135 | 2.65 |
| .95 | 30,400 | 103.1 | .324 | 0.0 | .0342 | -.1065 | 2.71 |
| 1.00 | 32,500 | 125.8 | .304 | 0.0 | .0336 | -.0965 | 2.89 |
| 1.05 | 34,500 | 147.7 | .297 | 0.0 | .0327 | -.0860 | 3.00 |
| 1.10 | 36,000 | 154.3 | .300 | 0.0 | .0316 | -.0795 | 3.08 |
| 1.15 | 38,000 | 151.8 | .305 | 0.0 | .0308 | -.0750 | 3.16 |
| 1.20 | 39,500 | 144.2 | .317 | 0.0 | .0299 | -.0725 | 3.21 |
| 1.40 | 43,750 | 118.1 | .340 | 0.0 | .0281 | -.0655 | 3.30 |
| 1.60 | 45,750 | 102.4 | .370 | 0.0 | .0267 | -.0585 | 3.26 |
| 1.80 | 46,700 | 95.5 | .400 | 0.0 | .0250 | -.0485 | 3.16 |
| 2.00 | 47,500 | 81.1 | .432 | 0.0 | .0236 | -.0435 | 3.03 |
| 2.20 | 52,000 | 75.2 | .470 | 0.0 | .0225 | -.0405 | 2.88 |
| 2.40 | 55,700 | 70.0 | .509 | 0.0 | .0218 | -.0390 | 2.82 |
| 2.60 | 59,300 | 65.7 | .556 | 0.0 | .0212 | -.0385 | 2.80 |
| 2.70 | 61,000 | 63.6 | .579 | 0.0 | .0211 | -.0385 | 2.88 |
| 2.70 | 61,169 | 63.6 | .580 | 0.0 | .0211 | -.0385 | 2.88 |
| 2.70 | 68,427 | 65.6 | .580 | 0.0 | .0211 | -.0385 | 2.88 |

*Table 3-B. B-2707 (P & WA) Performance Inputs (Reference Altitude)*

| MACH | $H_{REF}$ (ft) | $C_{D_{MIN}}$ x$10^4$ | K | $C_{L_o}$ | $C_{L_\alpha}$ | $C_{L_{\alpha=o}}$ | $\Delta C_{D_{F/\Delta H}}$ x$10^8$ |
|---|---|---|---|---|---|---|---|
| .26 | 35 | 630.1 | .142 | 0.20 | .0460 | .1170 | 2.50 |
| .40 | 1,501 | 80.6 | .202 | 0.035 | .0592 | -.1060 | 2.29 |
| .60 | 7,500 | 77.5 | .187 | 0.035 | .0537 | -.1205 | 2.40 |
| .80 | 23,000 | 78.5 | .190 | 0.035 | .0572 | -.1315 | 2.55 |
| .85 | 26,000 | 79.1 | .191 | 0.035 | .0580 | -.1340 | 2.74 |
| .90 | 28,200 | 87.8 | .350 | 0.0 | .0345 | -.1135 | 2.65 |
| .95 | 30,400 | 91.4 | .324 | 0.0 | .0342 | -.1065 | 2.71 |
| 1.00 | 32,500 | 119.5 | .304 | 0.0 | .0336 | -.0965 | 2.89 |
| 1.05 | 34,500 | 139.0 | .300 | 0.0 | .0327 | -.0860 | 3.00 |
| 1.10 | 36,000 | 144.0 | .300 | 0.0 | .0316 | -.0795 | 3.08 |
| 1.15 | 38,000 | 142.0 | .305 | 0.0 | .0308 | -.0750 | 3.16 |
| 1.20 | 39,500 | 139.0 | .315 | 0.0 | .0299 | -.0725 | 3.21 |
| 1.40 | 43,750 | 116.1 | .340 | 0.0 | .0281 | -.0655 | 3.30 |
| 1.60 | 45,750 | 102.2 | .370 | 0.0 | .0267 | -.0585 | 3.26 |
| 1.80 | 46,700 | 93.2 | .401 | 0.0 | .0250 | -.0485 | 3.16 |
| 2.00 | 47,500 | 80.2 | .432 | 0.0 | .0236 | -.0435 | 3.03 |
| 2.20 | 52,000 | 74.4 | .470 | 0.0 | .0225 | -.0405 | 2.88 |
| 2.40 | 55,700 | 69.7 | .509 | 0.0 | .0218 | -.0390 | 2.82 |
| 2.60 | 59,300 | 65.3 | .554 | 0.0 | .0212 | -.0385 | 2.80 |
| 2.70 | 61,000 | 63.5 | .580 | 0.0 | .0211 | -.0385 | 2.88 |
| 2.70 | 61,111 | 63.6 | .580 | 0.0 | .0211 | -.0385 | 2.88 |
| 2.70 | 69,314 | 65.8 | .580 | 0.0 | .0211 | -.0385 | 2.88 |

*Table 3-C. B-2707 (GE) Performance Inputs (Reference Altitude +10,000 Ft)*

| MACH | H ft | $C_{D_{MIN}}$ x10$^4$ | K | $C_{L_o}$ | $C_{L_\alpha}$ | $C_{L_{\alpha=o}}$ | $\Delta C_{D_{F/\Delta H}}$ x10$^8$ |
|---|---|---|---|---|---|---|---|
| .26 | 10,035 | 633.8 | .141 | 0.20 | .0460 | .1170 | 2.50 |
| .40 | 11,000 | 83.8 | .204 | 0.035 | .0502 | -.1060 | 2.29 |
| .60 | 17,500 | 81.2 | .198 | 0.035 | .0537 | -.1205 | 2.40 |
| .80 | 33,000 | 87.0 | .201 | 0.035 | .0572 | -.1315 | 2.55 |
| .85 | 36,000 | 89.0 | .201 | 0.035 | .0580 | -.1340 | 2.74 |
| .90 | 37,370 | 99.3 | .367 | 0.0 | .0345 | -.1135 | 2.65 |
| .95 | 40,000 | 105.7 | .350 | 0.0 | .0342 | -.1065 | 2.71 |
| 1.00 | 40,000 | 128.1 | .335 | 0.0 | .0336 | -.0965 | 2.89 |
| 1.05 | 40,100 | 149.4 | .324 | 0.0 | .0327 | -.0860 | 3.00 |
| 1.10 | 40,700 | 155.7 | .320 | 0.0 | .0316 | -.0795 | 3.08 |
| 1.15 | 41,500 | 152.9 | .317 | 0.0 | .0308 | -.0750 | 3.16 |
| 1.20 | 42,700 | 145.3 | .319 | 0.0 | .0299 | -.0725 | 3.21 |
| 1.40 | 48,200 | 119.6 | .360 | 0.0 | .0281 | -.0655 | 3.30 |
| 1.60 | 52,200 | 104.5 | .405 | 0.0 | .0267 | -.0585 | 3.26 |
| 1.80 | 55,000 | 98.1 | .445 | 0.0 | .0250 | -.0485 | 3.16 |
| 2.00 | 57,500 | 84.1 | .480 | 0.0 | .0236 | -.0435 | 3.03 |
| 2.20 | 62,000 | 78.1 | .520 | 0.0 | .0225 | -.0405 | 2.88 |
| 2.40 | 65,700 | 72.7 | .555 | 0.0 | .0218 | -.0390 | 2.82 |
| 2.60 | 69,200 | 68.4 | .585 | 0.0 | .0212 | -.0385 | 2.80 |
| 2.70 | 70,400 | 66.3 | .605 | 0.0 | .0211 | -.0385 | 2.88 |
| 2.70 | 71,169 | 66.4 | .610 | 0.0 | .0211 | -.0385 | 2.88 |
| 2.70 | 78,427 | 68.6 | .590 | 0.0 | .0211 | -.0385 | 2.88 |

*Table 3-D. B-2707 (P & WA) Performance Inputs (Reference Altitude +10,000 FT)*

| MACH | H (ft) | $C_{D_{MIN}}$ $x10^4$ | K | $C_{L_o}$ | $C_{L_\alpha}$ | $C_{L_{\alpha=o}}$ | $\Delta C_{D_{F/\Delta H}}$ $x10^8$ |
|---|---|---|---|---|---|---|---|
| .26 | 10,035 | 632.6 | .141 | 0.20 | .0460 | .1170 | 2.50 |
| .40 | 11,000 | 82.8 | .204 | 0.035 | .0502 | -.1060 | 2.29 |
| .60 | 17,500 | 79.9 | .198 | 0.035 | .0537 | -.1205 | 2.40 |
| .80 | 33,000 | 81.1 | .201 | 0.035 | .0572 | -.1315 | 2.55 |
| .85 | 36,000 | 81.8 | .201 | 0.035 | .0580 | -.1340 | 2.74 |
| .90 | 37,370 | 90.3 | .367 | 0.0 | .0345 | -.1135 | 2.65 |
| .95 | 40,000 | 94.0 | .350 | 0.0 | .0342 | -.1065 | 2.71 |
| 1.00 | 40,000 | 112.7 | .335 | 0.0 | .0336 | -.0965 | 2.89 |
| 1.05 | 40,100 | 140.7 | .324 | 0.0 | .0327 | -.0860 | 3.00 |
| 1.10 | 40,700 | 145.4 | .320 | 0.0 | .0316 | -.0795 | 3.08 |
| 1.15 | 41,500 | 143.1 | .317 | 0.0 | .0308 | -.0750 | 3.16 |
| 1.20 | 42,700 | 140.0 | .319 | 0.0 | .0299 | -.0725 | 3.21 |
| 1.40 | 48,200 | 117.6 | .360 | 0.0 | .0281 | -.0655 | 3.30 |
| 1.60 | 52,200 | 104.3 | .405 | 0.0 | .0267 | -.0585 | 3.26 |
| 1.80 | 55,000 | 95.8 | .445 | 0.0 | .0250 | -.0485 | 3.16 |
| 2.00 | 57,500 | 83.2 | .480 | 0.0 | .0236 | -.0435 | 3.03 |
| 2.20 | 62,000 | 77.3 | .520 | 0.0 | .0225 | -.0405 | 2.83 |
| 2.40 | 65,700 | 72.4 | .555 | 0.0 | .0218 | -.0390 | 2.82 |
| 2.60 | 69,200 | 68.0 | .585 | 0.0 | .0212 | -.0385 | 2.80 |
| 2.70 | 70,400 | 66.2 | .605 | 0.0 | .0211 | -.0385 | 2.88 |
| 2.70 | 71,111 | 66.4 | .610 | 0.0 | .0211 | -.0385 | 2.88 |
| 2.70 | 79,314 | 69.0 | .590 | 0.0 | .0211 | -.0385 | 2.88 |

*Table 3-E. B-2707 (GE) Performance Inputs (Minimum Altitude)*

| MACH | H (ft.) | $C_{D_{MIN}}$ x$10^4$ | K | $C_{L_O}$ | $C_{L_\alpha}$ | $C_{L_{\alpha=0}}$ | $\Delta C_{DF}/\Delta_H$ (X $10^8$) |
|---|---|---|---|---|---|---|---|
| .26 | 35 | 631.3 | .142 | 0.20 | .0460 | .1170 | 2.50 |
| .40 | 1,501 | 81.7 | .202 | 0.035 | .0502 | -.1060 | 2.29 |
| .60 | 7,500 | 78.7 | .189 | 0.035 | .0537 | -.1205 | 2.40 |
| .80 | 23,000 | 84.3 | .190 | 0.035 | .0572 | -.1315 | 2.55 |
| .85 | 25,000 | 86.1 | .186 | 0.035 | .0580 | -.1340 | 2.74 |
| .90 | 25,000 | 96.2 | .340 | 0.0 | .0345 | -.1135 | 2.65 |
| .95 | 25,000 | 101.8 | .318 | 0.0 | .0342 | -.1065 | 2.71 |
| 1.00 | 26,400 | 124.3 | .300 | 0.0 | .0336 | -.0965 | 2.89 |
| 1.05 | 27,900 | 146.1 | .297 | 0.0 | .0327 | -.0860 | 3.00 |
| 1.10 | 28,900 | 152.6 | .300 | 0.0 | .0316 | -.0795 | 3.08 |
| 1.15 | 30,100 | 149.8 | .305 | 0.0 | .0308 | -.0750 | 3.16 |
| 1.20 | 31,200 | 142.0 | .312 | 0.0 | .0299 | -.0725 | 3.21 |
| 1.40 | 35,300 | 115.4 | .340 | 0.0 | .0281 | -.0655 | 3.30 |
| 1.60 | 39,000 | 100.2 | .370 | 0.0 | .0267 | -.0585 | 3.26 |
| 1.80 | 43,200 | 94.5 | .400 | 0.0 | .0250 | -.0485 | 3.16 |
| 2.00 | 47,500 | 81.1 | .432 | 0.0 | .0236 | -.0435 | 3.03 |
| 2.20 | 52,000 | 75.2 | .470 | 0.0 | .0225 | -.0405 | 2.88 |
| 2.40 | 55,700 | 70.0 | .509 | 0.0 | .0218 | -.0390 | 2.82 |
| 2.60 | 59,300 | 65.7 | .556 | 0.0 | .0212 | -.0385 | 2.80 |
| 2.70 | 61,000 | 63.6 | .579 | 0.0 | .0211 | -.0385 | 2.88 |
| 2.70 | 61,169 | 63.6 | .580 | 0.0 | .0211 | -.0385 | 2.88 |
| 2.70 | 68,427 | 65.6 | .580 | 0.0 | .0211 | -.0385 | 2.88 |

Table I-5 B-2707 PSWA Performance Inputs Maximum A/B Rate

| MACH | H (ft) | $C_D$ MEN $N/m^2$ | N | $C_{L_0}$ | $C_{L_\alpha}$ | $C_{L_{\delta E=0}}$ | $\Delta C_{DF}$ MIL $\Delta C_{DR}$ |
|---|---|---|---|---|---|---|---|
| .85 | 35 | 630.1 | .342 | 0.00 | .0341 | .0000 | 2.81 |
| .90 | 1,501 | 60.5 | .302 | 0.000 | .0342 | -.0000 | 2.79 |
| .95 | 7,500 | 77.5 | .337 | 0.000 | .0337 | -.0000 | 2.81 |
| .90 | 20,000 | 76.5 | .333 | 0.000 | .0371 | -.0000 | 2.83 |
| .95 | 25,000 | 76.9 | .317 | 0.000 | .0350 | -.0000 | 2.74 |
| .90 | 22,000 | 67.0 | .340 | 0.0 | .0345 | -.0000 | 2.85 |
| .95 | 25,000 | 80.1 | .318 | 0.0 | .0341 | -.0000 | 2.71 |
| 1.00 | 26,400 | 105.0 | .306 | 0.0 | .0336 | -.0000 | 2.69 |
| 1.05 | 27,000 | 132.0 | .297 | 0.0 | .0327 | -.0000 | 2.66 |
| 1.10 | 29,900 | 142.3 | .306 | 0.0 | .0316 | -.0000 | 2.74 |
| 1.15 | 30,100 | 139.5 | .305 | 0.0 | .0309 | -.0000 | 2.76 |
| 1.20 | 31,200 | 136.7 | .312 | 0.0 | .0299 | -.0000 | 2.81 |
| 1.40 | 35,300 | 113.5 | .340 | 0.0 | .0281 | -.0000 | 3.30 |
| 1.60 | 39,000 | 100.2 | .370 | 0.0 | .0267 | -.0000 | 3.28 |
| 1.80 | 43,200 | 92.3 | .401 | 0.0 | .0250 | -.0000 | 3.16 |
| 2.00 | 47,500 | 80.2 | .432 | 0.0 | .0236 | -.0000 | 3.03 |
| 2.20 | 52,000 | 74.4 | .470 | 0.0 | .0225 | -.0000 | 2.88 |
| 2.40 | 55,700 | 69.7 | .509 | 0.0 | .0218 | -.0000 | 2.82 |
| 2.60 | 59,300 | 65.3 | .554 | 0.0 | .0212 | -.0000 | 2.80 |
| 2.70 | 61,000 | 63.5 | .580 | 0.0 | .0211 | -.0000 | 2.88 |
| 2.70 | 61,111 | 63.6 | .580 | 0.0 | .0211 | -.0000 | 2.88 |
| 2.70 | 69,314 | 65.8 | .580 | 0.0 | .0211 | -.0000 | 2.88 |

*Table 3-G. B-2707 (GE) Lift-Drag Characteristics 30 & 42 Degrees Sweep*

| MACH | $H_{REF}$ | $C_{DMIN}$ | K | $C_{LO}$ | $C_{L\alpha}$ | $C_{L_{\alpha=0}}$ | $\Delta CDF/\Delta H$ x $10^8$ | SWEEP | CONFIGURATION |
|---|---|---|---|---|---|---|---|---|---|
| .414 | 5,000 | .01590 | .200 | .10 | .0502 | -.106 | 2.29 | 42° T.O | SLATS AIR MANEUVER |
| .414 | 5,000 | .00832 | .186 | .04 | .0540 | -.033 | 2.31 | 30° LANDING | CLEAN AIR MAN. |
| .500 | 15,000 | .00837 | .180 | .04 | .0554 | -.034 | 2.63 | 30° HOLDING | CLEAN |
| .850 | 36,150 | .00899 | .183 | .035 | .0580 | -.134 | 3.50 | 42° CRUISE TO ALTERNATE | CLEAN |
| .850 | 33,300 | .00890 | .196 | .035 | .0580 | -.134 | 3.50 | 42° SUBSONIC CRUISE | CLEAN |

*Table 3-H. B-2707 (P & WA) Lift-Drag Characteristic 30 & 42 Degrees Sweep*

| MACH | $H_{REF}$ | $C_{DMIN}$ | K | $C_{LO}$ | $C_{L\alpha}$ | $C_{L_{\alpha=0}}$ | $\Delta CDF/\Delta H$ x $10^8$ | SWEEP | CONFIGURATION |
|---|---|---|---|---|---|---|---|---|---|
| .414 | 5,000 | .01580 | .200 | .10 | .0502 | -.106 | 2.29 | 42° T.O. | SLATS AIR MANEUVER |
| .414 | 5,000 | .00821 | .184 | .04 | .0540 | -.033 | 2.31 | 30° LANDING | CLEAN AIR MAN. |
| .500 | 15,000 | .00826 | .180 | .04 | .0554 | -.034 | 2.63 | 30° HOLDING | CLEAN |
| .850 | 36,150 | .00825 | .184 | .035 | .0580 | .-134 | 3.50 | 42° CRUISE TO ALTERNATE | CLEAN |
| .850 | 36,150 | .00825 | .195 | .035 | .0580 | -.134 | 3.50 | 42° SUBSONIC CRUISE | CLEAN |

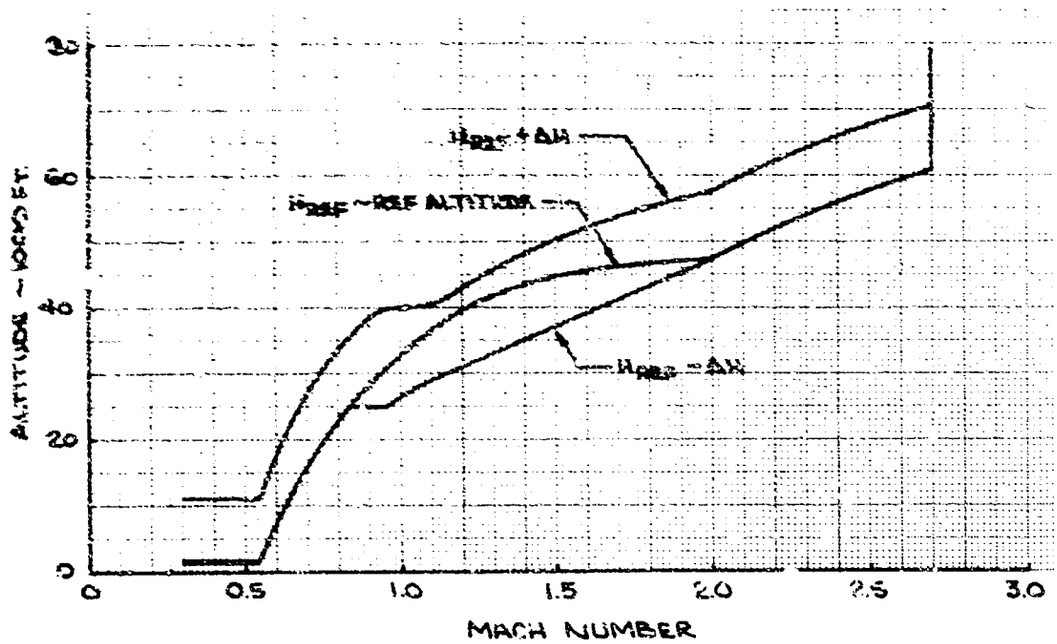


*Figure 3-6. B-2707 Climb Profiles*

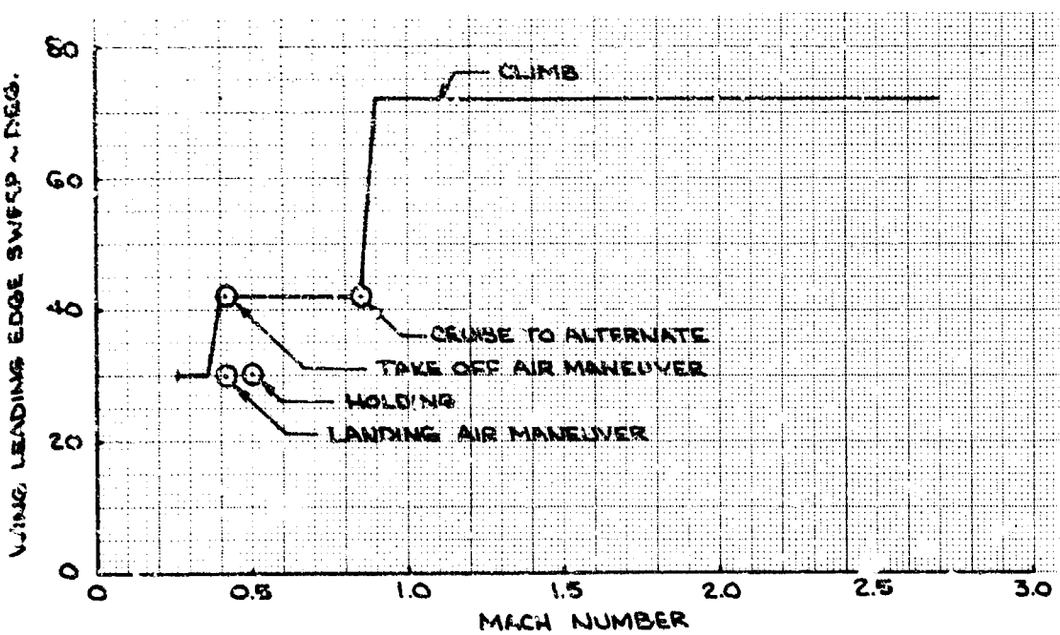


*Figure 3-7. B-2707 Sweep Schedules*

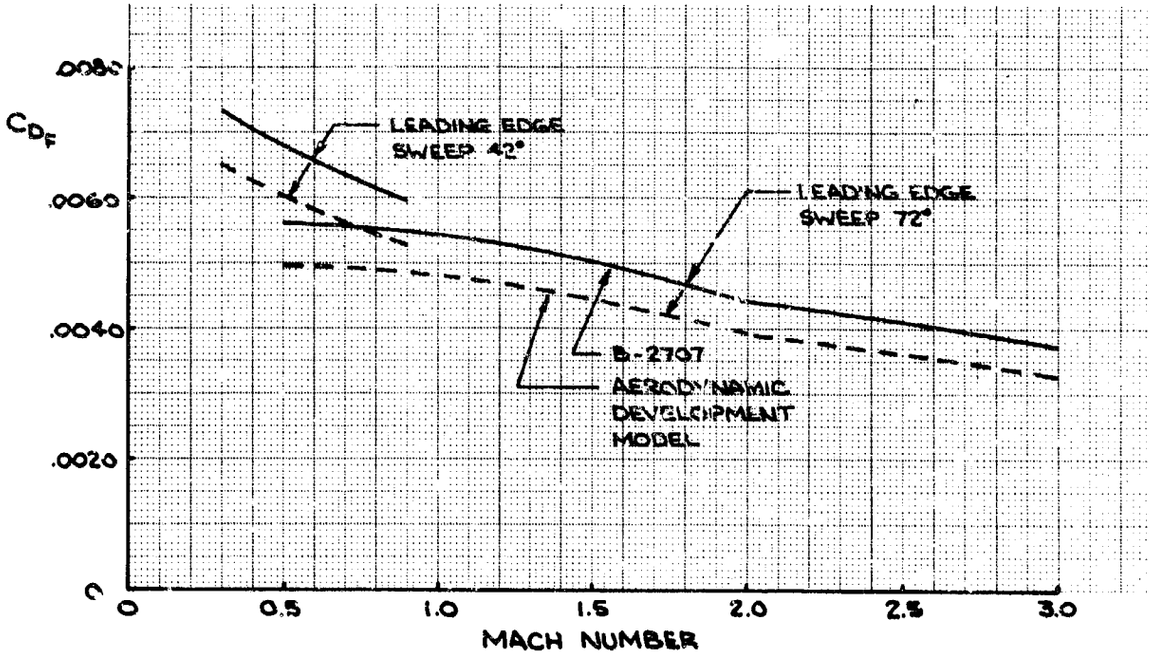


*Figure 3-8. Skin Friction Drag*

*Table 3-I. B-2707 Wetted Areas – Leading Edge Sweep – 72 Degrees*

| COMPONENT | WETTED AREA (Sq Ft) | | CHARACTERISTIC LENGTH (Ft) | |
|---|---|---|---|---|
| | GE | P&W | GE | P&W |
| Body | 9885 | 9885 | 306 | 306 |
| Wing | 14970 | 15047 | 93 | 93 |
| Nacelles | 2700 | 2300 | 35.9 | 28.7 |
| Horizontal Tail | (Included in Wing) | | | |
| Vertical Tail | 1750 | 1750 | 40 | 40 |
| Ventral | 402 | 402 | 40 | 40 |
| Fences | 226 | 276 | 40 | 50 |
| Total | 29933 | 29660 | | |

*Table 3-J. B-2707 Wetted Areas – Leading Edge Sweep – 42 Degrees*

| COMPONENT | WETTED AREA (Sq Ft) | | CHARACTERISTIC LENGTH (Ft) | |
|---|---|---|---|---|
| | GE | P&W | GE | P&W |
| Body | 9885 | 9885 | 306 | 306 |
| Wing | 12720 | 12797 | 58 | 58 |
| Nacelles | 2700 | 2300 | 35.9 | 28.7 |
| Horizontal Tail | 3085 | 3085 | 29 | 29 |
| Vertical Tail | 1750 | 1750 | 40 | 40 |
| Ventral | 402 | 402 | 40 | 40 |
| Fences | 226 | 276 | 40 | 50 |
| Total | 30768 | 30495 | | |

*Table 3-K. Aerodynamic Development Model Wetted Areas Leading Edge Sweep 72 Degrees*

| COMPONENT | WETTED AREA (Sq Ft) | | CHARACTERISTIC LENGTH (Ft) | |
|---|---|---|---|---|
| | GE | P&W | GE | P&W |
| Body | 8850 | 8850 | 306 | 306 |
| Wing | 16470 | 16530 | 95 | 95 |
| Nacelles | 2600 | 2300 | 35.9 | 28.7 |
| Horizontal Tail | | (Included in Wing) | | |
| Wing-Mounted Vertical Tails (2) | 1170 | 1170 | 35 | 35 |
| Body-Mounted Vertical Tail (1) | 650 | 650 | 25 | 25 |
| Ventral | 280 | 280 | 75 | 75 |
| Total | 30020 | 29700 | | |

*Table 3-L. Aerodynamic Development Model Wetted Areas Leading Edge Sweep 42 Degrees*

| COMPONENT | WETTED AREA (Sq Ft) | | CHARACTERISTIC LENGTH (Ft) | |
|---|---|---|---|---|
| | GE | P&W | GE | P&W |
| Body | 8850 | 8850 | 306 | 306 |
| Wing | 13996 | 14076 | 61 | 61 |
| Nacelles | 2600 | 2300 | 35.9 | 28.7 |
| Horizontal Tail | 3390 | 3390 | 30 | 30 |
| Wing-Mounted Vertical Tails (2) | 1179 | 1170 | 35 | 35 |
| Body-Mounted Vertical Tail (1) | 650 | 650 | 25 | 25 |
| Ventral | 280 | 280 | 75 | 75 |
| Total | 30936 | 30616 | | |

Table 3-M. Friction Drag Cha[illegible] 200 FT

| Mach Number | $\Delta C_{DF}$ $\Delta H$ |
|---|---|
| .4 | $2.29 \times 10^{-5}$ |
| .8 | $2.55 \times 10^{-5}$ |
| 1.0 | $2.89 \times 10^{-5}$ |
| 1.2 | $3.21 \times 10^{-5}$ |
| 2.0 | $3.03 \times 10^{-5}$ |
| 2.7 | $2.58 \times 10^{-5}$ |

At subsonic Mach numbers, the flat plate skin friction drag has to be increased by an increment of form drag due to thickness effects. The form drag increments for the B-2707 are listed in Table 3-N. Form drag increments have been obtained using the published data sheets of the Royal Aeronautical Society.

Table 3-N. B-2707 Form Drag

| Mach Number | $\Delta C_D$ | |
|---|---|---|
| | 42° Sweep | 72° Sweep |
| .4 | .00060 | .00035 |
| .6 | .00056 | .00033 |
| .8 | .00052 | .00033 |

3.1.2.2 Roughness and Miscellaneous Drag The calculations of skin friction drag have been based on the assumption that the skin of the airplane is smooth. A drag increment has been added to include the effects of:

- Surface waviness and manufacturing roughness.
- Miscellaneous protuberances not simulated on the wind tunnel models.
- Ram pressure and thrust recoveries of secondary air used for cooling, environmental control, etc.

Reference 2 contains a detailed description of the size and location of roughness items due to manufacturing tolerances, miscellaneous protuberances, and vents. The calculation of the drag for surface roughness and protuberances was based on test data for typical roughness elements. The general procedure was similar to that described in Ref. 3 which includes an extensive bibliography on test data for roughness elements. Since the publication of Ref. 3, more test data have become available and additional data from Refs. 4 to 7 have been used for the estimates of roughness drag. A summary of the surface roughness drag increments at Mach 2.70 is presented in Table 3-O. Detailed calculations for other Mach numbers are available. The drag, at Mach 2.7, of miscellaneous protuberances is listed in Table 3-P.

The drag of the environmental system is defined as the drag of that inlet air discharged from all areas other than the engine nozzles. External and internal air properties were determined for each exhaust nozzle, and these data were used to calculate ideal and estimated thrust recoveries. The ideal thrust recovery values were obtained by assuming isentropic flow. These values were then corrected using secondary air injection test data (Refs. 8 through 10), and skin friction increments due to the formation of secondary air boundary layers in the vicinity of each nozzle. In addition, drag components of the normal forces on inclined surfaces due to shock wave formation at supersonic Mach numbers (Refs. 11 through 13) were included in calculation of the estimated thrust recoveries. Total drag increments were obtained by subtracting ideal and estimated thrust recoveries from the ram drag of each inlet streamtube. An itemized summary of these calculations for Mach 2.7 is shown in Table 3-Q. Similar summaries and detailed calculations for other Mach numbers will be available.

The total drag increment for roughness, miscellaneous items, protuberances, etc., as a function of Mach number is shown in Fig. 3-9.

## *Table 3-0. Manufacturing Roughness Increment Drag Coefficients at Mach 2.7*

| ITEMS | $\Delta C_{D_R} \times 10^4$ |
|---|---|
| **Wing** | |
| Surface Waves | .1424 |
| Pivot Fairing Mismatch | .0165 |
| Pivot Access Doors | .0022 |
| Main Landing Gear Doors | .0058 |
| Wing Access Doors | .0043 |
| Skin Butt Joints | .0504 |
| Leading Edge Main Slat to Wing | .0225 |
| Leading Edge Fore Slat to Main Slat | .0100 |
| Leading Edge Slat Ends | .0133 |
| Trailing Edge Flaps to Wing | .0187 |
| Ailerons to Wing | .0083 |
| Spoilers to Wing | .0103 |
| Aft Flap to Stabilizer | .0288 |
| Inboard Flap Doors | .0137 |
| **Flap and Aileron Ends** | .0107 |
| **Fuselage** | |
| Surface Waves | .2216 |
| Cargo Doors | .0036 |
| Nose and Main Landing Gear Doors | .0122 |
| Entry and Galley Doors | .0190 |
| Escape Hatch and Doors | .0100 |
| Body Fuel Tank Doors | .0017 |
| Equipment Access Panels | .0008 |
| Auxiliary Drive System Door | .0020 |
| Hydraulic System Access Door | .0008 |
| Skin Butt Joints | .0289 |
| Cabin Windows | .0102 |
| Air Traffic Control Antenna | .0002 |
| Radome | .0010 |
| Canopy Windows | .0035 |
| Canopy Fairing | .0053 |
| **Horizontal Tail** | |
| Surface Waves | .0462 |
| Access Doors | .0017 |
| Thrust Reverser Doors | .0072 |
| Air Conditioning Access Panel | .0014 |
| Elevator to Horizontal Tail | .0021 |
| Skin Butt Joints | .0267 |
| Elevon Actuator Access Panels | .0036 |
| Auxiliary Drive System Panels | .0007 |
| Elevons to Horizontal Tail | .0072 |
| **Vertical Tail** | |
| Surface Waves | .0178 |
| Access Doors | .0009 |
| Skin Butt Joints | .0230 |
| Rudder to Vertical Tail | .0105 |
| **Ventral Fin** | |
| Skin Butt Joints | .0041 |
| Surface Waves | .0032 |
| **Propulsion Pods** | |
| Surface Waves (GE) | (.2398) |
| (P&W) | (.1550) |
| Power Take-Off Drive System Access Doors | .0013 |
| Oil Tank Filler Doors | .0014 |
| Skin Butt Joints | .0050 |
| Thrust Reverser Access Panels | .0021 |
| Diverter Doors | .0007 |
| Inlet By-Pass Doors | .0066 |
| Secondary Air/Thrust Reverser Doors (P&W) | (.0540) |
| Secondary Air Doors (GE) | (.0216) |
| Thrust Reverser Doors (GE) | (.0320) |
| Pressure Relief & Burnout Doors (GE) | (.0030) |
| (P & W) | (.0029) |

*Table 3-P. Miscellaneous Protuberance Incremental Drag Coefficients at Mach 2.70*

| Protuberances | $\Delta C_{D_R} \times 10^4$ |
|---|---|
| Nose Pitot Static Probe | .0639 |
| Keel Beam Chords | .0652 |
| Total Air Temperature Probes | .0649 |
| Galley Door Guide Plates | .0096 |
| VHF Antennae | .0530 |
| Fuselage Pitot Probes | .0148 |
| Angle of Attack Sensors | .0182 |
| Wing Fuel Tank Vent | .0001 |
| Vertical Tail Fuel Tank Vent | .0001 |
| Feel Computer Pitot Probes | .0079 |
| Tail Cone Fuel Jettison Nozzle | .0226 |
| Precipitation Static Dischargers (Blade Type) | .0400 |
| Precipitation Static Dischargers (Rod Type) | .0013 |
| **Protuberances on the Wind Tunnel Model** | |
| Actuator Fairings on Horizontal Tail | |
| Wing Pivot Fairings | |
| Landing Gear Fairings (on Fuselage and Wing) | |
| All Fences | |
| Wing Tip Fairings | |
| Wing Upper Surface Grooves | |
| Wing-Body Fairings | |

*Table 3-Q. Itemized Cooling Air-Quantities and Drags at Mach 2.7*

| ITEM | WEIGHT FLOW lb/min | IDEAL DRAG COEFFICIENT x $10^4$ | ESTIMATED DRAG COEFFICIENT x $10^4$ |
|---|---|---|---|
| Ram Drag | * | 1.228 | 1.228 |
| ACM Bearing & Separator Drain | 9.2 | -0.018 | -0.013 |
| Uncontrolled Leakage | 48.6 | 0 | 0 |
| Nose Wheel Well Cooling Air | 3.0 | -0.003 | 0.003 |
| Main Wheel Well Cooling Air | 16.0 | -0.016 | 0.014 |
| Accessory Drive System Cooling Air | 8.0 | -0.008 | 0.009 |
| Cabin Intrawall Air Exhaust (Inbd) | 152.2 | -0.262 | -0.188 |
| Cabin Intrawall Air Exhaust (Outbd) | 152.2 | -0.262 | -0.188 |
| Totals | 389.2* | | $\Delta C_D$=0.865 |

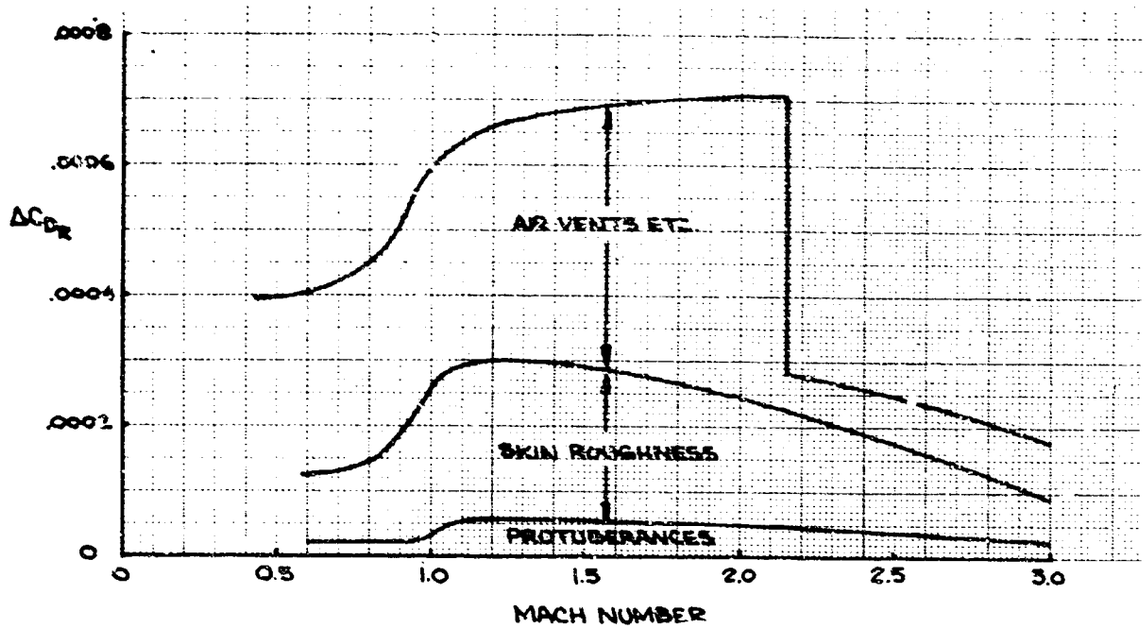


*Figure 3–9. Roughness and Miscellaneous Drag*

3.1.2.3 Wave Drag

The procedure used to calculate wave drag is an application of slender body theory in combination with the supersonic area rule. The geometric input data for the NASA Langley Computer Program P 7129 are given in Tables 3-R and 3-S. The computer program input tables indicate different inputs for GE and P&WA propulsion pods but since the calculated wave drag difference is well within the accuracy of the theory, only one drag level, applicable to both pods, has been shown in Fig. 3-10. The wing has a blunt base from wing buttock line 375 to wing buttock line 434. The drag increment shown on Fig. 3-11 has been estimated assuming that two-dimensional base pressure exists (Refs. 14 and 15).

3.1.2.4 Drag Due to Propulsion System Operation

The propulsion system increments for bleed drag, boattail drag, and additive drag, with the substantiation for these increments, are presented in Sec. 3 of Propulsion Report, Part A (V2-B2707-12). The propulsion drag increments and the corresponding engine airflow curves are repeated in Figs. 3-12 and 3-13. The greater part of the drag difference is caused by the accounting of nozzle boattail drag. For the P&WA engine, the drag of the nozzle is in the internal performance.

The effect of engine thrust on lift, drag, and pitching moment is shown in Fig. 3-14. The corrections are caused by the nonalignment of the thrust force with the thrust drag axis, as a function of airplane angle of attack, and for the moment changes caused by these forces. The propulsion pods have been designed with canted nozzles so that the thrust has a small component in the lift direction; this has a beneficial effect on drag. Particular care has been taken to simulate this feature on the pods of the wind tunnel models so the effect of thrust has also been included in the drag polars.

3.1.2.5 Aeroelastic Corrections and Trim Drag

Aeroelastic corrections are necessary because the theoretical drag analysis and the rigid model test data do not include the effects of airplane flexibility. The wind tunnel model duplicates the correct shape of the airplane at the design condition at Mach 2.7. Under all other conditions aeroelastic corrections have to be applied; these corrections have been calculated using linearized theory. The calculations have been programmed for a digital computer and the method is discussed in Par. 3.3.

Because the mission is carried out at near unit load factor, it has been assumed that, at each Mach number, lift coefficient is varied by changing altitude at unit load factor. Thus, each lift coefficient, at constant Mach number, corresponds to a particular altitude.

The corrections have been applied as follows:

The rigid pitching moment $C_{M_R}$ is corrected to a flexible moment $C_{M_F}$, at each lift coefficient, by the application of an increment $\Delta C_M$ such that

$$C_{M_F} = C_{M_R} + \Delta C_M$$

In Fig. 3-15, $\Delta C_M$ is shown plotted as a function of Mach number for various lift coefficients.

The aeroelastic corrections to angle of attack and drag are also a function of the elevator angle that is required to trim the flexible airplane (for simplicity, the elevon and elevator system are referred to as the elevator). The elevator angle is calculated from the equation:

$$\delta = \frac{C_{M_F}}{C_{M_{\delta_F}}}$$

where

$$C_{M_{\delta_F}} = \frac{C_{M_{\delta_F}}}{C_{M_{\delta_R}}} \quad C_{M_{\delta_R}}$$

= Flexible Elevator Efficiency

The ratio $C_{M_{\delta_F}} / C_{M_{\delta_R}}$ is shown in Fig. 3-18.

The rigid elevator effectiveness has been obtained from experiment; it is shown in Fig. 3-17 and discussed in Par. 3.1.1.3. Once $\delta$ is known, at any lift coefficient, the corrected angle of attack is obtained from:

$$\alpha_F = \alpha_R + \Delta\alpha_T + \frac{d\alpha}{d\delta}\delta$$

where

$\alpha_R$ = Rigid airplane angle of attack with undeflected elevator

$\alpha_F$ = Flexible airplane angle of attack with undeflected elevator

$\Delta\alpha = \left(\alpha_T - \alpha_R\right)_{\delta = 0}$

$\frac{d\alpha}{d\delta}$ = Rate of change of flexible airplane angle of attack with elevator angle.

The quantities $\Delta\alpha$ and $\frac{d\alpha}{d\delta}$ are shown in Figs. 3-18 and 3-19.

The drag coefficient of the trimmed flexible airplane, $C_{D_F}$, is determined in a similar way:

$$C_{D_F} \quad C_{D_R}(0) + \Delta C_{D_F} + \Delta C_{D_{TRIM}}$$

$C_{D_R}(\delta)$ is the drag of the rigid airplane with zero elevator deflection obtained from wind tunnel tests and/or theory, $C_{D_R}(\delta)$ is the drag at an elevator deflection $\delta$.

$$\Delta C_{D_F} = C_{D_F}(\delta) - C_{D_R}(\delta)$$

The elastic correction $\Delta C_{D_F}$ is shown in Fig. 3-20. The trim drag increment $\Delta C_{D_{TRIM}}$ is defined as the increment between the drag coefficient at zero elevator deflection $C_D(0)$ and the drag with the elevator deflected to the trimmed condition, lift coefficient being held constant. No attempts have been made to calculate the trim drag increment theoretically, and experimentally determined increments have been used to define the analytical drag polars. Trim drag increments are presented in Par. 3.1.3.

3.1.2.6 Drag Due to Lift

Drag due to lift has been calculated using several computer programs varying in complexity from the NASA-Ames program for the complete wing body (Ref. 16) to one which solves only the planar, thin wing problem. The latter method has been extended to subsonic speeds using ideas described in Ref. 17. This method is in agreement with NASA program 916.C (Ref. 18) at supersonic speeds and with vortex lattice methods in incompressible flow.

Figure 3-21 shows the proportion of theoretical leading edge thrust which has been included in the drag due to lift estimates; it varies from 0 at Mach 2.7 to 90 percent at low subsonic speeds. Figure 3-21 is based on test data presented in Refs. 19 and 20.

The nacelles on the model B-2707 have been designed to produce favorable lifting interference with the wing. The nacelle pressure field has been calculated by a method based upon the analysis described in Ref. 21.

Figure 3-22 shows the drag due to lift, reduced to symmetric envelope form and compared to flat wing and optimum surface envelopes.

The camber and twist is defined in Table 3-T in a form suitable for input to NASA Langley Computer Program 916C.

3.1.2.7 Theoretical Drag Polars

The drag polars resulting from the analytical buildup are compared with drag polars obtained by the extrapolation of wind tunnel data in Fig. 3-23. It is seen that the experimental polars show higher drag than the theory. Although the test data have not been corrected for boundary layer trip drag and for bluntness of the wind tunnel model nacelle lips and vertical tail leading edge, it is obvious that the full potential predicted by the theory has yet to be achieved. Further work is indicated, particularly on the drag due to lift; this is discussed in Par. 3.4.

*Table 3-R. B-2707 Wave Drag Program Inputs*

| | | | | | | | | | | |
|---|---|---|---|---|---|---|---|---|---|---|
| 0.0 | 2.5 | 10.0 | 25.0 | 40.0 | 50.0 | 60.0 | 75.0 | 90.0 | 100.0 | X/C |
| 92.10 | 5.625 | -4.0 | 179.05 | | | | | | | W1 |
| 129.39 | 9.86 | -3.5 | 140.36 | | | | | | | W2 |
| 141.0 | 12.24 | -3.2 | 128.83 | | | | | | | W3 |
| 151.03 | 15.5 | -2.8 | 118.55 | | | | | | | W4 |
| 164.93 | 20.0 | -2.4 | 105.2 | | | | | | | W5 |
| 193.53 | 31.25 | -1.1 | 73.54 | | | | | | | W6 |
| 199.56 | 31.26 | -1.1 | 47.10 | | | | | | | W7 |
| 214.65 | 36.17 | -0.5 | 39.03 | | | | | | | W8 |
| 248.10 | 47.04 | 0.8 | 24.52 | | | | | | | W9 |
| 266.0 | 52.87 | 1.5 | 0.0 | | | | | | | W10 |
| 0.0 | 0.24 | 0.55 | 0.88 | 1.07 | 1.13 | 1.11 | 0.87 | 0.36 | 0.0 | Z/C-1 |
| 0.0 | 0.41 | 0.87 | 1.40 | 1.57 | 1.46 | 1.28 | 0.88 | 0.35 | 0.0 | Z/C-2 |
| 0.0 | 0.45 | 1.02 | 1.70 | 1.75 | 1.60 | 1.35 | 0.90 | 0.36 | 0.0 | Z/C-3 |
| 0.0 | 0.45 | 0.89 | 1.40 | 1.75 | 1.75 | 1.50 | 0.87 | 0.35 | 0.0 | Z/C-4 |
| 0.0 | 0.44 | 0.87 | 1.28 | 1.40 | 1.39 | 1.29 | 0.88 | 0.35 | 0.0 | Z/C-5 |
| 0.0 | 0.44 | 0.87 | 1.28 | 1.40 | 1.39 | 1.29 | 0.88 | 0.35 | 0.0 | Z/C-6 |
| 0.0 | 0.51 | 1.10 | 1.69 | 2.00 | 2.12 | 2.17 | 2.18 | 2.06 | 1.88 | Z/C-7 |
| 0.0 | 0.46 | 0.91 | 1.34 | 1.49 | 1.50 | 1.44 | 1.12 | 0.54 | 0.0 | Z/C-8 |
| 0.0 | 0.46 | 0.91 | 1.34 | 1.49 | 1.50 | 1.44 | 1.12 | 0.54 | 0.0 | Z/C-9 |
| 0.0 | 0.46 | 0.91 | 1.34 | 1.49 | 1.50 | 1.44 | 1.12 | 0.54 | 0.0 | Z/C-10 |
| 0.0 | 10.0 | 20.0 | 30.0 | 40.0 | 50.0 | 60.0 | 70.0 | 80.0 | 90.0 | XFUS |
| 100.0 | 110.0 | 120.0 | 130.0 | 140.0 | 150.0 | 160.0 | 170.0 | 180.0 | 190.0 | XFUS |
| 200.0 | 210.0 | 220.0 | 230.0 | 240.0 | 250.0 | 260.0 | 270.0 | 280.0 | 306.0 | XFUS |
| 0.0 | 11.0 | 27.0 | 46.0 | 68.0 | 90.0 | 113.0 | 134.0 | 151.0 | 166.0 | FUSA |
| 176.0 | 182.0 | 183.0 | 178.0 | 169.0 | 159.0 | 152.0 | 147.0 | 144.0 | 143.0 | FUSA |
| 144.0 | 143.0 | 141.0 | 132.0 | 118.0 | 99.0 | 79.0 | 58.0 | 18.0 | 0.0 | FUSA |
| 0.0 | 12.0 | 24.0 | 25.0 | 26.0 | 27.0 | | | | | XACT |
| 0.0 | 1.026 | 0.0 | 0.0 | 0.0 | 0.0 | | | | | ACTR |
| 240.1 | 0.0 | 4.16 | 60.8 | 280.2 | 0.0 | 26.83 | 14.5 | | | FINLOC |
| 0.0 | 30.0 | 70.0 | 100.0 | | | | | | | FIN X/C |
| 0.0 | 1.50 | 1.50 | 0.0 | | | | | | | FIN Z/C |
| 246.33 | 31.25 | -1.0 | 26.70 | 270.33 | 45.00 | 0.50 | 7.75 | | | CANLOC |
| 0.0 | 37.5 | 62.5 | 100.0 | | | | | | | CAN X/C |
| 0.0 | 1.50 | 1.50 | 0.0 | | | | | | | CAN Z/C |

*G.E. NACELLES*

| | | | | | | | | | |
|---|---|---|---|---|---|---|---|---|---|
| 236.6 | 9.58 | -8.0 | 239.3 | 27.3 | -5.75 | 248.5* | 32.5* | 0.0* | PODLOC |
| 0.0 | 19.166 | 25.499 | 28.0 | 31.80 | 35.915 | | | | XPOD |
| 2.592 | 3.40 | 3.54 | 3.54 | 3.47 | 3.092 | | | | PODR |
| 0.0 | 19.166 | 25.499 | 28.0 | 31.80 | 35.915 | | | | XPOD |
| 2.592 | 3.40 | 3.54 | 3.54 | 3.47 | 3.092 | | | | PODR |

*P & WA NACELLES*

| | | | | | | | | | |
|---|---|---|---|---|---|---|---|---|---|
| 245.4 | 9.67 | -8.0 | 247.2 | 27.1 | -5.75 | 248.5* | 32.5* | 0.0* | PODLOC |
| 0.0 | 12.083 | 17.00 | 22.00 | 25.00 | 28.667 | | | | XPOD |
| 2.813 | 3.341 | 3.540 | 3.65 | 3.58 | 3.333 | | | | PODR |
| 0.0 | 12.083 | 17.00 | 22.00 | 25.00 | 28.667 | | | | XPOD |
| 2.813 | 3.341 | 3.540 | 3.65 | 3.58 | 3.333 | | | | PODR |

*NOTE: Actuator Fairing Input As a Nacelle.*

* *Actuator Origin*

*Table 3-S. Wave Drag Program Inputs for the Aerodynamic Development Model (GE)*

| | | | | | | | | | | |
|---|---|---|---|---|---|---|---|---|---|---|
| 0.0 | 2.5 | 10.0 | 25.0 | 40.0 | 50.0 | 60.0 | 75.0 | 90.0 | 100.0 | X/C |
| 83.03 | 6.67 | 0.0 | 180.95 | | | | | | | W1 |
| 114.53 | 10.33 | 0.8 | 150.82 | | | | | | | W2 |
| 127.73 | 12.83 | 1.0 | 138.56 | | | | | | | W3 |
| 192.01 | 31.25 | 4.5 | 81.44 | | | | | | | W4 |
| 192.03 | 31.26 | 4.5 | 49.49 | | | | | | | W5 |
| 224.07 | 41.67 | 6.2 | 35.88 | | | | | | | W6 |
| 247.51 | 49.28 | 7.5 | 25.69 | | | | | | | W7 |
| 258.83 | 82.96 | 8.2 | 20.76 | | | | | | | W8 |
| 274.08 | 57.92 | 9.0 | 0.0 | | | | | | | W9 |
| 0.0 | 0.85 | 1.60 | 2.01 | 2.03 | 1.95 | 1.72 | 1.18 | 0.50 | 0.0 | Z/C-1 |
| 0.0 | 0.35 | 0.88 | 1.34 | 1.49 | 1.49 | 1.35 | 0.98 | 0.43 | 0.0 | Z/C-2 |
| 0.0 | 0.36 | 0.85 | 1.30 | 1.43 | 1.40 | 1.29 | 0.92 | 0.42 | 0.0 | Z/C-3 |
| 0.0 | 0.44 | 0.88 | 1.28 | 1.40 | 1.39 | 1.29 | 0.90 | 0.35 | 0.0 | Z/C-4 |
| 0.0 | 0.58 | 1.12 | 1.74 | 2.08 | 2.21 | 2.27 | 2.28 | 2.21 | 2.06 | Z/C-5 |
| 0.0 | 0.44 | 0.78 | 1.15 | 1.25 | 1.25 | 1.21 | 0.95 | 0.46 | 0.0 | Z/C-6 |
| 0.0 | 0.44 | 0.78 | 1.15 | 1.25 | 1.25 | 1.21 | 0.95 | 0.46 | 0.0 | Z/C-7 |
| 0.0 | 0.44 | 0.78 | 1.15 | 1.25 | 1.25 | 1.21 | 0.95 | 0.46 | 0.0 | Z/C-8 |
| 0.0 | 0.44 | 0.78 | 1.15 | 1.25 | 1.25 | 1.21 | 0.95 | 0.46 | 0.0 | Z/C-9 |
| 0.0 | 10.0 | 20.0 | 30.0 | 40.0 | 50.0 | 60.0 | 70.0 | 80.0 | 90.0 | XFUS |
| 100.0 | 110.0 | 120.0 | 130.0 | 140.0 | 150.0 | 160.0 | 170.0 | 180.0 | 190.0 | XFUS |
| 200.0 | 210.0 | 220.0 | 230.0 | 240.0 | 250.0 | 260.0 | 270.0 | 290.0 | 306.0 | XFUS |
| 0.0 | 9.0 | 25.0 | 44.0 | 62.0 | 80.0 | 98.0 | 115.0 | 132.0 | 146.0 | FUSA |
| 154.0 | 158.0 | 157.0 | 155.0 | 151.0 | 145.0 | 139.0 | 133.0 | 128.0 | 124.0 | FUSA |
| 119.0 | 115.0 | 111.0 | 105.0 | 97.0 | 82.0 | 61.0 | 42.0 | 9.0 | 0.0 | FUSA |
| 237.0 | 10.0 | -3.33 | 243.5 | 27.10 | -0.50 | | | | | PODLOC |
| 0.0 | 19.166 | 25.449 | 28.0 | 31.8 | 35.915 | | | | | XPOD |
| 2.46 | 3.315 | 3.54 | 3.56 | 3.47 | 3.092 | | | | | PODR |
| 0.0 | 19.166 | 25.449 | 28.0 | 31.8 | 35.915 | | | | | XPOD |
| 2.46 | 3.315 | 3.54 | 3.56 | 3.47 | 3.092 | | | | | PODR |
| 237.0 | 26.0 | 4.83 | 40.0 | 274.0 | 26.0 | 17.33 | 6.67 | | | FINLOC |
| 0.0 | 37.5 | 62.5 | 100.0 | | | | | | | FIN X/C |
| 0.0 | 1.0 | 1.0 | 0.0 | | | | | | | FIN Z/C |
| 243.51 | 31.25 | 4.5 | 29.64 | 277.70 | 50.92 | 7.8 | 5.96 | | | CANLOC |
| 0.0 | 37.5 | 62.5 | 100.0 | | | | | | | CAN X/C |
| 0.0 | 1.5 | 1.5 | 0.0 | | | | | | | CAN Z/C |

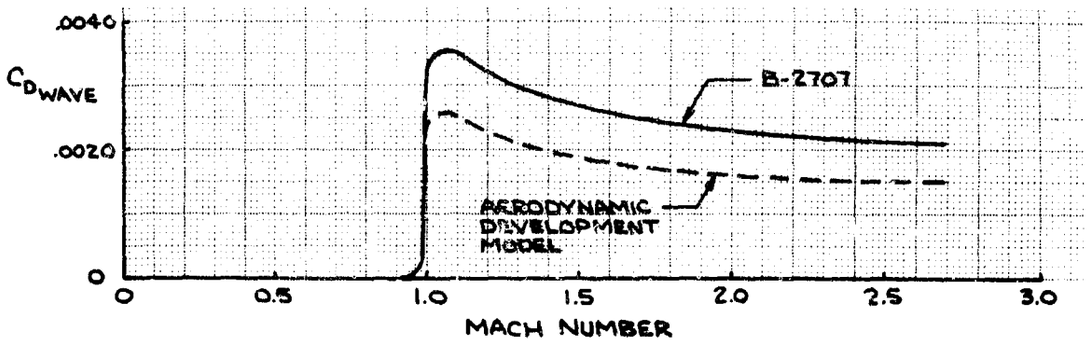


*Figure 3–10. Variation of Wave Drag with Mach Number*

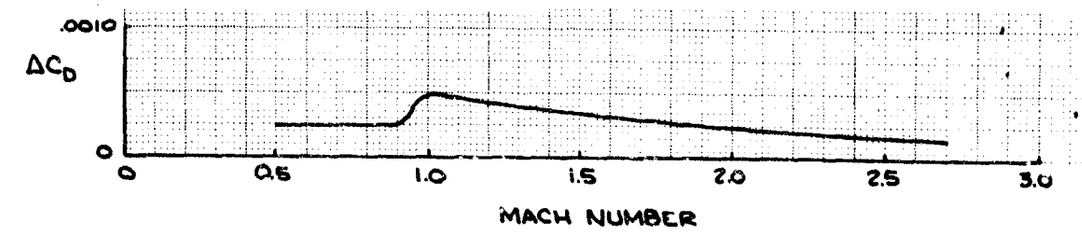


*Figure 3–11. Variation of Wing Gap Drag with Mach Number*

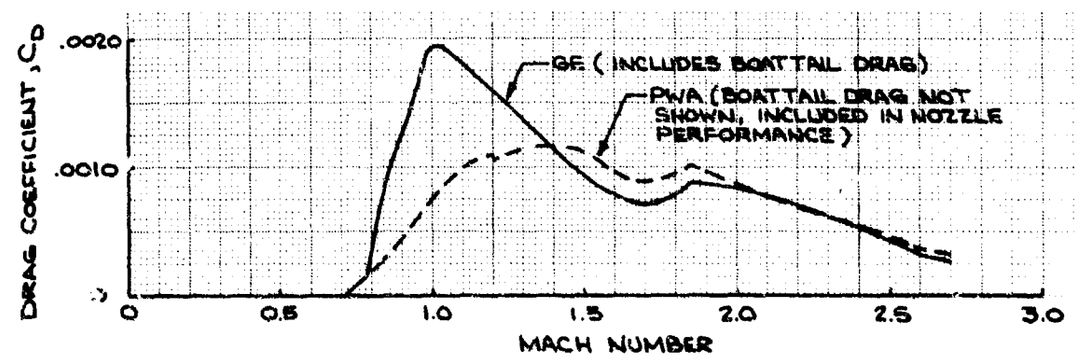


*Figure 3–12. Drag Due to Propulsion System*

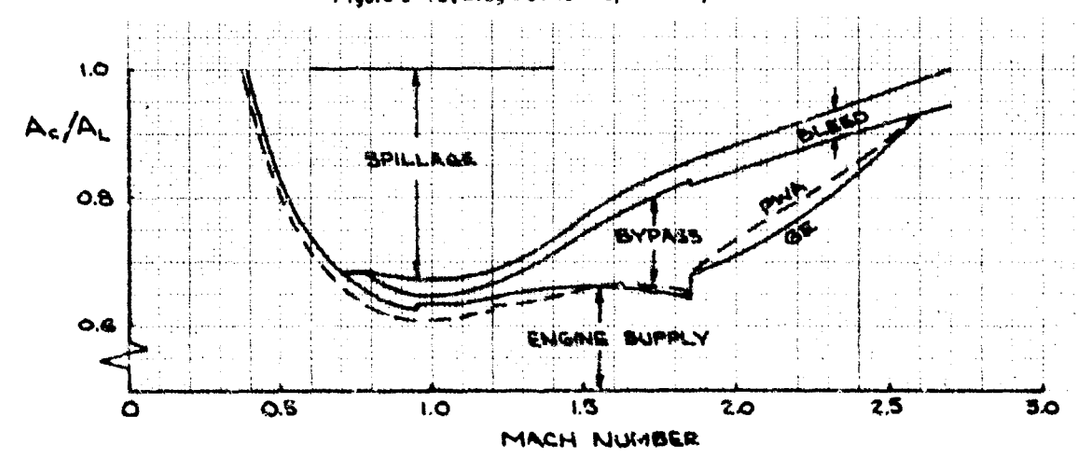


*Figure 3–13. Inlet Airflow Characteristics*

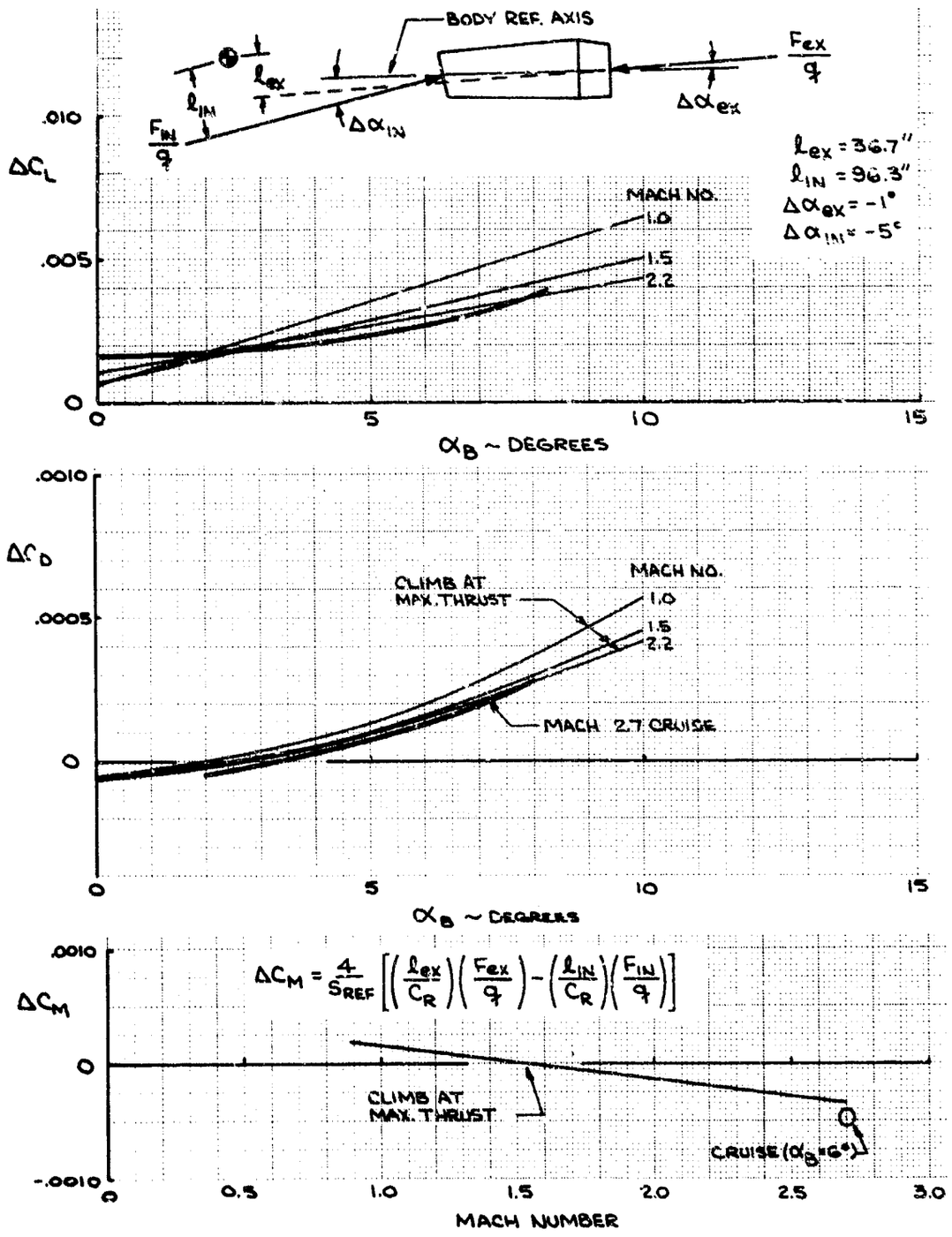


*Figure 3-14. Effect of Thrust on Aerodynamic Data*

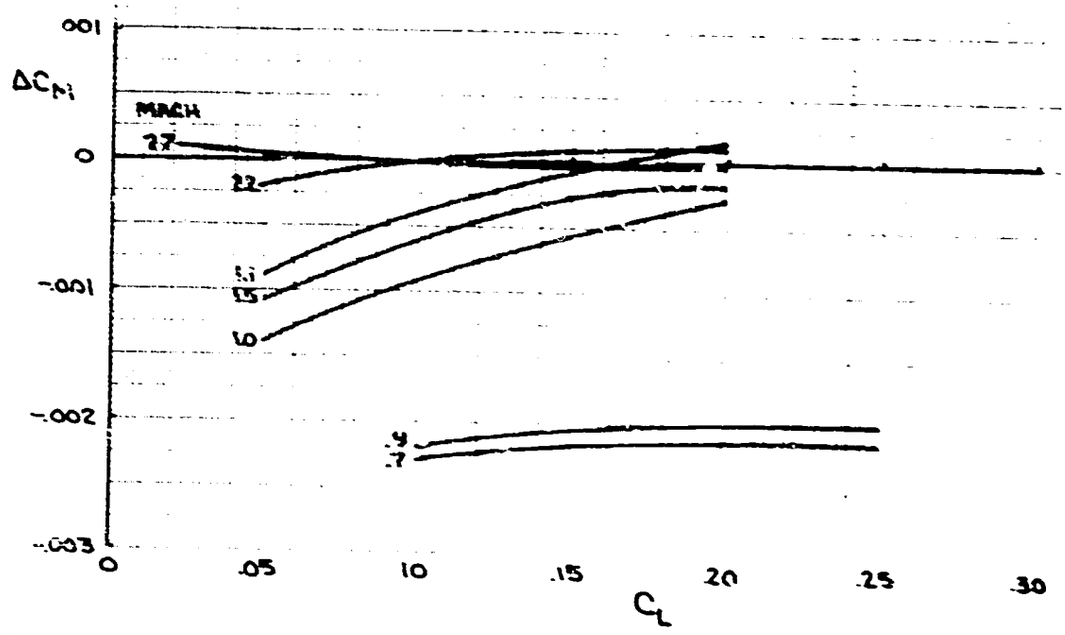


*Figure 3–15. (a) Aeroelastic Corrections to Rigid Pitching Moment Data – 72 Degrees Leading Edge Sweep*

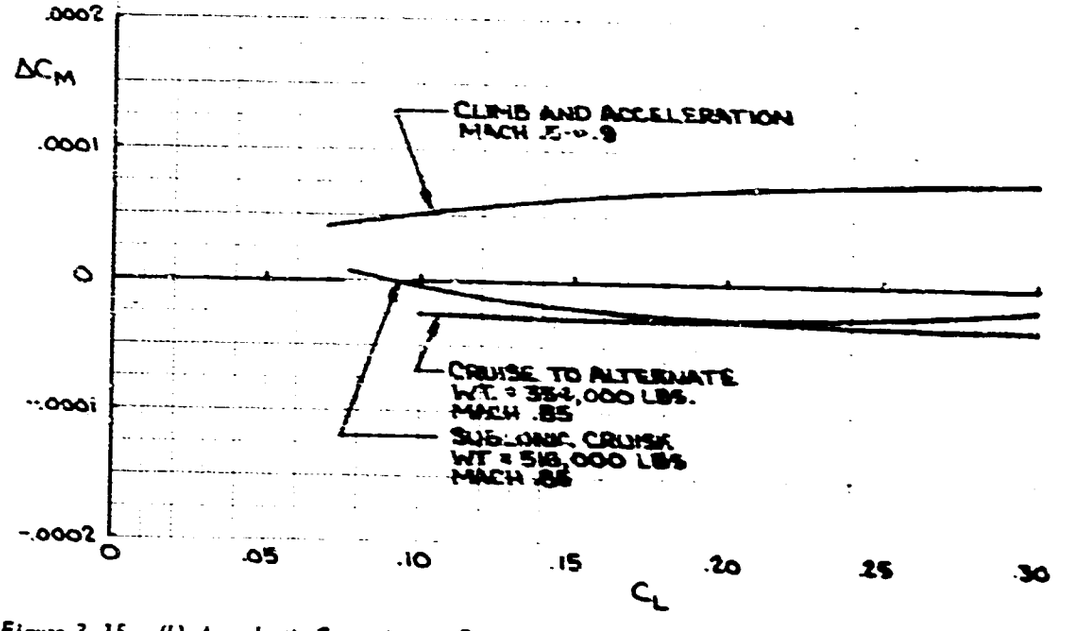


*Figure 3–15. (b) Aeroelastic Corrections to Rigid Pitching Moment Data – 42 Degrees Leading Edge Sweep*

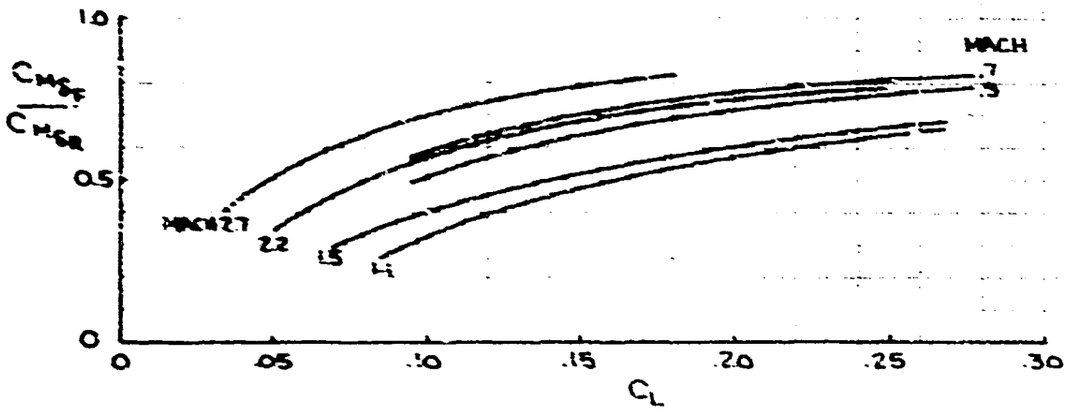


(a) 72 Degrees Leading Edge Sweep

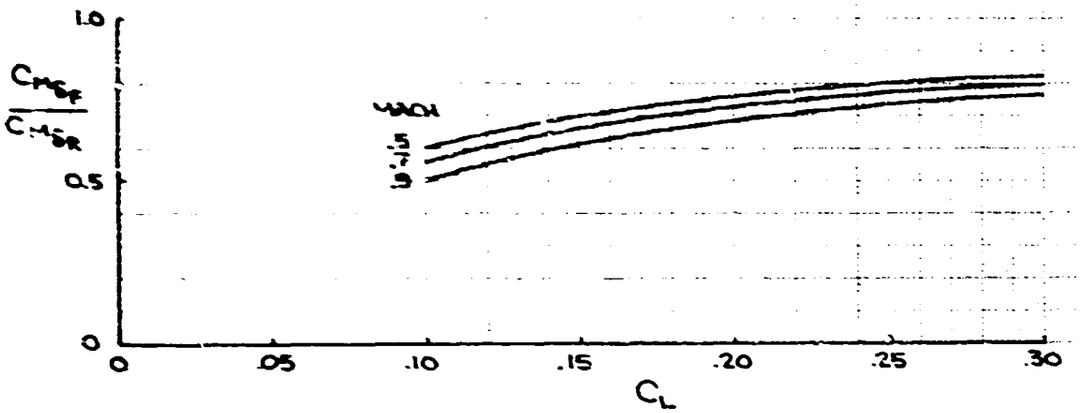


(b) 42 Degrees Leading Edge Sweep – Climb and Acceleration

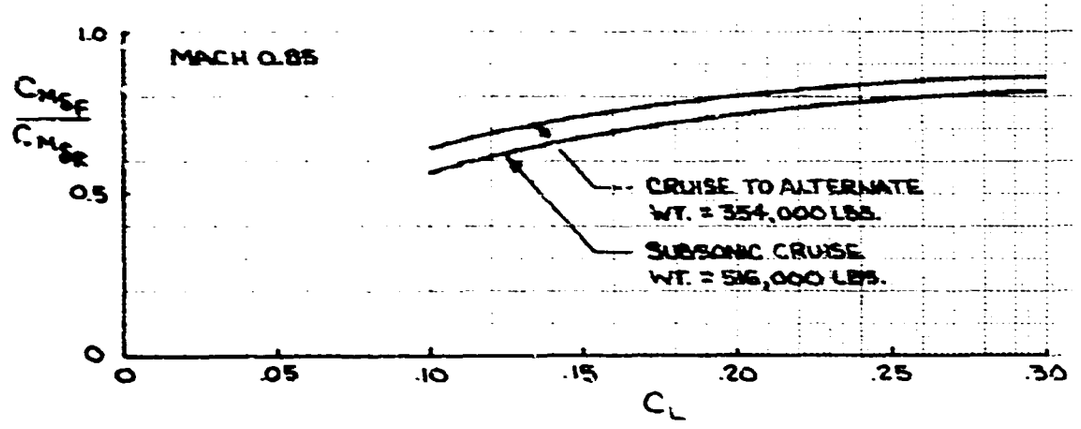


(c) 42 Degrees Leading Edge Sweep – Subsonic Missions

*Figure 3–16. Flexible Elevator Effectiveness*

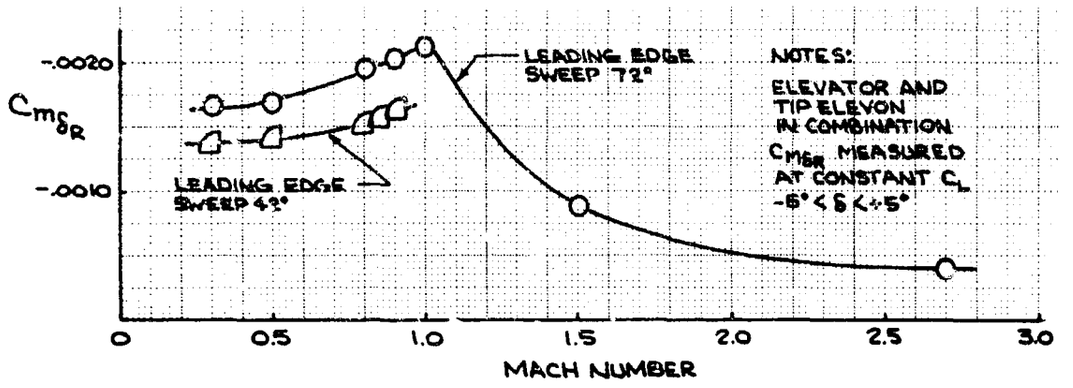


*Figure 3–17. Rigid Elevator Effectiveness*

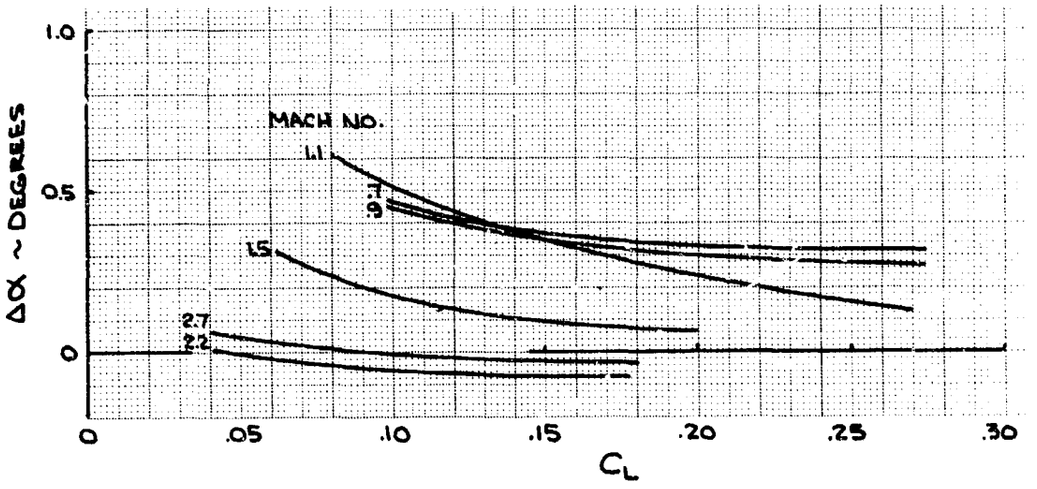


*Figure 3–18. Effect of Flexibility on Incidence – Leading Edge Sweep – 72 Degrees*

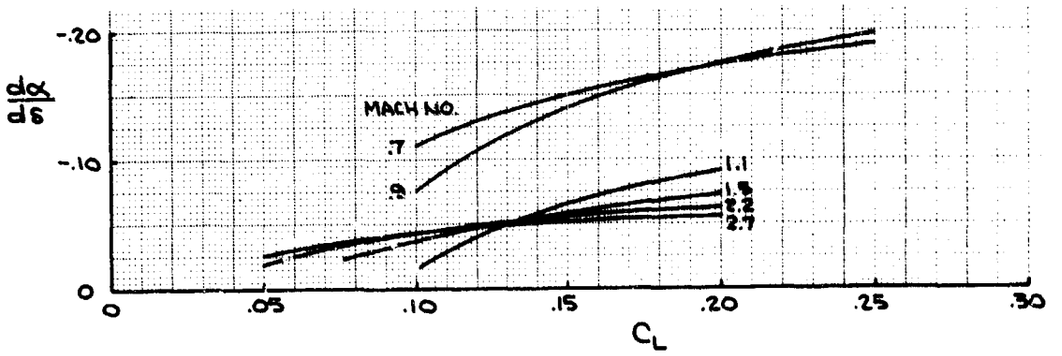


*Figure 3–19. Effect of Elevator Angle on Incidence – Leading Edge Sweep – 72 Degrees*

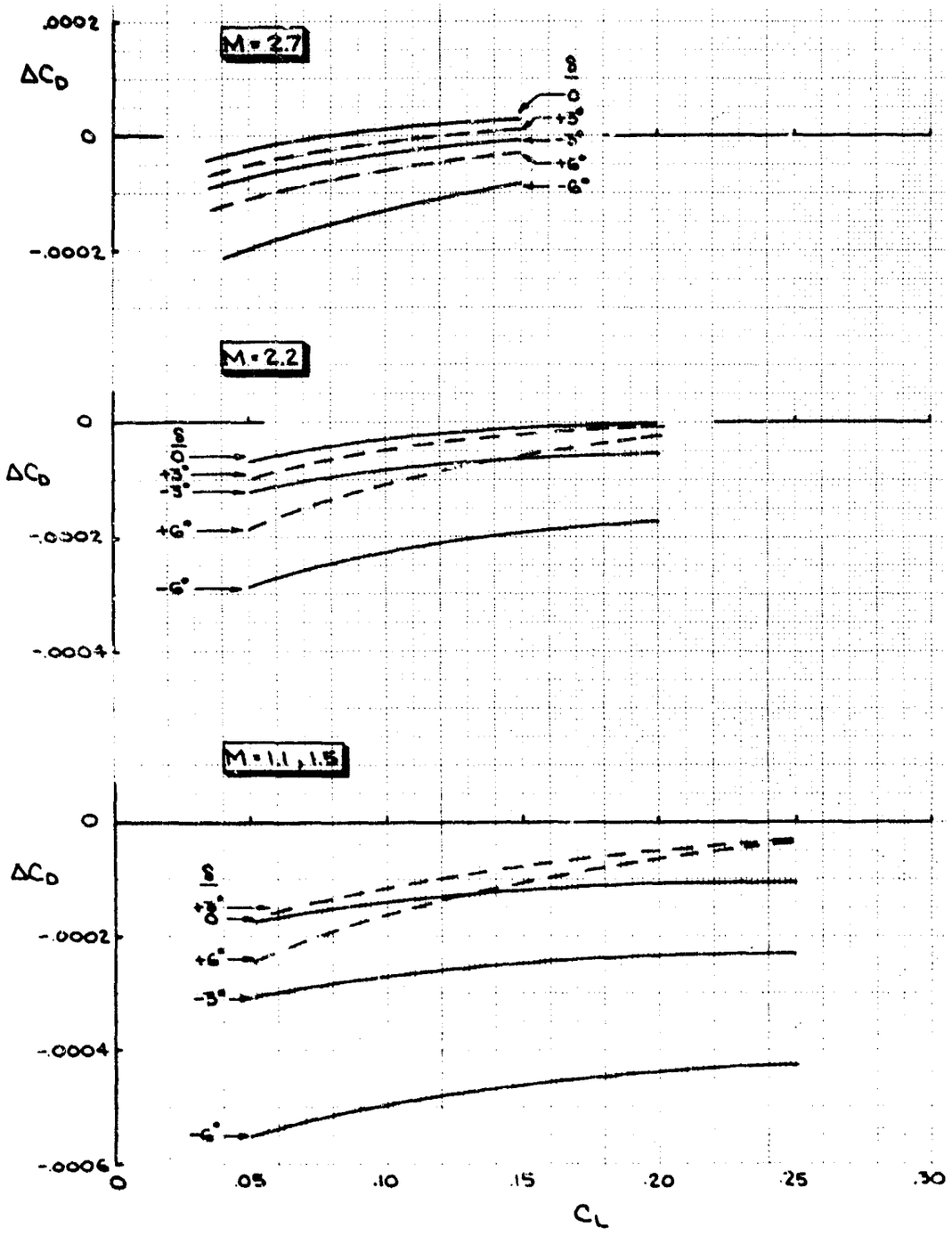


*Figure 3-70. Flexibility Correction to Drag*

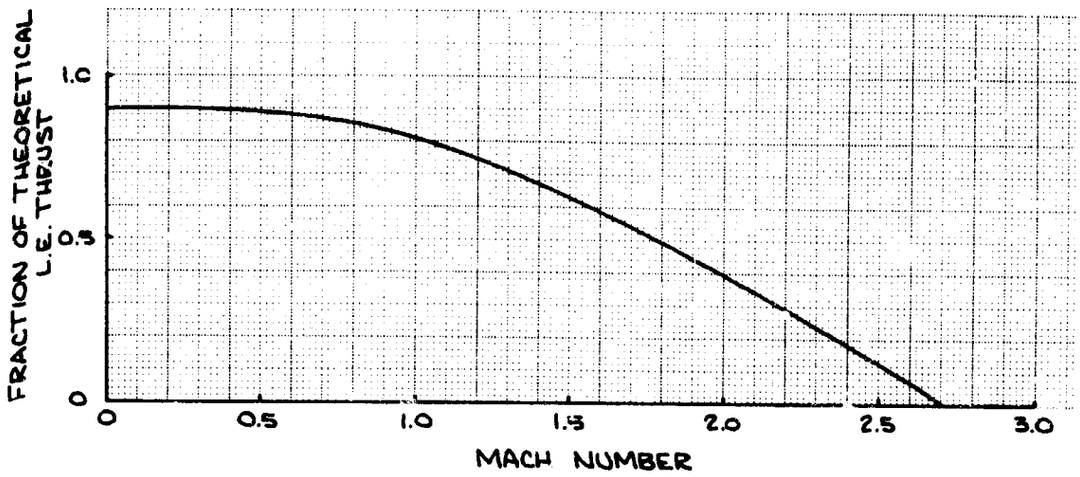


*Figure 3-21. Variation of Leading Edge Thrust with Mach Number at 72 Degrees Leading Edge Sweep*

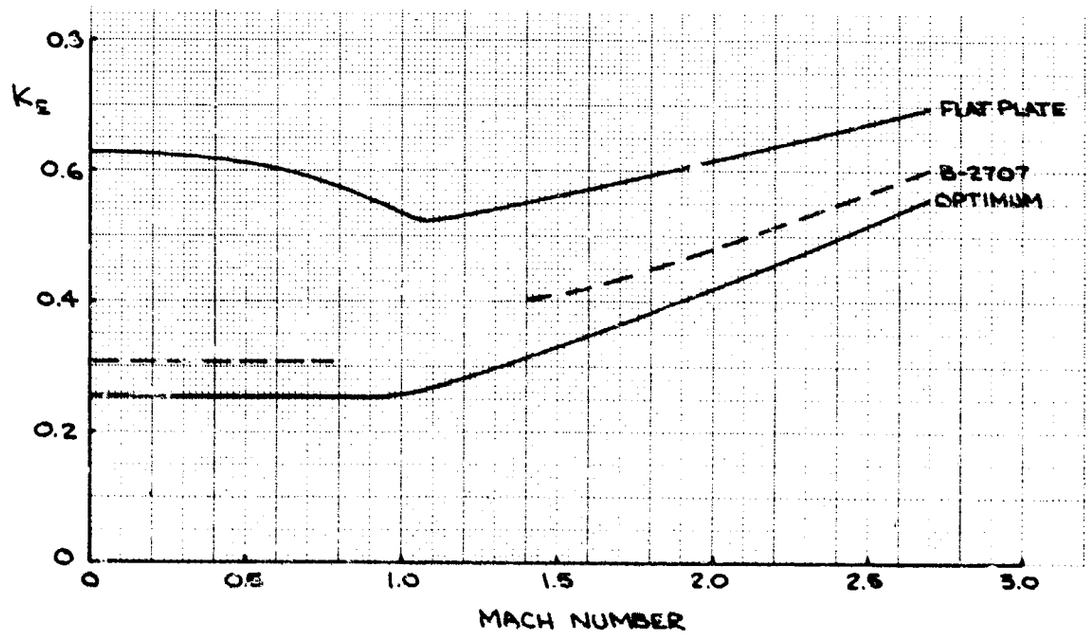


*Figure 3-22. B-2707 Symmetric Drag Due to Lift Variation*

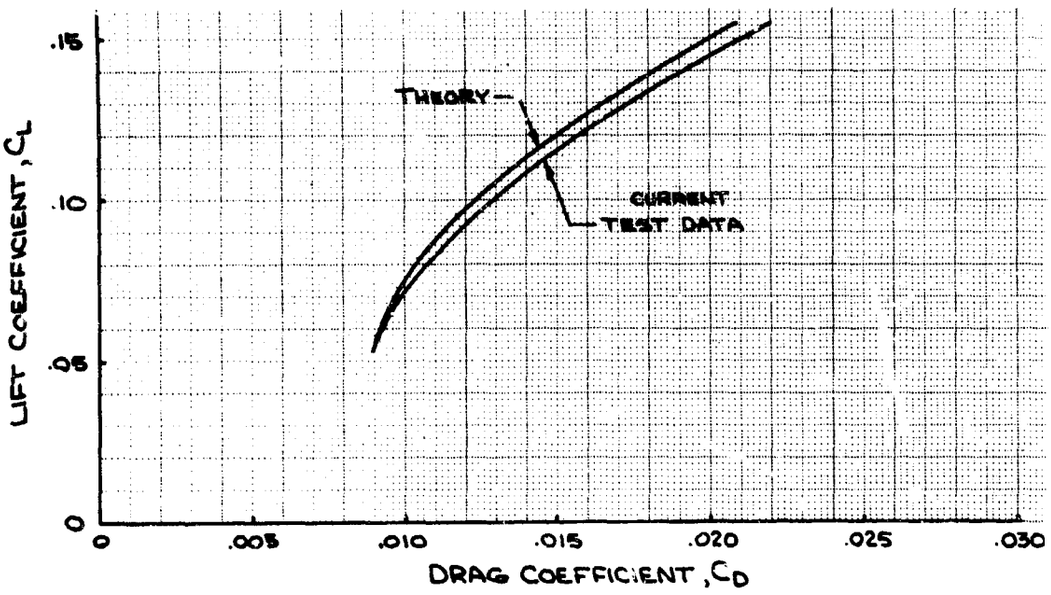


*Figure 3-23. (a) Comparison of Theory and Test — B-2707 - Mach 2.7*

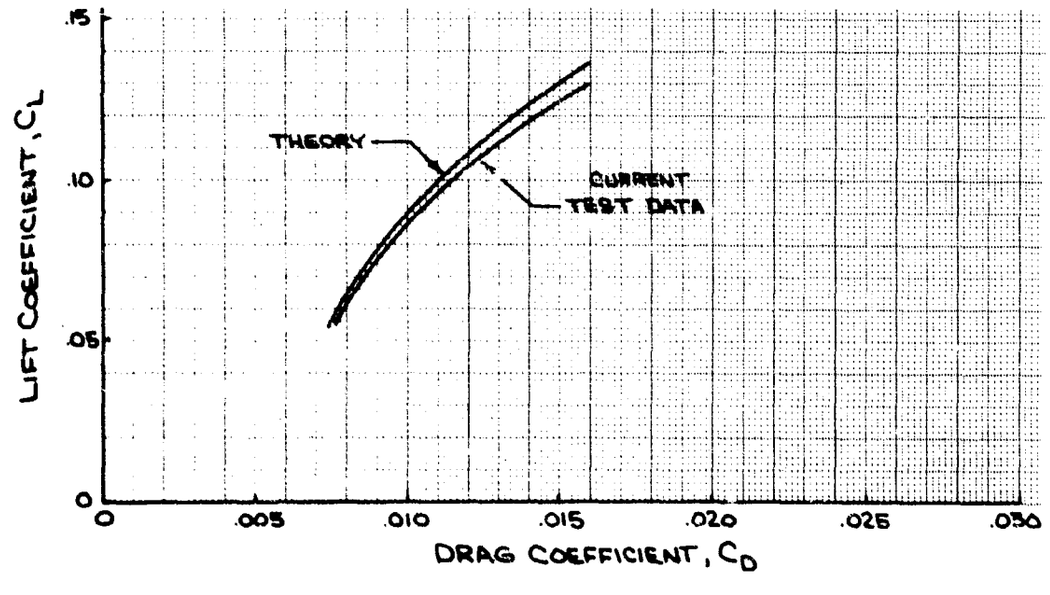


*Figure 3-23. (b) Comparison of Theory and Test - Aerodynamic Development Model -Mach 2.7*

3.1.3 Wind Tunnel Results

3.1.3.1 Wind Tunnel Models

The substantiation of the lift drag characteristics is based on wind tunnel results obtained with three wind tunnel models. For the range of Mach numbers from 0.9 to 2.7, where the airplane operates at a fixed 72 degrees of sweep, models SA-966 and SA-977 were used to represent the B-2707 and aerodynamic development model respectively. A reduced sweep of 42 degrees is used for lower Mach numbers and model SA-856 has been used to obtain transonic data for the B-2707. Model photographs are shown in Figs. 24 and 25. Three other force models of the B-2707, models SA-981, -983, and -984, together with relevant drawings and data, will be supplied to the FAA for evaluation. Although these models have been tested at Boeing, time did not permit incorporating the analysis of the data into this report; but this analysis will be available for evaluators' onsite inspection.

3.1.3.2 Test Procedures

The wind tunnel data were obtained in the Boeing 4- by 4-ft supersonic and 8- by 12-ft transonic wind tunnels. Nominal test conditions have been shown in Fig. 4-9 of Ref. 3. Standard test procedures have been used. Models are fitted with sparse transition trips to ensure turbulent boundary layers over all the surfaces of the model, but drag corrections are not applied for trip drag. The data are corrected for chamber and base pressures and also for internal nacelle drag. The models have been tested with nacelles of the correct external shape including a correct simulation of the boundary layer diverter. These nacelles are bent at the nozzle, in order to obtain a favorable thrust component in flight, but the internal ducts are straight and circular, so that the internal drag is an axial force transmitted to the model through shear stresses.

3.1.3.3 Extrapolation of Wind Tunnel Results to Full-Scale Flight Conditions

The full-scale drag polars have been obtained by adjusting the wind tunnel measurements to full-scale conditions. The corrections applied to the model data, to account for differences between the model and the airplane, are listed and described as follows:

- Scale effect corrections
- Drag due to surface roughness and miscellaneous items
- Wave drag
- Corrections due to propulsion system operation
- Aeroelastic corrections and trim drag

a. Scale Effect Corrections

The methods used to calculate skin friction and form drag have been discussed in Par. 3.1.2. These methods have been used to determine the corrections for the measured drag levels to account for the differences between the skin friction drag of the wind tunnel model at the test conditions, and that of the full-scale aircraft at the flight conditions. The corrections for the nominal mission are shown in Fig. 3-26 for a wing sweep of 72 degrees. The corrections for the wing sweep of 42 degrees are:

| Mach Number | Height (ft) | $C_D$ |
|---|---|---|
| 0.5 | 30,000 | 0.0039 |
| 0.8 | 30,000 | 0.0038 |
| 0.9 | 30,000 | 0.0037 |

A correction has been applied, for scale effect, to the polar shape at subsonic speeds. This correction has been defined, in terms of a parameter S, in Ref. 20. It was shown that S, which is a measure of the amount of leading edge suction, is a unique function of the Reynolds number of the leading edge. The variation of this Reynolds number as a function of Mach number in the wind tunnel (for the SA-856 model) and for the airplane is shown in Fig. 3-27. The parameter S is defined by the following equation:

$$S = \frac{C_L \tan\alpha - \left(C_D - C_{Dmin}\right)}{C_L \tan\alpha - A\int_0^1 d\left(\frac{y}{b/2}\right)}$$

It is the experimentally measured leading edge suction in percent of the total theoretical suction. With no suction the drag due to lift is $C_L \tan\alpha$; the drag due to lift for 100 percent suction is the second term in the denominator and for an elliptically loaded wing this would be $C_L{}^2/\pi A$, where A is the aspect ratio; the measured drag due to lift is $C_D - C_{D\,min}$. The parameter S was determined from the test data and an increment applied

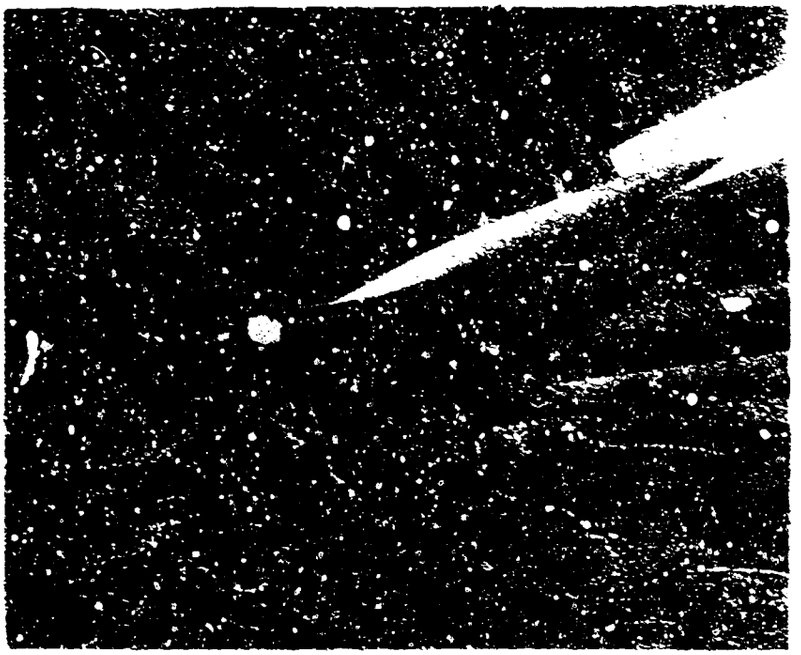

Figure 3-24. Transonic Wind Tunnel Model SA-836

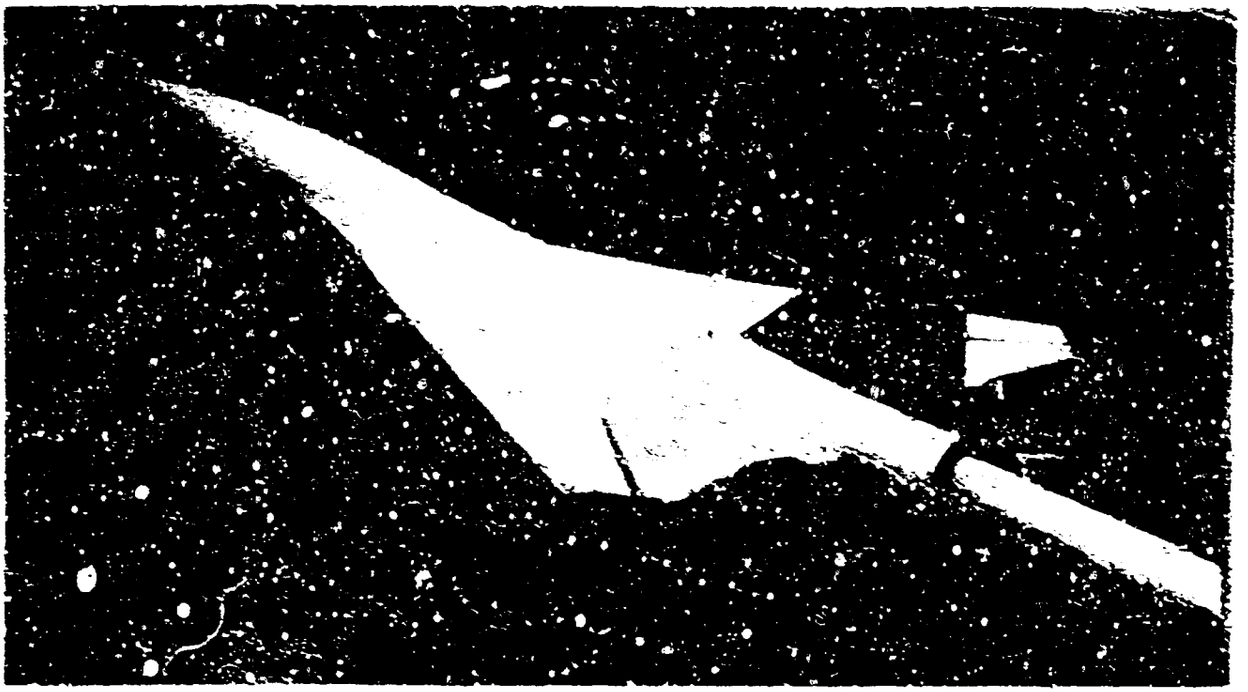

Figure 3-25. Supersonic Wind Tunnel Model SA-956

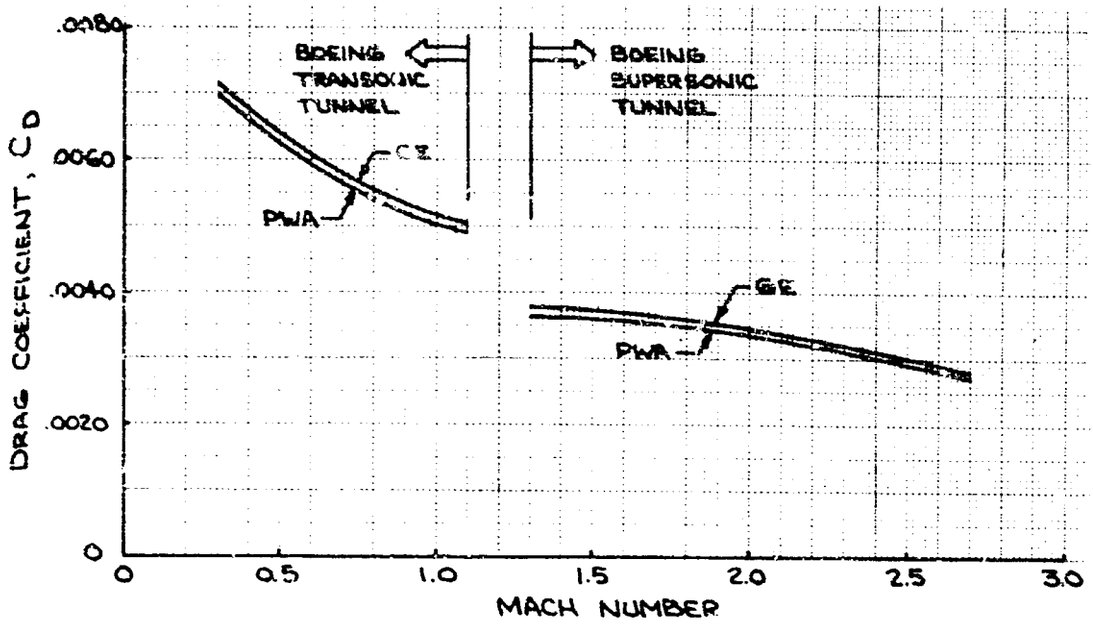


*Figure 3-26. Skin Friction Drag Correction*

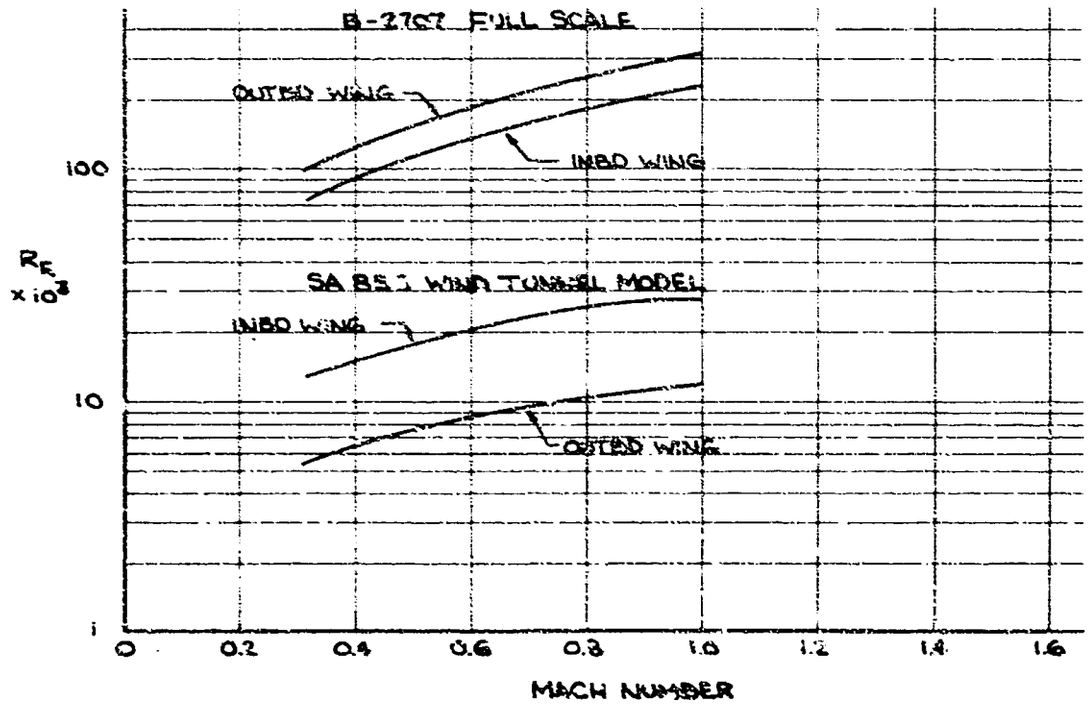


*Figure 3-27. Leading Edge Reynolds Number*

to it, for scale effect, based on the data shown in Fig. 7 of Ref. 20. The increment was obtained by entering that figure with the leading edge Reynolds Number for the average radius of the inboard wing portion, 72-degrees sweep, and also the average radius for the outboard wing portion, 42 degrees of sweep; and then averaging the two values of S that were obtained. The data in Fig. 7 of Ref. 20 were obtained at very small Mach numbers. Rather than assume that these would be valid at all Mach numbers, Fig. 3-28 was used to adjust them for Mach number; it being assumed that the probability of achieving an improvement in leading edge suction, due to scale effect, diminishes with increasing Mach number. The results are:

| Mach | S (Wind tunnel) | ΔS (From Ref. 19) | S (Full scale) |
|---|---|---|---|
| 0.5 | 74. | 12. | 86. |
| 0.7 | 74. | 9. | 83. |
| 0.9 | 46. | 7. | 53. |

The effect on the drag polar at Mach 0.85 is shown in Fig. 3-29.

b. Drag Due to Surface Roughness and Miscellaneous Items

The drag increments given in Par. 3.1.2.2 have been applied to the wind tunnel model drag level to account for surface roughness and the miscellaneous items listed and analyzed in Par. 3.1.2.2.

c. Wave Drag Corrections

A wave drag correction has been applied to the wind tunnel drag level to account for differences between the wind tunnel models and the aircraft. The major difference is in the afterbody, on the models, to accommodate a sting support system. The wave drag estimation procedure has been described in Par. 3.1.3 and the aircraft geometries in Tables 3-R, 3-S, and 3-T. Tables 3-U and 3-V define the geometry of the wind tunnel models. The thickness ratio of the wing of the SA 966 model is somewhat greater than on the airplane. The wave drag increments to be applied to the measured model drag coefficients are shown in Fig. 3-30. The geometry difference between the wind tunnel model and the airplane is the cause of a small change in aerodynamic center; the airplane being slightly less stable than the model. The data in Ref. 24 have been used to estimate this effect and the results are shown in Fig. 3-31.

d. Propulsion System Drag

The increments given in Par. 3.1.3 have been applied to the lift, drag, and pitching moment measured in the wind tunnel.

e. Aeroelastic Corrections and Trim Drag

The aeroelastic corrections presented in Figs. 3-15 to 3-20, Par. 3.1.2.5, have been applied to the wind tunnel lift, drag, and moment data. Trim drag was determined as follows:

(1) Data were transferred to the appropriate center of gravity position obtained from Fig. 3-32.

(2) Wind tunnel pitching moment data were corrected for engine thrust from Fig. 3-14.

(3) Wind tunnel data were corrected for fuselage aft closure from Fig. 3-31.

(4) Wind tunnel data were corrected for airplane flexibility as previously described (Fig. 3-15).

(5) Fig. 3-17 was used at the appropriate Mach number to determine the rigid elevator effectiveness. This has been obtained directly from test data at constant lift coefficients appropriate to the nominal flight profile; it is valid for small deflections (±5 degrees) only.

(6) Figure 3-16 was used at the appropriate Mach number and lift coefficient, to determine the ratio of flexible to rigid elevator effectiveness, to obtain the flexible elevator effectiveness.

(7) The deflection for trim was then determined by dividing the moment to trim by the flexible elevator effectiveness.

(8) Figures 3-33 and 3-34 present experimentally determined drag increments due to elevator deflections. Trim drag was obtained by entering these figures at the appropriate Mach number and lift coefficient, with the elevator deflection $\delta$ determined in preceding step (7).

Trim drag results for the airplane are shown in Figs. 3-35 to 3-38. The trim drag increment and elevator deflection, for the nominal mission, are shown in Figs. 3-35 to 3-36 as a function of Mach number. The effect of cg on the lift drag

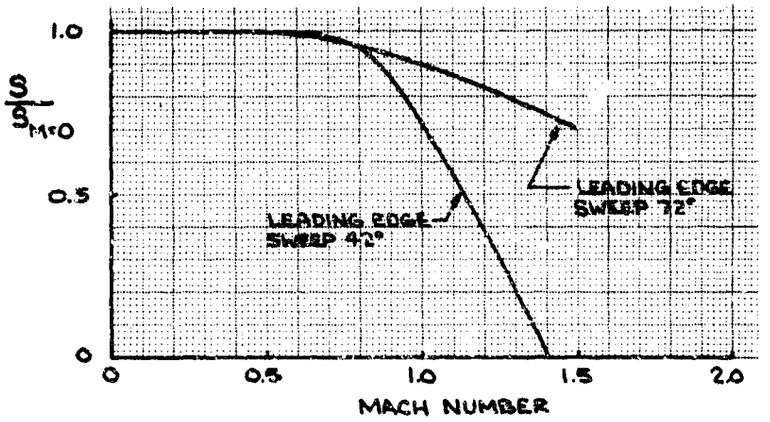


*Figure 3–28. Effect of Mach Number on Leading Edge Thrust*

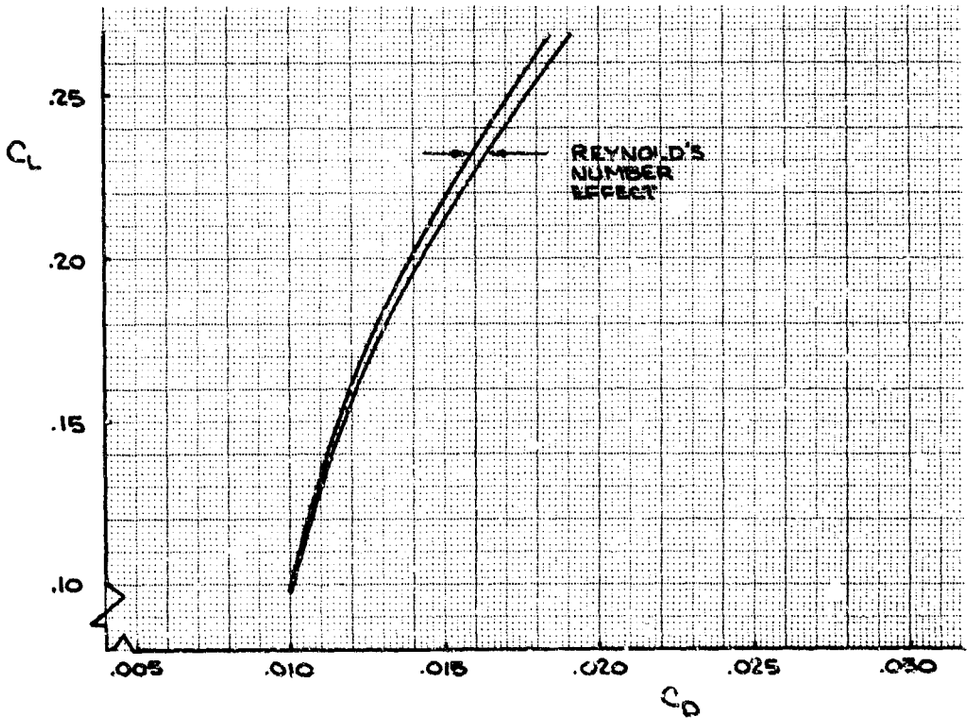


*Figure 3–29. Reynolds Number Effect on Drag Due to Lift at Mach .85*

*Table 3-T. 3-2707 Camber Line Ordinates (% Chord)*

| Percent Span / Percent Chord | 10.6 | 14.6 | 18.6 | 23.2 | 29.3 | 39.1 | 47.1 | 51.6 | 54.4 | 59.1 | 69.9 | 81.1 | 87.3 |
|---|---|---|---|---|---|---|---|---|---|---|---|---|---|
| 0 | 1.69 | 1.44 | 1.19 | .85 | .44 | -.28 | -.64 | -.71 | -.85 | -.83 | -.30 | 1.50 | 3.57 |
| 5 | 1.73 | 1.53 | 1.33 | 1.00 | .64 | .023 | -.32 | -.38 | -.54 | -.52 | .04 | 1.91 | 4.02 |
| 10 | 1.68 | 1.50 | 1.32 | 1.04 | .70 | .15 | -.15 | -.20 | -.35 | -.30 | .29 | 2.24 | 4.37 |
| 15 | 1.56 | 1.38 | 1.195 | .925 | .68 | .15 | -.08 | -.11 | -.24 | -.16 | .46 | 2.50 | 4.62 |
| 20 | 1.36 | 1.18 | 1.0 | .725 | .58 | .11 | -.78 | -.08 | -.15 | -.10 | .58 | 2.70 | 4.85 |
| 30 | .78 | .62 | .46 | .25 | .12 | -.105 | -.185 | -.15 | -.19 | -.08 | .74 | 3.01 | 5.25 |
| 40 | .08 | -.045 | -.17 | -.29 | -.35 | -.42 | -.41 | -.31 | -.31 | -.125 | .82 | 3.24 | 5.53 |
| 50 | -.72 | -.78 | -.83 | -.88 | -.85 | -.785 | -.63 | -.48 | -.42 | -.17 | .88 | 3.42 | 5.81 |
| 60 | -1.44 | -1.12 | -1.39 | -1.38 | -1.31 | -1.10 | -.87 | -.65 | -.53 | -.21 | .92 | 3.57 | 6.06 |
| 70 | -2.02 | -1.94 | -1.86 | -1.76 | -1.63 | -1.33 | -1.01 | -.85 | -.61 | -.26 | .95 | 3.69 | 6.28 |
| 80 | -2.42 | -2.31 | -2.27 | -2.06 | -1.87 | -1.49 | -1.14 | -1.09 | -.69 | -.31 | .98 | 3.79 | 6.49 |
| 90 | -2.64 | -2.52 | -2.74 | -2.23 | -2.02 | -1.60 | -1.18 | -1.37 | -.71 | -.34 | 1.02 | 3.86 | 6.67 |
| 100 | -2.70 | -2.59 | -3.27 | -2.30 | -2.11 | -1.65 | -1.25 | -1.70 | -.77 | -.36 | 1.05 | 3.93 | 6.88 |

| PLANFORM GEOMETRY | | | | | | | | |
|---|---|---|---|---|---|---|---|---|
| X (FT) | 0 | 17.2 | 30.5 | 47.4 | 63.1 | 76.8 | 131.5 | 162.7 |
| Y (FT) | 0 | 5.625 | 9.86 | 15.5 | 20.68 | 25.0 | 42.7 | 52.9 |
| CHORD (FT) | 169.75 | 150.5 | 136.1 | 118.7 | 103.4 | 90.6 | 42.5 | 0 (15.1) |

*Table 3–U. Model SA 966 Wave Drag Program Inputs*

| | | | | | | | | | | |
|---|---|---|---|---|---|---|---|---|---|---|
| 0. | 2.5 | 10. | 25. | 40. | 50. | 60. | 75. | 90. | 100. | X/C |
| 16.832 | 1.628 | -.731 | 32.723 | | | | | | | W1 |
| 23.647 | 1.802 | -.640 | 25.652 | | | | | | | W2 |
| 25.769 | 2.237 | -.585 | 23.545 | | | | | | | W3 |
| 27.602 | 2.833 | -.512 | 21.666 | | | | | | | W4 |
| 30.143 | 3.655 | -.439 | 19.226 | | | | | | | W5 |
| 36.466 | 5.711 | -.201 | 13.440 | | | | | | | W6 |
| 36.472 | 5.713 | -.201 | 8.608 | | | | | | | W7 |
| 39.229 | 6.610 | -.091 | 7.133 | | | | | | | W8 |
| 45.343 | 8.597 | .146 | 4.481 | | | | | | | W9 |
| 48.614 | 9.663 | .274 | 0.0 | | | | | | | W10 |
| 0.0 | 0.25 | 0.56 | 0.88 | 1.10 | 1.18 | 1.17 | 0.93 | 0.43 | 0.0 | Z/C-1 |
| 0.0 | 0.40 | 0.98 | 1.47 | 1.64 | 1.53 | 1.39 | 1.0 | 0.44 | 0.0 | Z/C-2 |
| 0.0 | 0.44 | 1.04 | 1.74 | 1.80 | 1.65 | 1.45 | 1.03 | 0.44 | 0.0 | Z/C-3 |
| 0.0 | 0.45 | 0.92 | 1.45 | 1.81 | 1.80 | 1.61 | 1.02 | 0.44 | 0.0 | Z/C-4 |
| 0.0 | 0.46 | 0.91 | 1.34 | 1.49 | 1.50 | 1.44 | 1.12 | 0.54 | 0.0 | Z/C-5 |
| 0.0 | 0.46 | 0.91 | 1.34 | 1.49 | 1.50 | 1.44 | 1.12 | 0.54 | 0.0 | Z/C-6 |
| 0.0 | 0.58 | 1.15 | 1.76 | 2.09 | 2.25 | 2.32 | 2.34 | 2.28 | 2.14 | Z/C-7 |
| 0.0 | 0.46 | 0.91 | 1.34 | 1.49 | 1.50 | 1.44 | 1.12 | 0.54 | 0.0 | Z/C-8 |
| 0.0 | 0.46 | 0.91 | 1.34 | 1.49 | 1.50 | 1.44 | 1.12 | 0.54 | 0.0 | Z/C-9 |
| 0.0 | 0.46 | 0.91 | 1.34 | 1.49 | 1.50 | 1.44 | 1.12 | 0.54 | 0.0 | Z/C-10 |
| 0.0 | 2.0 | 4.0 | 6.0 | 8.0 | 10.0 | 12.0 | 14.0 | 16.0 | 18.0 | XFUS |
| 20.0 | 22.0 | 24.0 | 26.0 | 28.0 | 30.0 | 32.0 | 34.0 | 36.0 | 38.0 | XFUS |
| 40.0 | 42.0 | 44.0 | 46.0 | 48.0 | 50.0 | 52.90 | | | | XFUS |
| 0.0 | 0.341 | 1.00 | 1.77 | 2.57 | 3.37 | 4.11 | 4.875 | 5.450 | 5.88 | FUSA |
| 6.08 | 6.12 | 5.95 | 5.58 | 5.23 | 5.01 | 4.84 | 4.81 | 4.82 | 4.81 | FUSA |
| 4.75 | 4.41 | 4.20 | 4.0 | 3.78 | 3.55 | 3.35 | | | | FUSA |
| 0.0 | 2.193 | 4.386 | 4.569 | 4.751 | 4.934 | | | | | XACT |
| 0.0 | 0.188 | 0.0 | 0.0 | 0.0 | 0.0 | | | | | ACTR |
| 44.502 | 0.0 | 1.127 | 8.401 | 50.387 | 0.0 | 6.077 | 2.100 | | | FINLOC |
| 0.0 | 37.5 | 62.5 | 100.0 | | | | | | | FIN X/C |
| 0.0 | 1.5 | 1.5 | 0.0 | | | | | | | FIN Z/C |
| 45.019 | 5.711 | -0.183 | 4.880 | 49.406 | 8.224 | 0.091 | 1.416 | | | CANLOC |
| 0.0 | 37.5 | 62.5 | 100.0 | | | | | | | CAN X/C |
| 0.0 | 1.50 | 1.50 | 0.0 | | | | | | | CAN Z/C |

***G.E. NACELLES***

| | | | | | | | | | |
|---|---|---|---|---|---|---|---|---|---|
| 43.241 | 1.751 | -1.462 | 43.734 | 4.989 | -1.051 | 45.416 | 5.940 | 0.0 | PODLOC |
| 0.0 | 3.503 | 4.660 | 5.117 | 5.812 | 6.56 | | | | XPOD |
| 0.474 | 0.621 | 0.647 | 0.647 | 0.634 | 0.565 | | | | PODR |
| 0.0 | 3.503 | 4.660 | 5.117 | 5.812 | 6.56 | | | | XPOD |
| 0.474 | 0.621 | 0.647 | 0.647 | 0.634 | 0.565 | | | | PODR |

***P & WA NACELLES***

| | | | | | | | | | |
|---|---|---|---|---|---|---|---|---|---|
| 44.849 | 1.767 | -1.462 | 45.178 | 4.953 | -1.051 | 45.416 | 5.940 | 0.0 | PODLOC |
| 0.0 | 2.208 | 3.107 | 4.021 | 4.569 | 5.239 | | | | XPOD |
| 0.514 | 0.611 | 0.647 | 0.667 | 0.654 | 0.609 | | | | PODR |
| 0.0 | 2.206 | 3.107 | 4.021 | 4.569 | 5.239 | | | | XPOD |
| 0.514 | 0.611 | 0.647 | 0.667 | 0.654 | 0.609 | | | | PODR |

*Table 3-V. Model SA 977 Wave Drag Program Inputs*

| | | | | | | | | | | |
|---|---|---|---|---|---|---|---|---|---|---|
| 0.0 | 2.5 | 10.0 | 25.0 | 40.0 | 50.0 | 60.0 | 75.0 | 90.0 | 100.0 | X/C |
| 14.94 | 1.20 | 0.0 | 32.57 | | | | | | | W1 |
| 20.62 | 1.859 | 0.144 | 27.15 | | | | | | | W2 |
| 22.99 | 2.309 | 0.180 | 24.94 | | | | | | | W3 |
| 34.56 | 5.625 | 0.810 | 14.66 | | | | | | | W4 |
| 34.56 | 5.626 | 0.810 | 8.908 | | | | | | | W5 |
| 40.33 | 7.501 | 1.116 | 6.458 | | | | | | | W6 |
| 44.55 | 8.870 | 1.350 | 4.624 | | | | | | | W7 |
| 46.59 | 9.533 | 1.476 | 3.737 | | | | | | | W8 |
| 49.33 | 10.426 | 1.620 | 0.0 | | | | | | | W9 |
| 0.0 | 0.85 | 1.60 | 2.01 | 2.03 | 1.95 | 1.72 | 1.18 | 0.50 | 0.0 | Z/C-1 |
| 0.0 | 0.35 | 0.88 | 1.34 | 1.49 | 1.49 | 1.35 | 0.98 | 0.43 | 0.0 | Z/C-2 |
| 0.0 | 0.36 | 0.85 | 1.30 | 1.43 | 1.40 | 1.29 | 0.92 | 0.42 | 0.0 | Z/C-3 |
| 0.0 | 0.44 | 0.88 | 1.28 | 1.40 | 1.39 | 1.29 | 0.90 | 0.35 | 0.0 | Z/C-4 |
| 0.0 | 0.58 | 1.12 | 1.74 | 2.08 | 2.21 | 2.27 | 2.28 | 2.21 | 2.06 | Z/C-5 |
| 0.0 | 0.44 | 0.78 | 1.15 | 1.25 | 1.25 | 1.21 | 0.95 | 0.46 | 0.0 | Z/C-6 |
| 0.0 | 0.44 | 0.78 | 1.15 | 1.25 | 1.25 | 1.21 | 0.95 | 0.46 | 0.0 | Z/C-7 |
| 0.0 | 0.44 | 0.78 | 1.15 | 1.25 | 1.25 | 1.21 | 0.95 | 0.46 | 0.0 | Z/C-8 |
| 0.0 | 0.44 | 0.78 | 1.15 | 1.25 | 1.25 | 1.21 | 0.95 | 0.46 | 0.0 | Z/C-9 |
| 0.0 | 1.80 | 3.60 | 5.40 | 7.20 | 9.00 | 10.8 | 12.6 | 14.4 | 16.2 | XFUS |
| 18.0 | 19.8 | 21.6 | 23.4 | 25.2 | 27.0 | 28.8 | 30.6 | 32.4 | 34.2 | XFUS |
| 36.0 | 37.8 | 39.6 | 41.4 | 43.2 | 45.0 | 46.8 | 48.6 | 52.2 | 55.08 | XFUS |
| 0.0 | 0.292 | 0.81 | 1.426 | 2.009 | 2.592 | 3.175 | 3.726 | 4.277 | 4.730 | FUSA |
| 4.990 | 5.119 | 5.086 | 5.022 | 4.892 | 4.698 | 4.536 | 4.406 | 4.309 | 4.212 | FUSA |
| 4.115 | 3.985 | 3.856 | 3.726 | 3.499 | 3.370 | 3.240 | 3.175 | 3.143 | 3.143 | FUSA |
| 42.66 | 4.68 | 0.869 | 7.20 | 49.32 | 4.68 | 3.119 | 1.201 | | | FINLOC |
| 0.0 | 37.5 | 62.5 | 100.0 | | | | | | | FIN X/C |
| 0.0 | 1.0 | 1.0 | 0.0 | | | | | | | FIN Z/C |
| 43.832 | 5.625 | 0.810 | 5.335 | 49.986 | 9.166 | 1.404 | 1.073 | | | CANLOC |
| 0.0 | 37.5 | 62.5 | 100.0 | | | | | | | CAN X/C |
| 0.0 | 1.5 | 1.5 | 0.0 | | | | | | | CAN Z/C |
| 42.66 | 1.800 | -.599 | 43.83 | 4.88 | -.10 | | | | | PODLOC |
| 0.0 | 3.450 | 4.59 | 5.04 | 5.72 | 6.46 | | | | | XPOD |
| 0.443 | 0.597 | 0.637 | 0.641 | 0.625 | 0.556 | | | | | PODR |
| 0.0 | 3.450 | 4.59 | 5.04 | 5.72 | 6.46 | | | | | XPOD |
| 0.443 | 0.597 | 0.637 | 0.641 | 0.625 | 0.556 | | | | | PODR |

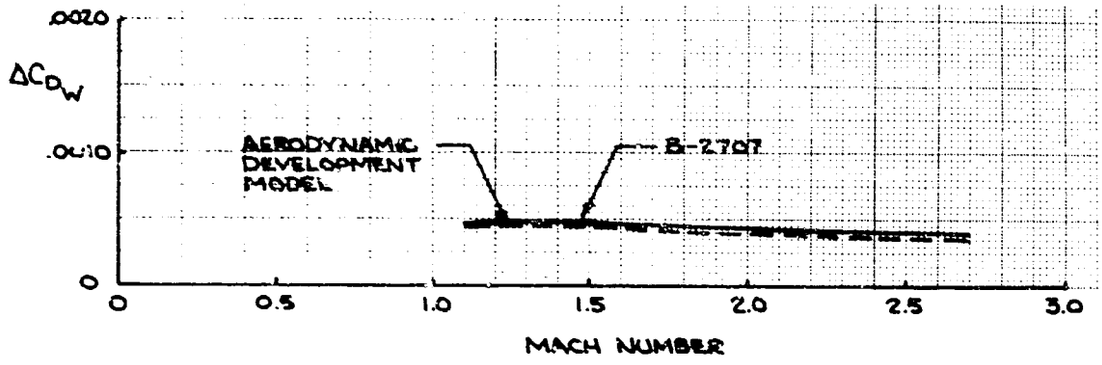


Figure 3-30 Wave Drag Correction

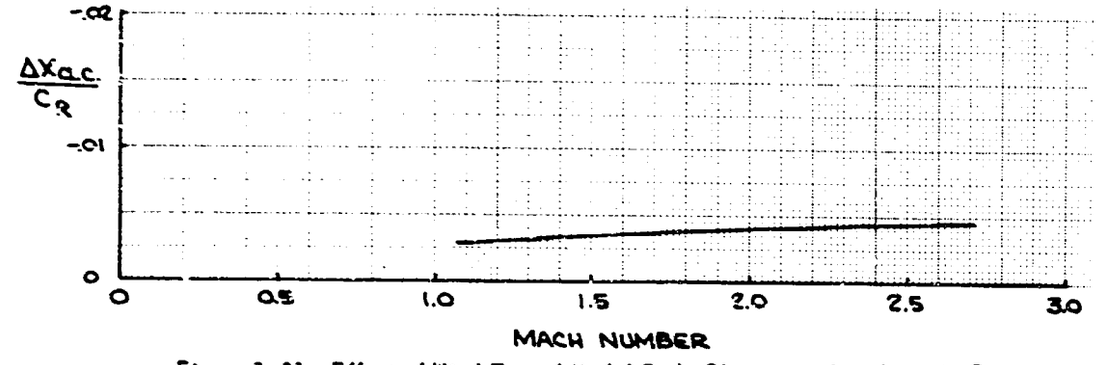


Figure 3-31. Effect of Wind Tunnel Model Body Closure on Aerodynamic Center

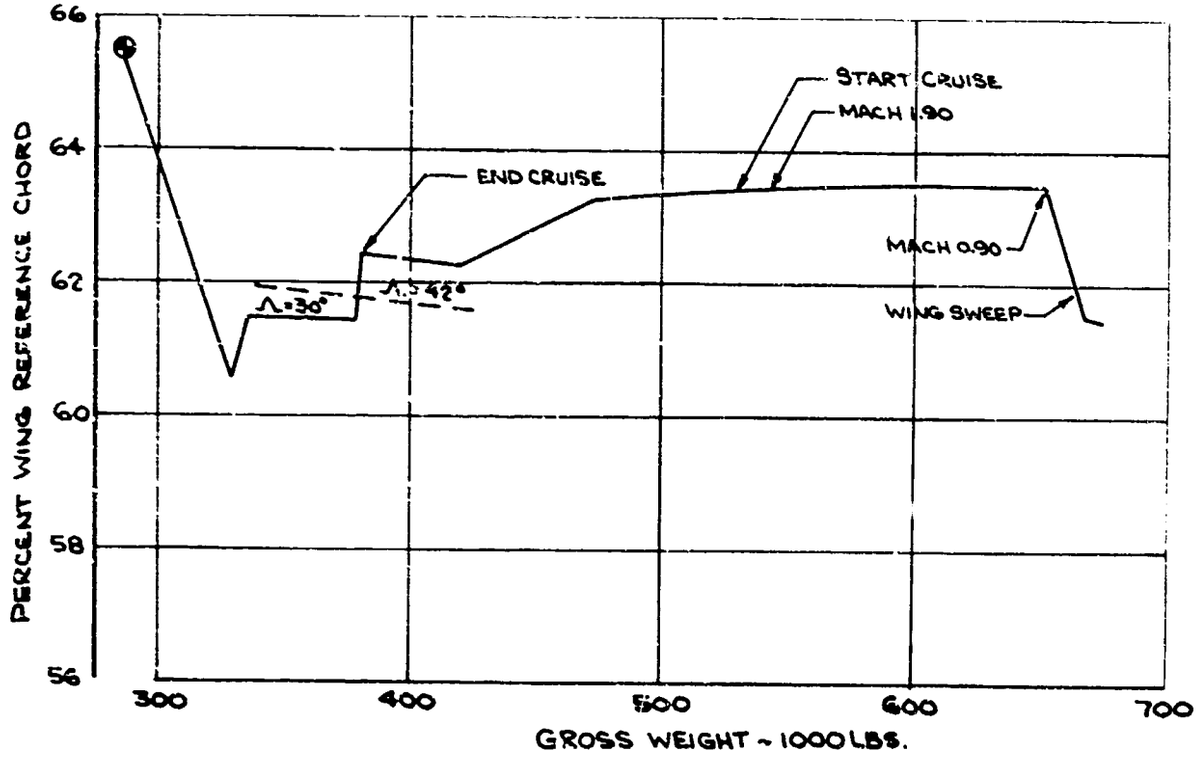


Figure 3-32. B-2707 Center of Gravity Location as a Function of Weight

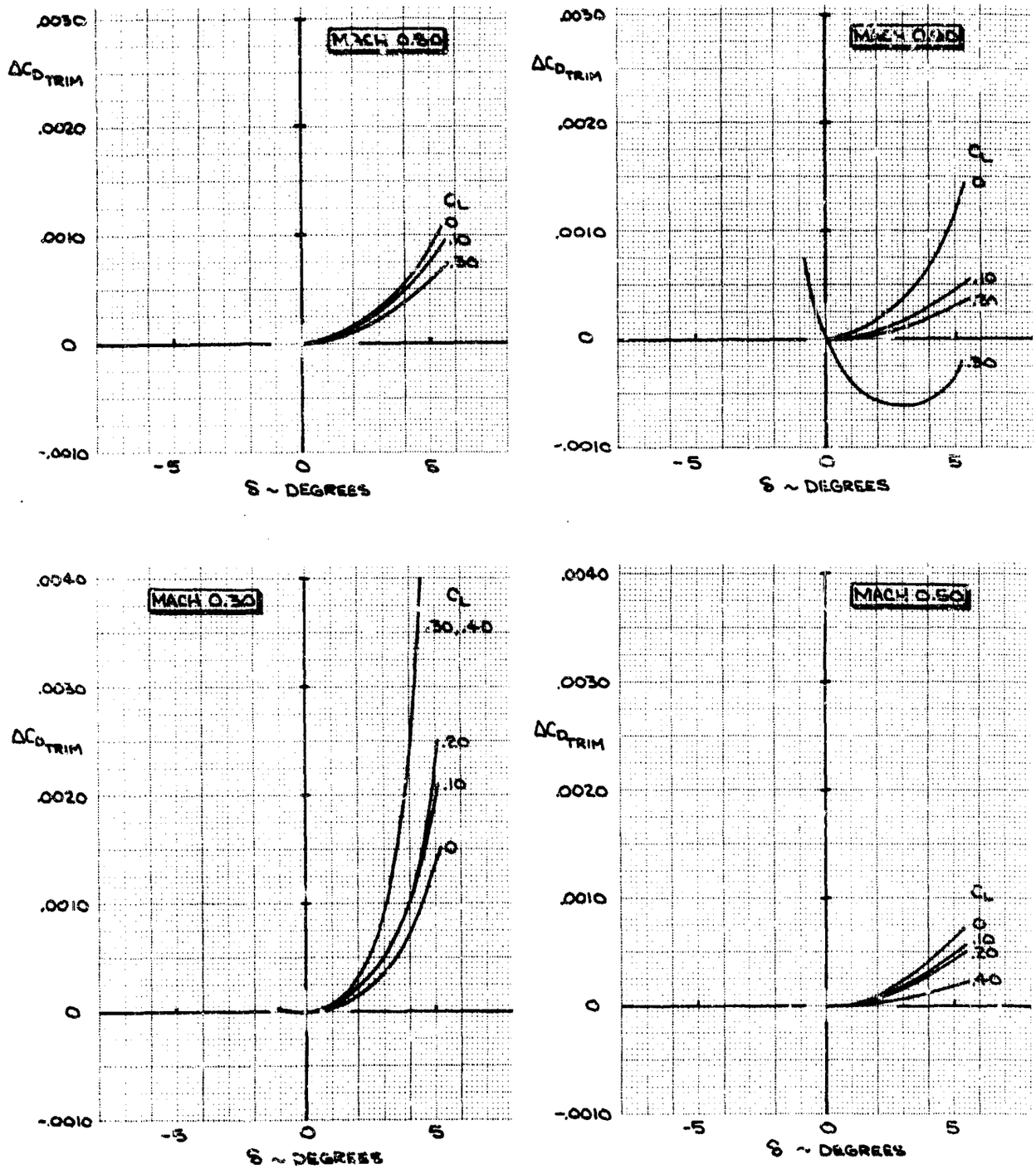


*Figure 3-33. Trim Drag at 42 Degrees Leading Edge Sweep*

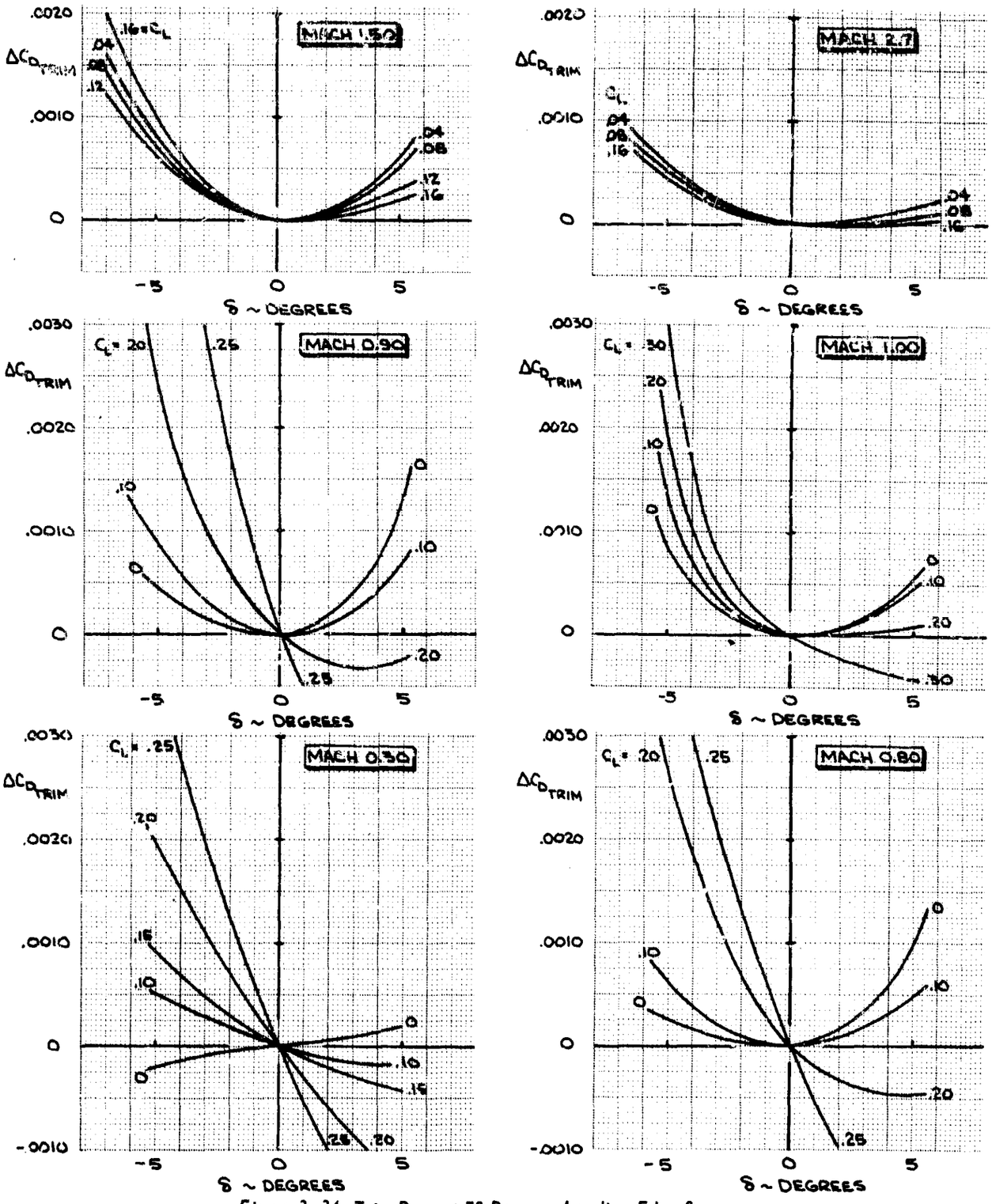


*Figure 3-34 Trim Drag at 72 Degrees Leading Edge Sweep*

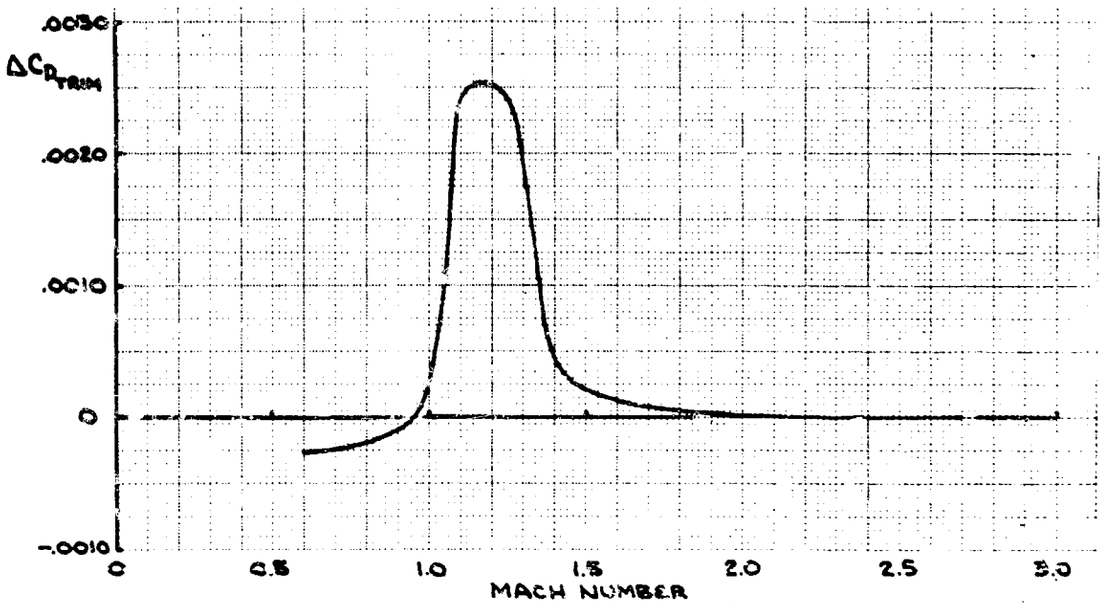


*Figure 3-35. Trim Drag Along the Climb Profile*

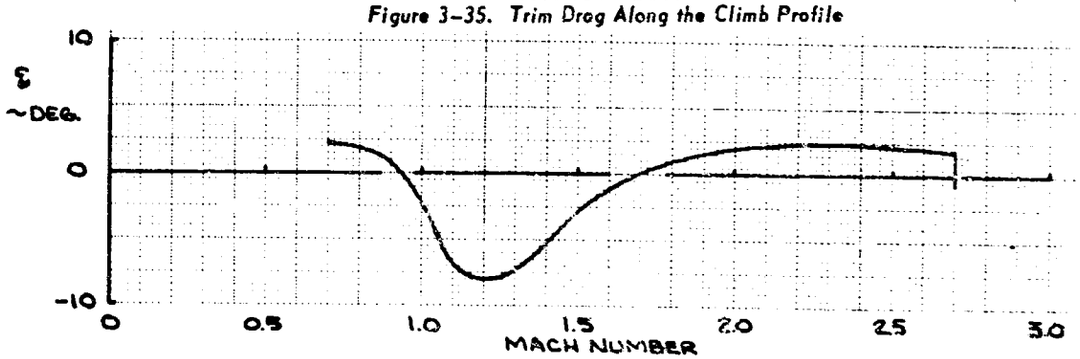


*Figure 3-36. Elevator Deflection to Trim*

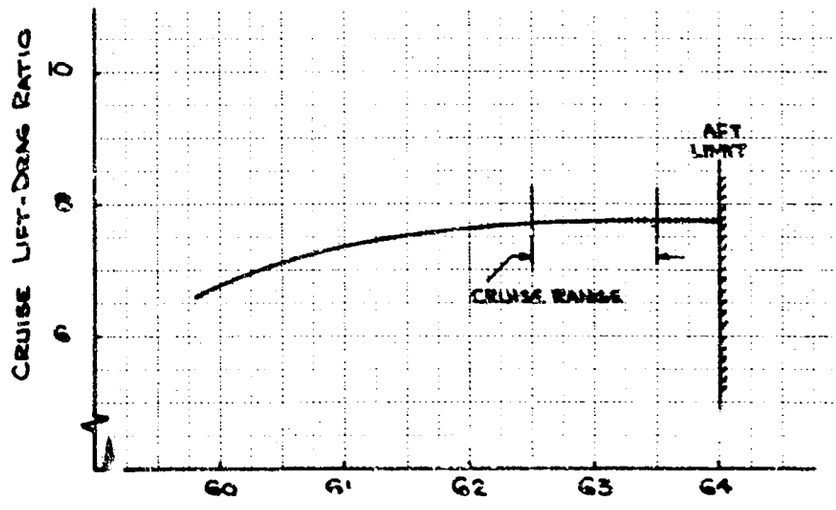


*Figure 3-37. Effect of Center of Gravity on Trim Drag*

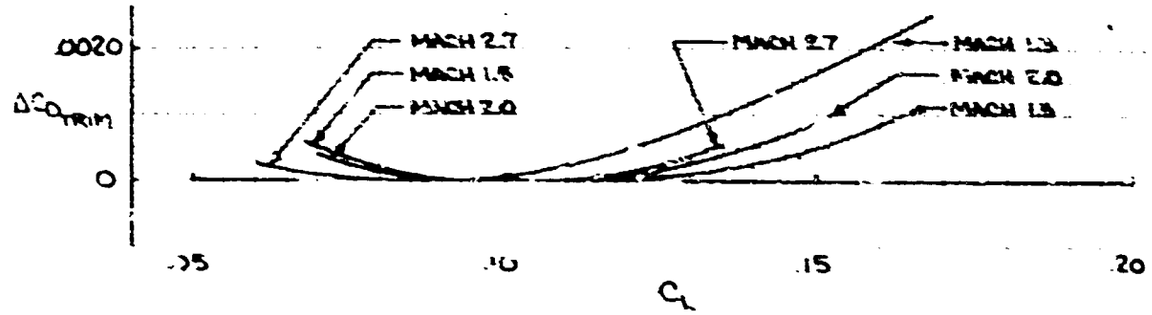


Figure 3-38. (a) Effect of Lift Coefficient on Trim Drag – Mach 1.3 to 2.7

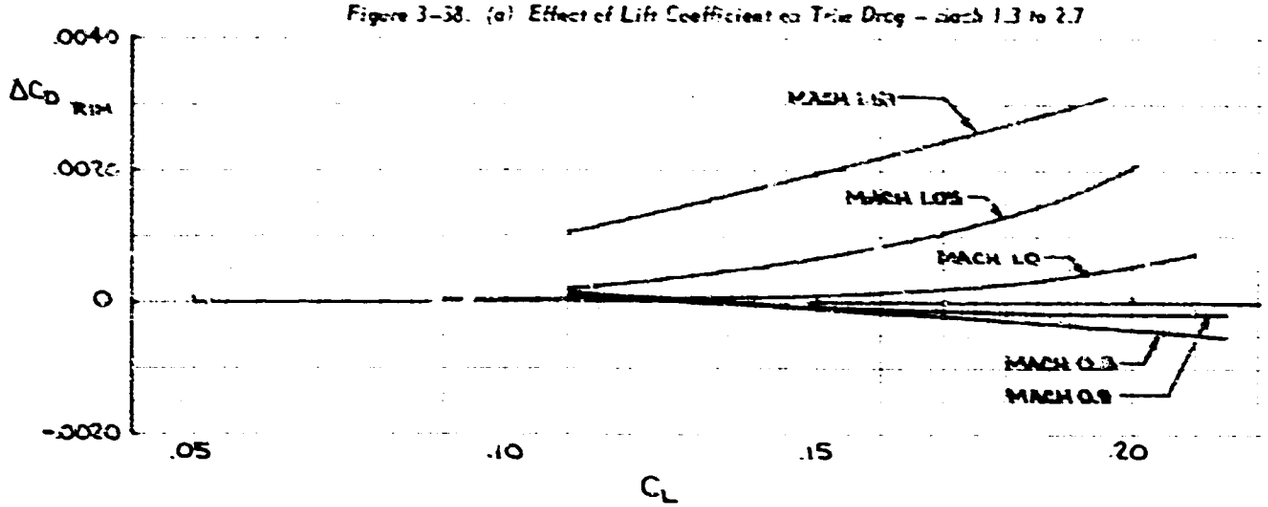


Figure 3-38. (b) Effect of Lift Coefficient on Trim Drag – Mach .8 to 1.1

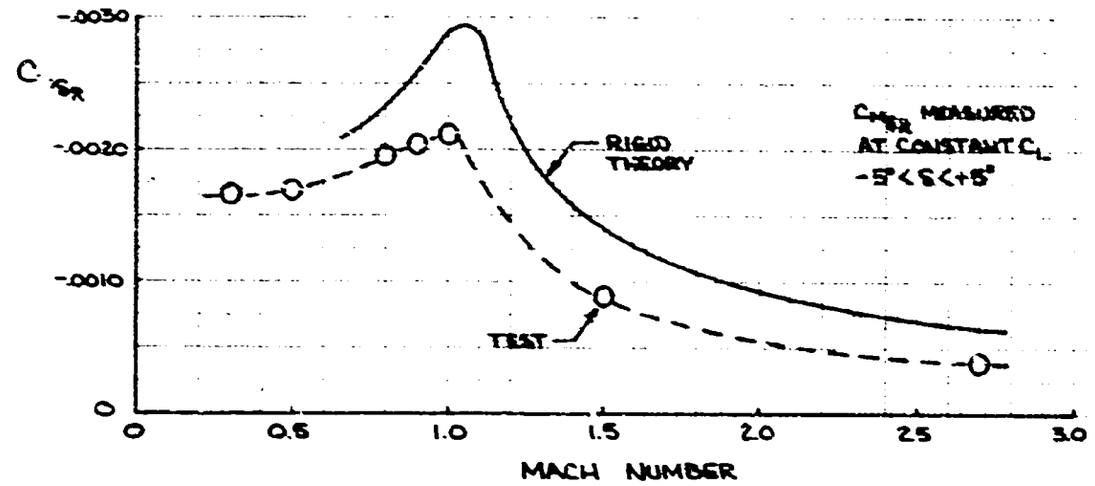


Figure 3-39. Comparison of Measured Elevator Effectiveness with Theory

ratio, at Mach 2.7 is sho n in Fig. 3-37 and the effect of lift coefficient on trim drag is shown in Fig. 3-38 at various Mach numbers.

In Fig. 3-39 the theoretically calculated values of $C_{M_{\delta_R}}$ are compared with the experimental values shown in Fig. 3-17. The poor agreement is surprising, particularly in the light of similar comparisons obtained during other Boeing and NASA tests. The reason for this is not fully understood now, and the measured value of $C_{M_{\delta_R}}$ have been used for trim drag calculations although this has resulted in trim drag penalties. Some measurements of the flexibility of the wind tunnel model have been made; they have indicated that the experimental values of $C_{M_{\delta_R}}$ might be small because of model flexibility. If this is verified, smaller deflections would be required to trim the airplane and further refinement of the wing camber and twist would be desirable.

3.1.3.4 Full-Scale Lift Drag Characteristics

The drag corrections itemized in the preceding paragraphs have been applied to the model data to account for differences between model and airplane conditions. Trimmed data for the flight profile of Fig. 3-6 are shown in Figs. 3-40 through 3-45. One set of data, applicable to both engines, is shown.

3.1.3.5 Comparisons of Installed Propulsion Pod Drag

A comparison has been made, at Mach 2.7, of the drag of GE and P&WA nacelle installations on the SA 966 wind tunnel model. Photographs are shown in Figs. 3-46 through 3-49. The design of the nacelles was based on information received from the engine manufacturers before July 1. Prior to that a careful survey had been carried out on the flow field below the wing of the model, to determine local flow directions, local Mach number, local boundary layer thickness, and the variation of these with angle of attack. The following criteria were applied to the design:

a. Inlet aligned into the local flow.

b. Boundary layer diverter deep enough to ensure that no boundary layer will enter the inlets and wide enough to enclose volume requirements.

c. Nozzle size determined by taking into account: internal efficiency, interference drag, skin friction drag, transonic boattail drag, and weight.

d. Nozzle exit flow direction determined by consideration of thrust, lift, sonic boom, and landing gear length considerations.

e. The nacelle had to enclose all volume requirements and the installation had to allow for thrust reverser operations.

Within these constraints the installations were designed for best drag. The design was based on analytical studies and augmented by development work in the wind tunnel. The wings of the wind tunnel models were so designed that the part affected by the interference from the nacelles was detachable; different wing designs were tested in the presence of GE and P&WA nacelles, respectively. Drag polars obtained for GE and P&WA installations are shown in Fig. 3-50. Because skin friction drag is accounted for separately, the drag data have been corrected by subtracting the skin friction drag. It is apparent that the drag difference between the engines, if any, is within the accuracy of the measurements.

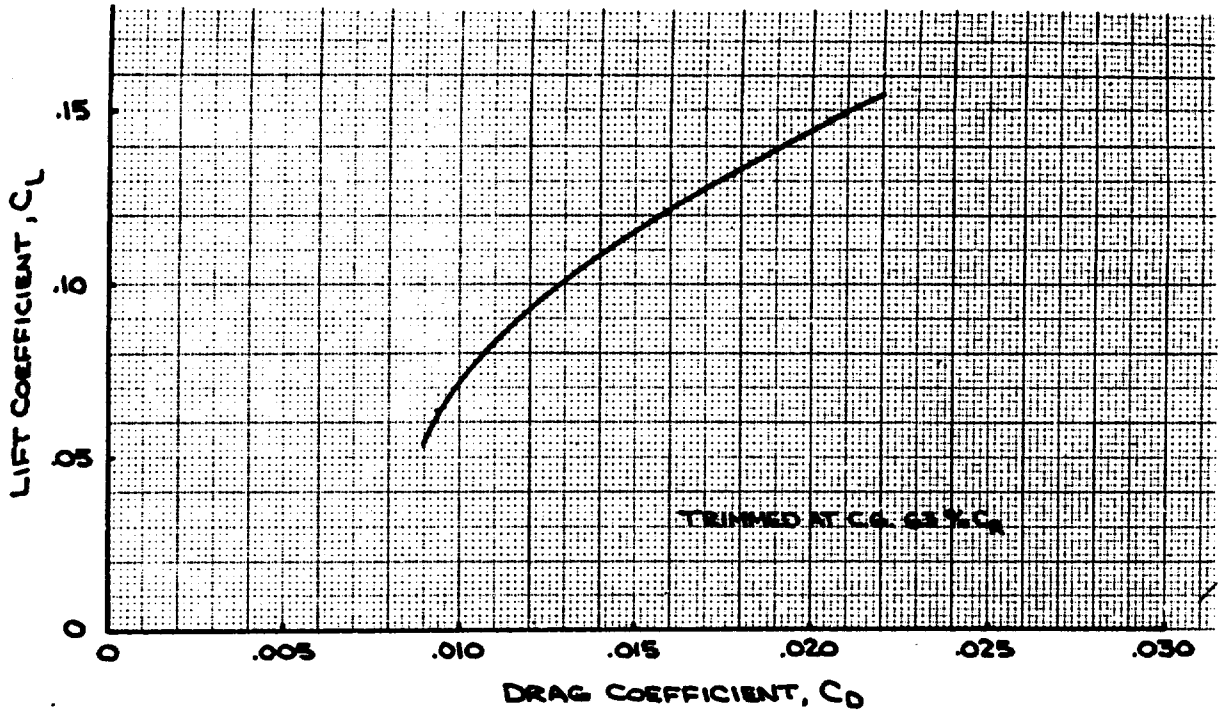


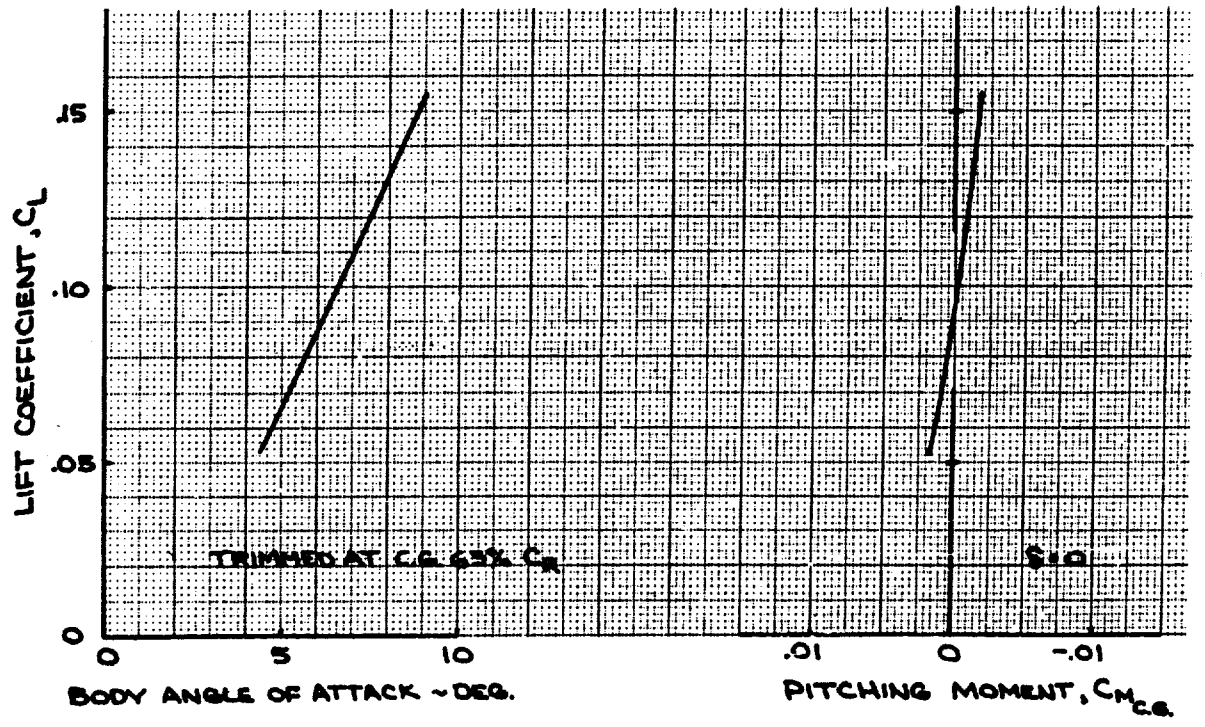


*Figure 3–40. Mach 2.7 B–2707 Aerodynamic Characteristics Leading Edge Sweep 72 Degrees – Current Data*

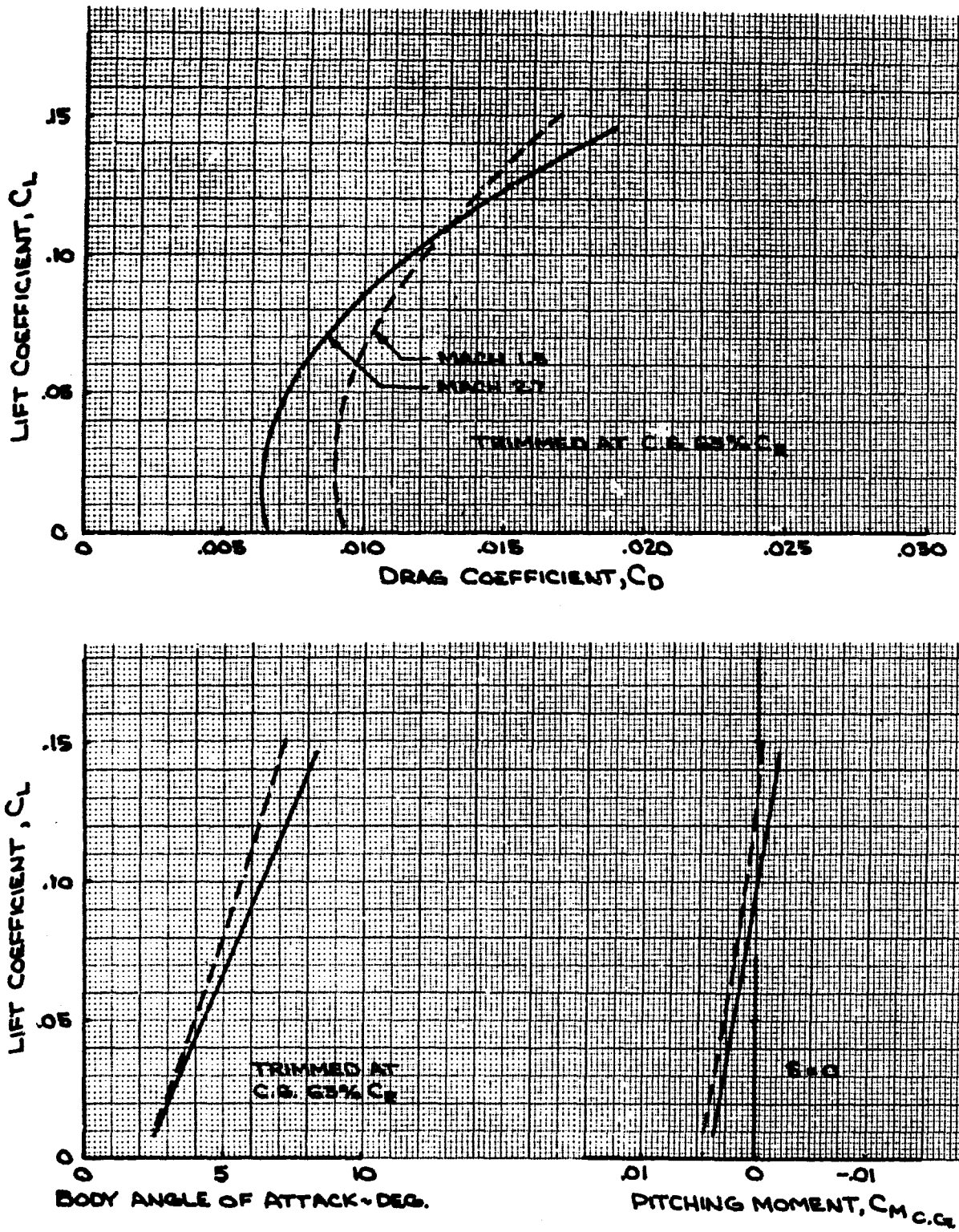


*Figure 3-41. Aerodynamic Development Model Aerodynamic Characteristics; Leading Edge Sweep- 72 Degrees*

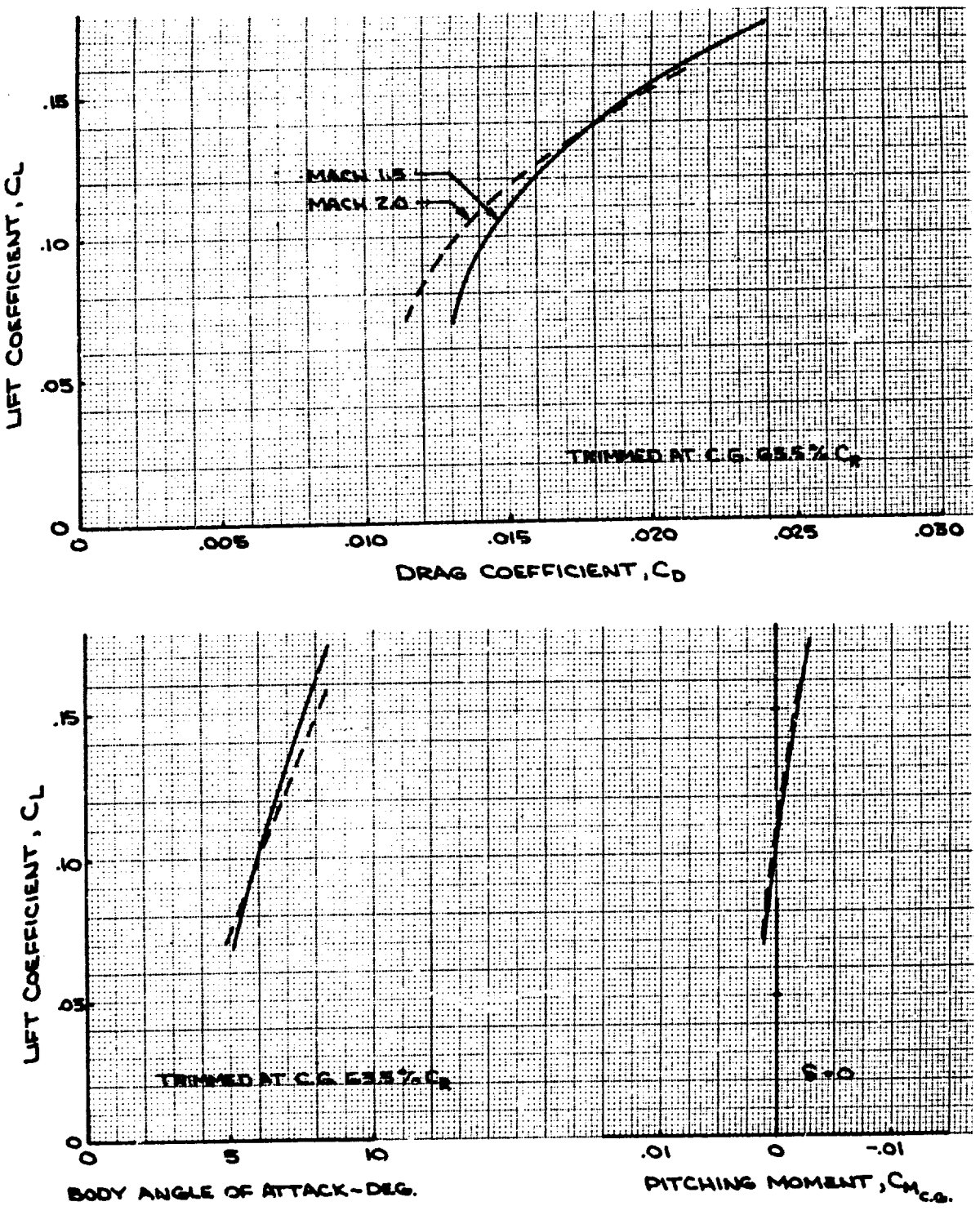


*Figure 3–42. B–2707 Configuration, Leading Edge Sweep 72 Degrees, Mach Numbers 2.0 and 1.5 Current Data*

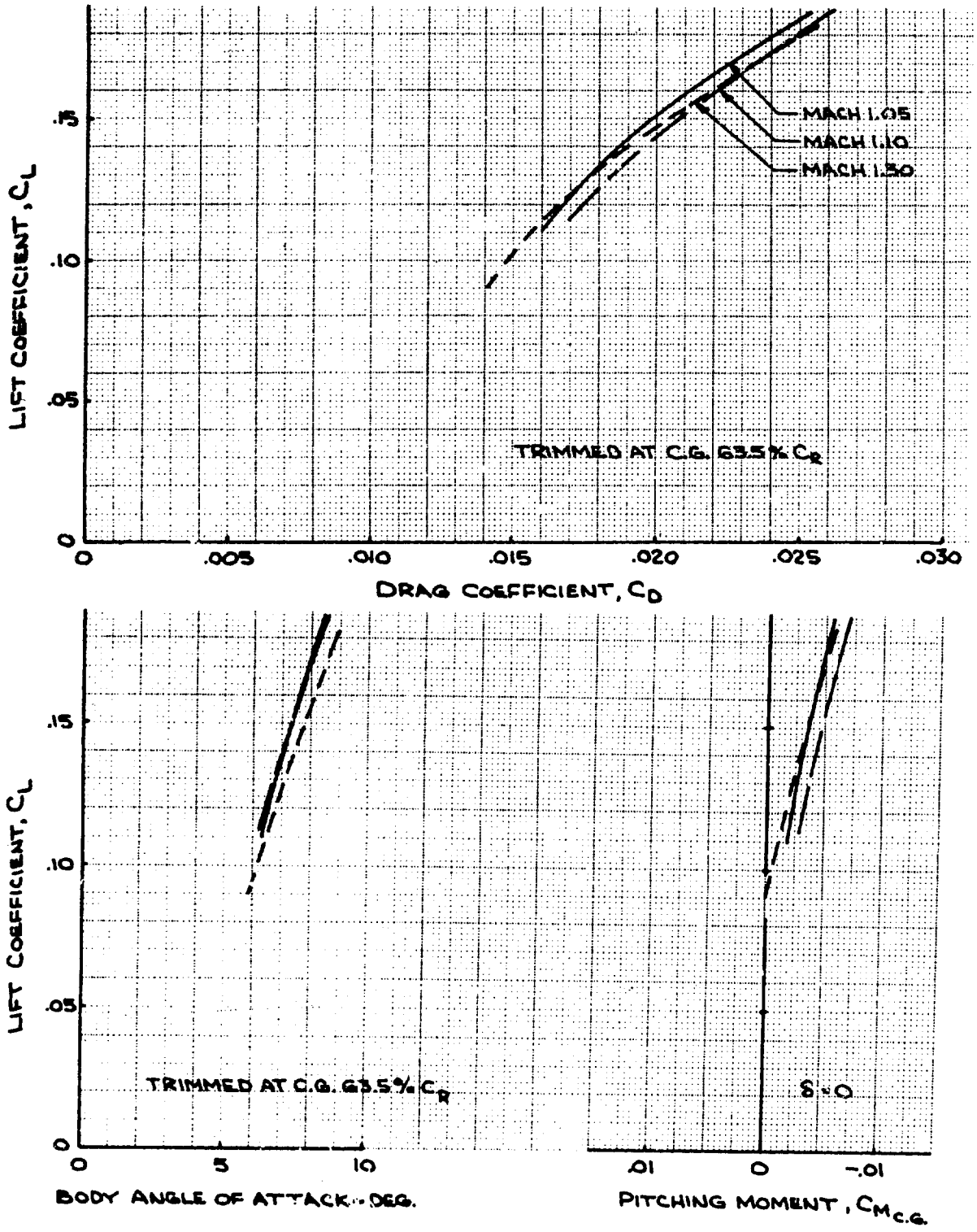


*Figure 3–43. B–2707 Configuration, Leading Edge Sweep 72 Degrees, Mach Numbers 1.3, 1.1, and 1.05 Current Data*

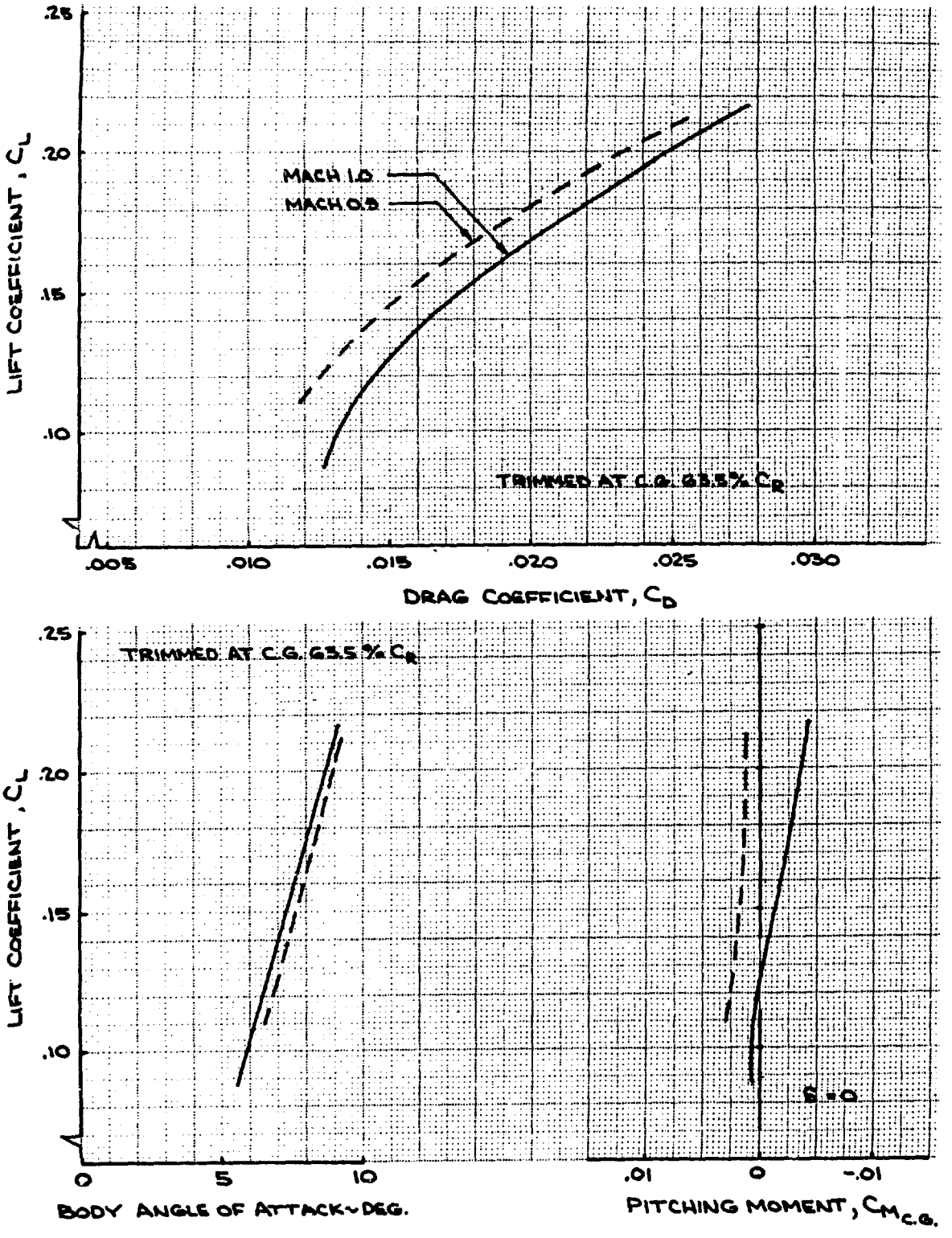


*Figure 3-44. B-2707 Configuration, Leading Edge Sweep 72 Degrees, Mach Numbers 1.0, .9 Current Data*

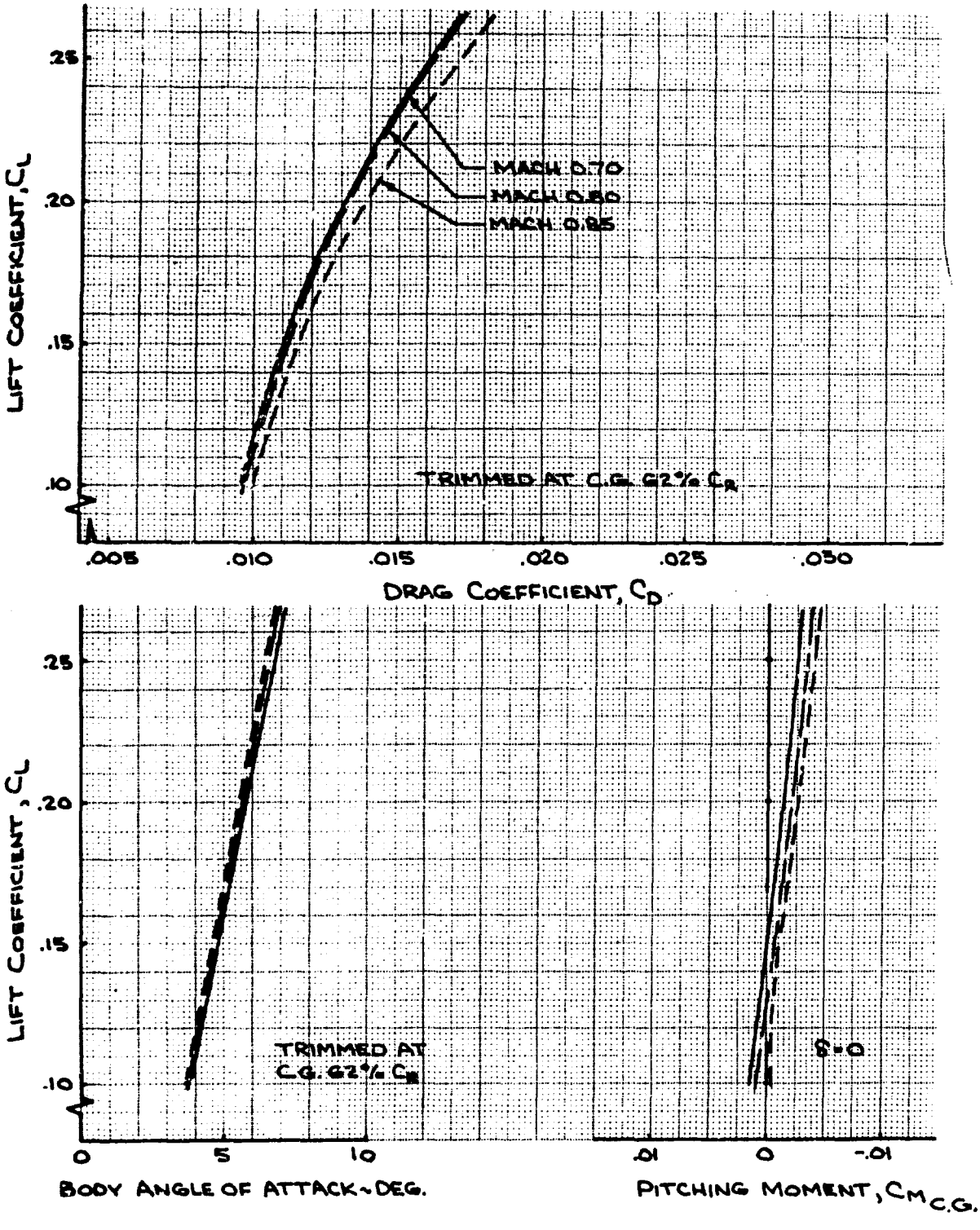


*Figure 3–45. B–2707 Configuration, Leading Edge Sweep 42 Degrees, Mach Numbers .7, .8, and .85, Current Data*

Figure 3–46. Supersonic Wind Tunnel Model GE Outboard Pod

Figure 3–47. Supersonic Wind Tunnel Model P & WA Inboard Pod

Figure 3–48. Thrust Reverser Simulation on Supersonic Model

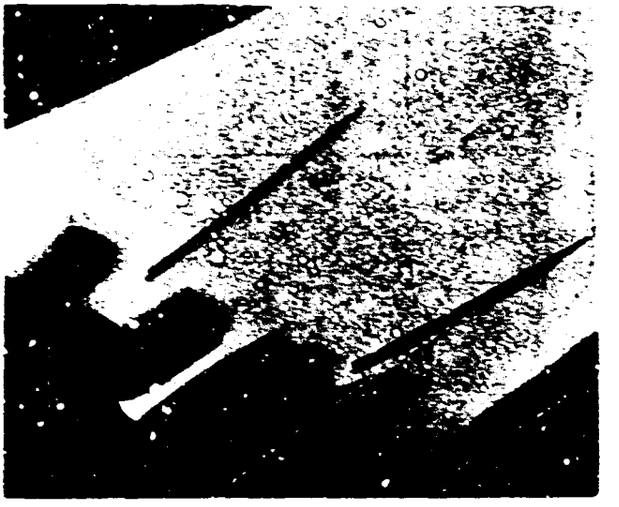

Figure 3–49. Nacelle Installation on SA 966 Supersonic Model

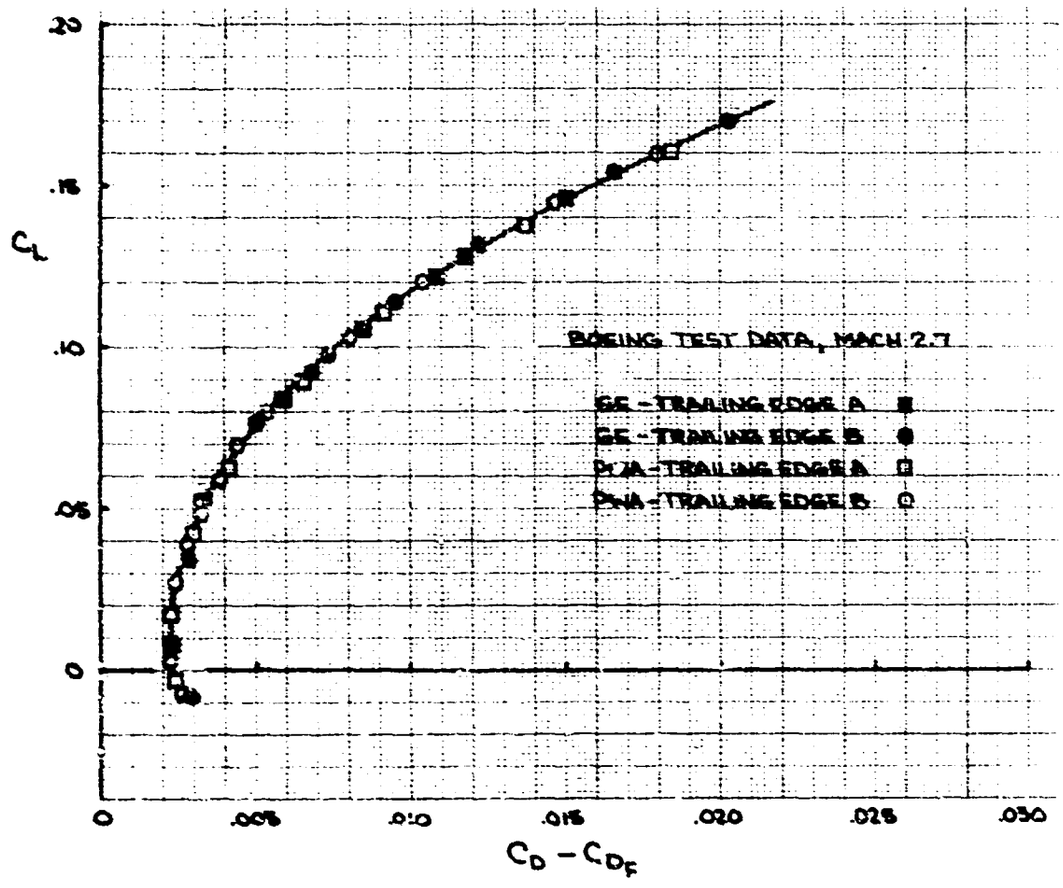


*Figure 3-50. Wind Tunnel Comparison of Installed Engine Drag*

3.2 TAKEOFF AND LANDING CONFIGURATIONS

Lift and drag of the model B-2707 applicable to takeoff and landing operations are substantiated in this paragraph. The close-coupled horizontal tail and longitudinal trim system in the low speed configuration at 30 degrees wing sweep call for a new approach to optimization. Analysis of preliminary test data leads to the conclusion that considerable improvements in trimmed lift and drag can be effected by design refinements, especially at the forward cg; these are being intensively studied. An estimate of the performance capabilities of the airplane with refinements has been made and has been used in calculating the takeoff and landing performance of the B-2707 airplane (shown in Sec. 2). Figure 3-51 is a summary plot comparing the aerodynamic characteristics with the current status. The estimated flight characteristics are based on preliminary wind tunnel model tests, with scale corrections and adjustments for geometry differences based on proven analytical techniques.

3.2.1 Airplane Geometry

3.2.1.1 Wing Geometry

Takeoff and landing operations are programmed using a wing leading edge sweepback angle of 30 degrees. The wing pivot location is chosen to give a favorable wing twist distribution at the 30-degree sweep angle.

Figure 3-52 shows a plan view of the airplane at the takeoff and landing wing sweepback angle of

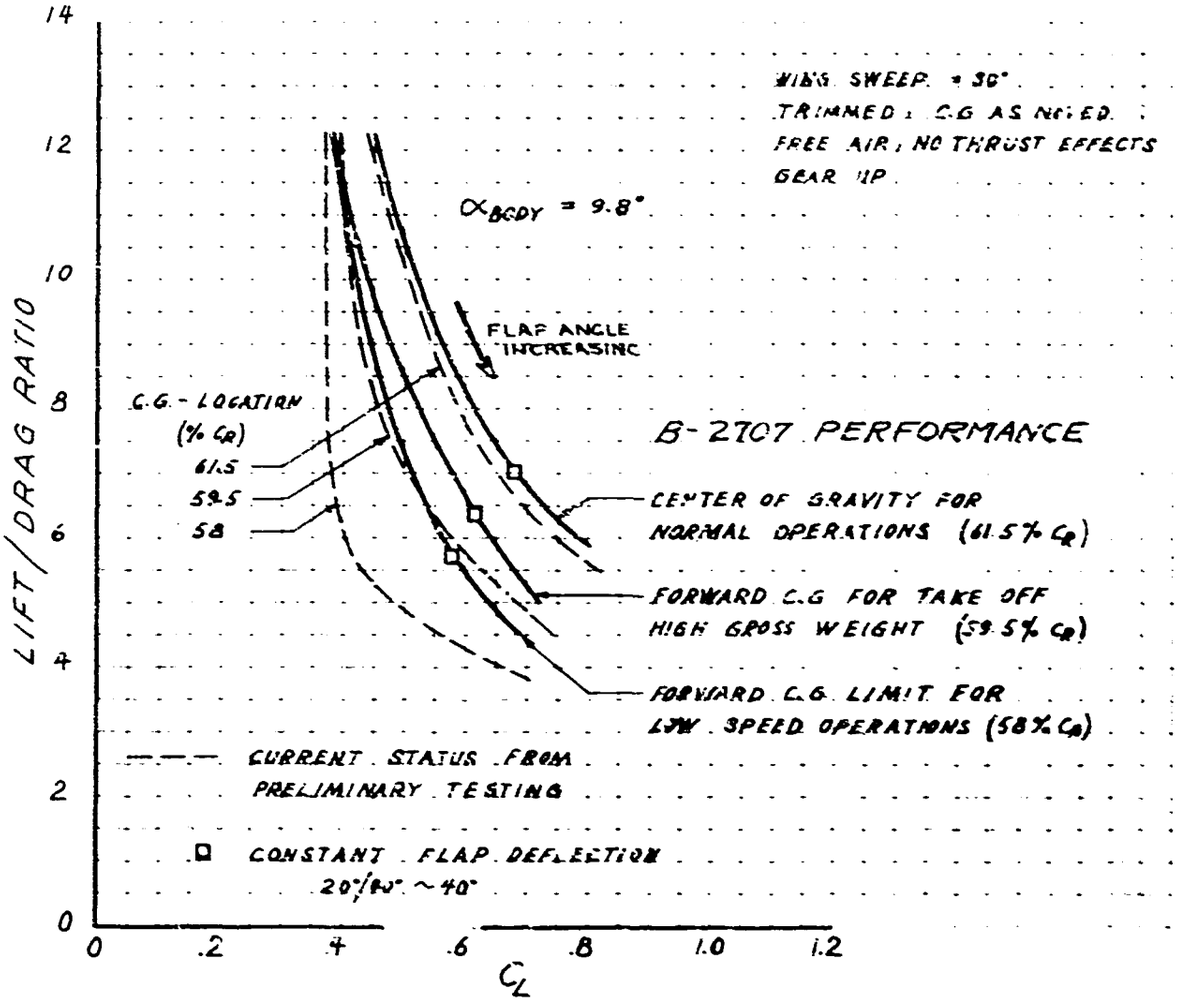


Figure 3-51. Performance Summary

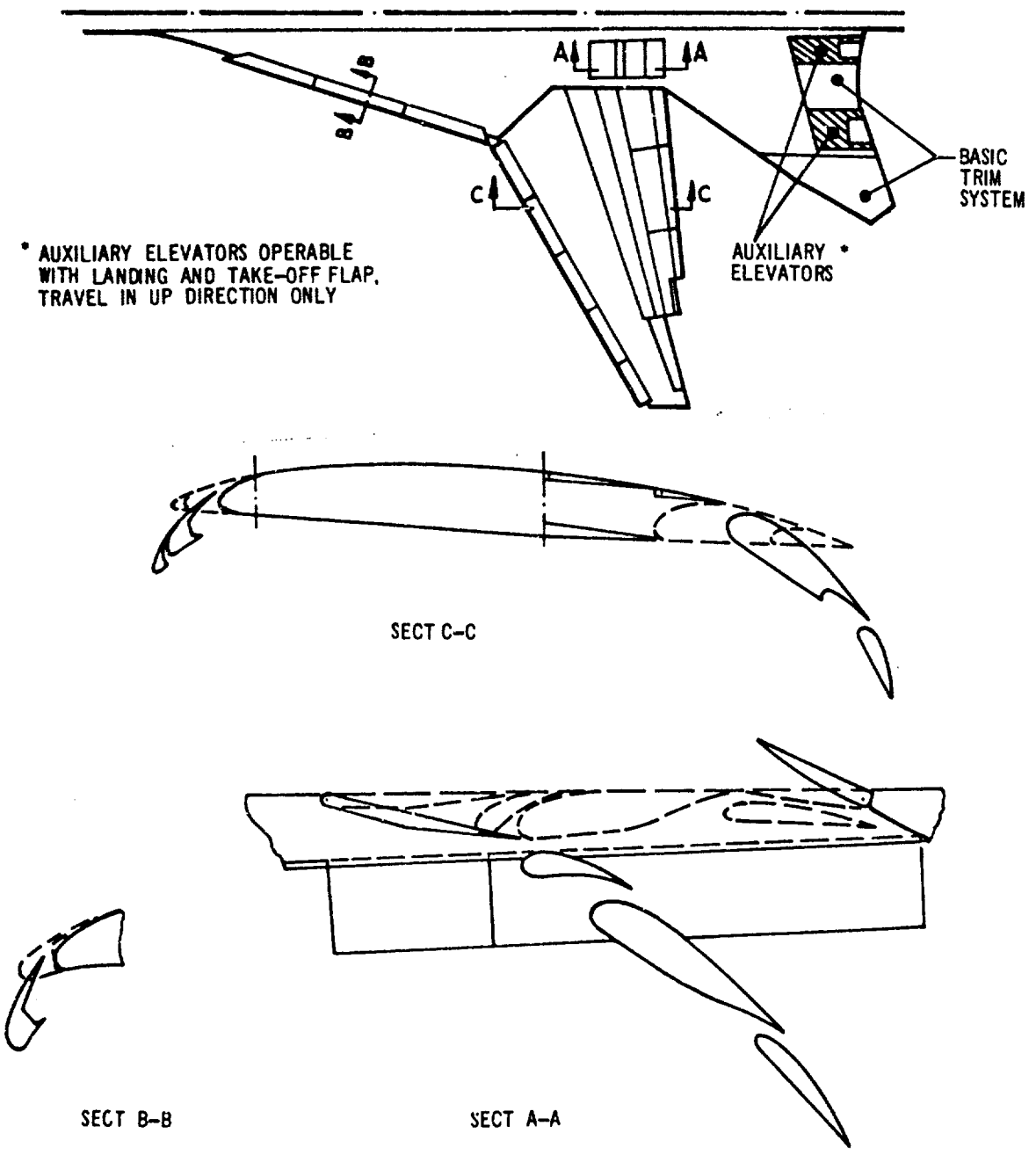


*Figure 3-52. Wing Flap and Slat Geometry*

30 degrees with section views depicting the slats and flaps.

The spanwise wing twist distribution at a typical 1-g takeoff climb condition is shown in Fig. 3-53. This is similar to that of the model 733-390, giving the same zero-lift angle, flaps up.

3.2.1.2 High Lift Devices
Development work on flaps and slats during Phases I and II has produced the very effective high lift system used on the B-2707 airplane. Trailing edge flaps on the outboard wing portion are double slotted for low drag. This flap was perfected in a NASA test program on the 1/5 scale model. Wing slats have a drooped nose to increase their efficiency. Inboard flaps are triple slotted like the powerful 727 airplane flaps. The leading edge slat on the fixed portion of the wing controls vortex development, increasing longitudinal stability, maximum lift coefficient, and lift to drag ratio.

Table 3-W lists the flap and slat deflections appropriate to takeoff and landing operations.

3.2.2 Airplane Characteristics

3.2.2.1 Performance Inputs
Lift and drag characteristics which have been used to calculate performance are estimated values which are well within the potential of the B-2707 airplane concept. These, or better levels of aerodynamic efficiency will be obtained through refinements to the configuration geometry in Phase III of the SST program. Trimmed lift and drag characteristics are affected by cg location, which can vary with loading according to the mission to be flown. It is convenient to quote representative takeoff and landing performance values, neglecting the many intricate loading variations which can have small effects on the numbers quoted. All generalized performance shown in Sec. 2.0 is based on the lift and drag curves of Figs. 3-54 and 3-55, applicable to a forward cg location of 59.5 percent $C_R$. All normal takeoffs and landings will be accomplished at cg locations

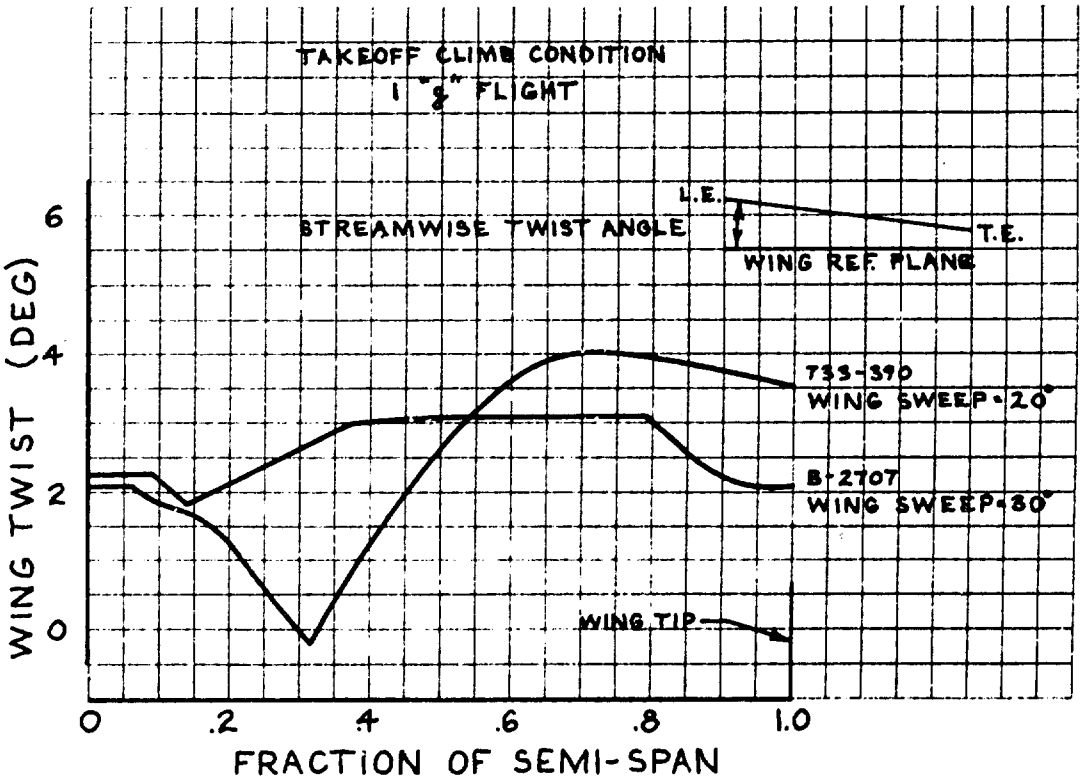


*Figure 3-53. Wing Twist at 30° Sweep*

*Table 3-W. Flap and Slat Angles for Low Speed Operations*

| | TRAILING EDGE FLAPS | | LEADING EDGE SLATS | |
|---|---|---|---|---|
| FLIGHT MODE | INBOARD FLAP | OUTER WING FLAPS | FIXED WING | OUTER WING |
| TAKEOFF & LANDING | 21°/40°/60° | 20°/40° | 35° | 20°/37.5° |
| ALTERNATE TAKEOFF | Up | 10°/20° | 28.5° | 11°/19.5° |
| CLIMB | UP | 5°/5° | 25° | 6°/10° |
| ALTERNATE LANDING | 21°/40°/60° | 30°/50° | 35° | 30°/55° |
| LANDING, WING SWEEP 72° | Up | Up | 25° | Nested Up |

NOTE: Flap and slat segment deflections are measured from the up datum, as shown below.

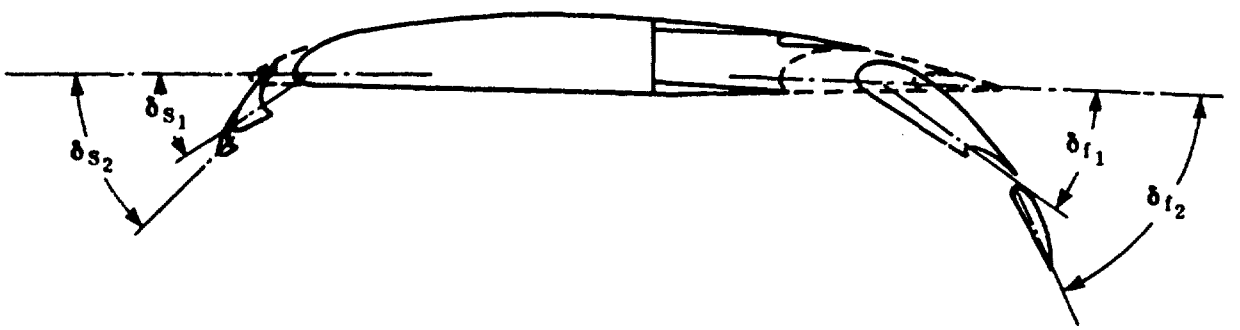

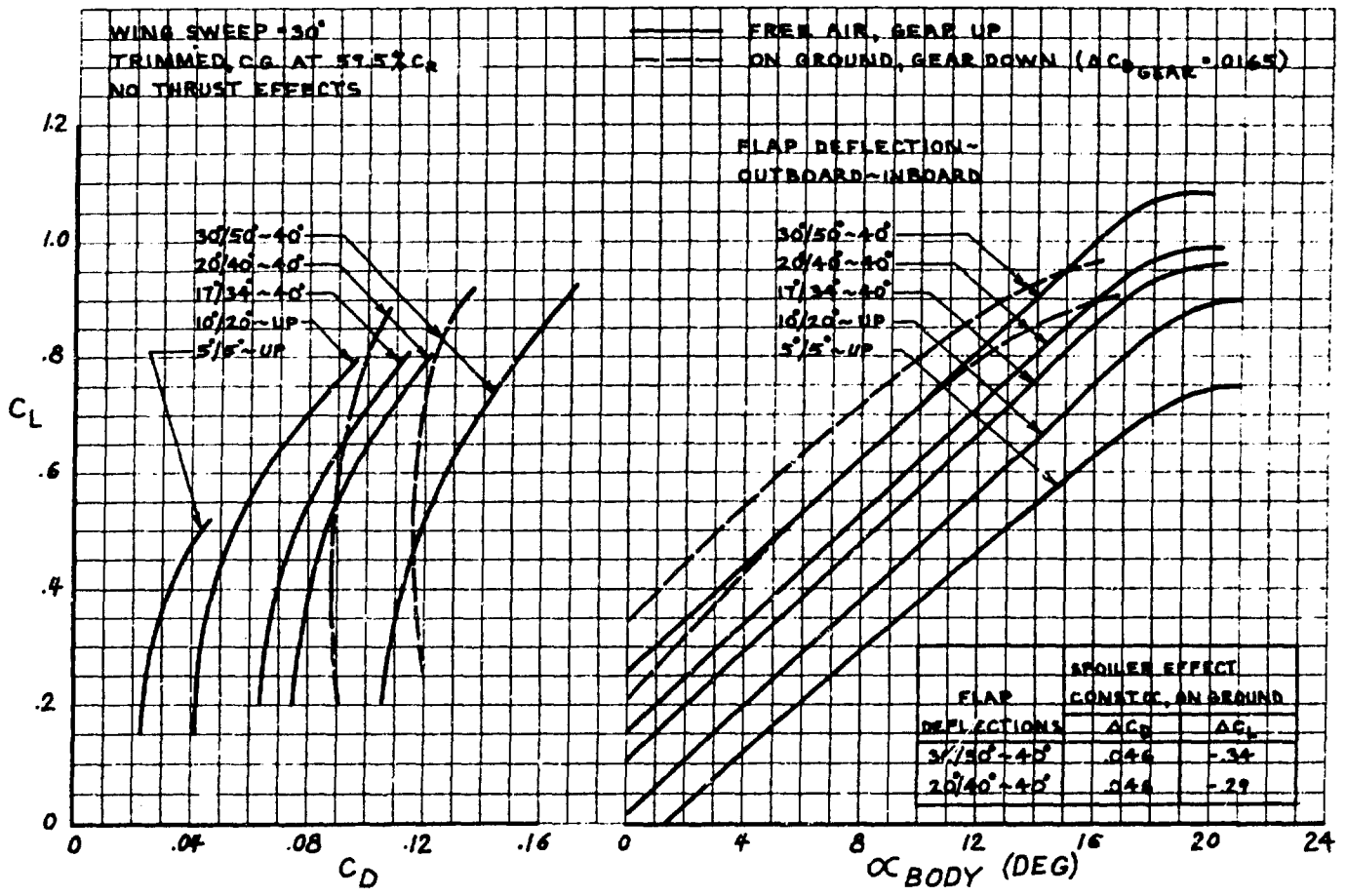


*Figure 3-54. B2707 Lift and Drag*

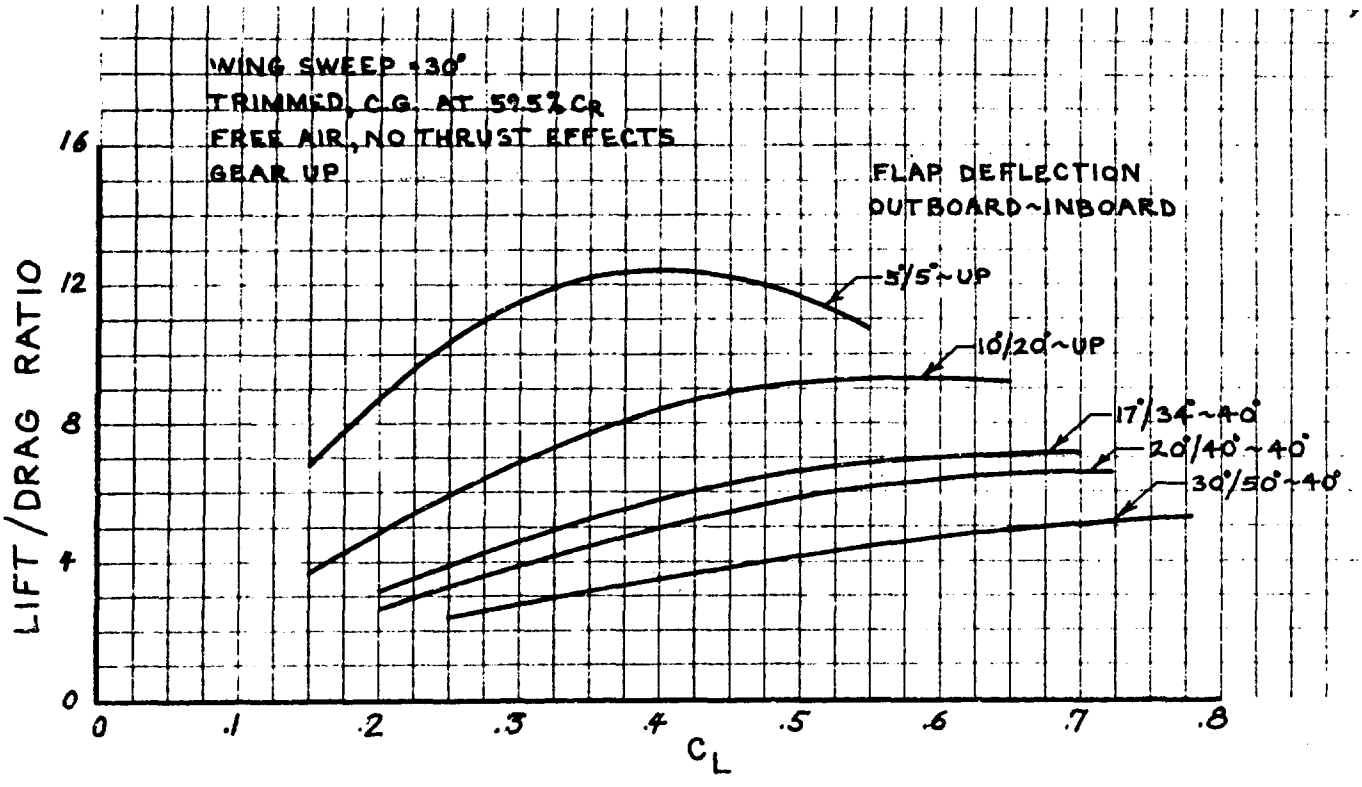


*Figure 3-55. B2707 Lift to Drag Ratio Curves*

of about 61.5 percent root chord, so the trades with varying cg location are illustrated for typical takeoff climb and landing approach angles of attack in Fig. 3-56.

Small friction drag differences between the GE and P&WA engine installations are within the accuracy to which the drag with flaps down can be determined, and have been ignored.

Thrust effects on lift and drag, which are not included in the graphical data are accounted for by solving for the lift coefficient in terms of angle of attack, normal load factor, and thrust to weight ratio, using equations shown in Fig. 3-57.

Table 3-X lists representative lift, drag, and angle of attack values used for takeoff and landing; these have been selected to provide adequate margins for controllability, maneuvering, gust encounters, inadvertent speed changes and abuse.

Stalling characteristics of the B-2707 in the takeoff and landing configurations will be similar to those of many jet airplanes now in service. The airplane characteristics will be entirely conventional. It will be possible to establish both the decelerating stall speed ($\frac{dv}{dt}$ = -1 kn/sec) used as reference in the current FAR regulations, and the 1-g load factor minimum speed under essentially steady state conditions. This latter will occur at the angle of attack for $C_{L_{Max}}$, about 20 degrees, and will be about 5 percent faster than the stall speed, as it is on present airplanes.

Because of the conventional angle of attack at which the minimum and stall speeds will be reached, the minimum demonstrated speed for operations in the sense of Ref. 23 will be the stall speed. In the discussions which follow, operating speeds are related to either the stall speed or the 1-g minimum speed as appropriate.

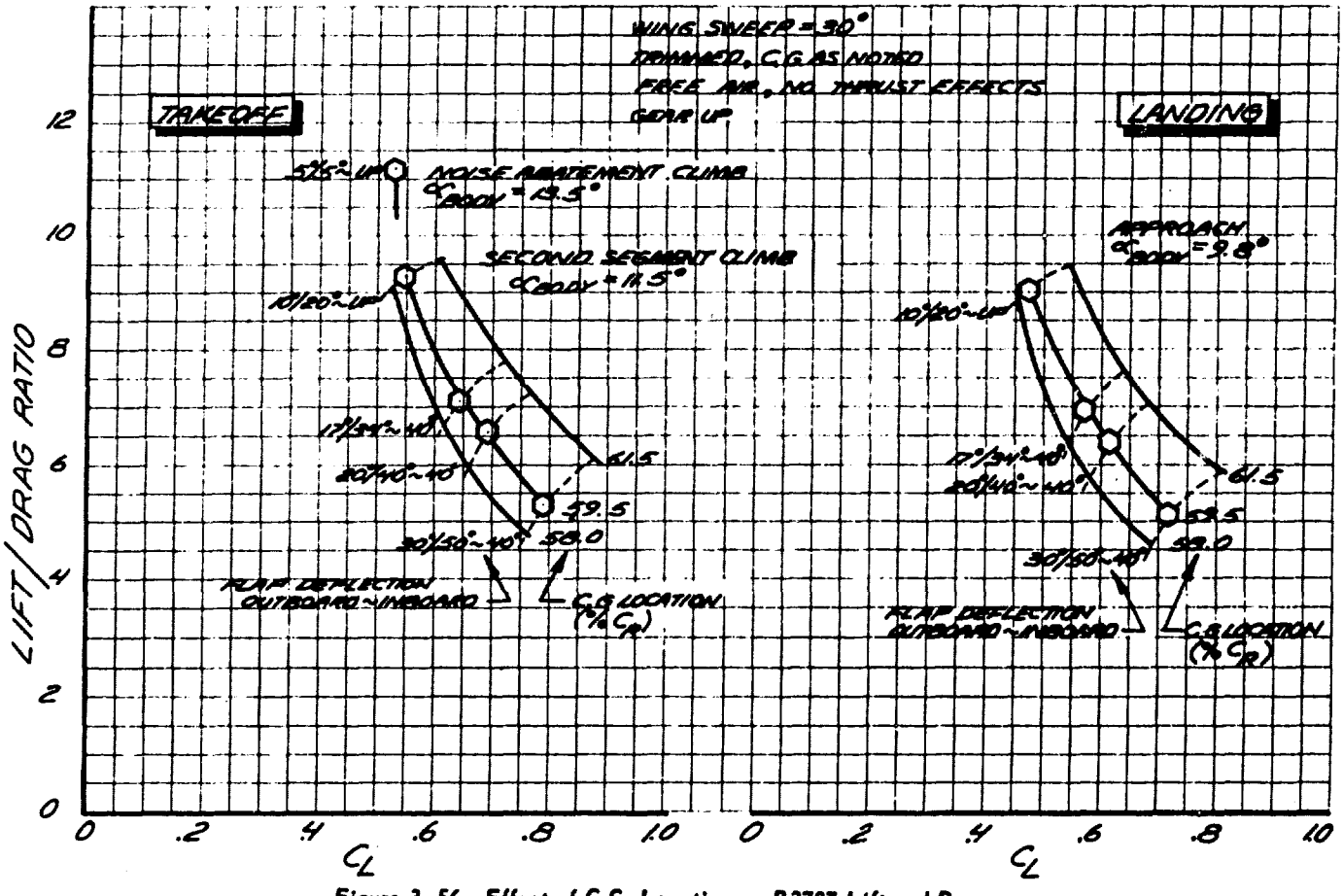


Figure 3-56. Effect of C.G. Location on B2707 Lift and Drag

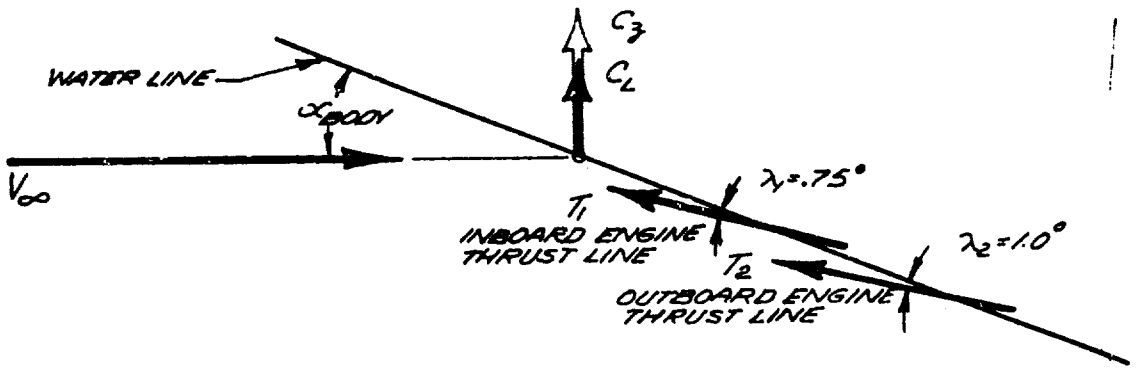


$$C_Z = C_L + \frac{T_1}{qS}\sin(\alpha_B - \lambda_1) + \frac{T_2}{qS}\sin(\alpha_B - \lambda_2)$$

ALSO

$$C_Z qS = nW$$

ELIMINATING $qS$

$$C_Z = C_L + C_Z\left[\frac{T_1}{nW}\sin(\alpha_B - \lambda_1) + \frac{T_2}{nW}\sin(\alpha_B - \lambda_2)\right]$$

FINALLY

$$\frac{C_Z}{C_L} = \frac{1}{\left[1 - \frac{T_1}{nW}\sin(\alpha_B - \lambda_1) - \frac{T_2}{nW}\sin(\alpha_B - \lambda_2)\right]}$$

EQUATION NEGLECTS;
(a) DIFFERENCE IN LINE OF ACTION OF INLET AND GROSS THRUST VECTORS. I.E. $T_1$ AND $T_2$ ARE NET THRUST VECTORS
(b) 1.1°(AVERAGE) TOE-IN OF THE GROSS THRUST AXIS IN THE PLANVIEW

WHERE
$C_L$ = LIFT COEFFICIENT = LIFT/$qS$
$T_1$ = NET THRUST VECTOR OF INBOARD ENGINES
$T_2$ = NET THRUST VECTOR OF OUTBOARD ENGINES
$\alpha_B$ = BODY ANGLE OF ATTACK
$\lambda_1$ AND $\lambda_2$ = INCLINATION OF THRUST AXES WITH REFERENCE TO WATER LINE
$n$ = NORMAL LOAD FACTOR
$W$ = AIRPLANE WEIGHT

FOR EQUILIBRIUM CONDITIONS, WINGS LEVEL

$$n = \cos\gamma + \frac{V\dot{\theta}}{g}, = 1 \text{ FOR LEVEL FLIGHT}$$

WHERE
$\gamma$ = FLIGHT PATH ANGLE
$\dot{\theta}$ = PITCH RATE
$g$ = ACCELERATION OF GRAVITY

Figure 3-57. Lift Coefficient with Thrust Effects

*Table 3-X. B2707 Takeoff and Landing Operation*

| Flight Condition | T/W | Flap Deflection Outboard ~ Inboard (Deg) | $\alpha$ Body (Deg) | $C_L$ No Thrust Effects | $C_D$ No Thrust Effects | $C_L$ Including Thrust Effects |
|---|---|---|---|---|---|---|
| Lift Off In ground effect Gear down | .308 * | 20/40 ~ 40 | 10 | .725 | .0945 | .76 |
| Approach Free Air Gear Down | —— | 20/40 ~ 40 | 9.8 | .615 | .1130 | —— |
| | | 30/50 ~ 40 | 9.8 | .710 | .1565 | —— |
| Touchdown In ground effect Gear down | —— | 20/40 ~ 40 | 8.4 | .650 | .0905 | —— |
| | | 30/50 ~ 40 | 8.4 | .750 | .1200 | —— |

* MAX. AUG. THRUST, SEA LEVEL ~ 86°F, TAKEOFF AT MAX. DESIGN TAXI WEIGHT, 675,000 LB.

3.2.2.2 Takeoff

The primary takeoff flap angle for most airports is 20/40 degrees. Larger and smaller deflections will be defined to meet unique airport requirements such as high-altitude airports, or runways where normal standards for field length and community noise require further optimization. In all cases a liftoff attitude of 10 degrees (body reference water line) is recommended. Liftoff speed for the maximum taxi weight of 675,000 lb is 169 kn estimated airspeed (EAS) using the primary flap setting.

Maximum pitch attitude, with gear oleos fully extended and the tail skid touching the runway is 11.5 degrees, so that an early rotation to tail skid contact will permit liftoff at about 96 percent of the normal speed. Rotation characteristics are described in Par. 4.1.1.1.

Table 3-Y shows some of the significant minimum operating margins achieved during takeoff for the chosen operating mode. Minimum requirements of the current Federal Aviation Regulations are shown in parentheses where applicable.

Figure 3-58 illustrates the takeoff operating speeds in more detail, showing their variation with thrust-to-weight ratio. Margins are equal to or greater than the current minima in all cases.

Airworthiness standards for application to supersonic transport operations are under continuous review, with the objective of ensuring satisfactory operating margins in all circumstances, together with a high degree of efficiency. Comparing the presently proposed operating margins with the current regulations is, therefore, largely a matter of convenience. Future changes may be made in operating procedures when found to be desirable.

3.2.2.3 Landing

The flap angle to be used for landing must be a compromise determined by the requirements for good visibility, low speed, and an acceptable noise level throughout the approach. Maximum flap deflection is 30/50 degrees.

*Table 3-Y. Minimum Operating Margins – Takeoff*

| OPERATING MARGIN | NORMAL LIFTOFF $\alpha_{BODY} = 10°$ | | MINIMUM LIFT OFF SPEED, $\alpha_{BODY} = 11.5°$ Tail Skid Contacting Runway | |
|---|---|---|---|---|
| | Ground Effect | Free Air | Ground Effect | Free Air |
| $\Delta\alpha$ to 1 "g" stall at $V_{LOF}$ | 6° | 10° | 4.5° | 8.5° |
| Increment in normal load factor to 1 "g" stall $\Delta n$ Minimum, liftoff to 35 ft | 0.28 | —— | 0.12 | —— |
| Increment in normal load factor to 1 "g" stall $\Delta n$ 2nd Segment climb | .35 (0.3 typical) | | | |
| $\frac{V_2}{V_{LOF}}$ Critical engine inoperative, most adverse loading | 1.043 | | | |
| $\frac{V_2}{V_{S_{F.A.R.}}}$ Critical engine inoperative, most adverse loading | 1.225 (1.2) | | | |
| $\frac{V_2}{V_{MIN\ LEVEL\ FLIGHT}}$ Critical engine inoperative, most adverse loading, gear extended | 1.21 | | | |

Values in Parentheses Result From Meeting Current F.A.R. Operating Minimums

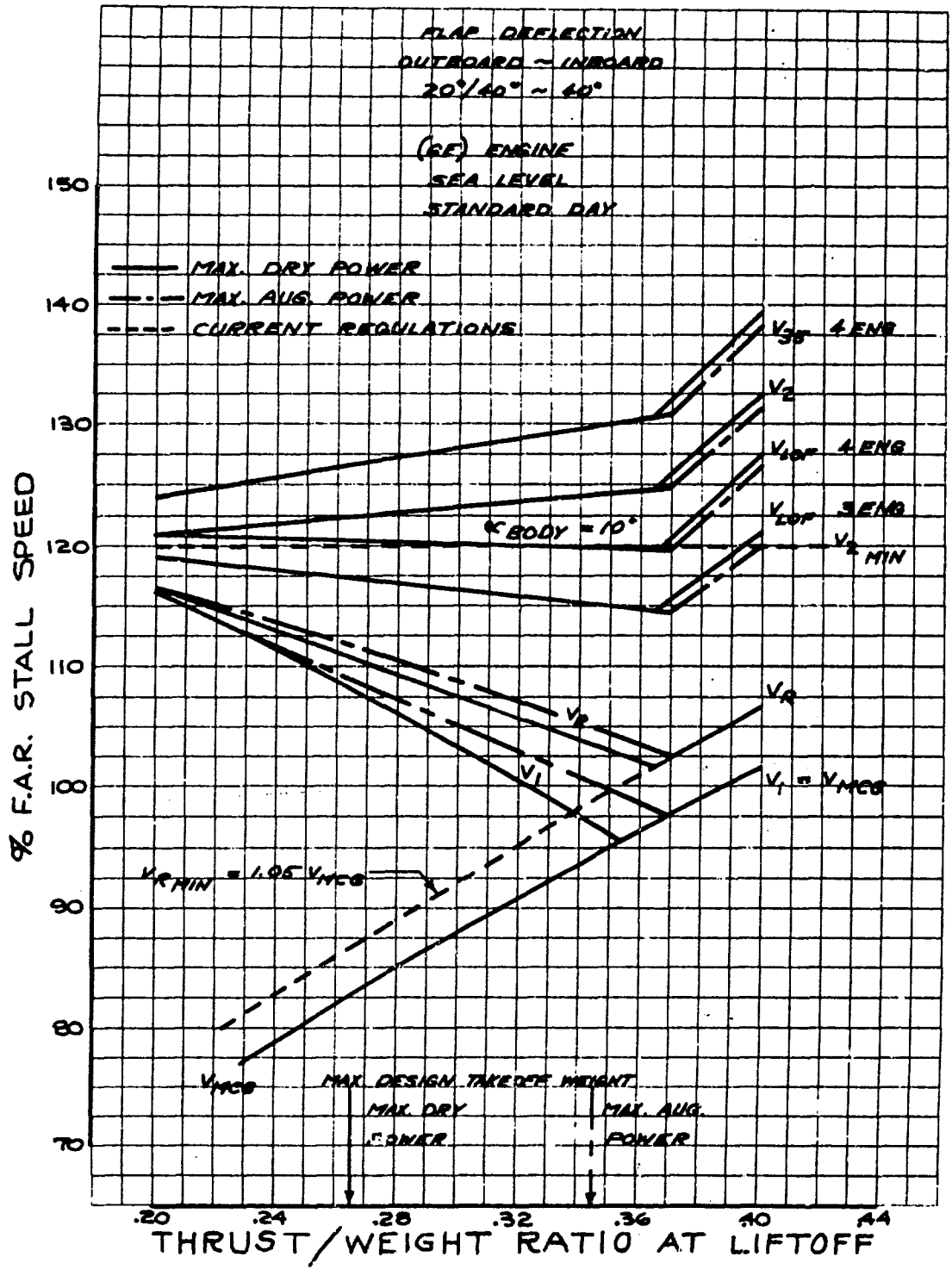


*Figure 3–58. Takeoff Speeds*

A representative approach condition is flaps 20/40 degrees, angle of attack 9.8 degrees measured to the reference body water line. (This gives a body attitude of 6.8 degrees nose up when descending with a 3-degree glide slope.) The approach speed will be 1.35 $V_{S_{FAR}}$, at a $C_L$ of 0.62 leaving a margin of 0.6-g incremental normal acceleration to the 1-g stall for maneuvering. Body attitude at landing will be about 8.4 degrees. Tail drag angle is 11.5 degrees, leaving a normal clearance of 3.1 degrees of pitch rotation (42 inches actual clearance to the tail skid).

3.2.2.4 Landing With 72-Degrees Wing Sweep
In low speed flight at 72 degrees of wing sweep, the inboard wing portion leading edge slat (the strake slat) will be deflected 25 degrees down. This provides satisfactory pitch stability with an aft cg limit of 64 percent root chord. The wing high lift flaps cannot be used at this sweep angle.

Trimmed lift and drag curves are shown Fig. 3-59 for a representative cg position of 62 percent $C_R$.

An approach speed of 205 kn has been recommended to ensure good handling characteristics. This results in an approach attitude of 9 degrees at 350,000 lb weight, using a 3-degree glide slope. Body attitude at touchdown will be just over 10 degrees.

Future improvements in control and stability characteristics could permit the approach speed to be reduced to about 185 kn with a body attitude of 10.5 degrees. Touchdown would then be about 176 kn at 11.5 degrees body attitude, the tail skid scrape angle.

3.2.3 Wind Tunnel Tests and Results
The test data used to derive preliminary estimates of takeoff and landing performance were obtained on a 0.0371 scale model, closely simulating the proposal configuration in all important respects except wing twist. Tests were made in the University of Washington Aeronautical Laboratory 8- by 12-ft wind tunnel, at a Reynolds number of $4.87 \times 10^6$, based on the model root chord reference length. Photographs of the model are shown in Figs. 3-60 and 3-61.

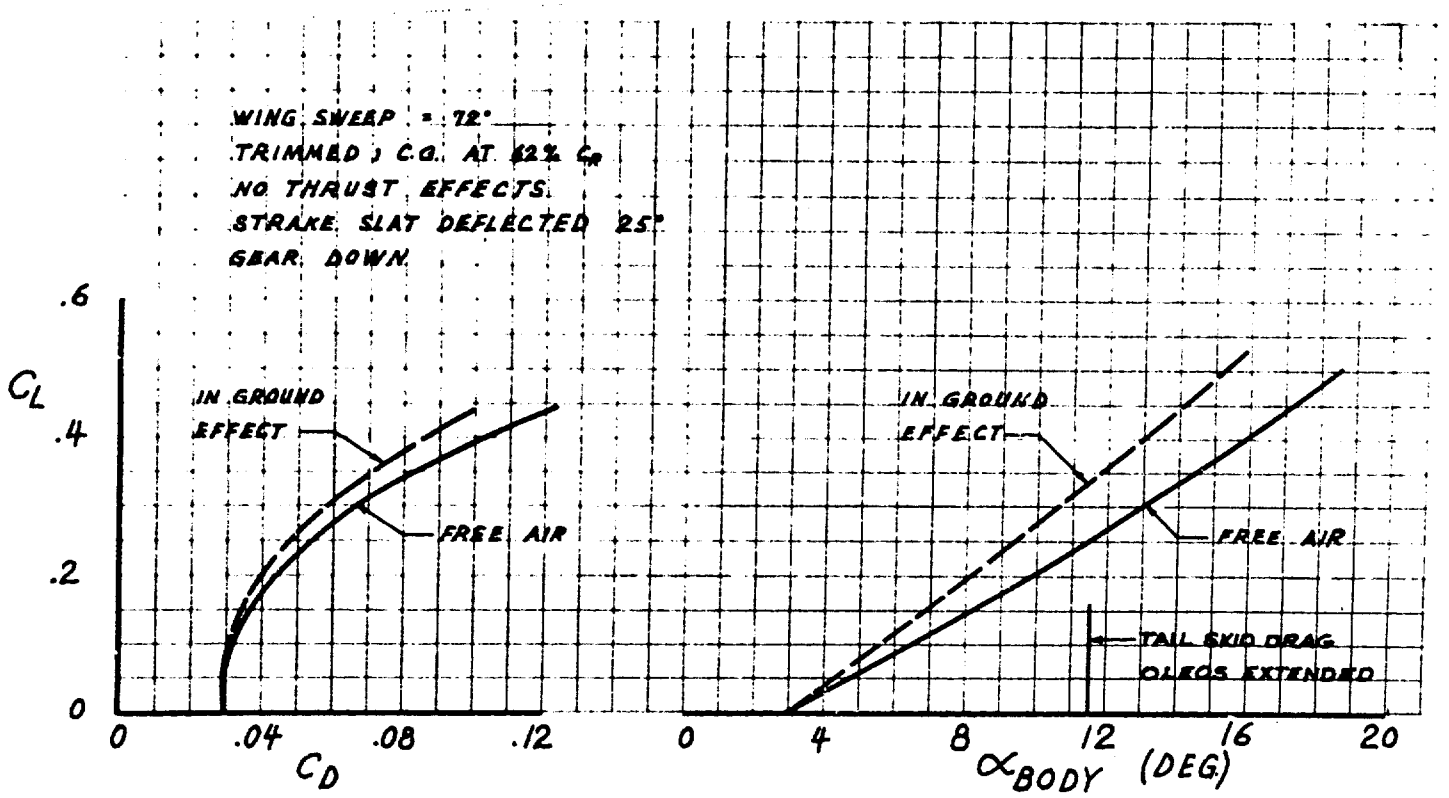


*Figure 3-59. Lift and Drag for Landing, Wing Sweep 72 Degrees*

TAKEOFF CONFIGURATION

WING SWEEP 72°

*Figure 3–60. Low Speed Wind Tunnel Model*

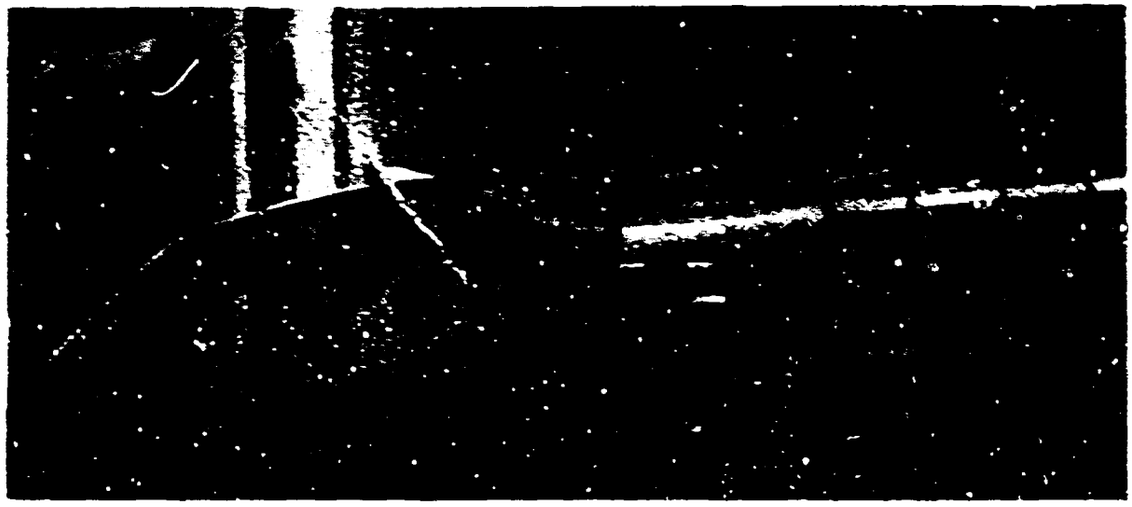

CLOSEUP OF LEADING
EDGE SLATS

*Figure 3-61. Low Speed Wind Tunnel Model*

A new low-speed wind tunnel aeroelastic development model of the 2707-300 has been constructed. It will be submitted to the FAA for evaluation testing in the NASA. A matching program using this and other models will be used to explore configuration refinements. A photograph of the FAA evaluation model is Fig. 3-62.

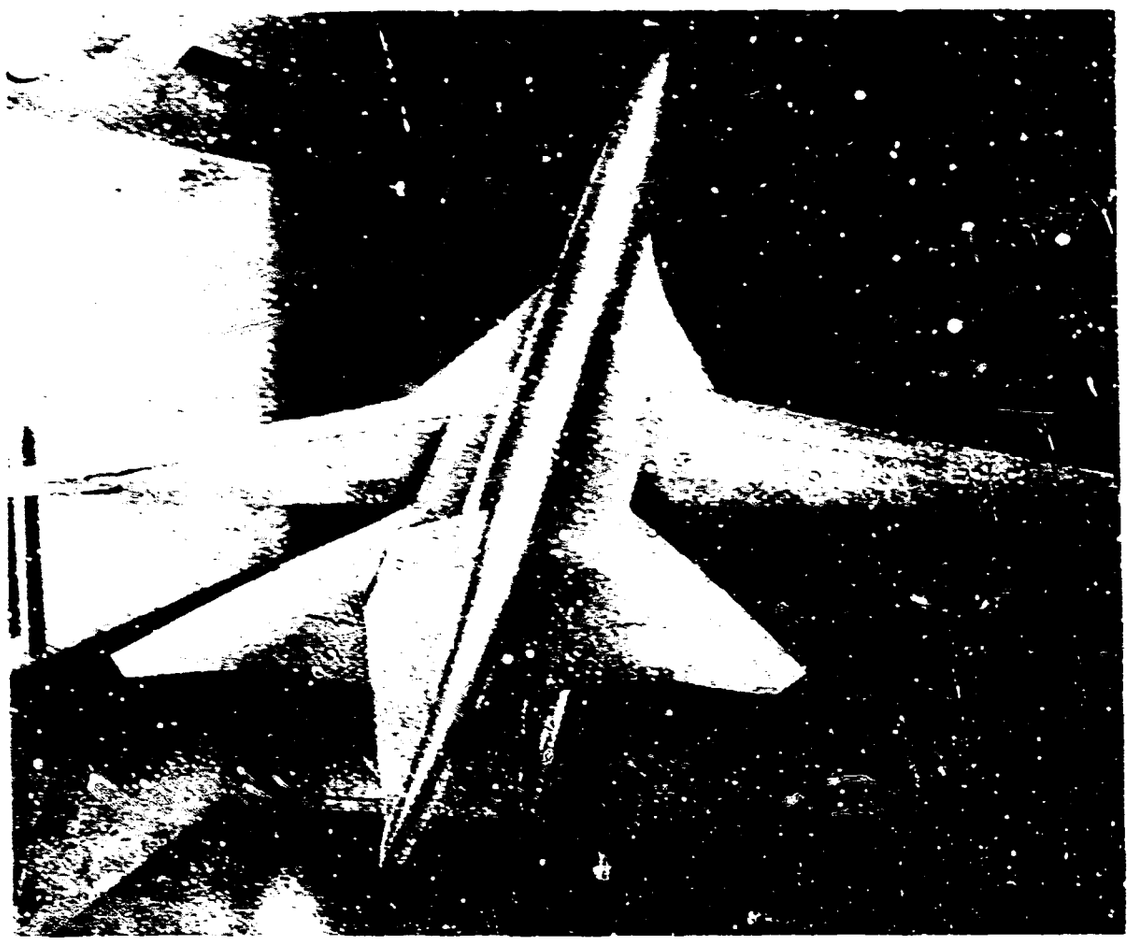

*Figure 3-62. FAA Evaluation Model*

The preliminary model twist distribution resulted from an adaption of a 733-390 model to the new configuration, expediting development testing. Lifting surface theory has been used to estimate corrections for the wing twist differences. These corrections have been applied to the test data, making it representative of the proposal airplane, and are as follows:

$$\Delta\alpha_{BODY} = -2.87°$$

$$\Delta C_M = -0.0085$$

$$\Delta\alpha_{Tail} = -1° \text{ per } C_L$$

All these are applicable with tail off, at 30-degrees wing sweep, and corresponding corrections have been added to data obtained with tail on. Drag values have been further adjusted by $\Delta C_D = -0.0116$, allowing for mounting tares and Reynolds effect on skin friction.

Test data, including these adjustments, are shown in Fig. 3-62 (with tail off) and Fig. 3-64 (tail on) for a range of wing flap angles. Moment data is given in Fig. 3-63.

Model data used to analyze landings with 72-degrees wing sweep, shown in Fig. 3-66, are taken from tests in the Boeing Transonic Wind Tunnel. The model has a representative wing twist distribution, but the data have been corrected for wing incidence setting on the body and for tare and Reynolds effect on drag:

$$\Delta\alpha_{BODY} = -0.5°$$

$$\Delta C_D = -0.0020$$

Trimmed lift and drag curves for landing at 72-degree wing sweep, shown in Fig. 3-59 were derived from further tests with the elevator angle varying. Trimmed performance curves

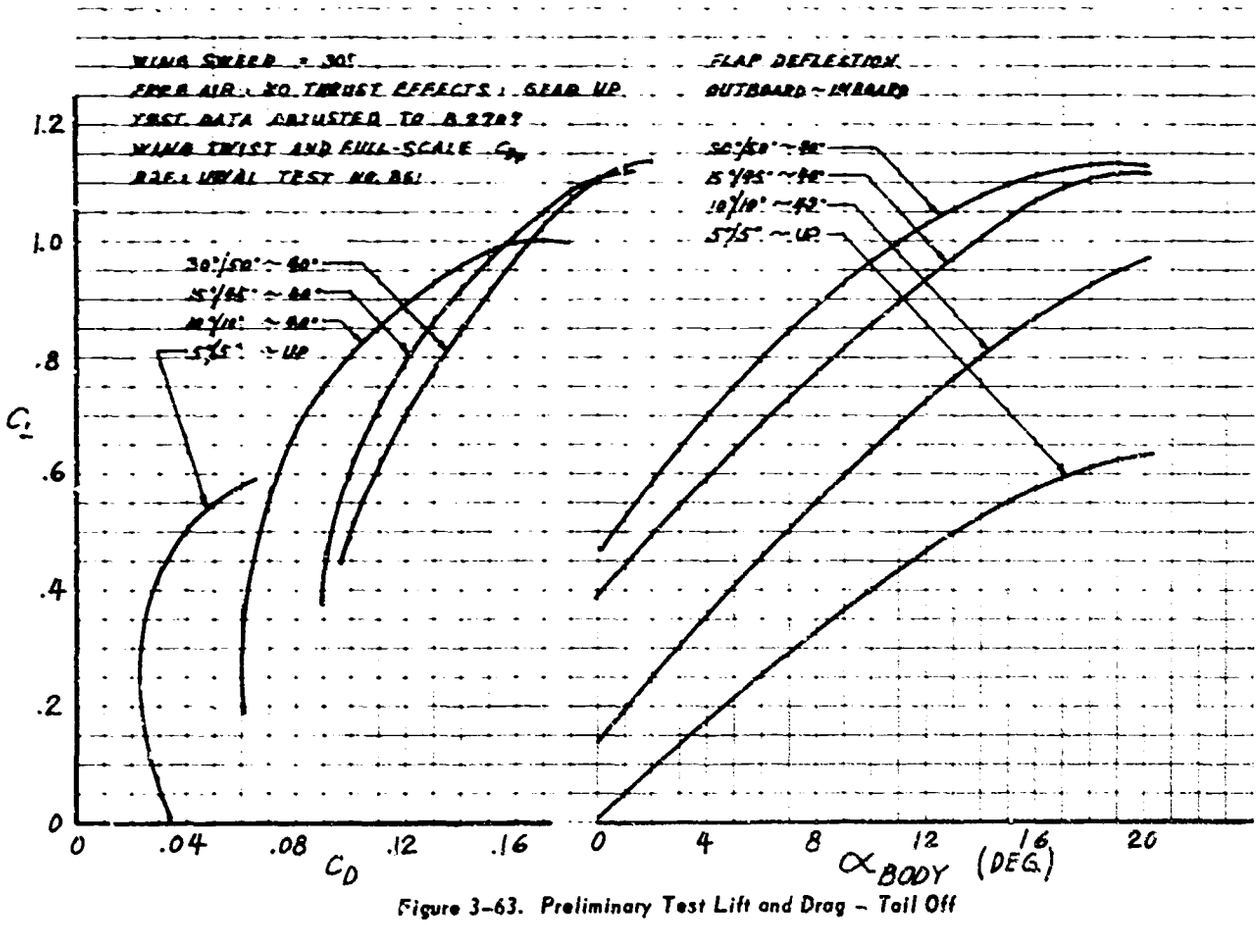


Figure 3-63. Preliminary Test Lift and Drag – Tail Off

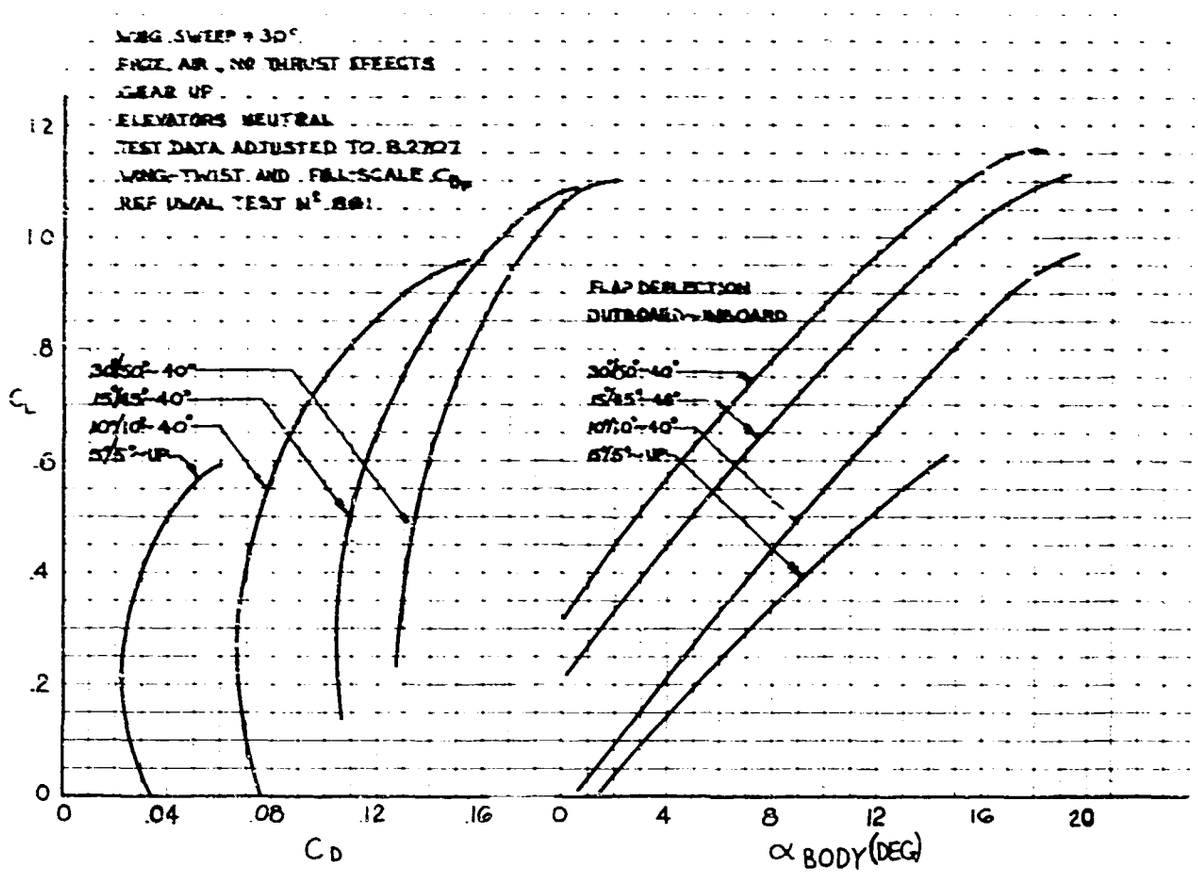


*Figure 3-64. Preliminary Test Lift and Drag – Tail On*

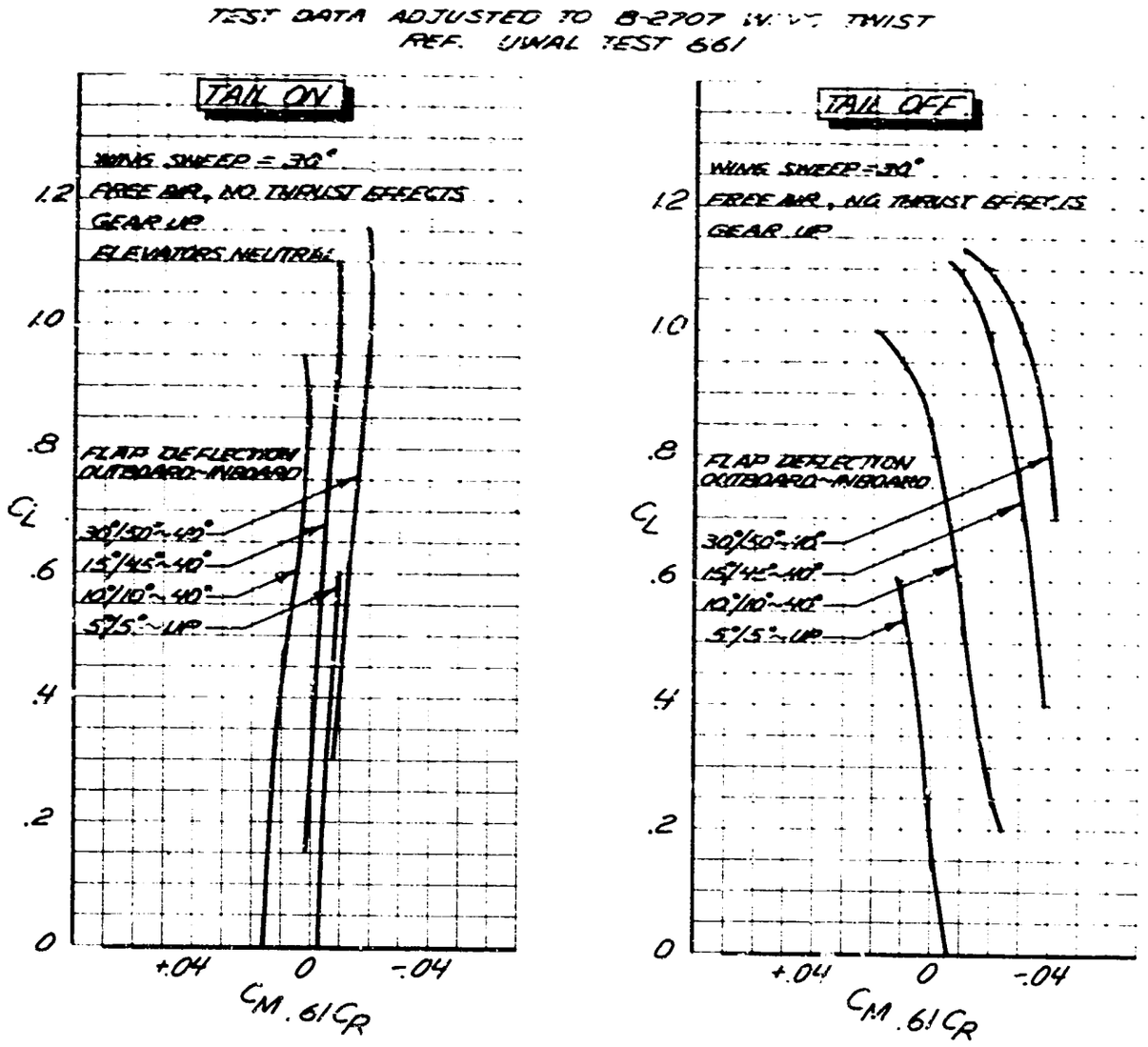


Figure 3-65. Preliminary Test Pitching Moments

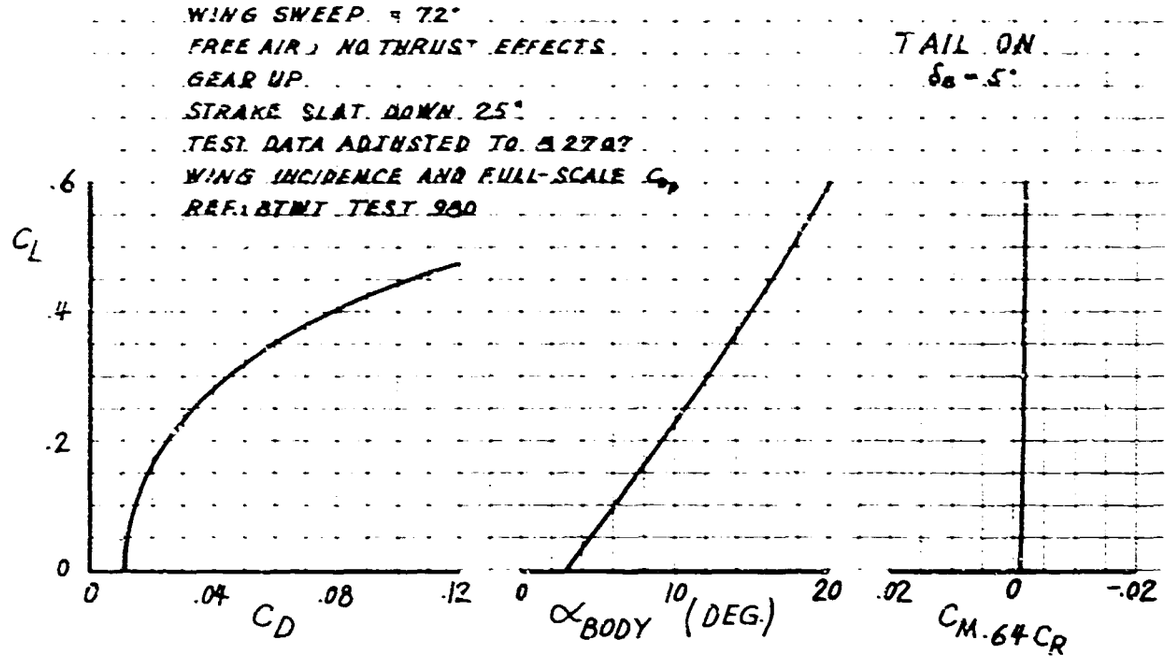


*Figure 3-66. Wind Tunnel Data, Wing Sweep 72 Degrees*

for 30-degree wing sweep were also derived, and are shown for the takeoff and landing forward center-of-gravity limits in Figs. 3-67 and 3-68. An analysis of the lift and drag increments for trim is made in Par. 3.2.5 to define the configuration features that are amenable to refinement. The performance levels of the B-2707 airplane include the effects of such refinements.

3.2.4 Aeroelastic and Scale Corrections

3.2.4.1 Lift

Previous proposal documents used empirical corrections to lift in developing full-scale airplane characteristics from small-scale model test data. This use is justified because of the basic similarity between the SST and present day jet transports in the takeoff and landing configurations. The so called scale effects established empirically are, in fact, the sum of two effects:

a. Viscous effects on lift slope due to the large difference between model and flight Reynolds numbers.

b. Wing, flap, and control surface deflections relative to the test model geometry, varying with the airloads applied to the airplane, and affecting the lift at any given angle of attack.

The airplane lift slope, at 1-g flight conditions, is increased by the corrections for these effects. The flap and control installations are designed to eliminate adverse blow back effects on lift for the chosen design condition.

Pending completion of aeroelastic design studies on the B-2707 (see Par. 3.3), the empirically derived 7-percent factor on lift slope and $C_{L_{MAX}}$ (Phase I Proposal, Par. C6.2.5 Volume A-V, D6-2400-11) gives a good indication of the probable effect. Figure 3-69 shows the estimated scale and aeroelastic effects on rigid model data for a representative flap angle. The most significant scale effect is that on the maximum lift coefficient, which is the only one included in the present estimates of the B-2707 airplane performance.

3.2.4.2 Drag

Full-scale airplane drag is estimated by the buildup technique explained in Par. 3.1.2. Table 3-Z shows the drag elements for a rep-

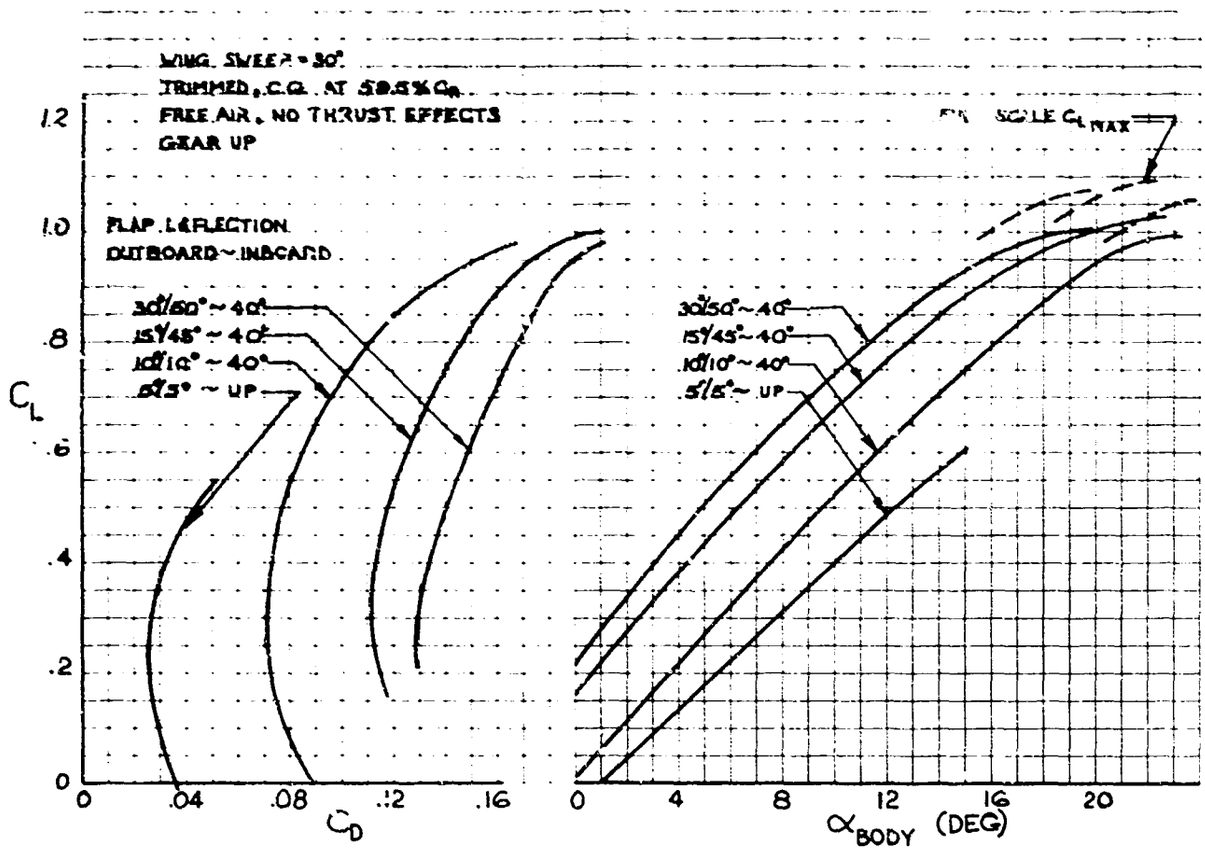


*Figure 3-67. B2707 Performance-Current Status, C. G. at 59.5% $C_R$*

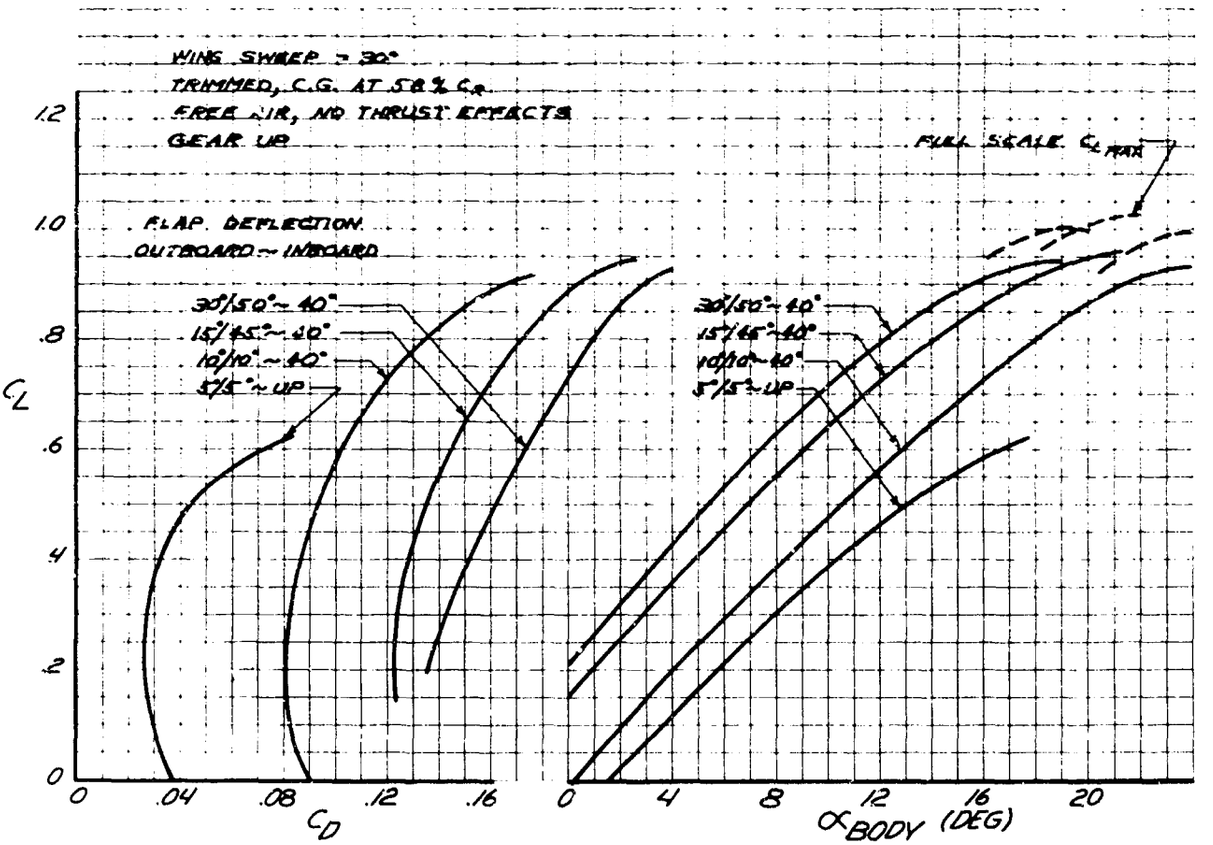


Figure 3-68. B2707 Performance–Current Status, C. G. at 58% $C_R$

resentative low-speed flight condition for the clean airplane. Small differences are apparent in the drags with the GE and the P&WA engines.

The tare and scale correction to wind-tunnel model drag values, $\Delta C_D$ of the previous section, was the difference between the model $C_{D_{MIN}}$ and the estimated full-scale value.

3.2.5 Analysis of Performance

A highly effective double slotted wing flap system has been adopted for the airplane, with leading edge slats for stall control. These high lift devices have been developed by wind-tunnel testing at Boeing and at the NASA. The triple-slotted inboard flap is of similar design to that of the 727 airplane.

Analysis of model test data to date reveals certain areas for potential improvement in the trimmed lift and drag, especially at the forward cg. The pitch trim system is the key to better performance. The data points to two factors susceptible to improvement by refinements in design:

a. An interference between the closely-coupled wing and tail, giving a small effective tail arm for trimming the wing body pitching moments.

b. High tail drags, indicating near zero leading edge suction on the tail; this feature is sensitive to Reynolds number as well as tail section geometry.

3.2.5.1 Effective Tail Arm and Trim Lift Loss

With a conventional small tail set well behind the wing, the tail lift force which trims the airplane in pitch has a center of pressure at, or slightly behind, the tail quarter chord point. For a large tail like that of the B-2707, the center of lift depends upon the spanwise loading, which in turn is determined by the wing downwash distribution, the dynamic pressure distribution, and the tail twist. Since the tail is a low aspect ratio surface, and because the trimming is accomplished by elevators and elevons, the design goal is to place the point of action of the trim lift to be behind the tail quarter chord point. Preliminary testing shows that the tail lift is centered forward of this point, as shown in Fig. 3-70. From this it can be surmised that much of the download induced on the tail from the wing downwash field, is inboard, near the body and consequently centered well forward. The wing chordwise loadings might also be affected by the close-coupled tail.

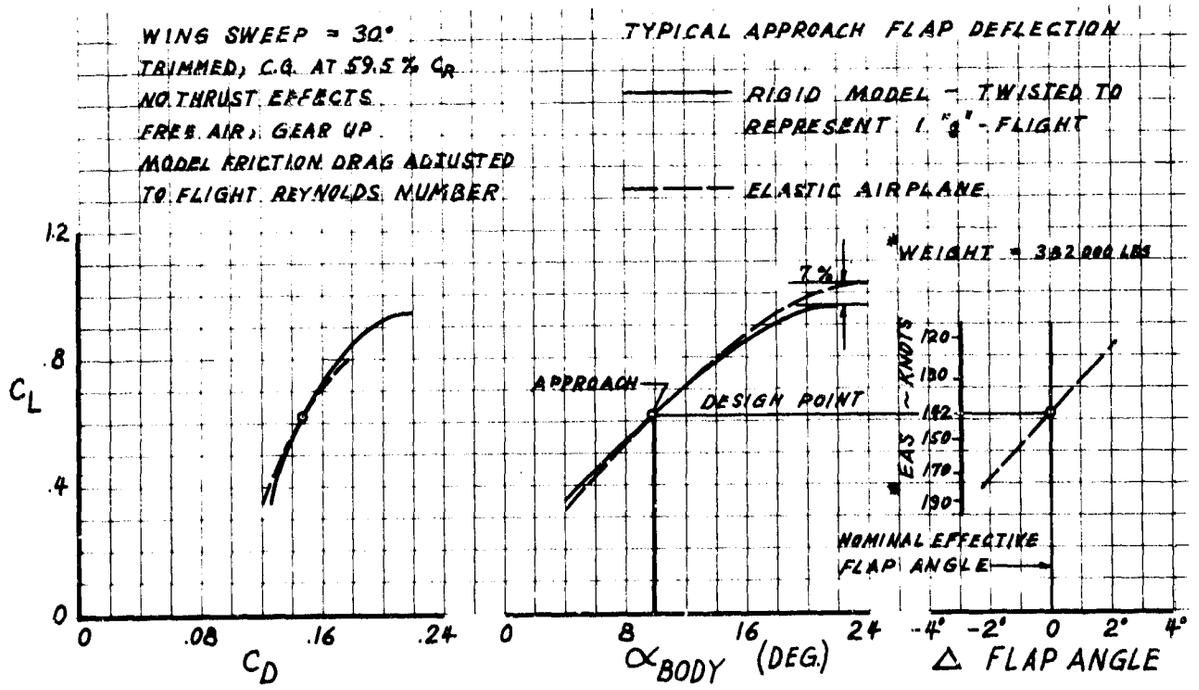


Figure 3-69. Typical Scale Effects

*Table 3-Z. Airplane Minimum Parasite Drag*

($\Lambda$=30°, $S_{ref}$ = 9000 ft$^2$)

AVERAGE TAKEOFF AND LANDING FLIGHT CONDITION

V= 150 Kn, Sea Level, Re/Foot = 1.5x10$^6$
Flaps and Slats Up

| ITEM | WETTED AREA (Ft$^2$) | | $\lambda C_f$ | | $\Lambda f$ (Ft$^2$) | |
|---|---|---|---|---|---|---|
| BODY | 9885 | | .00178 | | 17.60 | |
| WING | 12800 | | .00254 | | 32.50 | |
| HORIZ. TAIL | 3085 | | .00259 | | 8.00 | |
| VERT. TAIL | 1890 | | .00249 | | 4.70 | |
| VENTRAL | 355 | | .00245 | | 0.87 | |
| SURFACE GAPS | | | | | 5.96 | |
| INTERFERENCE | | | | | 4.98 | |
| MISCELLANEOUS | | | | | 3.87 | |
| ENGINE | (GE) | (P&WA) | (GE) | (P&WA) | (GE) | (P&WA) |
| NACELLES | 2700 | 2300 | .00229 | .00233 | 6.18 | 5.36 |
| FENCES | 226 | 276 | .00245 | .00238 | 0.55 | 0.66 |
| TOTAL | 31,018 | 30,668 | | | 85.20 | 84.50 |
| | | | $C_{D_{P_{MIN}}}$ = | | .00947 | .00939 |

Figure 3-70 shows:

a. The tail lift center of pressure range determined experimentally, the quarter MAC and pitch-trim load centers of pressure estimated for a flat surface in a uniform stream.

b. Actual effective value of tail arm ratio $\frac{C_R}{l_t}$ for several flap angles. This quantity is defined by the approximation

$$\Delta C_{L_{\text{to trim}}} = C_{M_{\text{to be trimmed}}} X \left(\frac{C_R}{l_t}\right)$$

c. Numerical values of the trimming lift loss as a function of wing flap angle.

It is concluded that the lift loss in trimming the wing pitching moments is unexpectedly large in the current configuration data. This may be reduced considerably by design refinements. An aerodynamic development program described in Par. 3.4.2 is underway to study means of improving trim lift and drag. Some refinements that appear likely to increase the effective tail arm are:

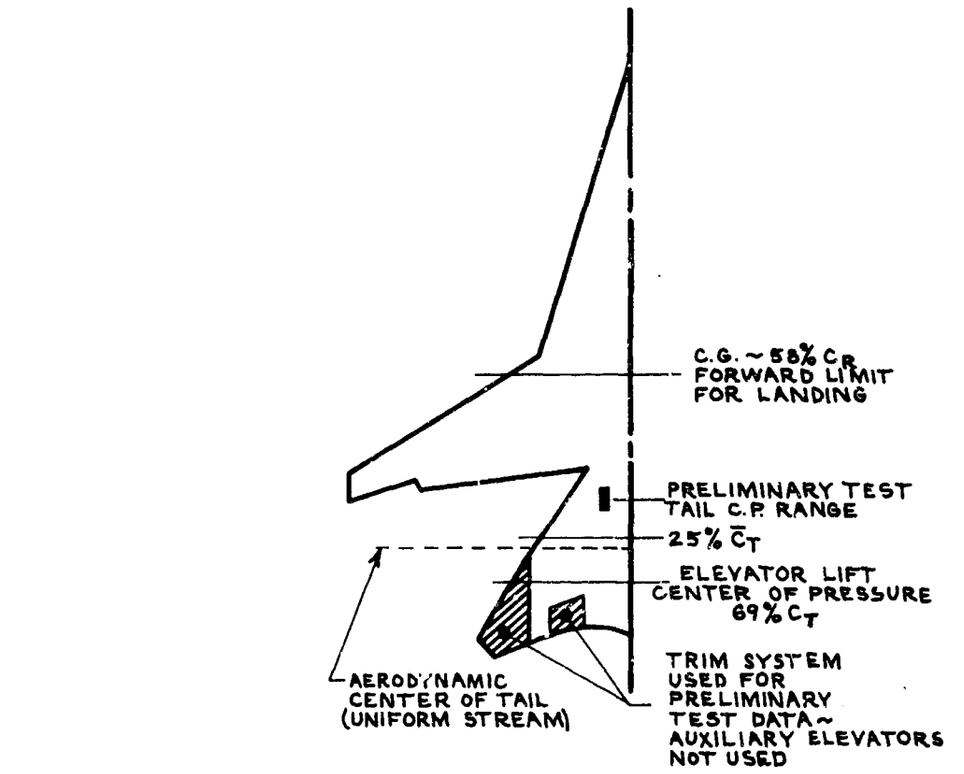


PRELIMINARY WIND TUNNEL TEST DATA

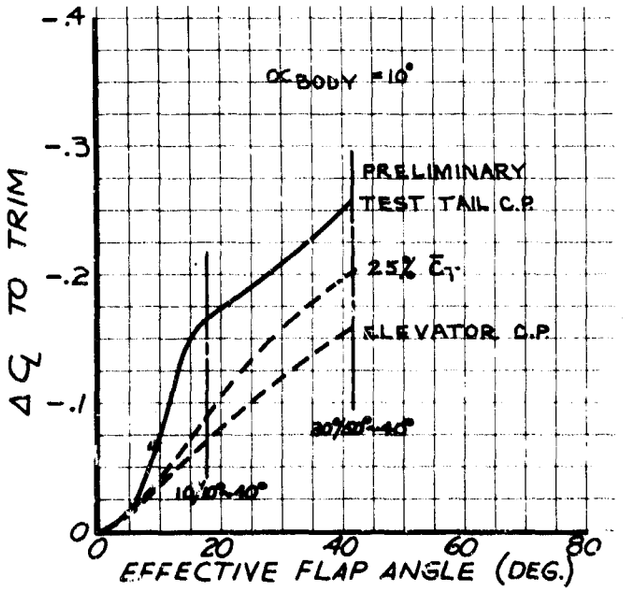


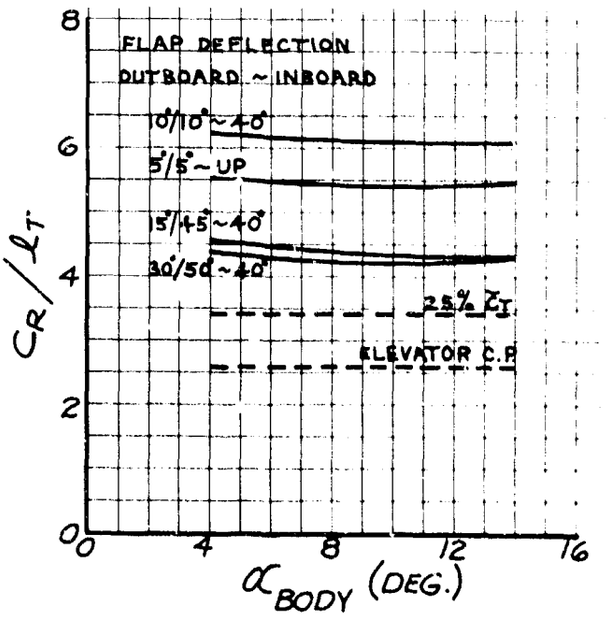


*Figure 3-70. Trim Lift and Tail Center of Pressure*

a. Changing the relative main flap and aft flap deflection angles, thus changing the downwash and wake characteristics.

b. Spanwise grading of the flap angles.

c. Nose camber (leading edge up) in the tail.

d. More trailing edge reflex in the tail.

e. Increased washout toward the tail tips.

It is necessary to reconcile any geometry changes to the tail with the requirements for wing-to-tail closure and efficient supersonic and subsonic cruise; nevertheless, it is believed that much may be done to improve the tail efficiency during takeoff and landing. Figure 3-73 shows large potential performance gains.

3.2.5.2 Tail Drag

Tail on and tail off data have been analyzed using the equations shown in Fig. 3-71 to determine the mean downwash angles, tail lift, and tail drag relationships, which are shown in Fig. 3-72. Tail lift and drag in this figure are referred to the wing reference area, 9,000 sq ft, for convenience. These quantities may be multiplied by 3.63 to refer them to the exposed tail area of 2,478 sq ft. The downwash at the tail is practically independent of flap angle when plotted against wing lift coefficient. The tail lift and drag curves vary in normal fashion with pitch control angle $\delta_e$, the deflection of the elevator and elevon surfaces. Reference to the plot of $C_{D\ tail}$ against $(C_L)^2$ tail, on which lines of $\frac{(C_L)^2}{\pi AF}$ and $\frac{(C_L)^2}{C_{L_\alpha}}$ have been drawn representing full leading edge suction and zero suction respectively, shows that very little suction is being realized.

The apparent leading edge suction force on the tail surface is, of course, related to the lift distribution on the tail, and it is doubtful if the ideal value could ever be realized, even with optimum

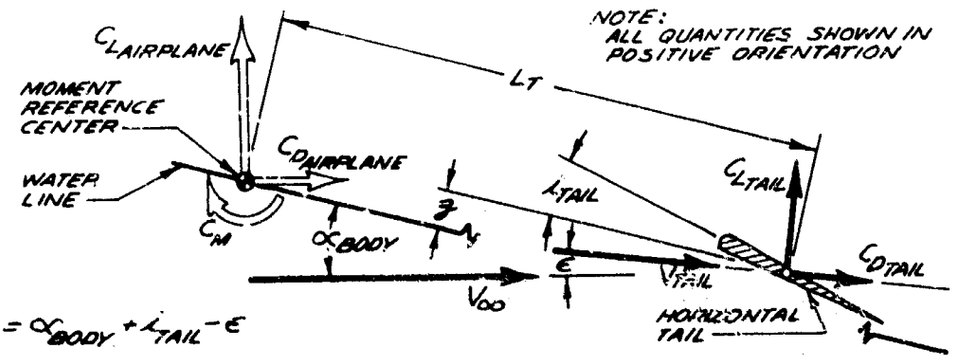


- $\alpha_{TAIL} = \alpha_{BODY} + i_{TAIL} - \epsilon$
- $\Delta C_{L_{AIRPLANE\ DUE\ TO\ TAIL\ INPUT}} = C_{L_{TAIL}} \cos\epsilon - C_{D_{TAIL}} \sin\epsilon$
- $\Delta C_{D_{AIRPLANE\ DUE\ TO\ TAIL\ INPUT}} = C_{L_{TAIL}} \sin\epsilon + C_{D_{TAIL}} \cos\epsilon$
- $\Delta C_{M_{INPUT\ BY\ TAIL}} = -\ell_T/c_R \left( C_{L_{TAIL}} \cos\phi + C_{D_{TAIL}} \sin\phi \right) + z/c_R \left( -C_{L_{TAIL}} \sin\phi + C_{D_{TAIL}} \cos\phi \right)$

WHERE $\phi = \alpha_{BODY} - \epsilon$

NOTE: TAIL COEFFICIENTS ARE REFERRED TO WING REFERENCE AREA, 9000 FT$^2$

Figure 3-71. Horizontal Tail Force and Moment Equations

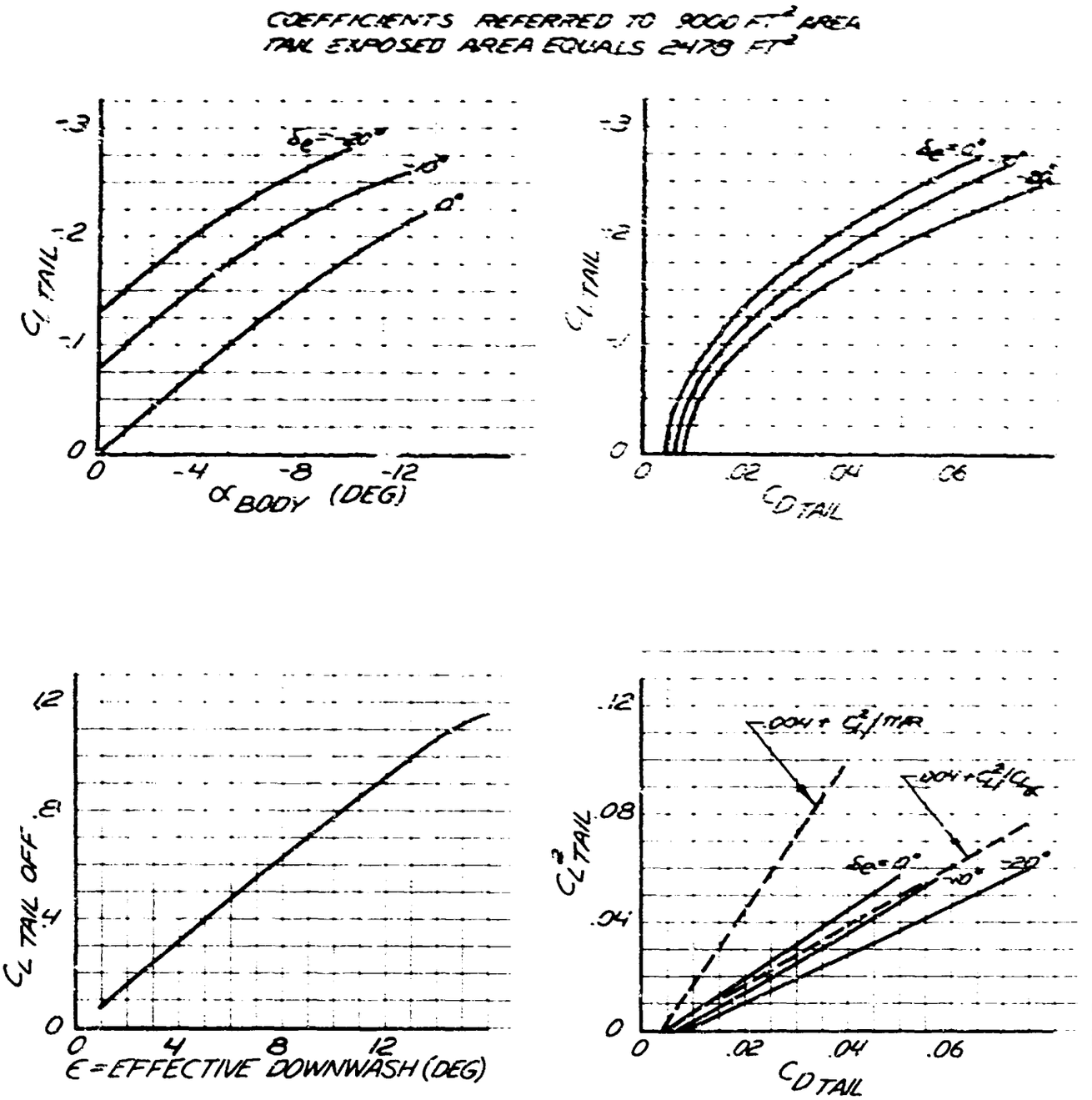


*Figure 3-72. Model Tail Lift and Drag Characteristics*

section geometry. However, two factors hold promise for improved values at full scale on a refined version of the airplane. These are:

a. Leading edge suction force improves sharply on swept wings having rounded leading edges as Reynolds number is increased. This has been proved by NASA tests. (See Ref. 20.) The model test Reynolds number was below the critical value defined in that reference. The same paper also shows considerable drag reductions from judicious use of twist and leading edge camber. A design goal of 40 percent theoretical suction appears reasonable.

b. The wing tail design study discussed in Par. 3.4.2 will show where the greatest drag benefits accrue from appropriate local section changes; a larger effective tail arm, once realized, ensures large reductions in tail drag by reducing tail lift and trim control deflections required.

3.2.6 Effects of Tail Refinements

Figure 3-73 illustrates potential low-speed performance improvement from refinements to the horizontal stabilizer and pitch trim system design. It shows airplane lift and drag effects from moving the effective tail trim force center of pressure aft. The illustration is for one flap angle and one angle of attack for clarity; similar improvements occur for other conditions. Effects are shown for two tail center-of-pressure positions:

a. At the exposed tail quarter mean aerodynamic chord, believed to be readily attainable.

b. At 69 percent of the tail mean aerodynamic chord, a position which pertains if all the trim force is generated by the elevator and moving tip.

3.2.7 Influence of cg Position and of cg Margin
Trimmed lift and drag are directly influenced by fore and aft location of the airplane center of gravity. The best usable performance is obtained when the center of gravity is as far aft as airplane handling considerations will allow.

The variable-sweep wing offers another means to control the cg margin. If wing sweep programming is carefully correlated with airplane load distribution, it is possible to ensure takeoff and landing operations with small cg margins under all conditions.

The effects of cg position on L/D ratio and $C_L$ are shown in Fig. 3-74 for a 10-degree angle of attack, representative of takeoff and landing operations. If the cg margin is controlled by reducing wing sweep angle, the performance gains will be somewhat increased because of the increased wing span.

Figure 3-75 summarizes the performance for all flap deflections, as affected by cg margin and effective tail arm. This shows the tremendous performance potential of the B-2707 airplane configuration, and supports the input lift and drag levels used to estimate production airplane takeoff and landing performance.

3.3 AEROELASTIC ANALYSIS METHODS
Careful consideration has been given to aeroelastic effects in the development of the B-2707 configuration. Extensive analyses, trade studies, and experimental programs have supported the design. While the aeroelastic effects are very important, none has been found to pose a serious problem; however, it is essential that the effects can be accurately calculated. Having this capability, aeroelasticity becomes a routine design consideration.

The calculations principally are made to:

a. Determine aeroelastic effects on the lift, drag, stability, and control characteristics of the airplane.

b. Define a manufacturing jig shape for the structure such that the desired flight shape is attained while the airplane deflects under normal flight loads.

c. Determine flexibility corrections to the rigid model wind-tunnel test data.

In the paragraphs following, analytical and experimental methods are discussed and some typical test data presented. Specific, detailed flexibility effects on the B-2707 lift, drag, stability, and control characteristics are found in Par. 3.1 and Sec. 4.

3.3.1 Analytical Methods
Aeroelastic deflections and resulting incremental air loads are caused by aerodynamic and inertia (including gravity) loads on the airplane. Schematic loading situation is shown in Fig. 3-76.

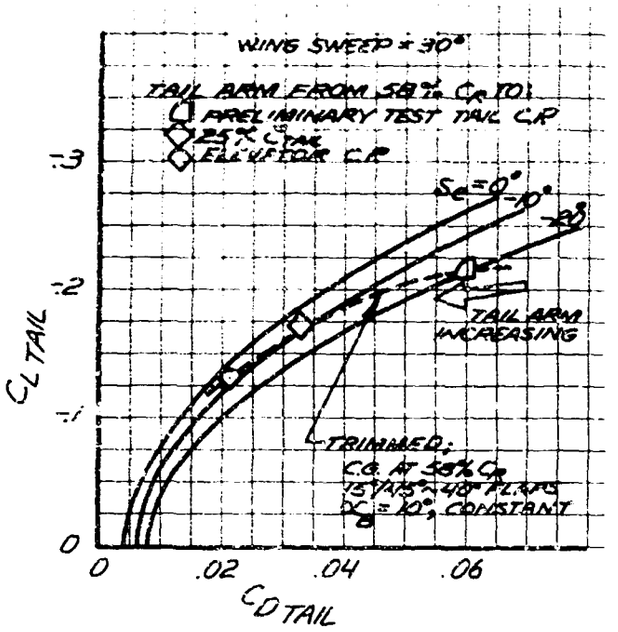


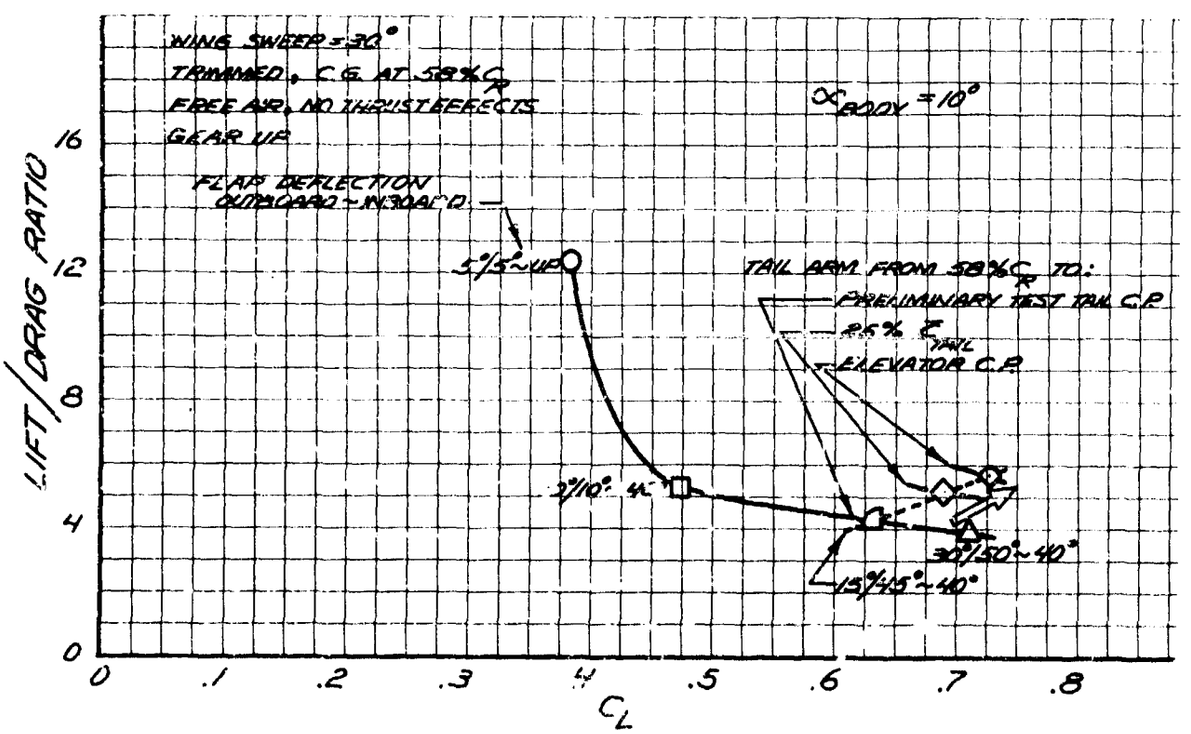


*Figure 3-73. Tail Arm Effect on Lift and Drag*

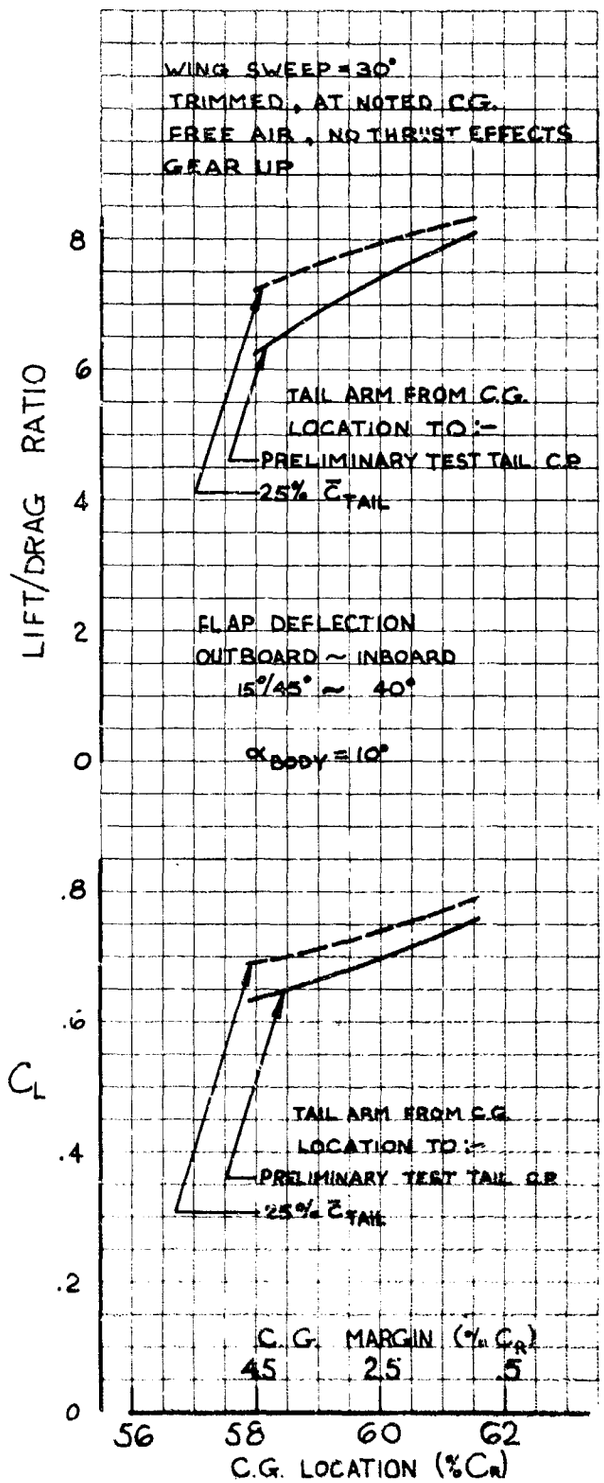


*Figure 3-74. C. G. Effect on Lift and Drag*

The overall flexibility effects depend on the structural stiffness and on the magnitude and distribution of loads over the complete airplane. For illustrative purposes it is convenient to think of the total aeroelastic effect as the sum of effects of each airplane component: forebody, aftbody, wing, and tail.

Consider the forebody deflections as indicated in Fig. 3-77. Air loads tend to bend the forebody upward, increasing its angle of attack and lift by an incremental amount. On the other hand, inertia loads tend to bend the forebody downward, decreasing its angle of attack and lift. The combined loading results in some intermediate position. Often for the forebody, inertia dominates, so that Case II in the figure is representative. For this case, as the airplane angle of attack increases during a maneuver, the incremental loss in lift due to forebody flexibility results in a nose down pitching moment increasing airplane stability. The other components can be viewed in a similar manner to study their individual effects.

No general statement can be made as to whether the aeroelastic effects of the various components will be stabilizing or destabilizing. Wing and tail can go either way or change with Mach number and airplane loading. The forebody and aftbody are usually, but not always, stabilizing. To determine effects accurately, a careful aeroelastic analysis for each situation is essential, taking into account the airplane geometry, structural characteristics, Mach number, loading condition, and other pertinent factors.

Current methods of aeroelastic analysis have evolved from experience gained in the company's subsonic military and commercial airplane programs, and from the supersonic IM99 which was investigated in considerable detail, including longitudinal and lateral stability and control effects. While the fundamental approach has not changed appreciably, there has been a continuous improvement in the accuracy of methods. This is a result of better aerodynamic pressure distribution prediction methods and of more accurate and complete structural representation of the airplane. To use the better and more detailed aerodynamic and structural data, computer programs have been developed which process the lengthy and involved calculations rapidly.

It is anticipated that improvement in analysis methods will continue; for example, Boeing is

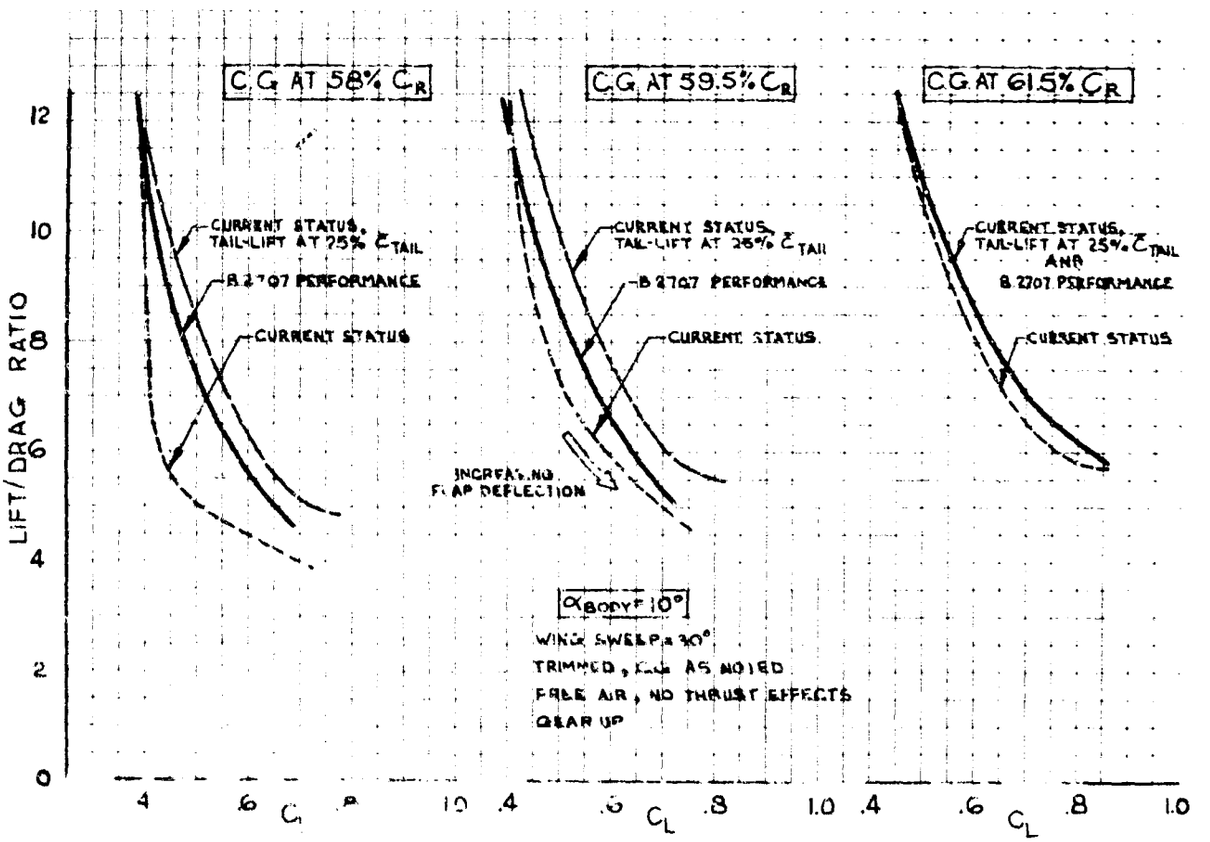


*Figure 3-75. Developed Performance Potential of B 2707*

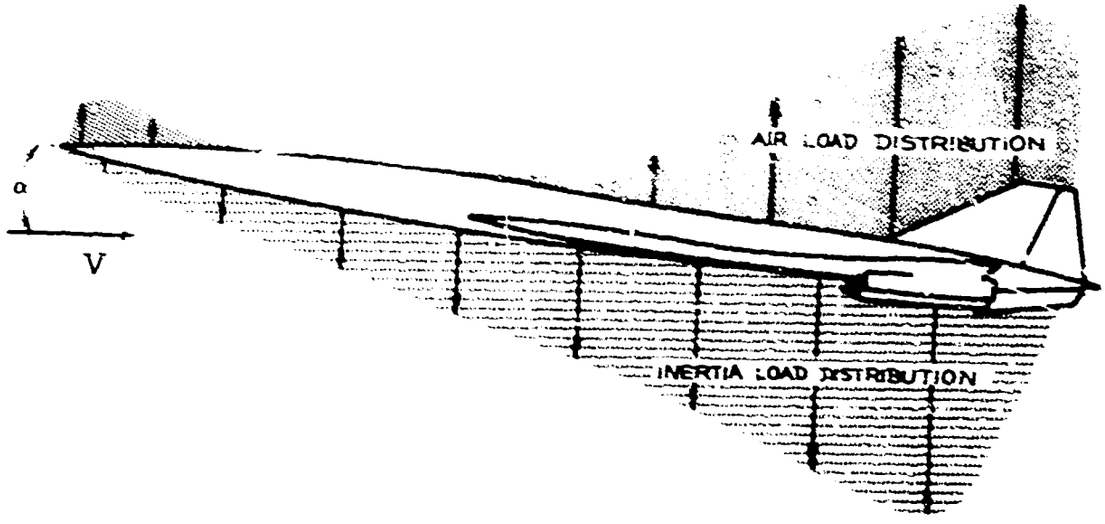


*Figure 3–76. Schematic Air and Inertia Loads on a Rigid Airplane*

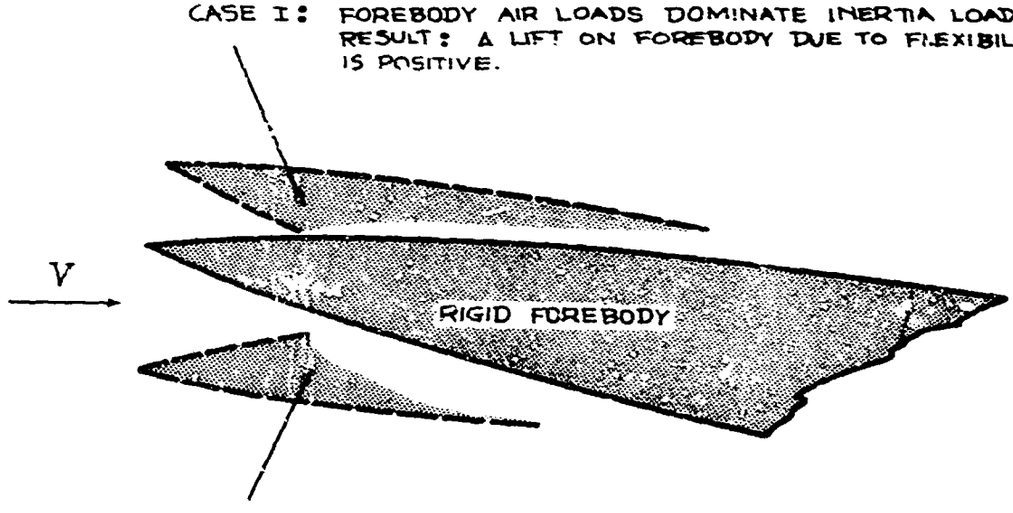


*Figure 3–77. Typical Forebody Aeroelastic Deflections and Resulting Incremental Air Loads*

currently working on a 2-yr research program to analyze methods for calculating stability characteristics of large elastic airplanes. This program is being carried out under the NASA Ames Contract NAS 2-3662. Applicable results are being integrated into the B-2707 program.

Two main computer programs were used in support of B-2707 design development and for preparation of proposal data. These programs calculate the aerodynamic influence coefficients for subsonic, transonic, and supersonic flow as a preliminary step to calculating the aeroelastic effects. The programs require inputs of airplane geometry, structural flexibility, mass distribution, and nacelle interference pressure distribution.

The geometric inputs define the airplane planform, camber lines, and the aerodynamic panel breakdown for the airplane. A typical panel breakdown is shown in Fig. 3-78. The paneling system is arranged to be consistent with the control surface planform shape so that effects of control surface angular position can be included in the calculations. This is done by adding the control surface angular position, relative to its zero position, to the basic camber slope of the surface.

The elastic properties of the wing, body, and tail are represented by two structural influence coefficient matrices (flexibility matrices). One matrix gives the change in position of each panel control point due to unit loads at the other panel control points. The other matrix gives the change in panel slope at each panel control point due to unit loads at the other panel control points.

The mass distribution is determined in accordance with the paneling of the airplane. A number of separate distributions are superimposed to permit convenient investigation of variations in fuel, cargo, and component mass distribution.

The aerodynamic properties of the wing, body, and tail are represented by an aerodynamic influence coefficient matrix. The elements of this matrix relate the lift on each panel to a unit angle of attack on the other panels. Interference effects are accounted for in the theory.

The computations are made for panel loads of the elastic airplane, $P_E$, for a load factor, $\eta$, dynamic pressure, q, and incidence, i.

$$\left|P_E\right| = \left|B\right|^{-1} q \left( \left[A\right] \left( \left|1\right| i + \left|\theta\right| - \eta \left[F\right] \left|W\right| \right) + \left[S\right] \left|P_n\right| \right)$$

where

$$\left|B\right| = \left|1\right| - q \left[A\right] \left[F\right]$$

and

$\left|\theta\right|$ = initial panel slopes

$\left[S\right]$ = diagonal matrix of panel areas

$\left|P_n\right|$ = panel pressures due to nacelles

$\left[F\right]$ = slope flexibility matrix

$\left|W\right|$ = mass distribution matrix

$\left[A\right]$ = aerodynamic matrix

The deflections at the control points, $\left|\delta\right|$, are found as

$$\left|\delta\right| = \left[F_1\right] \left( \left|P_E\right| - \eta \left|W\right| \right)$$

where

$\left|F_1\right|$ = deflection flexibility matrix

Once the panel loads on the elastic airplane have been found, the forces and moments on the airplane are readily computed. For computation of stability derivatives that involve a variation in incidence angle such as roll damping, $C_{l_p}$, or pitch damping, $C_{m_q}$, the proper distribution of incidence is obtained by changing the column matrix $\left|\theta\right|$.

Calculations to find the manufacturing jig shape are made by introducing the design condition elastic loads, dynamic pressure, load factor, incidence, and mass distribution into the above equations. They are then solved for the deflections which are subtracted from the design shape.

The experience of the company in using these methods to predict the aeroelastic characteristics of large airplanes has been generally successful. The structural influence coefficients have been accurately predicted and confirmed by full-scale

test. The aerodynamic coefficients have been more difficult to estimate accurately before full-scale test. For this reason, B-2707 aerodynamic data will be verified by pressure model tests. Means are being developed for the rapid inclusion of wind tunnel data into the aerodynamic matrices.

The major influence of elastic distortions on the dynamics of the airplane motion have been accounted for through modification of the aerodynamic derivatives. An exception to this approach was made for one study that included the dynamics of the forward fuselage. The excitation of the first cantilever mode was determined, including the aerodynamic perturbations. This analysis was carried out to ascertain the accelerations at the pilot's station as compared to center-of-gravity accelerations resulting from maneuvering gust and engine-out conditions.

3.3.2 Experimental Investigations

Considerable work has been done in exploring the effects of aeroelasticity by means of flexible model wind-tunnel testing. The tests, with supporting analyses, have been found to substantiate the analytical methods previously described.

The question of model scaling immediately arises in models simulating flexibility. True scaling for all conditions cannot be accomplished because of limitations on available model materials and the range of test facility conditions. The approach taken is to match directly the model and full-scale Mach number and dynamic pressure. The model structure is designed so that flexibilities (similar nondimensional deflections) between the model and full-scale airplane are simulated. Mass scaling to obtain the proper inertial loading has not been attempted because a model material with sufficient density is not available. Even if a suitable material were available, mass scaling would apply only for a single loading condition. The best procedure is to depend on analytical methods to account for inertial effects. These calculations are easy, accurate, and allow the investigation of any desired loading factor and mass distribution. They are also used to adjust the test results for the actual model mass distribution which in general is different than the desired airplane mass distribution. It is necessary to test at several facilities to cover the airplane flight envelope properly as a result of matching the model and airplane dynamic pressures and Mach numbers on a one-to-one basis, (See Figure 3-79).

The objectives of initial flexible model tests were to check the analytical methods and to develop advanced model construction techniques. For this reason, it was decided to build the model with a single fixed wing sweep angle and to make only the wing flexible. Features of the wing construction are shown in Fig. 3-80. Pictures showing the model during test are shown in Fig. 3-81. The rather large wing tip deflection at high angle of attack is easily seen by comparing the pictures.

Typical data for the tests are shown in Fig. 3-82. Also shown are data for a so-called rigid model which is found to be not perfectly rigid. The theory compares very closely with both the flexible model data and rigid model test data, thus substantiating the analytical methods.

A new model, now near completion and scheduled to begin tests in September 1966, was designed to represent the B-2707 configuration. This model is of more sophisticated design than earlier models. It has interchangeable flexible and rigid components to enable investigation of singular and combined component flexibility effects. It will be used to investigate:

a. The effects of flexible wing and horizontal tail.

b. The effects of wing to tail structural ties.

c. The effect of wing sweep angle.

d. The effect of flexible control surfaces; flaps, elevators, and elevons.

3.4 AERODYNAMIC DEVELOPMENT PROGRAM

The aerodynamic development program consists of analytical and experimental work that will insure that technological and state-of-the-art improvements are considered and incorporated in the refinement of the B-2707. It is discussed under two headings: cruise configuration and takeoff and landing configuration. This program is part of the overall Phase III program Integrated Test Program, V4B-2707-11.

3.4.1 Cruise Configuration

Boeing has worked closely with the NASA in the establishment of the present state of the art in supersonic aerodynamic research. Through the years, practical methods have been developed and these have been applied to the design of high

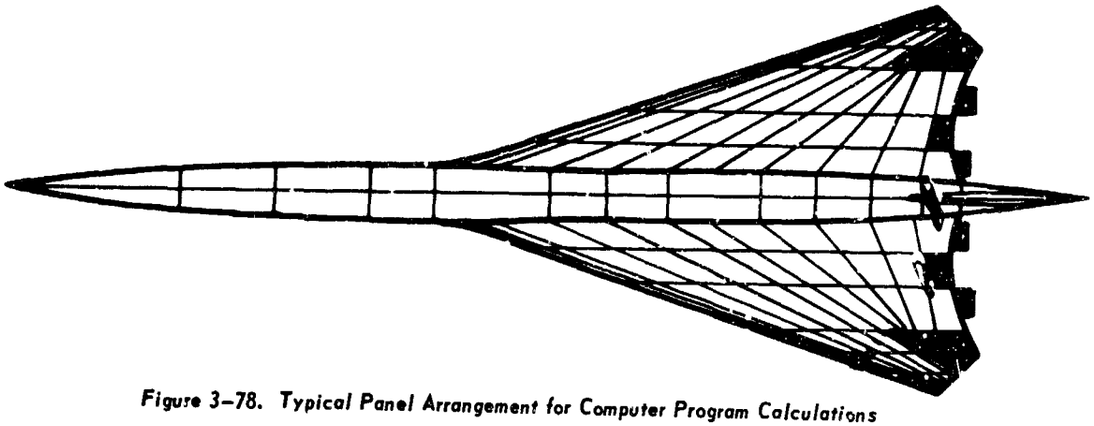

*Figure 3-78. Typical Panel Arrangement for Computer Program Calculations*

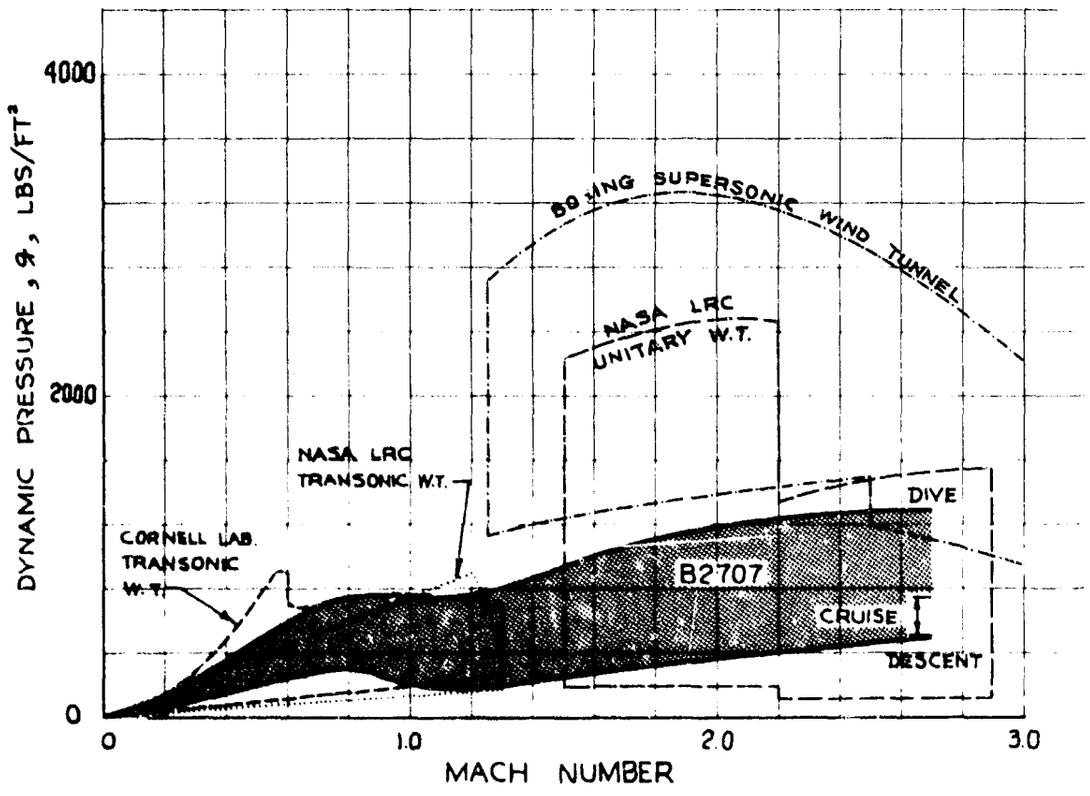


*Figure 3-79. Test Condition Coverage For Flexible Model Testing*

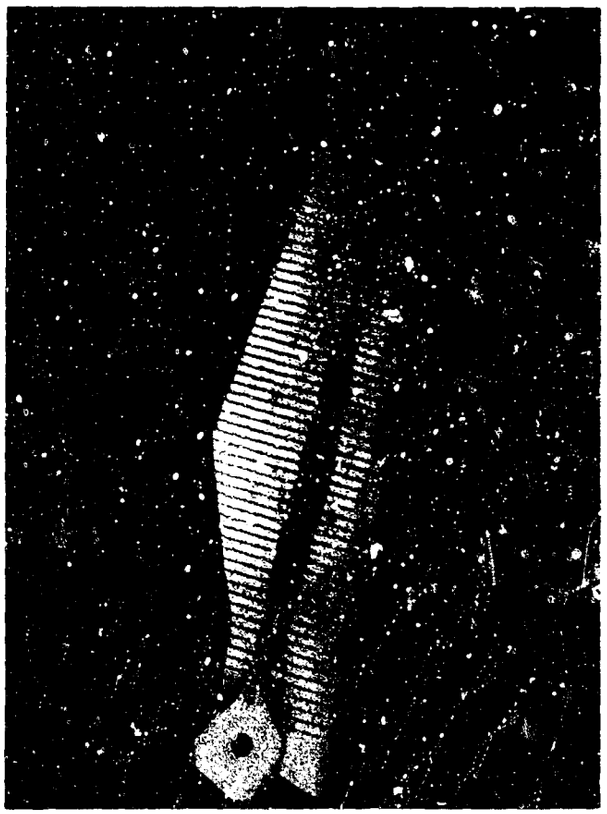

*Figure 3–80. Typical Construction for Flexible Model Wing*

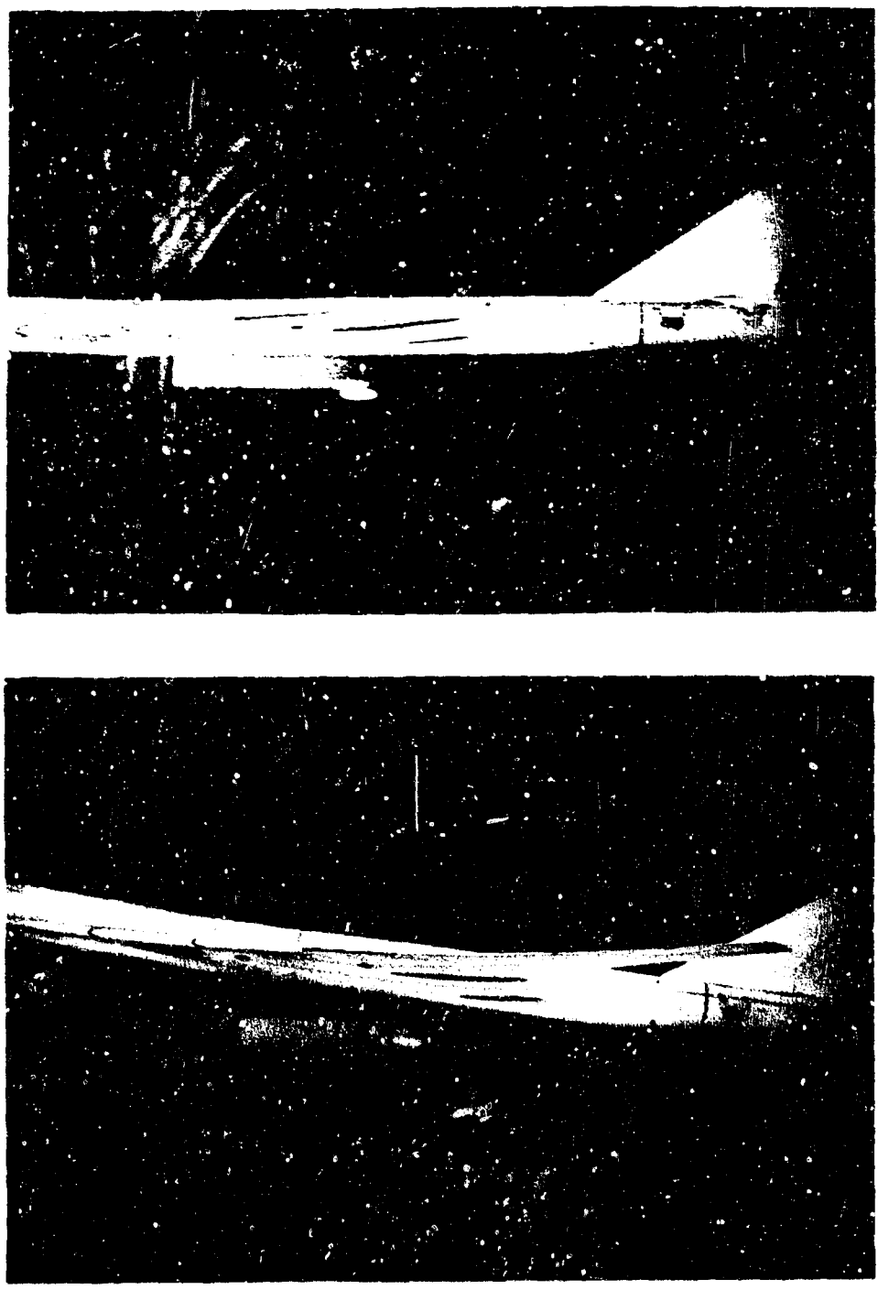

*Figure 3-81. Wing Deflection on Model During Wind Tunnel Test*

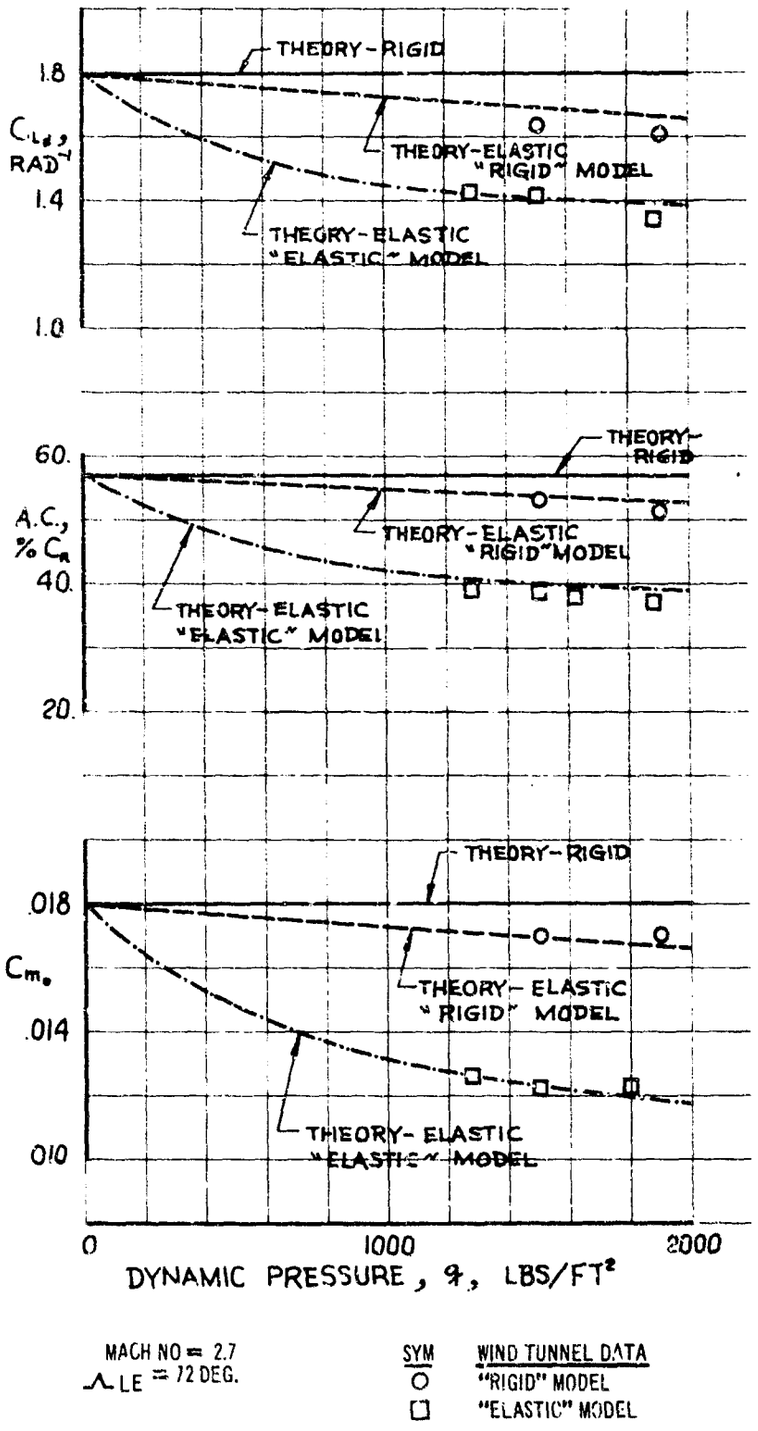


*Figure 3–82. Comparison of Flexible Model Test Data With Calculated Data*

efficiency supersonic configurations. The methods will be refined through continued test correlations and used in future investigations. General areas of investigation will include continued development and improvement of wing camber surfaces for low drag, fuselage design studies to improve drag and sonic boom, and skin friction and base drag reduction studies. A comprehensive program of aeroelastic research will also be carried on.

a. Drag Due to Lift Reduction

Figure 3-83 compares the drag polar of the wind tunnel model of the B-2707 and a theoretical drag polar (as calculated by small disturbance theory) for a minimum drag wing of the identical planform. It is seen that large drag improvements are possible. Some part of this potential improvement is achievable through wing camber and twist refinement. Several computer programs have been developed and are now available. One of these uses combinations of up to 15 different loadings, on any given wing, and will allow the design of wing surfaces optimized with many arbitrary constraints. Already, experimental evidence is in hand to indicate that better drag-due-to-lift characteristics can be obtained through camber and twist development. Figure 3-84 shows that, at Mach 2.7, a wind-tunnel model has achieved drag-due-to-lift reduction equivalent to an increase of approximately 0.2 in lift-to-drag-ratio. This has been obtained with a camber surface designed for a three-loading optimum similar to that tested on the NASA SCAT 15F Model. Time did not permit incorporating this wing into the series of models designed to simulate the B-2707.

A novel approach to drag-due-to-lift reduction has been discussed in Ref. 24. In this approach, airplane wave drag is optimized at the lifting condition. A computer program that accomplishes this optimization using area rule concepts is in use at Boeing. Another program, using the classical approach to the lifting wing body problem is under continuous development. This latter work has been discussed in Ref. 16. These analysis methods are being applied to the detail design of the wing body combination.

Drag-due-to-lift reduction is possible not only by camber and twist design but also by wing planform changes. Such a planform change has been defined for the aerodynamic development model. Planform changes require, however, considerations of structural design and aerodynamic stability. Careful tradeoff studies will be conducted to determine the overall effects of planform changes.

An extensive wind-tunnel test program has been defined to correlate analysis and to accomplish the necessary tailoring and refinement.

b. Fuselage Design Studies

Fuselage drag is an important percentage of the total airplane drag and the aerodynamic design of the fuselage requires careful attention. It is intended to carry out a number of fuselage design studies that will have the objectives of drag reduction and increase in useful volume. Different interior arrangements are being studied and a continuous contact with the airlines is being maintained in order to achieve a design that will combine a high aerodynamic efficiency with maximum passenger appeal.

Several alternate bodies for the B-2707 have already been designed and tested in the wind tunnel. These have a more nearly ideal longitudinal area variation that will allow a wider, deeper body forward, coupled with the minimum acceptable width aft (four- or five-abreast seating). Initial airline reaction has been enthusiastic because of the unusual interior arrangements that are possible, including such features as seven- or eight-abreast seating and two aisles with only one or two seats per seat unit. The body drag increments are equal to or less than that of the B-2707, depending on the minimum acceptable cross section. Refinement of these bodies will be continued.

c. Skin Friction Drag and Other Drag Studies

Skin friction drag is still the largest fraction of the airplane zero lift drag and it is necessary to carry out research in this area. It has been shown in Ref. 25, that surface flow injection is an effective means of drag reduction. Tradeoff studies will be carried out to examine the effects of local blowing on the airplane. In addition, it has been shown that small amounts of bleed air are powerful means for base drag reduction; this fact will be studied further. More data on skin friction will also be obtained through flight test measurements. Knowledge of skin friction coefficients and of the state of the boundary layer can also lead to indirect drag reduction by changes in the design of the camber surface. The design will thus benefit from these flight studies.

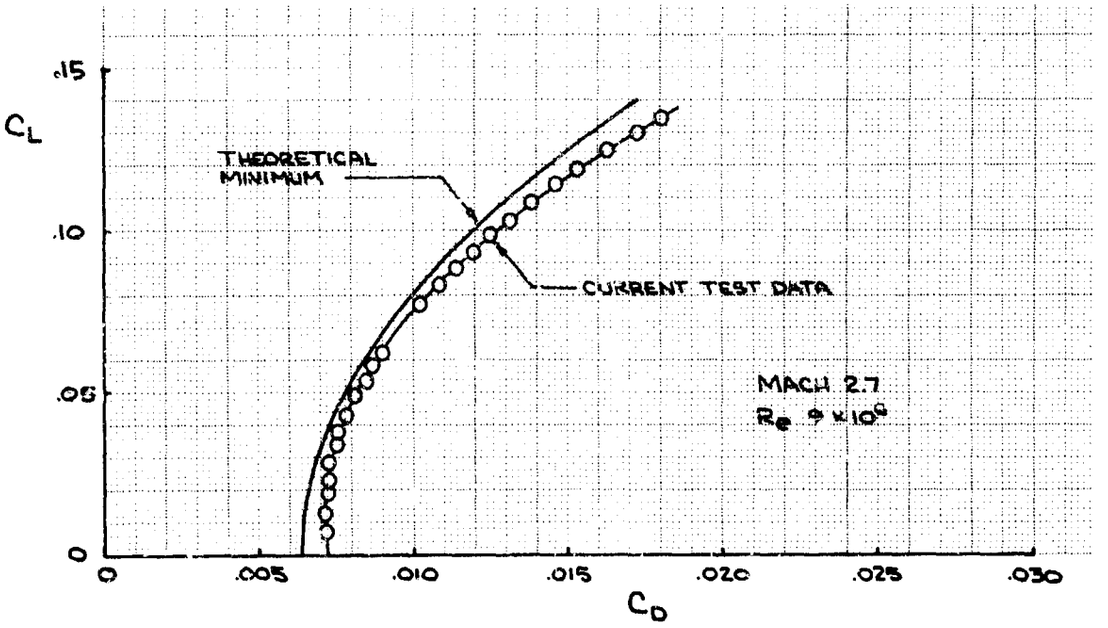


*Figure 3-83. B-2707 – Drag Due To Lift Improvement*

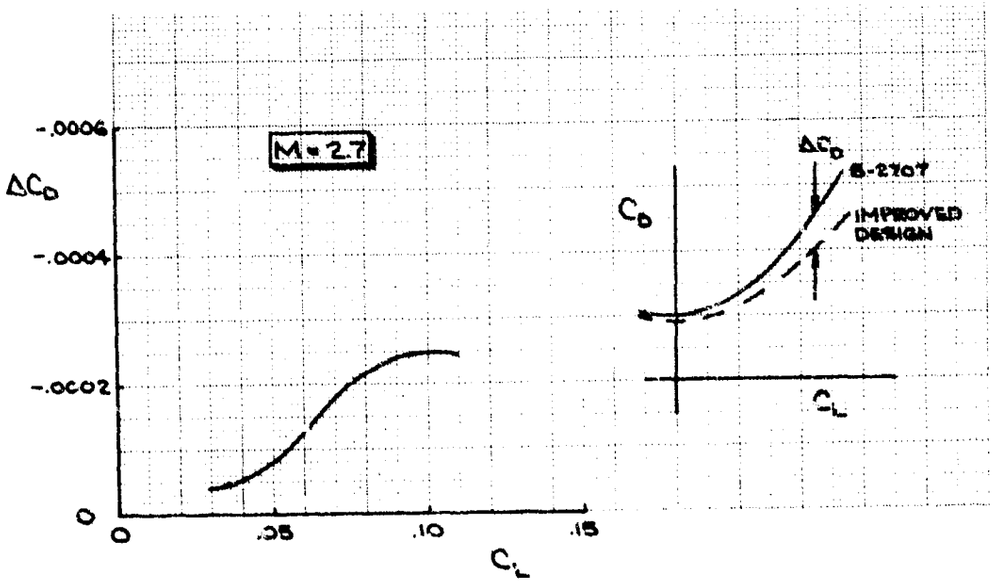


*Figure 3-84. Effect of Camber Refinement on Drag Due to Lift*

d. Aeroelastic Research

Aeroelastic research studies are being conducted to improve the design efficiency of the supersonic transport through evaluation of all the elastic benefits and penalties. Theoretical studies as well as experimental investigations with flexible wind tunnel models are being carried out. A detailed discussion of the aeroelastic program is in Par. 3.3.

3.4.2 Takeoff and Landing Configurations

The program is planned to achieve maximum trimmed lift and lift-to-drag ratios and to investigate the use of direct lift control for landing and takeoff operations. As already stated in Par. 3.2, one way to improve performance is to reduce the tail down load to trim the airplane, which has the further benefit of minimizing the horizontal stabilizer drag.

Careful control of center-of-gravity location and the wing sweep angle programmed for low-speed operations, contributes to performance optimization in all flight regimes. System design studies are being conducted in these areas.

Parallel studies to refine the airplane geometry for optimum aerodynamic efficiency will add to the airplane capability and will include:

a. Flap and slat development, using theoretical and test techniques to maximize effectiveness and minimize drags. Boundary layer control studies will be included.

b. Further wing lofting studies to optimize low-speed attitudes within the dictates of the required high-speed wing design.

c. The wing body tail optimization study will be a wind-tunnel test program supported by lifting surface theory. The approach is as follows:

(1) Survey the flow field (downwash and dynamic pressure distributions).

(2) Set up a vortex lattice system representing the wing body flap combination; adjust as necessary to match the experimental downwash field.

(3) Add the horizontal tail representation to the vortex lattice system.

(4) Make systematic variations to wing, flap, and tail geometry to study their effects and to minimize unfavorable wing tail interference.

## 4.0 STABILITY AND CONTROL


| | | Page |
|---|---|---|
| 4.1 | CONTROL AND TRIM | 145 |
| 4.2 | STATIC STABILITY | 179 |
| 4.3 | DYNAMIC STABILITY | 210 |
| 4.4 | CROSS-COUPLING CHARACTERISTICS | 230 |
| 4.5 | EMERGENCY OPERATIONS | 231 |

# 4.0 STABILITY AND CONTROL

Tests and analyses conducted to date show that with normal systems development the production airplane will have stability and control characteristics that ensure the high levels of safety and the good handling qualities required for commercial transport operation.

The B-2707 design concept of integrated wing and horizontal tail, with the engines mounted aft below the tail, eliminates the tail temperature and the jet exhaust interference effects at the tail experienced by past configurations. Tail span and area are increased and the length is reduced (relative to past SST configurations) so that the same effective tail volume coefficient is maintained.

Substantial size increase over past configurations and the change in mass distribution, caused by aft-mounted engines, have caused the basic airplane to become quite sluggish. Stability and control studies indicate that increased reliance must be placed on stability and control augmentation to achieve good handling qualities as airplanes increase in size and inertia. Areas where current data show that stability and control improvements are required in order to achieve the desired characteristics throughout the flight envelope are indicated in the following paragraphs. New control concepts are being explored to improve this situation; for example, direct lift control holds promise of improving low speed airplane response to pilot inputs for high-inertia, close-coupled configurations.

The stability and control analysis presented herein is based on the B-2707 configuration. Areas where further improvements are expected during the development program are pointed out. Flight control and stability augmentation systems design and operation are described in detail in Systems Report, Part B, V2-B2707-11. Airplane control capabilities, stability, and handling qualities for normal and emergency operations are described in this section; the aerodynamic design requirements for the controls and augmentation system are discussed in Sec. 5.0.

The control system is illustrated in Sec. 5.0. Aerodynamic coefficients are based on the gross wing plus tail planform area, root chord, or span, where the wing area is 9,000 sq ft, the root chord is 157.58 ft and the wing span is 105.67 ft. A detailed geometric description of the airplane and definitions of nomenclature are given in Appendix A.

## 4.1 CONTROL AND TRIM

The flight control system of the B-2707 combines the pitch and roll controls on the horizontal tail for wings-back operation. For the more critical low speed, wings-forward operation, the horizontal tail controls provide pitch control only. A conventional aileron and spoiler system provides the powerful roll control needed for the demanding landing approach task. The low speed control arrangement is thus similar to that of current jet transports. The control ability to maneuver and trim the airplane is discussed in the following paragraphs.

### 4.1.1 Longitudinal Control

The airplane is controlled longitudinally during all-flaps-up flight by segmented elevator surfaces on the tail between the engine nacelles, operating with large tail tip elevon surfaces that share roll and pitch control functions when the wings are fully swept. For wings-forward flight, the full authority of the tip elevons is assigned to pitch control. For flaps-down flight, the pitch control is augmented by large upward-moving elevator surfaces above the engine nacelles.

The critical design requirements for sizing the longitudinal controls are the forward cg limits, takeoff rotation, landing configuration stall, and landing flare control. High speed maneuvering flight dictates hydraulic system hinge moment capabilities and tail structural torsion and bending stiffness. Takeoff rotation is aided by a unique landing gear design that incorporates a manifolding system to maintain equal oleo pressures between the front main and aft main gears during the initial rotation. The manifolding system moves the location of the equivalent single reaction force well forward of the aft gear, relieving the pitch control requirements, and simultaneously preventing an overloading of the aft main gear struts and tires. Additional low speed pitch control capability is considered desirable for takeoff and landing at extreme forward center-of-gravity conditions; means of improving the control, such

as control surface modifications and small retractable canard surfaces far forward, are being explored.

Current data indicate that greater high speed control capability is required. Longitudinal control capability is affected by the variation of aeroelastic effects, aerodynamic center, and zero lift pitching moment with Mach number, altitude, and wing sweep and by hydraulic control power. Continuous design refinement with emphasis on the judicious tailoring of these effects will lead to a greatly improved control capability.

4.1.1.1 Takeoff Rotation

Control requirements for takeoff rotation are compared with longitudinal control capabilities in Fig. 4-1. Airplane loading for the normal mission will place the takeoff center of gravity at 61-1/2 percent of the wing root chord ($C_R$). Takeoff rotation control is seen to be adequate to meet the 169-kn design liftoff speed at this loading condition for the maximum takeoff gross weight. The most critical loading condition for takeoff control is the extreme forward cg loading case where the cg can be as far forward as 59-1/2 percent $C_R$; however, for this case the fuel can be transferred from the forward auxiliary tanks to the aft auxiliary tanks before takeoff thereby locating the cg at 61-1/2 percent $C_R$. For takeoff at the forward cg limit, either increased takeoff speed or improved pitch control are required. A 5-kn speed increase plus a modest increase in control provide adequate rotation control at the forward loading condition (59-1/2 percent $C_R$). Wind tunnel testing has shown that one way to achieve this increase in control effectiveness is by adding a 20 percent chord split flap to the elevator and deflecting the leading edge of the tip elevon up at 10 percent of the chord. Analyses also show that reducing takeoff wing sweep to 20 degrees would permit rotation for takeoff at the forward cg limit at 174-kn liftoff speed with existing control capability. Approximate takeoff rotation time histories are shown for comparison purposes in Figs. 4-2 and 4-3. The time histories, as well as the rotation summary in Fig. 4-1, employ normal control rotation techniques. A 5-sec interval was maintained between the rotation and liftoff speeds, to

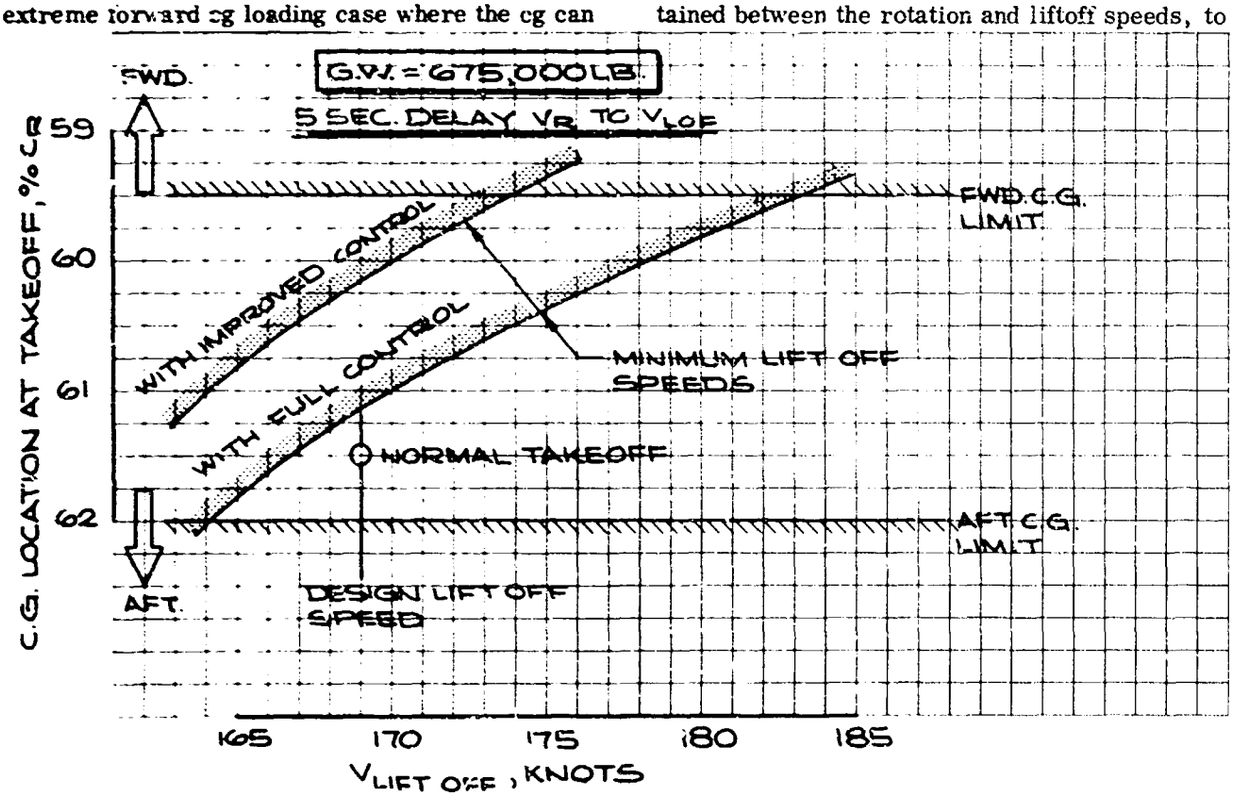


*Figure 4-1. Takeoff Rotation Control Capability*

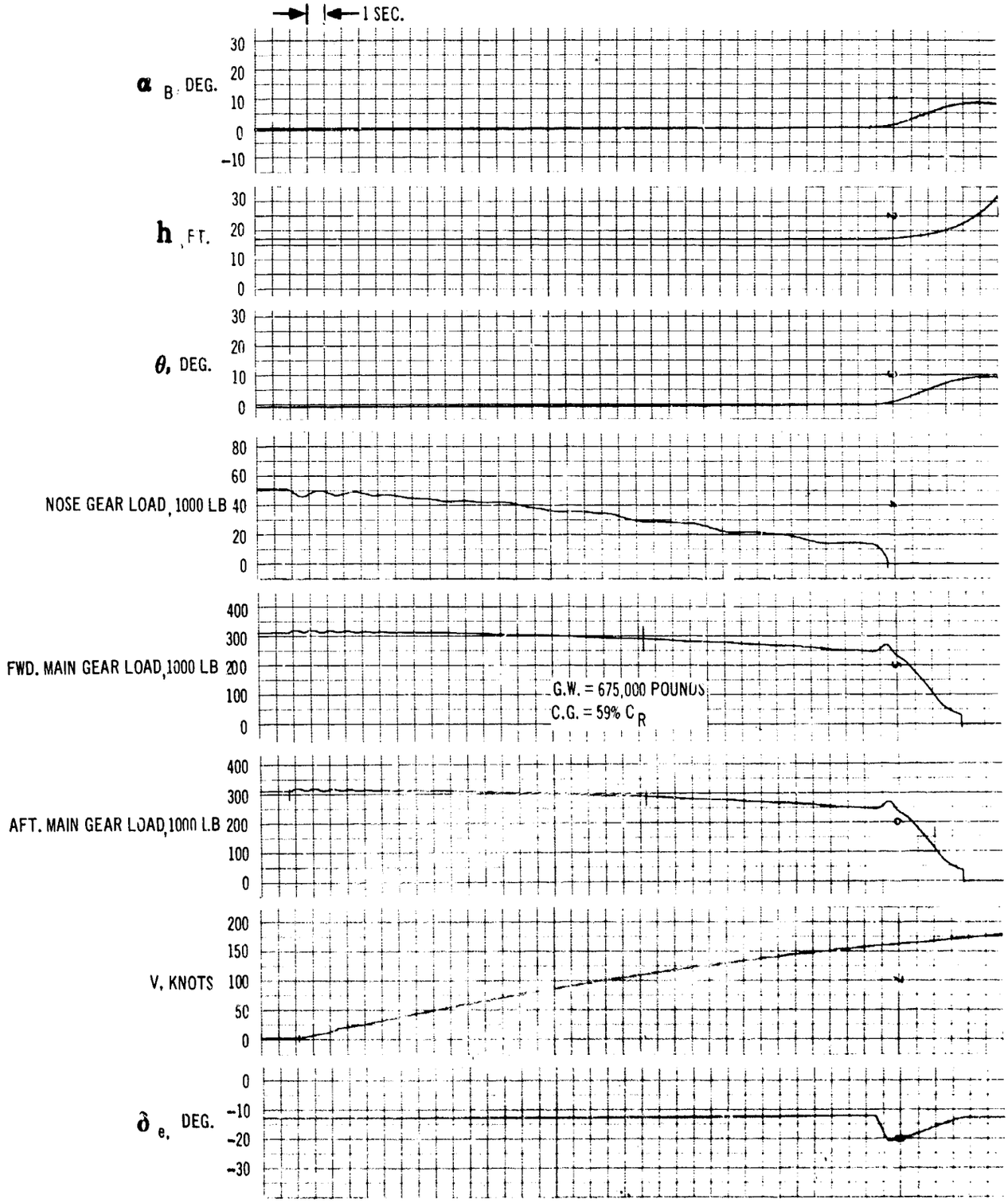


*Figure 4-2. Takeoff With 4 Degrees Manifolded Main Gear*

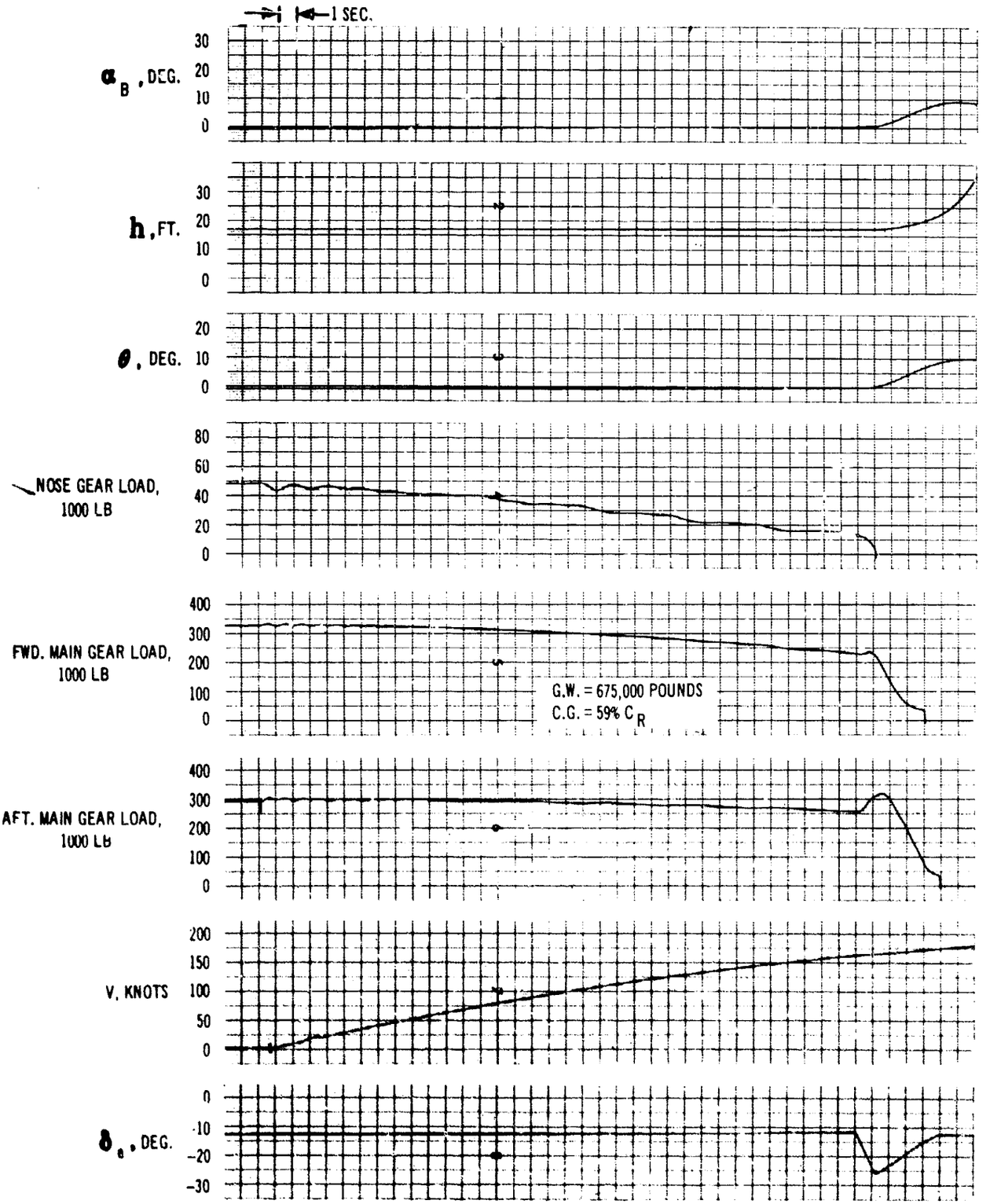


*Figure 4-3. Takeoff Without Gear Manifolding*

provide adequate time to allow an easily controllable pitch rate at the liftoff attitude; this eliminates any tendency for the pilot to overrotate or hunt for the desired attitude. A shorter time interval between liftoff and rotation speeds would require slightly less control for initial rotation, because of the higher dynamic pressure.

The effect of manifolding is illustrated by comparing Figs. 4-2 and 4-3. Manifolding reduces the amount of control required by 19 percent.

4.1.1.2 Landing Approach Control

Longitudinal control in the landing approach configuration is shown for two critical conditions in Fig. 4-4. Sufficient control is available to stall the airplane at forward cg, and to push over from well above the stall at aft cg. The nonlinear stability at high angle of attack shown in the figure is discussed in Par. 4.2. Longitudinal control in ground effect is shown in Fig. 4-5. Full nose up control remains adequate to compensate for the increased negative $C_{M_O}$ in ground effect. The 24-ft cg height corresponds to the altitude just prior to touchdown. Little excess control power beyond trim is required in the landing flare because of the increase in total airplane lift from ground effect.

The variation of control moment with control deflection is shown in Fig. 4-6. Also included is the improved effectiveness due to the control, as discussed in Par. 4.1.1.1.

Landing flare capability has been evaluated to ensure that an adequate margin of control is available beyond normal static trim requirements. Time histories of landing flares are shown in Figs. 4-7 through 4-9 for normal and for very steep approaches. All flares were accomplished at the forward cg limit, using full elevator control. An unpiloted analog computer mechanization of the three longitudinal degrees of freedom similar to that employed in the takeoff rotation analysis was used to obtain the time histories. Aerodynamic characteristics in the simulation included the nonlinear influence of ground effect on lift, drag, and pitching moment, and gear reactions included damping and nonlinear spring rates. Satisfactory flare maneuvers were considered accomplished in the study when the following conditions were met at touchdown: sink rate was reduced to 2 to 4 fps, and the pitch rate and vertical acceleration were near zero. Flares shown in Figs. 4-7 and 4-8 were made with throttle setting held at the level required to maintain the approach flight path before flare initiation. At a cg height of 25 ft thrust was reduced to zero. The thrust reduction, with accompanying speed loss, was used to simulate the most severe flare maneuver from the standpoint of control input. Flare from a normal 3-degree glide slope (Fig. 4-7) required a small nose up command to initiate the flare, followed by an increasing control deflection to counter the nose down moment from ground effect. Flares initiated from a high sink rate (Fig. 4-8) required more pitch command in the early part of the flare. The normal flare technique of adjusting thrust during the flare to maintain constant speed was employed for the time history in Fig. 4-9. This resulted in less pitch attitude buildup during the flare, and was accomplished with reduced control deflection.

Longitudinal control developed by the current wind tunnel model is marginal for landing flare; however, the control modifications discussed above, or a reduction in wing leading edge sweep to 20 degrees for landings, would provide a large margin of control for maneuver and flare.

Improved low speed pitch response is possible through the use of direct lift control. The B-2707 geometry is compatible with such a development.

The recent U.S. Navy tests using wing flaps for direct lift control on an F-8 airplane have shown marked improvement in pilot opinion of flying qualities and precision in accomplishing the very demanding carrier landing task. These results encourage applying direct lift control to the B-2707 or other large transport airplanes to improve landing approach and flare path control.

The data of Fig. 4-10, obtained during flap development testing, indicate the incremental lift that is readily obtainable. More important for direct lift consideration, the pitching moment curves indicate that the downwash change at the tail with flap deflection produces nearly complete self-trimming.

An alternate means of direct lift control would be to use symmetric spoiler deflection about some partially deflected position. Some preliminary experimentation has already been done by NASA Ames Research Center on the use of spoilers for direct lift control on a large subsonic transport, both in ground-based simulation and in actual flight. The results were promising. Figure 4-10

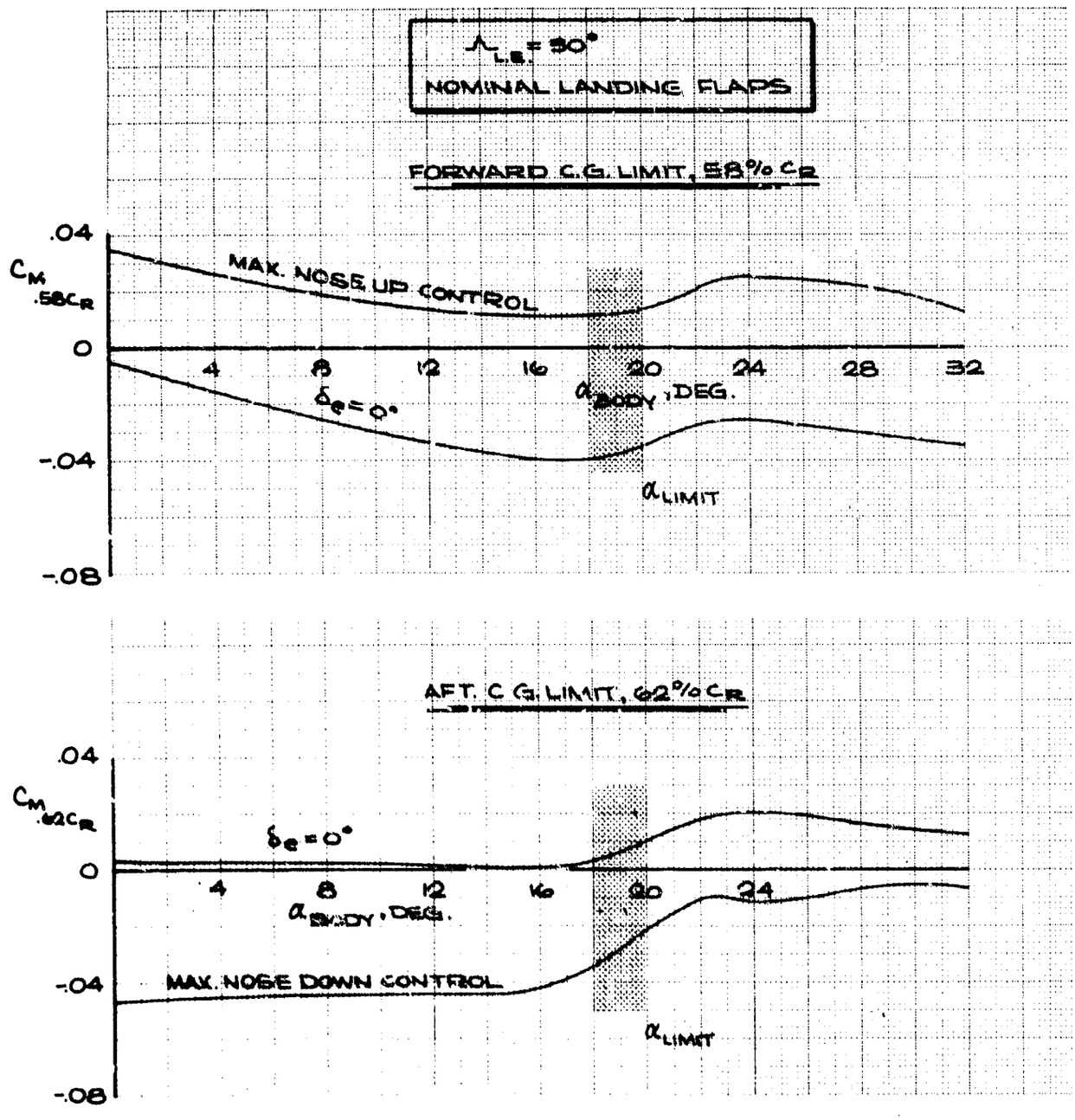


*Figure 4-4. Landing Control, No Ground Effect*

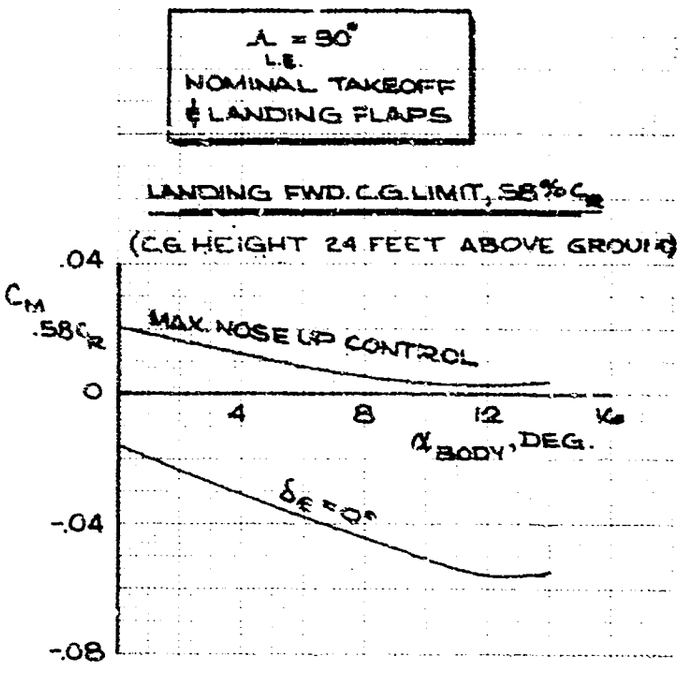


*Figure 4-5. Landing Control, In Ground Effect*

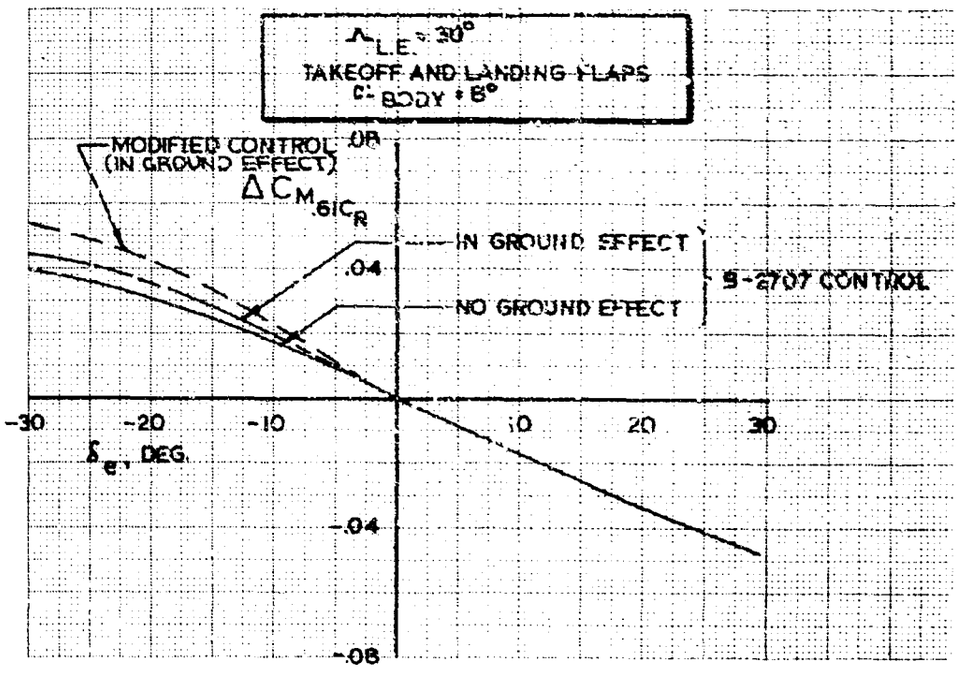


*Figure 4-6. Low Speed Control Power*

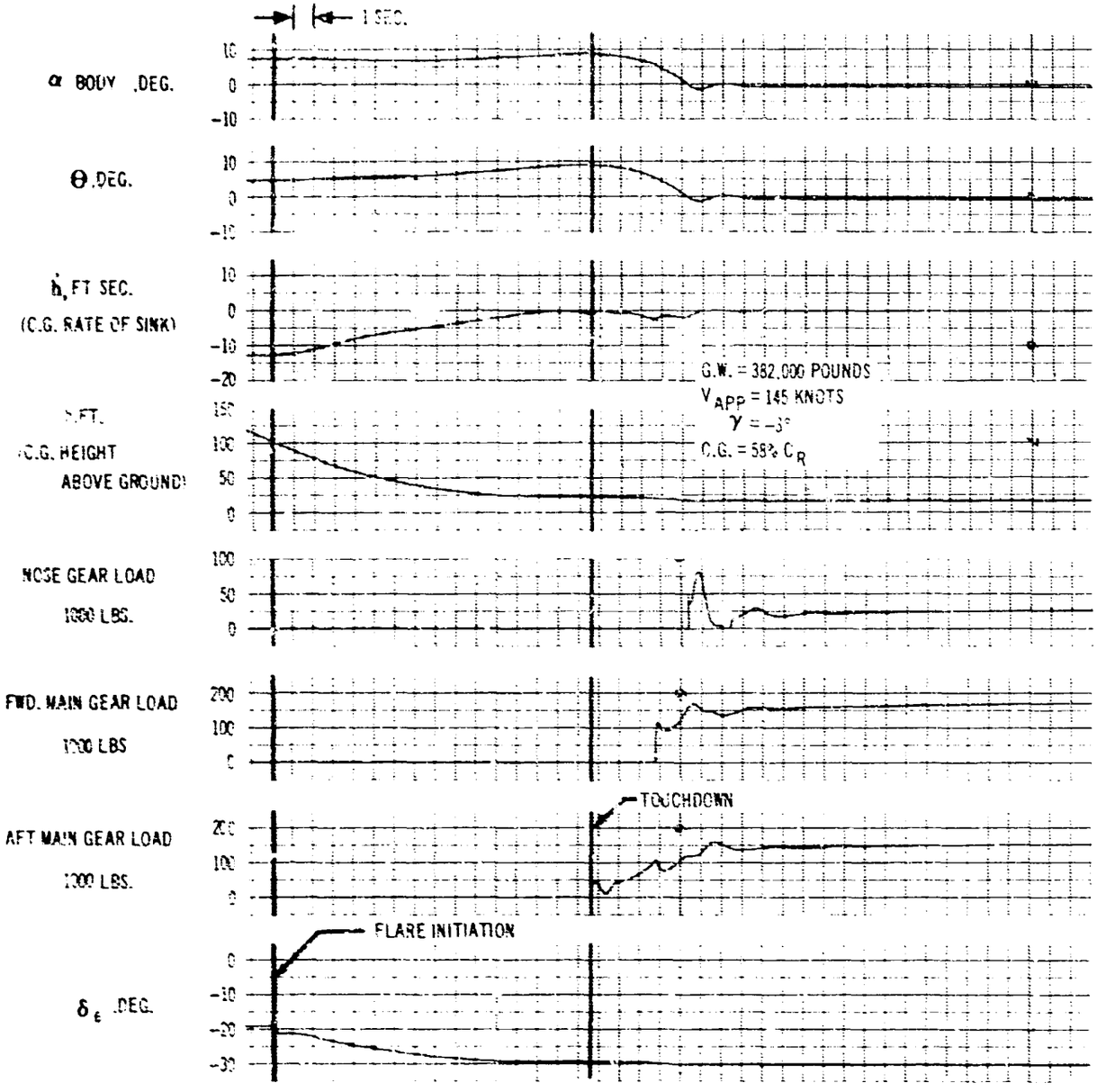


*Figure 4-7. Landing Flare From Normal Approach*

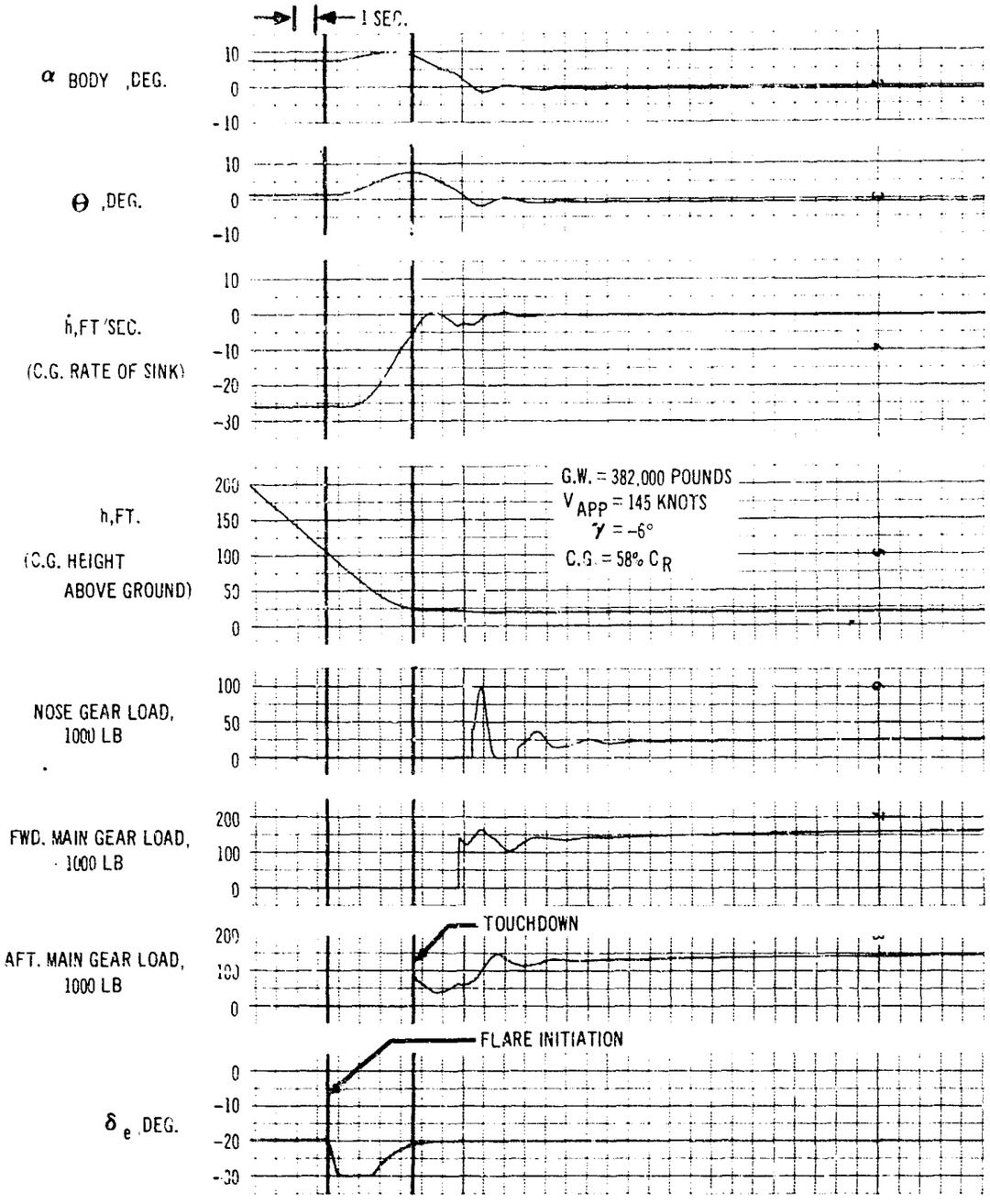


*Figure 4-8. Landing Flare From Steep Approach*

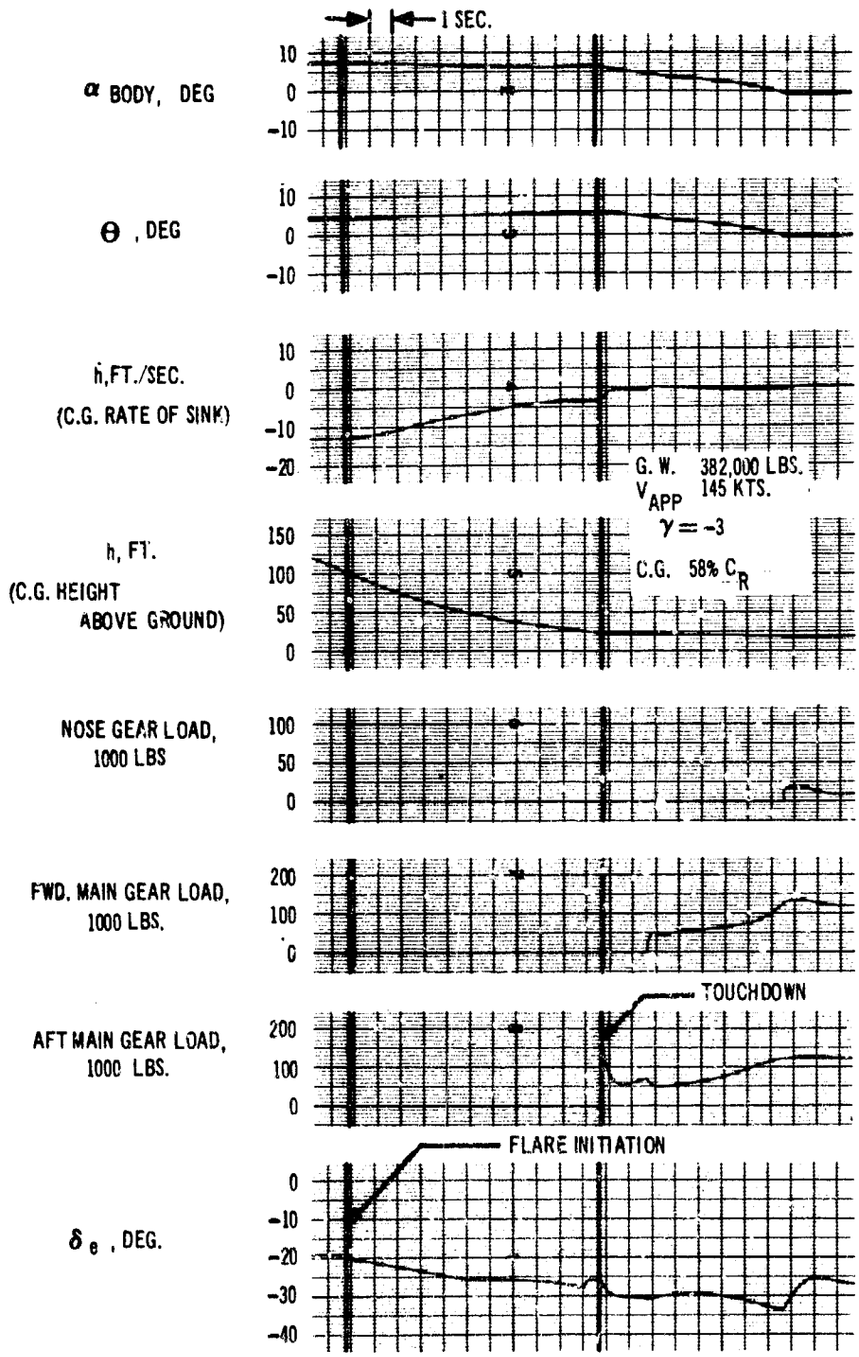


*Figure 4-9. Landing Flare From Normal Approach, Constant Speed*

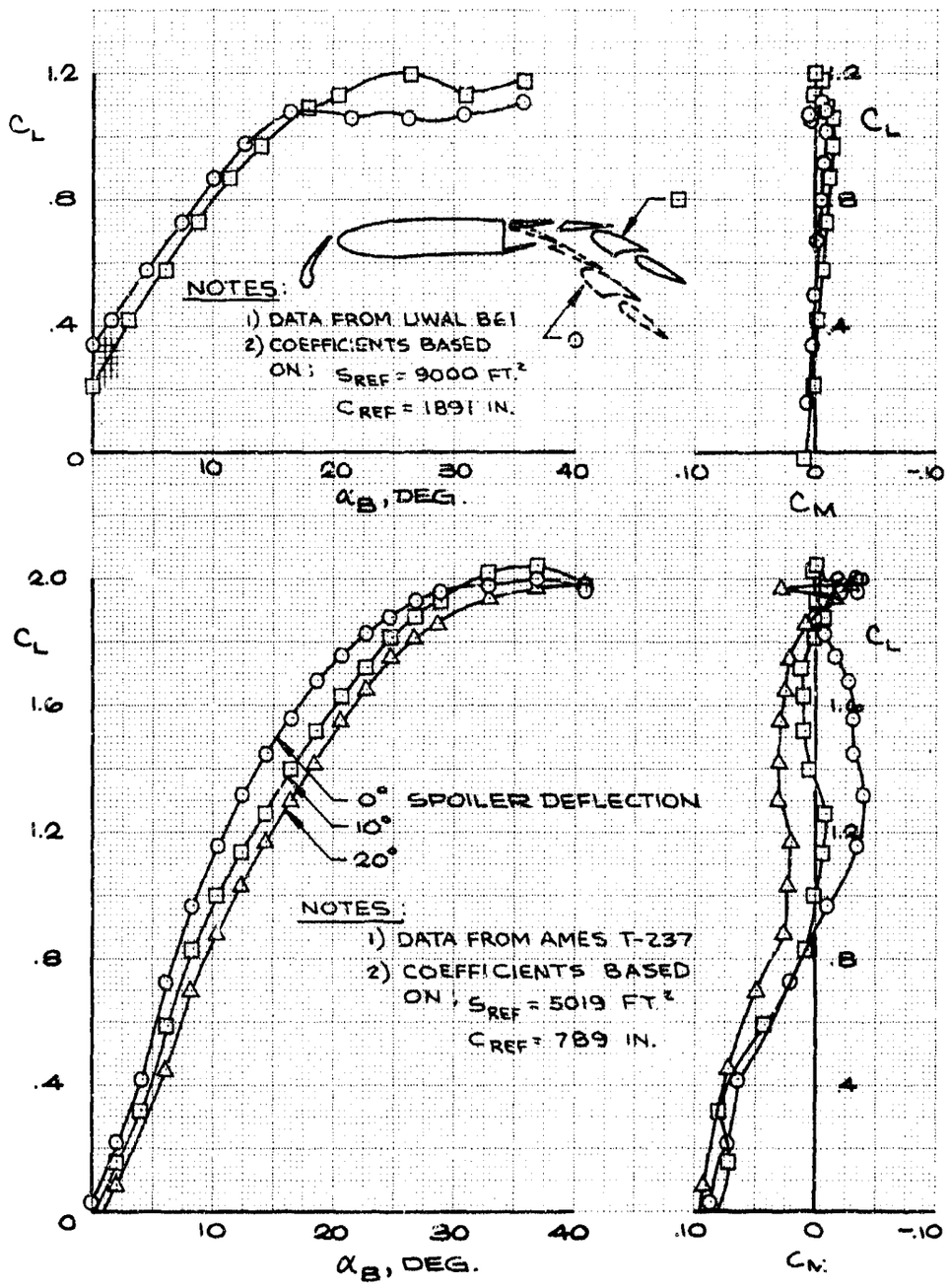


*Figure 4–10. Effect of Spoiler and Flap Deflection on Lift and Trim*

shows small spoiler deflection effects on an earlier SST configuration taken from large scale tests in the Ames Research Center 40-ft by 80-ft wind tunnel. Adequate lift increments for direct lift control are obtainable with moderate spoiler deflections, and the pitching moments are within the capability of a reasonable trim interconnect gearing. Direct lift control is being studied for the B-2707 as a possible improvement.

4.1.1.3 Low Speed Control, Flaps Up

Flaps up longitudinal control, Fig. 4-11, is adequate to stall the airplane at forward cg and push over from stall at aft cg. The moderate instability shown at aft cg is discussed in Par. 4.2. Longitudinal control for wings aft landing is shown in Fig. 4-12.

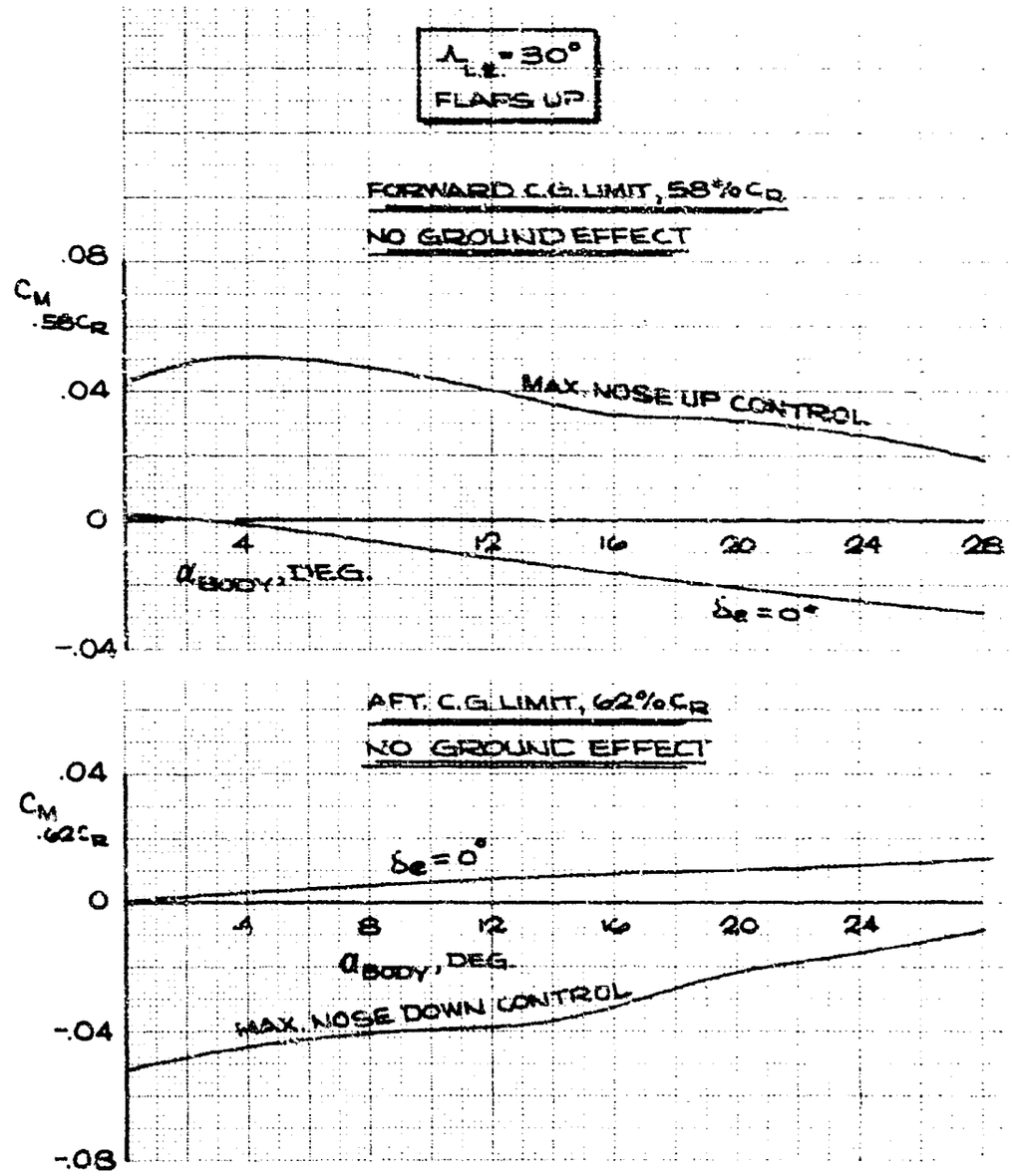


*Figure 4-11. Low Speed Control, Flaps Up*

***Table 4-A. Low Speed Trim Changes***

| Initial Trim Conditions | | | | Configuration Change | Parameter Held Constant | $\Delta\delta_e$ Trim Change Degrees | |
|---|---|---|---|---|---|---|---|
| Configuration | Speed, Knots | Power | Flaps | | | Forward C.G., .58 $C_R$ | Aft. C.G., .62 $C_R$ |
| Maximum Landing Weigh' $\Lambda = 30^o$ | 1.4 Vs 189.5 | Off | Up | Extend Landing Flaps | 1.4 Vs | -10.4 | -1.5 |
| | 1.4 Vs 157.0 | Off | Takeoff Flaps | Retract Flaps | 1.4 Vs | +10.4 | +1.5 |
| | 1.4 Vs 189.5 | Off | Up | Max. Aug. T.O. Power | 1.4 Vs | + 2.0 | +2.0 |
| | 1.4 Vs 157.0 | Off | Landing Flaps | Max. Aug. T.O. Power | 1.4 Vs | + 2.5 | +2.5 |
| | 1.4 Vs 157.0 | Off | Landing Flaps | Gear Down | Speed | Negligible | |
| | 1.3 Vs 145.8 | Off | Landing Flaps | Max Dry Thrust-Flaps Up, Max. L/D | Altitude | +12.2 | +3.5 |
| | 1.4 Vs 157.0 | Off | Landing Flaps | Speed Change To 1.1 Vs (123. KTS) | Altitude | - 5.4 | -1.25 |
| | 1.4 Vs 157.0 | Off | Landing Flaps | Speed Change To $V_{F.E.}$ (195. KTS) | Altitude | + 5.9 | +0.25 |
| G.W. = 627,000 LBS $\Lambda = 30^o$ | 1.4 Vs 230.0 | On | Up | Sweep Wing To $\Lambda = 72^o$ | Maintain Climbout Acceleration ($\Delta$V=115. KTS) | 0 (C.G. At .59 $C_R$) | -2.5 |

4.1.1.4 Low Speed Trim Changes
Elevator deflections measured from initial trim required to control significant configuration changes are presented in Table 4-A. The trim changes are small for all conditions except those involving wing flap retraction or extension. Elevator trimming with flap actuation will be gradual due to the slow rate of operation for the flaps. No control force changes will be felt by the pilot because of the automatic trim feature in the stability augmentation system.

4.1.1.5 Flight Envelope Trim Requirements
The control surface deflections required to trim the airplane in steady level flight are shown in Fig. 4-13 for climb, $V_{MO}$ descent and dive conditions throughout the flight envelope. Control deflections for the elevator and tip elevon surfaces are shown at forward and aft center of gravity limits and also for the normal cg variations experienced during flight. The required trim angles are moderate for all except transonic conditions at forward cg's where stability margins and $C_{M_o}$'s are at their maximum levels. Studies are in progress to tailor the $C_{M_o}$ variation with Mach number to minimize the trim requirements at all conditions. These studies include experimentation with body shape variation, wing twist and camber, strake fairing, and the effects of a small canard trimming surface.

The control requirements for trim and maneuver shown herein are based on wind tunnel test data and not on tests of the models submitted for FAA evaluation. No accounting has been made for model control surface flexibility although subsequent analysis indicates that the effects of model flexibility may be significant. Estimates of control surface effectiveness based on these results may be somewhat conservative.

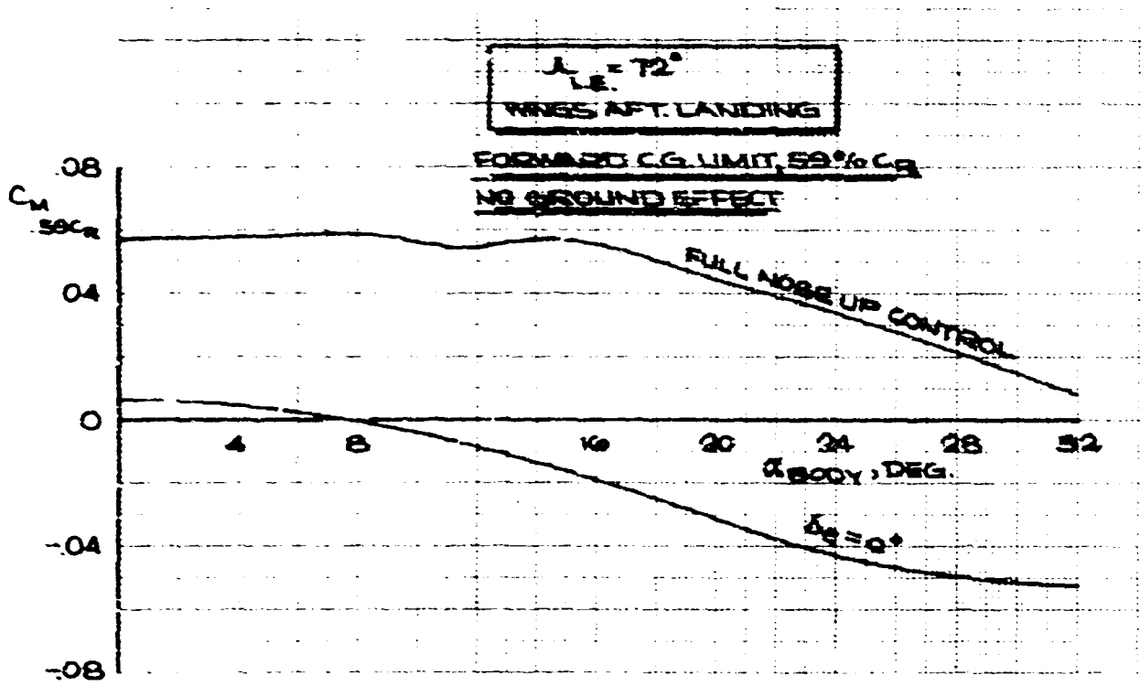


Figure 4-12. Low Speed Control, Wings Aft Landing

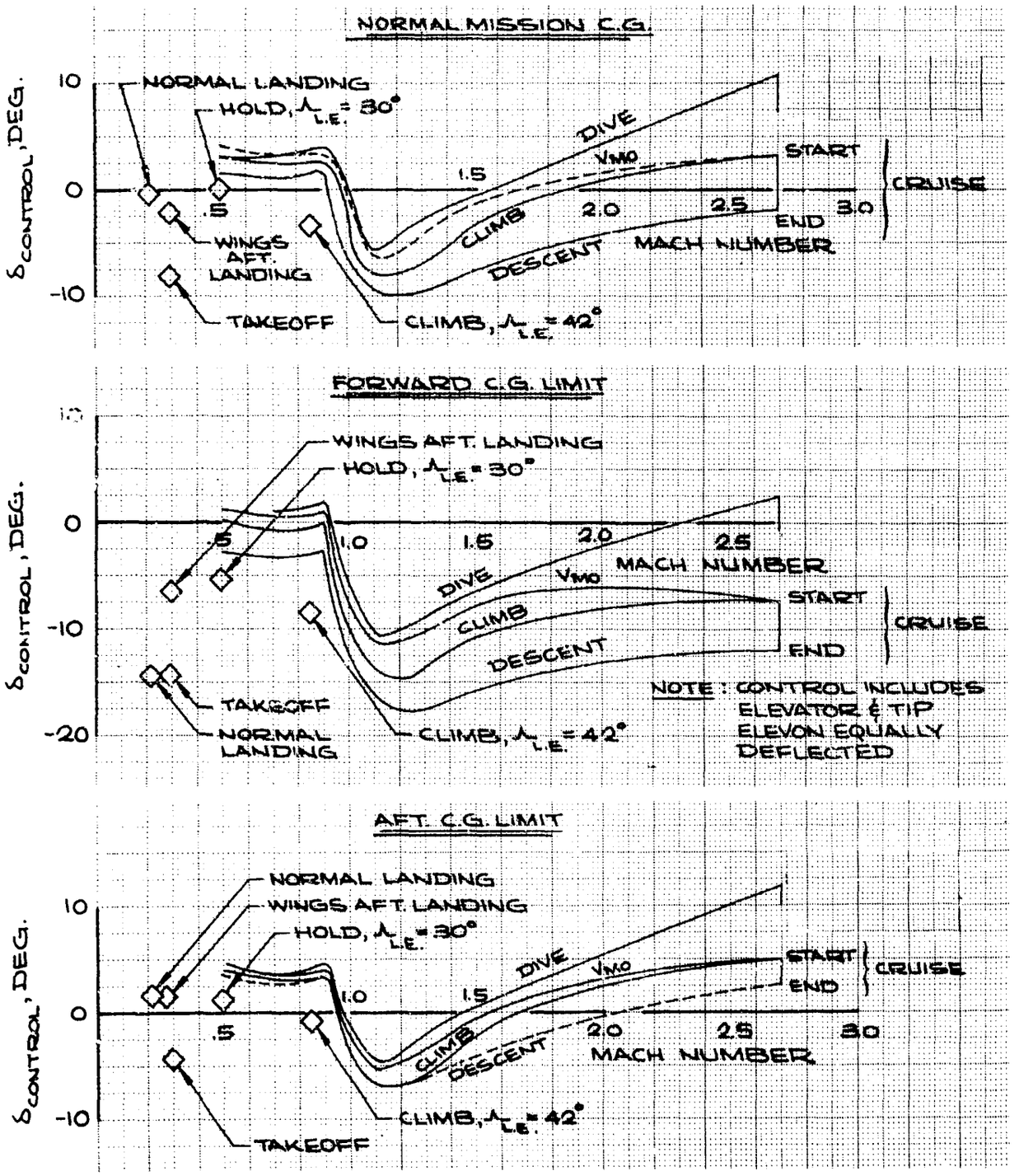


*Figure 4-13. Longitudinal Trim Characteristics*

The method of determining the control surface trim angles is as follows:

$$\delta = \frac{\Delta C_{M_{C.G.}}}{\left(C_{M_\delta}\right)_{\text{constant } C_L}^{\text{flexible}}} \quad \text{where,}$$

$$\left(C_{M_\delta}\right)_{\text{const. } C_L}^{\text{flex.}} = \left(C_{M_\delta}\right)_{\text{const. } \alpha}^{\text{rigid}} \left(\frac{M_E}{M_R}\right)_\delta + \left(C_{L_\delta}\right)^{\text{rigid}} \left(\frac{L_E}{L_R}\right)_\delta \left(X_S - .64\right),$$

$X_S = X_{a.c.}$ (rigid aerodynamic center)

$+ \Delta X_{a.c.}$ (flexibility effect),

$$\left(\frac{M_E}{M_R}\right)_\delta = \left(\frac{C_{M_\delta}}{C_{M_\delta}}\right)_{\text{rigid}}^{\text{flex.}}, \quad \left(\frac{L_E}{L_R}\right)_\delta = \left(\frac{C_{L_\delta}}{C_{L_\delta}}\right)_{\text{rigid}}^{\text{flex.}} \text{ and}$$

$\Delta C_{M_{C.G.}} = \Delta C_M$ [at flight $C_L$ from pitching moment data at mean reference point $- C_{L_{\text{flight}}} (.64 - X_{C.G.})$] + $\Delta C_{M_O}$ (flexibility correction on $C_M$ at $C_L = 0$) + $\Delta C_M$ (flexibility corrections on aerodynamic center) + $\Delta C_{M_{\text{thrust}}}$.

The rigid aerodynamic centers, aeroelastic corrections, and thrust effects employed in the above calculations are presented in Par. 4.2.1.

The trim control requirements versus Mach number in Fig. 4-13 show negative speed stability (control versus M or V) for transonic operation. Acceptable control force versus speed characteristics will be provided throughout the flight envelope by the longitudinal stability augmentation system.

4.1.1.6 Maneuver Capability

The ability of the airplane to develop positive load factor is shown in Fig. 4-14. Good maneuver capability is seen to exist when operating at normal mission center of gravity. The airplane is capable of developing load factor in excess of the 2.5 g structural limit for most flight conditions. At forward cg's, however, the maneuver load factor capability shown is considered marginal, and will improve through the development refinement (Par. 4.1.1). Boeing flight simulator studies indicate requirement for 2.0 to 2.5 g load factor capability at maximum dive speeds for recovery from upset maneuvers. Consideration is also given to operating with failed hydraulic systems, where hinge moment limitation on control deflections will further restrict maneuverability, as discussed in Par. 4.5.

Studies are in progress to expand the longitudinal maneuver capabilities of the airplane considering both the normal operation and flight with single or dual hydraulic system failures. This work will investigate $C_{M_o}$ tailoring and elimination of control deflection restrictions imposed by large aerodynamic hinge moments and hydraulic power limitation.

Longitudinal control surface effectiveness is summarized in Figs. 4-15 through 4-21; aeroelastic corrections are shown in Par. 4.2.1. The following method is used to compute maneuver capability:

$$\frac{d\delta}{dn} = \frac{C_{L_{\text{trim}}} \left(X_M - X_{C.G.}\right)}{\left(C_{M_\delta}\right)_{\text{constant } C_L}^{\text{flexible}}} \quad \text{where}$$

$X_M$ = flexible airplane maneuver point, and

$\left(C_{M_\delta}\right)_{\text{const. } C_L}^{\text{flex.}}$ = flexible control parameter

$$= \left(C_{M_\delta}\right)_{\text{const } \alpha}^{\text{rigid}} \left(\frac{M_E}{M_R}\right)_\delta + \left(C_{L_\delta}\right)^{\text{rigid}} \left(\frac{L_E}{L_R}\right)_\delta \left(X_M - .64\right)$$

Maneuver capability equations continued on next page:

Maneuver capability equations concluded

$$\Delta n = \frac{(\Delta\delta)_{\text{effective}}}{\frac{d\delta}{dn}} \quad \text{where}$$

$$(\Delta\delta)_{\text{effect.}} = K_3(\Delta\delta)_{\text{tip elevon}} + K_4(\Delta\delta)_{\text{elevator}}$$

and $(\Delta\delta)_{\text{tip elevon or elevator}} = \delta_{\text{available}}$ (maximum deflection available as limited by hinge moments) $- \delta_{\text{trim}}$

4.1.2 Lateral Control

A conventional aileron and spoiler system is used for roll control during wings-forward, flaps-down flight. The ailerons are phased out as wing flaps are retracted, and tail tip elevons are partially phased in. At low and intermediate sweep conditions, flaps up, roll control is provided by the segmented wing spoiler system and partial tip elevons. As the wings are swept aft, the outboard wing spoilers lose effectiveness and the tail tip elevon surfaces are phased fully into the lateral control system. The outermost wing wing spoiler segments are simultaneously phased out as lateral controls. The roll control system at wing sweep 72 degrees consists of the tip elevons, which also retain a longitudinal control function, and the four most effective wing spoiler segments. The large tip elevon surfaces provide between 75 percent and 90 percent of the effective rolling moment of the total lateral system. A mechanical rudder interconnect is incorporated into the design, operating with the elevons at all flaps-up conditions to minimize the adverse yaw characteristics of the elevons. The wing spoilers augment the elevon rolling moments and also reduce the adverse yaw effects of the roll control system. The pitch effects of both spoiler and elevons are negligible. Phasing of the various elements in the lateral control system and the rudder interconnect are described in Sec. 5.0. Airplane dynamic response to roll control inputs and cross-coupling characteristics are discussed in Pars. 4.3 and 4.4 of this section.

4.1.2.1 Roll Performance

The lateral control surfaces have been sized to satisfy the roll control performance requirements developed in the Phase II-C studies. Figure 4-22 shows that the roll performance for coordinated (single degree of freedom) rolls meets the proposed requirements for representative flight cases which encompass the airplane's flight regime. The plot is in the form of maximum steady state roll rate attainable versus bank angle obtainable in 1 sec after application of full wheel by the pilot, using maximum lateral control deflections available from the 1g trim setting. Control surface rates are the maximum design values for all hydraulic systems operating. The airplane roll time constant which indicates the dynamic characteristics of the roll response is noted for each flight case. Long roll time constants, in excess of 2.0 sec, are typical at transonic and supersonic flight conditions for the unaugmented airplane. Roll response augmentation (Par. 4.3) is incorporated to improve roll damping and reduce overshoot to obtain satisfactory handling qualities at all flight conditions. At subsonic conditions, the variable sweep concept inherently provides short roll time constants and good control response characteristics.

For flight at high load factor conditions, pitch control authority for the elevons can restrict the available deflection for roll control. Figure 4-23 shows single degree of freedom rolls for the eight standard flight conditions for the airplane in a 1g maneuver ($n = 2$); at low speed where $n = 2$ is not possible, the case chosen is the stall. All conditions satisfy the emergency boundaries. Flight simulator testing will be conducted to evaluate roll performance in high-g maneuvers.

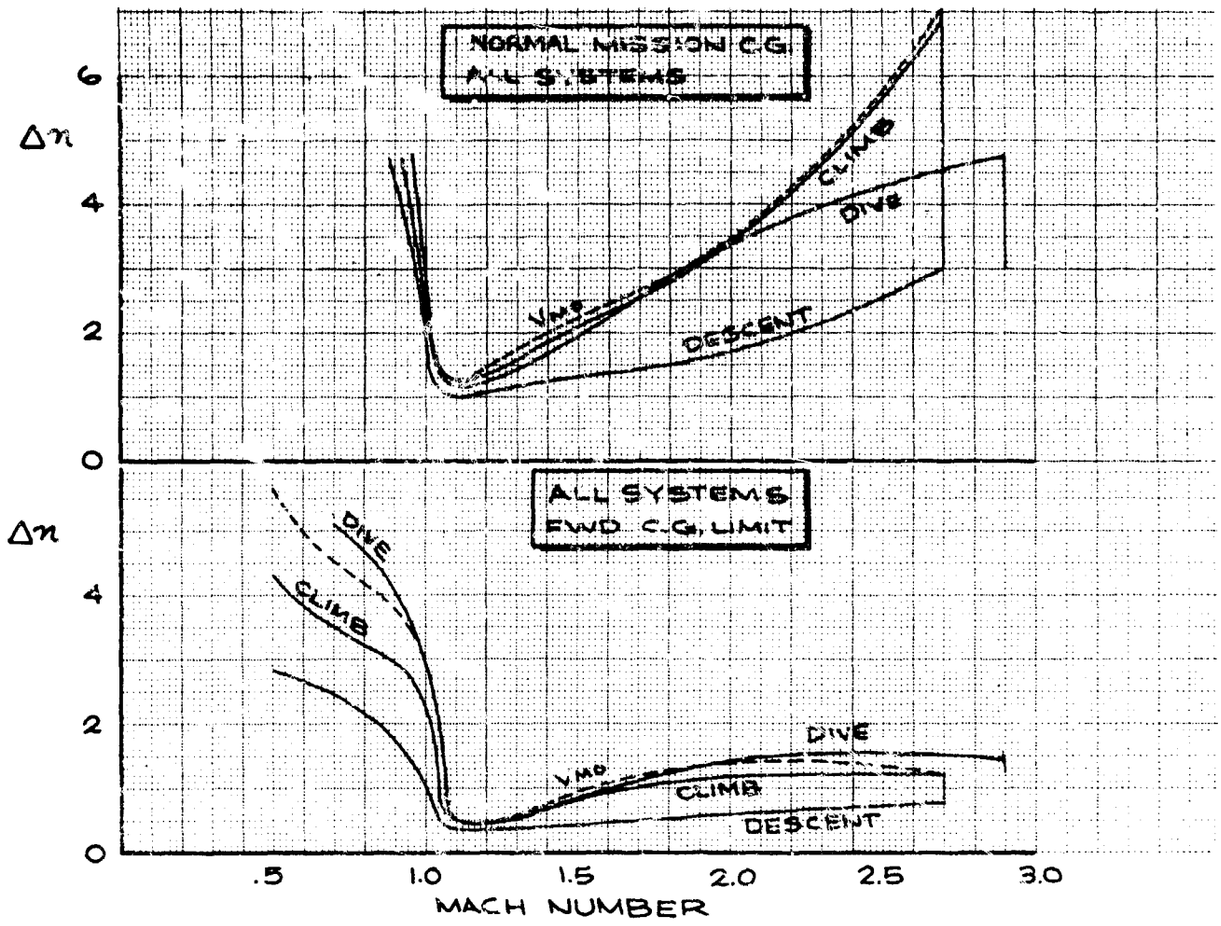


*Figure 4–14. Maneuver Capability*

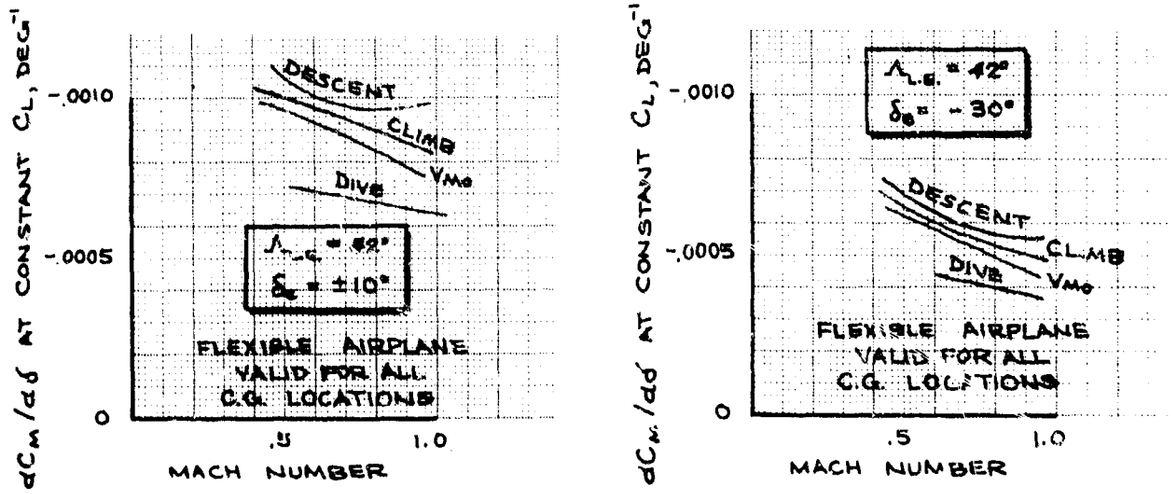


*Figure 4–15. Longitudinal Control Effectiveness, Λ = 42 Degrees*

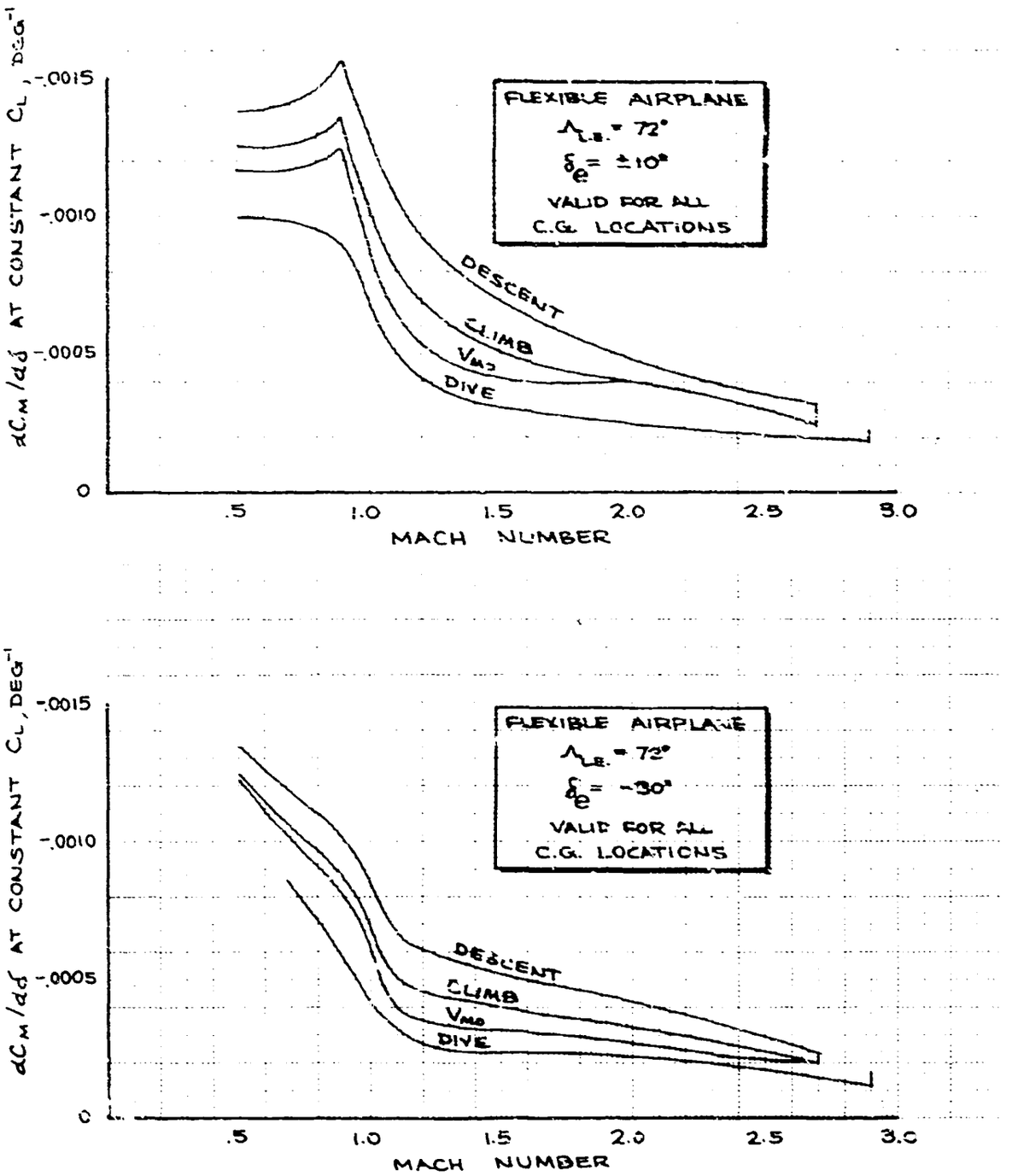


*Figure 4–16. Longitudinal Control Effectiveness, Λ = 72 Degrees*

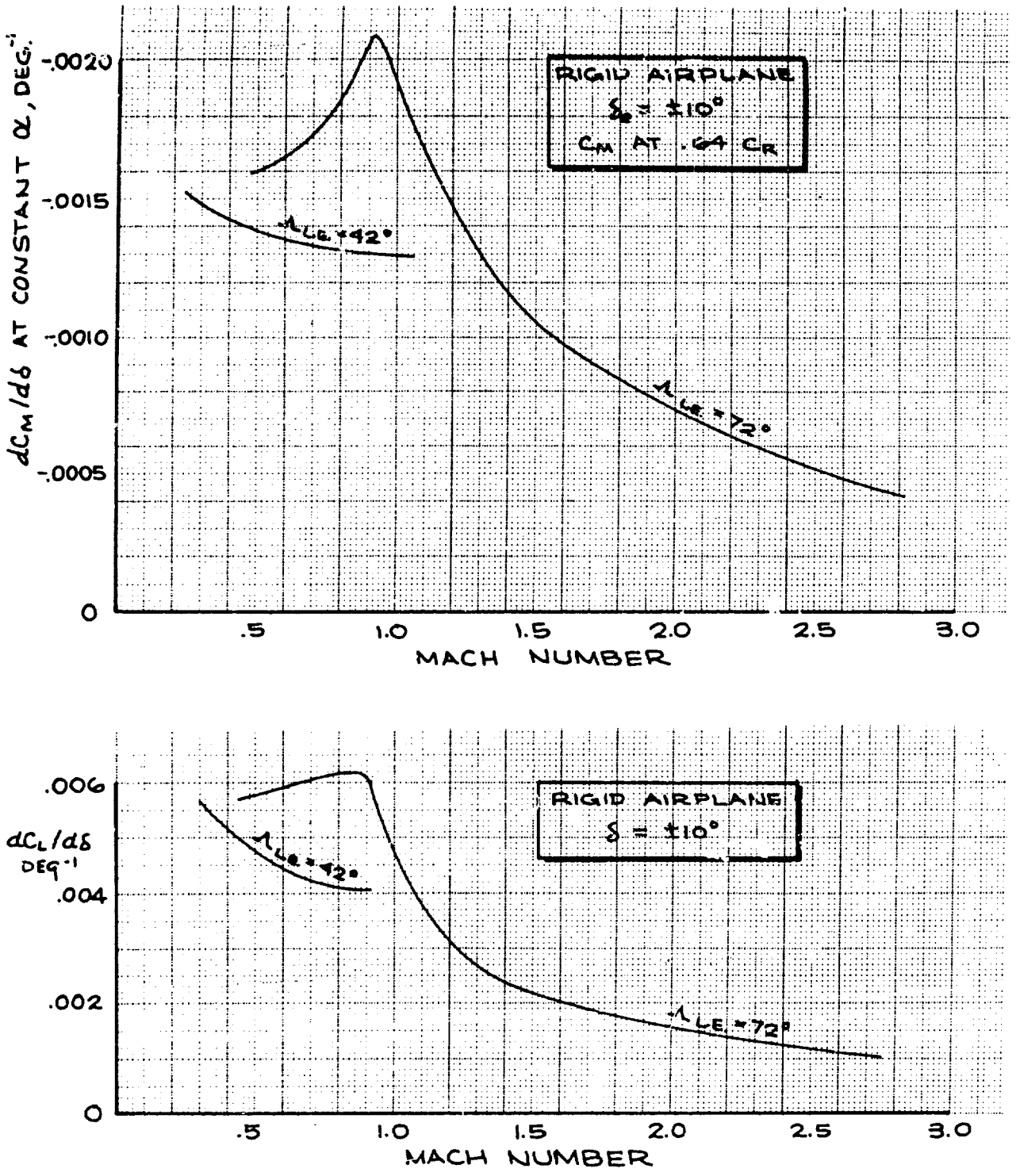


*Figure 4–17. Longitudinal Control Effectiveness , Trim, Rigid Airplane*

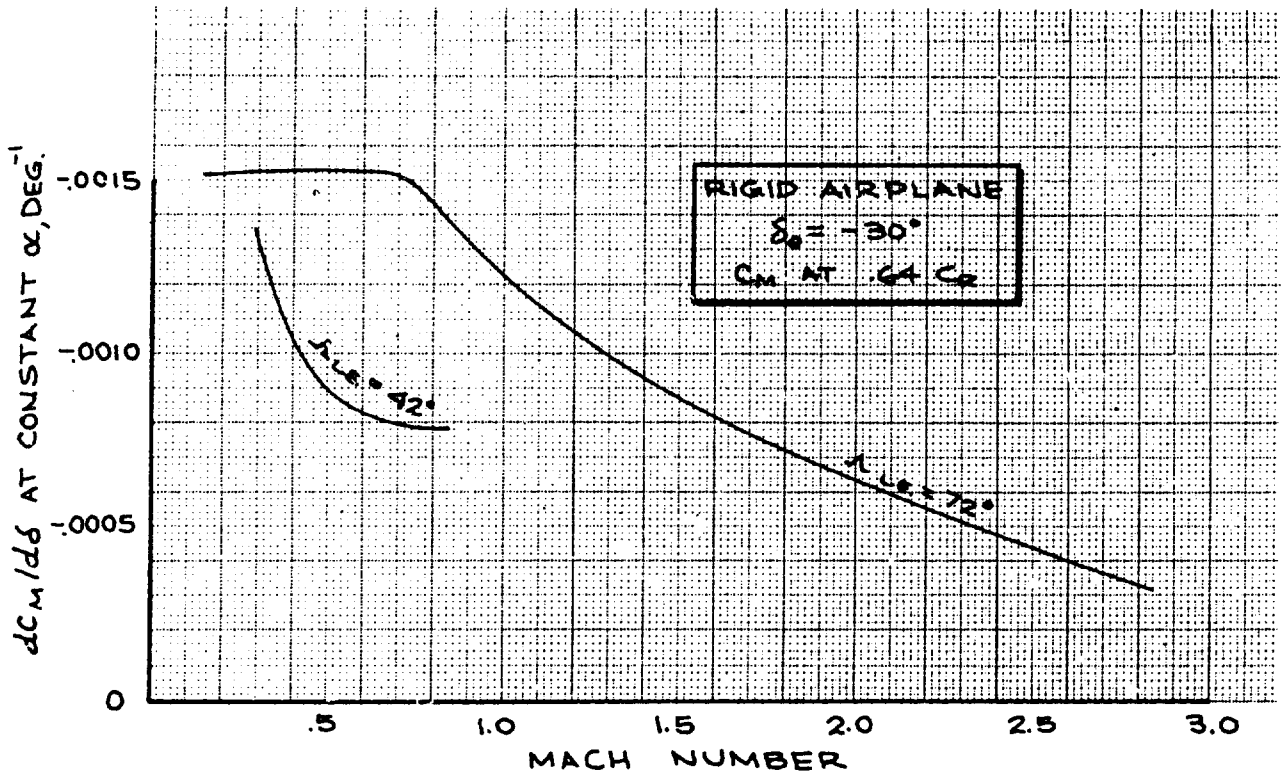


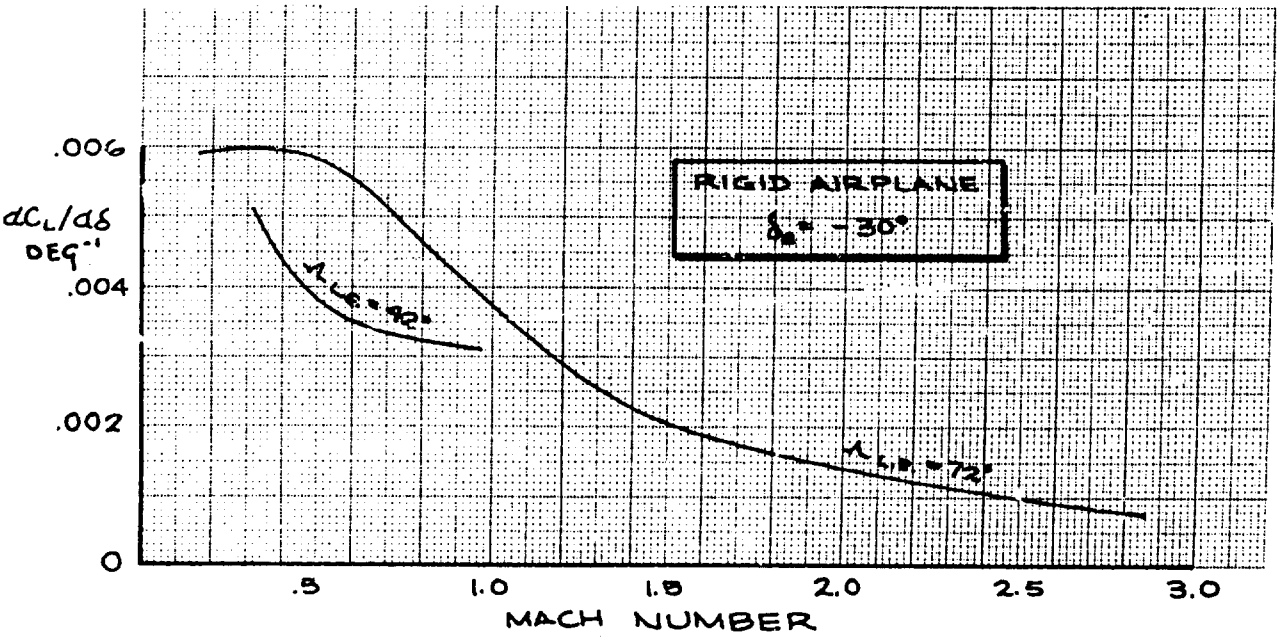


*Figure 4–18. Longitudinal Control Effectiveness, Control, Rigid Airplane*

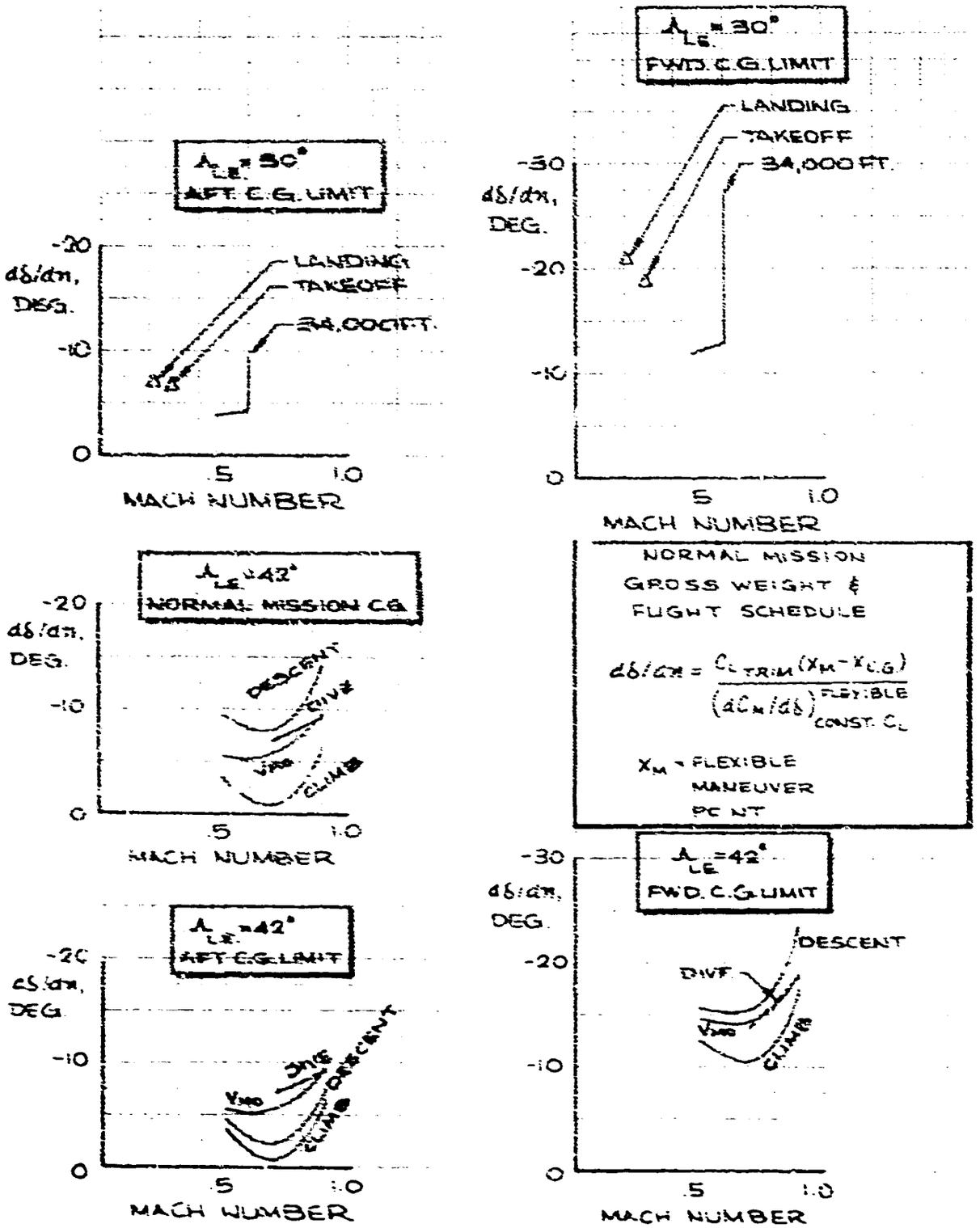


Figure 4-19. Longitudinal Control For g, Wing Forward

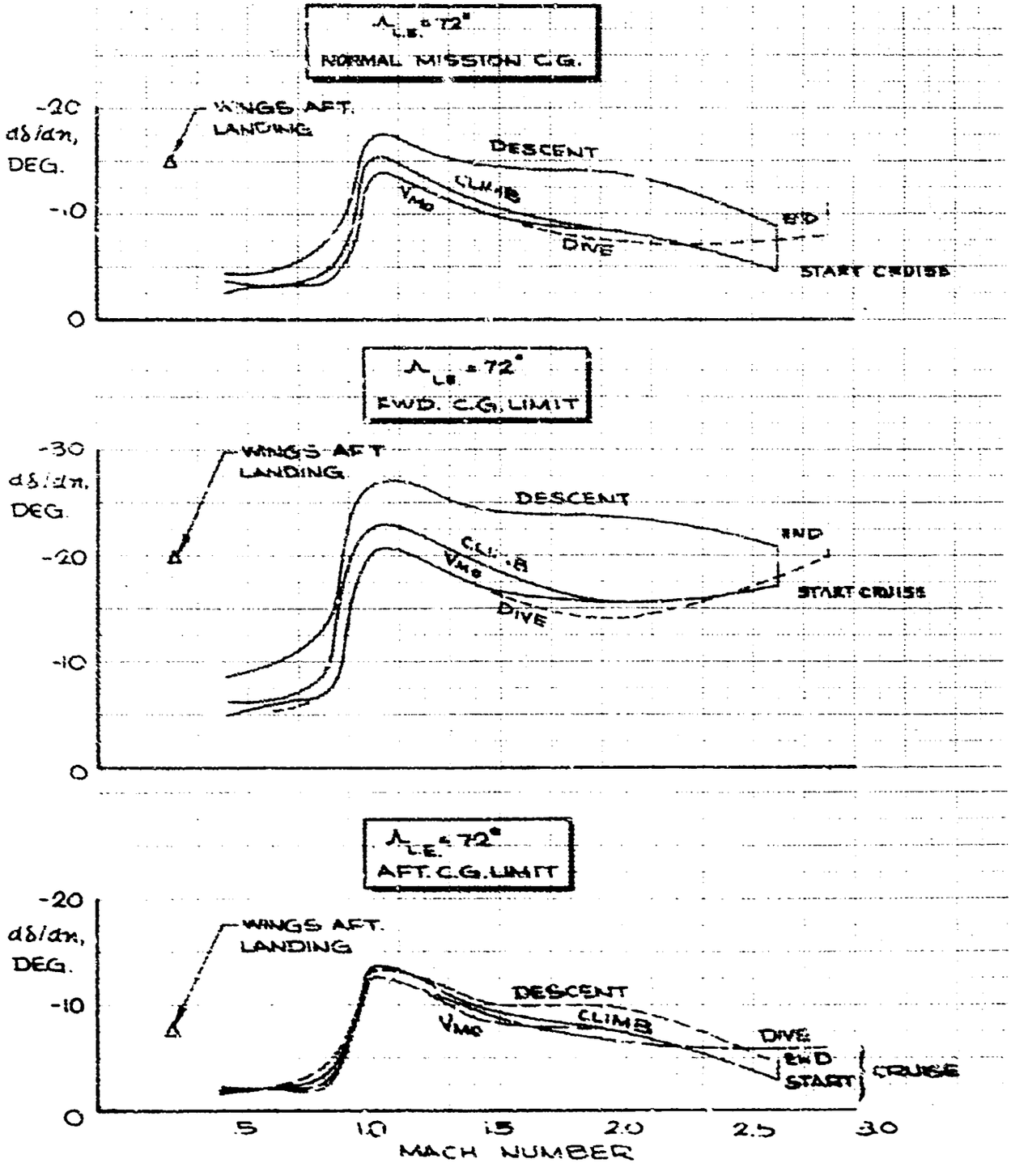


*Figure 4-20. Longitudinal Control Per g, Wings Aft*

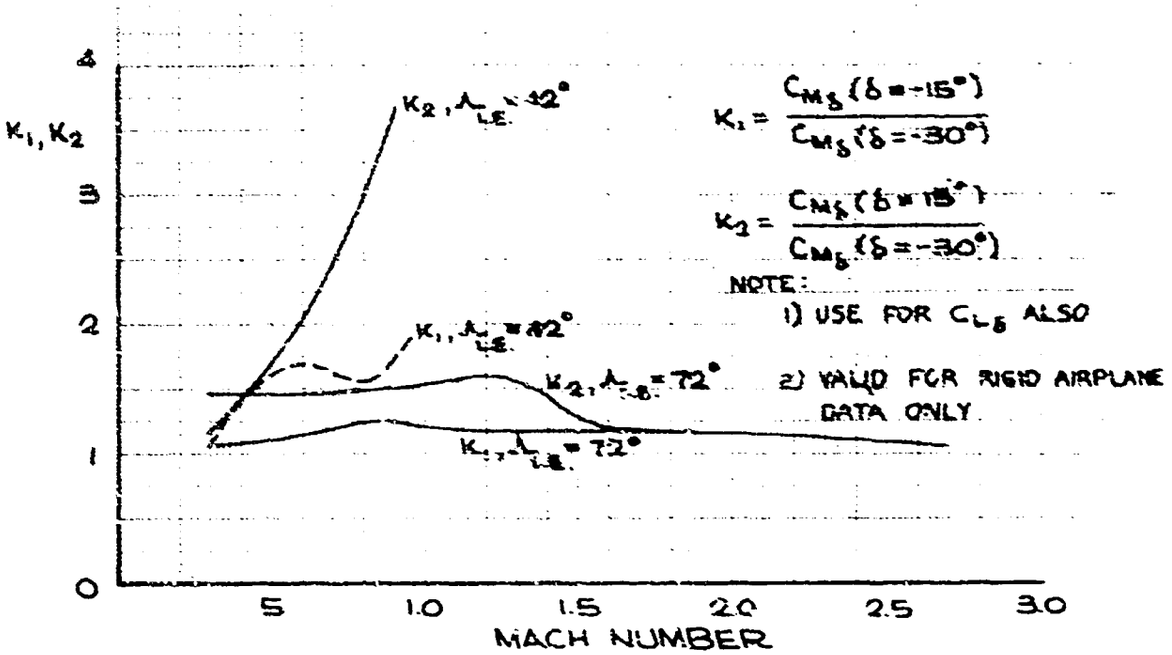


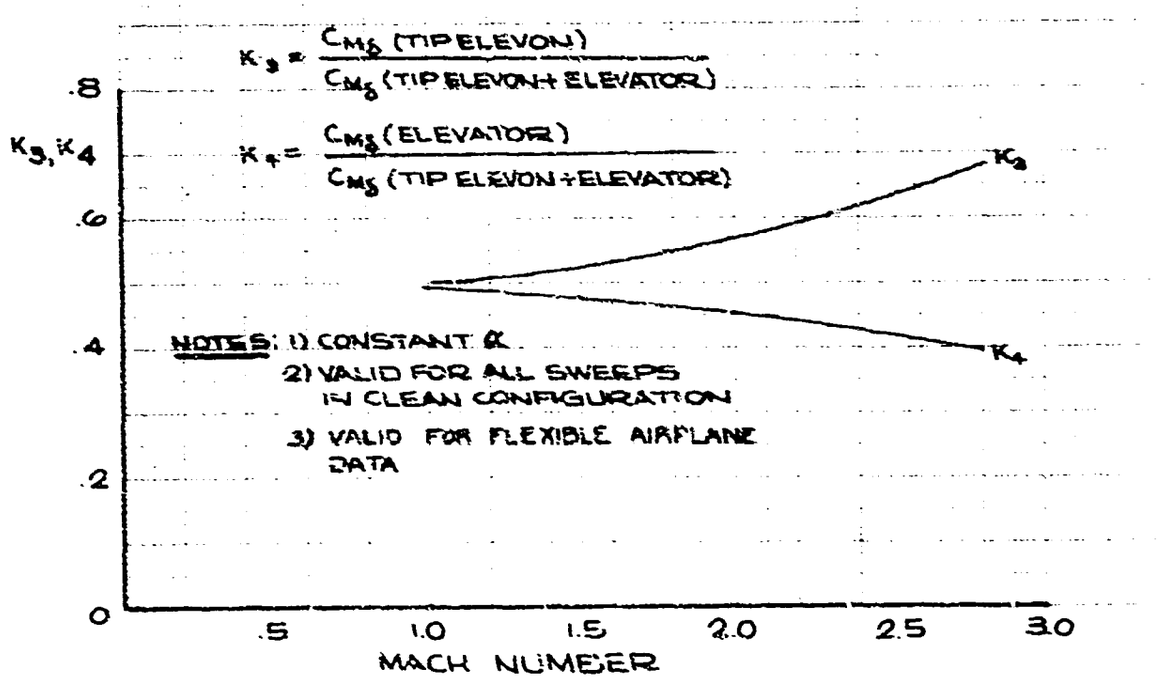


*Figure 4-21. Longitudinal Control Effectiveness Factors*

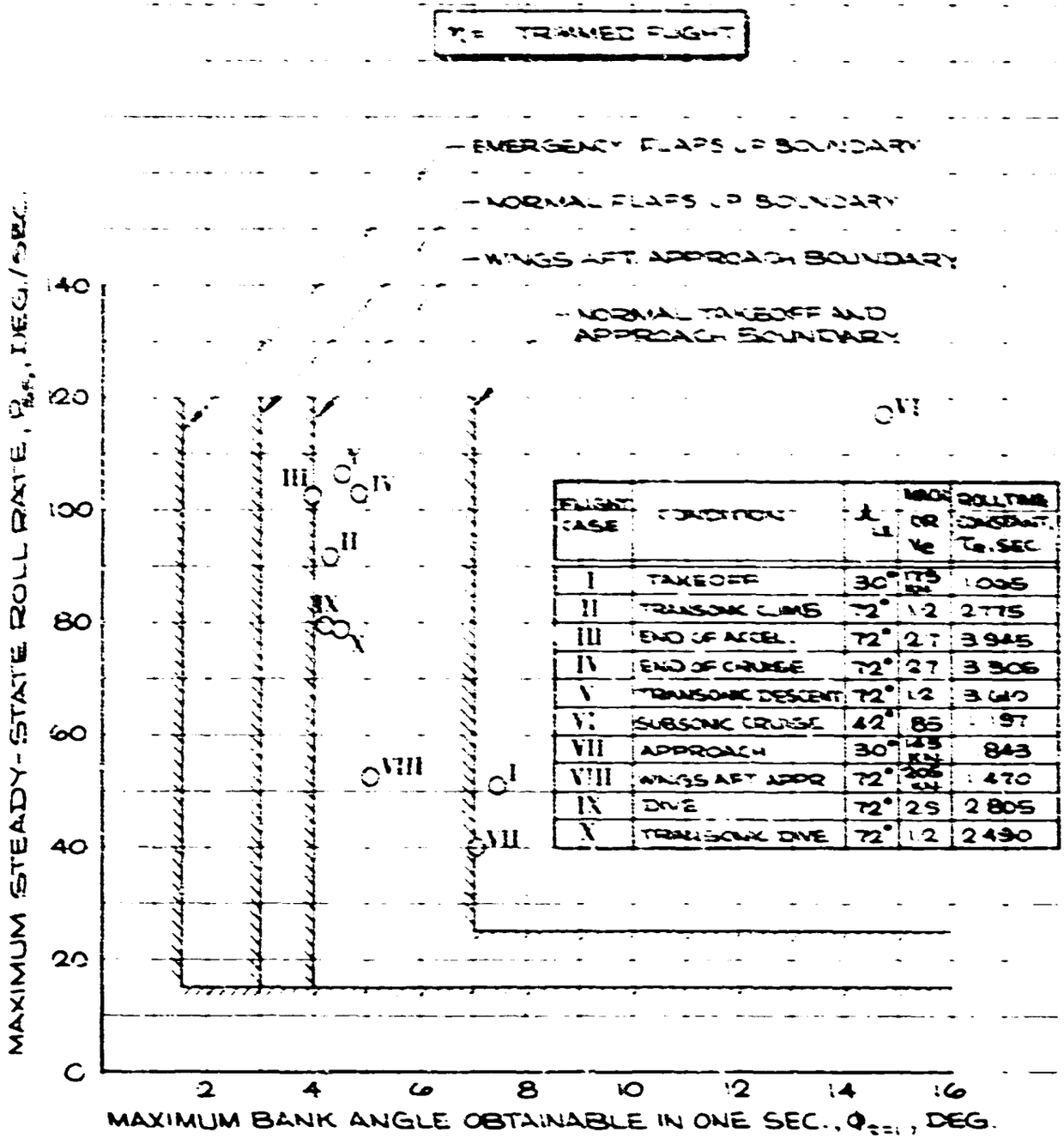


| FLIGHT CASE | CONDITION | $\delta_{TE}$ | MACH OR $V_e$ | ROLL TIME CONSTANT $T_R$, SEC |
|---|---|---|---|---|
| I | TAKEOFF | 30° | 175 KEAS | 1.035 |
| II | TRANSONIC CLIMB | 72° | 1.2 | 2.775 |
| III | END OF ACCEL. | 72° | 2.7 | 3.945 |
| IV | END OF CRUISE | 72° | 2.7 | 3.906 |
| V | TRANSONIC DESCENT | 72° | 1.2 | 3.640 |
| VI | SUBSONIC CRUISE | 42° | .85 | .97 |
| VII | APPROACH | 30° | 225 KEAS | .843 |
| VIII | WINGS AFT APPR | 72° | 206 KEAS | .470 |
| IX | DIVE | 72° | 2.5 | 2.805 |
| X | TRANSONIC DIVE | 72° | 1.2 | 2.490 |

Figure 4–22. Roll Performance

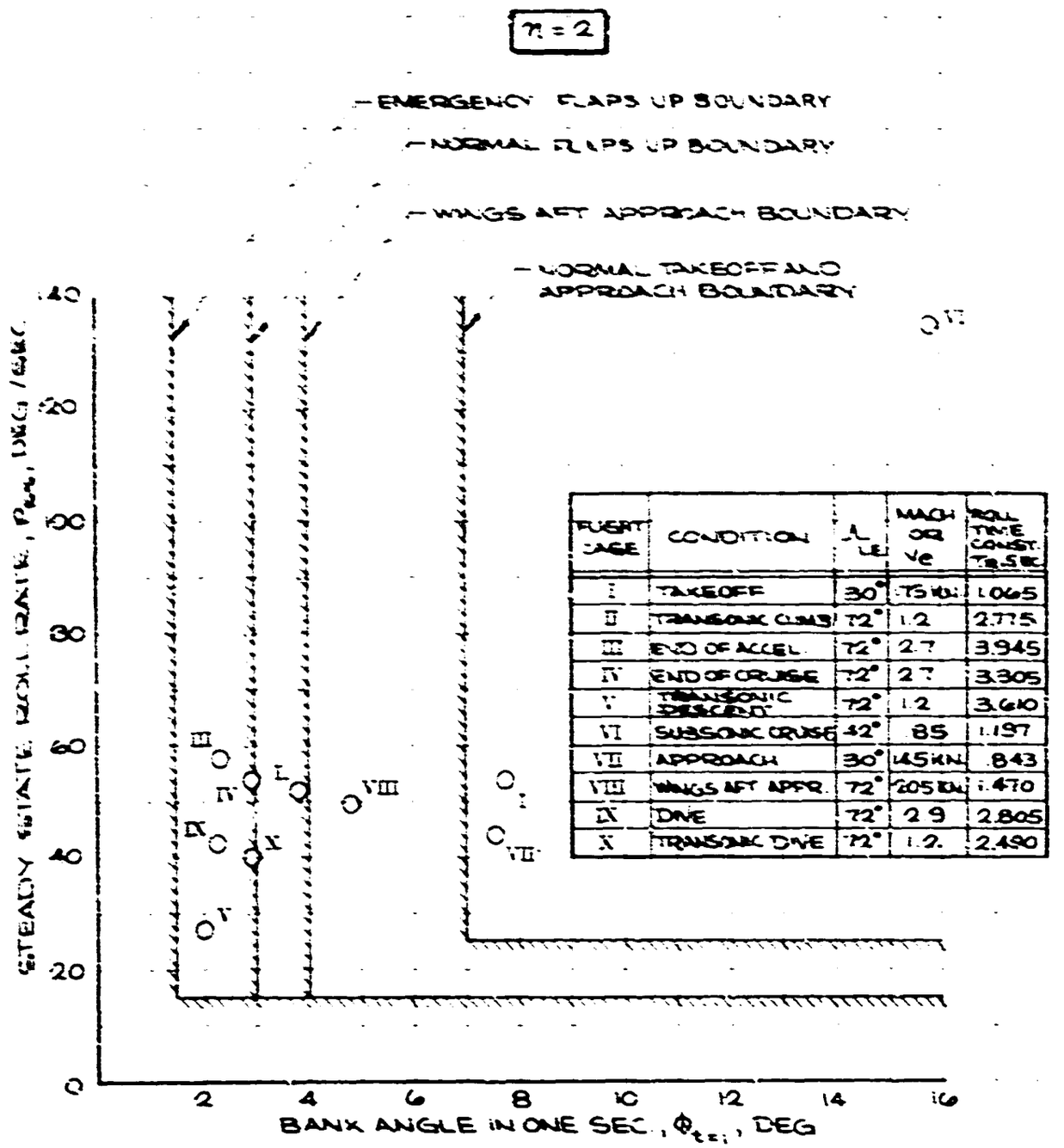


| FLIGHT CASE | CONDITION | $\Lambda_{LE}$ | MACH OR $V_e$ | ROLL TIME CONST. $T_R$, SEC |
|---|---|---|---|---|
| I | TAKEOFF | 30° | 175 KN. | 1.065 |
| II | TRANSONIC CLIMB | 72° | 1.2 | 2.775 |
| III | END OF ACCEL. | 72° | 2.7 | 3.945 |
| IV | END OF CRUISE | 72° | 2.7 | 3.305 |
| V | TRANSONIC DESCENT | 72° | 1.2 | 3.610 |
| VI | SUBSONIC CRUISE | 42° | .85 | 1.197 |
| VII | APPROACH | 30° | 145 KN. | .843 |
| VIII | WINGS AFT APPR. | 72° | 205 KN. | 1.470 |
| IX | DIVE | 72° | 2.9 | 2.805 |
| X | TRANSONIC DIVE | 72° | 1.2. | 2.490 |

Figure 4-23. Roll Performance in Maneuvering Flight

Good lateral control capability in sideslip is associated with the lateral-directional stability characteristics inherent for the variable sweep airplane in the low sweep, large span, landing configuration shown in Fig. 4-24. Lateral controllability is not degraded appreciably up to the maximum sideslip angles attainable with full rudder deflection. This is caused by the combination of small dihedral effect, roll due to sideslip, and powerful lateral control provided in the low sweep configuration.

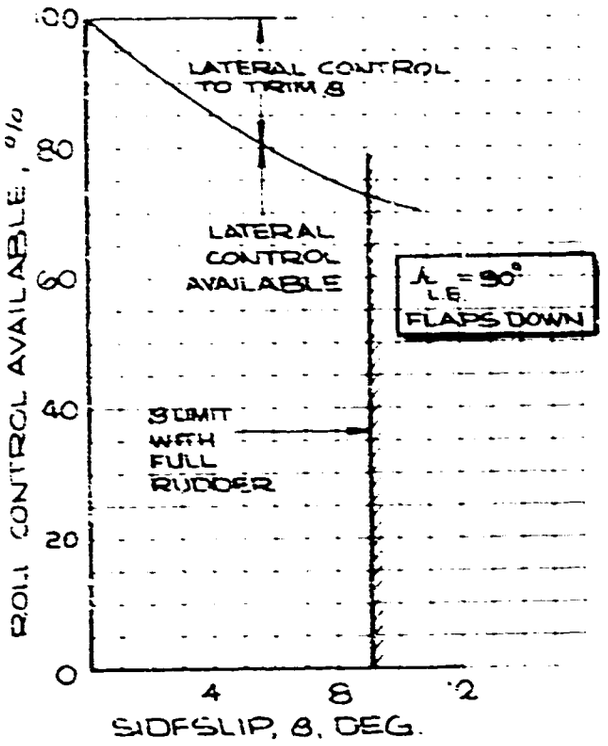


*Figure 4-24. Roll Control in Sideslip*

The rolling moment available per unit control wheel deflection is shown in Fig. 4-25 for the rigid and flexible airplane, along the $V_{MO}$ climb cruise and descent profiles, at dive placard speeds, and in landing conditions. The damping in roll, $C_{lp}$, is plotted versus Mach number for the rigid and flexible airplane for these same flight conditions in Fig. 4-26. Rigid airplane control effectiveness and yawing moment characteristics are shown in Figs. 4-27 through 4-29 as a function of angle of attack for representative Mach number and sweep conditions. The capability of maintaining positive roll control well beyond stall or limit angle of attack is evident especially in the low speed, flaps down operation. These data show the adverse yaw characteristics of the tip elevon controls. Cross-coupling introduced by these adverse yaw characteristics is discussed in Par. 4.4.

Wind tunnel test results show that the elevon provides essentially linear effectiveness from zero deflection to large deflections. These data are shown in Fig. 4-30.

Figures 4-31 through 4-33 present the airplane aeroelastic corrections to be applied to the rigid controls data in the form:

$$(C_l)_\delta^{\text{flexible}} = (C_l)_\delta^{\text{rigid}} \left(\frac{R_E}{R_R}\right)_\delta \quad \text{for aileron,}$$

elevon and spoiler and

$$(C_n)_\delta^{\text{flexible}} = (C_n)_\delta^{\text{rigid}} \left(\frac{R_E}{R_R}\right)_\delta \quad \text{for aileron and}$$

elevon, where $\left(\frac{R_E}{R_R}\right)_\delta$ is the aeroelastic roll

factor for the control.

No aeroelastic corrections are applied to the side force terms which are assumed rigid for all controls. No aeroelastic correction is applied to the rigid spoiler yaw term ($C_{n_\delta}$) since the reduction in parasite drag of the spoiler due to wing flexibility is approximately matched by increased induced wing drag with wing flexibility. Conversely, an aeroelastic correction is applied to the rigid aileron and elevon yaw effects ($C_{n_\delta}$) since the yawing moment arises from the induced drag difference between left and right surfaces deflected antisymmetrically.

Roll damping equations are on next text page.

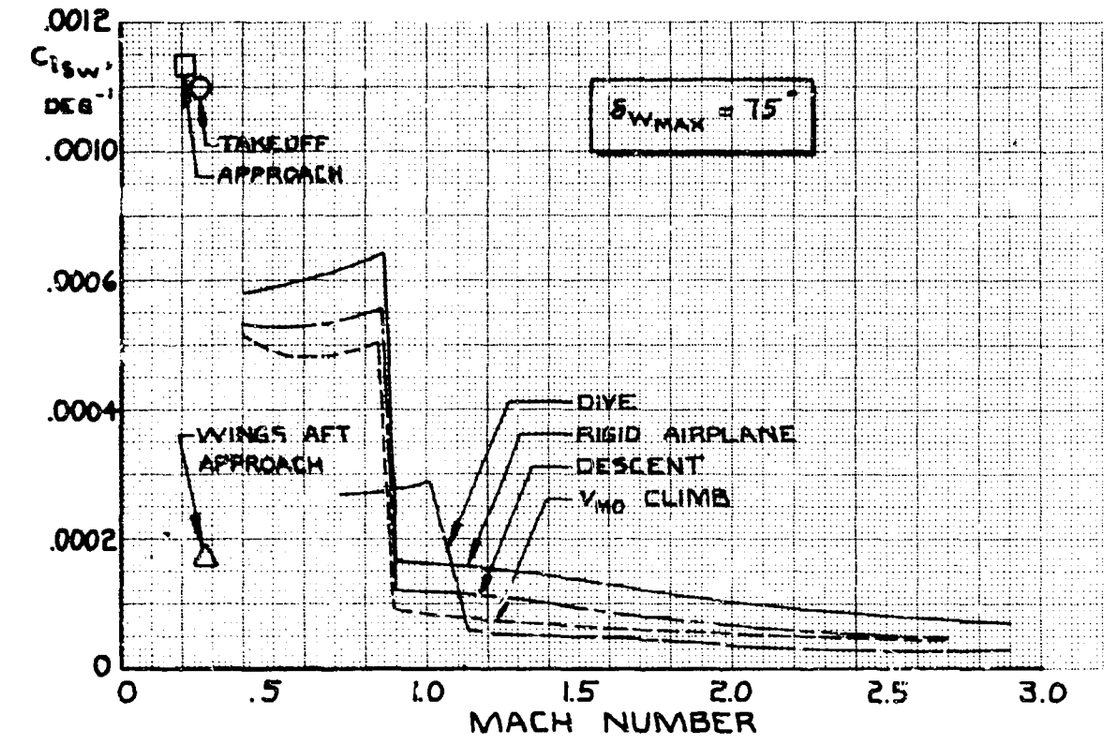


*Figure 4–25. Rolling Moment Per Unit Wheel Deflection*

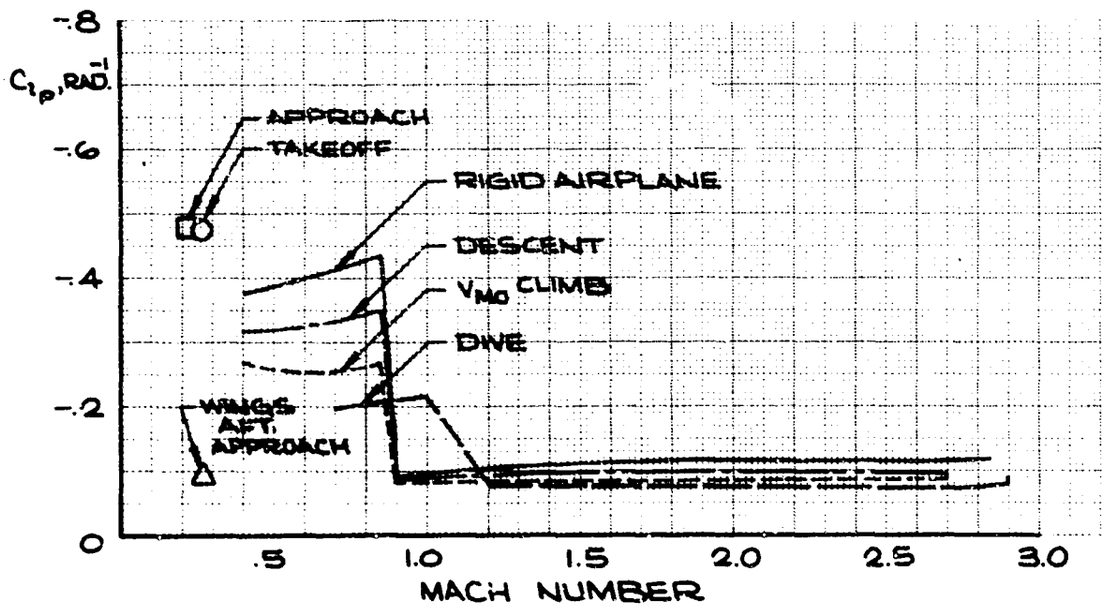


*Figure 4–26. Roll Dampina Derivative*

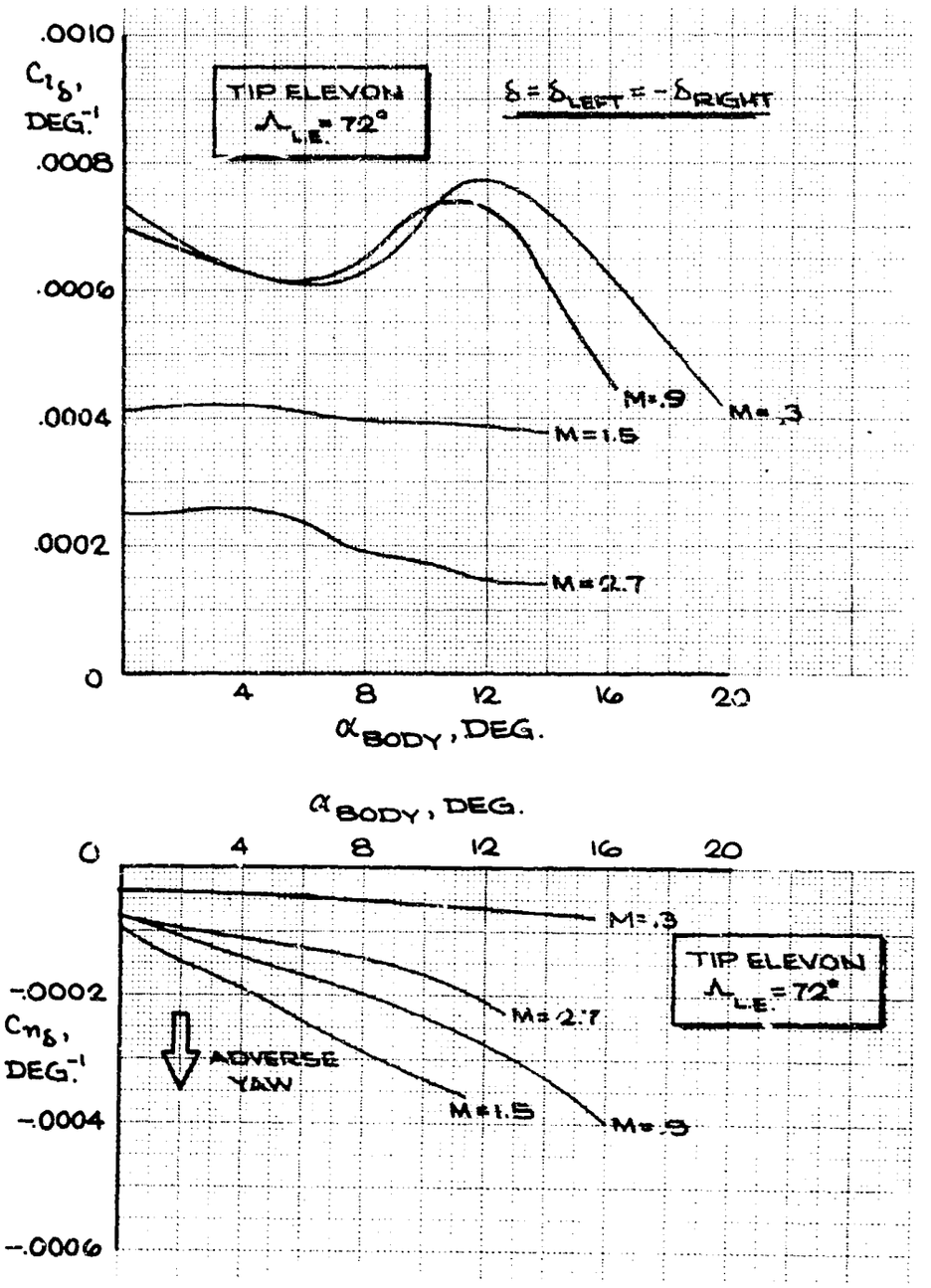


*Figure 4-27. Tip Elevon Effectiveness, Rigid Airplane*

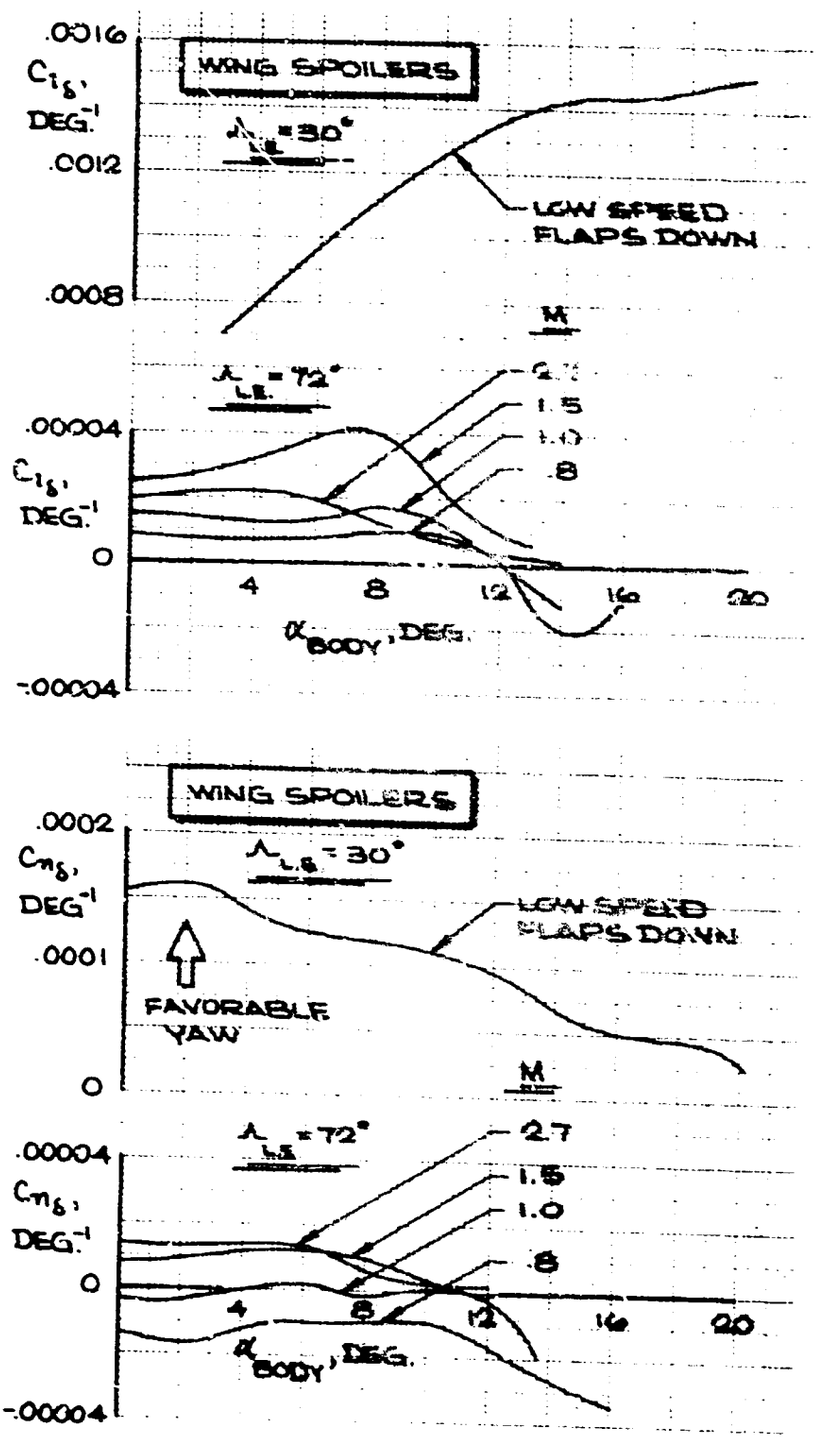


*Figure 4-28. Wing Spoiler Effectiveness, Rigid Airplane*

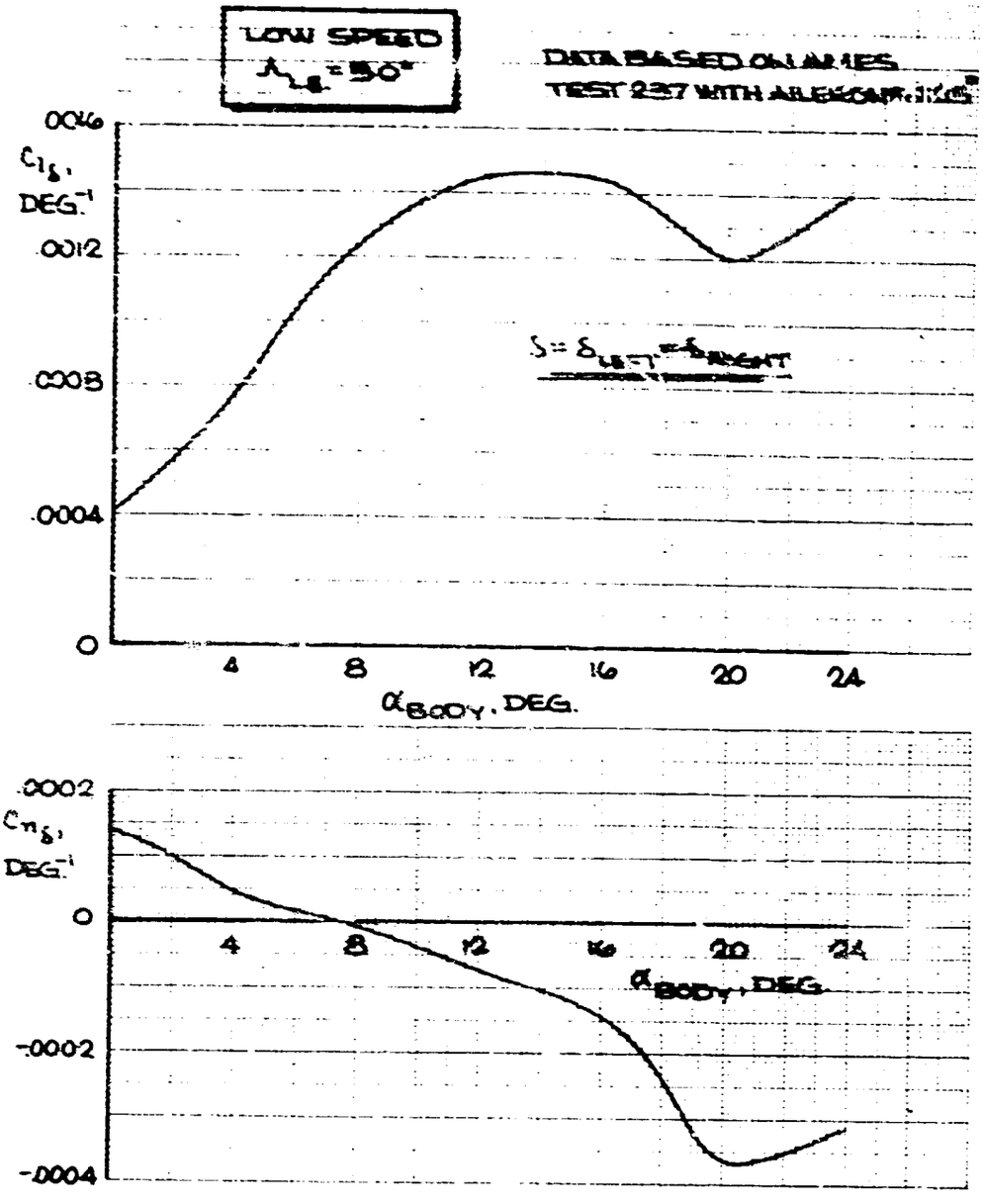


*Figure 4–29. Wing Aileron Effectiveness, Rigid Airplane*

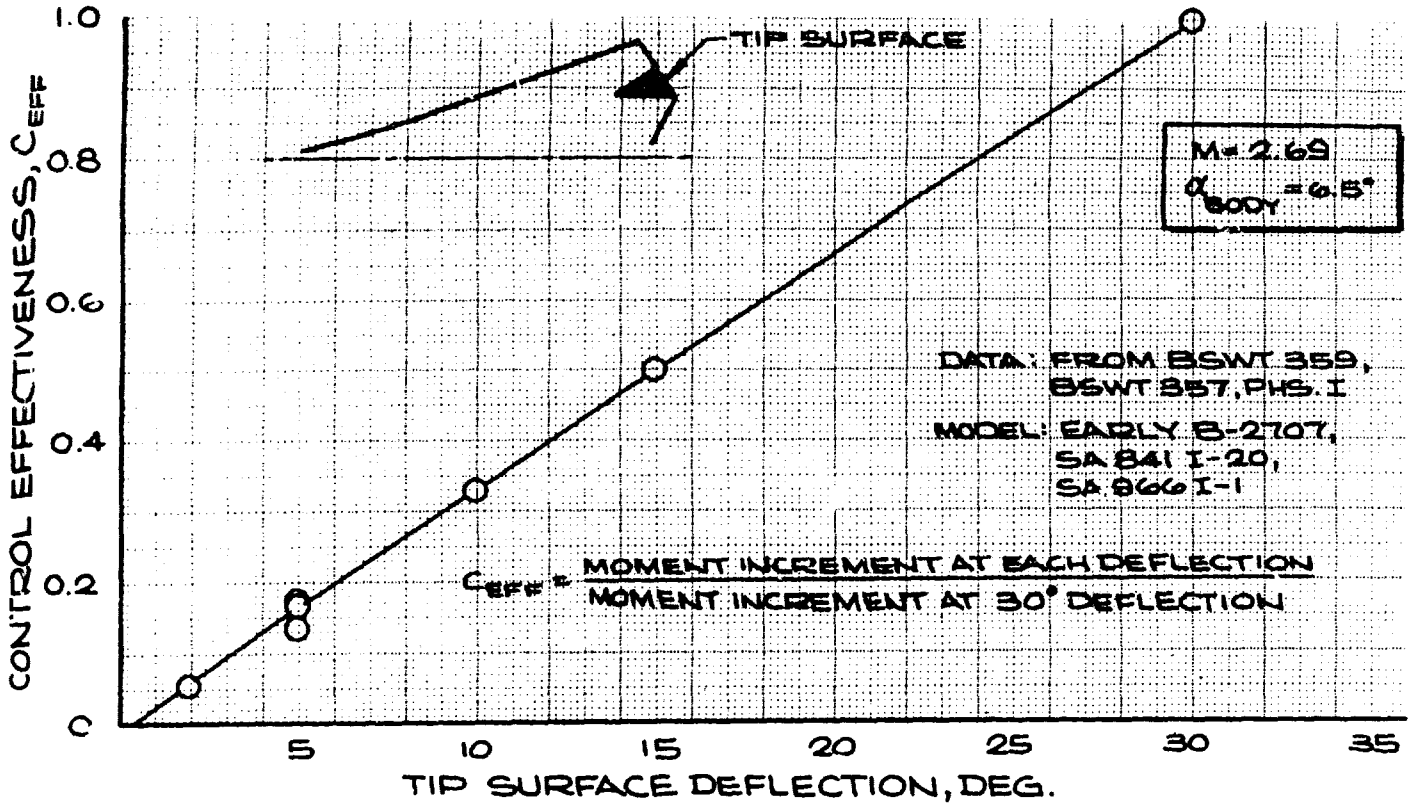


*Figure 4-30. Tip Elevon Effectiveness*

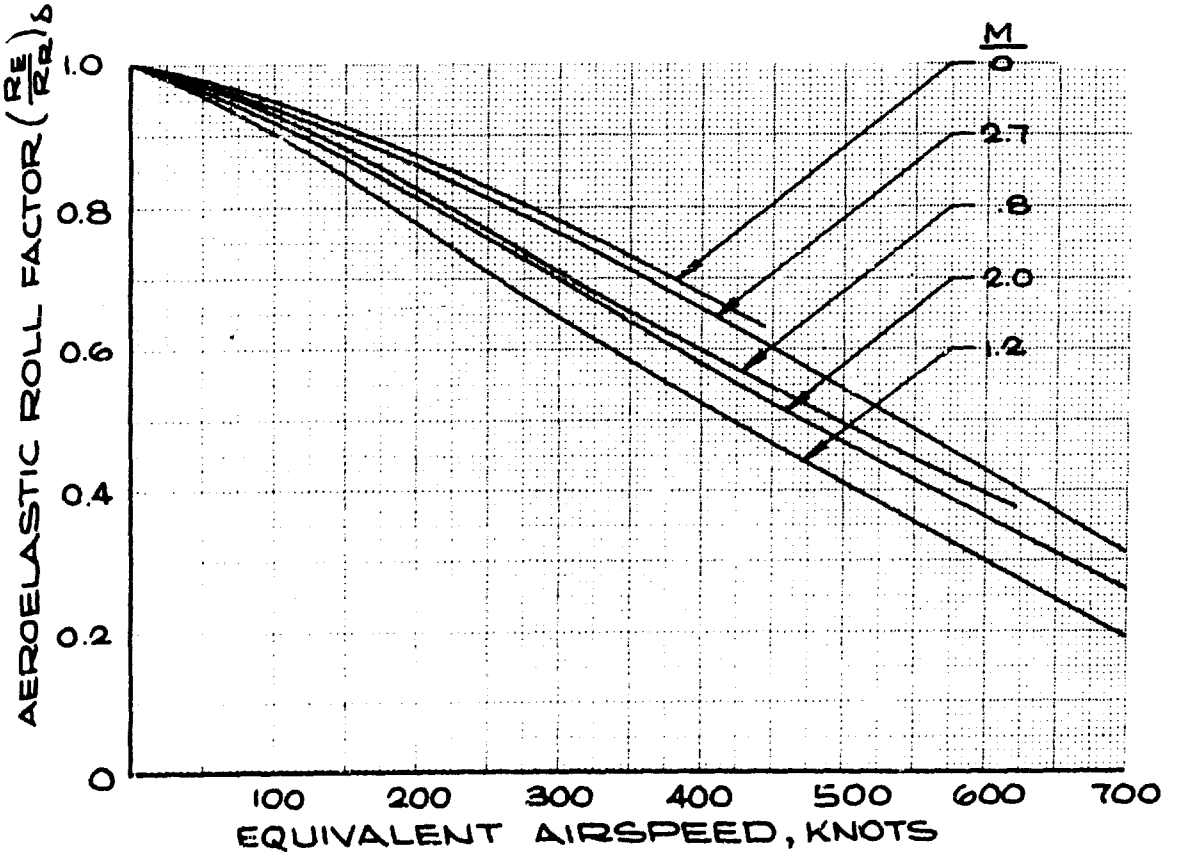


*Figure 4-31. Aeroelastic Factor for Tip Elevon*

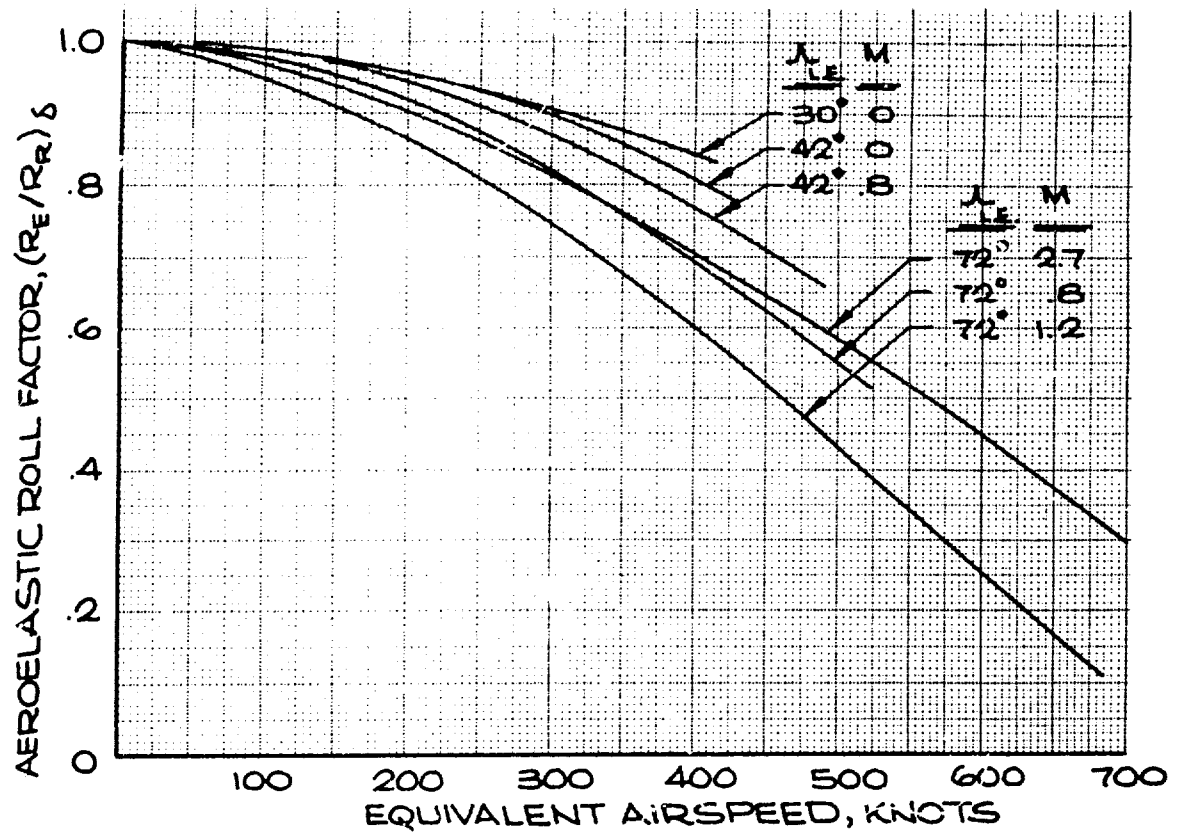


*Figure 4–32. Aeroelastic Factor for Wing Spoilers*

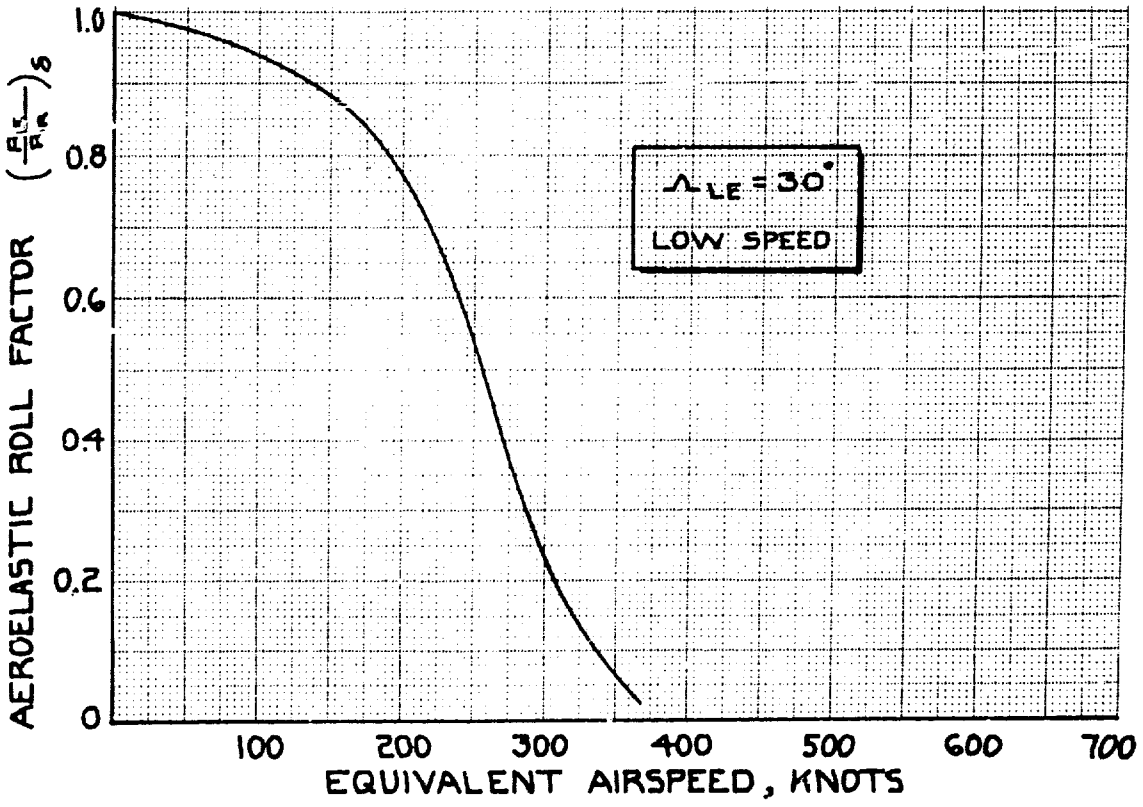


*Figure 4–33. Aeroelastic Factor for Wing Allerons*

The rigid roll damping coefficient $C_{l_p}$ is corrected as follows:

$$(C_{l_p})^{\text{flexible}} = (C_{l_p})^{\text{rigid}} \left(\frac{R_E}{R_R}\right)_p \text{ where}$$

$\left(\frac{R_E}{R_R}\right)_p$ is the aeroelastic factor on roll damping and shown in Fig. 4-34

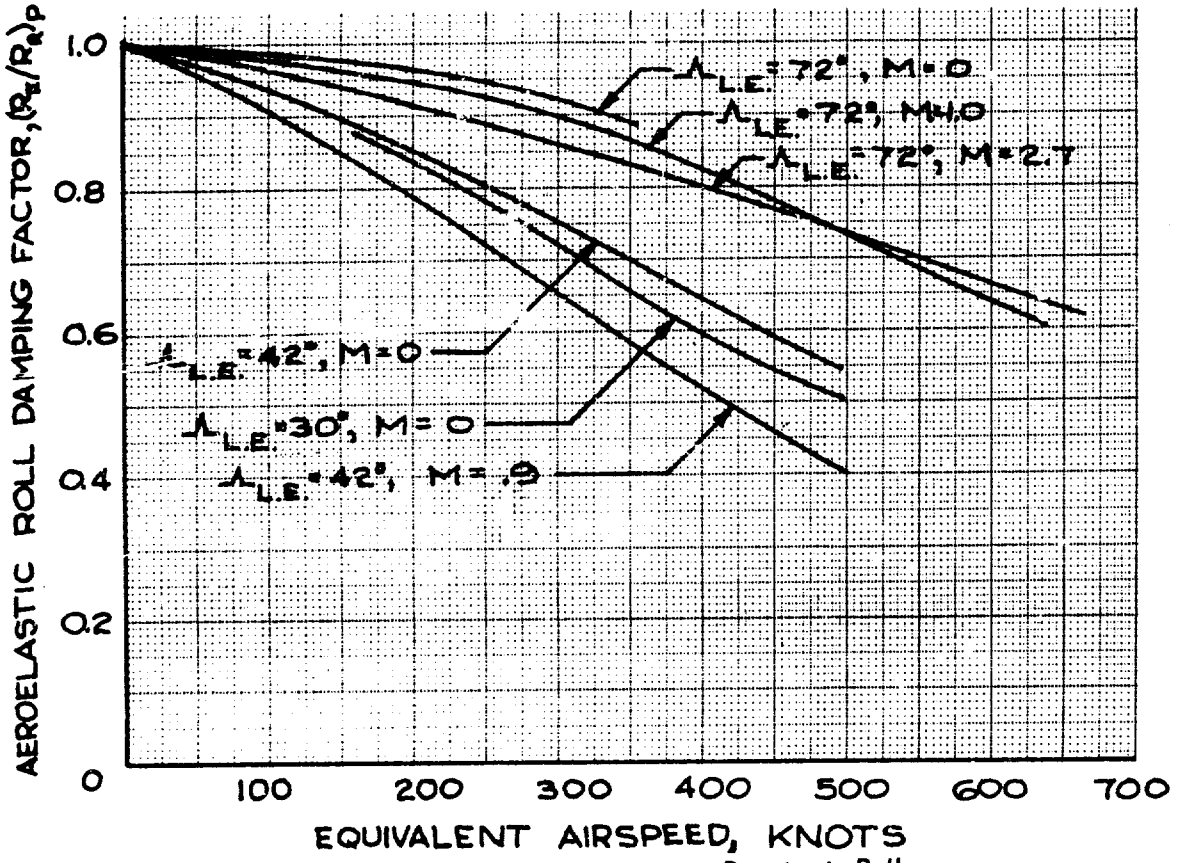


*Figure 4-34. Aeroelastic Factor on Damping in Roll*

4.1.3 Directional Control

Directional control is provided by a single piece rudder mounted on the low aspect ratio vertical tail. The rudder is powered by a triple hydraulic system and has control stops to limit rudder deflection. The deflection limits are controlled by wing flap position and wing sweep, as described in Sec. 5.0. The rudder is sized to provide adequate control for the critical single engine failure at takeoff, and has the capability of controlling landings in 90-degree crosswinds greater than 30 kn.

Figure 4-35 shows the ability of controls to handle the critical single engine failure at takeoff Full rudder, applied to trim the asymmetric thrust and windmill drag, provides values for minimum control speed, $V_{MC}$ (on ground, no nosewheel steering), of 132.5 kn for the B-2707 (GE) with engines at full afterburner thrust, and $V_{MC}$ = 115 kn with maximum dry thrust. The $V_{MC}$ speeds are 130kn and 115kn for the B-2707 (P&WA) with engines at maximum and 80 percent of maximum augmented thrust. A comparison with the FAR requirement shows that ample control margin is provided at normal takeoff weights. With maximum dry thrust B-2707 (GE) or 80 percent maximum augmented thrust with B-2707 (P&WA), adequate margins are provided for weights as low as 520,000 lb.

The crosswind landing capability is shown in Fig. 4-36. Full rudder produces 9.2 degrees of sideslip. About 30 percent of the lateral control

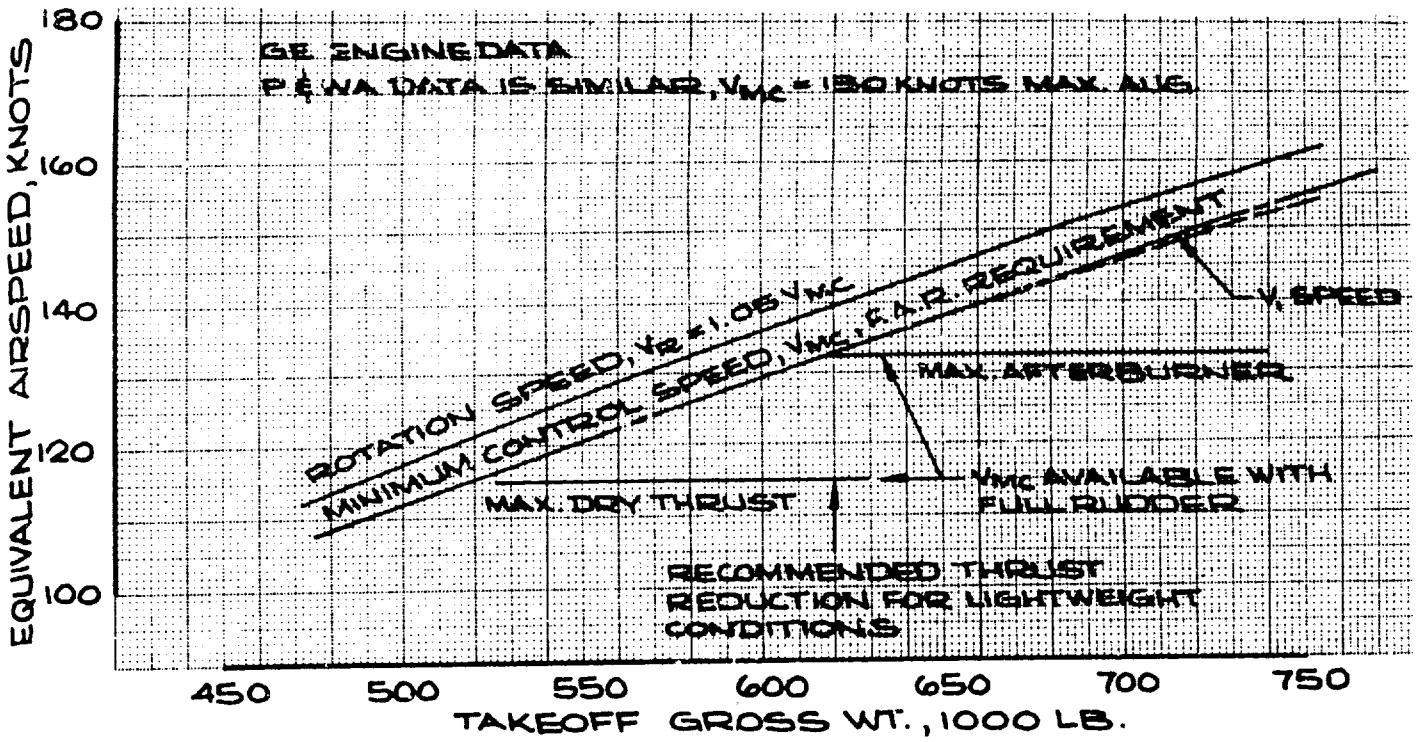


*Figure 4-35. Takeoff Minimum Control Speeds*

apability is required to maintain wings level ar. 4.1.2). The 9.2-degree sideslip provides 33.1 kn, 90-degree crosswind capability equivaent to 13.2 degrees of sideslip, with the assumption at the airplane can be landed comfortably with degrees of crab remaining at touchdown. Crosswind velocities are normally quoted at the tower eight of 50 ft; application of the standard FAR indshear correction (Fig. 4-37) gives a crosswind capability of 36.6 kn measured at tower levation. The 36.6-kn, 90-degree crosswind apability quoted for the B-2707 follows the rocedure of determining crosswind landing apabilities developed in certification of commerial jet transports. Crosswind control capability determined by computing the maximum sideslip eveloped with full rudder and adding to this degrees of crab on the gear, which is the ractical limit of crab that can be taken comfortbly by the gear at touchdown. Boeing experience demonstrating crosswind landings and the evelopment of this criteria for establishing aximum crosswind landing capabilities are escribed in Ref. 26.

igid and elastic rudder effects are shown in igs. 4-38 and 4-39. Figure 4-40 presents the udder aeroelastic data that is used to correct ne rigid data as follows:

$$\left[C_{(\ )_{\delta_r}}\right]_{\text{flexible}} = \left[C_{(\ )_{\delta_r}}\right]_{\text{rigid}} \left(\frac{M}{M_R}\right)_r \left(K_{BB}\right)_{\text{vert.}}$$

where $\left(\frac{M_E}{M_R}\right)_r$ is the aeroelastic factor on rudder effectiveness due to vertical tail flexibility, and

$K_{BB}$ vertical is the aeroelastic factor on rudder effectiveness due to body side bending,

$\left(K_{BB}\right)_{\text{vertical}}$ is shown in Par. 4.2.2.

## 4.2 STATIC STABILITY

### 4.2.1 Longitudinal Static Stability

The large span, close-coupled tail arrangement of the airplane provides essentially linear stability characteristics for all flight conditions except low speed. At Mach numbers less than about 0.5, pitch instabilities exist at angles of attack near stall. An angle of attack warning and control system (Systems Report, Part B, V2-B2707-11) has been designed for the B-2707 to prevent inadvertent exposure to extreme attitudes at all flight conditions. Wing and strake leading edge slats eliminate instabilities for all wing sweeps, flaps up. However, moderate pitch up exists for

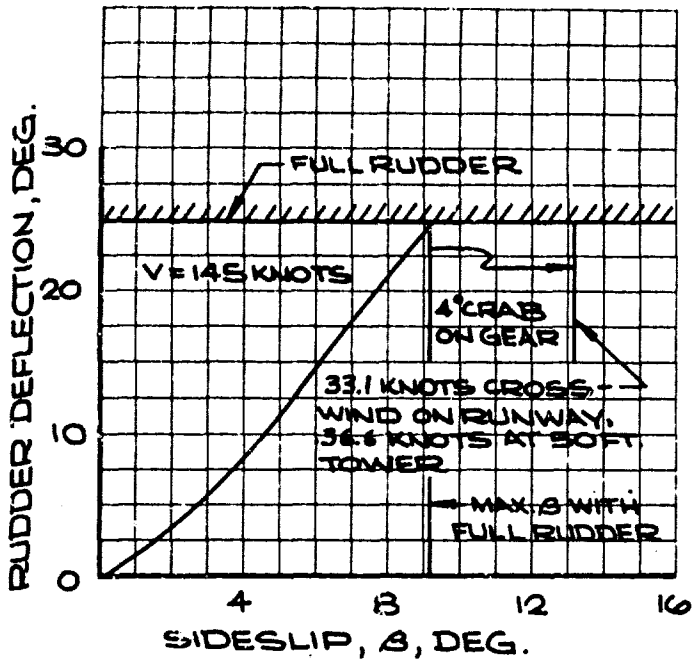


*Figure 4–36. Rudder Control, Crosswind Landing*

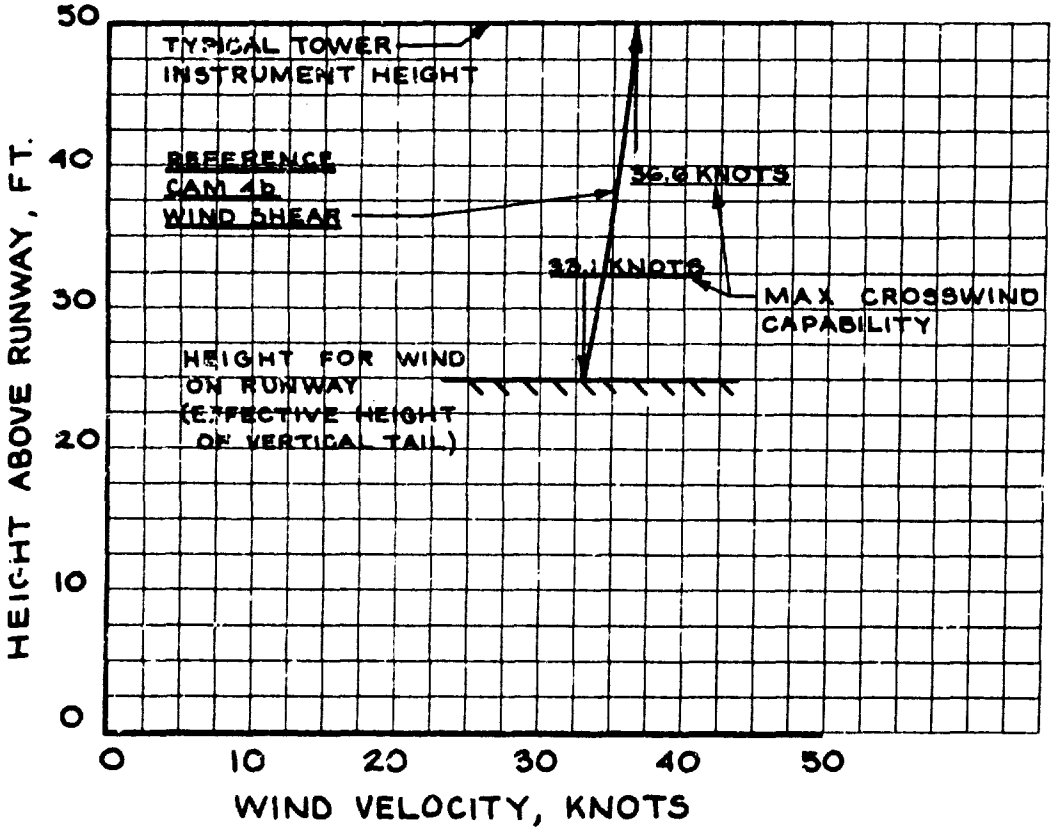


*Figure 4–37. Wind Shear Effect*

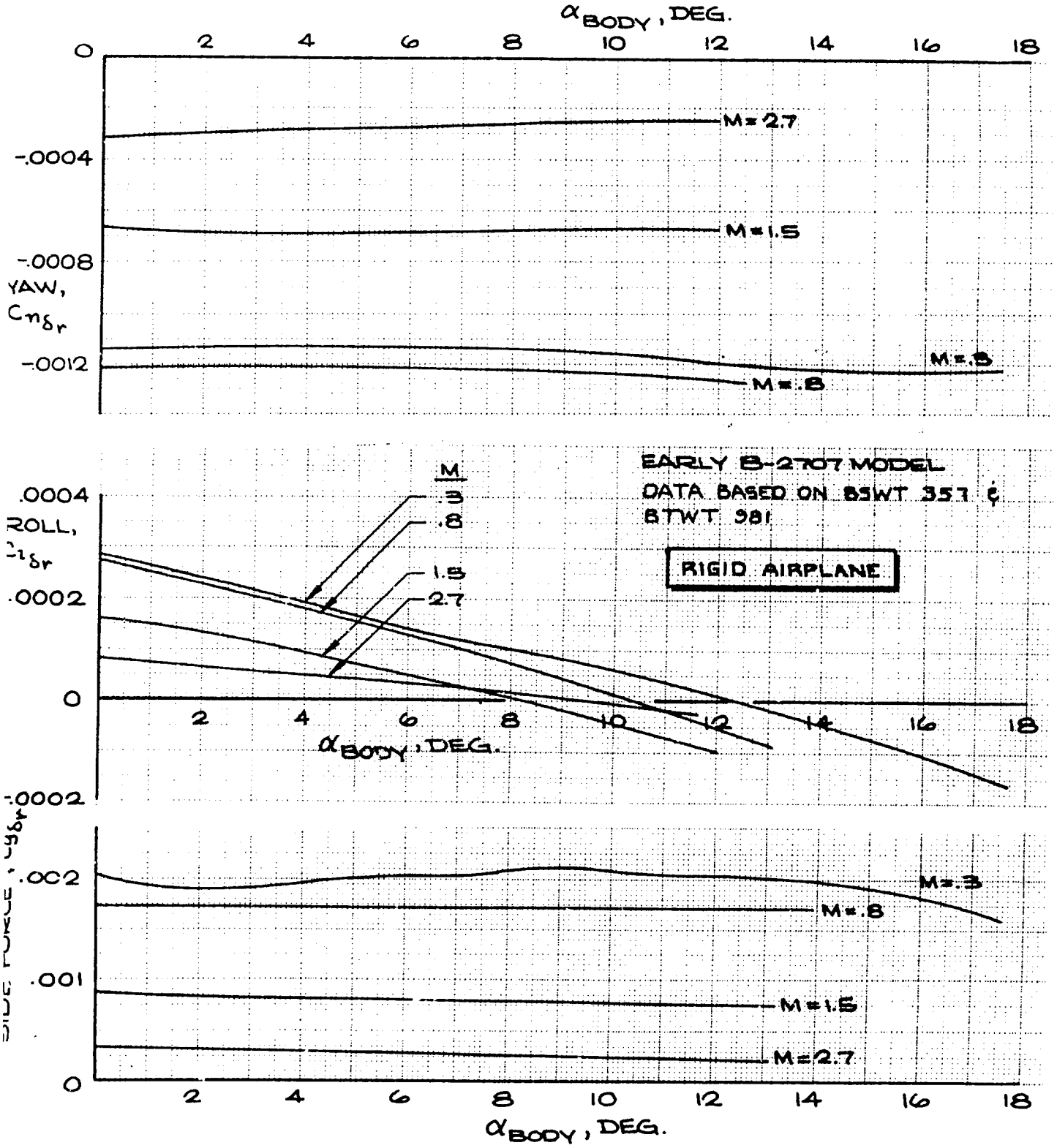


*Figure 4–38. Rudder Effectiveness, Rigid Airplane*

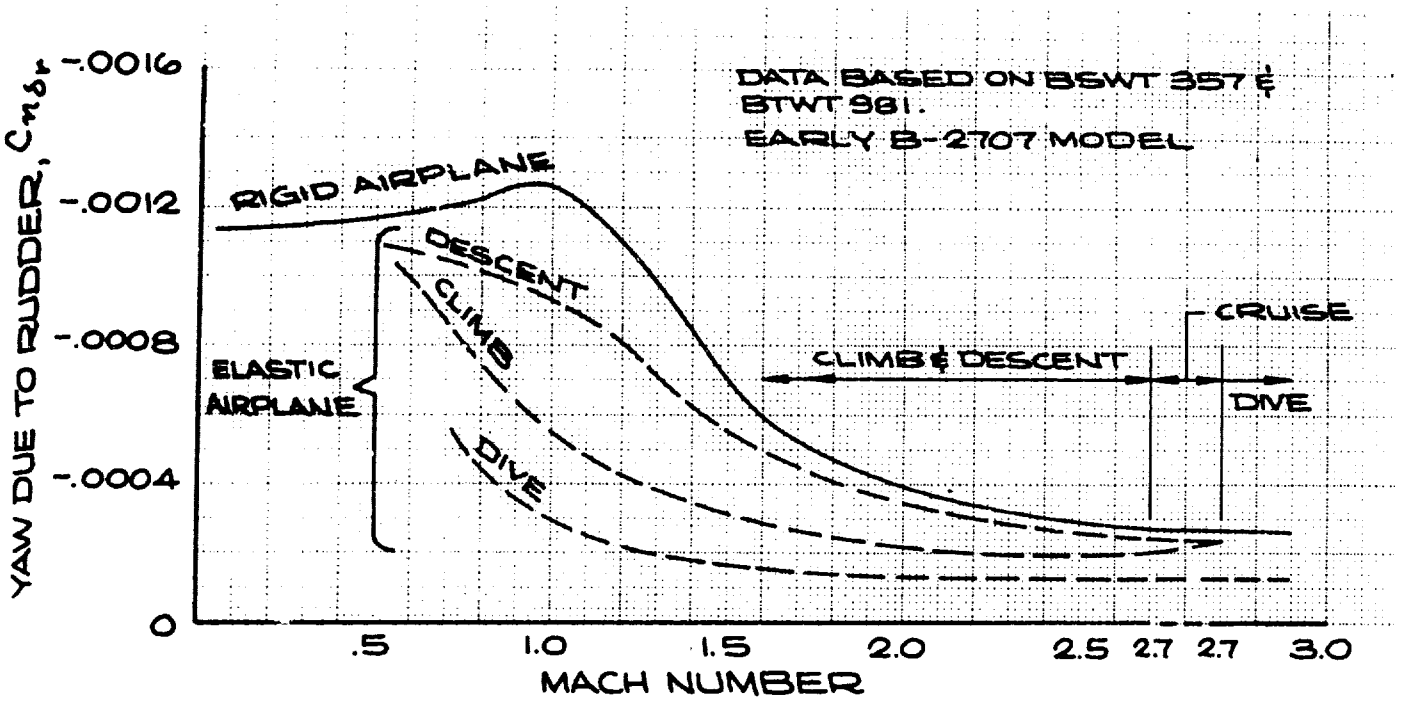


*Figure 4–39. Rudder Effectiveness, Flexible Airplane*

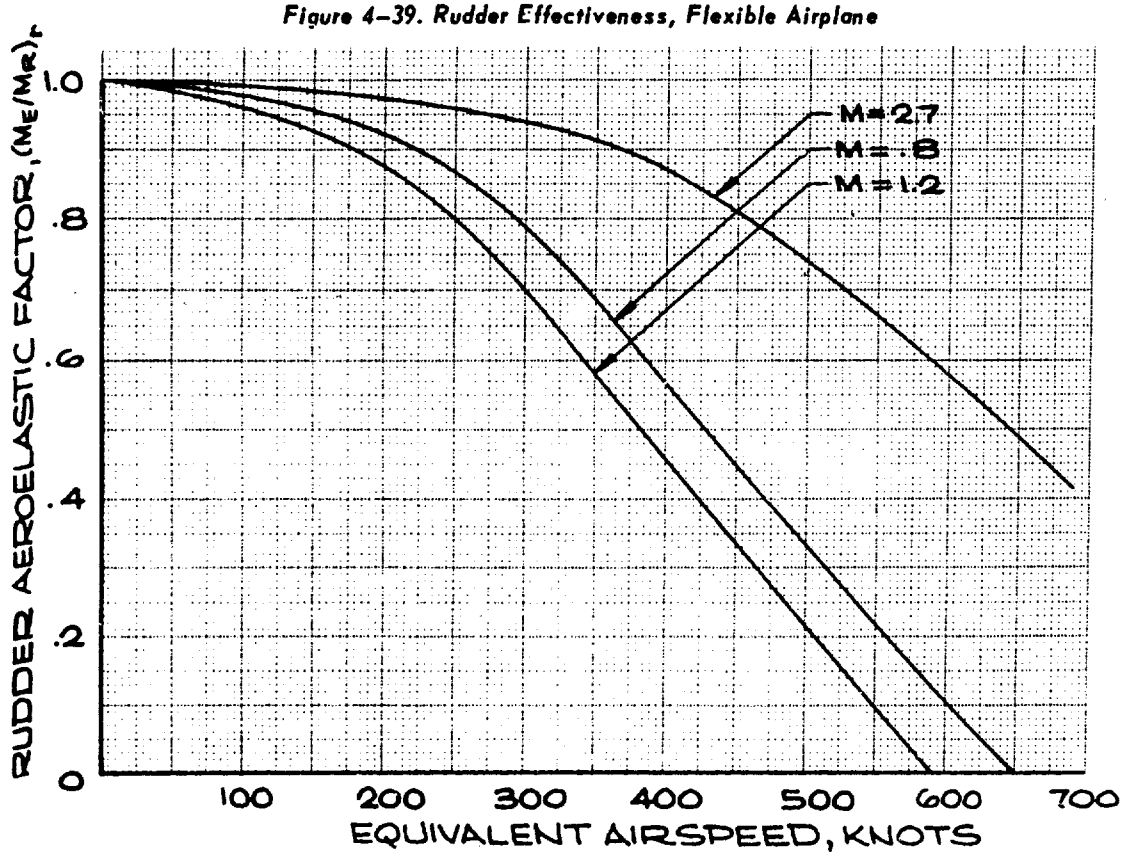


*Figure 4–40. Aeroelastic Factor for Rudder*

flaps down. Additional aerodynamic improvements will be explored in case they should be required to eliminate stall pitch up for flaps-down operation.

Placing engines aft on the B-2707 has caused a relatively far aft longitudinal balance. Considerable effort has been directed toward placing the stability center of gravity limits as far aft as possible to simplify airplane loading and fuel system management. The airplane has been balanced with low stability margins at subsonic conditions to achieve the desired longitudinal balance. Analytical studies and flight simulator testing have shown that acceptable airplane handling qualities are provided with these low stability margins. Handling qualities with and without stability augmentation are discussed in Par. 4.3 (See also Refs. 27 through 32).

4.2.1.1 Stability Margins

Figure 4-41 shows the flexible airplane static and maneuver neutral point computed for conditions of Mach number and dynamic pressure which are the most critical from the standpoint of minimum stability margins. The stability is compared with the aft center of gravity limits which are 62 percent $C_R$ for 30-degree sweep, 63 percent $C_R$ for 42-degree sweep, and 64 percent $C_R$ at 72-degree sweep.

The airplane is stable at all conditions except 30-degrees sweep, where static stability is about 1 percent $C_R$ negative. This condition of instability is considered unsatisfactory and will be corrected. Available means of correction include adjusting airplane balance to move the aft cg limit forward, increasing the minimum flaps-up sweep to about 35 degrees, and improving the tail design. Subsonic operation below 0.6 Mach number at all wing sweeps requires that the strake leading edge slats be down to eliminate instabilities at moderate to high angles of attack. At low wing sweeps, the wing leading edge slats are down at Mach numbers less than 0.45 to provide satisfactory stability.

Figure 4-42 shows the variation of airplane center of gravity during the nominal mission. Figures 4-43 through 4-56 show longitudinal stability characteristics at various wing sweeps for representative Mach numbers.

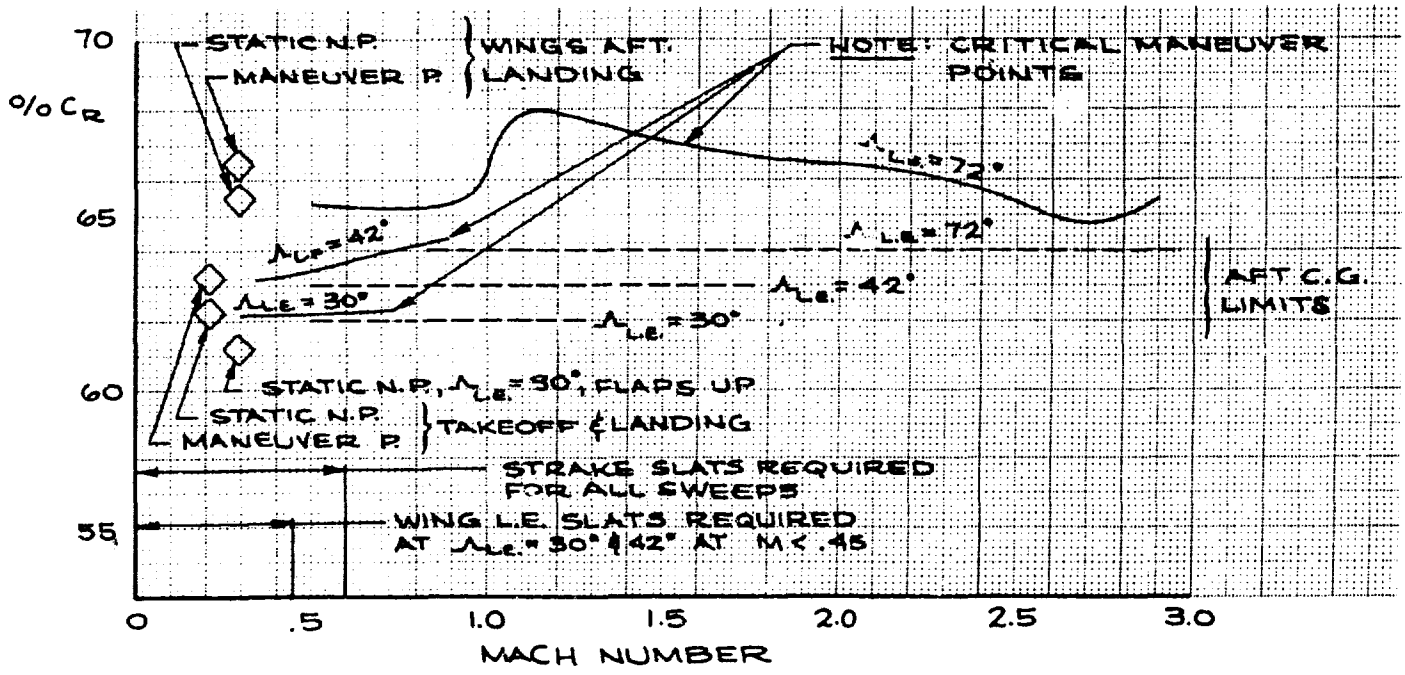


*Figure 4-41. Longitudinal Stability Neutral Points*

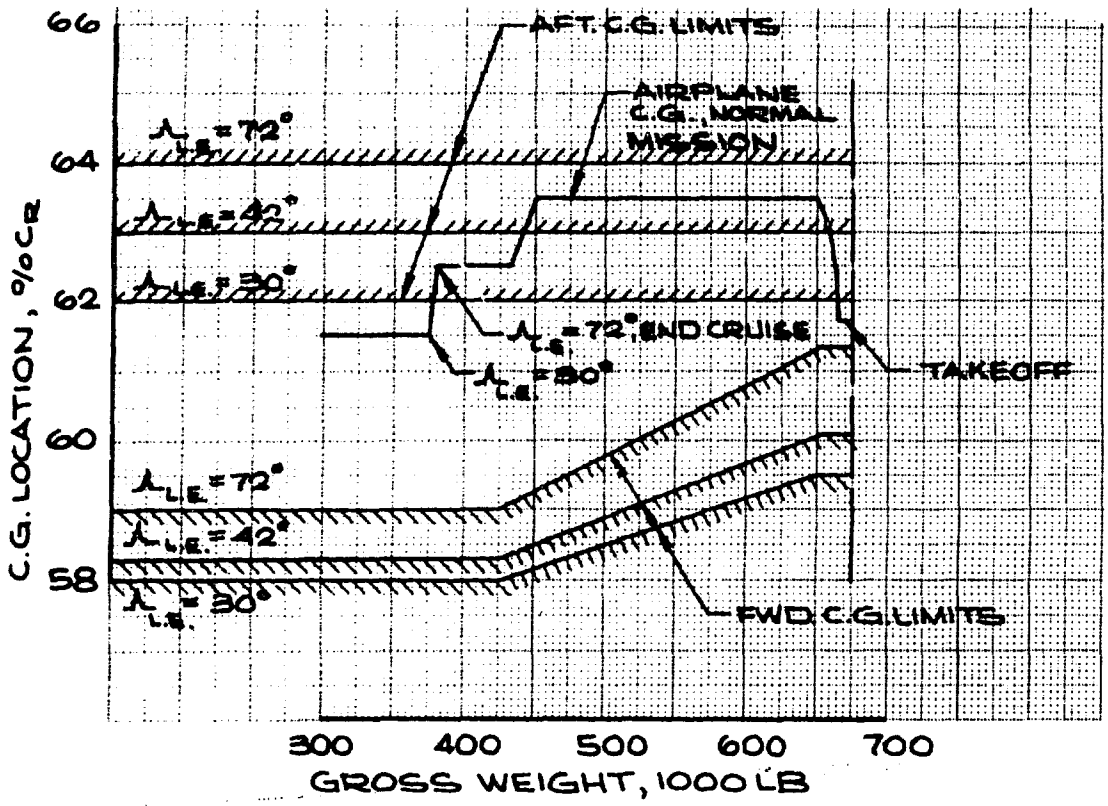


*Figure 4-42. Center of Gravity Limits and Variations*

The maneuver stability neutral points have been determined from model test data corrected for full-scale aeroelastic and wing body tail damping. The following equation is employed:

$X_M$ = flexible airplane maneuver point

$X_M = X_{a.c.}$ (rigid aerodynamic center)
$+ \Delta X_{a.c.}$ (flexibility effect)
$+ \Delta X_{a.c.}$ (damping effect).

The aeroelastic corrections, damping effects, and thrust effects on stability are shown in Figs. 4-43 through 4-67.

4.2.1.2 Flaps-Down Static Stability
Stability characteristics in and out of ground effect are shown in Figs. 4-43 and 4-44 for the landing flap configuration. Low stability margins and moderate pitch up are evident. Handling qualities analyses and flight simulator testing have demonstrated that handling characteristics are insensitive to static stability margin within the range of low margins that are practical for SST design. The airplane response in pitch is inherently sluggish because of the effect of high moment of inertia about the pitch axis. Increasing the static margin by the limited amounts that are practical from the standpoint of airplane balance and trim drag has no discernible effect on handling qualities. Stall demonstrations in the flight simulator have shown the airplane attitude to be controllable in the pitch up region for either slow or rapid stall entry rates. Dynamic longitudinal handling characteristics and stall testing in the simulator are discussed in Par. 4.3.

Recent wind tunnel testing has demonstrated methods to eliminate pitch up in the low speed regi n. Figures 4-45 and 4-46 show linear stability characteristics up to the maximum angle of attack tested, 33.5 degrees, which is about 14 degrees above the stall. This was accomplished through readjustment of the wing

lift distribution by retraction of outboard flaps, and by eliminating vortex flow development on the strake by folding up an outboard section of the strake. Design studies and wind-tunnel testing in this area are continuing in order to eliminate longitudinal instabilities. The angle of attack warning and control system will prevent inadvertent exposure to extreme attitudes at all flight conditions. The design goal, however, is to achieve inherent pitch down stability through and beyond stall.

4.2.1.3 Flaps Up Static Stability

Acceptable stability characteristics are provided with strake and wing leading edge slats down for all conditions except 30-degree sweep at the aft cg limit (62 percent $C_R$). Stability characteristics at 30-, 42- and 72-degree wing sweep at subsonic Mach numbers are shown in Figs. 4-47 through 4-53. Figure 4-47 shows the low speed 30-degree sweep stability at the aft cg limit with strake and wing slats down. The improvement in high angle of attack stability with wing and strake leading edge slats is shown in Figs. 4-49 and 4-50.

Good stability characteristics are provided at all wing sweeps for high subsonic and supersonic Mach numbers. Wind tunnel model test data for transonic and supersonic conditions are shown in Figs. 4-54 through 4-56.

4.2.1.4 Aeroelastic Corrections and Reference Flight Data

Structural aeroelastic effects on longitudinal stability and control effectiveness are substantially changed from those of previous configurations. The integration of wing and tail has provided deeper structure which has greatly reduced wing bending and twisting associated with the destabilizing forward shift of aerodynamic center. Forebody and aft body bending under inertia loading, during maneuvering flight, are stabilizing. The net effect of aeroelasticity at low and intermediate wing sweeps will increase the stability slightly.

Aeroelastic effects pertinent to longitudinal stability and control are summarized in Figs. 4-61 through 4-66. A detailed discussion of methods for determining structural aeroelastic effects is presented in Par. 3.3 of this document.

Reference data used in evaluating stability and control, such as operating lift coefficients, weights, and speed profiles, are presented in Figs. 4-67 through 4-71.

4.2.2 Lateral-Directional Static Stability

The low aspect ratio planform of the vertical tail has been selected to minimize aeroelastic stability losses at high airspeeds with minimum weight and drag. Tail size is dictated by the requirement for rudder control capability to ensure safe minimum control speed, $V_{MC}$, with critical engine failure on takeoff. This tail sizing has been found to provide ample static directional stability within the airplane flight envelope, with the possible exception of high angle of attack operation at Mach numbers in excess of 2.4. At high supersonic Mach numbers the stabilizing effect of top body-mounted vertical tails decreases as they become submerged in the forebody and wing wakes at high angles of attack. The level of $C_{n_\beta}$ required at high angle of attack is not clearly defined at this stage of the design development. Consideration of airplane dynamics indicates that the airplane will be dynamically stable even with unstable $C_{n_\beta}$ due to the inertia characteristics and the high level of positive dihedral effect, $C_{l_\beta}$. Examination of the Dutch roll stability approximation parameter, $C_{n_{\beta dyn}}$, indicates that high levels of dynamic directional stability will continue to exist at high angle of attack even where static $C_{n_\beta}$ is negative: for example, at an angle of attack of 14 degrees and at Mach number 2.7.

$$C_{n_{\beta_{dyn}}} = \frac{C_{n_\beta} + \left(I_{xz}/I_{xx}\right) C_{l_\beta}}{1 - \left(I^2_{xz}/I_{xx}\, I_{zz}\right)}$$

$$C_{n_{\beta_{dyn}}} = 0.00248$$

The above approximation indicates positive Dutch roll damping. However, it does not consider the rotary derivatives or the effects introduced by the pilot in the control loop when attempting to hold wings level. If increased static directional stability is required, it will be proviced by stabilizing surfaces mounted below the aft body, horizontal tail, or nacelles, or by location of top-mounted vertical tails outboard in good airflow regions on the horizontal tail. As previously discussed in Par. 4.2.1, the airplane is protected against inadvertent exposure to angles of attack greater than 12 degrees by an angle of attack warning and control system.

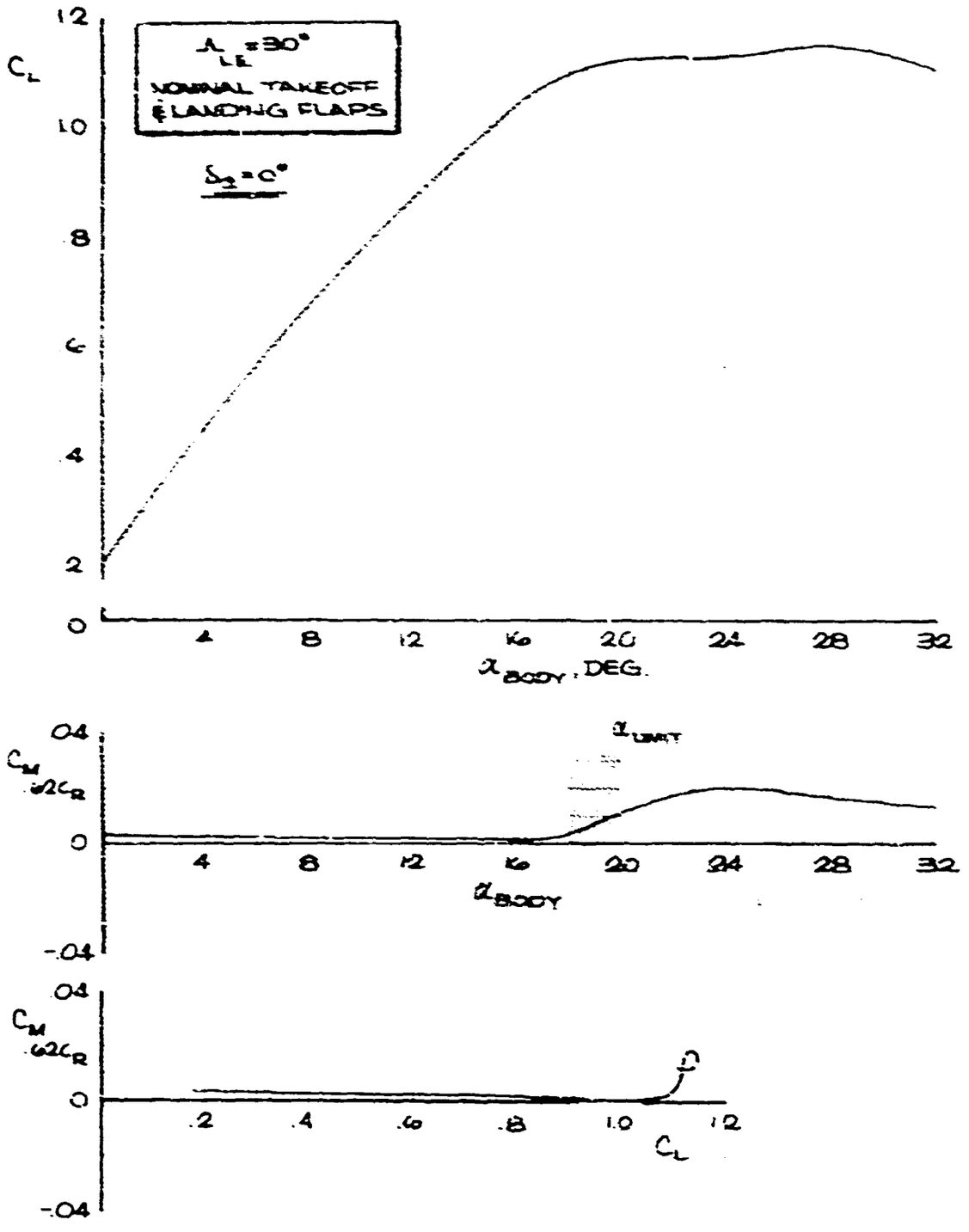


*Figure 4-33. Landing Stability, No Ground Effect*

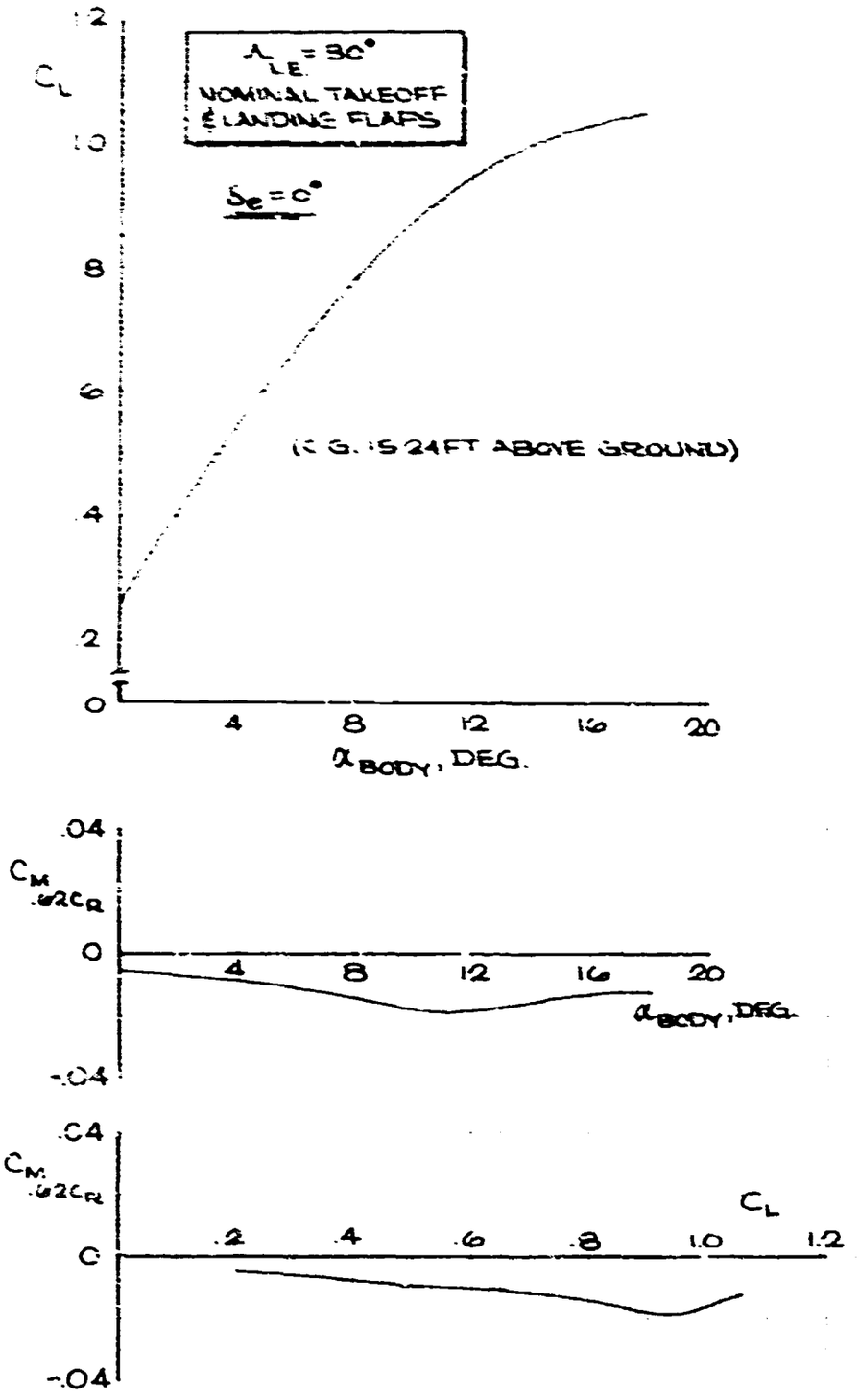


*Figure 4–44. Landing Stability, in Ground Effect*

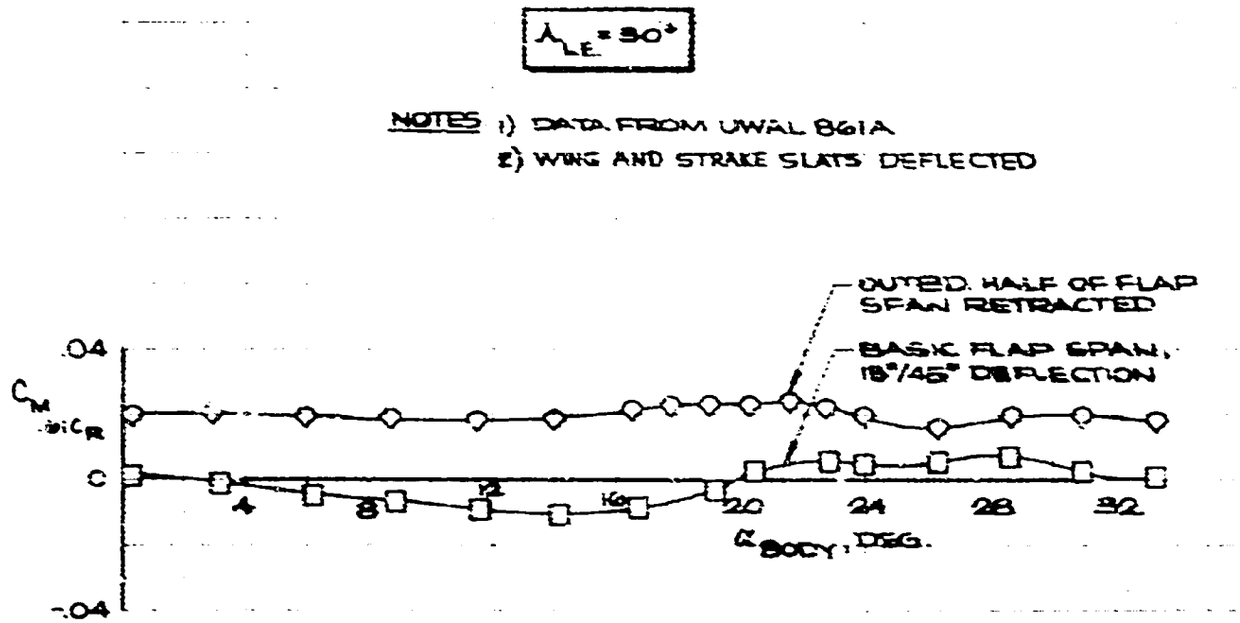


Figure 4-45. Effect of Flap Span

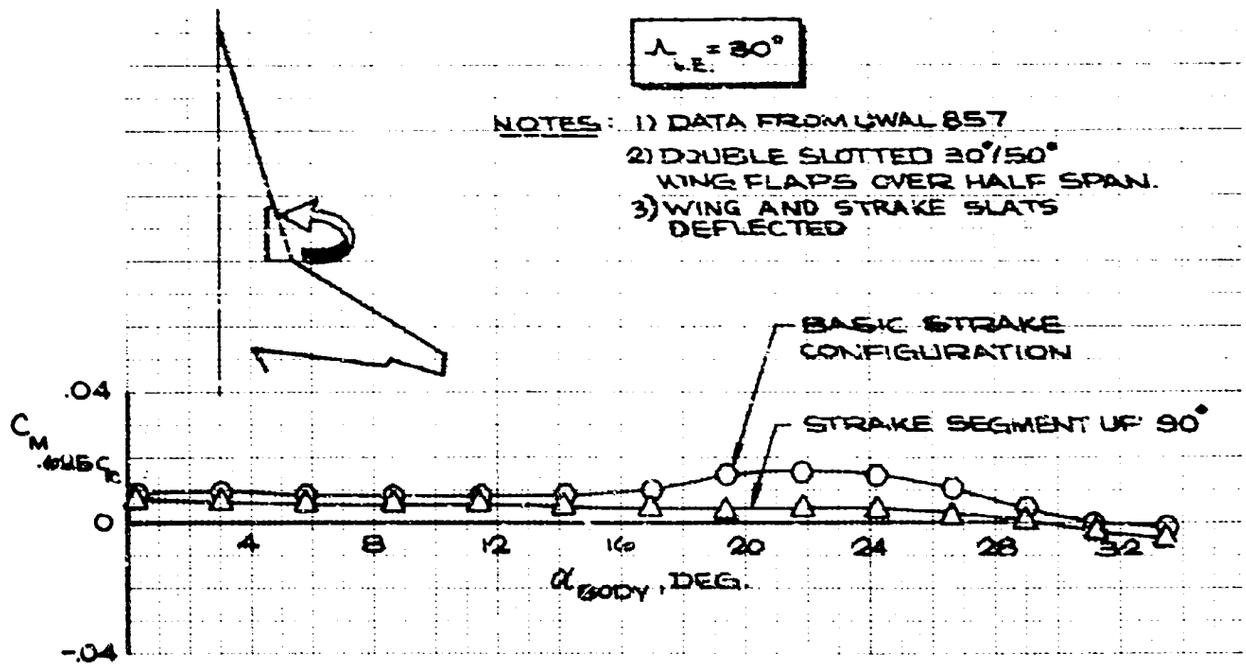


Figure 4-46. Effect of Strake Segment Rotation

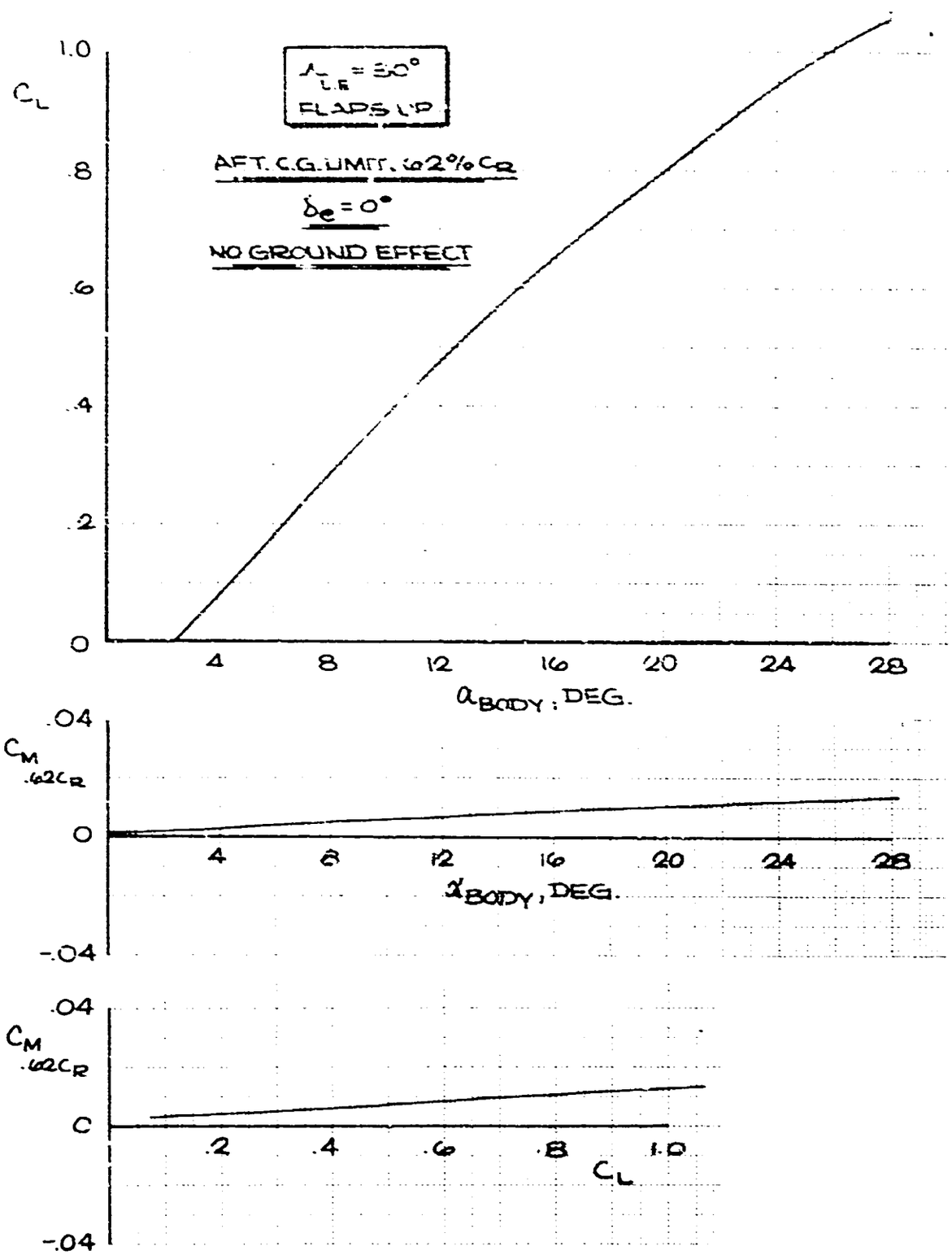


*Figure 4–47. Low Speed Stability, Flaps Up, No Ground Effect*

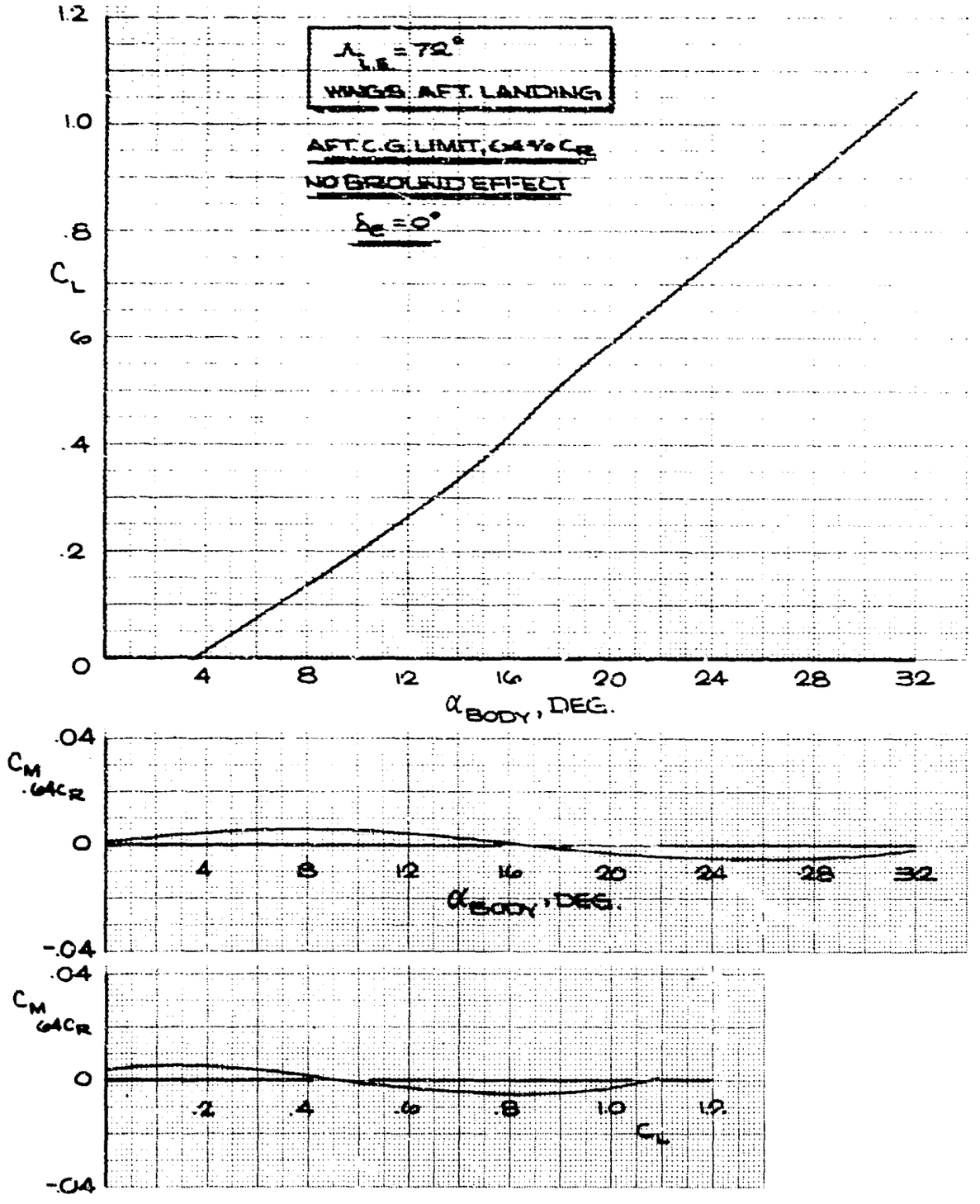


*Figure 4-38. Low Speed Stability, Wings Aft Landing*

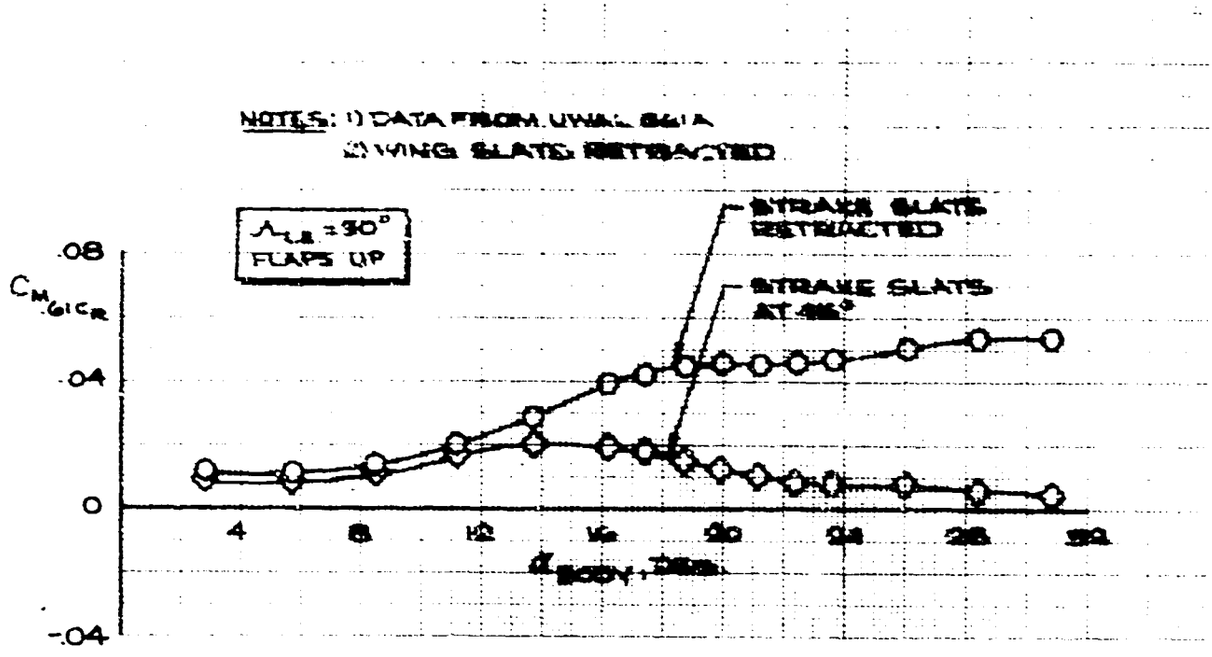


*Figure 4-49. Effect of Strake Slats*

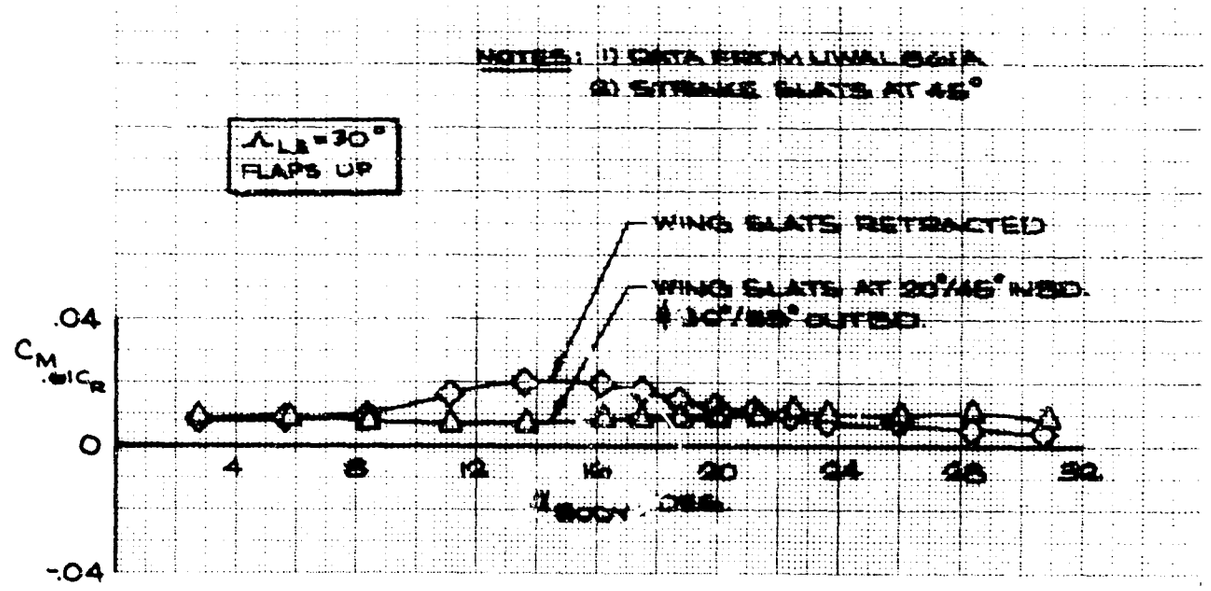


*Figure 4-50. Effect of Wing Slats*

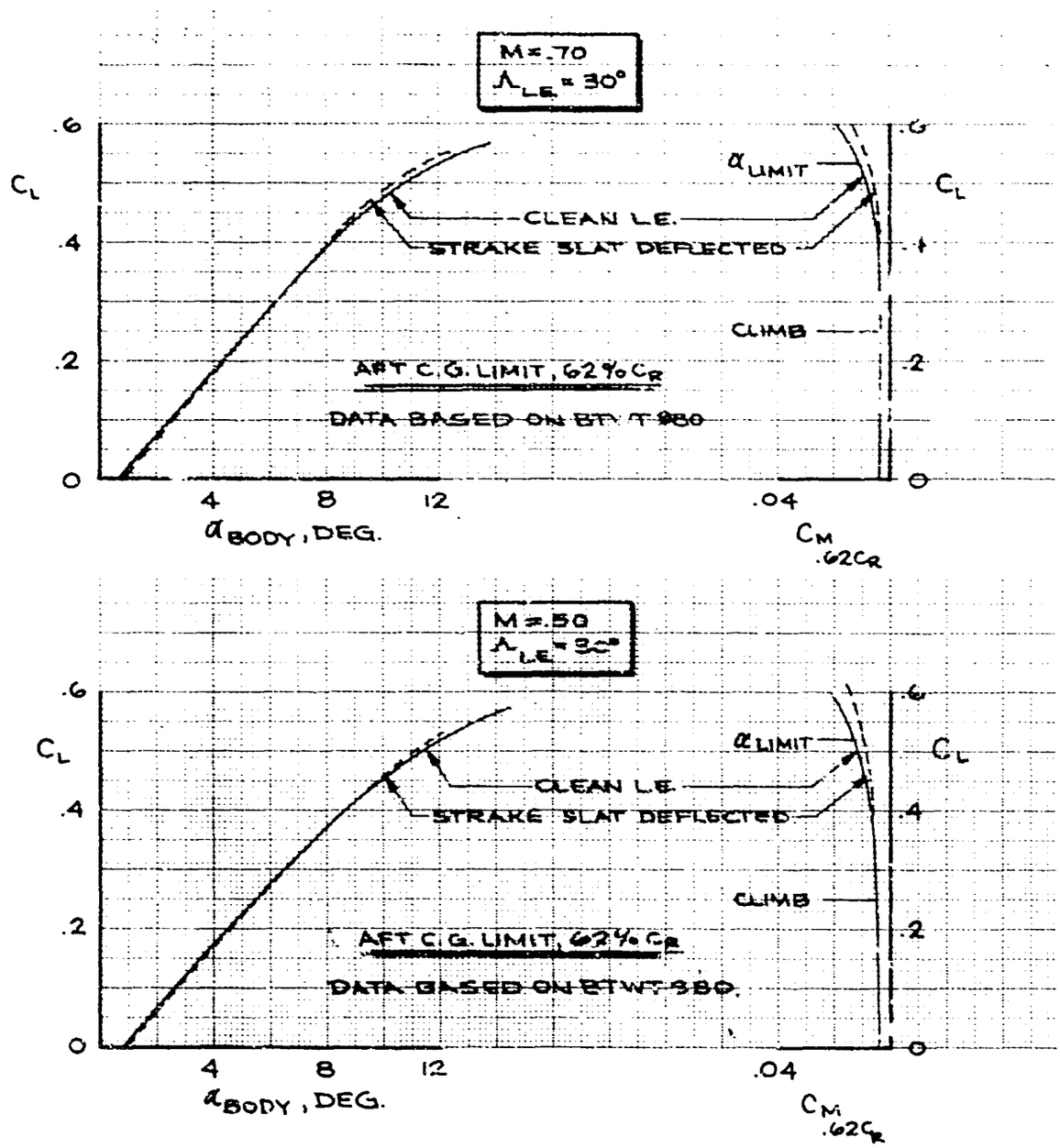


*Figure 4-51. Longitudinal Stability Characteristics, $\Lambda$ = 30 Degrees*

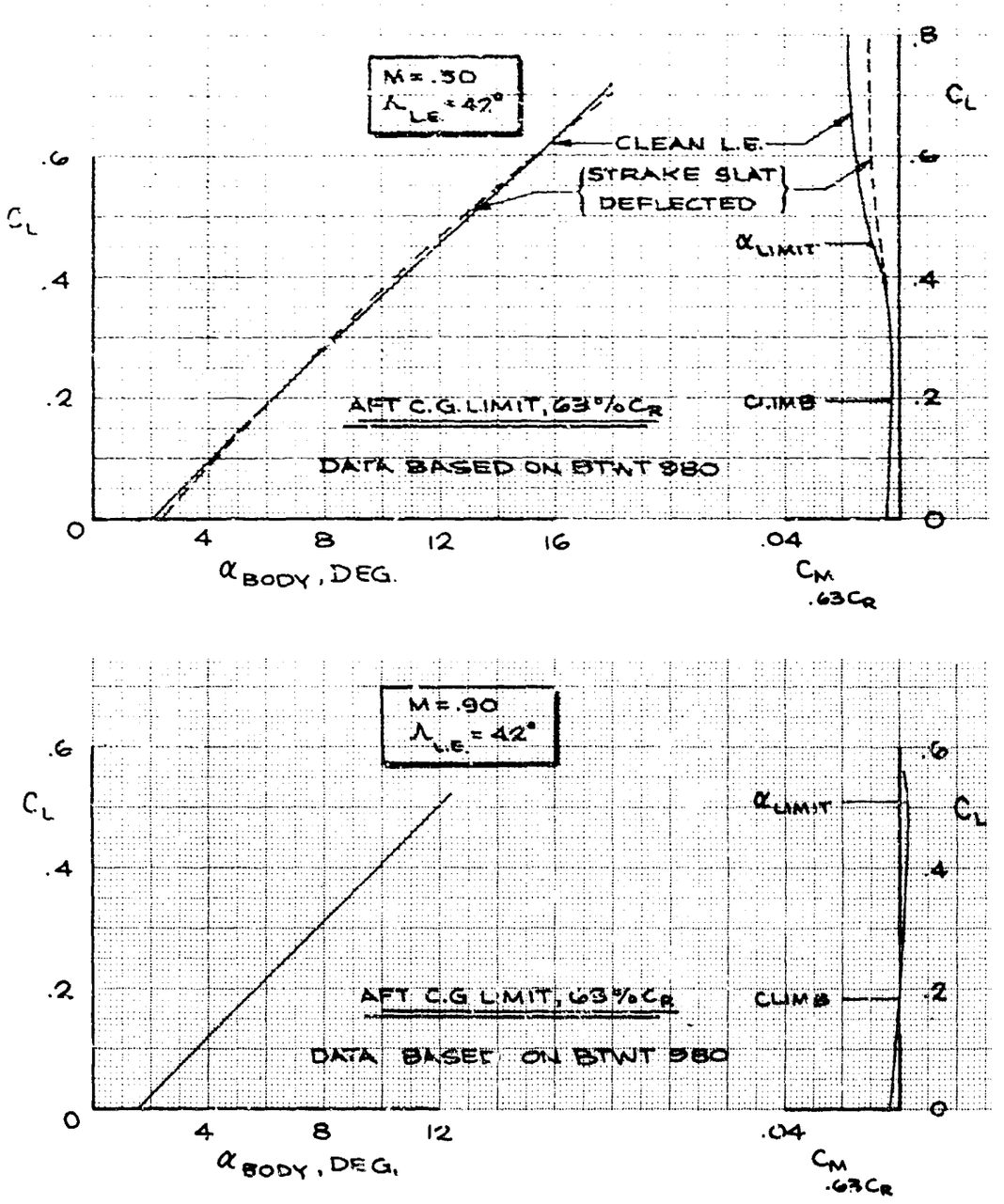


*Figure 4–52. Longitudinal Stability Characteristics, $\Lambda$ = 42 Degrees*

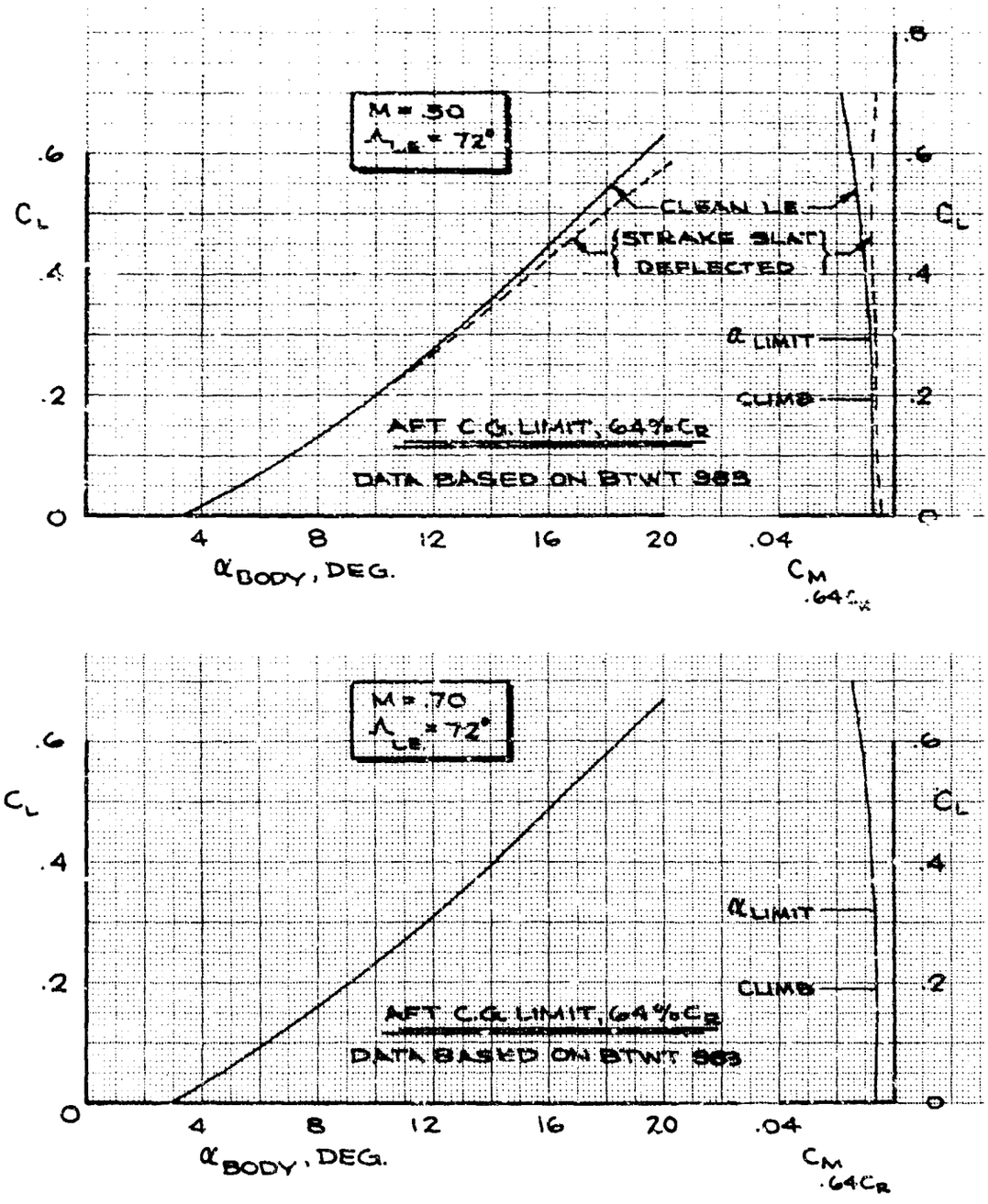


*Figure 4-53. Longitudinal Stability Characteristics, $\Lambda$ = 72 Degrees, M =.5, .7*

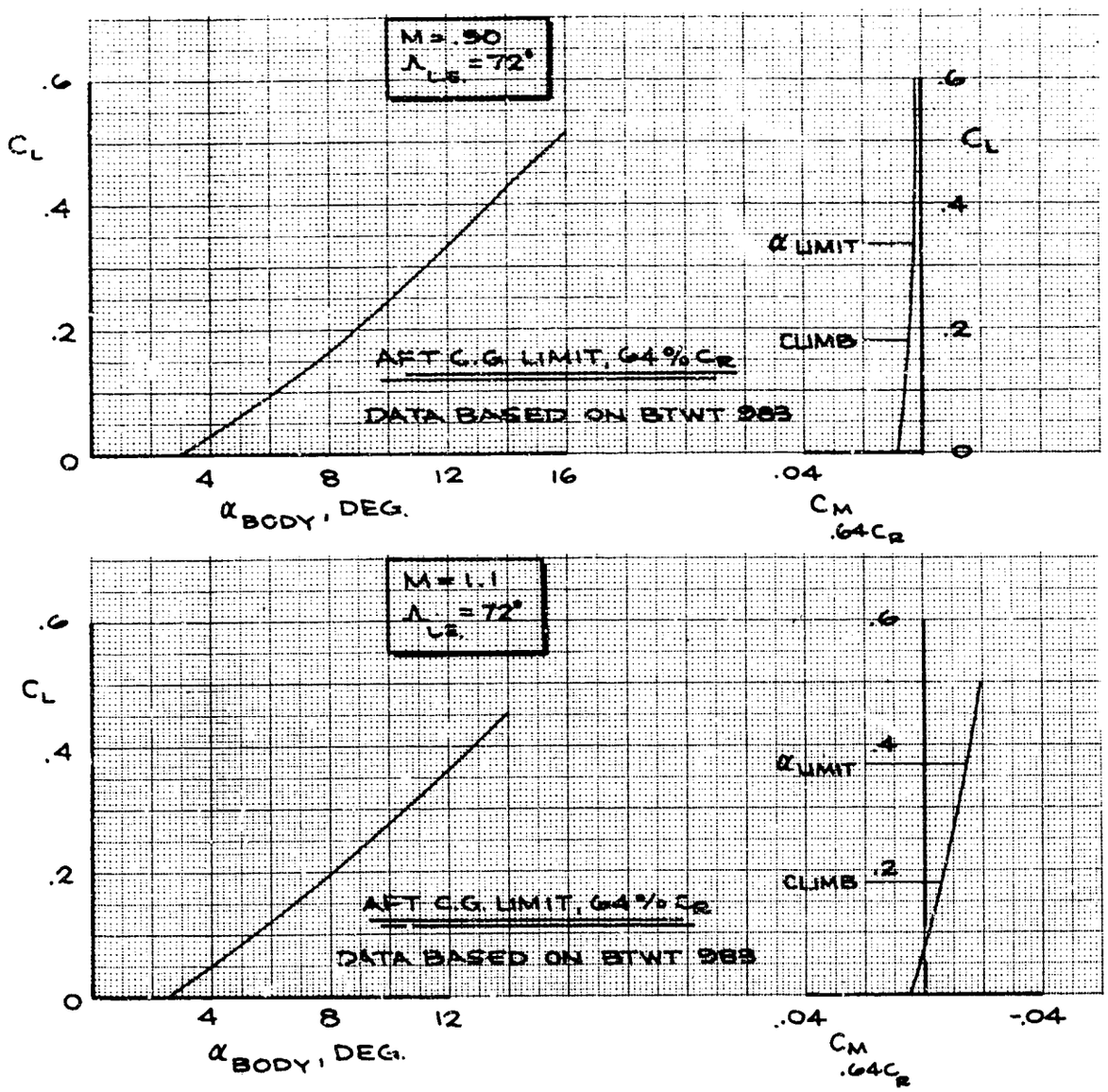


*Figure 4–54. Longitudinal Stability Characteristics, $\Lambda$ = 72 Degrees, M = .9, 1.1*

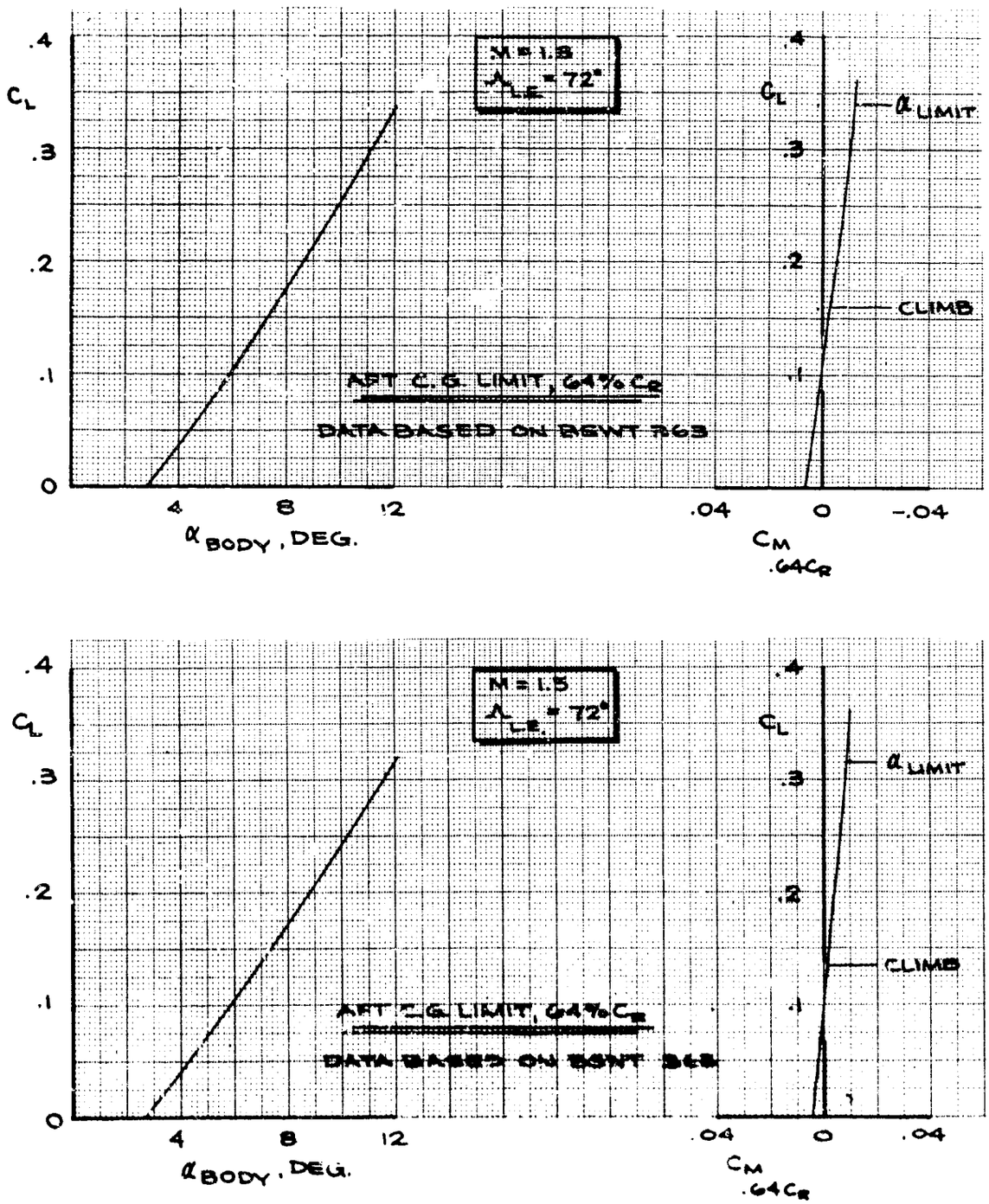


*Figure 4-55. Longitudinal Stability Characteristics, $\Lambda$ = 72 Degrees, M = 1.3, 1.5*

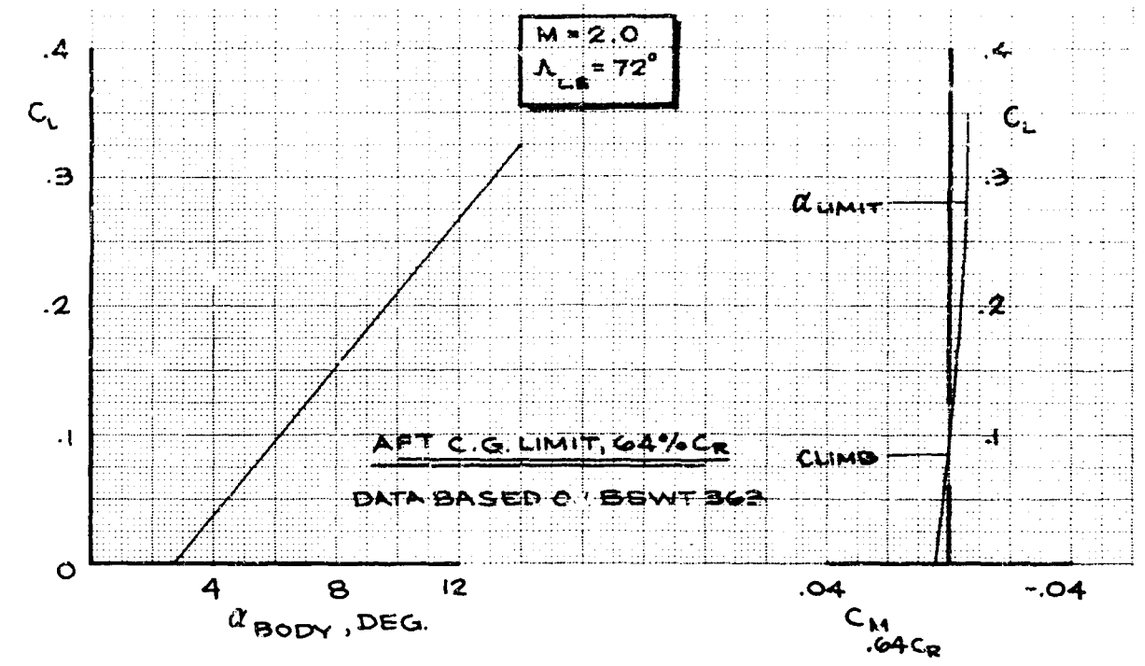


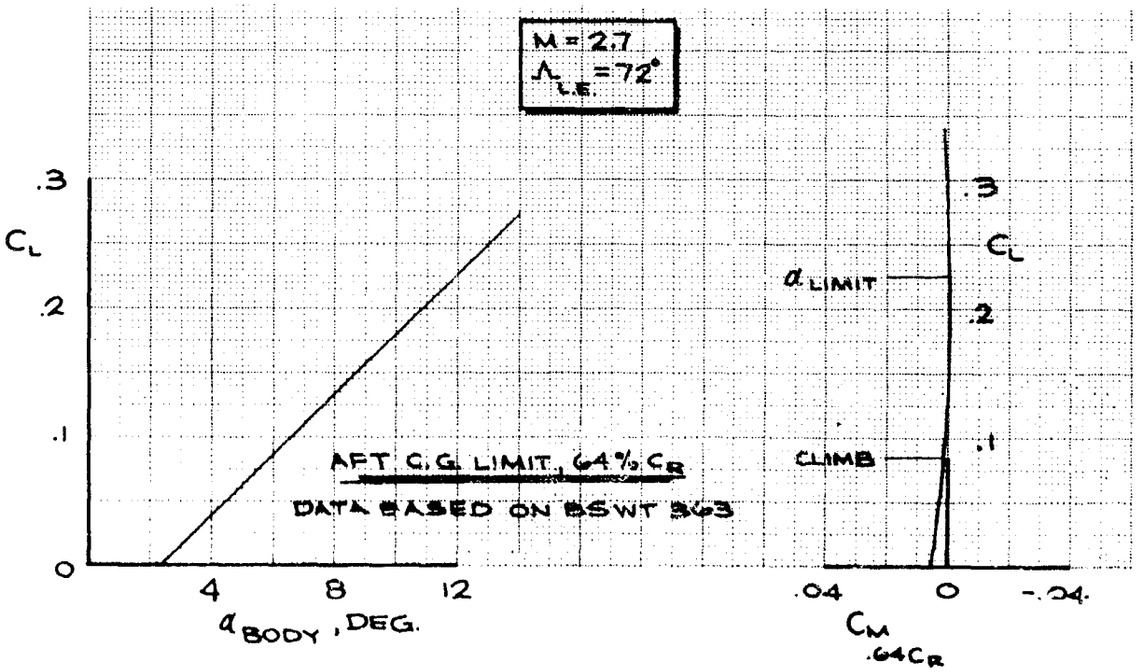


*Figure 4-56. Longitudinal Stability Characteristics, $\Lambda$ = 72 Degrees, M=2.0, 2.7*

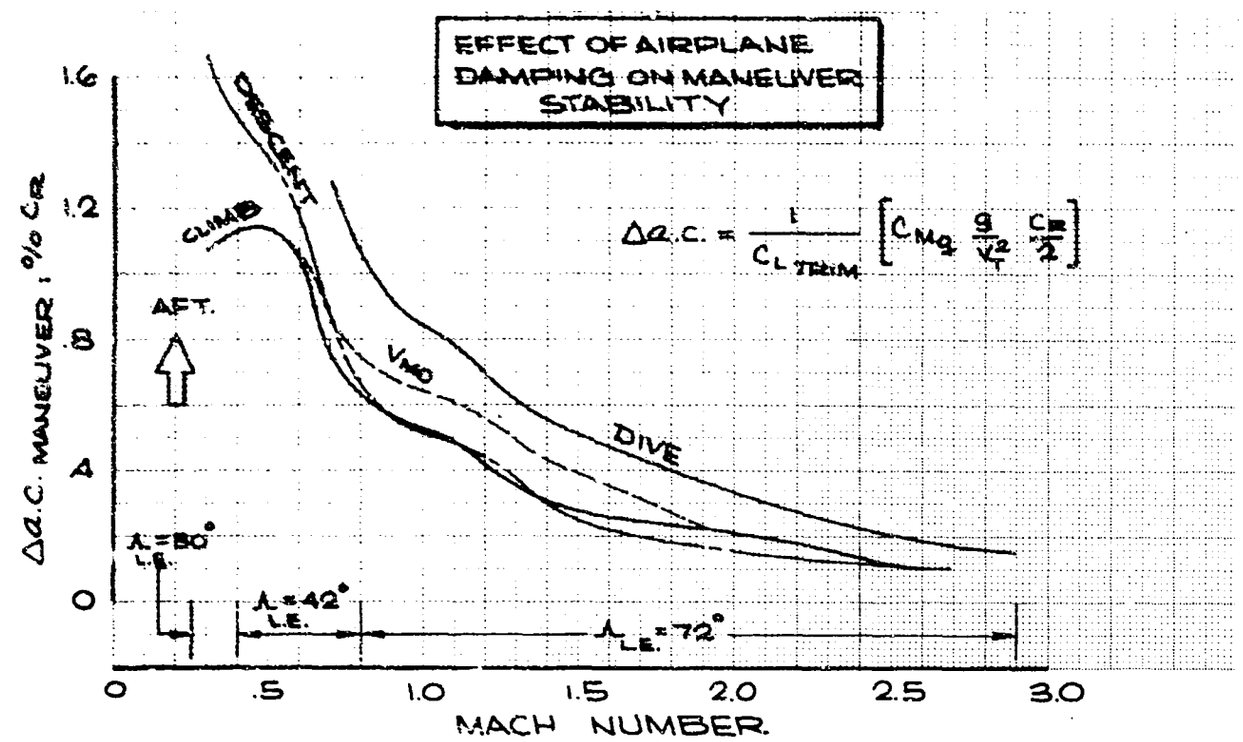


*Figure 4–57. Aerodynamic Center Shift Due to Pitch Damping*

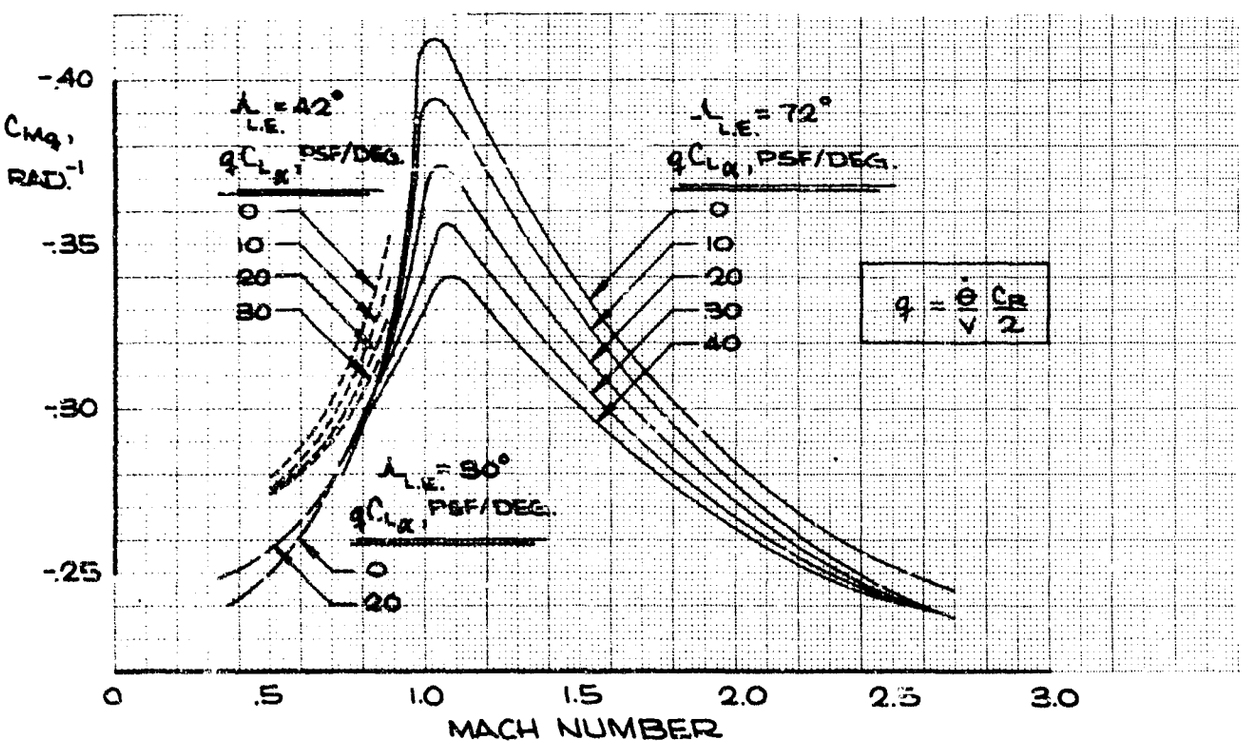


*Figure 4–58. Pitching Moment Due to Pitch Rate*

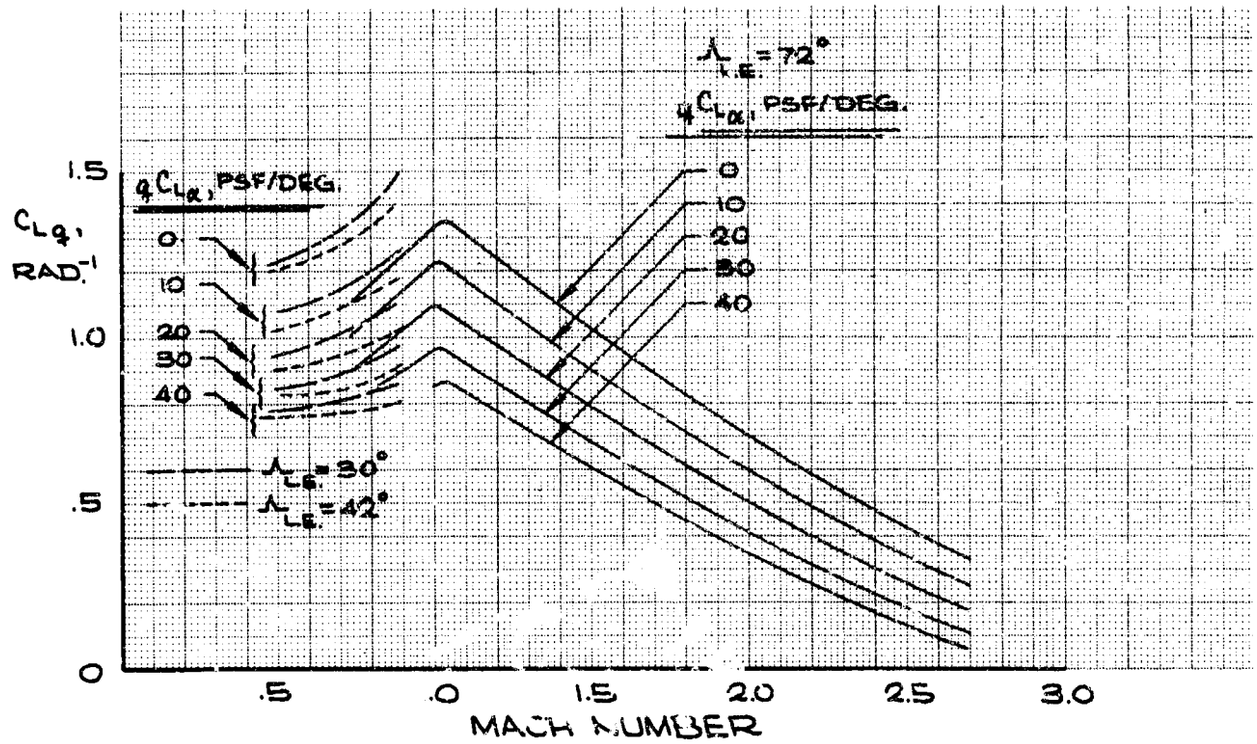


*Figure 4-59. Lift Due to Pitch Rate*

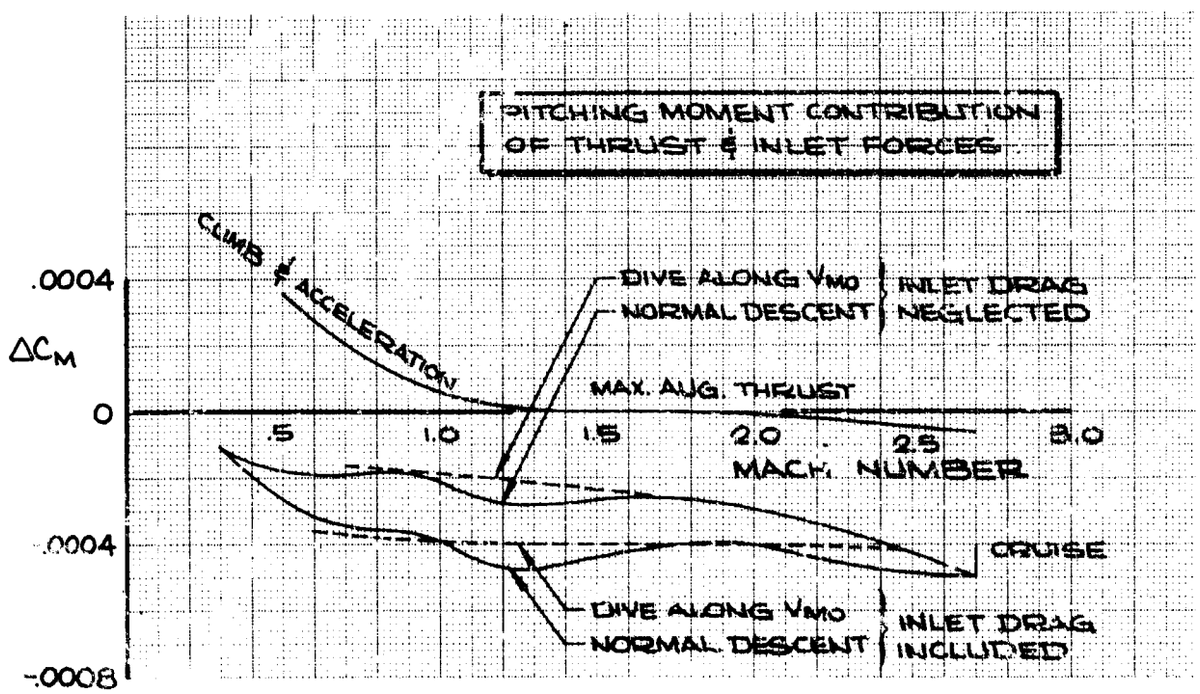


*Figure 4-60. Pitching Moment Contribution of Thrust and Inlet Forces*

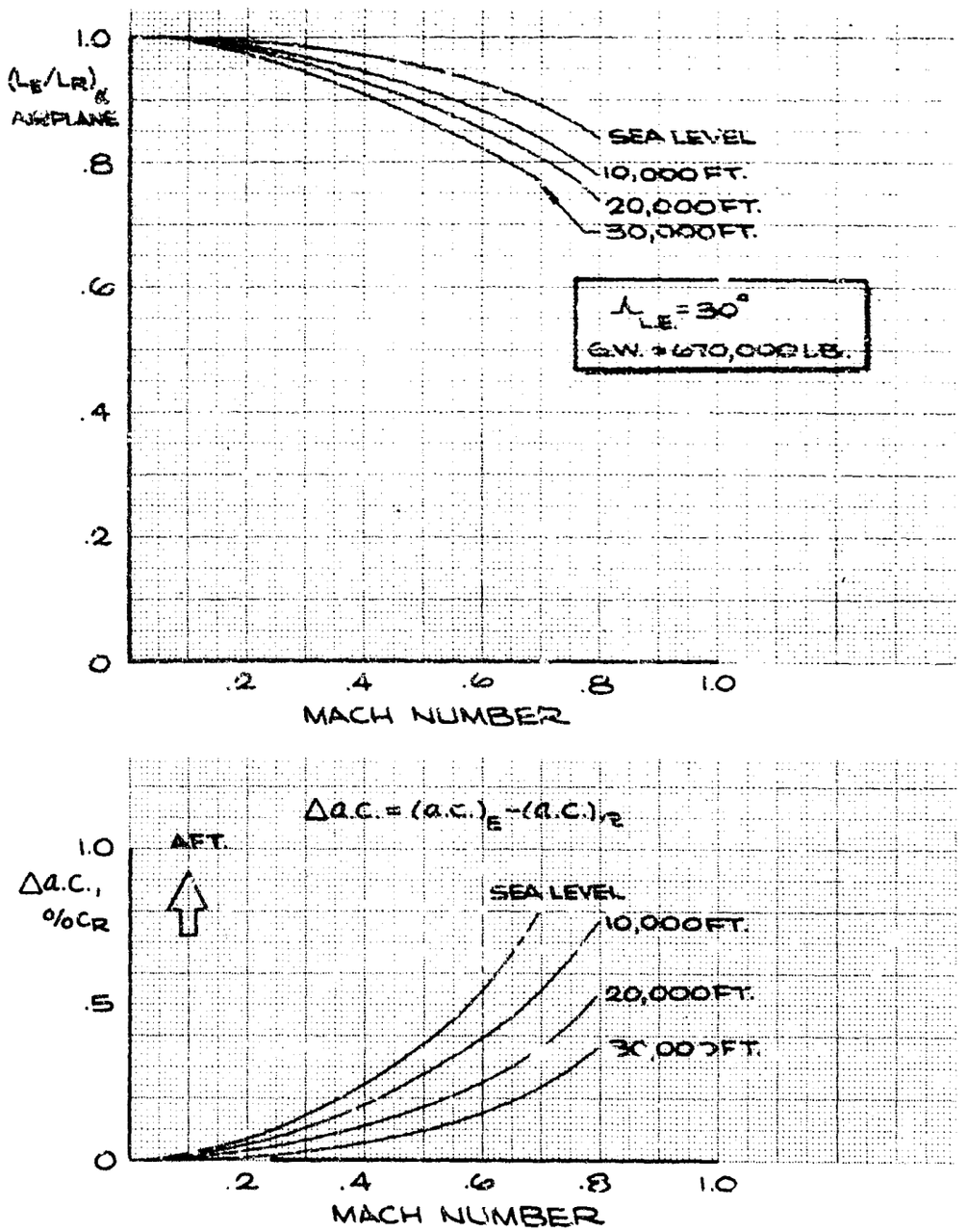


*Figure 4-61. Aeroelastic Effects, $\Lambda$ = 30 Degrees*

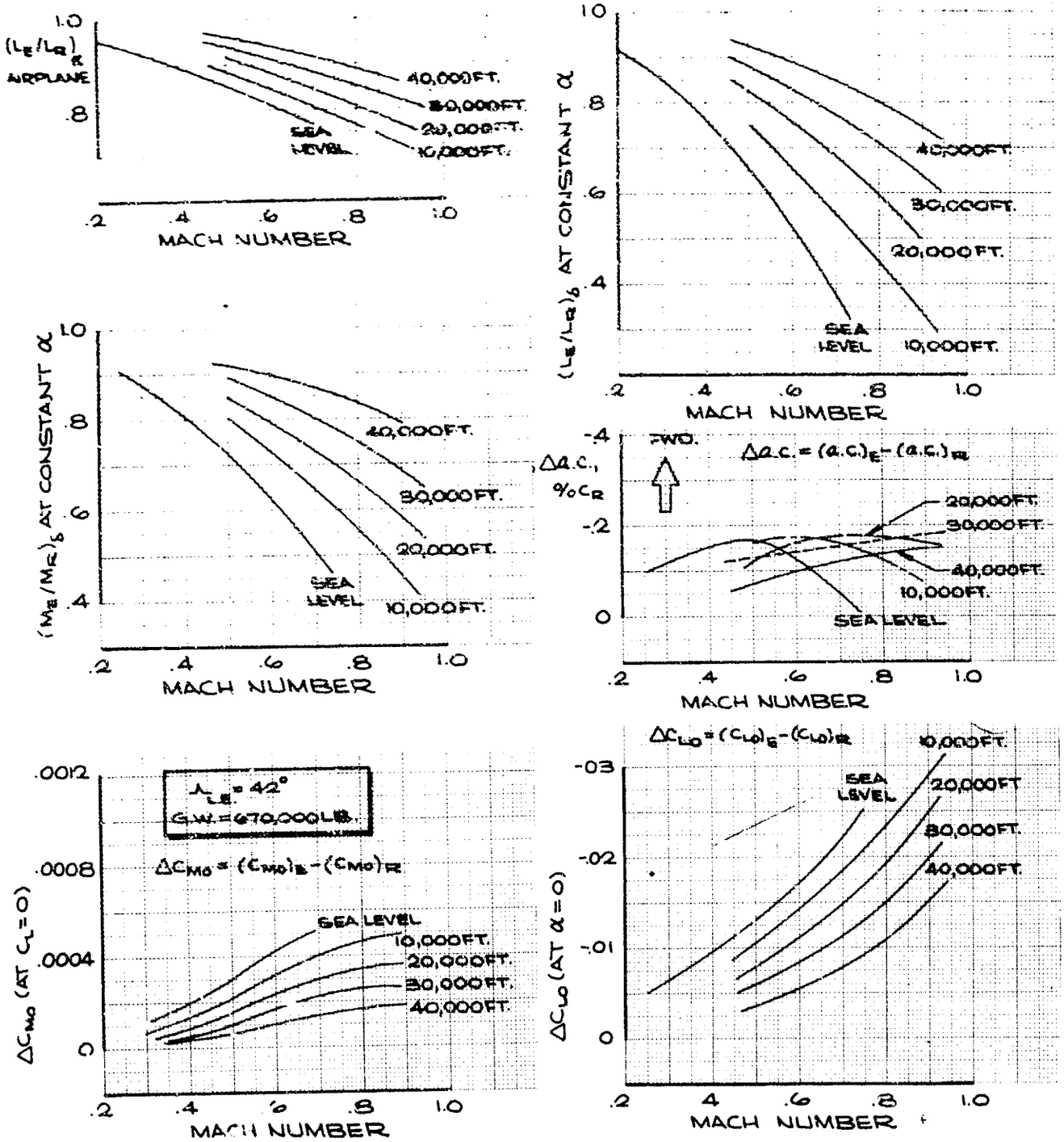


*Figure 4–62. Aeroelastic Effects, $\Lambda$ = 42 Degrees*

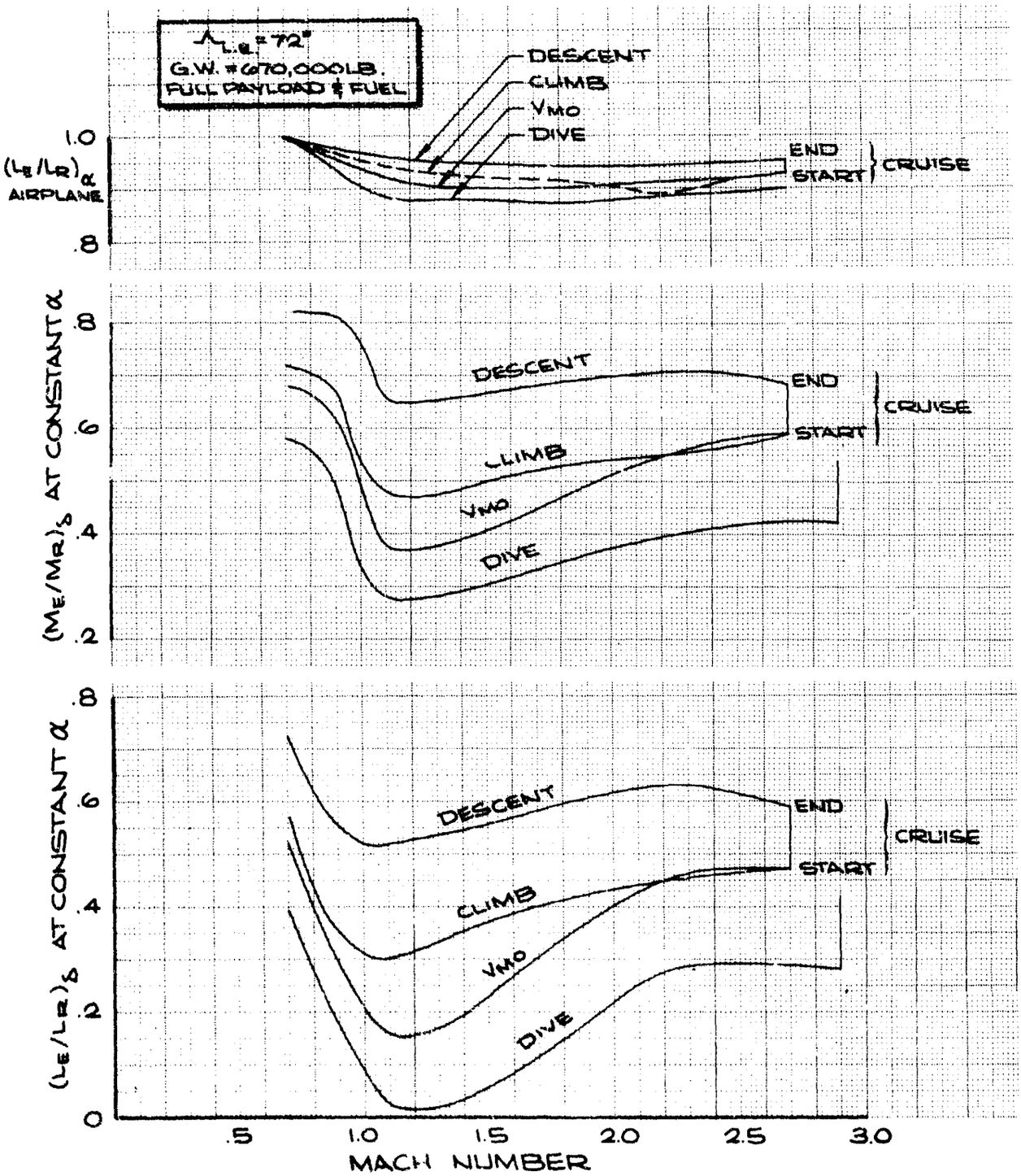


*Figure 4-63. Aeroelastic Effects, $\Lambda$ = 72 Degrees, Factors*

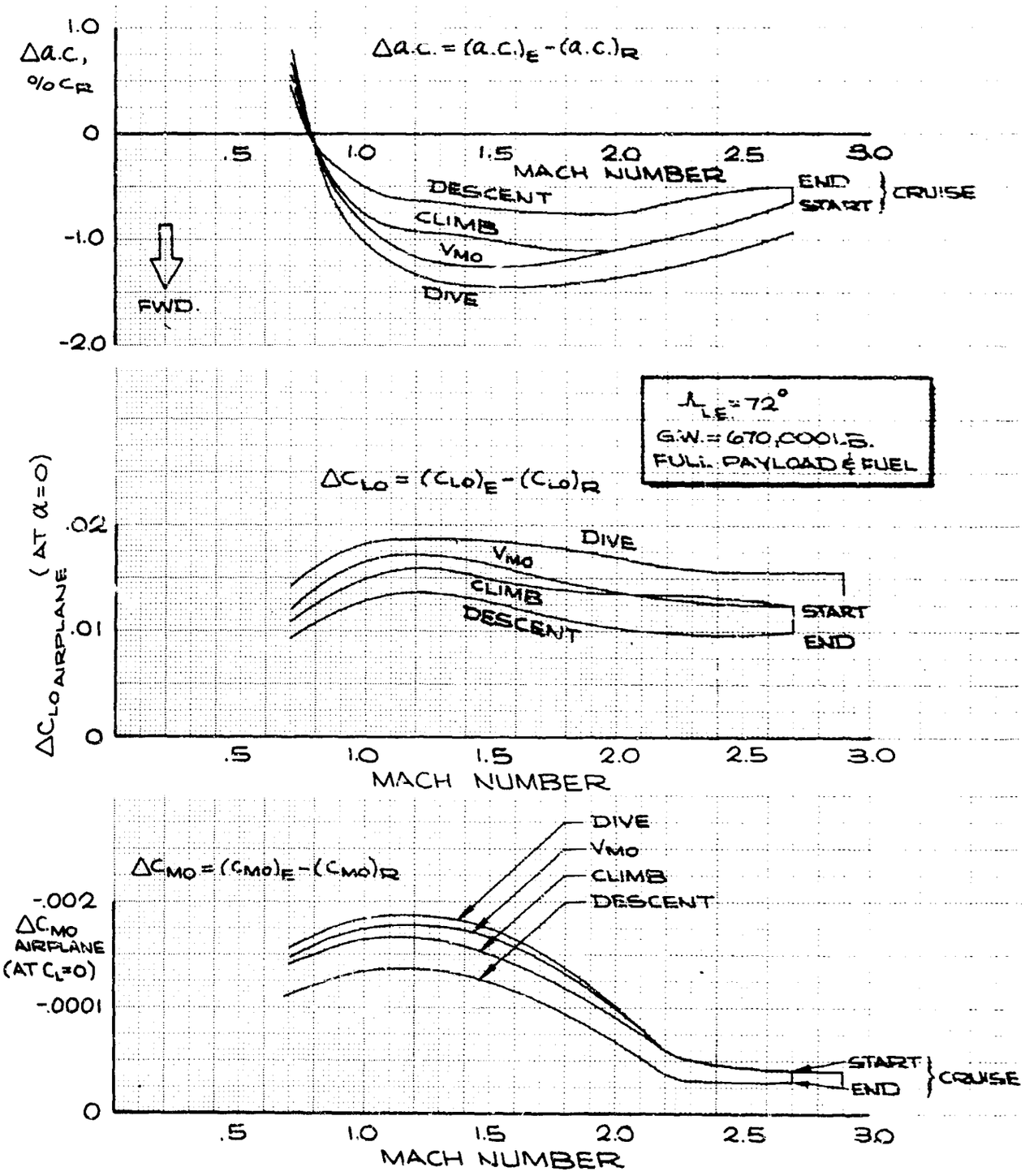


*Figure 4–64. Aeroelastic Effects, Λ = 72 Degrees, Increments*

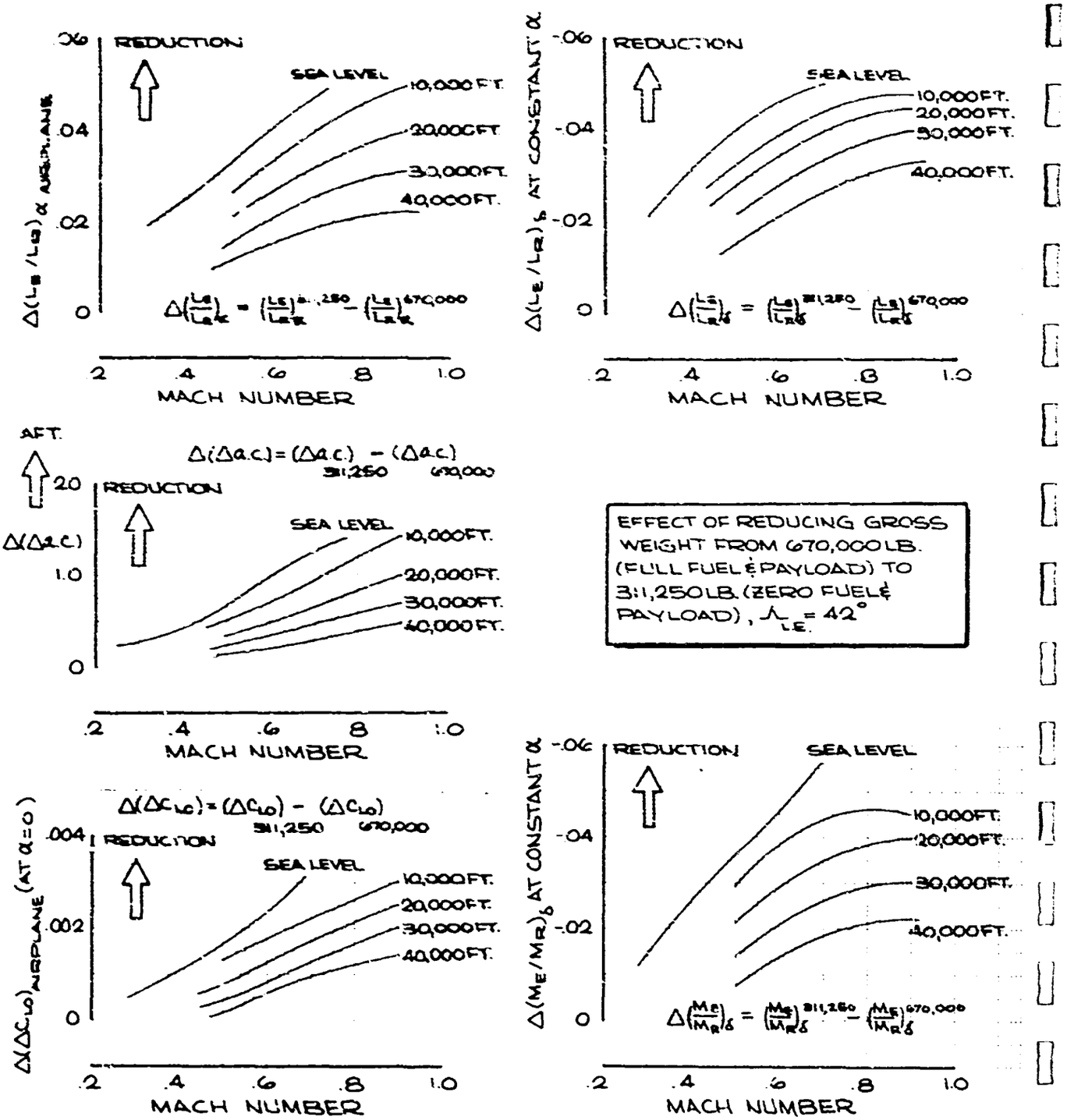


*Figure 4–65. Effect of Changing Airplane Weight on Aeroelastic Effects, Λ = 42 Degrees*

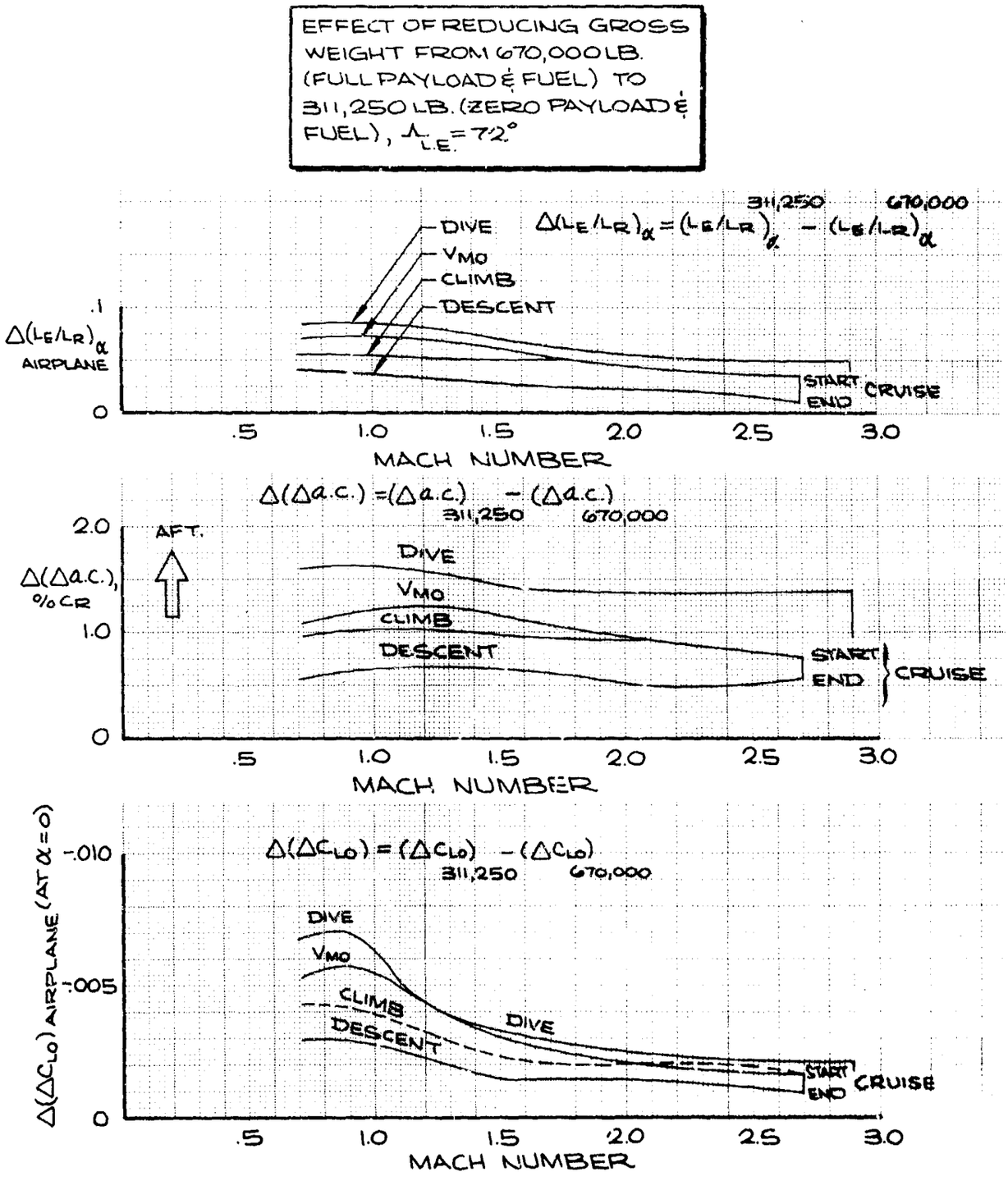


*Figure 4-66. Effect of Changing Airplane Weight on Aeroelastic Effects, Λ = 72 Degrees*

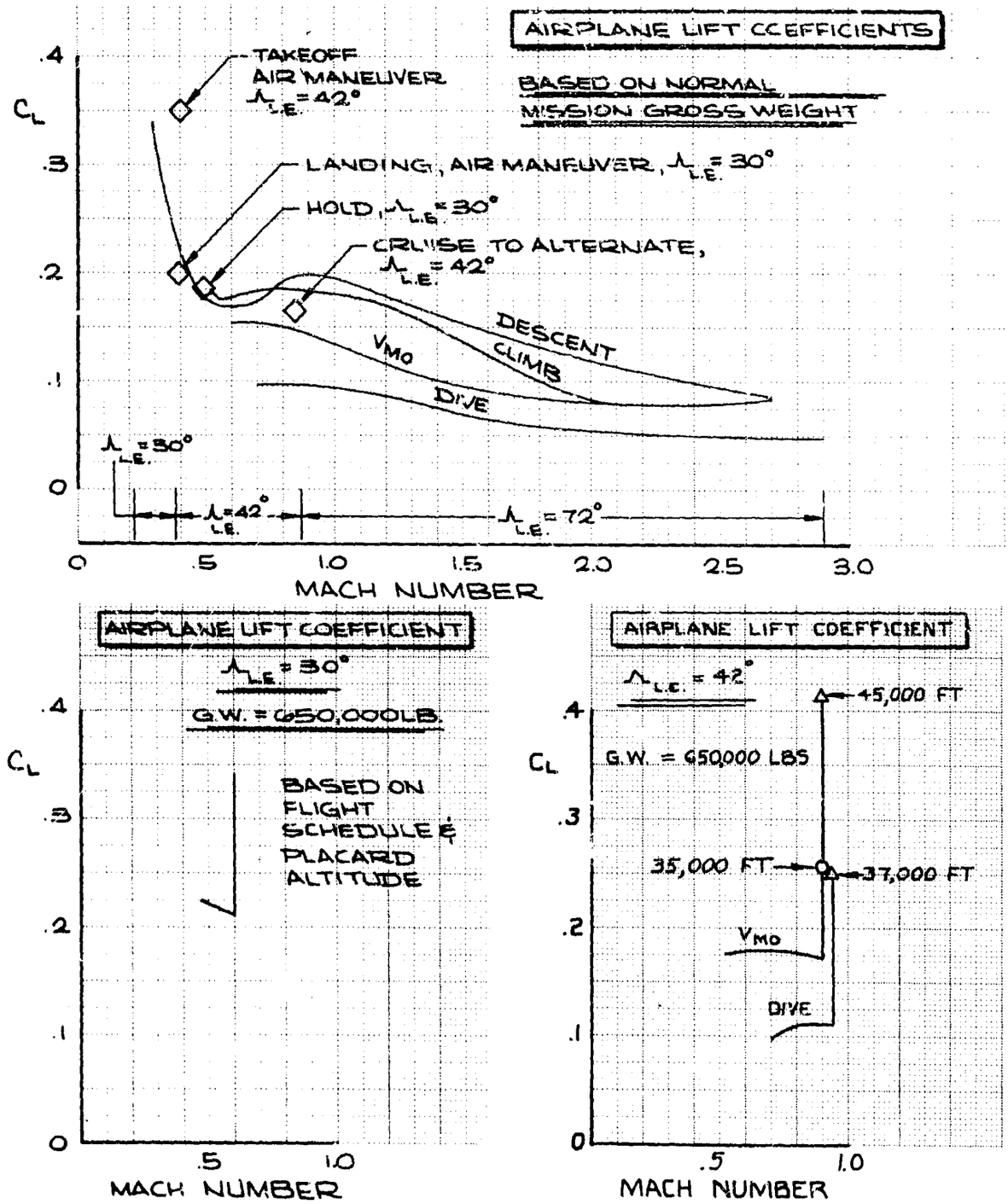


*Figure 4-67. Flexible Airplane Lift Coefficients*

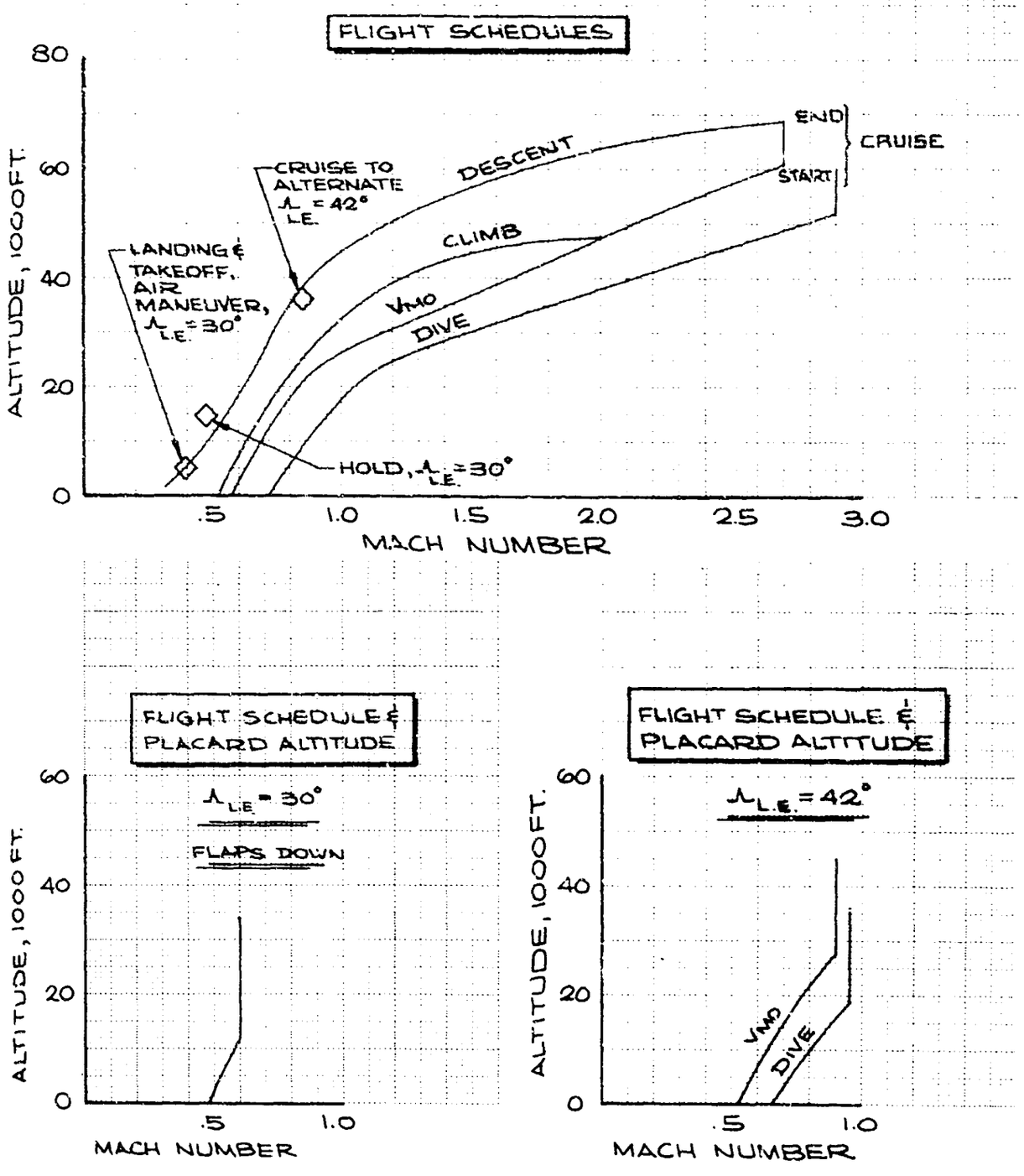


*Figure 4-68. Airplane Flight Schedules*

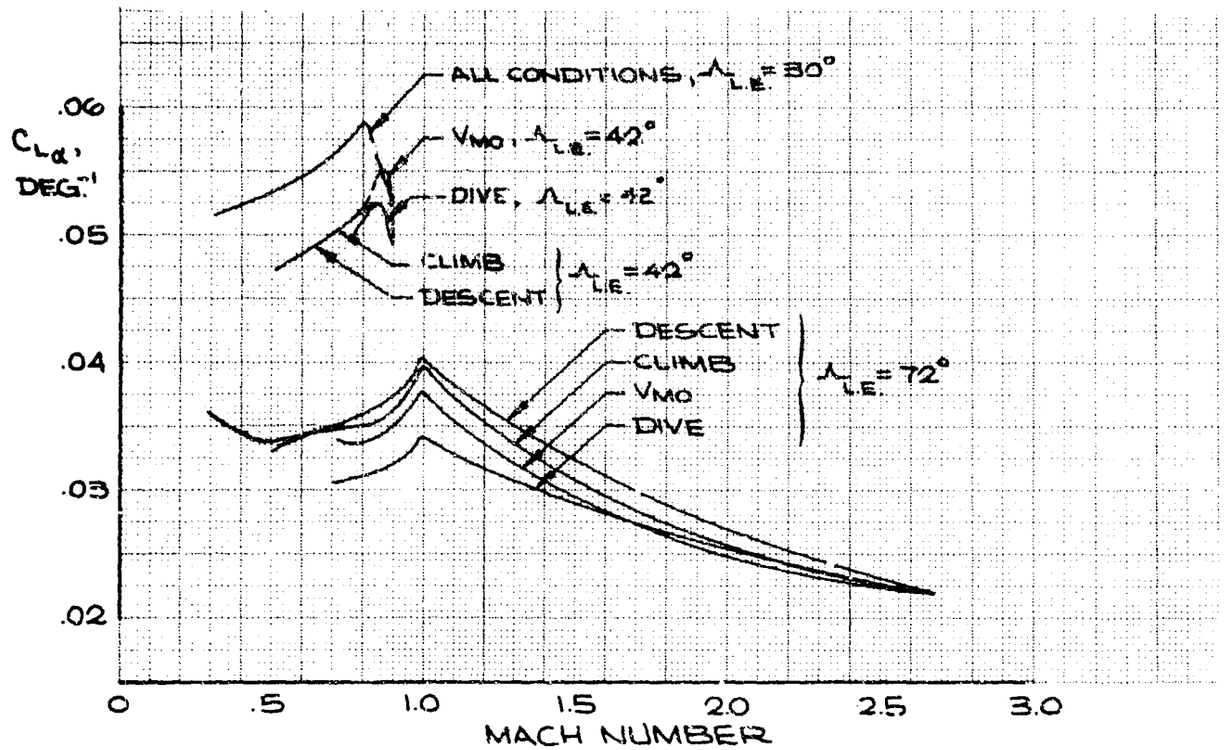


*Figure 4-69. Lift Curve Slope, Rigid Airplane*

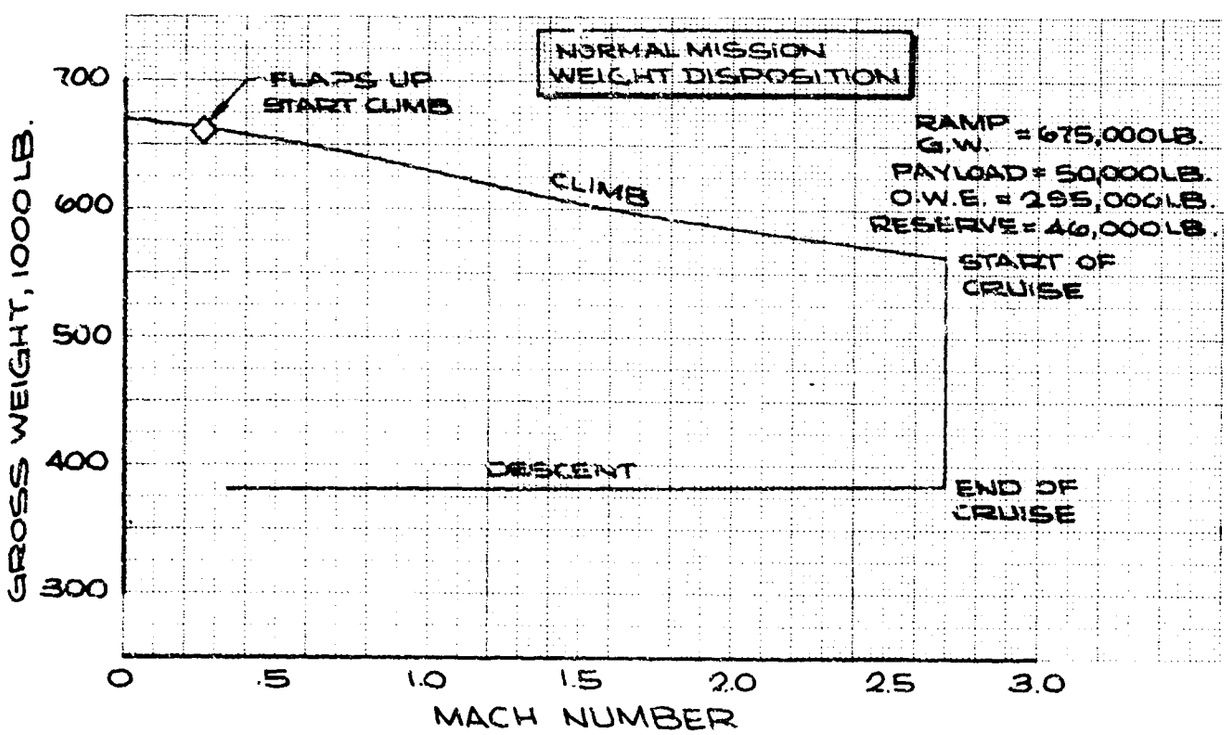


*Figure 4-70. Normal Mission Weight Disposition*

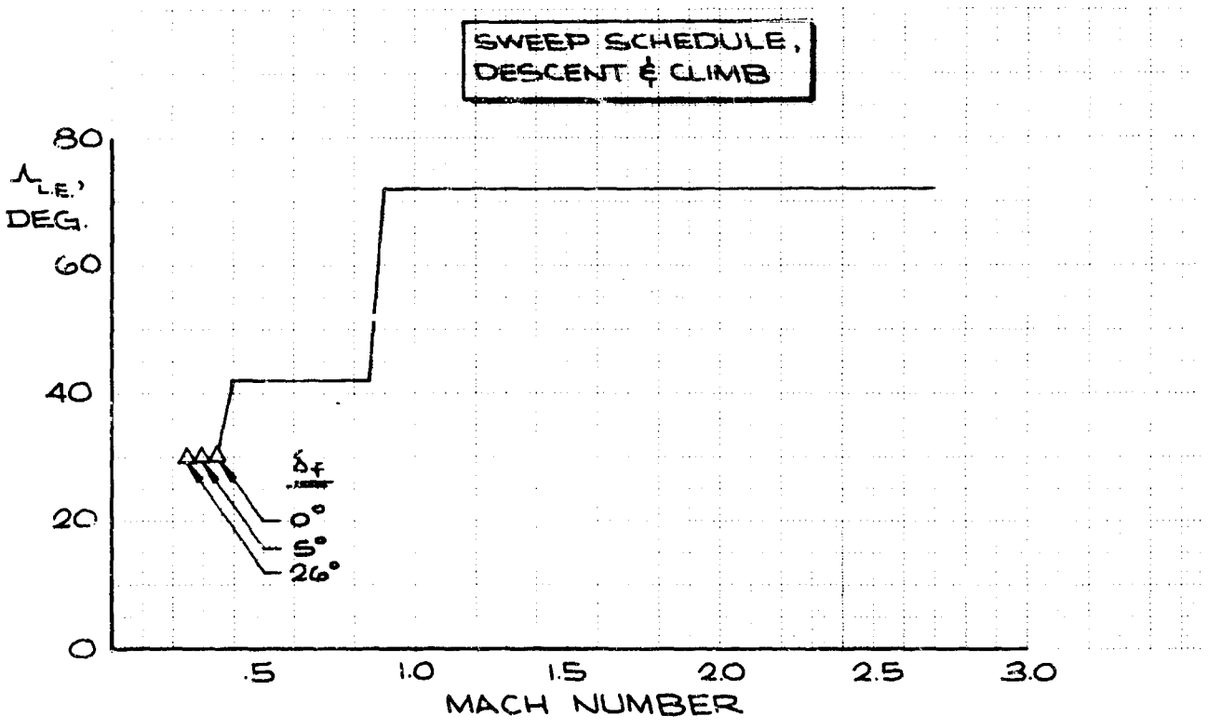


*Figure 4-71. Wing Sweep Schedule*

Directional stability at the 2.7 $M_{MO}$ placard altitude is shown for the flexible airplane in Fig. 4-72 as a function of airplane angle of attack. This flight condition is the most critical from the standpoint of $C_{n_\beta}$ deterioration with angle of attack. A folding vertical fin has been wind tunnel tested and can provide positive directional stability to attitudes above 2.5 load factor as shown in Fig. 4-72.

Studies are in progress to evaluate the dynamic transients with the estimated control cross-coupling characteristics and the elevon rudder interconnect. These will include nonlinearities of $C_{n_\beta}$ with both angle of attack and sideslip angle. The results of these studies will be available for the onsite evaluation.

Directional stability in the 30-degree sweep landing configuration is shown in Fig. 4-73. Good characteristics exist up to very high angles of attack, well beyond wing stall. These test data were obtained at low Reynolds number, and therefore may change at full scale Reynolds number due to differences in forebody flow separation. Correlation with flight Reynolds number characteristics will be provided by testing small models in pressure tunnels and by testing the large 1/5 scale model in the NASA Ames 40-ft by 80-ft wind tunnel. If directional stability problems exist at full scale conditions, they probably can be corrected by proper placement of small forebody strakes to induce flow separation similar to that occurring at low Reynolds number. Figure 4-74 shows the airplane directional stability versus Mach number over the normal flight range. The effect of flexibility is seen to be small, due to the stiff vertical tail and aft body.

Lateral stability, $C_{l_\beta}$, is shown over the Mach range in Fig. 4-75 for the flexible airplane at 1-g normal load factor conditions. These characteristics are based on rigid model data without aeroelastic corrections, since tests of a 72-degree sweep model with a flexible wing have shown little effect of wing flexibility on $C_{l_\beta}$ for a wide range of dynamic pressures. The changes in wing dihedral due to wing bending were evidently com-

pensated for by the unloading of the wing tip through bending. Figure 4-76 shows the wind tunnel data for the elastic model.

The variation of lateral stability with angle of attack is shown in Fig. 4-77 for several combinations of Mach number and wing sweep. Directional stability and side force characteristics are shown in Figs. 4-78 and 4-79. It is seen that directional stability at Mach 2.7 is a function of both angle of attack and sideslip.

The aeroelastic correction factors for the rigid lateral-directional stability data are presented in Figs. 4-80 and 4-81. The following equations indicate the manner of application of the aeroelastic data to obtain flexible airplane effects.

$$\left(\Delta C_{n_\beta}\right)^{\text{flexible}}_{\substack{\text{vertical}\\ \text{tail}}} = \left(\Delta C_{n_\beta}\right)^{\text{rigid}}_{\substack{\text{vert.}\\ \text{tail}}} \left(\frac{L_E}{L_R}\right)^2_V \left(K_{BB}\right)_{\text{vert.}}$$

$$\left(\Delta C_{n_\beta}\right)^{\text{flexible}}_{\substack{\text{ventral}\\ \text{fin}}} = \left(\Delta C_{n_\beta}\right)^{\text{rigid}}_{\substack{\text{ventral}\\ \text{fin}}} \left(K_{BB}\right)_{\text{ventral}}$$

$$\left(\Delta C_{Y_\beta}\right)^{\text{flexible}}_{\substack{\text{vertical}\\ \text{tail}}} = \left(\Delta C_{Y_\beta}\right)^{\text{rigid}}_{\substack{\text{vert.}\\ \text{tail}}} \left(\frac{L_E}{L_R}\right)^2_V \left(K_{BB}\right)_{\text{vert.}}$$

No aeroelastic corrections were applied to the body, nacelles, and horizontal tail contributions to airplane directional stability or side force effects. In addition, no aeroelastic corrections were applied for the wing and ventral fin contributions to side force, or for the wing contribution to directional stability.

## 4.3 DYNAMIC STABILITY

Preliminary dynamic analyses and flight simulator evaluations of the B-2707 have been conducted to evaluate unaugmented airplane handling qualities, control capabilities, stability augmentation systems, and emergency operations. These studies have shown that there are practical solutions available for all cases in which control problems exist or where improvements in handling characteristics are desired. The airplane has demonstrated that it is sufficiently tractable to permit safe deceleration, descent, and landing in the event of complete failure of the stability augmentation systems. However, the simulator tests have emphasized the need for stability and control response augmentation and improved instrument displays to ensure good handling qualities at all flight conditions.

### 4.3.1 Longitudinal Dynamics

Longitudinal handling qualities of the unaugmented airplane are characterized by sluggish pitch response which is well damped at low speeds and lightly damped at high speeds. These character-

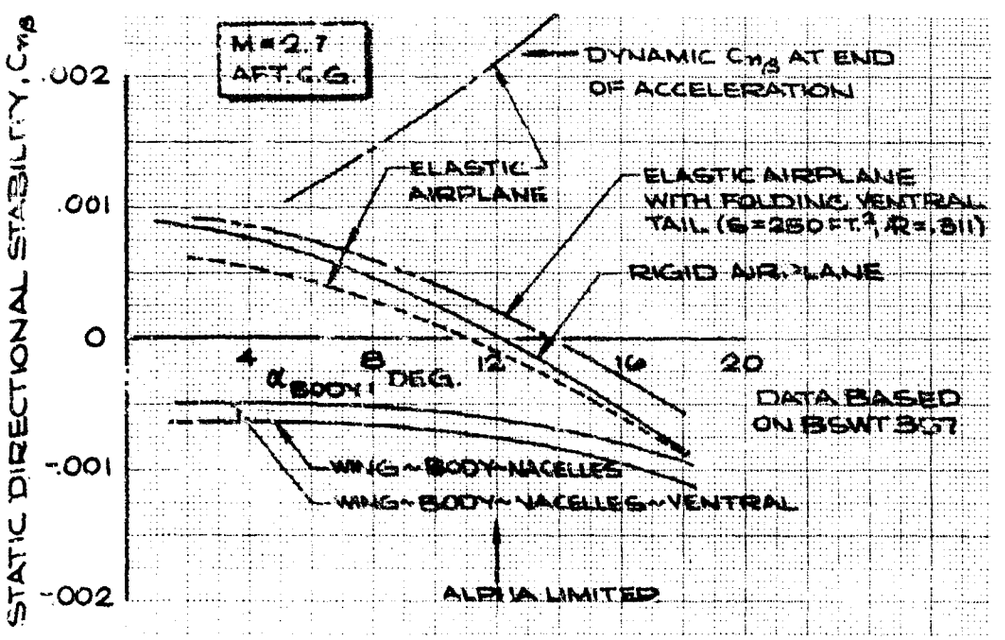


*Figure 4-72 Mach 2.7 Directional Stability*

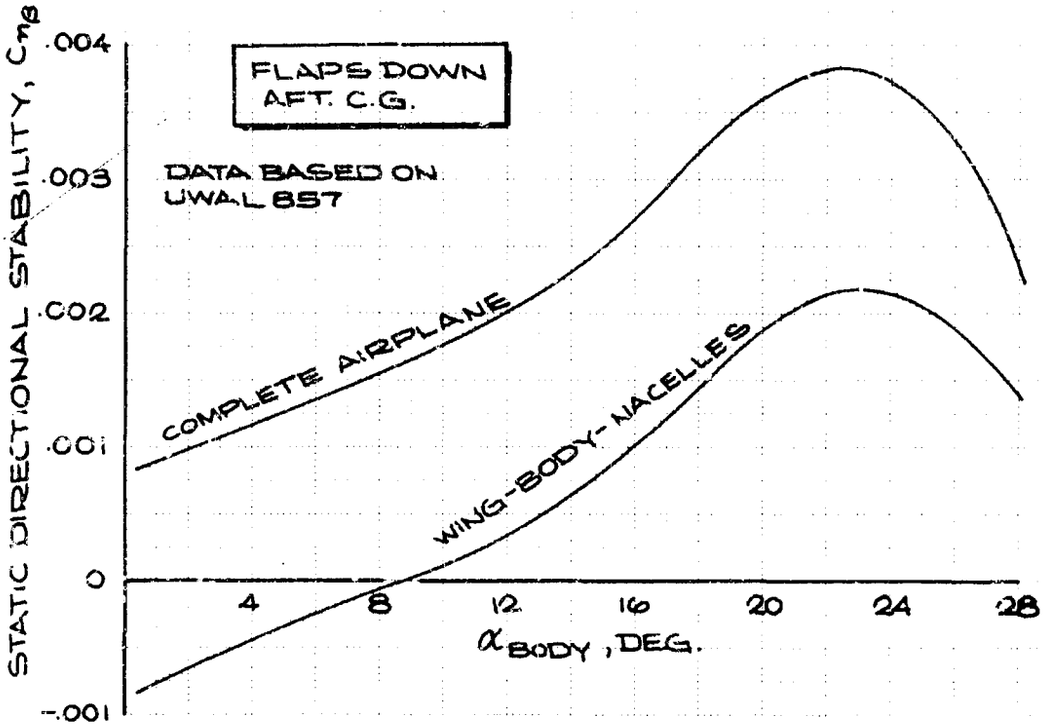


*Figure 4-73. Directional Stability, Landing*

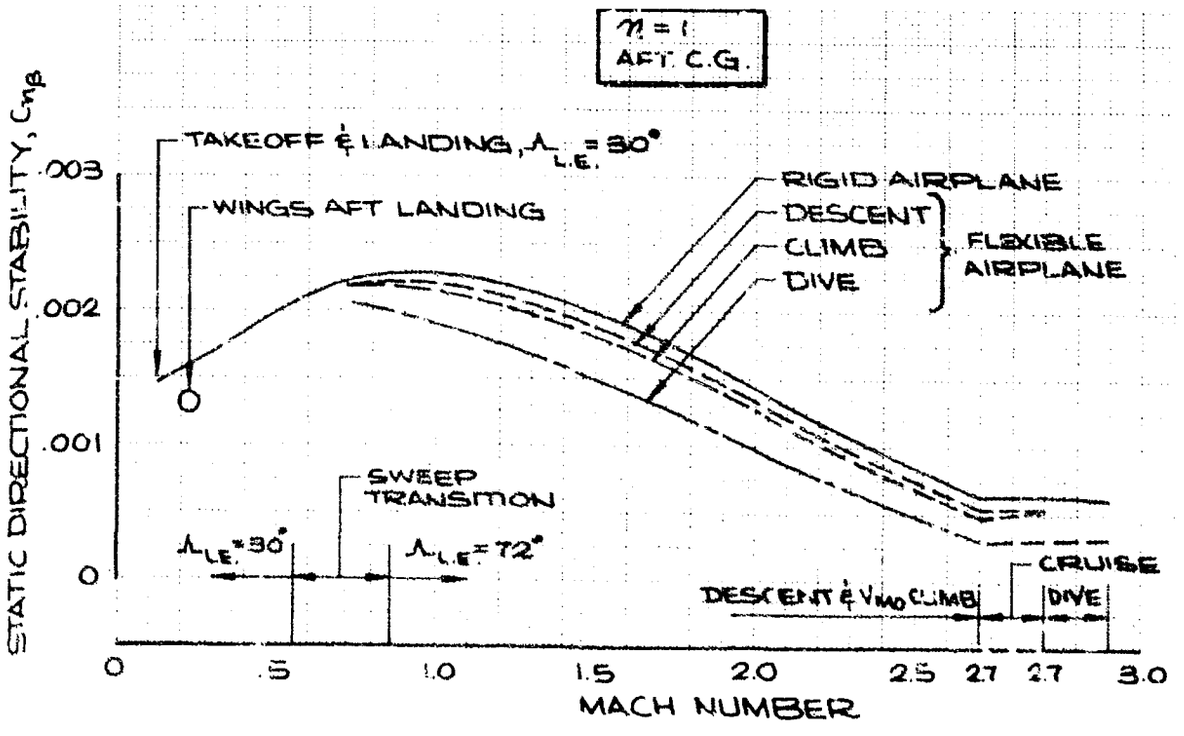


*Figure 4-74. Directional Stability Vs. Mach Number*

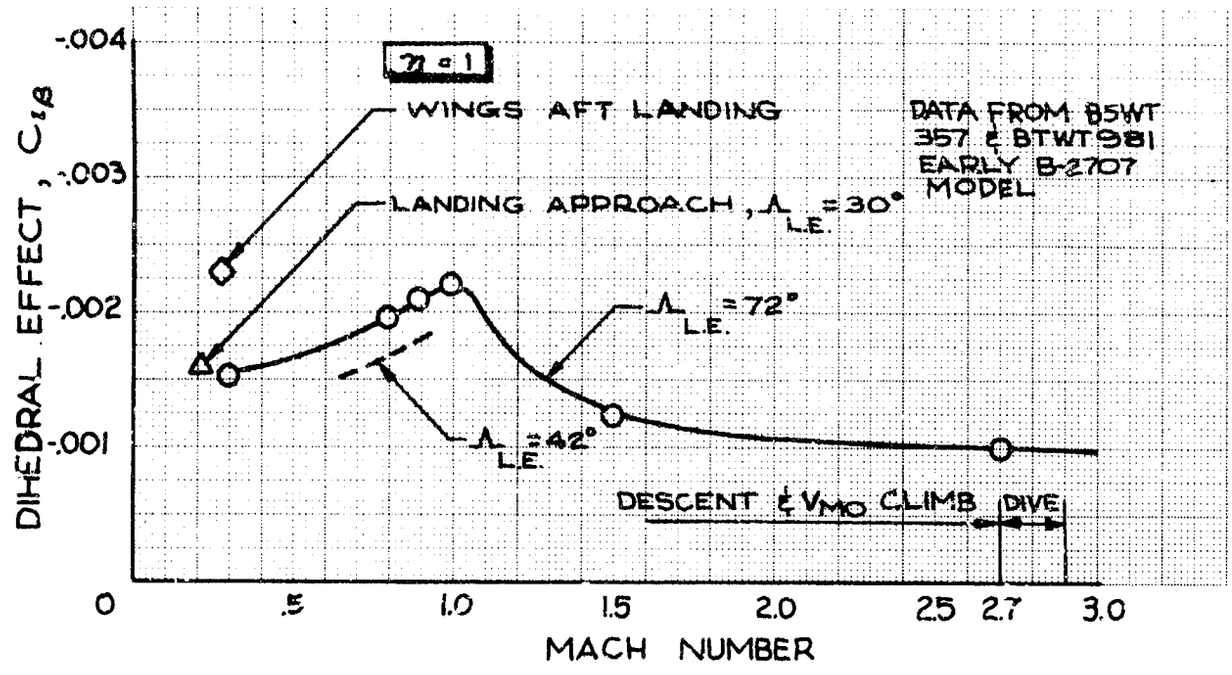


*Figure 4–75. Dihedral Effect*

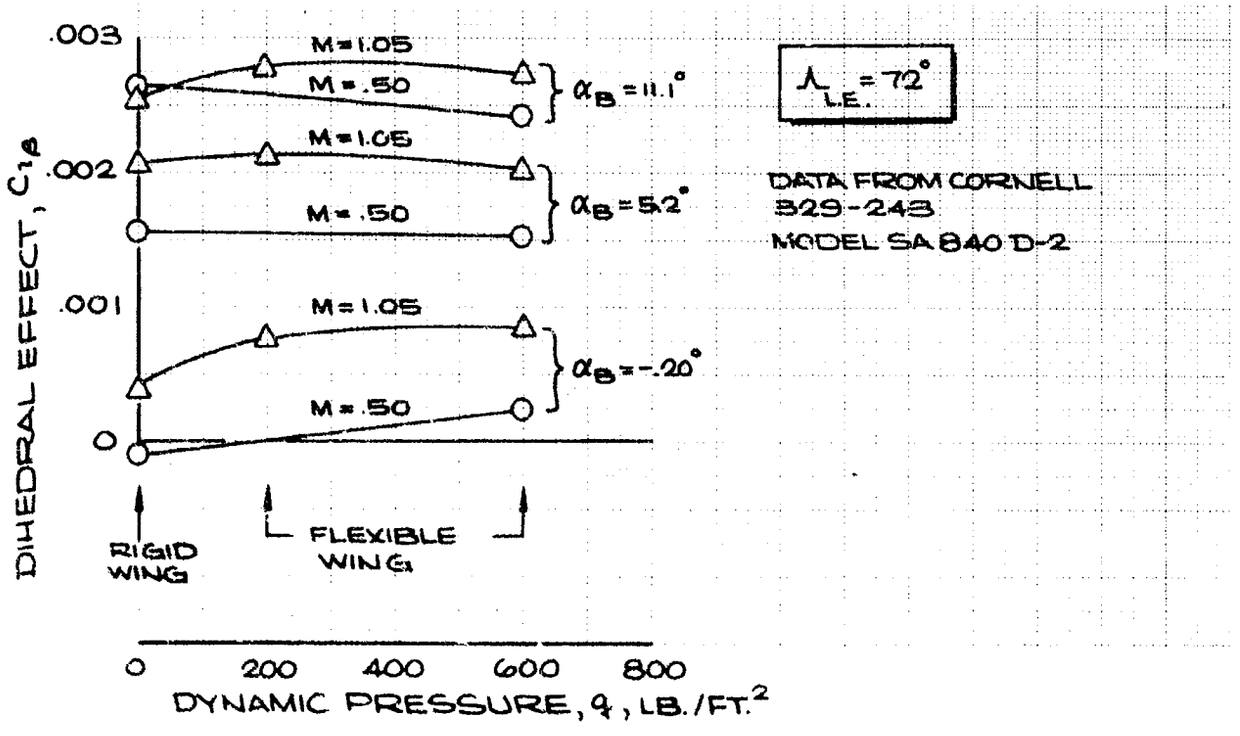


*Figure 4–76. Effect of Wing Flexibility on Dihedral Effect*

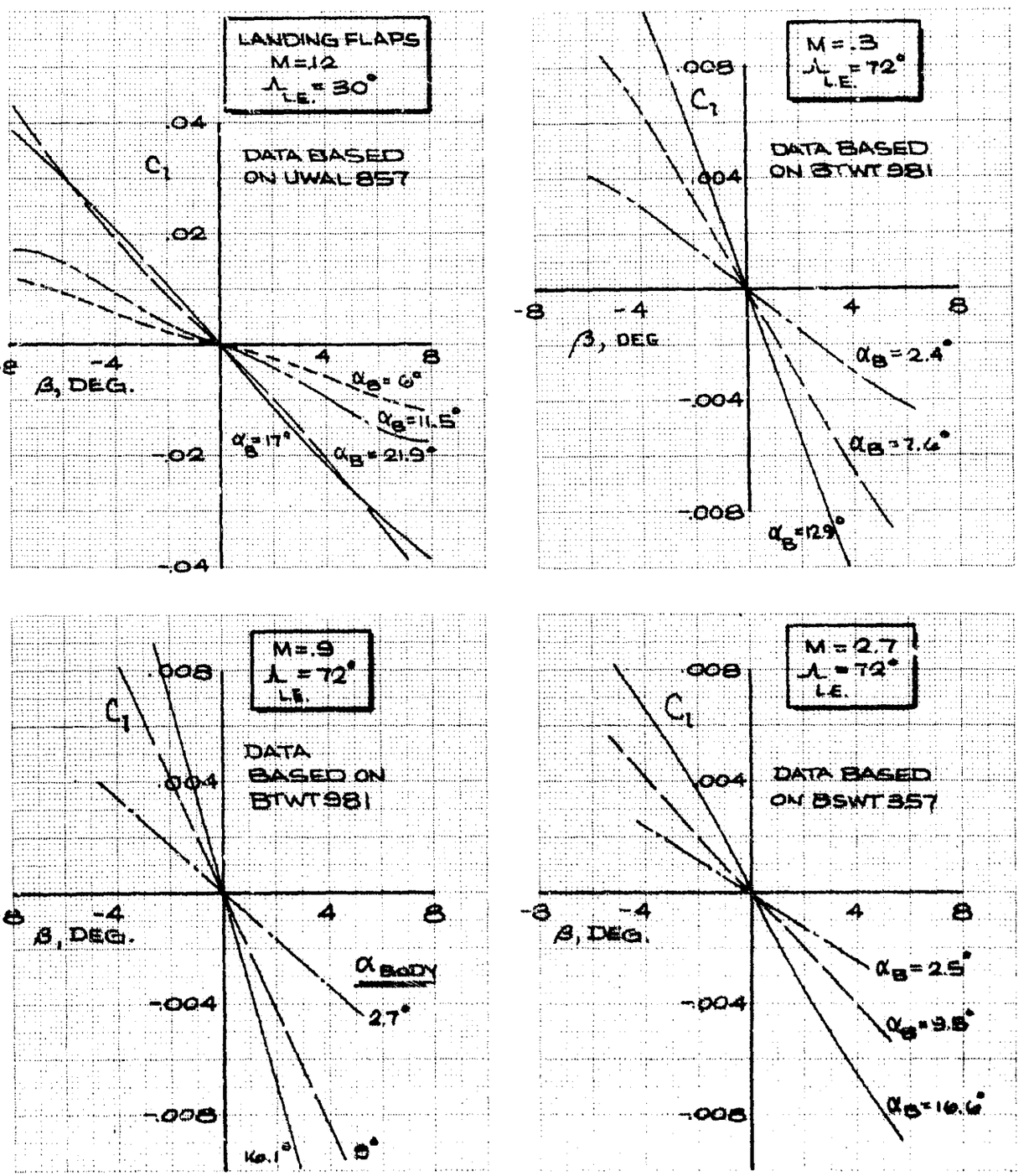


*Figure 4-77. Rigid Airplane Dihedral Effect*

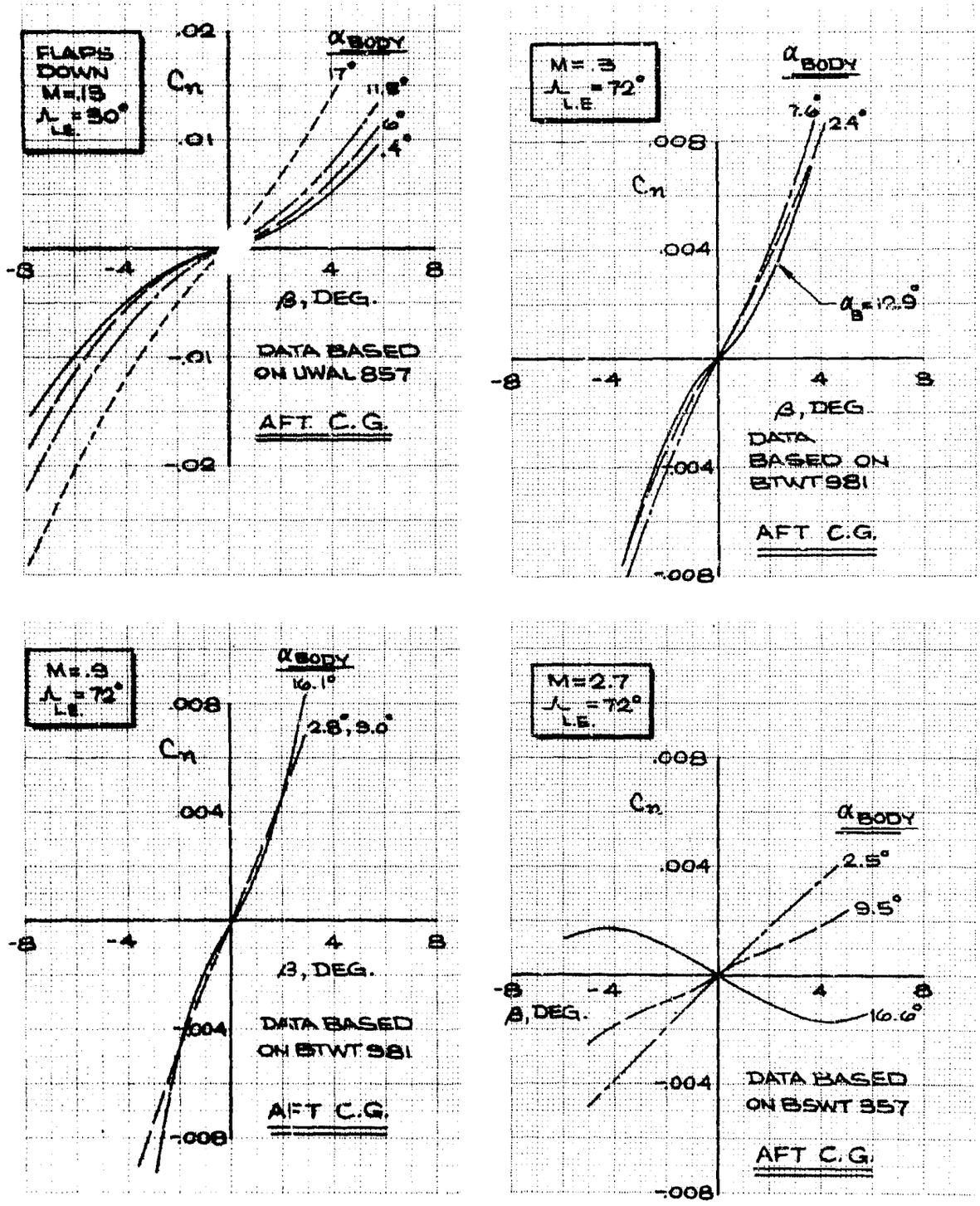


*Figure 4–78. Rigid Airplane Directional Stability*

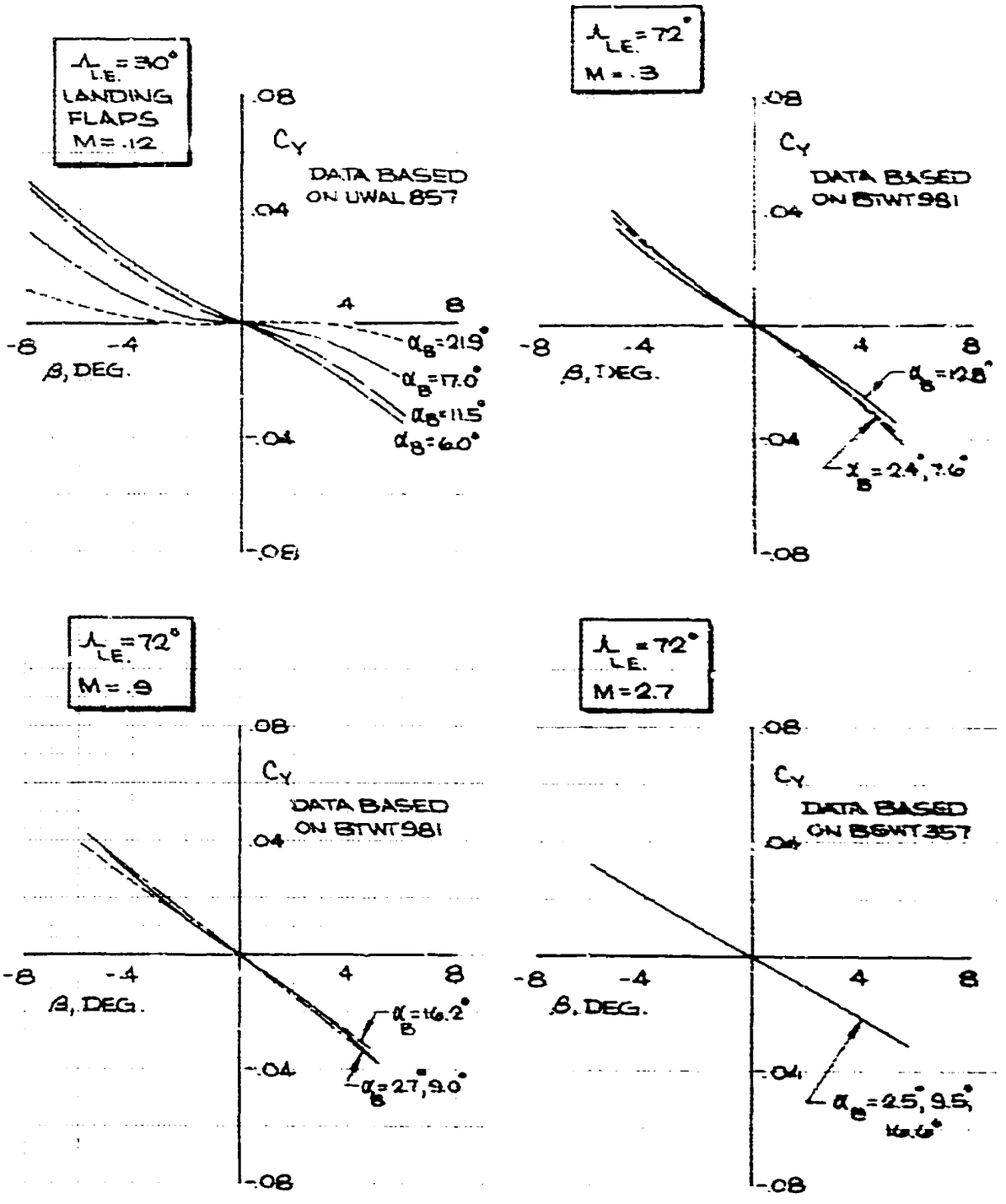


*Figure 4-79. Rigid Airplane Side Force Characteristics*

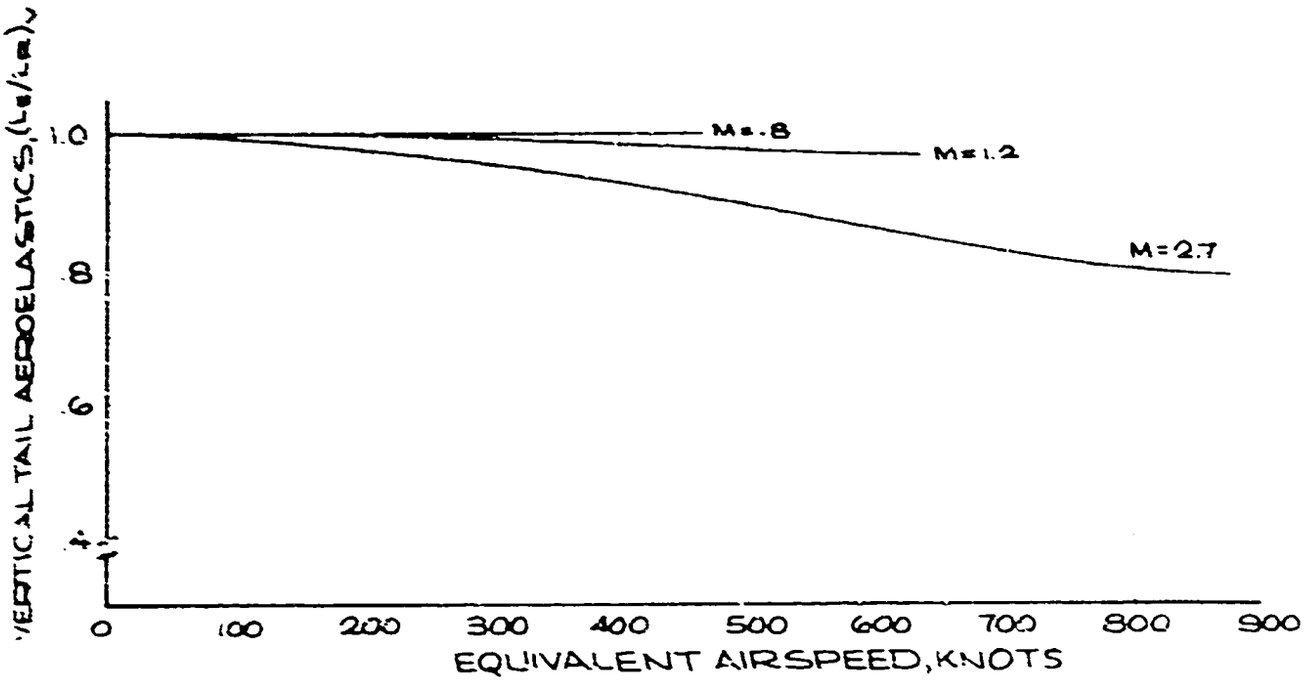


*Figure 4-80. Aeroelastic Factor for Vertical Tail*

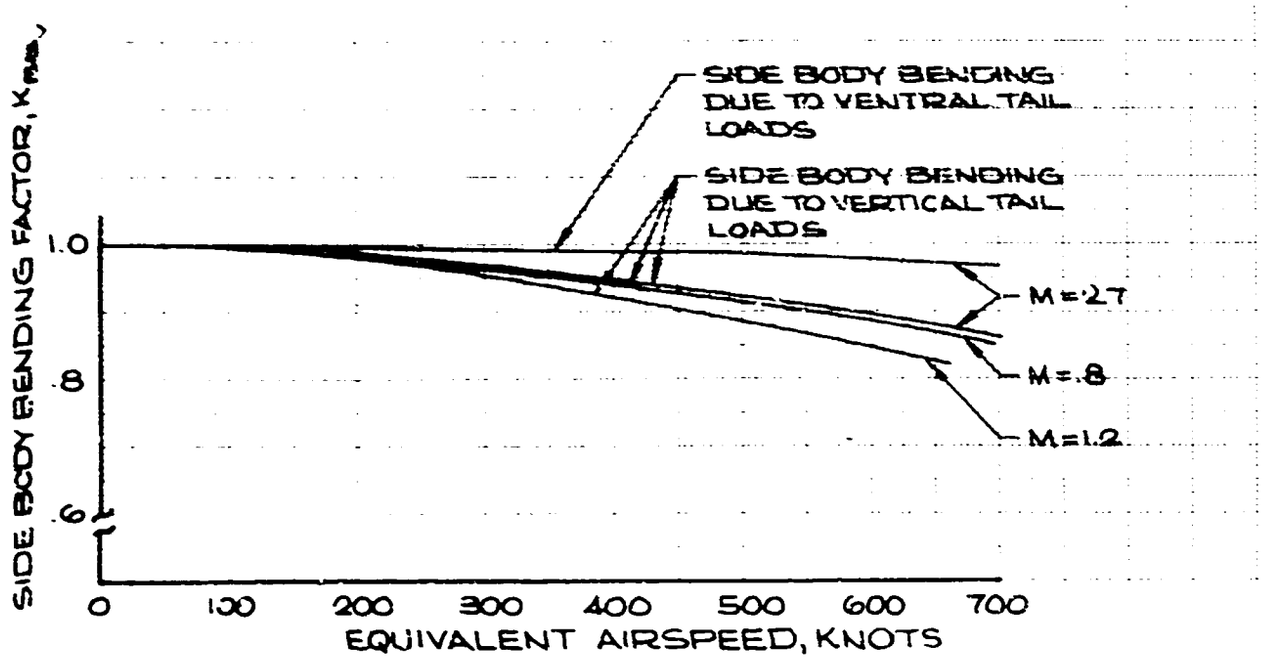


*Figure 4-81. Body Bending Due to Vertical Tail Loads*

istics are inherent in high-inertia configurations. Good handling qualities will be provided by pitch response augmentation and improved attitude display. Pilot effort is high without pitch response augmentation; however, the low frequency character of the motion eliminates any tendency toward pilot induced oscillations or other undesirable characteristics. There is some concern that, for low speed operation, better flight path response to control input may be required than that which can be attained with the conventional elevator controls and the stability augmentation system. Direct lift control is being studied as a possible method of providing further improvement in low speed flight path control (Par. 4.1.1.2). The dynamic characteristics of the airplane with conventional control system, with and without stability augmentation, are discussed in the following paragraphs.

4.3.1.1 Unaugmented Airplane

The longitudinal dynamic characteristics of the unaugmented B-2707 at eight significant flight conditions are presented in the form of Bode plots of the pitch rate to elevator deflection transfer function in Fig. 4-82. The significance of this form of presentation in terms of the more conventional static and dynamic stability parameters is shown in Fig. 4-83. This format was chosen to be compatible with the discussion of the augmented airplane characteristics. It is also consistent with the stability augmentation system design objectives shown in the preliminary procurement specification for the automatic flight control system. A great deal of analytical and flight simulator work has been done to establish and present airplane handling qualities criteria in the way most useful to groups within and outside the company who are engaged in the analysis, synthesis, and design of the automatic flight control system. The results have shown the desirability of presenting dynamic stability and response criteria in the frequency domain.

Figure 4-82 shows that the airplane short period frequencies remain essentially constant throughout the normal flight range, but the damping varies from heavy at the landing approach condition (VII) to light at the end of cruise condition (IV). The light damping at the high speed flight conditions is apparent to the pilot as a pitch rate overshoot. There is general agreement among pilots

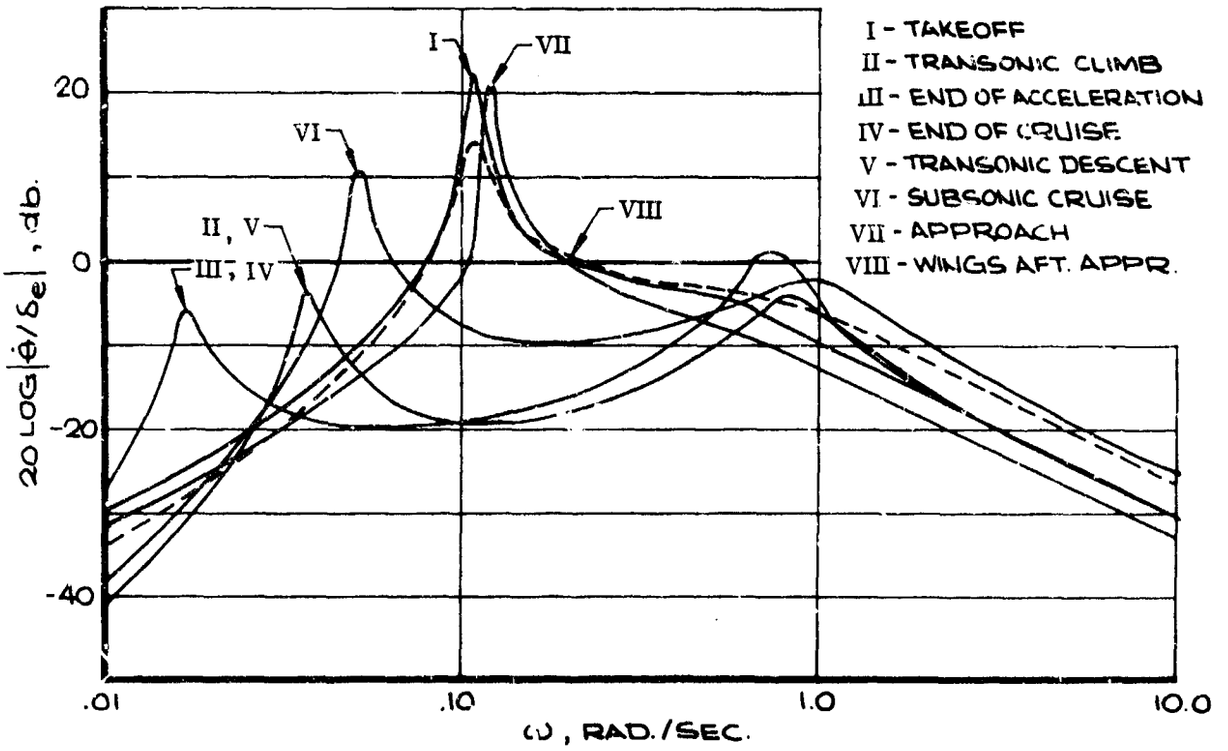


*Figure 4-82. Frequency Response Diagrams, Unaugmented Airplane*

who have flown the simulator that the unaugmented airplane is sluggish and lightly damped at high speeds and overdamped at low speeds. The low frequency portion of the curves exhibit the typical lightly damped phugoid characteristic with the break frequency of the mode varying roughly as a function of true airspeed. The low damping of this mode does not present any particular problem but does add to the pilot workload when the task is to arrive at a precise pitch attitude.

4.3.1.2 Augmented Airplane

Figure 4-84 presents the criterion on which the pitch axis portion of the stability augmentation system has been synthesized. This criterion has several important features:

a. The maximum deviation allowable up to the high frequency break point is 2.5 db, which precludes any lightly damped modes in the closed-loop control response.

b. The high frequency break point which establishes the effective short period frequency was selected at 1.6 rad/sec (0.255 cps). Flight simulator experience has shown this to be a good compromise value for jet transport operation since it provides adequate response characteristics without imposing a severe requirement for control system rates.

c. At the low frequency end of the diagram the solid lines represent the criterion for high speed operation. The criterion demands a constant pitch rate output to control input down to very low frequencies. This characteristic suppresses the airplane's natural phugoid mode or speed stability characteristics as, in the absence of pilot command, the pitch rate is held near zero. Flight simulator studies showed a requirement for a moderate level of static stability at low speeds. The dashed lines on Fig. 4-84 represent the change made to the criterion at the low frequency portion of the diagram to achieve this end; the low frequency component of the commanded pitch rate is washed out and a fixed control input is required to hold the airplane at an attitude different from trim. When a control input is released the attitude returns to trim without overshoot. The location of the low frequency break point fixes the level of apparent static stability.

The response due to control input is not the same as the response due to external disturbances. It is also specified that airplane oscillations due to these disturbances should damp to 0.2 amplitude in one cycle. This also has the effect of greatly reducing trim changes due to configuration changes.

An augmentation system approximating the above criterion was tested on the flight simulator at

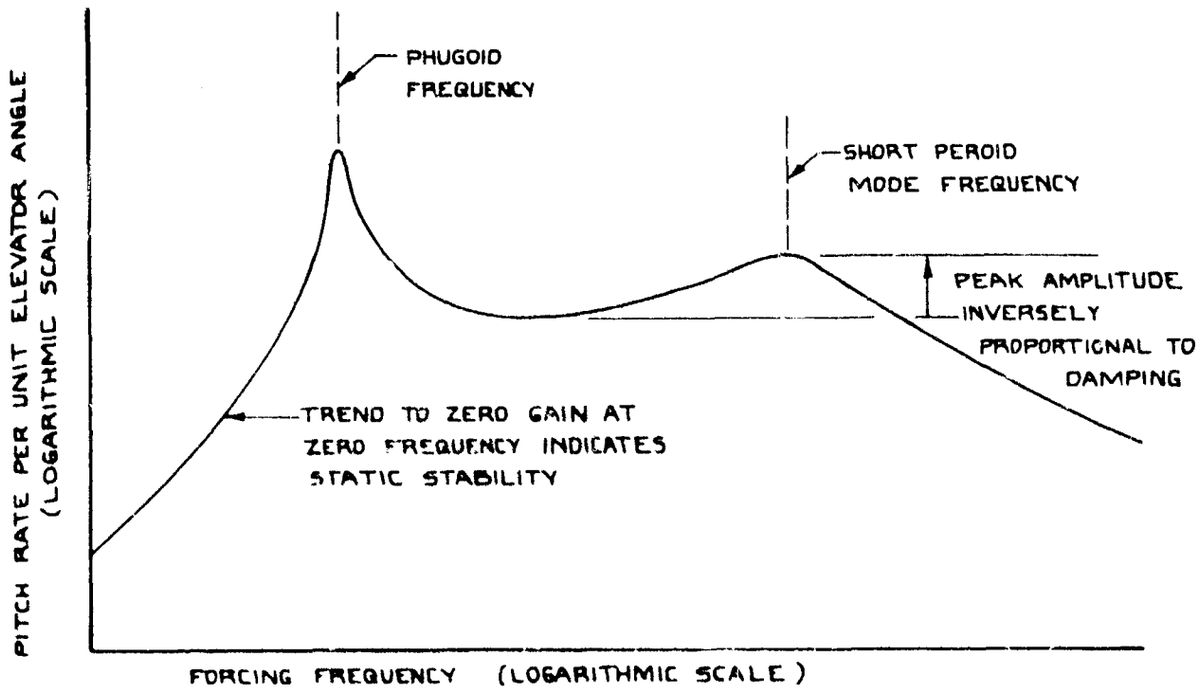


*Figure 4-83. Frequency Response Sample Diagram*

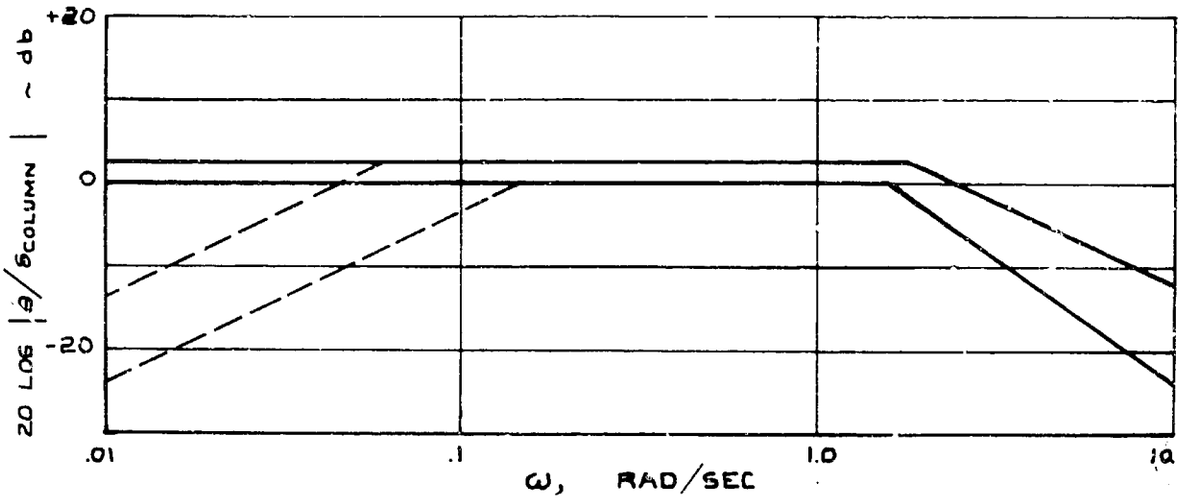


*Figure 4-84. Pitch Axis Augmentation Design Criteria*

various flight conditions. The resulting airplane response characteristics were satisfactory. Flight simulator and analytical studies are continuing in order to improve the criterion and to ensure that the airplane will possess good control response characteristics throughout the flight envelope.

4.3.1.3 Flight Simulation of Stalls

A series of stalls was performed in a flight simulator evaluation of the flaps down pitching moment characteristics of the airplane at high angles of attack without the angle of attack warning and control system operative. The simulation included the complete nonlinear lift, drag, pitching moment, and elevator characteristics as a function of angle of attack. Time histories of two stalls are presented in Figs. 4-85 and 4-86. The first figure presents the unaugmented airplane and shows that the small nonlinearity in the pitch curve is easily controllable through the stall and that there is not a large increase of pitch rate or of angle of attack rate as the minimum speed point is traversed. The second trace for the airplane with the pitch axis augmented shows about the same characteristics, except for the increase in elevator activity ordered by the SAS to improve the airplane response to control input. In either case, the stall speed could be demonstrated with no unusual control action required to complete the recovery.

4.3.2 Lateral-Directional Dynamics

The lateral-directional oscillatory characteristics of the B-2707 are illustrated in Figs. 4-87 and 4-88. Figure 4-88 presents time histories of sideslip releases for the eight representative flight conditions tabulated in Par. 4.3.3. The B-2707 is inertially a very slender airplane and, unaugmented, exhibits the mode shape ($\phi/\beta$) typical of such an inertia distribution. The ratio $\phi/\beta$ varies from about 2 in the transonic flight conditions to near 5 at the end of cruise.

The large yaw inertia of the airplane produces a lateral-directional oscillation natural frequency that is somewhat lower than that exhibited by current large jet transports.

There is no generally accepted criterion at present for the damping of lateral-directional oscillations for this class of airplane. However, this mode is primarily a nuisance motion and its acceptability is best determined in terms of the time to damp. A tentative criterion of 5 sec to one-half amplitude has been selected for the augmented airplane. The time required to damp to some specified amplitude is proportional to the product $\zeta_d\omega_d$, and the handling quality of the airplane is approximately constant along a line of constant time to damp, i.e., constant $\zeta_d\omega_d$. Figure 4-87 shows the frequency and damping ratio for each of the eight representative flight conditions with lines of 10 sec to one-half amplitude ($\zeta_d\omega_d = 0.069$) and 5 sec to one-half amplitude ($\zeta_d\omega_d = 0.0138$).

The time histories of Fig. 4-88 illustrate the improvement in time to damp provided by the

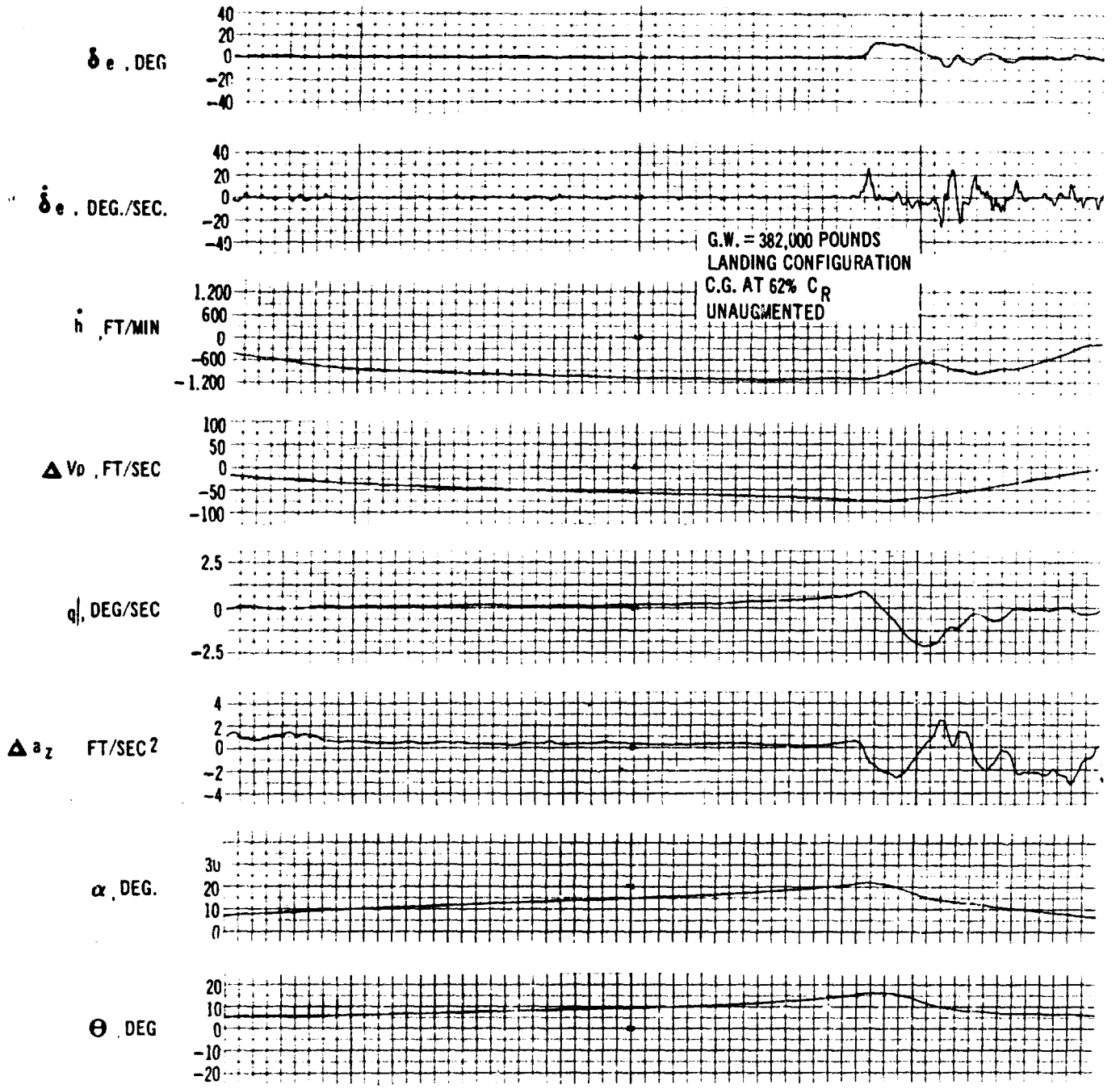


*Figure 4-85. Stall Demonstration, Unaugmented Airplane*

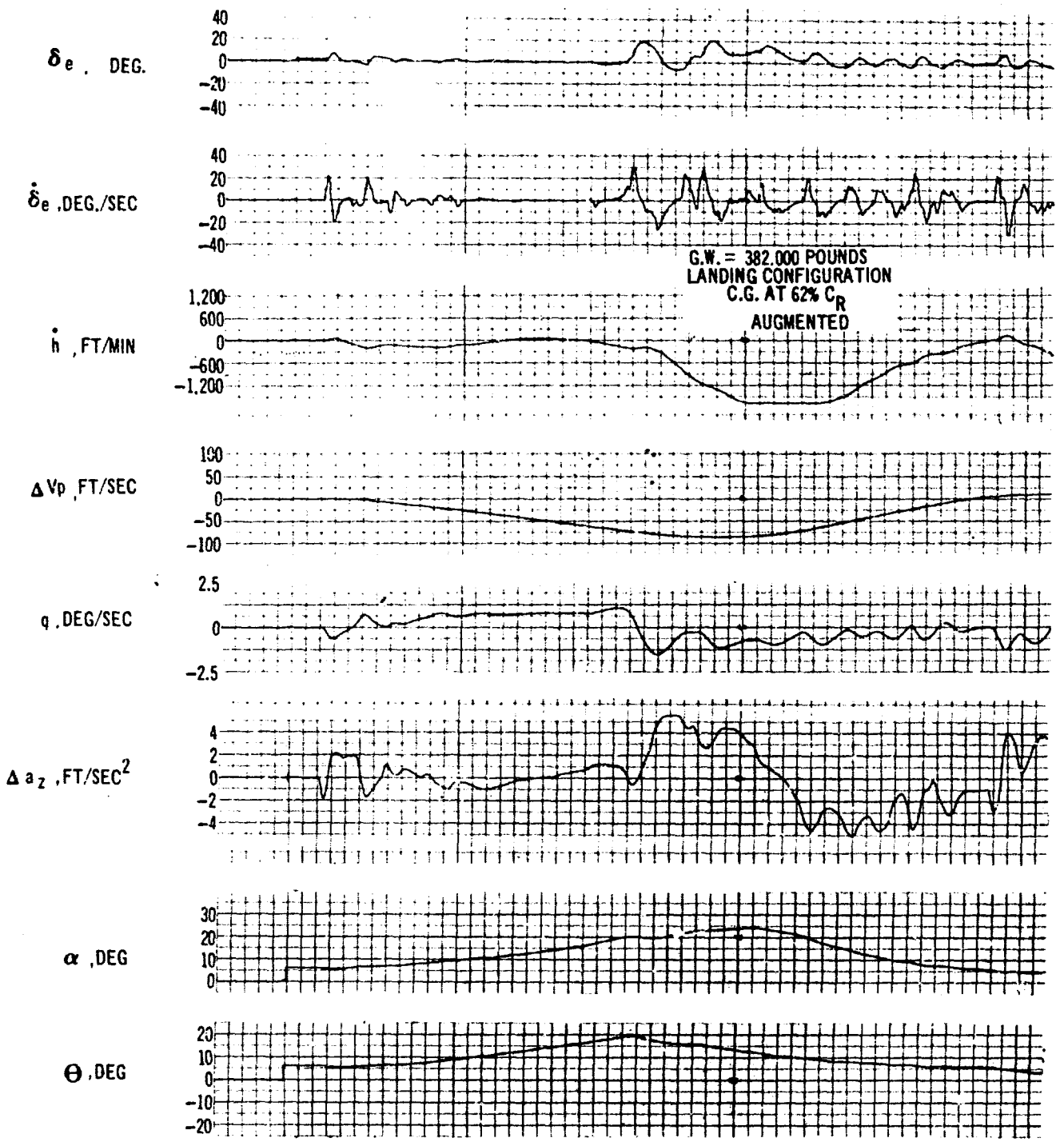


*Figure 4-86. Stall Demonstration, Augmented Airplane*

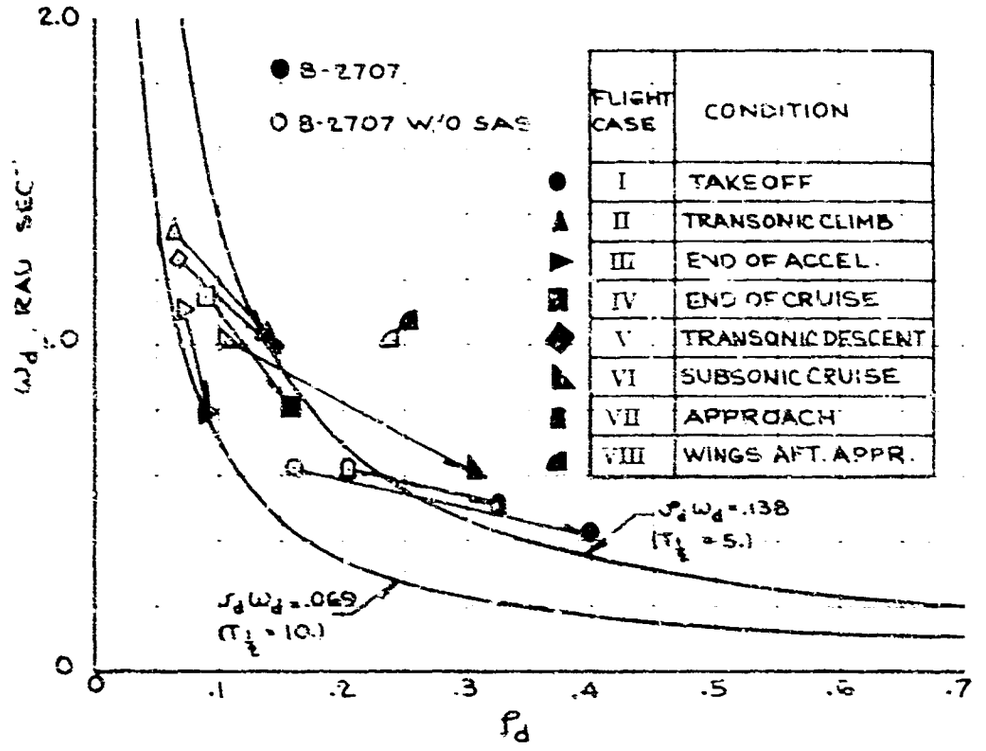


*Figure 4-87. Lateral-Directional Oscillatory Characteristics*

present mechanization of the SAS. The system changes the period as well as the damping ratio. The shaded symbols of Fig. 4-87 represent the B-2707 with SAS operating, and as observed on the time histories, exhibit lower frequencies and higher damping ratios than the airplane with SAS off. Continuing development of the SAS will produce satisfactory characteristics at all flight conditions.

4.3.3 Response to Lateral Control

Figure 4-89 illustrates the response of the B-2707 in supersonic cruise, and transonic descent, to a step application of the pilot's wheel to less than maximum deflection, i.e., normal control operation, and to maximum deflection. Normal use of the control allows the SAS to utilize the elevons to increase the damping, which improves the quality of the bank angle response. However, full control is available at maximum deflection, and provides the greater roll response shown.

Figure 4-90 shows the bank angle response for subsonic cruise (42-degree sweep) and landing approach (30-degree sweep, flaps down). This is response to partial control and illustrates the powerful lateral control available at these flight conditions.

4.3.4 Dynamic Stability Data

Tables 4-B and 4-C summarize dynamic stability characteristics and stability derivative data applicable to the eight flight conditions selected for analysis.

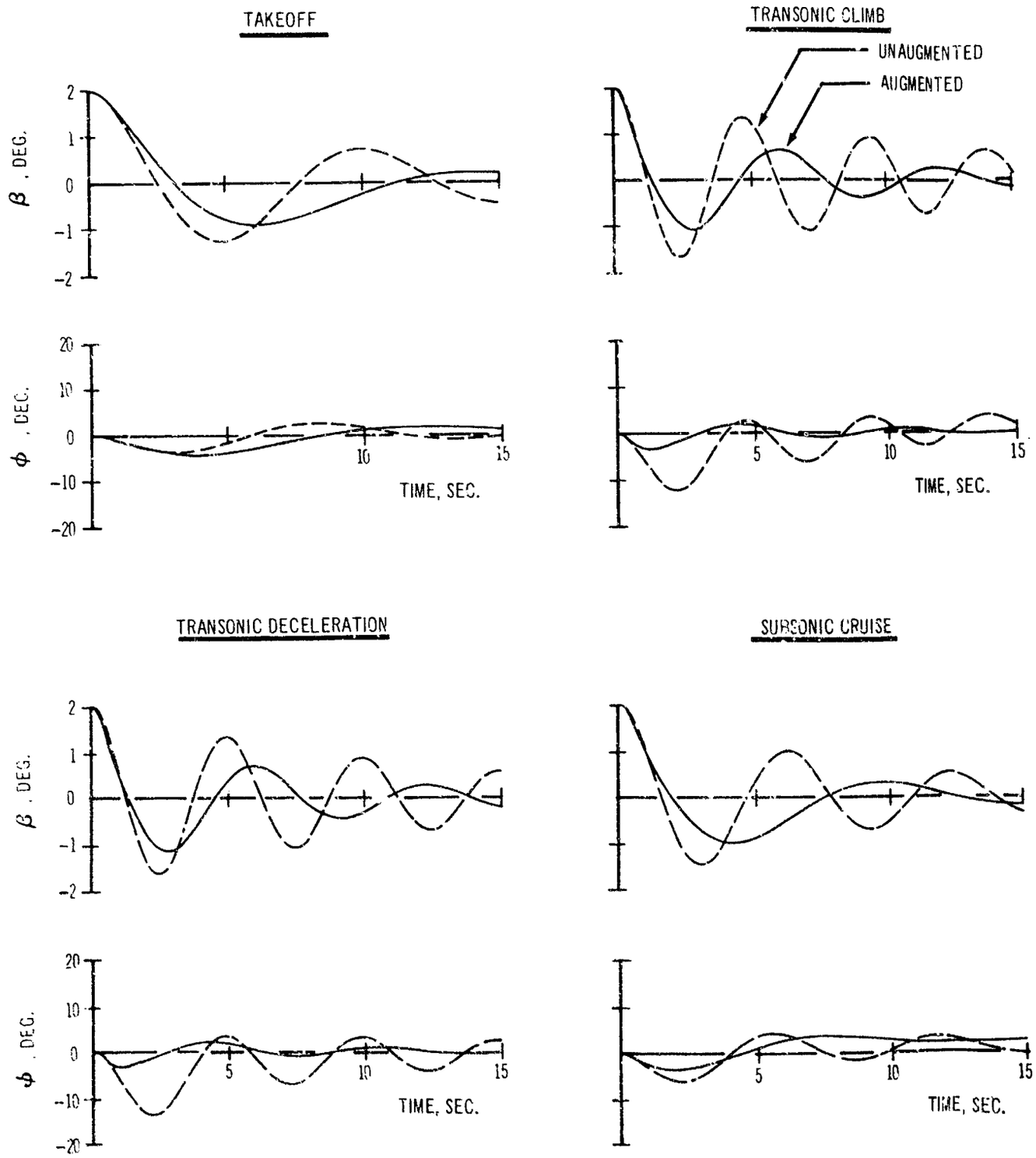
TAKEOFF
TRANSONIC CLIMB
UNAUGMENTED
AUGMENTED
β, DEG.
φ, DEG.
TIME, SEC.
TRANSONIC DECELERATION
SUBSONIC CRUISE

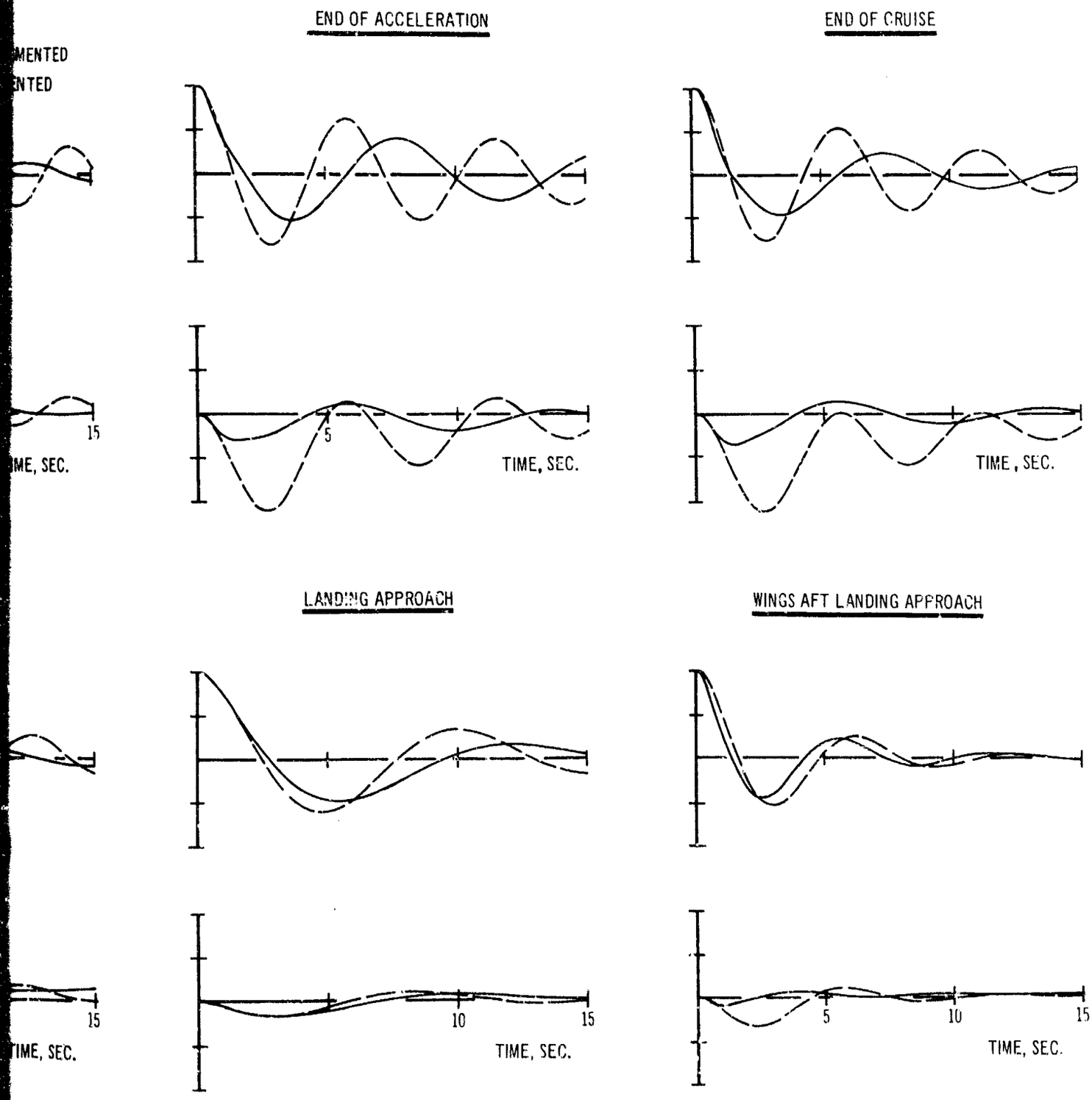


*Figure 4–88. β –Releases, Augmented and Unaugmented Airplane*

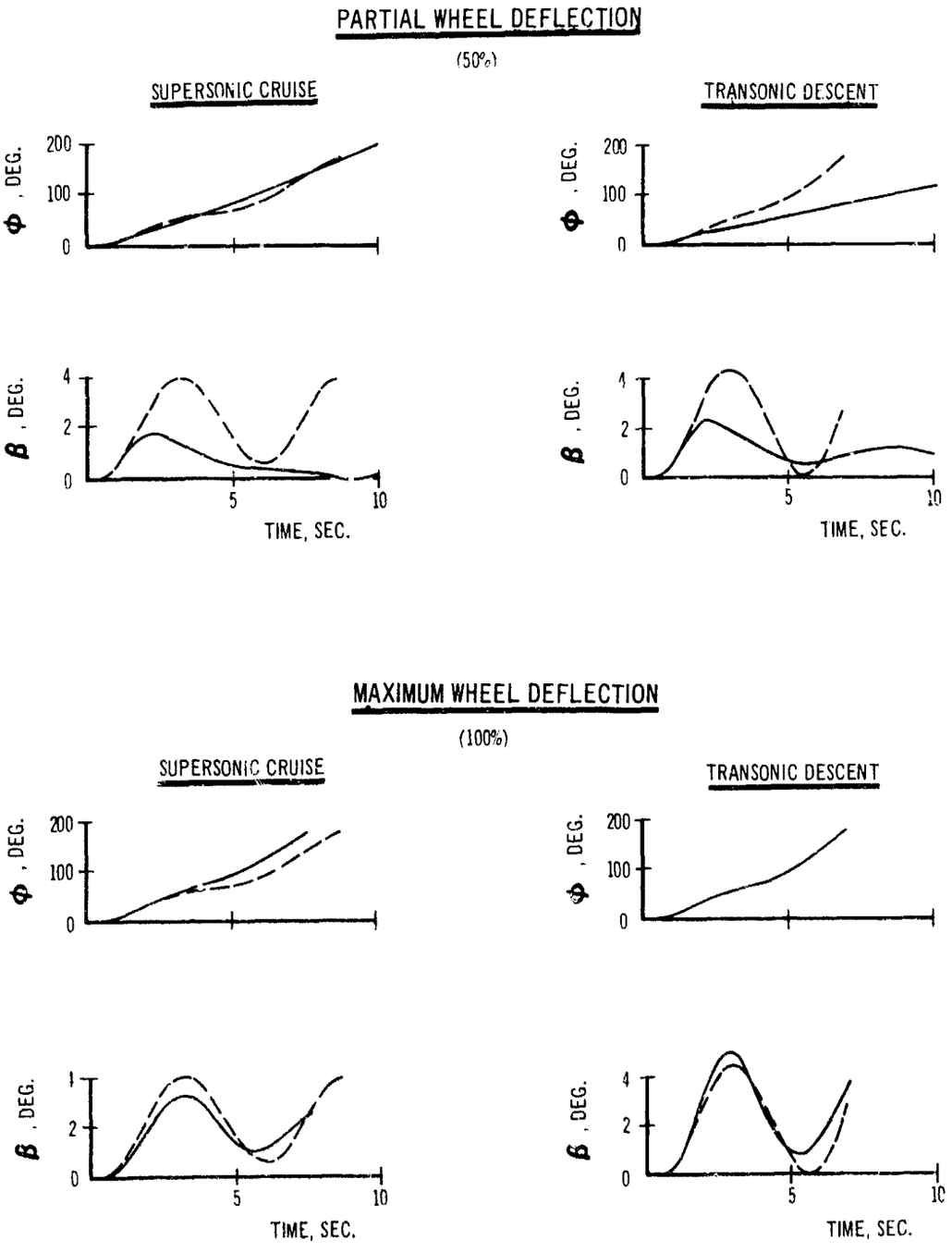


*Figure 4-89. Response to Control Wheel Deflection, Cruise Configuration*

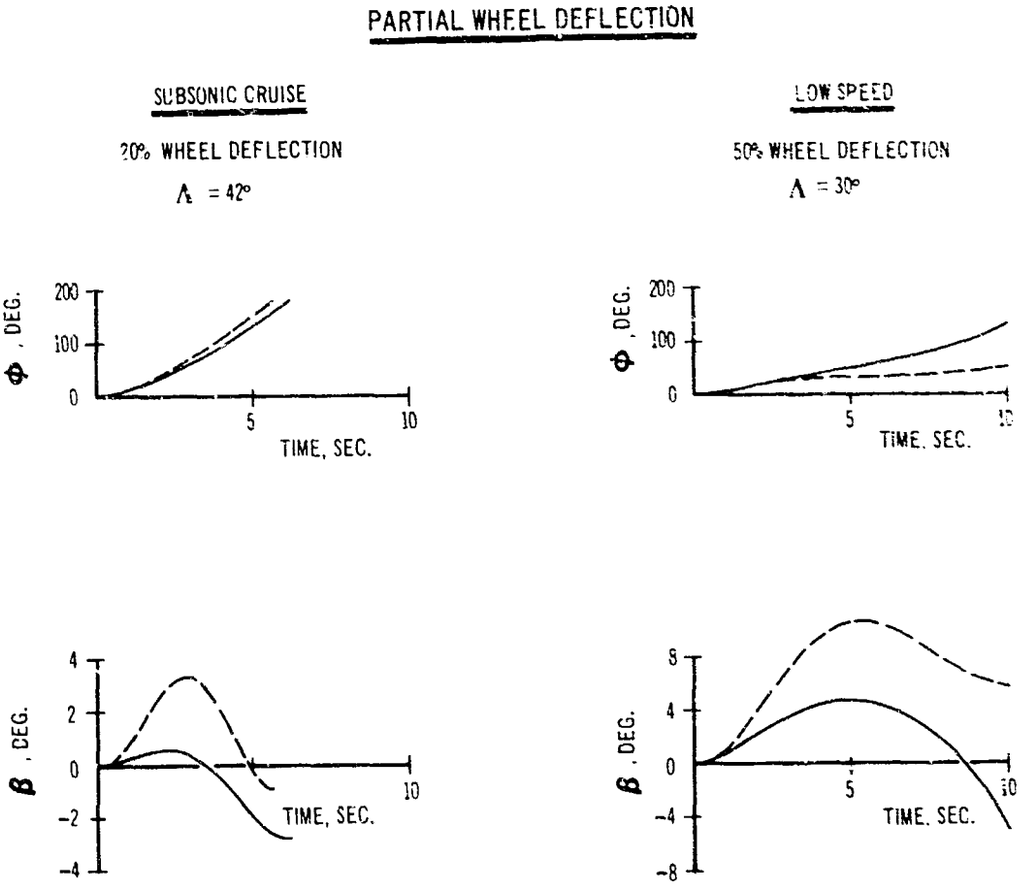


*Figure 4-90. Response to Control Wheel Deflection, Wings Forward*

| FLIGHT CONDITION | GW 1000 LB | C.G. LOC % CR | $A_{L.E.}$ DEG | ALTITUDE FT | $V_e$ FT SEC | q LBS $FT^{-2}$ | MACH NO. | $I_{XX}$ | $I_{YY}$ $NM^{-4}$ sec |
|---|---|---|---|---|---|---|---|---|---|
| I | 670 | 61.7 | 31 | Sea Level | 367 | 113 | .278 | 11.13 | 46.5 |
| II | 614.8 | 63.5 | 72 | 40,513 | 1,162 | 387 | 1.8 | 5.23 | 43.3 |
| III | 574.1 | 63.5 | 72 | 51,217 | 2,611 | 735.5 | 2.7 | 4.52 | 47.1 |
| IV | 555.2 | 62.1 | 72 | 51,300 | 2,630 | 473.5 | 2.7 | 2.81 | 42.3 |
| V | 387.6 | 62.1 | 72 | 52,600 | 1,163 | 216.3 | 1.2 | 2.51 | 42.4 |
| VI | 650 | 62.3 | 42 | 34,000 | 845 | 323 | .85 | 5.80 | 47.2 |
| VII | 581 | 61.1 | 30 | Sea Level | 244 | 71 | .219 | 4.27 | 41.1 |
| VIII | 340 | 62.2 | 72 | Sea Level | 346 | 142 | .312 | 2.61 | 38.1 |

| FLIGHT CONDITION | $C_{l_\beta}$ RAD.$^{-1}$ | $C_{l_p}$ RAD.$^{-1}$ | $C_{l_r}$ RAD.$^{-1}$ | $C_{l_{\delta_W}}$ RAD.$^{-1}$ | $C_{l_{\delta_R}}$ RAD.$^{-1}$ | $C_{l_{\delta_A}}$ RAD.$^{-1}$ | $C_{l_{\delta_{SP}}}$ RAD.$^{-1}$ | $C_{l_{\delta_{TIP}}}$ RAD.$^{-1}$ | $C_{l_\beta}$ RAD. |
|---|---|---|---|---|---|---|---|---|---|
| I | -.159 | -.530 | .531 | .0682 | 0 | .0682 | .0755 | - | .355 |
| II | -.095 | -.0969 | .0385 | .00539 | .00097 | - | .00135 | .0180 | .111 |
| III | -.0573 | -.0832 | .0105 | .00229 | .00126 | - | .00063 | .00739 | .059 |
| IV | -.0579 | -.0903 | .0110 | .00264 | .00149 | - | .00092 | .00831 | .057 |
| V | -.095 | -.101 | .0384 | .00641 | .00132 | - | .00120 | .0212 | .122 |
| VI | -.0091 | -.275 | .335 | .0309 | .00430 | - | .00441 | .0249 | .127 |
| VII | -.159 | -.547 | .211 | .0647 | .00372 | .0693 | .0696 | - | .055 |
| VIII | -.0888 | -.112 | .115 | .0103 | .00103 | - | .000229 | .0384 | .09 |

| MACH NO. | $i_{XX}$ | $i_{YY}$ | $i_{ZZ}$ | $i_{XZ}$ | $\alpha_{TRIM}$ | $\delta_{TRIM}$ | $C_{D_\alpha}$ | $C_{L_\alpha}$ | $C_{L_\delta}$ | $C_{L_{\delta_{elev.}}}$ | $C_{L_{\delta_{aux}}}$ |
|---|---|---|---|---|---|---|---|---|---|---|---|
| | $X 10^{-5}$ SLUG-FT$^2$ | | | | DEG | DEG | RAD.$^{-1}$ | RAD.$^{-1}$ | RAD.$^{-1}$ | RAD.$^{-1}$ | RAD.$^{-1}$ |
| .276 | 10.43 | 45.6 | 56.0 | .70 | 12.0 | -5.0 | .297 | 3.152 | .135 | .060 | |
| 1.2 | 5.23 | 45.0 | 52.5 | .65 | 5.4 | -5.0 | .193 | 2.040 | .0266 | - | |
| 1.7 | 4.62 | 47.5 | 51.5 | .62 | 5.6 | -3.25 | .093 | 1.215 | .0108 | - | |
| 2.7 | 3.83 | 41.9 | 44.1 | .51 | 6.9 | -2.0 | .101 | 1.238 | .0135 | - | |
| 1.2 | 2.83 | 41.9 | 44.1 | .50 | 8.5 | -10.0 | .227 | 2.103 | .0453 | - | |
| .85 | 3.62 | 47.2 | 55.9 | .71 | 6.9 | -3.2 | .151 | 2.521 | .087 | - | |
| .219 | 4.27 | 41.2 | 44.2 | .25 | 9.5 | -.5 | . 29 | 3.152 | .132 | .0625 | |
| .315 | 3.61 | 39.7 | 41.0 | .29 | 11.5 | -2.0 | . 35 | 1.948 | .152 | .0693 | |

| $C_{l_{\delta_{SP}}}$ RAD.$^{-1}$ | $C_{l_{\delta_{TIP}}}$ RAD.$^{-1}$ | $C_{n_\beta}$ RAD.$^{-1}$ | $C_{n_p}$ RAD.$^{-1}$ | $C_{n_r}$ RAD.$^{-1}$ | $C_{n_{\delta_W}}$ RAD.$^{-1}$ | $C_{n_{\delta_R}}$ RAD.$^{-1}$ | $C_{n_{\delta_A}}$ RAD.$^{-1}$ | $C_{n_{\delta_{SP}}}$ RAD.$^{-1}$ | $C_{n_{\delta_{TIP}}}$ RAD.$^{-1}$ | $C_{Y_\beta}$ RAD.$^{-1}$ | R |
|---|---|---|---|---|---|---|---|---|---|---|---|
| .0755 | - | .0837 | -.072 | -.226 | -.00206 | -.063 | -.00355 | +.0054 | - | -.201 | |
| .00103 | .0180 | .117 | -.0111 | -.220 | -.00052 | -.0295 | - | -.00029 | -.00860 | -.350 | |
| .00063 | .00739 | .029 | -.0068 | -.182 | -.00011 | -.0115 | - | -.00169 | -.00430 | -.275 | |
| .00092 | .00831 | .0315 | -.0066 | -.187 | -.000057 | -.0138 | - | +.00080 | -.00493 | -.287 | |
| .00120 | .0212 | .122 | -.0115 | -.219 | -.000057 | -.0458 | - | +.00029 | -.0101 | -.355 | |
| .00441 | .0249 | .127 | -.0231 | -.196 | -.00424 | -.0524 | - | +.00613 | -.00722 | -.327 | |
| .0696 | - | .0837 | -.0812 | -.239 | -.00315 | -.0630 | -.00178 | +.0630 | - | -.229 | |
| .000229 | .0384 | .09 | -.0172 | -.186 | -.00195 | -.0615 | - | -.000802 | -.00298 | -.344 | |

*Table 4-B. Airplane Stability Derivatives*

| | $C_{L_\delta}$ RAD.$^{-1}$ | $C_{L_{\delta\ \text{elev.}}}$ aux RAD.$^{-1}$ | $C_{L_{\delta\ TIP}}$ RAD.$^{-1}$ | $C_{M_\alpha}$ RAD.$^{-1}$ | $C_{M_{\dot\alpha}}$ RAD.$^{-1}$ | $C_{M_q}$ RAD.$^{-1}$ | $C_{M_{\delta\ \text{elev.}}}$ RAD.$^{-1}$ | $C_{M_{\delta\ e\ \text{aux}}}$ RAD.$^{-1}$ | $C_{M_{\delta\ TIP}}$ RAD.$^{-1}$ |
|---|---|---|---|---|---|---|---|---|---|
| | .135 | .060 | .189 | -.0258 | -.08 | -.255 | -.0361 | -.0160 | -.0504 |
| | .0266 | - | .0266 | -.105 | 0 | -.38 | -.0189 | - | -.0189 |
| | .0108 | - | .0175 | -.0447 | 0 | -.236 | -.00510 | - | -.00963 |
| | .0135 | - | .0220 | -.0619 | 0 | -.238 | -.00596 | - | -.0113 |
| | .0453 | - | .0453 | -.147 | 0 | -.390 | -.0261 | - | -.0261 |
| | .087 | - | .0702 | -.0636 | 0 | -.33 | -.0281 | - | -.0264 |
| | .132 | .0625 | .156 | -.0430 | -.10 | -.33 | -.0363 | -.0172 | -.0430 |
| | .152 | .0693 | .152 | -.0573 | 0 | -.26 | -.0458 | -.0210 | -.0458 |

| | $C_{n_{\delta\ TIP}}$ RAD.$^{-1}$ | $C_{Y_\beta}$ RAD.$^{-1}$ | $C_{Y_P}$ RAD.$^{-1}$ | $C_{Y_r}$ RAD.$^{-1}$ | $C_{Y_{\delta_W}}$ RAD.$^{-1}$ | $C_{Y_{\delta_R}}$ RAD.$^{-1}$ | $C_{Y_{\delta_{SP}}}$ RAD.$^{-1}$ | | |
|---|---|---|---|---|---|---|---|---|---|
| | - | -.201 | .202 | .009 | -.00007 | .115 | -.00011 | | |
| 29 | -.00860 | -.350 | .435 | .153 | -.00007 | .0315 | -.00011 | | |
| 39 | -.00430 | -.275 | .189 | .0773 | -.00010 | .0120 | -.00017 | | |
| 30 | -.00493 | -.287 | .190 | .0825 | -.00010 | .0149 | -.00017 | | |
| 29 | -.0101 | -.355 | .435 | .151 | -.00007 | .0544 | -.00011 | | |
| 13 | -.00722 | -.327 | .147 | .051 | -.00029 | .0802 | -.00046 | | |
| 0 | - | -.229 | .177 | .054 | -.00007 | .120 | -.00011 | | |
| C2 | -.00298 | -.344 | .0938 | .0737 | -.0021 | .115 | -.00355 | | |

C

*Table 4–C. Dynamic Parameters*

| FLIGHT CONDITION | DUTCH ROLL | | | | | SPIRAL |
|---|---|---|---|---|---|---|
| | $\zeta_d$ | $T_{1/2}$ | $f_{n_d}$ | $\frac{\lvert\phi\rvert}{\lvert\beta\rvert}$ | $\frac{\omega_\phi}{\omega_d}$ | $T_{1/2}$ ($T_2$) |
| I | .154 | 7.46 | .096 | 2.56 | .691 | (86.4) |
| II | .0638 | 8.29 | .209 | 4.26 | .658 | 30.8 |
| III | .0905 | 6.81 | .179 | 7.26 | .541 | 26.3 |
| IV | .0995 | 5.97 | .186 | 7.14 | .481 | 27.0 |
| V | .0742 | 7.26 | .205 | 4.78 | .591 | 40.1 |
| VI | .0946 | 6.89 | .169 | 3.05 | .903 | (38.7) |
| VII | .131 | 8.99 | .0940 | 2.32 | .646 | 31.9 |
| VIII | .265 | 2.46 | .169 | 3.92 | .589 | 36.1 |

| FLIGHT CONDITION | SHORT PERIOD | | PHUGOID | |
|---|---|---|---|---|
| | $f_{n_{s.p.}}$ | $\zeta_{s.p.}$ | $P_d$ | $\zeta_p$ |
| I | .0743 | .880 | 67.8 | .0738 |
| II | .179 | .270 | 166.6 | .0836 |
| III | .162 | .167 | 375.5 | .0875 |
| IV | .163 | .143 | 355.1 | .0869 |
| V | .170 | .231 | 164.7 | .0854 |
| VI | .136 | .421 | 128.9 | .0302 |
| VII | .091 | .950 | 58.4 | .107 |
| VIII | .115 | .715 | 64.8 | .0975 |

## 4.4 CROSS-COUPLING CHARACTERISTICS

The lateral control system is described in Sec. 5. The tip elevons, employed as the primary roll control surfaces at large wing sweep angles, exhibit adverse yaw characteristics. Figure 4-91 illustrates the $C_n/C_l$ ratio of the tip elevon at Mach 2.7. The addition of the spoiler improves the control system yaw characteristics by providing additional rolling moment as well as favorable yawing moment. At moderate to low angles of attack the improvement is significant. The further addition of 4 degrees of rudder (rudder-elevon interconnect) provides a $C_n/C_l$ ratio of approximately zero for the Mach 2.7 cruise condition. The $C_n/C_l$ ratio is essentially constant with wheel deflection. Modifications to the control system such as an unswept spoiler on the wing or additional rudder interconnect will improve the $C_n/C_l$ variation with angle of attack.

The lateral control for low speed, flaps-down flight consists of ailerons and spoilers. Fig. 4-91

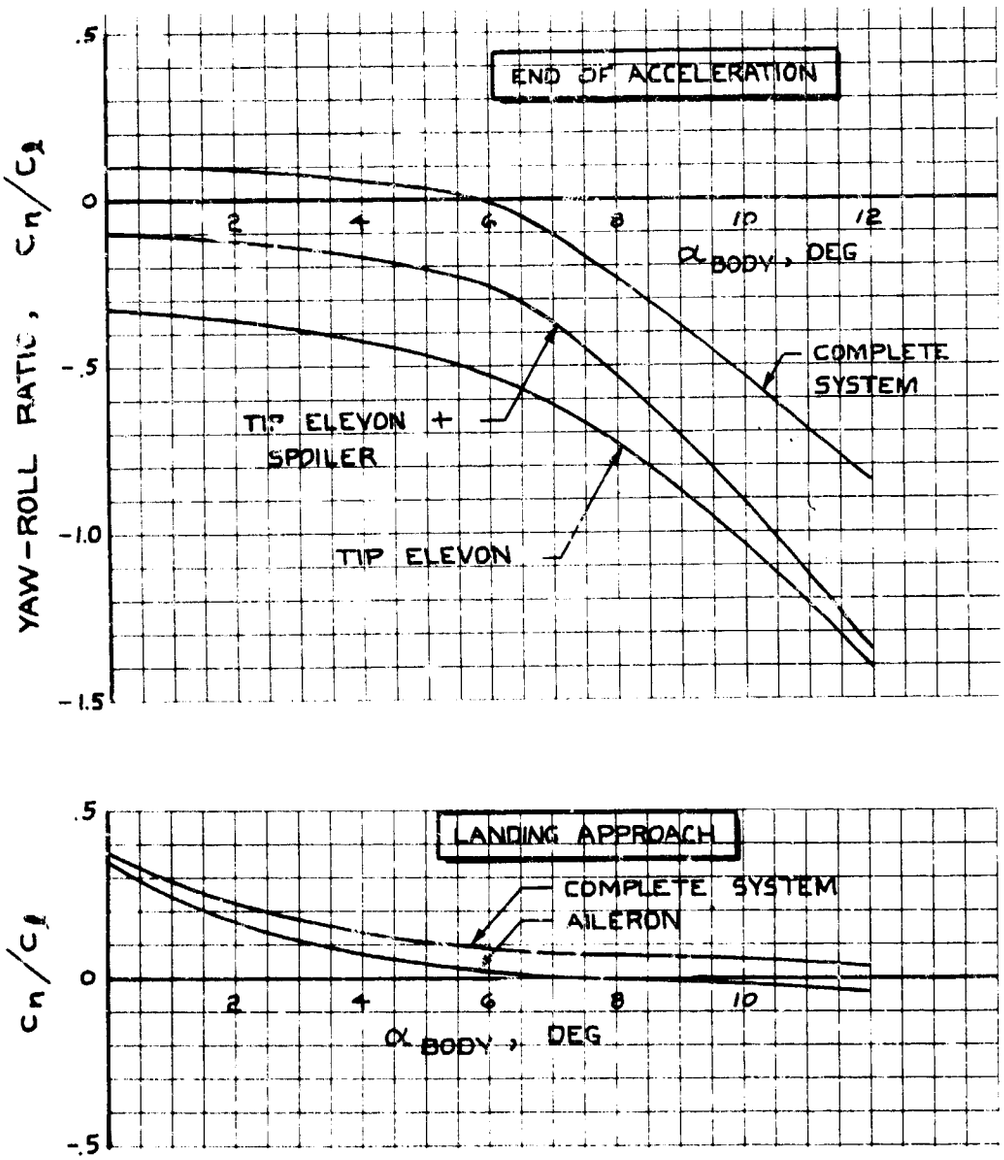


*Figure 4-91. Yaw Due to Lateral Control*

shows a favorable $C_n/C_l$ ratio for a wide range of angle of attack. The data shown correspond to full wheel deflection; as at cruise, $C_n/C_l$ is essentially invariant with wheel deflection.

The roll-yaw parameter, $\omega_\phi/\omega_d$, is shown for maximum lateral control at the eight representative flight conditions in Fig. 4-92. The characteristics illustrated are considered satisfactory but not optimum at all flight conditions. Further studies will be directed toward improving the basic roll-yaw coupling.

## 4.5 EMERGENCY OPERATIONS

A high level of reliability is provided in critical airplane systems through design concepts and redundancy. The flight control system will provide a margin of controllability to ensure safe operation in the event of system failures that affect airplane handling characteristics. These include single or multiple engine or inlet failures, flight control and trim system failures, stability augmentation failures, fuel system failures, and failures of the wing sweep system.

### 4.5.1 Engine Failure on Takeoff

Sufficient rudder control has been provided to ensure a safe margin between the minimum control speed, $V_{MC}$, and takeoff rotation speed. Rudder control for safe $V_{MC}$ speed is the critical design point for sizing the rudder surface area, and as such it is discussed in Par. 4.1.5.

### 4.5.2 Steady State Engine Failures, Enroute

The rudder deflection range has been selected to provide complete trim of the asymmetric yawing moment associated with the failure of two engines on one side (engine windmilling, inlets started, bypass doors open). Figure 4-93 shows the capability of the rudder to trim the airplane in these conditions throughout the normal flight envelope.

### 4.5.3 Abrupt Engine Inlet Failures, Supersonic Speeds

The severity of the engine inlet failure problem at supersonic speeds is governed by several factors: the level of asymmetric thrust, the aerodynamic forces and moments generated by shock expulsion in supersonic flight, and the

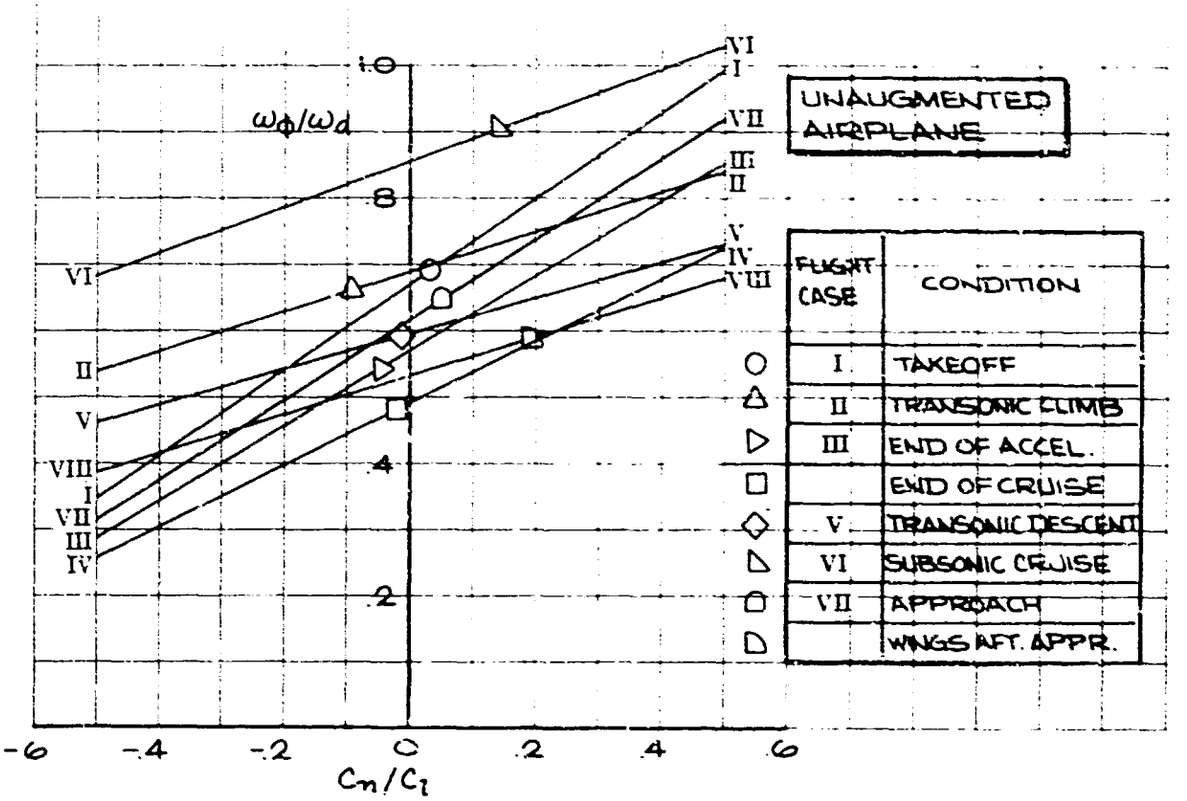


*Figure 4-92 Roll – Yaw Coupling Parameter, Eight Flight Conditions*

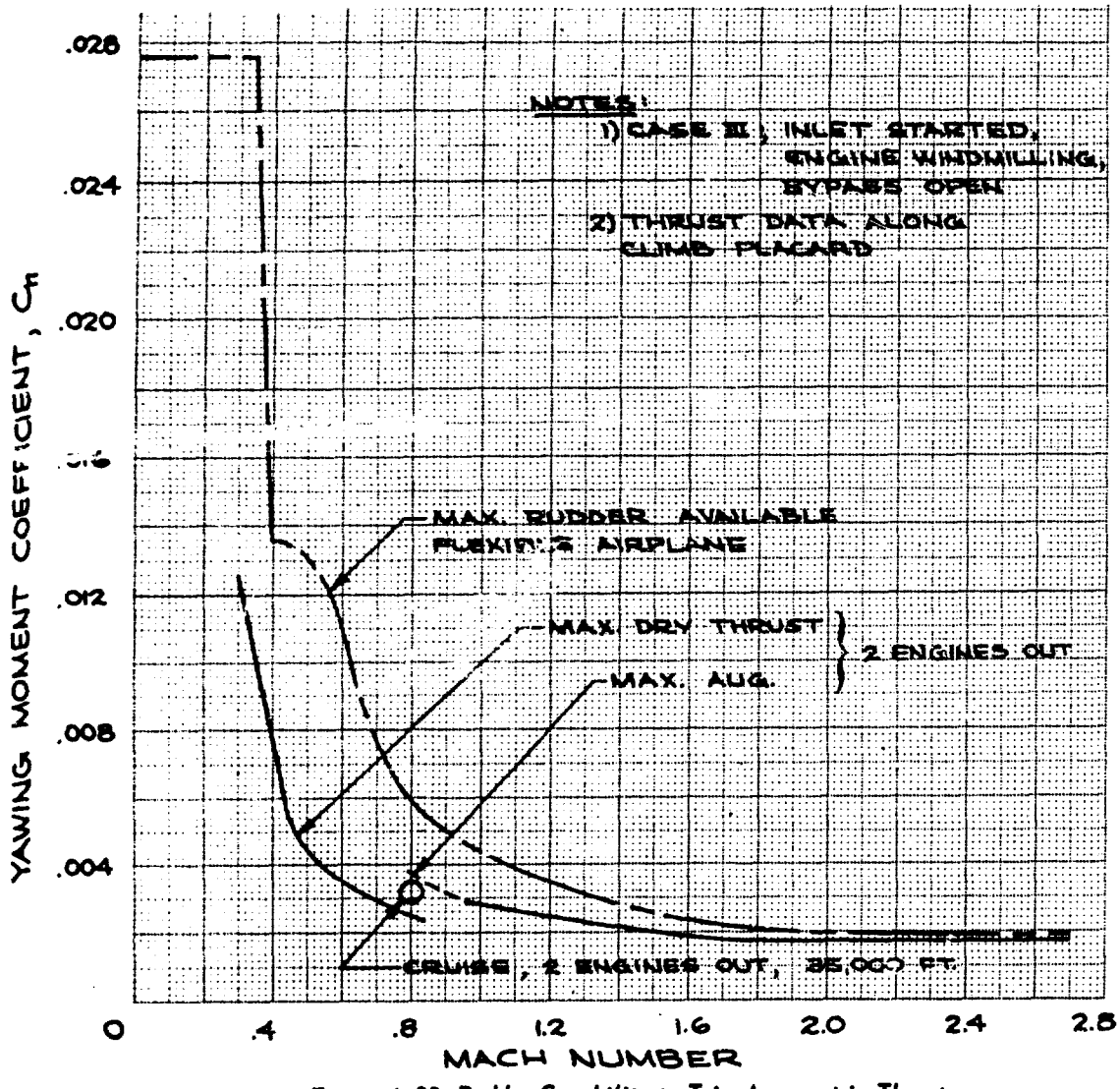


*Figure 4-93. Rudder Capability to Trim Asymmetric Thrust*

lateral control capabilities and cross-coupling characteristics.

The aerodynamic forces and moments associated with partial or complete engine/inlet failure were measured in the Boeing supersonic wind tunnel at the critical Mach 2.7 condition and at Mach 2.0. Additional testing is scheduled at other flight conditions.

Aerodynamic data from wind tunnel tests are shown in Fig. 4-94 for 2.7 Mach number. The data have been adjusted to include the effects of recent inlet changes. Four cases are presented:

a. Case I, inlet unstarted and buzzing

b. Case II, inlet started, bypass open, engine running.

c. Case III, inlet started, bypass open, engine windmilling.

d. Case IV, inlet unstarted, bypass open, engine rotor stopped.

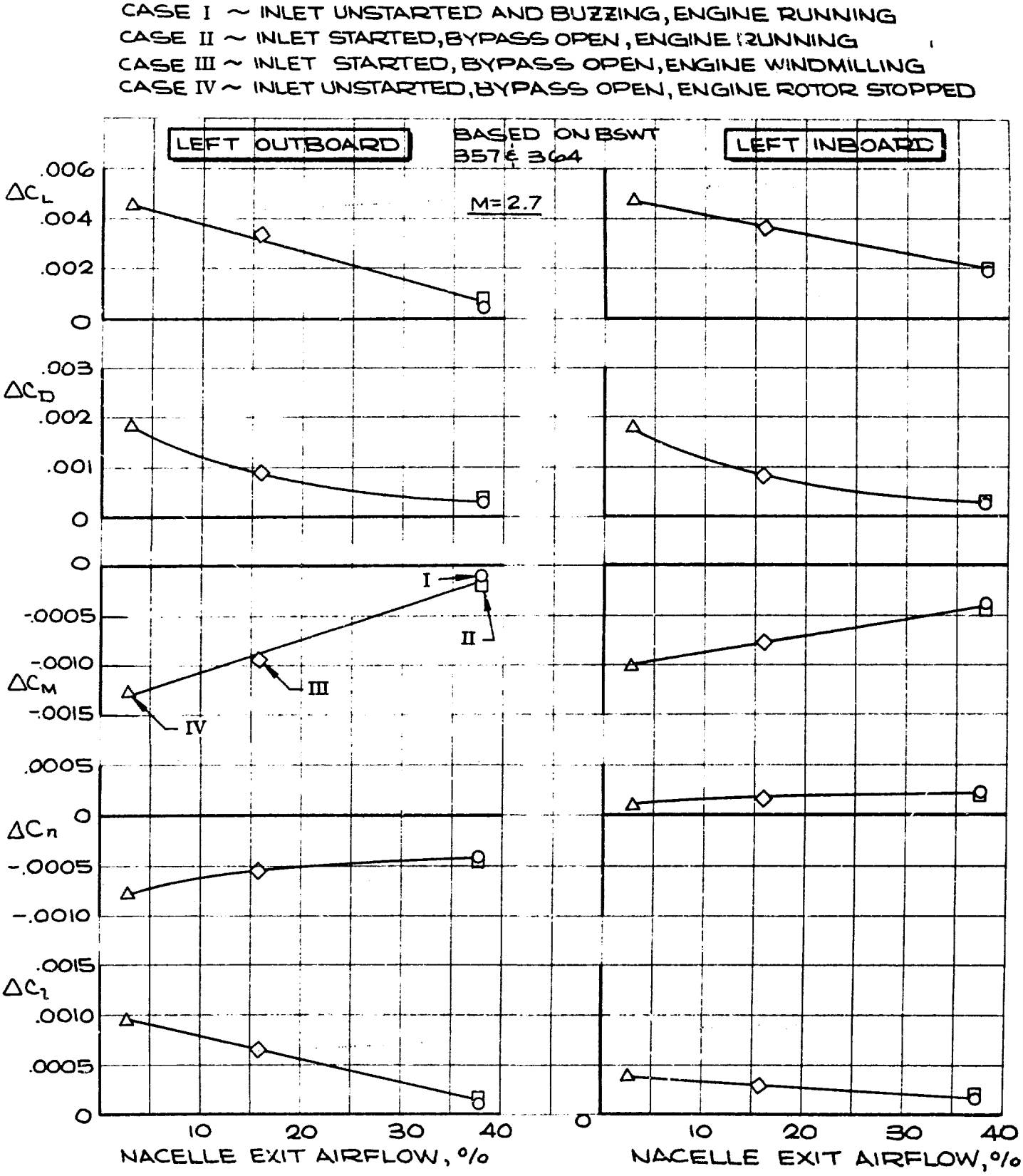


*Figure 4-94. Wind Tunnel Test Data, Propulsion Failure Effects*

4.5.3.1 Propulsion Failures
Four propulsion system failures were chosen for analysis of airplane handling problems following engine/inlet failure at Mach 2.7. These four failures are described as follows:

a. Failure A. Inlet unstart followed by automatic restart. This is a normal operational response of the inlet control to some excessive internal or external disturbance. Single and multiple failures were examined with the most extreme case being a simultaneous unstart of all four engines.

b. Failure B. Inlet unstart with no restart, followed by engine shutdown. A malfunction in the inlet control could cause an unstart which, if the pilot could not obtain a manual restart, would result in engine shutdown to windmill 10 sec after unstart.

c. Failure C. Engine shutdown. This condition represents an engine malfunction with the inlet remaining started.

d. Failure D. Engine failure followed by the rotor stopping and inlet unstart. This is the most extreme failure case in which a massive mechanical failure causes almost complete blocking of engine airflow and the inlet is forced into an unstarted condition. Both single and multiple failures were examined for this case.

The most critical failure conditions are those resulting in asymmetric thrust and drag forces acting to yaw the airplane. Single and double engine failures on one side produce strong yawing moments toward the failed engine. The resulting sideslip induces rolling moments toward the failed engine due to the large dihedral effect of the highly swept wing. The pilot is sensitive to bank angle change and will apply lateral wheel control in the proper direction to level the wings. If the lateral control provides strong rolling moment and very little cross-coupling in yaw, the airplane is readily brought under control. The B-2707 lateral control system with rudder interconnect is being designed to provide the desired roll response characteristics to ensure safe operation for the most extreme engine/inlet failure conditions.

Fixed base simulator testing was conducted to examine both the uncontrolled and the piloted transient response of the airplane to propulsion system failure. The responses of the augmented airplane to each of the failures are shown in Fig. 4-95, for cases where no corrective control is applied. For the most severe case (Failure D) the bank angle reaches 20 degrees in 12.3 sec following the complete failure of the outboard engine.

Simulated engine failures with the pilot applying corrective control are shown in Fig. 4-96. These were single outboard engine failures with stability augmentation operative. In each case, the pilot easily controlled the airplane disturbance with the lateral control; no rudder pedal inputs or thrust retarding on opposite engines was required.

Simulator tests showed difficulty in handling the Dutch roll oscillations created by engine failure disturbance. Directional stability was increased by the addition of increased ventral surface area (folding ventral fin) as discussed in Par. 4.2.2. Simulator testing of the most severe engine failure cases showed that this increase in directional stability enabled the pilot to control the airplane satisfactorily without the aid of the SAS. As shown in Fig. 4-97 for the worst double engine failure case, the pilot was able to control the bank angle to within ±8 degrees and sideslip to ±1 degree.

Engine/inlet failure studies are continuing with wind tunnel testing, computer studies, and flight simulator tests. The Boeing criterion for satisfactory airplane handling in these emergencies is that the pilot must be able to control the most severe cases with lateral control only, with or without the assistance of the stability augmentation system.

4.5.4 Wing Sweep Failure
The inability to sweep the wings forward for landing is an extremely remote possibility. In this case the ability to correct for crosswinds during landing is limited by the large dihedral effect and low roll control power. Figure 4-98 summarizes the roll performance available for a crosswind landing with the wings fully swept. With 4 degrees of crab on the landing gear, the maximum tolerable 90-degree crosswind velocity is 21 kn at tower height. The roll performance in this condition is based on attaining 4 degrees bank angle in 1 sec. The wind shear correction for tower height is shown in Fig. 4-99.

4.5.5 Control System Failures

4.5.5.1 Longitudinal Control
The ability to maneuver the airplane with single

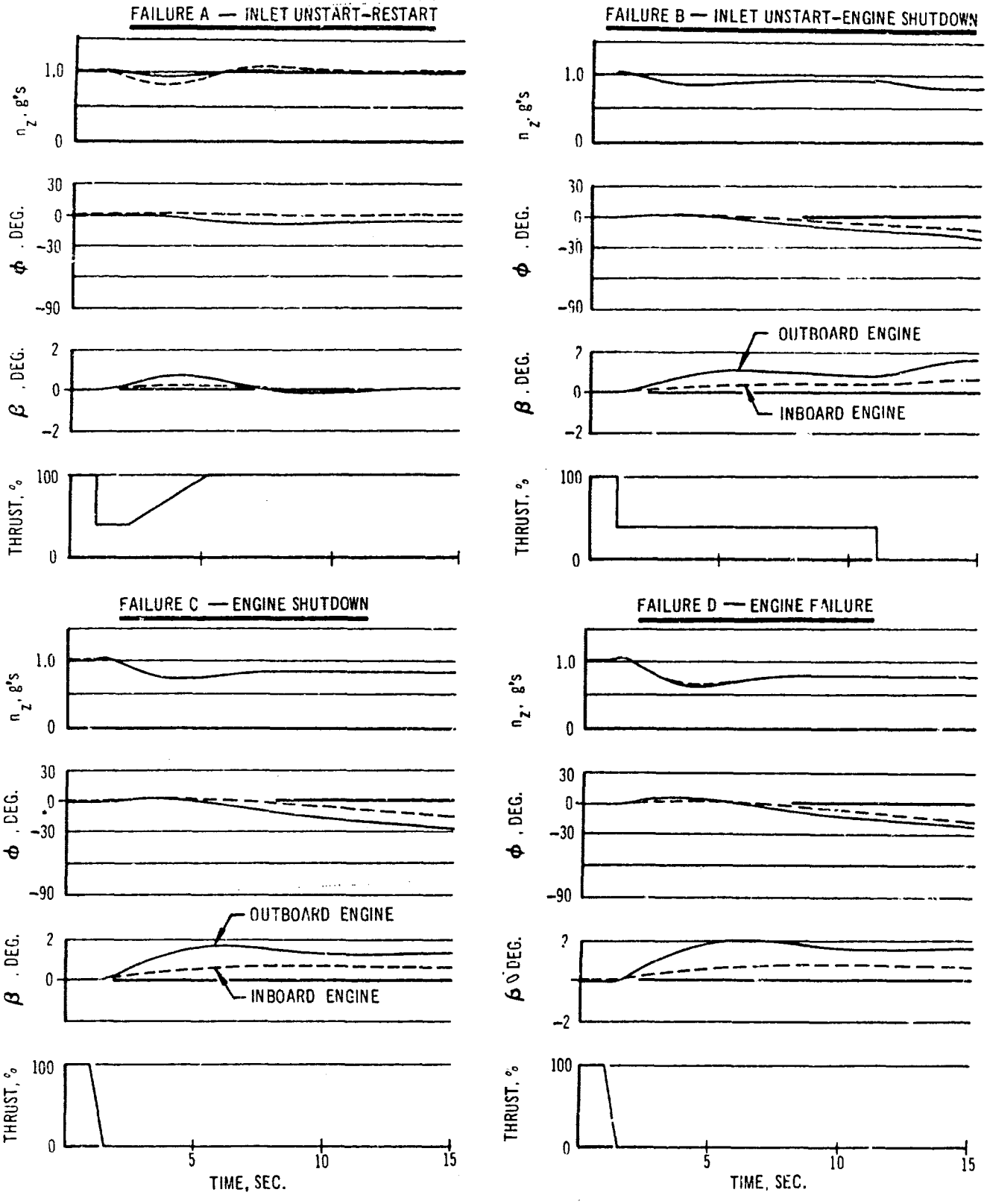


*Figure 4–95. Response to Single Propulsion Failure, No Pilot Correction, Augmented*

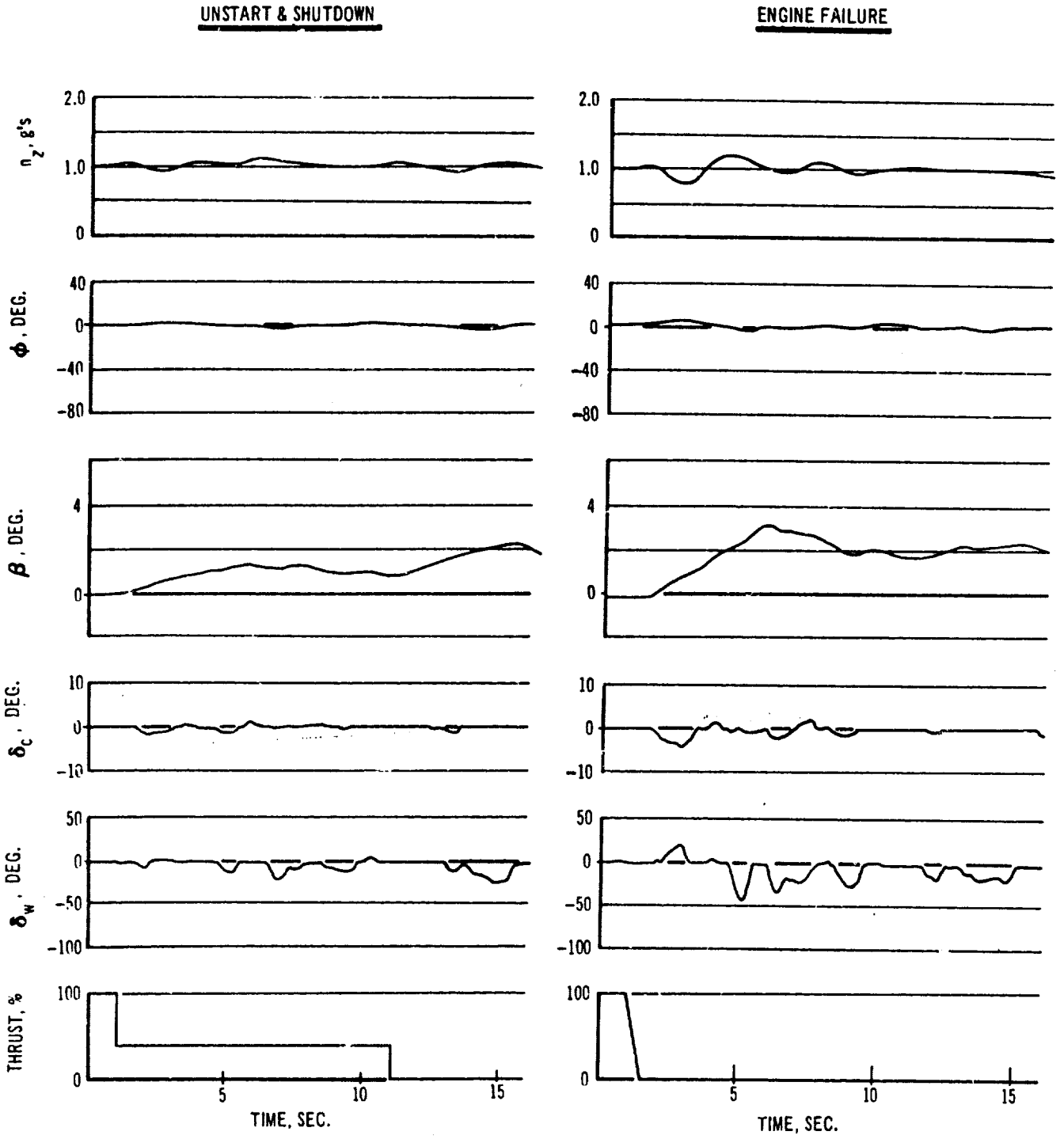


*Figure 4-96. Single Propulsion Failure, With Pilot Corrective Action*

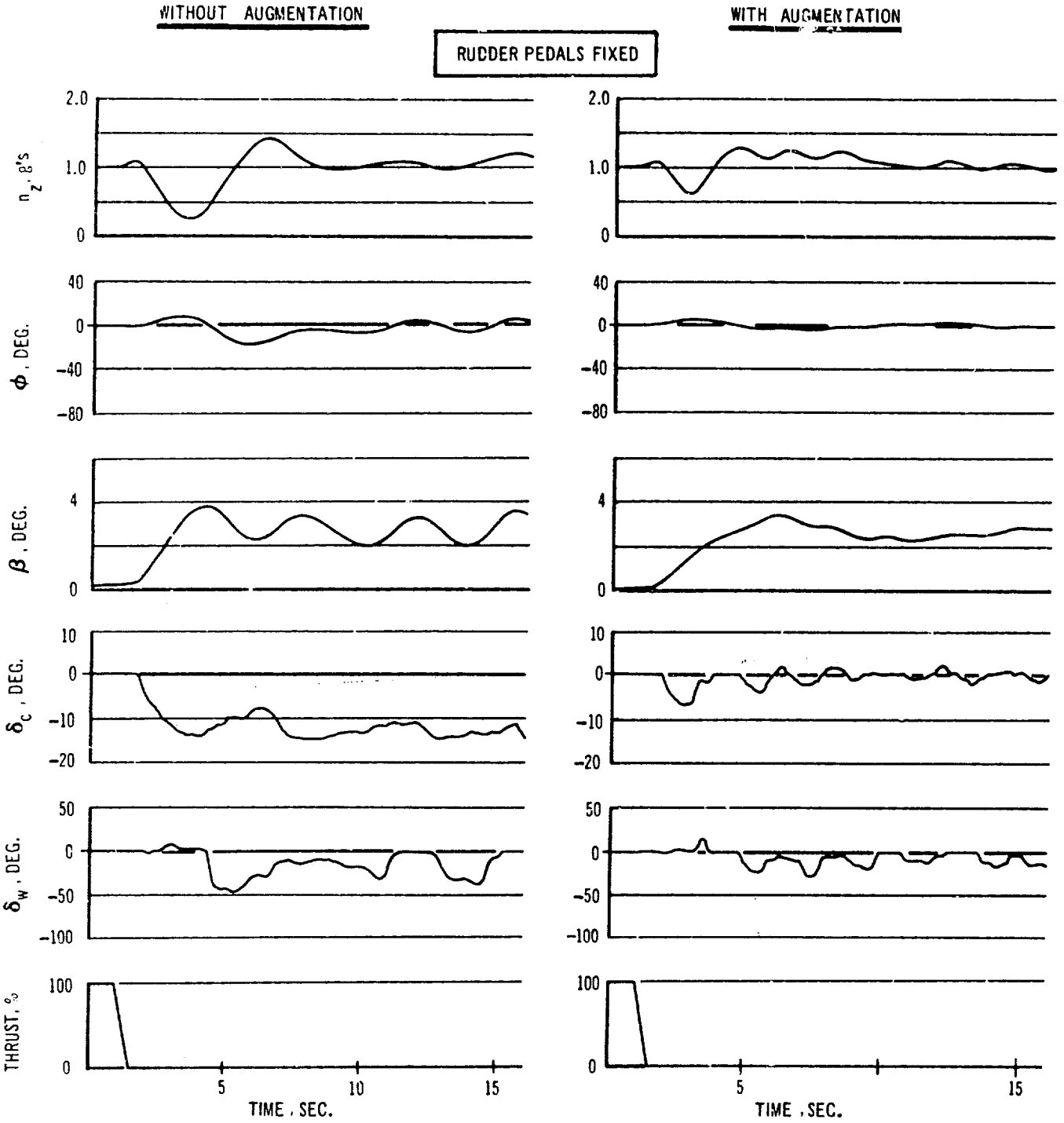


*Figure 4-97. Double Engine Failure, With Pilot Corrective Action, Improved Directional Stability*

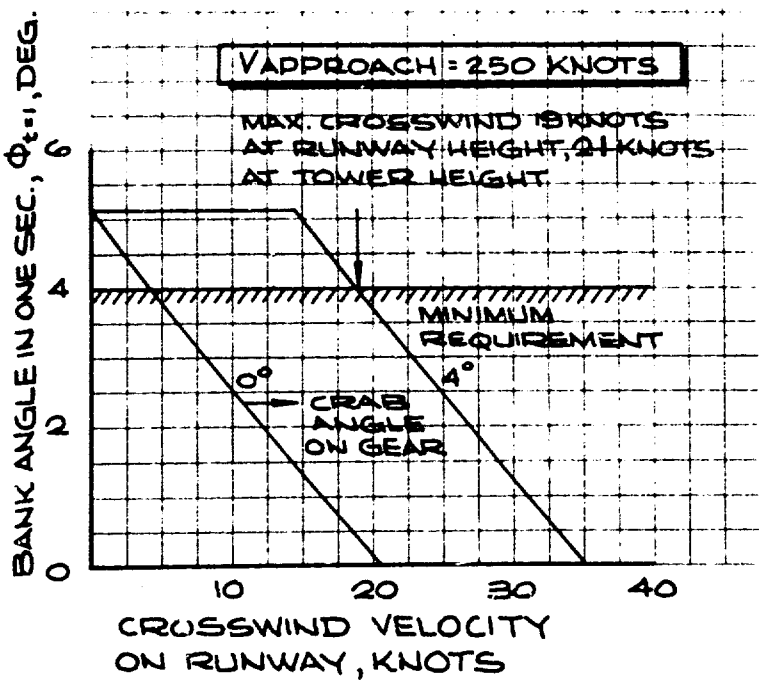


*Figure 4-98. Roll Performance, Wings Aft Landing*

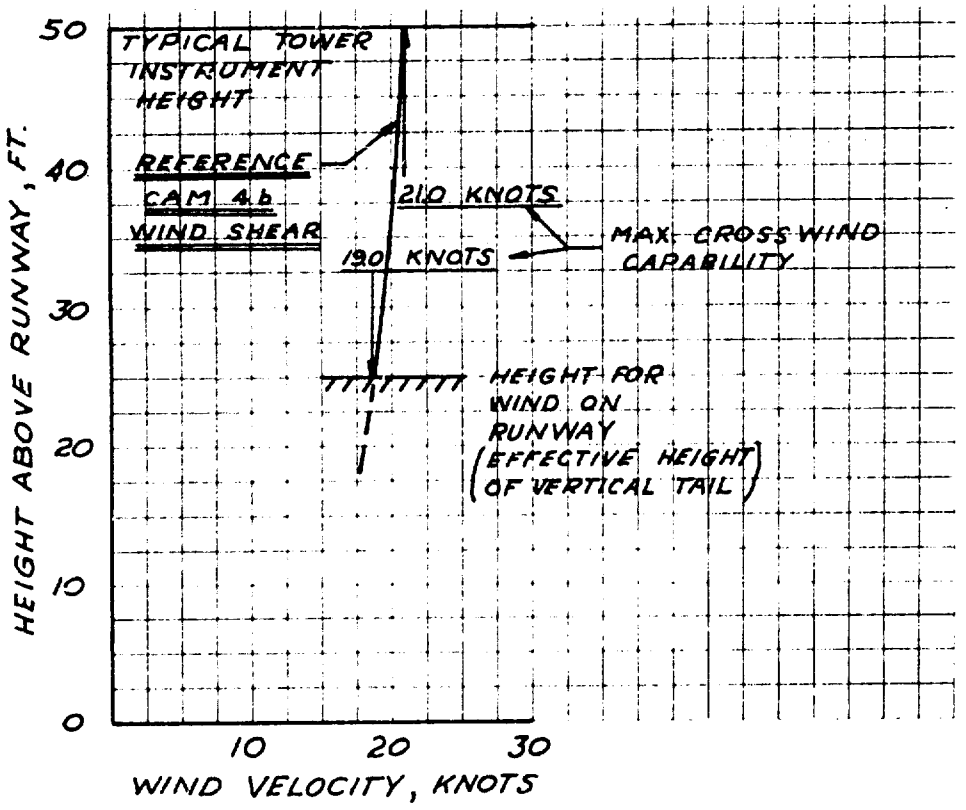


*Figure 4-99. Wind Shear Effect*

and dual hydraulic system failures is shown in Figs. 4-100 and 4-101. Adequate maneuver capability is seen to exist for all conditions except operations with forward cg's at supersonic Mach numbers. The existing hydraulic control power partially limits elevator travel with all hydraulic systems operating, and severely limits surface deflection with one or two systems failed (Sec. 5.0). Thus, maneuver capability becomes marginal at extreme forward cg's with system failures. Improved maneuver capabilities will be developed to provide a substantial margin of safety for operating with failed hydraulic systems. The design goal is to provide the ability to continue supersonic cruise following a single system failure, with the assurance that a safe deceleration and descent can be made following a subsequent, second, hydraulic system failure. It is considered that adequate maneuver capability will be provided with the ability to develop 1.5 g normal acceleration at $V_D$ with only one hydraulic system operative while at the most critical center of gravity loading.

4.5.5.2 Lateral Control

Lateral control performance under single and double hydraulic system failure is summarized in Fig. 4-102, which shows steady state roll rate and bank angle in 1 sec capabilities for coordinated single degree of freedom rolls. The selected roll performance requirements for emergency conditions are shown compared with the roll performance provided for the failure conditions for eight flight conditions. Adequate roll control is provided in all cases for either two systems operating or one system operating.

4.5.5.3 Directional Control

No limitation in available rudder deflection occurs up to Mach 0.85 with either single or double system failure (Fig. 4-103). At higher speeds the available rudder deflection is limited by reduced hydraulic power following system failure. However, sufficient directional control capability remains to trim sideslip to zero with one hydraulic system failed and an outboard engine inoperative with maximum thrust on the other engines. With two engines failed and maximum thrust on the remaining engines, a small residual sideslip (less than 1 degree) remains with full available rudder trim for either two hydraulic systems failed or one system failed. Directional control capabilities for these emergency operations are considered satisfactory.

4.5.5.4 Trim Systems

The parallel trim system design precludes runaway trim about any control axis, Systems Report, Part B, V2-B2707-11. Even if failures of this nature could occur, pilots control forces are such that the runaway trim could be overpowered.

4.5.5.5 Fuel System Failure

The fuel system is described in Propulsion Report Part B, V2-B2707-13. Unbalance of the airplane due to fuel system failures is an extremely remote possibility because of the fuel transfer system redundancy. Fuel transfer is not employed to maintain the airplane within stability limits in any case, but only to ensure minimum trim drag.

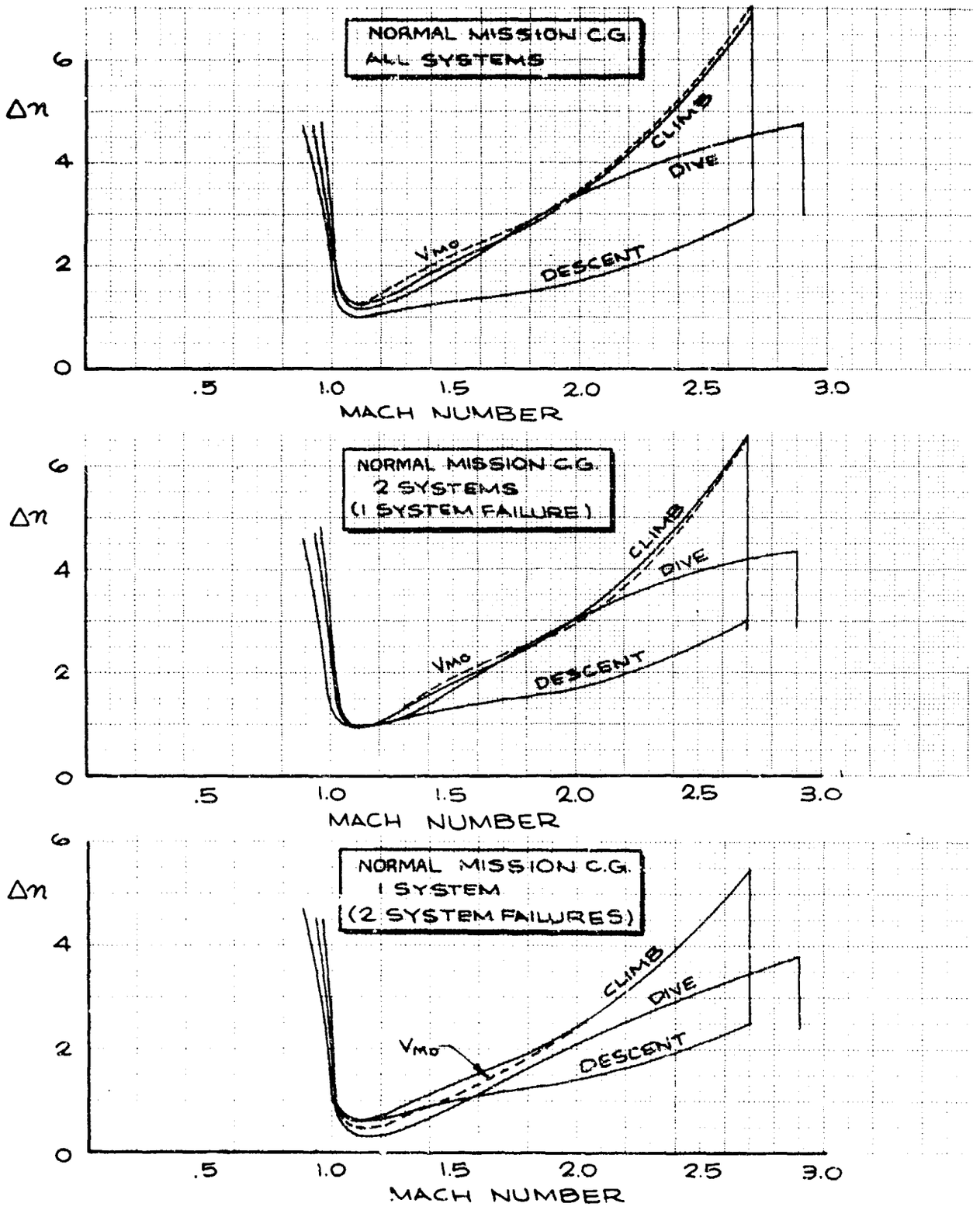


*Figure 4–100. Maneuver Capability With Control System Failures, Normal Mission C.G.*

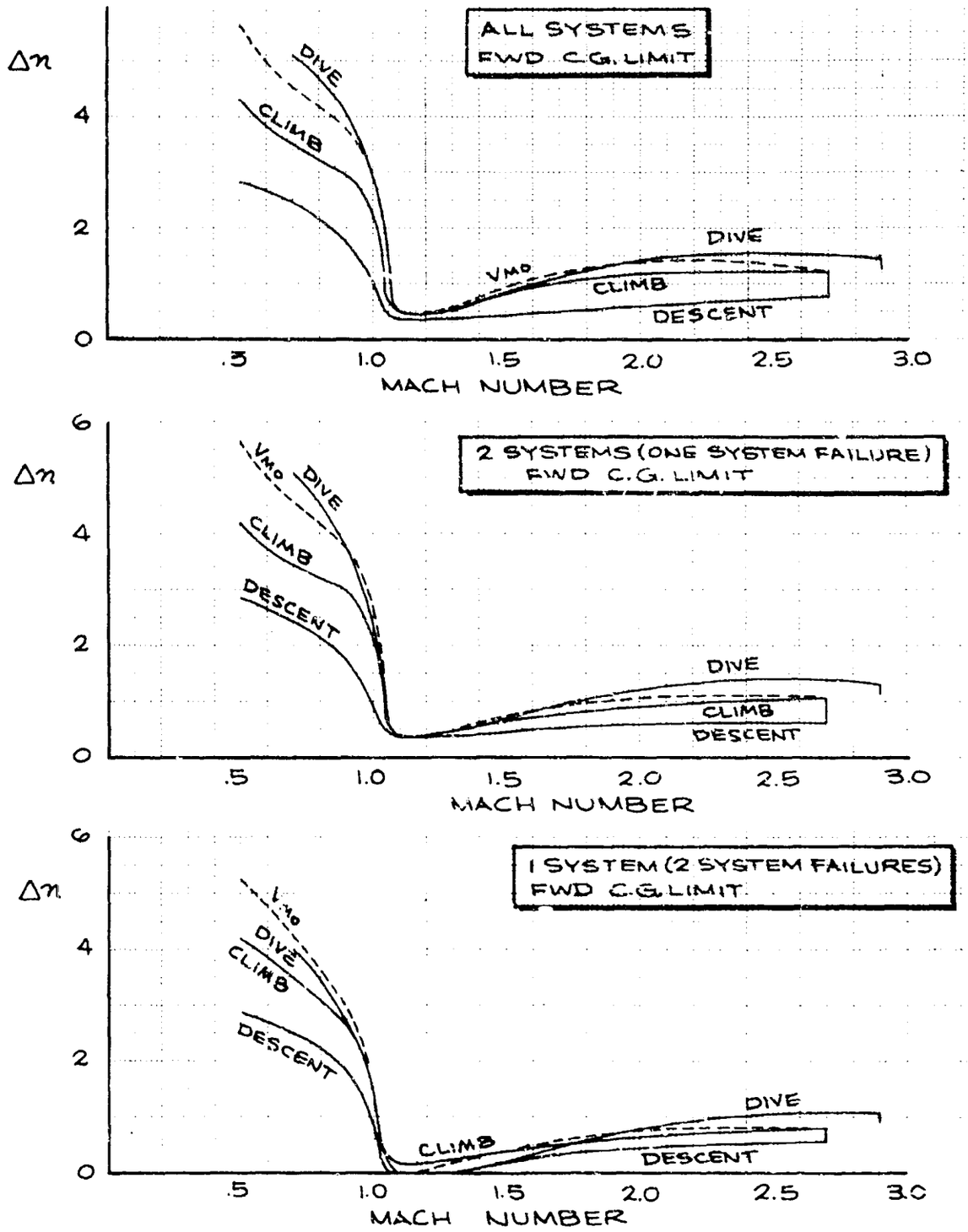


*Figure 4–101. Maneuver Capability With Control System Failures, Forward C.G. Limit*

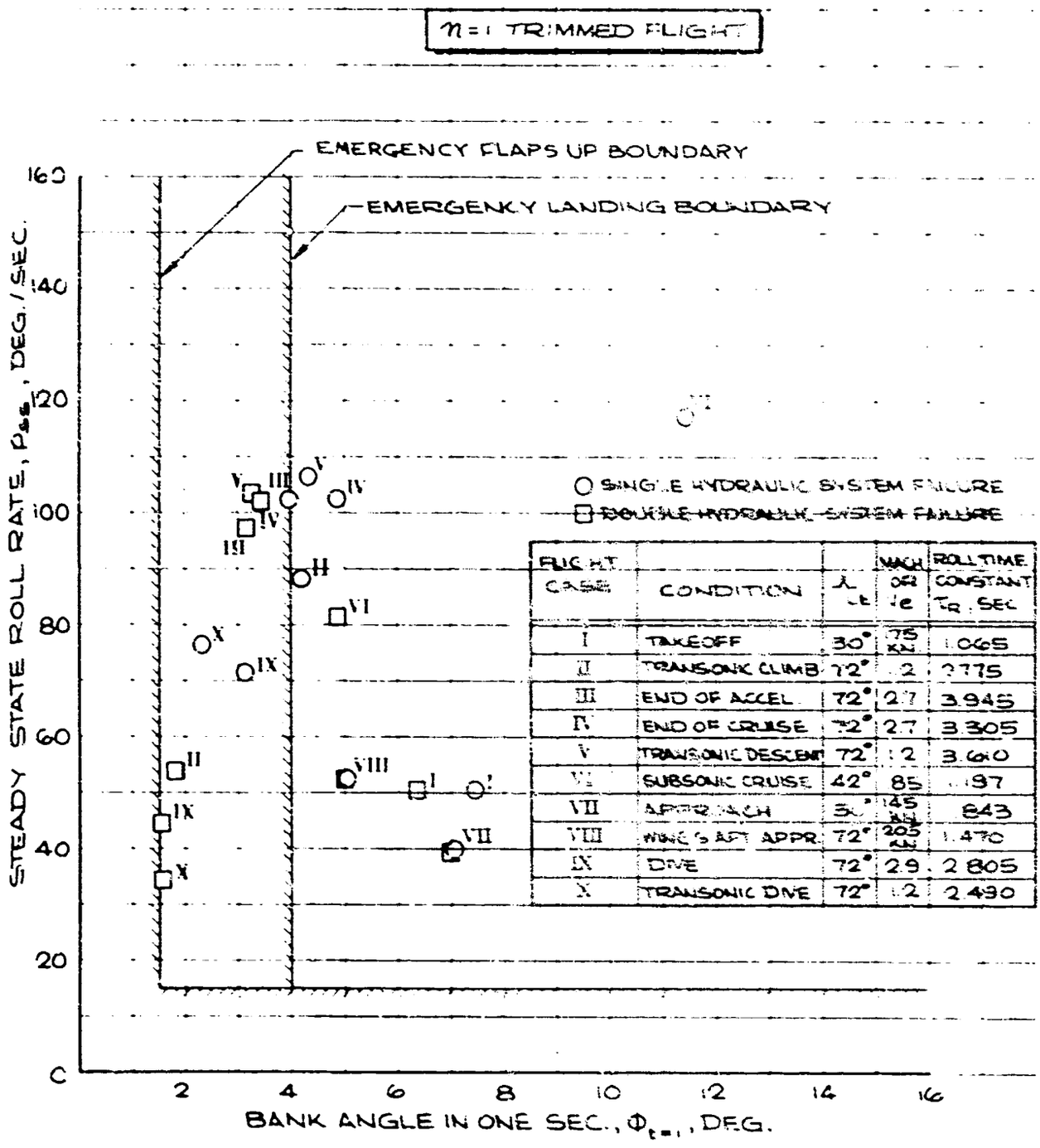


| FLIG HT CASE | CONDITION | $\lambda_{ct}$ | MACH OR $V_e$ | ROLL TIME CONSTANT $\tau_R$, SEC |
|---|---|---|---|---|
| I | TAKEOFF | 30° | 175 KN | 1.065 |
| II | TRANSONIC CLIMB | 72° | .2 | 2775 |
| III | END OF ACCEL | 72° | 2.7 | 3.945 |
| IV | END OF CRUISE | 72° | 2.7 | 3.305 |
| V | TRANSONIC DESCENT | 72° | .2 | 3.610 |
| VI | SUBSONIC CRUISE | 42° | .85 | .97 |
| VII | APPROACH | 30° | 145 KN | 843 |
| VIII | WING'S AFT APPR. | 72° | 205 KN | 1.470 |
| IX | DIVE | 72° | 2.9 | 2.805 |
| X | TRANSONIC DIVE | 72° | .2 | 2.490 |

*Figure 4-102. Roll Performance with Control System Failures*

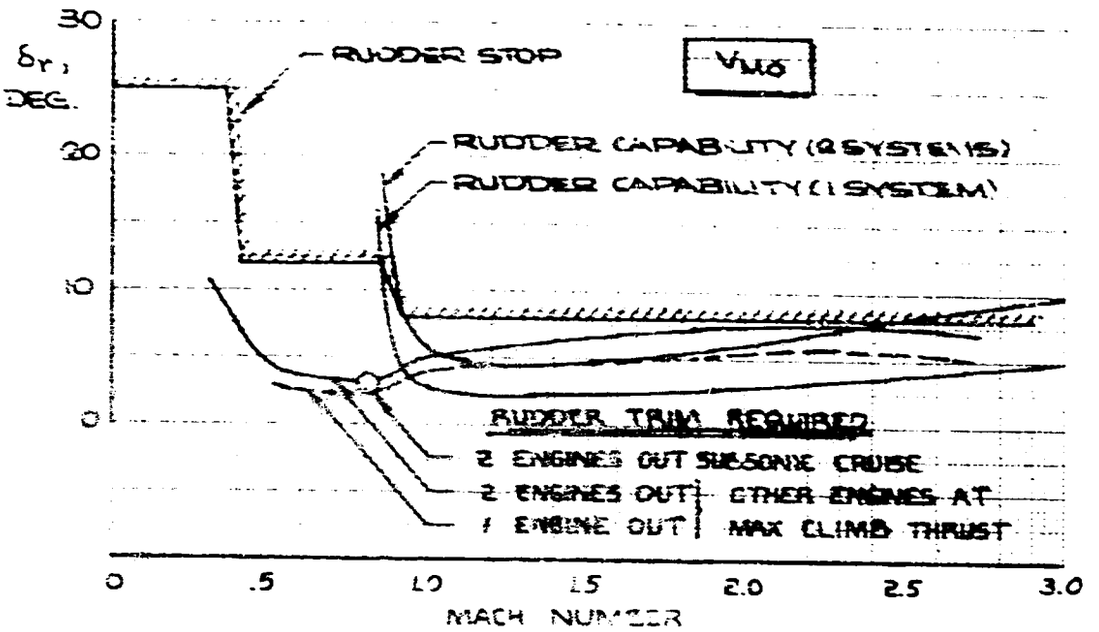


*Figure 4-103. Rudder Capability With Control System Failures*

## 5.0 FLIGHT CONTROLS AND STABILITY AUGMENTATION SYSTEM


| | | Page |
|---|---|---|
| 5.1 | PRIMARY FLIGHT CONTROL SYSTEM | 245 |
| 5.2 | SECONDARY FLIGHT CONTROL SYSTEM | 254 |
| 5.3 | STABILITY AUGMENTATION SYSTEM | 254 |

# 5.0 FLIGHT CONTROLS AND STABILITY AUGMENTATION SYSTEM

The basic features of the B-2707 flight controls subsystem are determined by the large size and variable geometry characteristics of the airplane and by the requirements for high safety and reliability. These requirements are met through the inclusion of such items as the electric command system, triplicated hydraulic actuation of the primary control surfaces, and multichannel SAS on all control axes. The functional characteristics and aerodynamic design requirements of the flight control system are described in this section. Systems Report, Part B (V2-B2707-11) provides a detailed description of the design features of the control systems. The control surfaces and their high speed and low speed functions are shown in Fig. 5-1.

## 5.1 PRIMARY FLIGHT CONTROL SYSTEM

Primary flight control is obtained from aerodynamic control surfaces driven by hydraulic power control packages in response to pilot inputs through conventional control columns and rudder pedals. The aerodynamic control surfaces consist of elevons, elevators, and auxiliary elevators for longitudinal control, ailerons and spoilers for low speed lateral control, elevons and spoilers for high speed lateral control, and a rudder for directional control. The normal mode of operation of the longitudinal and lateral axes employs an electric command system. If the electric command system becomes inoperative, a backup mechanical cable system will take over the control functions. Pilots' rudder input is transmitted to the rudder surface actuator by mechanical cables. Various hydraulic, electronic, and mechanical redundancy arrangements are used to achieve a fail-operational design.

### 5.1.1 Electric Command System, Pitch and Roll Axes

An electric command system is provided to compensate for the compliance, inertia, hysteresis, and friction associated with mechanical cable systems. The electric command is the normal control mode for the primary flight control longitudinal and lateral axes and is backed up by a mechanical cable system. Electric signals proportional to the force applied to the control column are produced by force transducers. After filtering and gain scheduling, these electric signals are fed to the hydraulic master servos. The master servos drive the surface actuators and also back drive the mechanical cable system which repositions the control columns. Triple redundant electric command channels in each axis ensure fail-operational capability upon the first failure and fail-passive upon the second failure. A control panel for the electric command system is located in the flight deck which allows separate axis and channel selection and engagement. Trimming is accomplished by electrically biasing the center point of the master servo and simultaneously biasing the center point of the mechanical feel and centering spring. The trim motor drives the trim screw which positions the mechanical feel spring center point. A position transducer provides an electrical input to the master servo, thus providing coordination between the electrical and mechanical system trim points.

### 5.1.2 Longitudinal Control System

The output action of the longitudinal master servo is mechanically transmitted to the actuator valves of the elevators, auxiliary elevators, and, through a mixer unit which combines longitudinal and lateral inputs, to the elevons. The auxiliary elevators are operative only when the flaps are in the takeoff or landing position. Longitudinal SAS signals from the SAS servo are combined mechanically with pilot inputs by a summing linkage.

### 5.1.3 Lateral Control System

The lateral master servo output is transmitted to the elevons through the mixer unit which combines the lateral and longitudinal inputs. The lateral master servo output also drives the actuators of the four inboard spoiler panels on each wing; when the wings are at sweep angles less than 60 degrees, it drives all spoiler panels. When the wing flaps are extended to takeoff or landing position, the ailerons are also driven by the lateral control system. Gearing of the lateral control surfaces as a function of wing sweep and flap position is shown in Fig. 5-2. The relative longitudinal and lateral control gearing of the elevons is shown in Fig. 5-3. The longitudinal input to the elevon always has priority over the lateral input; i.e. if a control position is commanded outside the boundary of Fig. 5-3, the longitudinal deflection commanded is produced and the lateral command uses the remaining surface deflection to the maximum of 30 degrees.

*Low Speed Configuration*

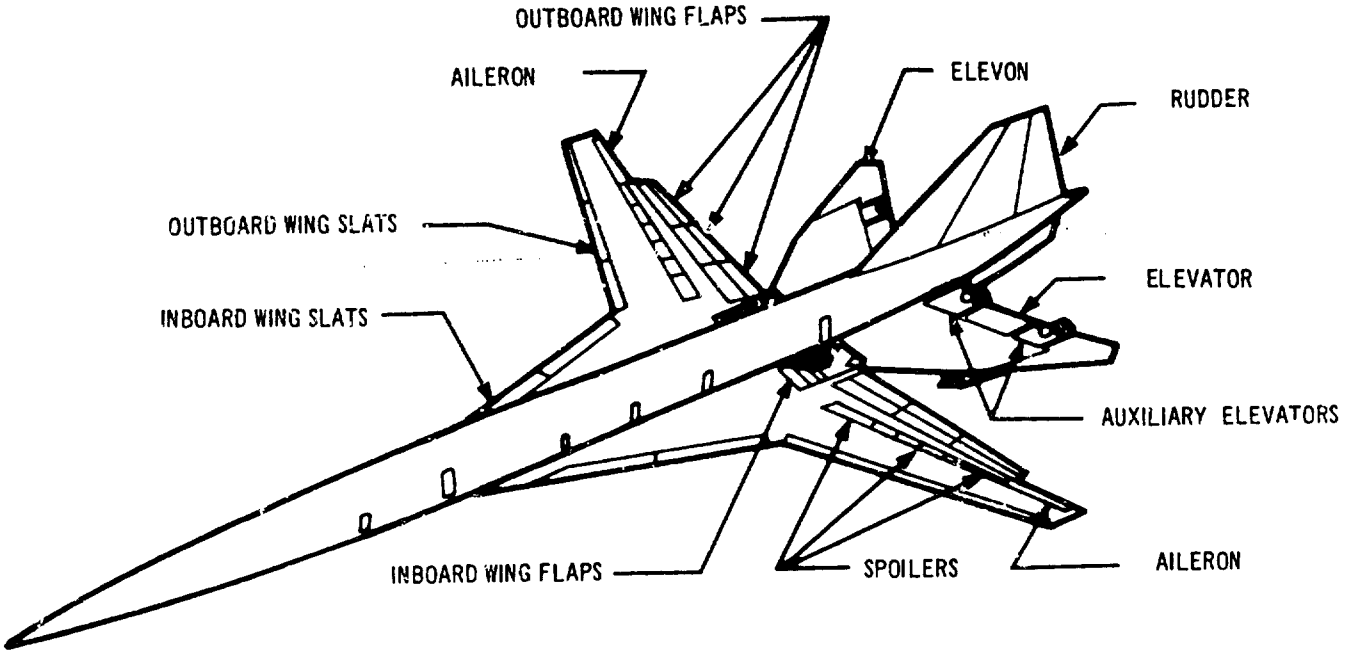


*Cruise Configuration*

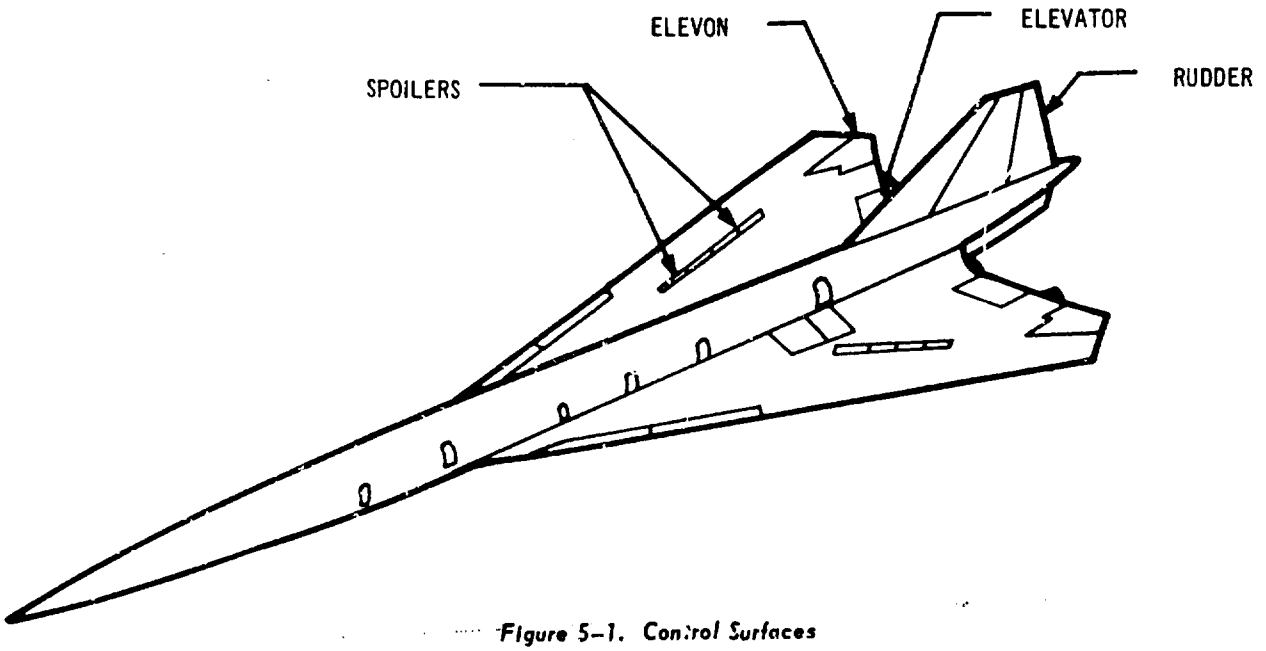


*Figure 5-1. Control Surfaces*

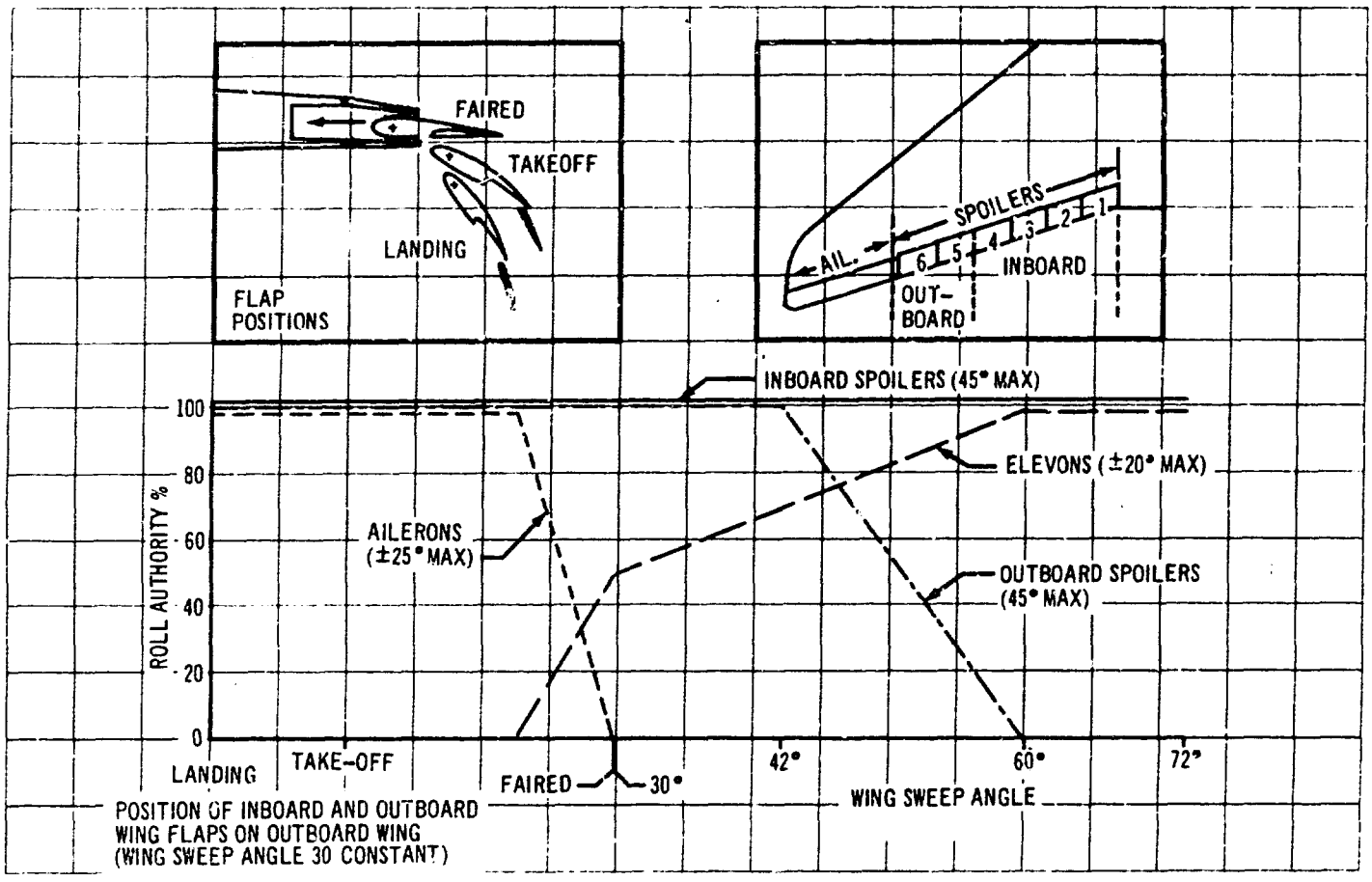


*Figure 5–2. Lateral Control Programming*

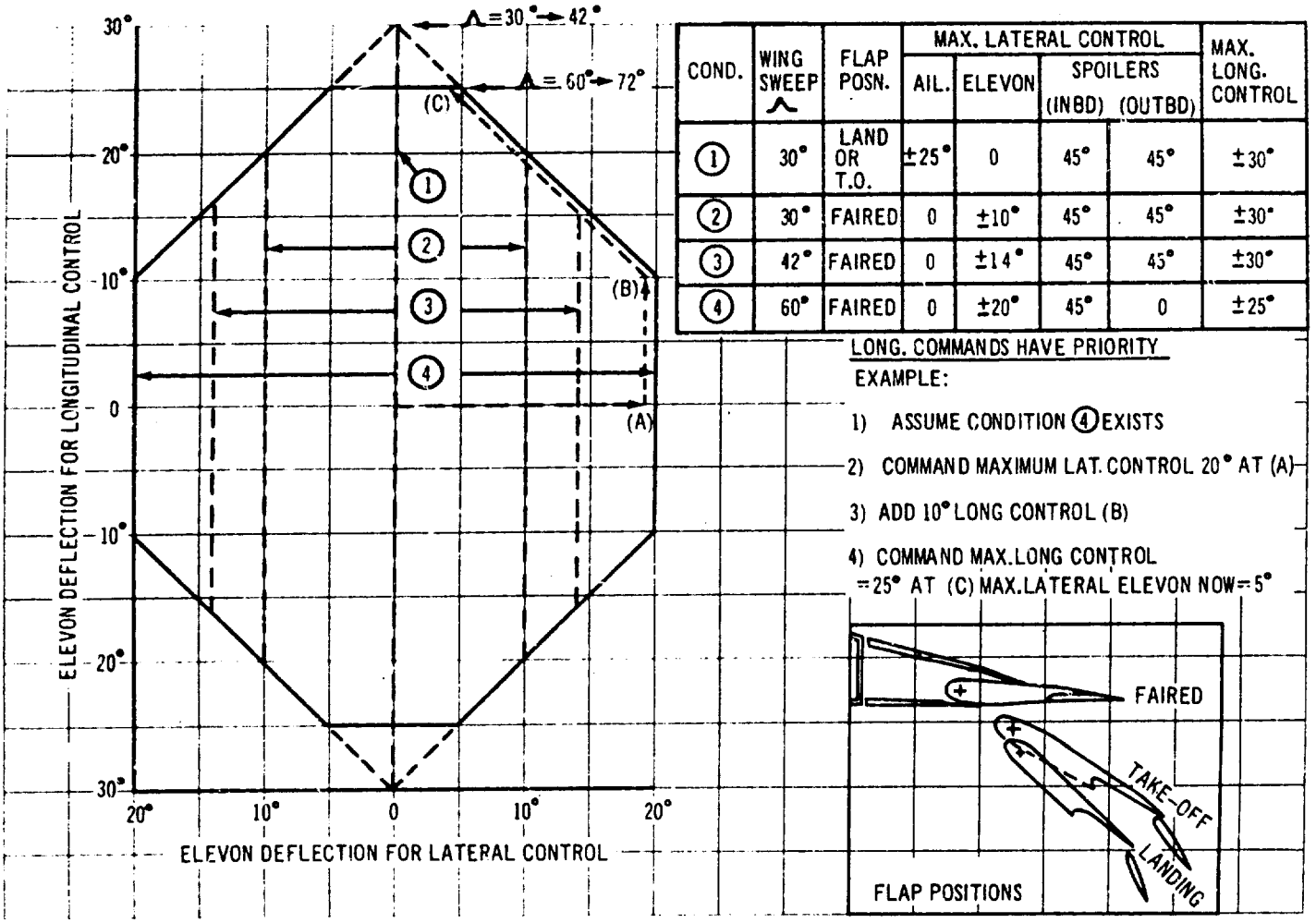


| COND. | WING SWEEP Λ | FLAP POSN. | MAX. LATERAL CONTROL | | | | MAX. LONG. CONTROL |
|---|---|---|---|---|---|---|---|
| | | | AIL. | ELEVON | SPOILERS (INBD) | SPOILERS (OUTBD) | |
| ① | 30° | LAND OR T.O. | ±25° | 0 | 45° | 45° | ±30° |
| ② | 30° | FAIRED | 0 | ±10° | 45° | 45° | ±30° |
| ③ | 42° | FAIRED | 0 | ±14° | 45° | 45° | ±30° |
| ④ | 60° | FAIRED | 0 | ±20° | 45° | 0 | ±25° |

LONG. COMMANDS HAVE PRIORITY

EXAMPLE:

1) ASSUME CONDITION ④ EXISTS

2) COMMAND MAXIMUM LAT. CONTROL 20° AT (A)

3) ADD 10° LONG CONTROL (B)

4) COMMAND MAX. LONG CONTROL =25° AT (C) MAX. LATERAL ELEVON NOW=5°




*Figure 5-3. Elevon Mix-Longitudinal / Lateral Control*

Lateral SAS servo signals are transmitted only to the elevon surfaces; thus the lateral SAS effectiveness is faded to zero when the flaps are extended and the lateral input to the elevons is zeroed. As described in Par. 5.1.1, trimming is accomplished by biasing the center point of the lateral master servo. The control output of the master servo to the spoilers has a trim cancelling input introduced to avoid deflecting the spoiler panels for trim.

5.1.4 Directional Control System

The directional control system is mechanically controlled and hydraulically powered. Commands to the rudder actuator package are received from flight deck controls, the stability augmentation system, and the lateral control system. Rudder trim is provided by moving the location of the centering point for the artificial feel spring. Rudder authority is limited by mechanical stops in the control linkage to the actuators which are introduced as a function of flap position and wing sweep. The stability augmentation system inputs and turn coordination commands from the lateral control system are added to the pilot control inputs in the mechanical mixer. SAS and turn coordination inputs do not produce flight deck control motion.

5.1.5 Control Surfaces

The primary control surfaces are shown in Fig. 5-1. Pitch control is obtained from the elevators, elevons, and, in takeoff and landing configuration, from the auxiliary elevators. Lateral control is produced by differential deflection of the elevons and by the eight inboard wing spoiler panels in the supersonic cruise configuration. As the wings are extended to the subsonic cruise position, the remaining wing spoilers become operative. When the wings are fully forward to the 30-degree sweep position and the high lift devices extended, the elevons revert to pitch control only and the ailerons are operated for additional low speed lateral control. Table 5-A tabulates the control surface deflections, rates, and actuation. The pitch and roll control surfaces have fixed deflection limits, unless otherwise limited by actuator hinge moment capability. To limit the maneuver loads, the rudder deflection is limited by mechanical stops in the actuator input linkage which are adjusted as a function of flap and wing sweep as shown in Fig. 5-4. The high speed deflection limit can be withdrawn by a pilot operated override for the emergency wings aft landing condition.

Control surface deflection rate requirements have been estimated from various dynamic analyses and simulation studies. Lateral control surface rates are determined by high speed roll response requirements, longitudinal surface rates by landing approach maneuver, and rudder rates by control of abrupt engine failure. The specified rates are conservative and further refinement will be made.

Control surface hinge moments have been estimated for all primary control surfaces to establish the actuation component sizing and power requirements. These hinge moment values are preliminary and further refinement and wind tunnel testing will be performed in Phase III to establish final design values. No aerelastic corrections have been applied to the hinge moment data presented herein; this is a conservative approach.

Elevator hinge moments shown in Fig. 5-5 are based on National Advisory Committee for Aeronautics data (Ref. 34) for the Mach No. range 0.75 to 1.96 and Boeing wind tunnel data (BSWT 357) at M = 1.5 and 2.7. The NACA data are for a 60-degree delta wing configuration with a mid-span elevator and the Boeing data for a configuration closely approximating the B-2707. The agreement between the two sets of data is good, shown in Fig. 5-5. For zero elevator deflections, the hinge moment is zero at an approximately 6-degree angle of attack for the B-2707 configuration at M = 1.5 and 2.7. This angle of attack for zero hinge moment has been assumed for all Mach numbers since angle of attack effects are relatively unimportant in determining the maximum surface hinge moments which occur in the M = 1.2 region. Hinge moments for the low speed auxiliary elevators are assumed to be similar to the elevator moments.

Data from several sources on tip control surfaces have been correlated to estimate the elevon hinge moments. These data are for a variety of hinge line locations and tip shapes, shown in Fig. 5-6. The correlating parameter used for these data was $S_{fl}/S_c$; the ratio of area forward of the hinge line to total control surface area. Zero hinge moment is assumed to occur at a 6-degree angle of attack and at zero deflection which is the case for the elevator. The effect of unporting the tip control from behind the wing at low deflections on the hinge moments is unkown at this time, but as is shown in

*Table 5-A. Primary Flight Controls, Travels, Rates, and Power*

| | | Longitudinal Control | | | Speed Brakes | Lateral Control | | | Directional Control |
|---|---|---|---|---|---|---|---|---|---|
| Wing Sweep | Flap | Primary Elevator | Aux Elevators | Elevons | Spoilers | Spoilers | Ailerons | Elevons | Rudder |
| 30° | T.O. or Landing | ±30° | 0 - 30° | ±30° | 0 - 45° (All Panels) | 0 - 45° (All Panels) | ±25° | 0 | ±25° |
| 30° | Faired | ±30° | 0 | ±30° | 0 - 45° (All Panels) | 0 - 45° (All Panels) | 0 | ±10° | ±12° |
| 42° | Faired | ±30° | 0 | ±30° | 0 - 45° (All Panels) | 0 - 45° (All Panels) | 0 | ±14° | ±12° |
| 72° | Faired | ±30° | 0 | ±25° | 0 - 45° (8 Inboard Panels) | 0 - 45° (8 Inboard Panels) | 0 | ±20° | ± 8° |
| Maximum Surface Rate (Deg/Sec) | 1.5 | 25 | 25 | 25 | 60 | 60 | 50 | 25 | 25 |
| [1] Max. Design Hinge Mom. (In. Lb.) | | 2,840,000 | 514,000 [2] | 3,200,000 | 980,000 [3] | 490,000 [4] | 340,000 | 3,200,000 | 1,250,000 |
| Control Surface Actuators — Total Number | | 18 [5] | 10 | 6 | 36 | 36 | 6 | 6 | 3 |
| Control Surface Actuators — Bore (In.) | | 4.33 | 3.14 | 7.225 | 2.5 | 2.5 | — | 7.225 | 6.88 |
| Control Surface Actuators — Stroke (In.) | | 6.25 | 3.1 | 18.0 | 5.42 | 5.42 | — | 18.0 | 11.0 |
| Flow/Hyd System (GPM, | | 108.0 | 17.6 | 115.2 | 110.4 | 55.2 | 27.0 | 115.2 | 50.5 |

[1] Stalling Hinge Moment with One Hydraulic System
[2] Total for Inboard & Outboard Auxiliary Elevators
[3] Total for 12 Spoilers
[4] Total for 6 Spoilers
[5] Each Actuator has Two Cylinders & Pistons

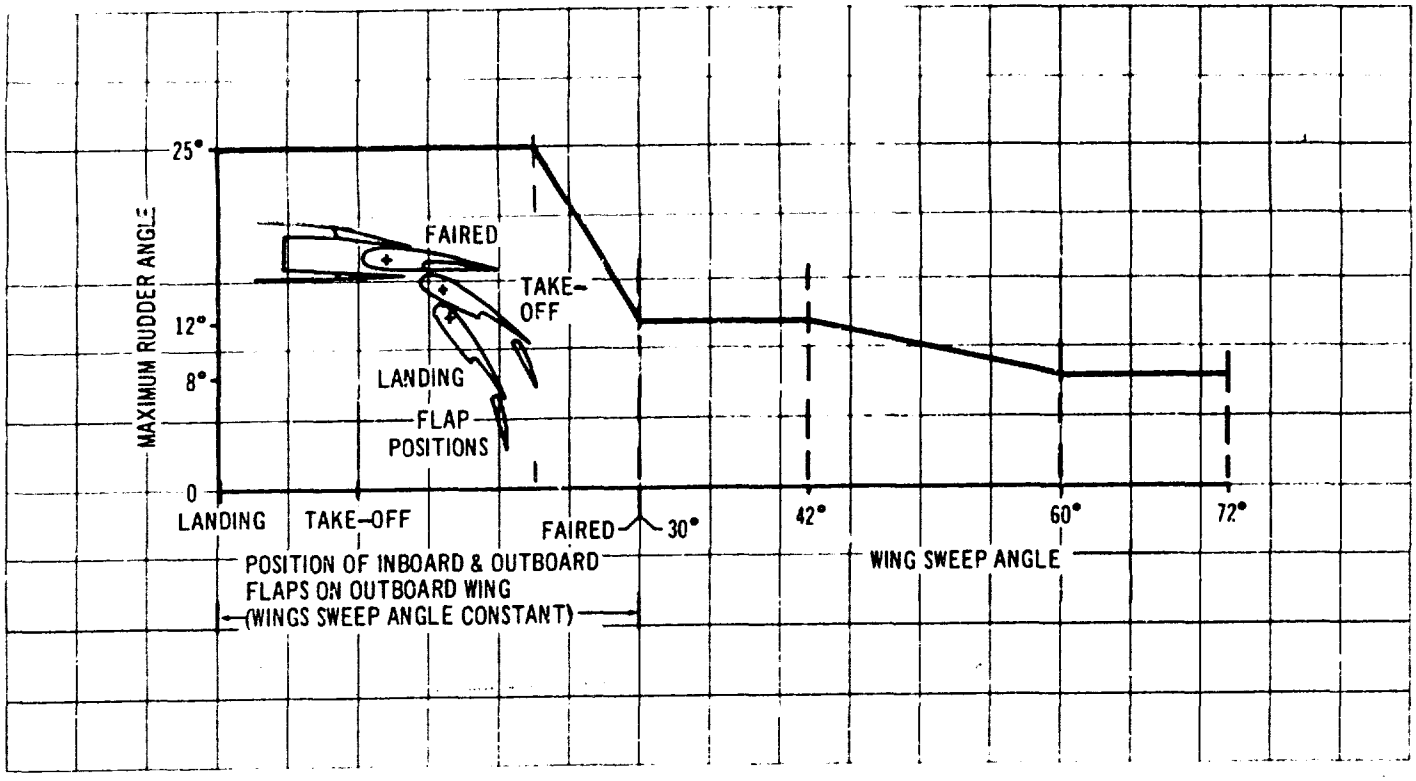


*Figure 5-4. Rudder Travel Limiting*

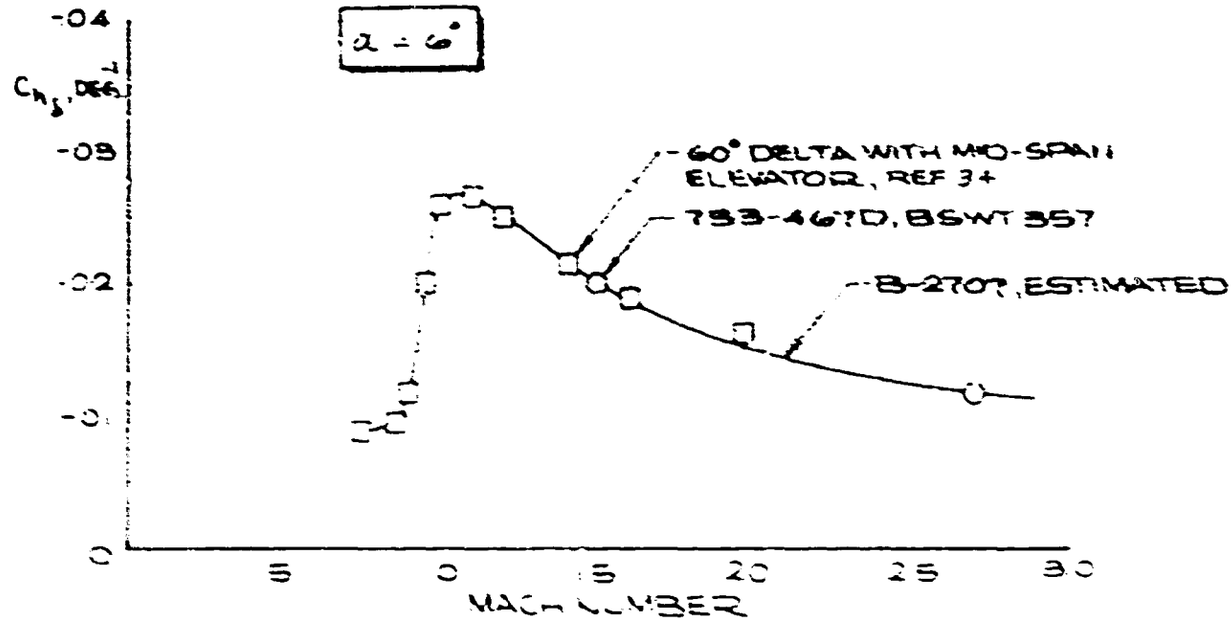


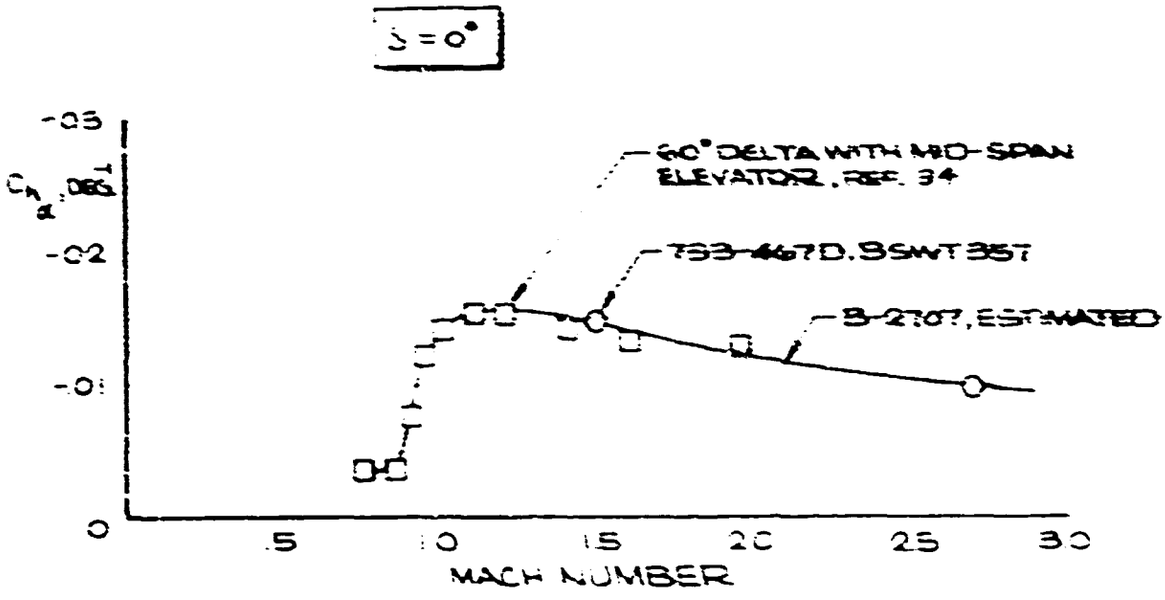


Figure 3-5. Elevator Hinge Moment Characteristics

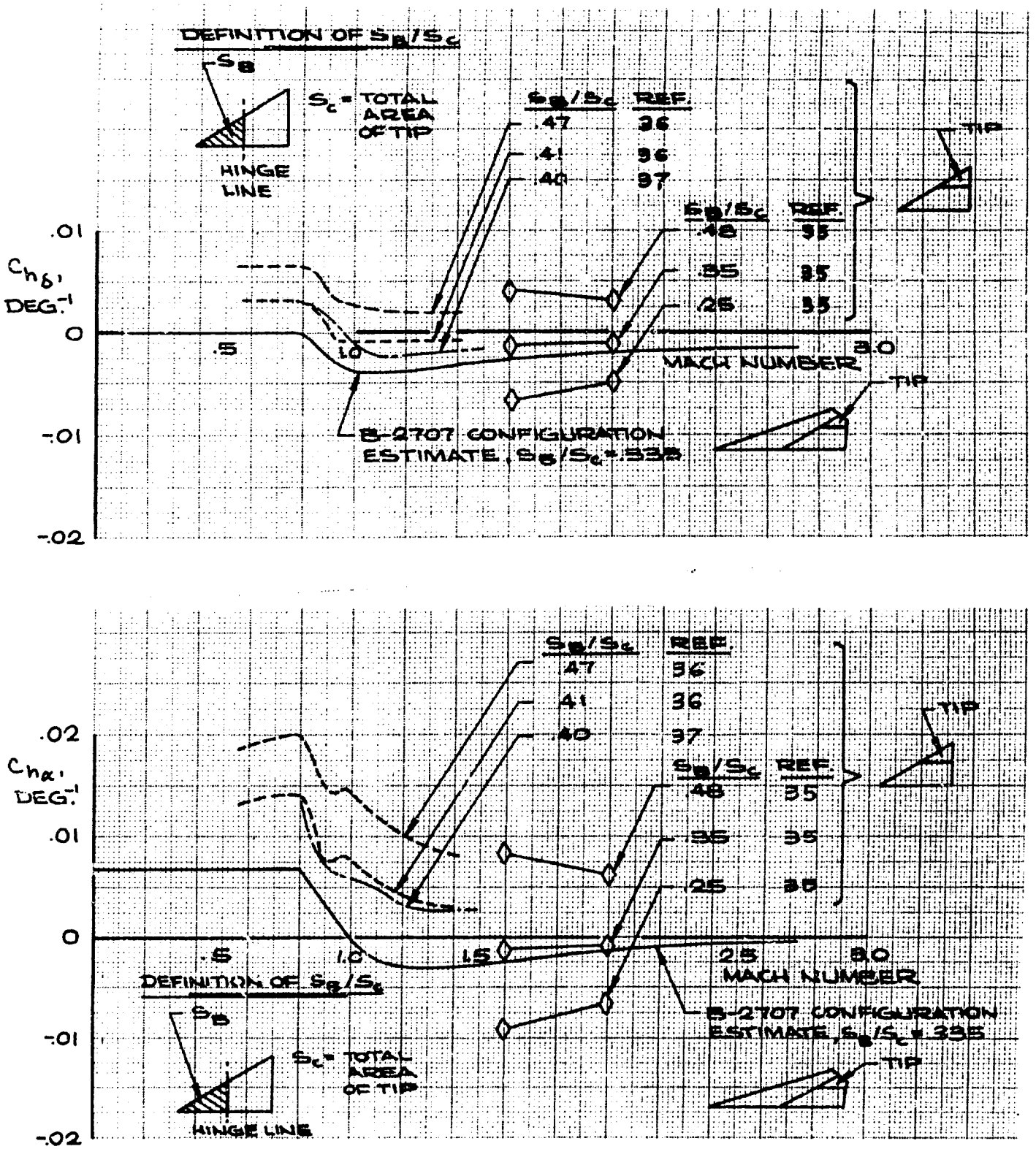


*Figure 5-6. Elevon Hinge Moment Characteristics*

Sec. 4.0 the surface effectiveness is substantially linear in the small deflection range, and the hinge moment characteristics would be expected to be fairly linear. In any event, little effect is expected on the maximum hinge moments at large deflection.

The spoiler and aileron hold-down hinge moment coefficients and hinge moment coefficients caused by deflection are shown in Fig. 5-7. Spoiler deflection hinge moment characteristics are based on NACA data and Boeing wind tunnel test data referenced in Fig. 5-7. Low speed, flaps down spoiler, and aileron, and flaps up spoiler characteristics are based on model 727 wind tunnel test data (UWAL 692) adjusted for sweep angle changes. High speed spoiler characteristics are based on wind tunnel tests (BSWT 320) with spoilers similar to the current B-2707 configuration. Hold-down hinge moment requirements for the spoilers and ailerons are based on low speed, flaps down model 727 wind tunnel data (UWAL 692) and high subsonic pressure model data on the 733-290 configuration, from NASA Ames Unitary test 143. The large hold-down loads indicated are caused by high local negative pressures caused by high circulation with flaps down at low speeds and by the leading edge vortex at high speed and high angles of attack with the wings at 72-degree sweep.

The estimated rudder hinge moment data shown in Fig. 5-8 are based on the referenced NACA data and low speed estimates using the methods of Ref. 22.

Elevon and elevator deflection capability is shown along $V_{MO}$ and $V_D$ placards in Fig. 5-9 and also along normal climb and descent schedules in Fig. 5-10. Full control surface deflection is available with all systems operating within the normal flight envelope. Moderate loss in maximum deflection occurs if one hydraulic system fails. At the maximum operating speed ($V_{MO}$), the ability of the airplane to maneuver to its structural limits is only slightly restricted by control hinge moments in the low supersonic speed range; maneuver capability, although reduced, appears adequate with a failed system. Analysis based on current data indicates that the control surface deflections available are marginal for upset recovery at $V_D$ with forward CG. Improvements in control effectiveness will be developed as discussed in Section 4.0.

Spoiler control deflection capabilities are shown in Fig. 5-11 at $V_{MO}$ and $V_D$ at wing sweeps of 42 degrees and 72 degrees. At design dive speed, the deflection capability is only slightly limited at 72 degrees sweep and about half deflection is available at 42-degree sweep where full deflection is not needed to meet requirements. Single system capability (two failures) is shown in Fig. 5-12. Sufficient spoiler deflection is available for lateral balance and bank angle corrections for all conditions.

Rudder hinge moment, adequate to give essentially full deflection to the surface stops, is available at all speeds as shown in Fig. 5-13. The two-engine-out enroute directional control requirement is not compromised by rudder actuation power.

## 5.2 SECONDARY FLIGHT CONTROL SYSTEM

### 5.2.1 Wing Sweep Control

The wing sweep control mechanism is described in Systems Report, Part B, V2-B2707-11. Wing sweep rates are 0.7 degree per second for increasing sweep and 0.35 degree per second for decreasing sweep. These rates were chosen to be compatible with the airplane accelerations and decelerations along normal flight profiles. Trim changes with wing sweep are moderate, as shown by the data in Sec. 4.0 and in normal operation are compensated by the SAS. The system has multiple power sources and load paths for safety and reliability of operation as described in V2-B2707-11.

### 5.2.2 High Lift Devices

The high lift devices consist of leading edge slats and trailing edge flaps on both the inboard fixed portion and outboard variable sweep portion of the wing. The details of flap and slat drive mechanisms are described in V2-B2707-11. The leading and trailing edge flap extension is scheduled with wing sweep as shown in Fig. 5-14. An override mechanism allows inboard slat extension with the wings at 72-degree sweep for the emergency wings aft landing condition.

## 5.3 STABILITY AUGMENTATION SYSTEM

### 5.3.1 General Description

A stability augmentation system is provided on all three primary control axes to improve handling qualities and reduce the variation in airplane response characteristics with loading and flight condition. Besides improving the handling qualities, the SAS provides gust loads alleviation, turn coordination, and inner loop damping for the autopilot. The stability augmentation system

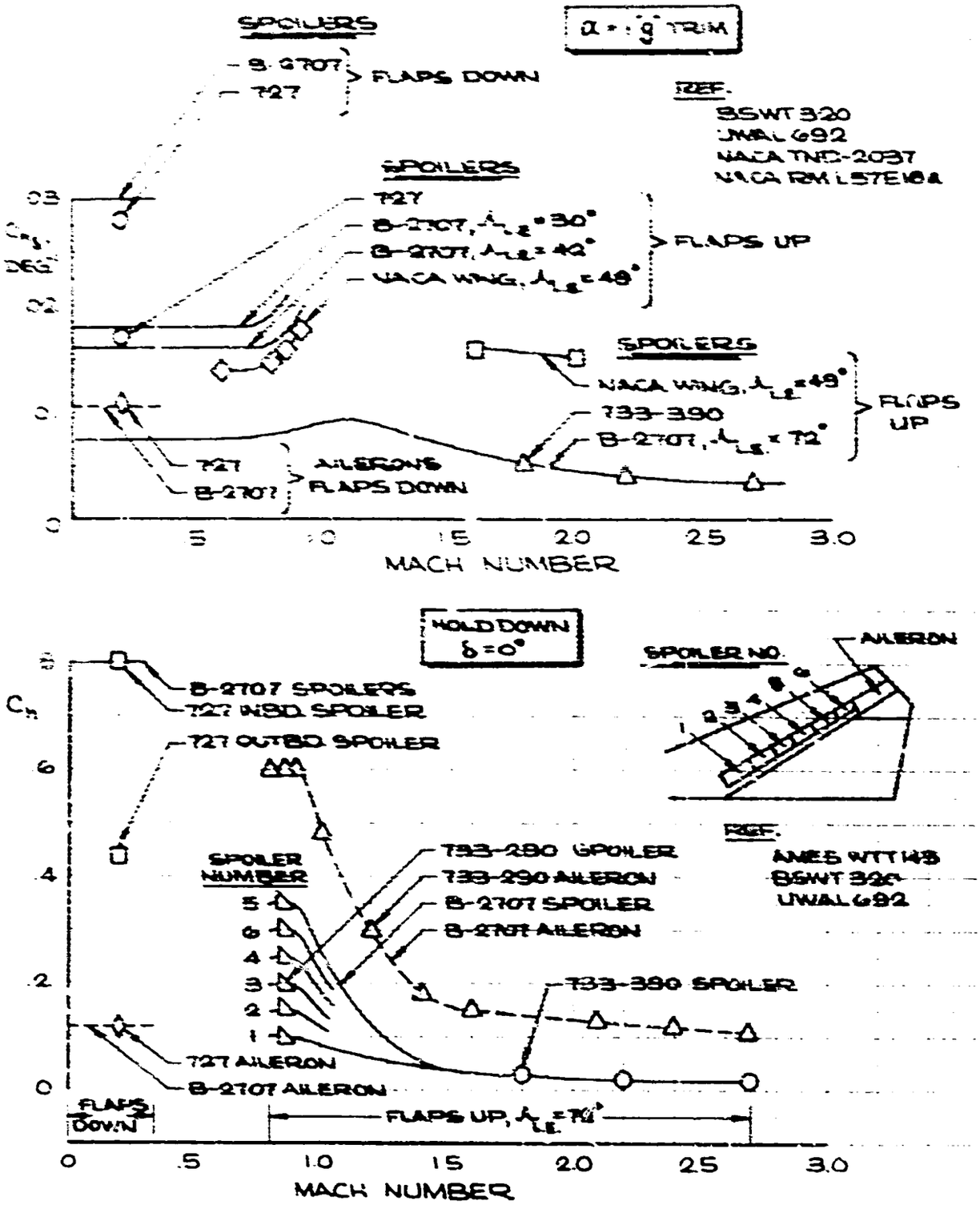


*Figure 5-7. Aileron and Spoiler Hinge Moment Characteristics*

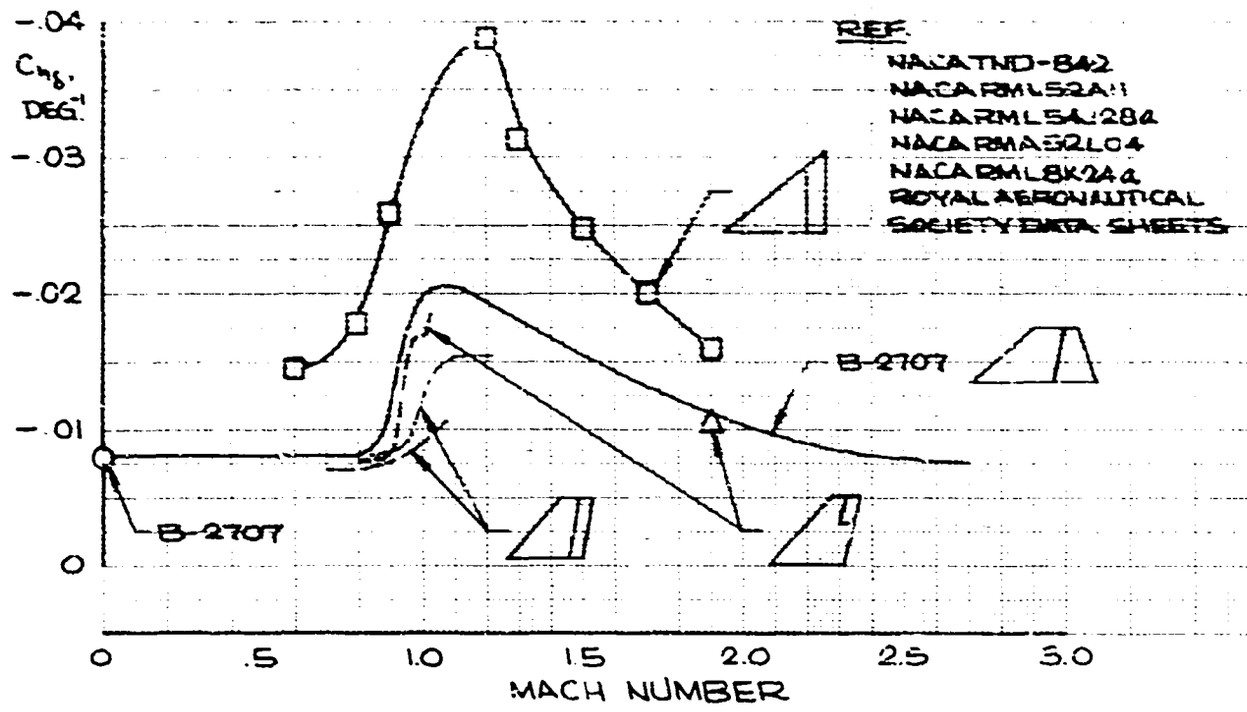


*Figure 5–8. Rudder Hinge Moment Characteristics*

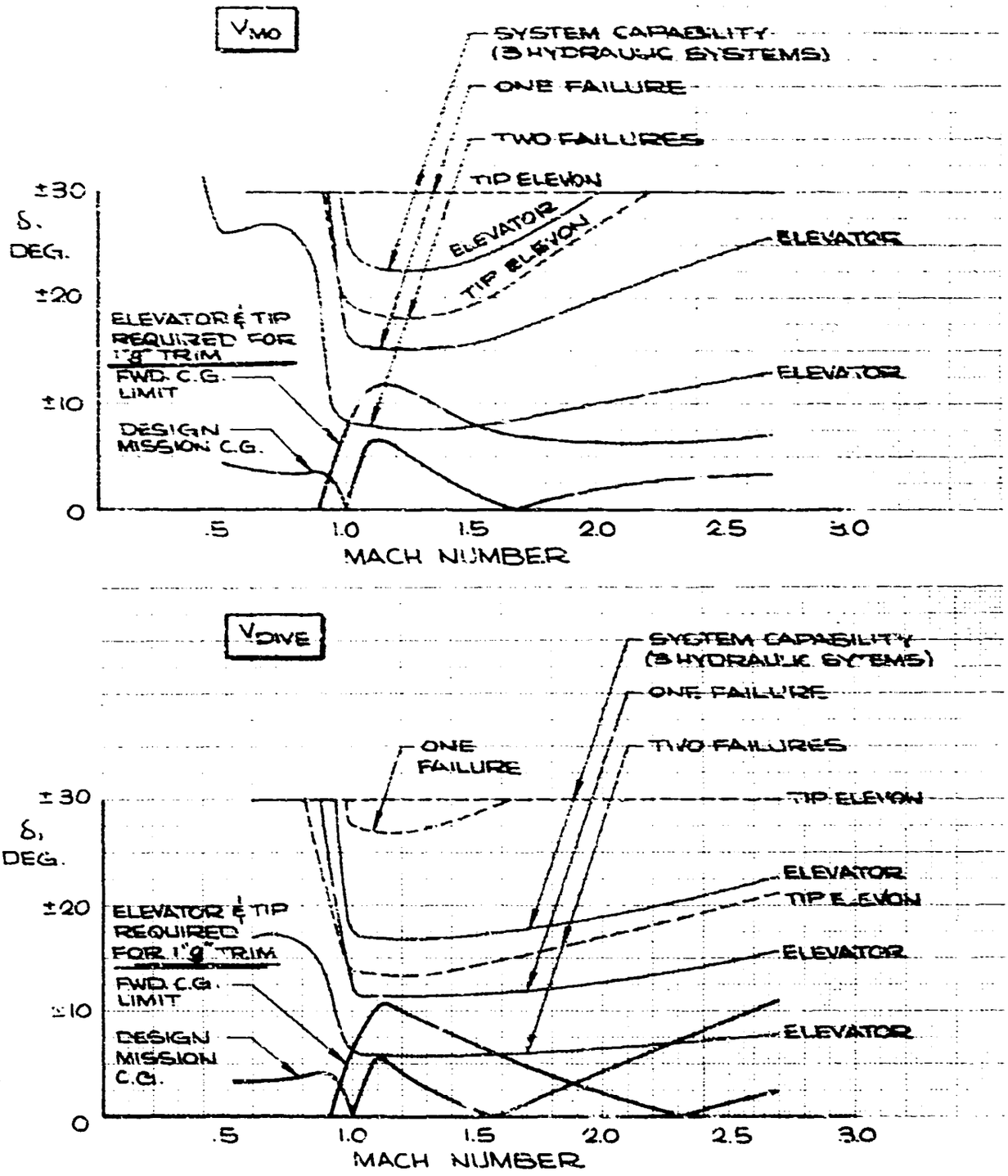


*Figure 5-9 Elevator and Elevon Deflection Capability ($V_{DIVE}$ and $V_{MO}$)*

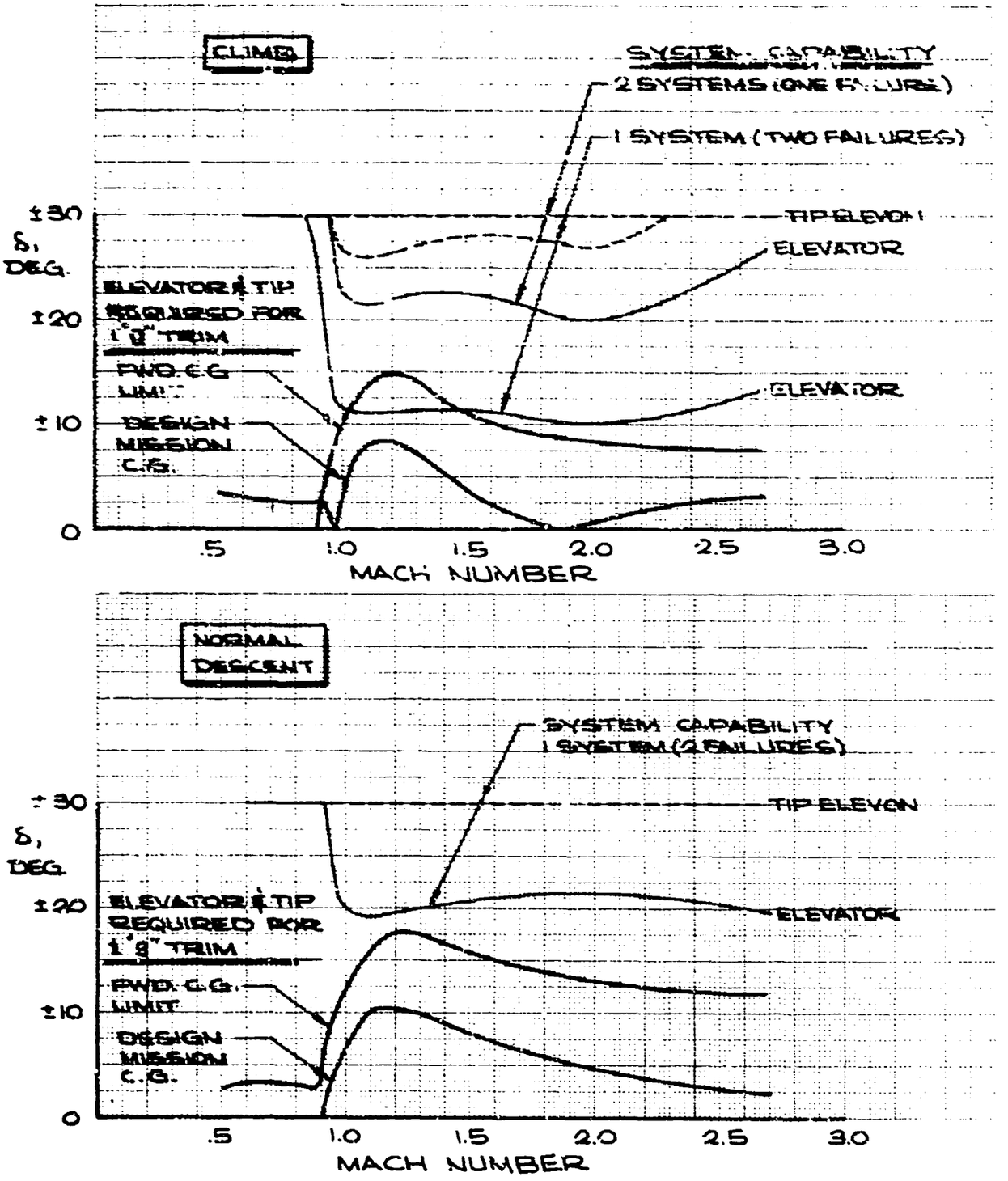


*Figure 5-10. Elevator and Elevon Deflection Capability (Climb and Descent)*

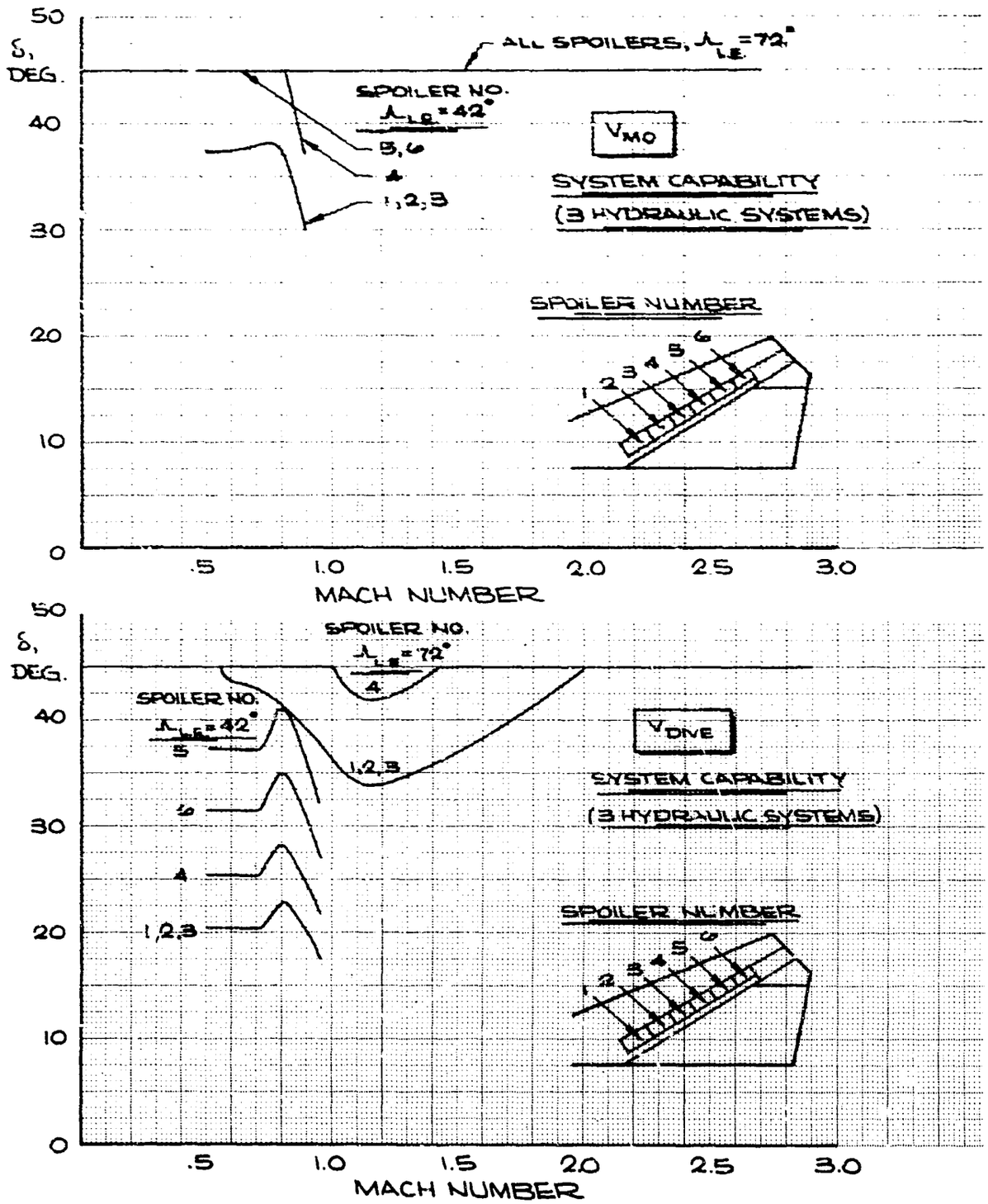


*Figure 5–11. Spoiler Deflection Capability (All Systems)*

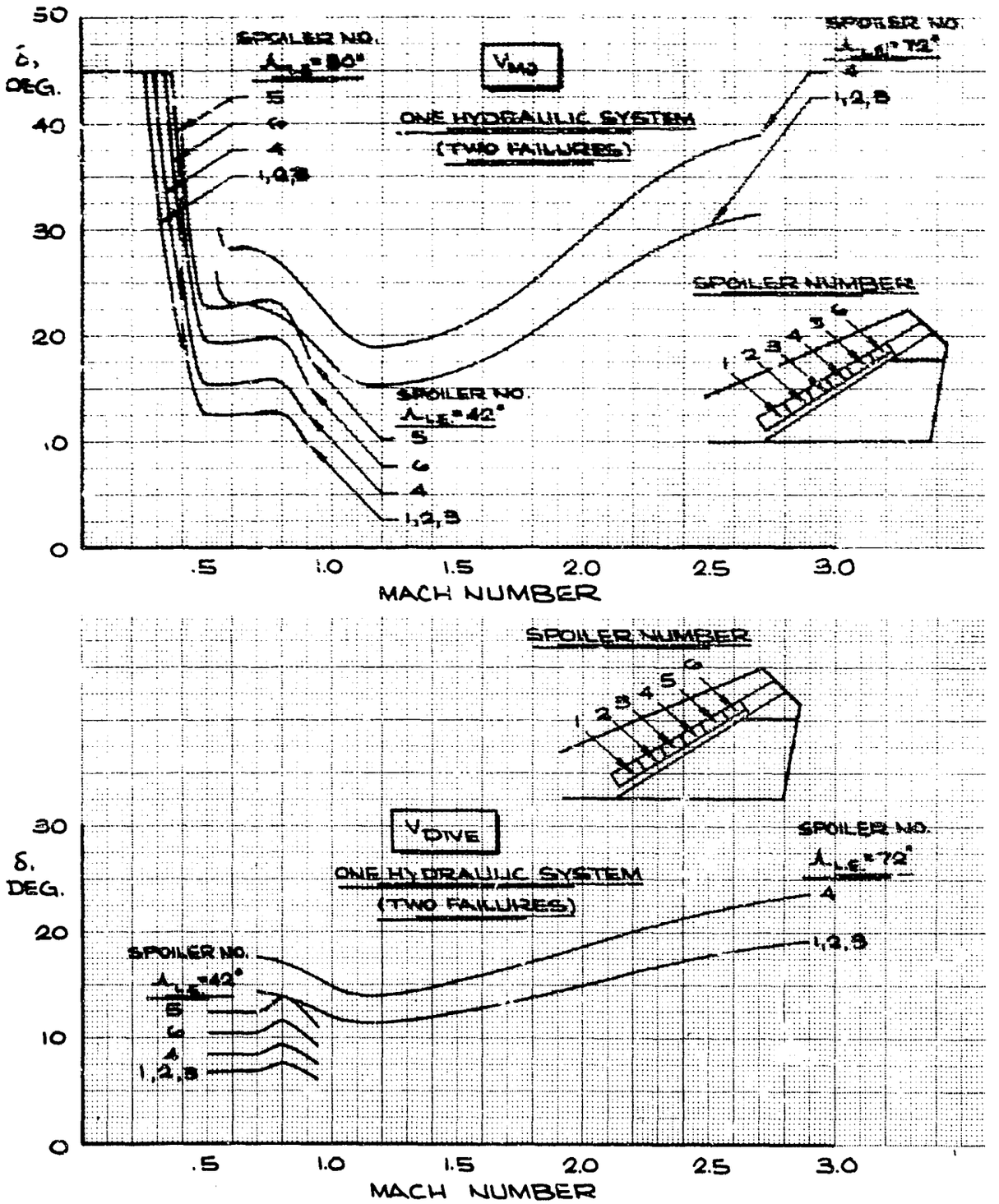


*Figure 5-12. Spoiler Detection Capability (One System)*

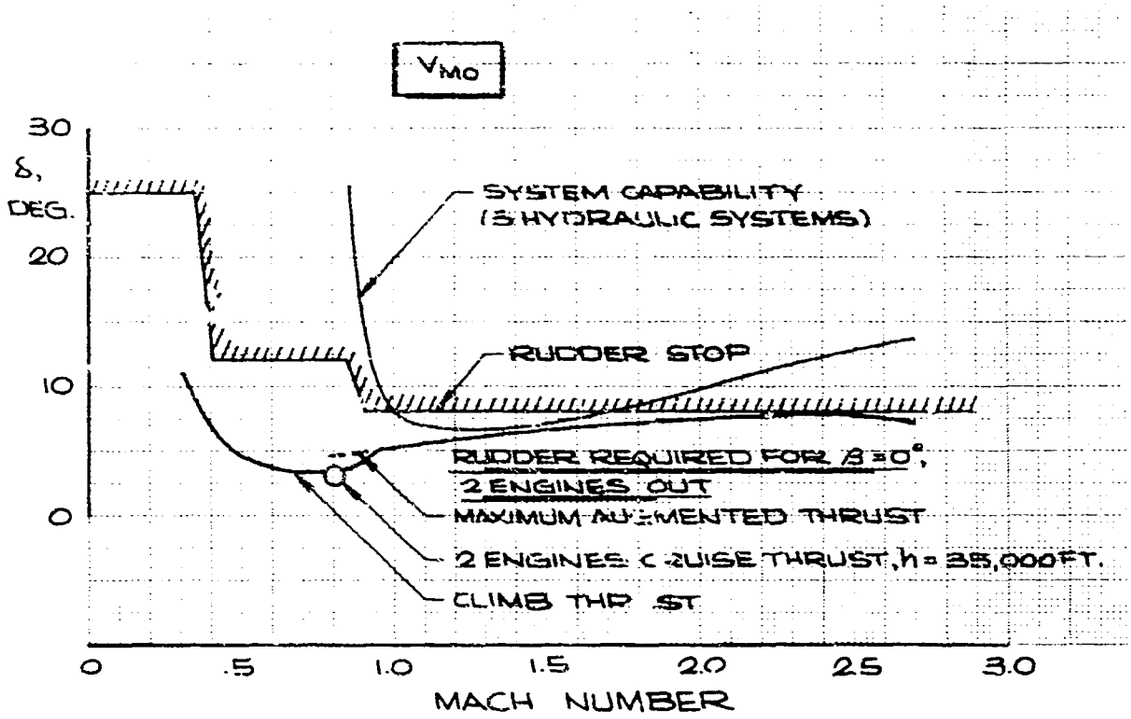


*Figure 5–13. Rudder Deflection Capability*

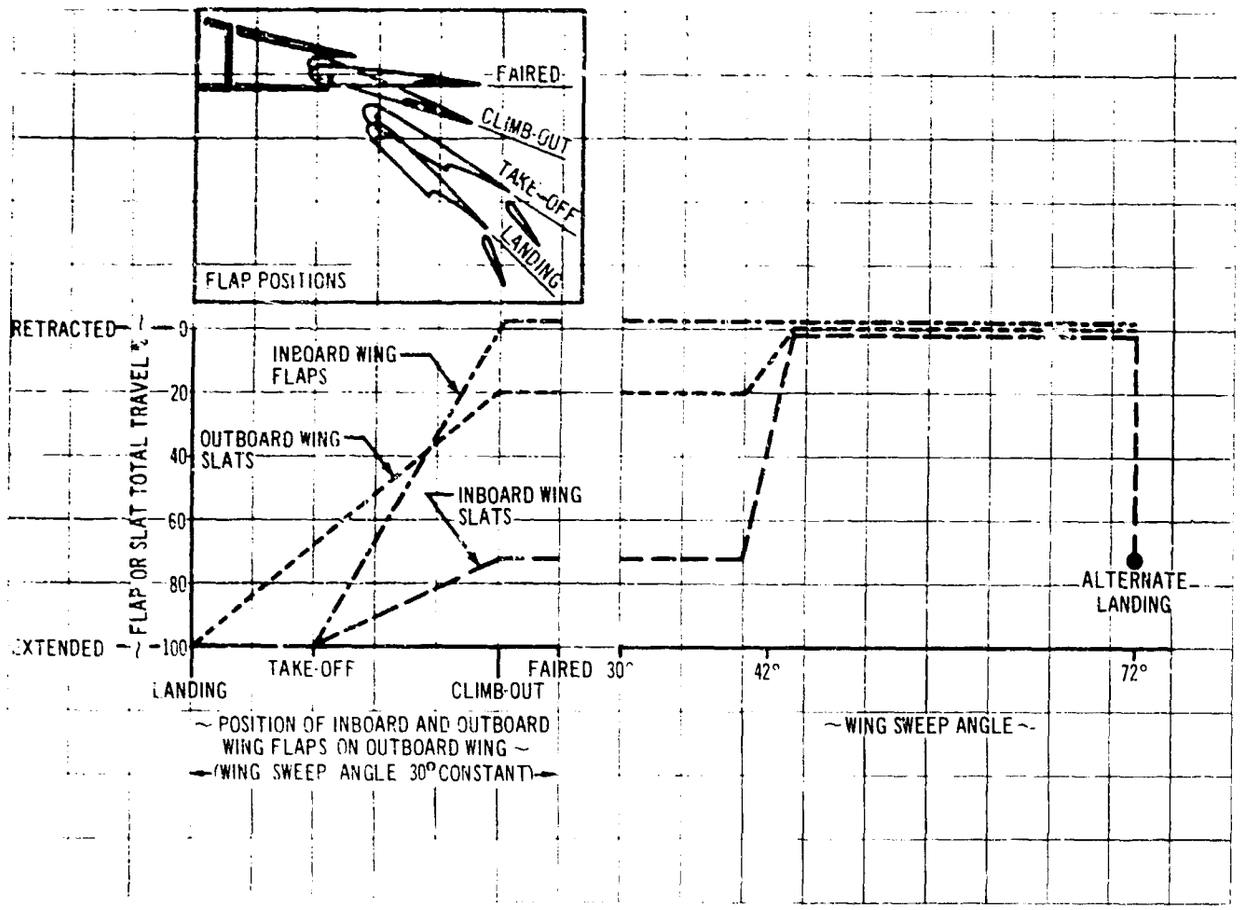


*Figure 5-14. Slat and Flap Programming*

pitch and roll axes provide series inputs to the elevators and elevons, and the yaw axis provides a series input to the rudder. The SAS pitch axis also provides an automatic trim signal which positions the control column. Triple force summed series actuators are used in each axis to provide fail-operational characteristics. The pitch and the yaw axes have four separate channels of sensors and electronics, and a servo monitor. This provides fail-operational characteristics after both the first and the second failure. The roll axis has three separate channels and is fail-operational after the first failure.

5.3.2 Pitch Axis

5.3.2.1 System Functional Characteristics Figure 5-15 is a functional block diagram of the pitch axis of the SAS which also shows the relationship with the electric command and trim systems. The pitch axis of the SAS is essentially a pitch rate feedback system with command augmentation. The SAS feedback and electric command combine to give an airplane response to control input which is heavily damped and has minimum variation with flight condition. When the applied control force is reduced to zero, the pitch rate command is zero and the airplane remains at the new attitude. This characteristic is referred to as platform stability.

Pilot command inputs to the SAS are measured at the output position of the pitch master servo and are shaped by the prefilter to give a pitch rate command signal. Body mounted rate gyros measure the airplane pitch rate, resulting in a pitch rate error signal. This signal is then shaped by the compensation filter to give a SAS pitch axis servo position command. This servo provides a series input which is added mechanically to the pitch master servo position. The resulting servo output linkage movement then positions the pitch control surfaces by means of the surface actuators.

The steady pitch rate developed for a given change in pitch master servo position is fixed for all flight conditions. This simplifies the gain scheduling in the electric command system required to give near constant stick force per g characteristics. Scheduling for CG shift and variation in control effectiveness is therefore not required. Electric command system gain scheduling and the resultant stick force per g characteristics are shown in Fig. 5-16.

Because the augmented airplane has platform stability, the pitch axis of the SAS produces a control deflection to balance moment changes caused by flap deflection or wing sweep. To minimize the SAS servo authority required, automatic trimming is provided within the SAS and therefore a slow drift in attitude occurs if the SAS is providing a balancing moment. Automatic trimming minimizes this drift.

Manual trim commands move the feel center and the pitch master servo is positioned accordingly. This master servo position change is sensed by the SAS pitch axis command augmentation and interpreted as a pitch rate command. Whether the column is controlled by the force sensors or by the trim system the airplane responds in the same manner.

To prevent the automatic trim being interpreted as manual trim command, an electronic counterpart is generated within the SAS computer to balance the change in the master servo position signal. The components of the automatic trim function are a threshold detector, a pulse generator to command the trim stepping motor, and an electronic model of the trim motor and master servo. The same pulses are integrated by the trim stepping motor and the pulse counting circuitry of the electronic model so that the two systems track identically. This integrator is also used for pre-engage synchronization. The basic platform stability mode of the pitch axis of the SAS has characteristics similar to those of a stick steering system. It exhibits neutral speed stability, i.e. changes in speed do not cause pitch attitude changes and do not require the pilot to hold a steady force proportional to the speed change. For many modes of flight, neutral speed stability simplifies the central problem; however, for landing approach and low speed operation, it may be desirable to have positive speed stability. A separate speed stability mode is provided within the pitch SAS which may be selected for these cases. When this mode is engaged, an airspeed error signal with an airspeed rate damping signal is introduced which opposes the command augmentation signals and provides ideal speed stability characteristics.

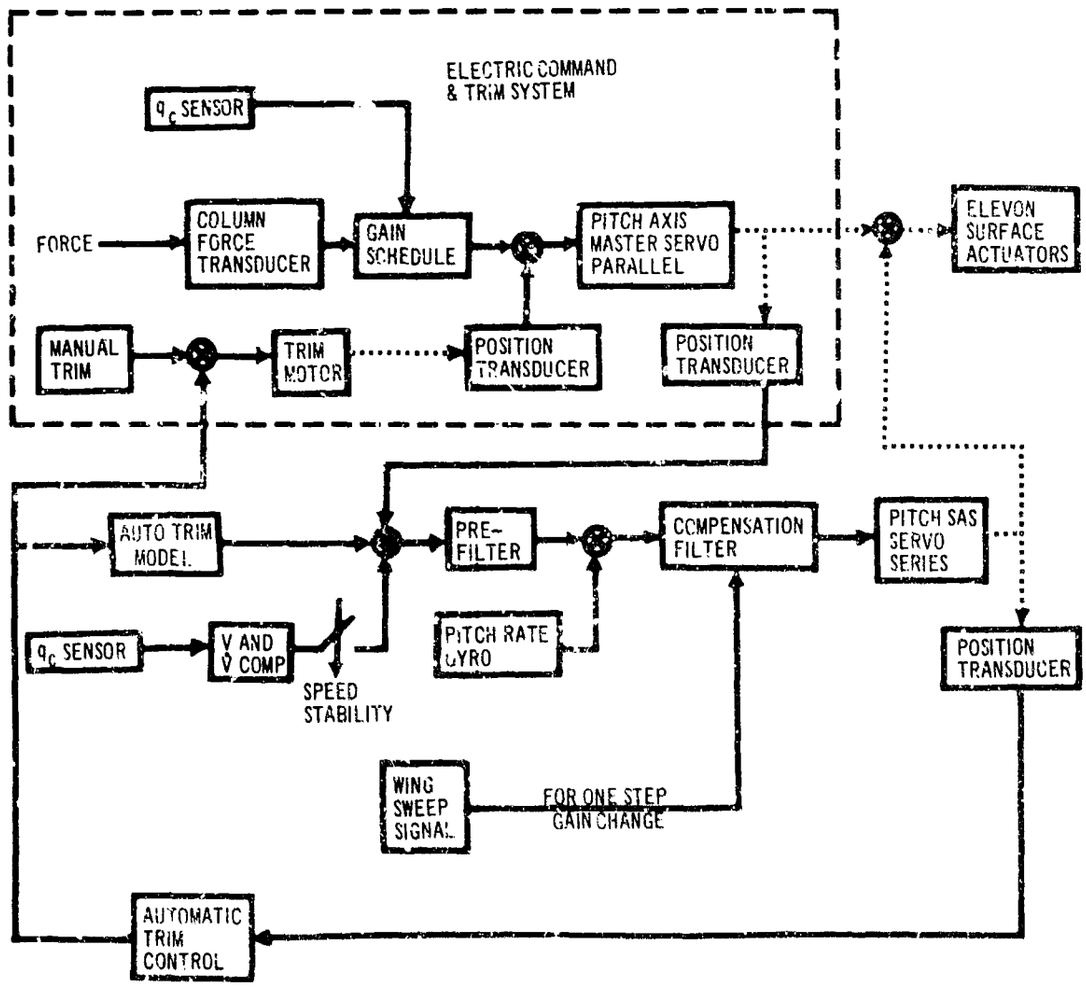


*Figure 5-15. SAS Pitch Axis Functional Diagram*

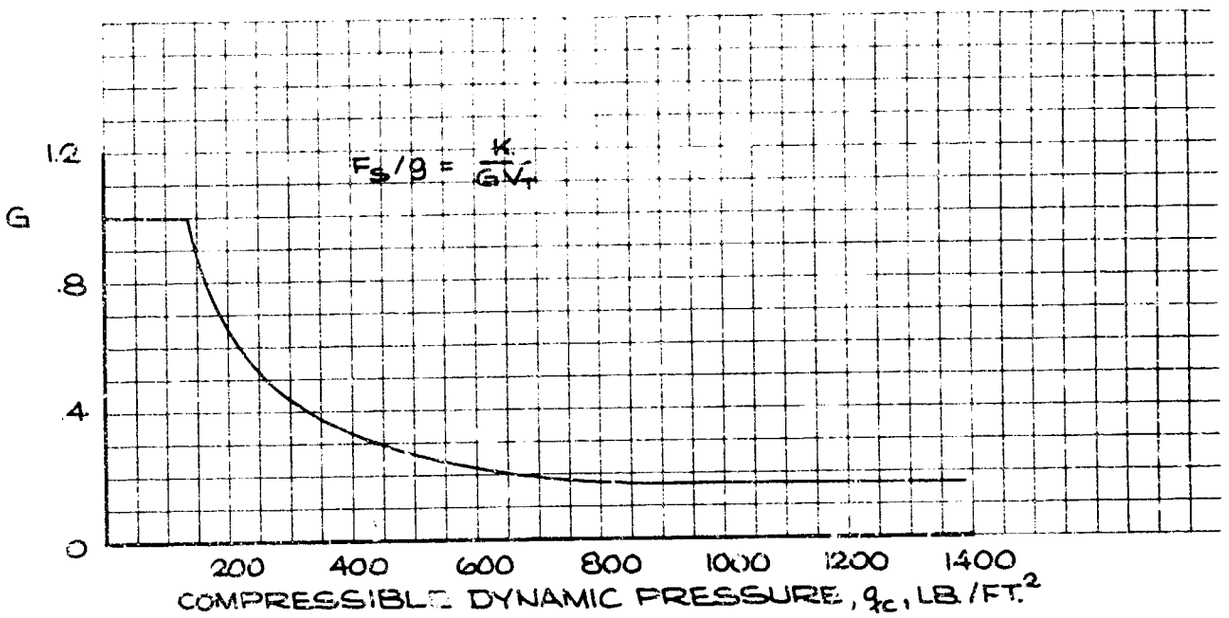


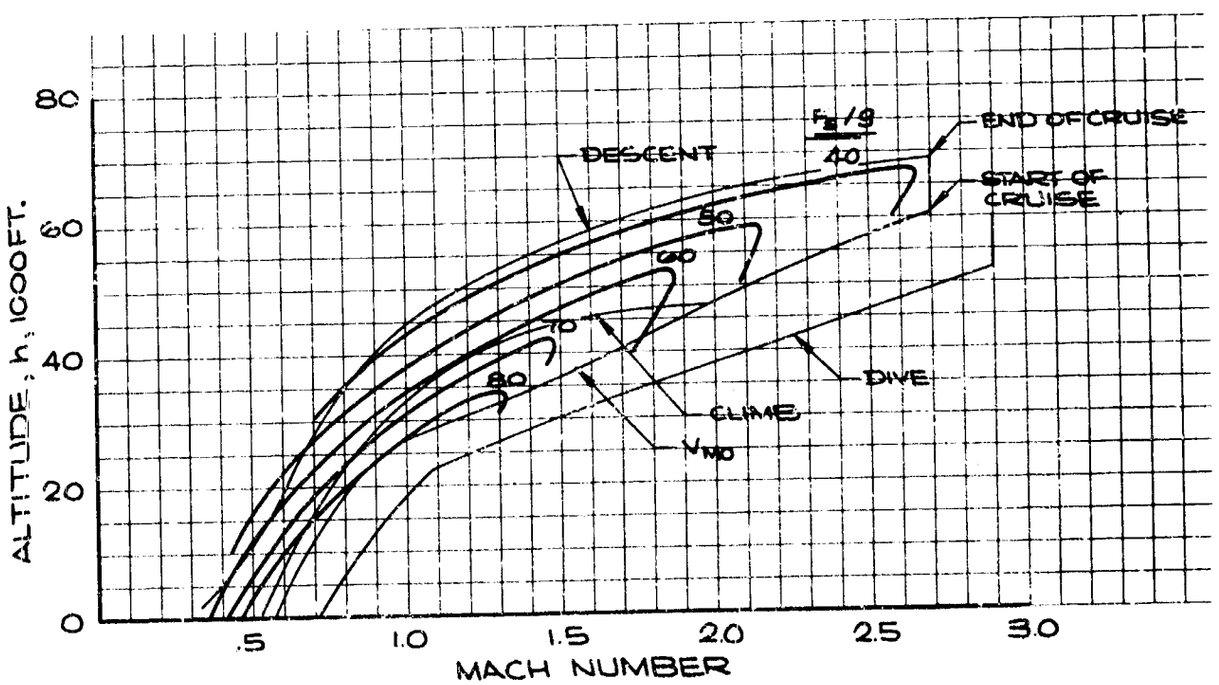


*Figure 5-16. Stick Force Per g*

The air data required for this mode are computed within the SAS using the same dynamic pressure signals as used for electric command gain scheduling. This part of the system will be fail-operational upon the first failure and fail-passive for the second failure.

Loads alleviation is provided by the SAS pitch axis through damping of the short period. By eliminating the large pitch rate overshoot, which is characteristic of the unaugmented airplane response to a step command, a slow well damped normal acceleration response is obtained at high speed. This reduces the maneuver loads induced by the pilot when he is making small path corrections. Structural loads for design maneuver cases are considered for both SAS on and off (Airframe Design Report, Part C, V2-B2707-7).

Electronic filtering of the SAS feedback loops is relied upon to prevent excitation of the flexible body modes. An initial attempt to provide one compensation filter suitable for all flight conditions resulted in too much gain at high frequencies. With two compensation filters, one for the wings forward flight conditions and another for the wings aft conditions, the desired high-frequency cutoff is attained. This transition is made as a function of wing sweep position.

5.3.2.2 Response to Command and Disturbance The longitudinal response of the augmented airplane to step command inputs and to step vertical gusts is shown in Figs. 5-17 and 5-18. Unaugmented airplane responses are shown for comparison. These traces show the master servo and series servo position responses as well as the surface deflection. Note that the pitch rate response to step command for the augmented airplane has similar characteristics at all flight conditions. The large pitch rate overshoot of the unaugmented airplane response at high speed is eliminated by the SAS. The longitudinal SAS authority is determined by the requirements of the landing approach flight condition to be ±15 degrees at 30-degree sweep and is reduced to ±8 degrees at sweep angles greater than 40 degrees. SAS actuators have a 30 radian per second break frequency and will have rate capability for full-stroke operation at this frequency.

The pitch axis SAS design resulted from the synthesis of a fixed-gain system providing good handling qualities at all flight conditions. The design method was developed by Horowitz. As applied to the Boeing SST, the design causes the pitch rate due to command input to approach a specified ideal amplitude frequency response for all flight conditions and all frequencies.

The basic assumption is that an ideal pitch rate transfer function is known and may be expressed as a Bode plot. In the actual synthesis, a band or envelope of a specified width in decibels is used as the criterion rather than a single curve. If the amplitude responses for all flight conditions of the augmented airplane lie inside the envelope at all frequencies, the airplane will exhibit satisfactory handling qualities at all flight conditions.

In order to avoid flexible mode coupling, it is necessary to reduce the gain at the higher frequencies. This is achieved by dividing the flight conditions into two groups, one group for the wings forward flight condition and another group for the wings aft conditions. An analysis of the airframe SAS structural coupling, including five flexible modes, has been completed using aerodynamic and structural data from an earlier configuration with satisfactory results. This analysis is presently being repeated with B-2707 aerodynamic and structural characteristics and will be reported in Development Data Document D6A-10339-1.

5.3.3 Roll Axis

5.3.3.1 System Functional Characteristics Figure 5-19 is a functional block diagram of the roll axis of the SAS. The roll axis of the SAS is a roll rate feedback system with command augmentation. The electric command and SAS work together so that in response to an applied wheel force a steady roll rate is developed. Roll rate feedback and command augmentation are included to produce good roll command response.

No gain change is required in the roll axis command because the control gains are varied by the mechanical programming of elevons, spoilers, and ailerons with wing sweep and flap extension as described in Par. 5.1.3.

5.3.3.2 Response to Command and Disturbance The lateral-directional responses of the augmented and unaugmented airplane to step wheel inputs are shown in Fig. 5-20. These traces are obtained with the longitudinal SAS operating. Response to an initial value of sideslip is shown in Fig. 5-21.

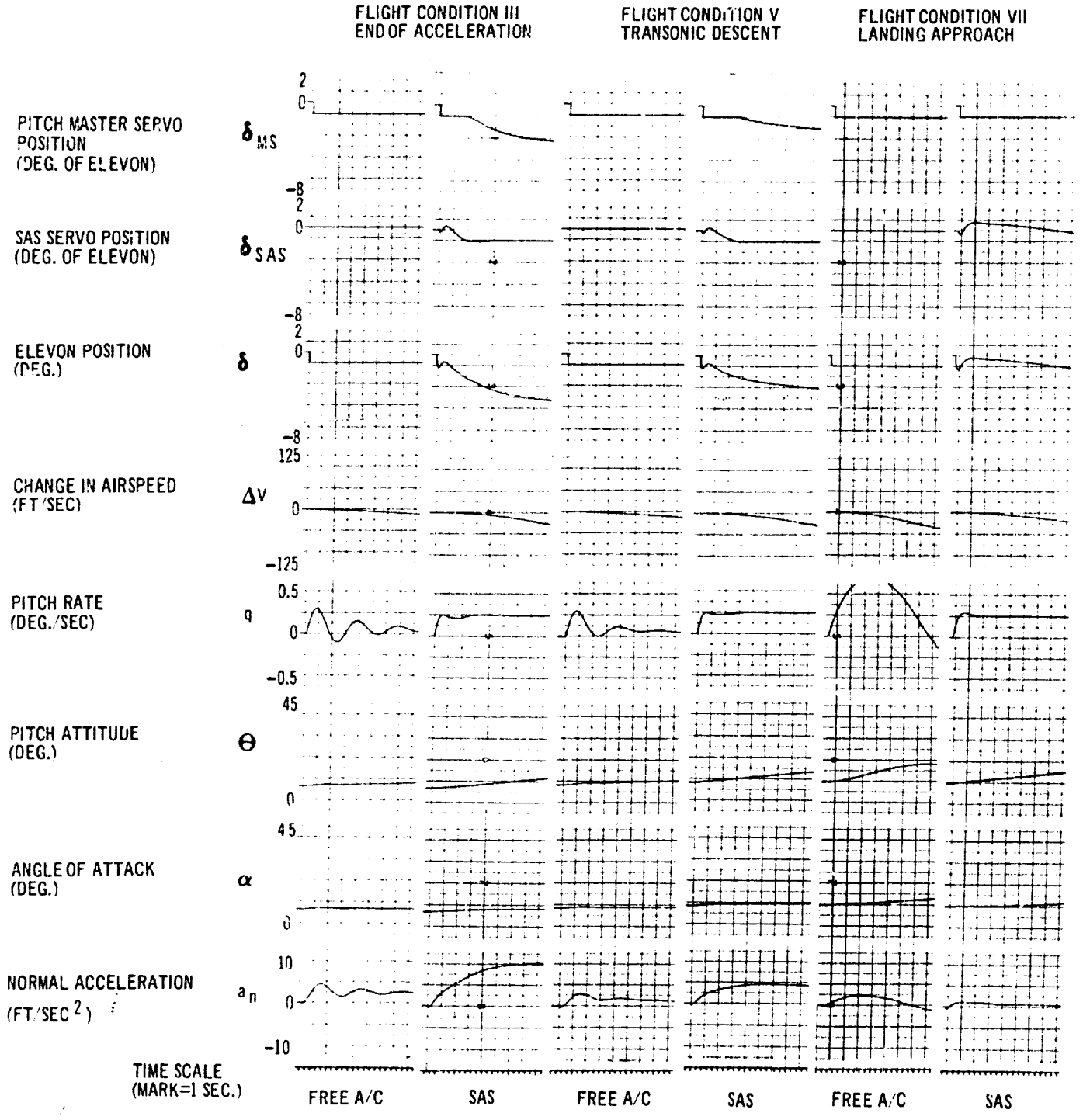


*Figure 5–17. Longitudinal Response to Step Command*

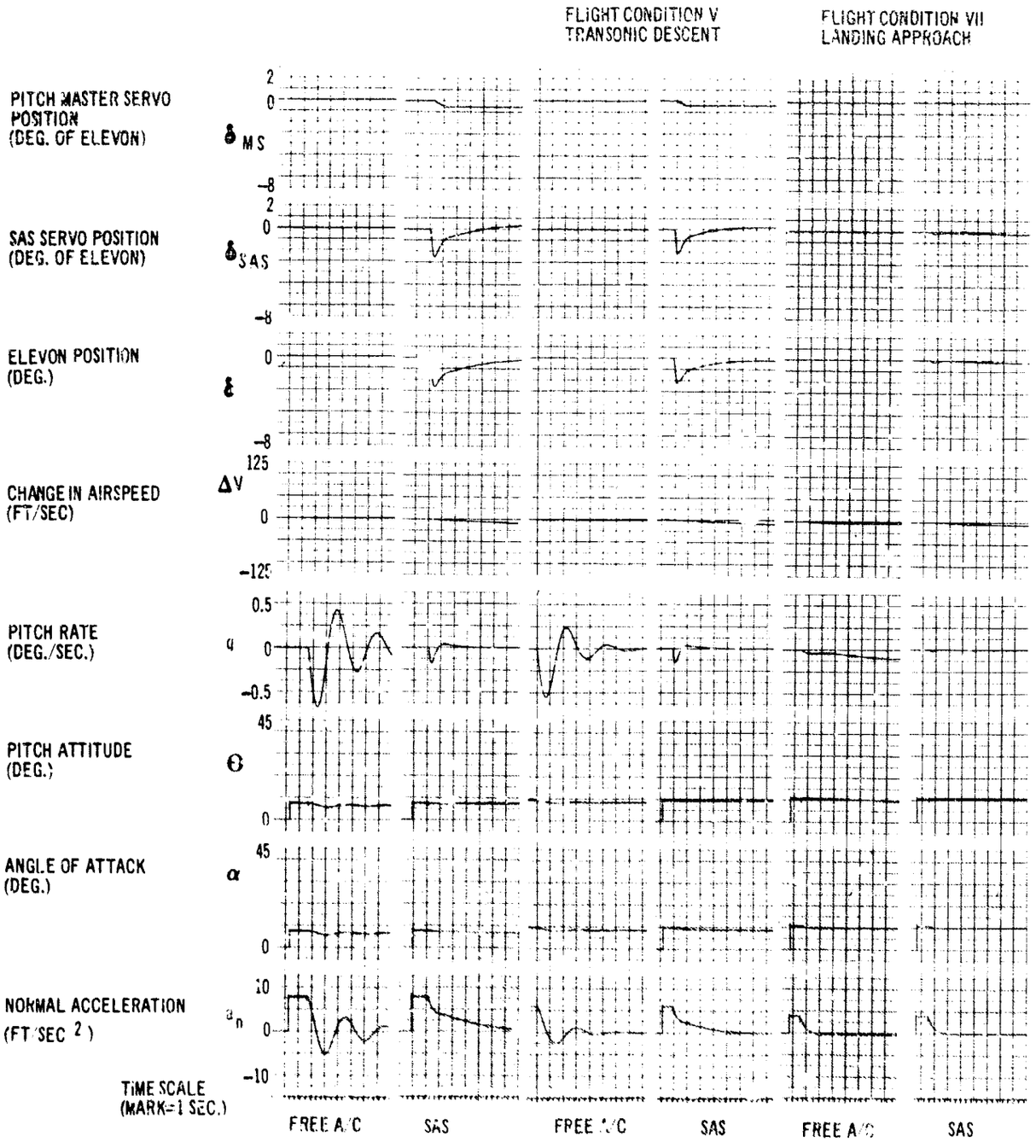


*Figure 5-18. Longitudinal Response to Step Gusts*

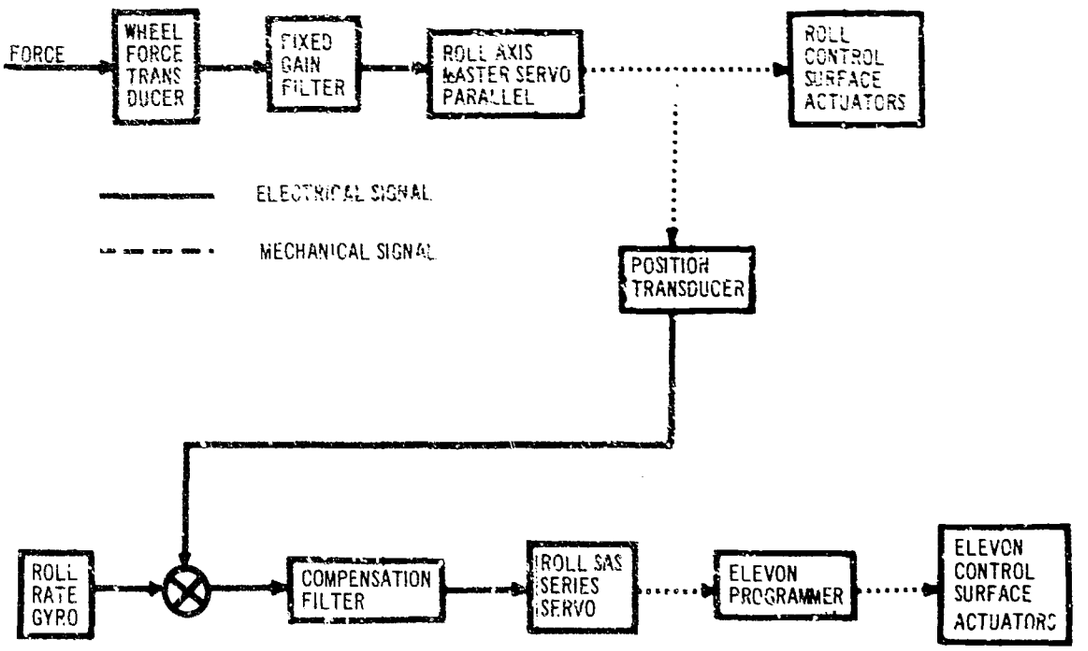


*Figure 5–19. SAS Roll Axis Functional Diagram*

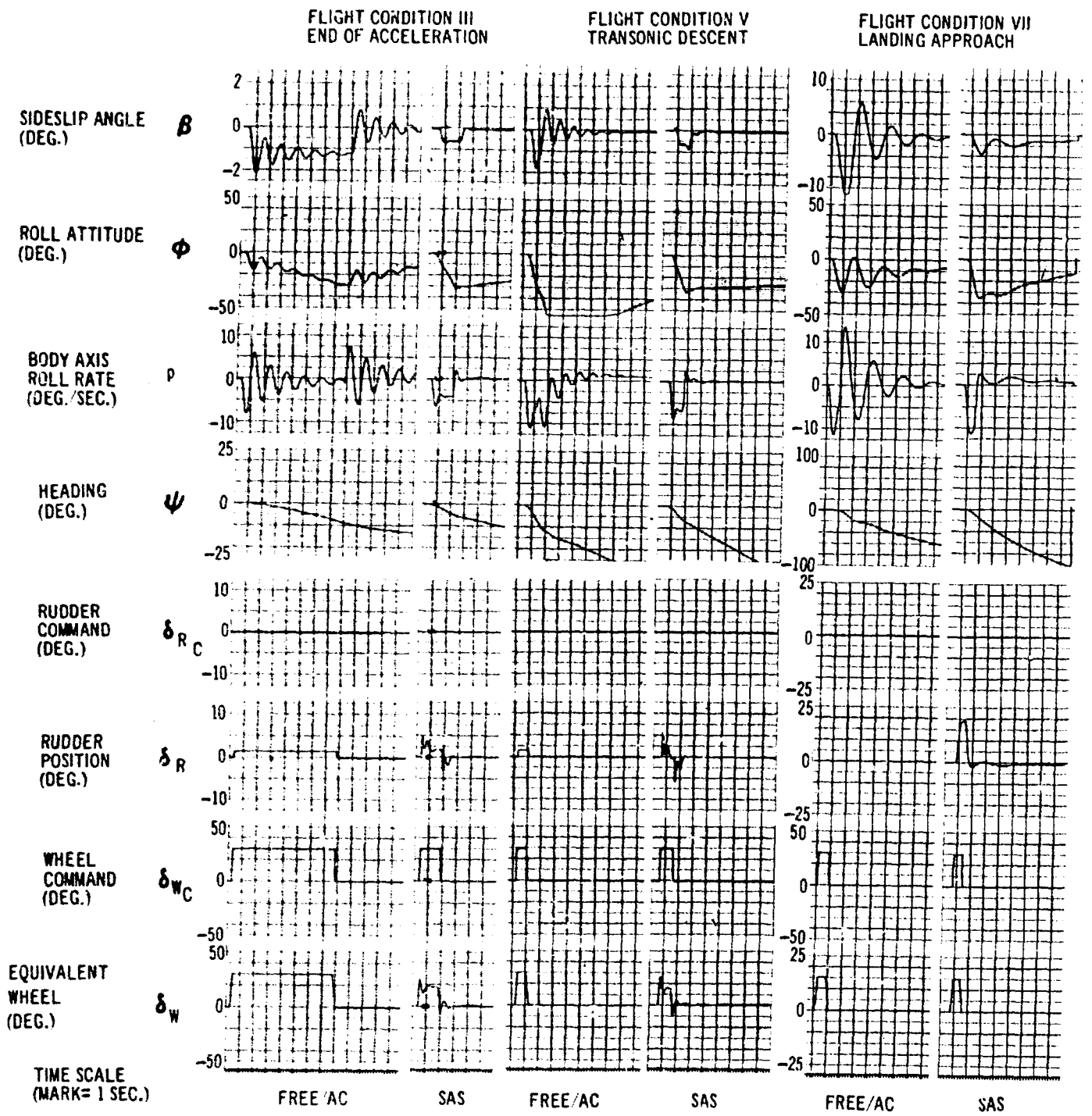


*Figure 5-20. Lateral – Directional Response to Step Command*

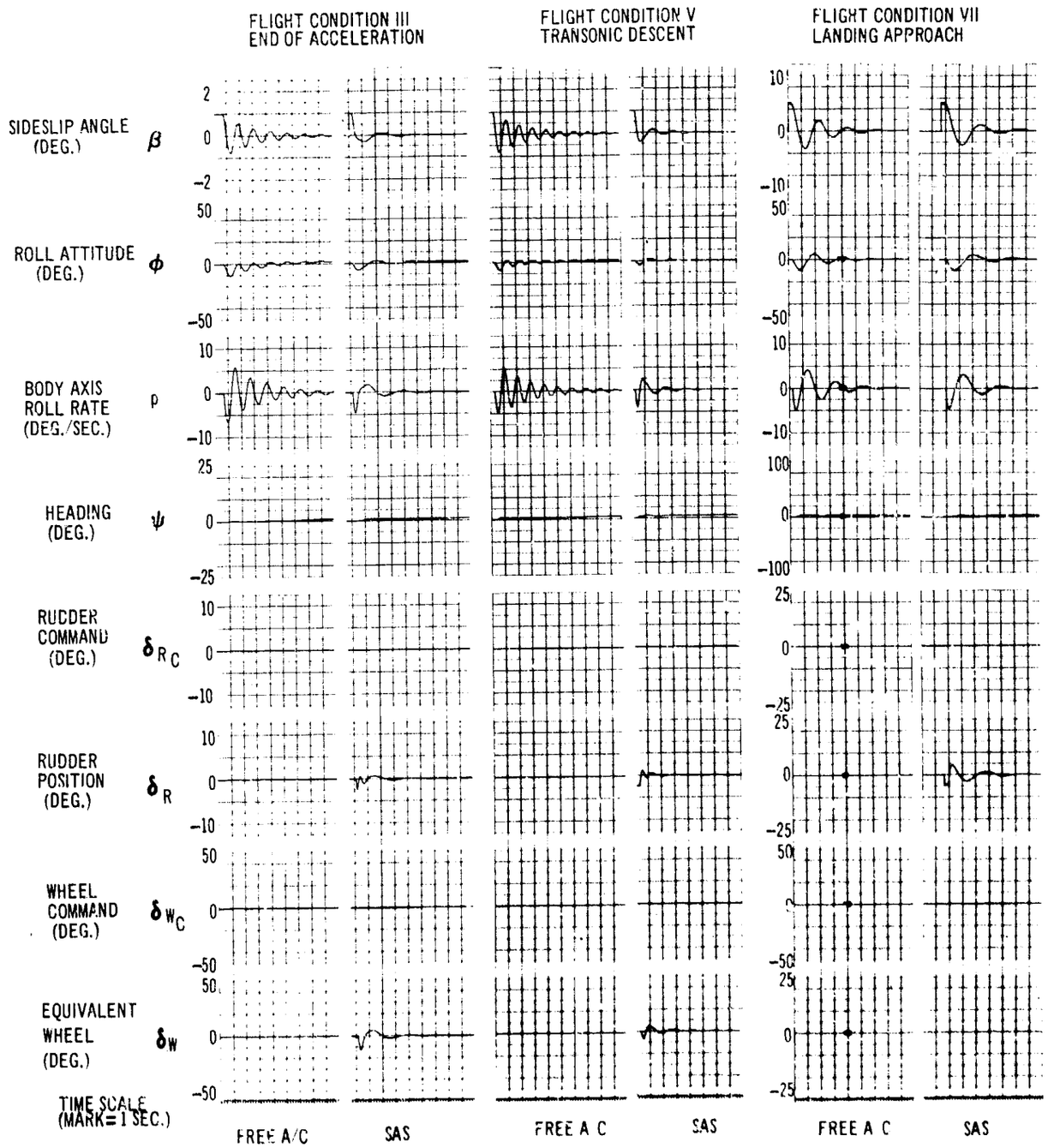


*Figure 5-21. Lateral – Directional Response to Step Sideslip*

5.3.4 Yaw Axis

5.3.4.1 System Functional Characteristics
Figure 5-22 is a functional block diagram of the yaw axis of the SAS. Suitably filtered roll rate feedback results in good Dutch roll damping and a substantial decrease in roll time constant. This roll rate signal is gain scheduled as a function of compressible dynamic pressure ($q_c$). A limited signal from a body-mounted lateral accelerometer provides directional static augmentation and reduces sideslip angles in maneuvers. The mechanical gearing between elevons and rudder deflection is augmented in the SAS by a shaped electrical signal. This signal, like the mechanical interconnection, is gain scheduled by wing sweep.

Improvement in Dutch roll damping by the use of roll rate feedback into rudder is demonstrated by the root locus diagram shown in Fig. 5-23. By filtering roll rate with a washout and lag network, the position of the spiral mode is moved toward the origin (neutral spiral stability) and the roll time constant is reduced.

5.3.4.2 Response to Command
The sideslip angle developed in the response to a pulse wheel command is shown in Fig. 5-24.

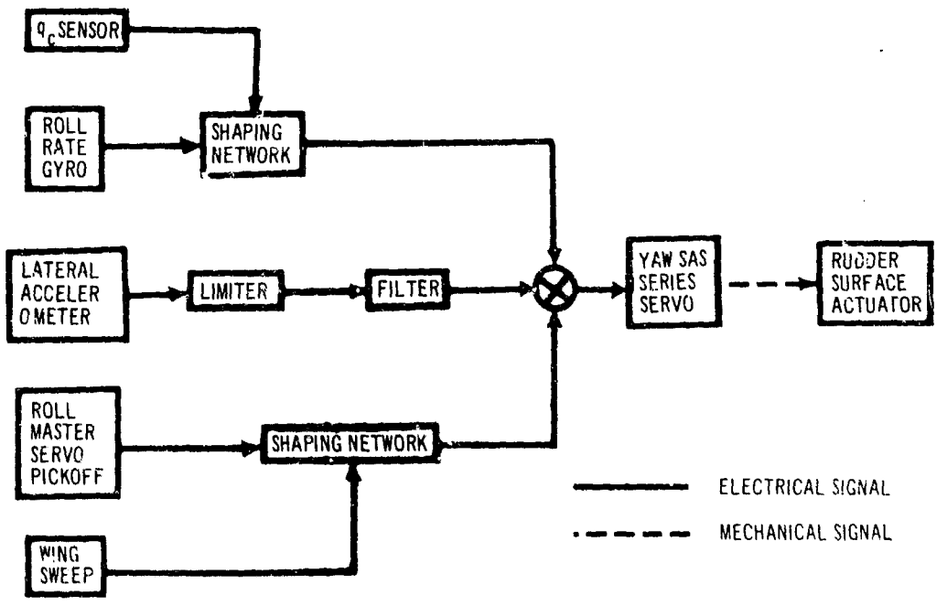


*Figure 5-22. SAS Yaw Axis Functional Diagram*

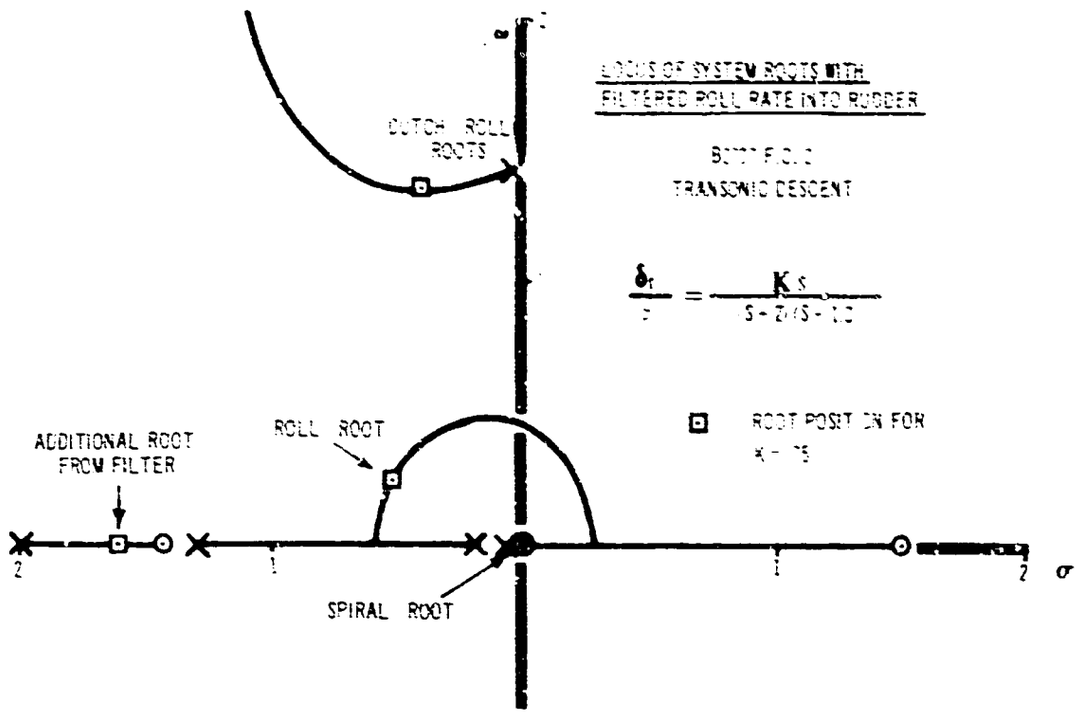


*Figure 5–23. Root Locus Roll–Yaw SAS*

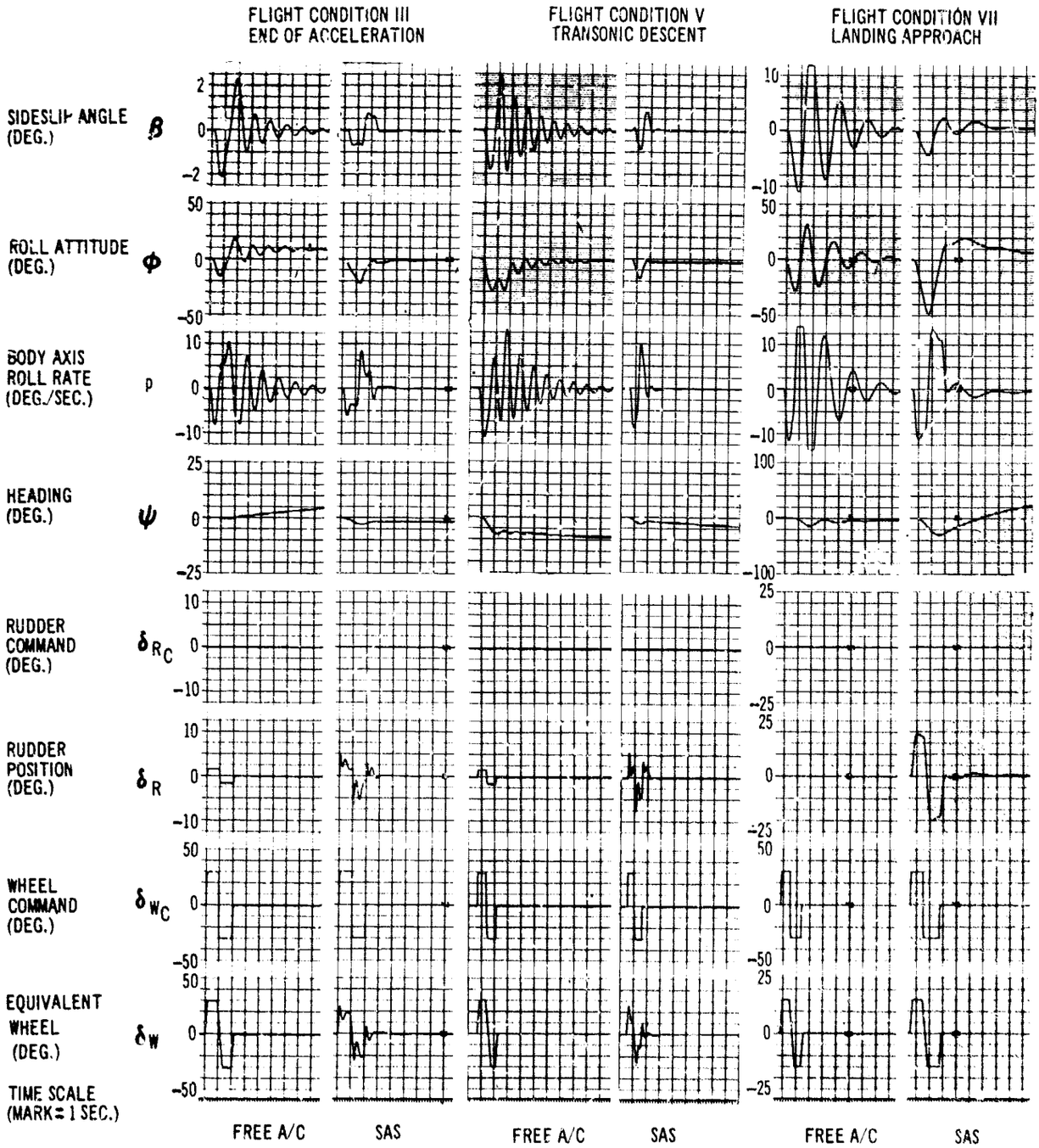


*Figure 5-24. Yaw Response in Abrupt Roll Maneuvers*

## SYMBOLS

### Coefficients and Derivatives

| | |
|---|---|
| $C_D$ | Drag coefficient, drag/qS |
| $C_h$ | Hinge moment coefficient, H. M. $/qS_c c_c$ |
| $C_L$ | Lift coefficient, Lift/qS |
| $C_l$ | Rolling moment coefficient, rolling moment/qSb |
| $C_m$, $C_M$ | Pitching moment coefficient, pitching moment/qSc |
| $C_n$ | Yawing moment coefficient, yawing moment/qSb |
| $C_Y$ | Side-force coefficient, side force/qS |
| $C_{h_\alpha}$ | Hinge moment coefficient due to angle of attack, $\partial C_h/\partial\alpha$ |
| $C_{h_\delta}$ | Hinge moment coefficient due to surface deflection, $\partial C_h/\partial\delta$ |
| $C_{L_\alpha}$ | Lift-curve slope, $\partial C_L/\partial\alpha$ |
| $C_{L_\delta}$ | Lift coefficient due to surface deflection, $\partial C_L/\partial\delta$ |
| $C_{l_\beta}$ | Effective dihedral derivative, $\partial C_l/\partial\beta$ |
| $C_{l_\delta}$ | Roll control power derivative, $\partial C_l/\partial\delta$ |
| $C_{l_p}$ | Rolling moment coefficient due to rolling velocity, $\partial C_l/\partial(pb/2V)$ |
| $C_{l_r}$ | Rolling moment coefficient due to yawing velocity, $\partial C_l/\partial(rb/2V)$ |
| $C_{m_\alpha}$ | Static longitudinal stability derivative, $\partial C_m/\partial\alpha$ |
| $C_{m_{\dot\alpha}}$ | Pitching moment coefficient due to angle-of-attack rate $\partial C_m/\partial(\dot\alpha c/2V)$ |
| $C_{m_\delta}$ | Pitch control power derivative, $\partial Cm/\partial\delta$ |
| $C_{m_q}$ | Pitching moment coefficient due to pitching velocity, $\partial C_m/\partial(qc/2V)$ |
| $C_{n_\beta}$ | Static directional stability derivative, $\partial C_n/\partial\beta$ |
| $C_{n_\delta}$ | Yawing moment coefficient due to surface deflection, $\partial C_n/\partial\delta$ |
| $C_{n_p}$ | Yawing moment coefficient due to rolling velocity, $\partial C_n/\partial(pb/2V)$ |

| | |
|---|---|
| $C_{n_r}$ | Yawing moment coefficient due to yawing velocity, $\partial C_n / \partial (rb/2V)$ |
| $C_{Y_\beta}$ | Side-force derivative, $\partial C_Y / \partial \beta$ |
| $C_{Y_\delta}$ | Side-force coefficient due to surface deflection, $\partial C_Y / \partial \delta$ |
| $C_{Y_p}$ | Side-force coefficient due to rolling velocity, $\partial C_Y / \partial (pb/2V)$ |
| $C_{Y_r}$ | Side-force coefficient due to yawing velocity, $\partial C_Y / \partial (rb/2V)$ |
| $\dot{h}$ | Rate of change of altitude |
| $\dot{\delta}$ | Rate of change of surface deflection |
| $\dot{\theta}$ | Pitch rate, $d\theta/dt$ |
| $\ddot{\theta}$ | Pitch acceleration, $\frac{d^2\theta}{dt}2$ |

## General

| | |
|---|---|
| a | Acceleration |
| a.c. | Aerodynamic center |
| AR | Aspect ratio $b^2/S$ |
| b | Wing span |
| BSWT | Boeing supersonic wind tunnel |
| BTWT | Boeing transonic wind tunnel |
| c | Chord |
| $C_R$ | Reference chord: root chord at basic 72° sweep wing planform |
| $C_{1/2}$ | Cycles to half amplitude |
| C.G.; CG; cg | Center of gravity |
| db | Decibels |
| $F_s$ | Stick force, pounds |
| $f_n$ | Undamped natural frequency |
| g | Gravitational constant, 32.2 $fps^2$ |
| G.W. | Gross weight |
| H.M. | Control surface hinge moment |
| h | Altitude |
| I | Moment of inertia, slug-$feet^2$ |

| | |
|---|---|
| K | Control surface effectiveness parameter |
| $K_{bB}$ | Body aeroelastic factor |
| LE | Leading edge |
| $L_E/L_R$ | Aerodynamic surface aeroelastic factor |
| M | Mach number, moment |
| $M_E/M_R$ | Aerodynamic surface aeroelastic factor |
| $M_D$ | Mach number, dive placard |
| $M_{MO}$ | Mach number, maximum operating |
| n | Load factor, g's |
| $n_{z_\alpha}$ | Change in load factor per degree of angle of attack |
| N. P. | Neutral point |
| P | Damped period, pressure |
| PNdb | Perceived noise, decibels |
| p | Rolling velocity |
| q | Dynamic pressure, pitching velocity |
| $q_c$ | Compressible dynamic pressure |
| r | Yawing velocity, rotation |
| $R_E/R_R$ | Aerodynamic surface aeroelastic factor |
| S | Area |
| s | Laplace operator |
| SAS | Stability augmentation system |
| SST | Supersonic transport |
| TE | Trailing edge |
| UWAL | University of Washington Aeronautical Laboratory |
| V | Velocity |
| $V_{APP}$ | Velocity during landing approach |
| $V_D$ | Velocity at dive placard |
| $V_e$ | Equivalent airspeed |
| $V_{LOF}$ | Liftoff speed |
| $V_{LNDG}$ | Velocity at touchdown |
| $V_{MC}$ | Minimum control velocity |
| $V_{MCG}$ | Minimum control speed with critical engine failed, on ground |

| | |
|---|---|
| $V_{MO}$ | Maximum operating velocity |
| $V_{MU}$ | Minimum unstick velocity |
| $V_P$ | Path velocity |
| $V_R$ | Velocity at start of rotation |
| $V_S$ | Velocity at stall |
| $\bar{V}_H$ | Horizontal tail volume coefficient, $\frac{l_H S_H}{\bar{c} S_W}$ |
| $\bar{V}_v$ | Vertical tail volume coefficient, $\frac{l_V S_V}{b S_W}$ |
| $\bar{V}_u$ | Ventral volume coefficient, $\frac{l_{VEN} S_{VEN}}{b S_W}$ |
| $V_2$ | Takeoff speed at 35 feet height above runway, with critical engine failed |
| $V_{35}$ | Takeoff speed at 35 feet height, all engines operating |
| $\alpha$ | Angle of attack of horizontal reference line |
| $\beta$ | Sideslip angle |
| $\Delta$ | Increment |
| $\delta$ | Surface deflection |
| $\zeta$ | Damping ratio |
| $\theta$ | Angle between the horizontal reference line and the horizon, panel slope |
| $\Lambda_{LE}$; $\wedge$ | Leading edge sweep angle |
| $\lambda$ | Taper ratio, $c_t/c_r$ |
| $\rho$ | Air density |
| $\sigma$ | Density ratio, $\rho_h/\rho_o$ |
| $\tau$ | Time constant |
| $\phi$ | Roll angle |
| $\psi$ | Yaw angle |
| $\omega_\phi$ | Undamped natural frequency derived from the numerator of the bank angle to aileron transfer function |
| $\omega_d$ | Dutch roll undamped natural frequency |

## Subscripts

| | |
|---|---|
| a | Aileron |
| aux. | Auxiliary |
| B | Body |
| c | Control column; control surface |
| d | Dutch roll |
| E | Elastic |
| f | Flap |
| H | Horizontal stabilizer |
| ILS | Instrument landing system |
| MAX | Maximum |
| O | Reference; free stream; at zero lift |
| P | Phugoid |
| r | Rudder, root |
| R | Rigid, reference |
| S | Stall |
| s | Spoiler |
| ss | Steady state |
| S.P. | Short period |
| t | Tip |
| T | Tail |
| trim | Trim condition |
| V | Vertical |
| VEN | Ventral |
| w | Wing; wheel |
| XX, YY, ZZ, XZ | Moment of inertia axis designation |
| z | Along z -axis |

Other nomenclature is defined in text.

## REFERENCES


1. FAA Letter to Mr. M. L. Pennell from Mr. Gordon Bain, "Sonic Boom Calculation Methods to be Used for Phase II-A Evaluation", September 8, 1964

2. Boeing Document, D6A10368-1, Aerodynamic Smoothness and Alignment Requirements, Vents, and Protuberances, 1966

3. Commercial Supersonic Transport Program, Phase II-A Comprehensive Report, The Boeing Company, Volume V-A, Book 1, Aerodynamics

4. Jay Fox, "Surface Pressure and Turbulent Airflow in Transverse Rectangular Notches", NASA TN D-2501, November 1964

5. R. L. Roensch, Investigation of Skin Friction Drag on Practical Construction Surfaces for Supersonic Transport, Douglas Aircraft Company, FDL-TDR 64-74, August 1964

6. John B. Peterson Jr. and Albert L. Braslow, "Implications of the Effects of Surface Temperature and Imperfections on Supersonic Operations", NASA SP-83, May 1965, pp. 227-233

7. K. R. Czarnecki, "The Problem of Roughness Drag at Supersonic Speeds", NASA SP-124, May 1966, pp. 455-468

8. A. R. Vick, An Investigation to Determine the Discharge and Thrust Characteristics of Auxiliary-Air Outlets for Stream Mach Number of 3.25, NASA TN D-1478, October 1962

9. P. E. Dewey and A. R. Vick, An Investigation of the Discharge and Drag Characteristics of Auxiliary-Air Outlets Discharging into a Transonic Stream, NACA TN 3466, July 1955

10. D. C. Anderson, Efficiency of Flush and Protruding Oblique Exhaust Nozzles with and without External Flow, United Aircraft Corp., Report R-0955-22, October 1957

11. J. E. Broadwell, "Analysis of the Fluid Mechanics of Secondary Injection for Thrust Vector Control", AIAA Journal, Vol. 1, No. 5, May 1963

12. J. E. Broadwell, "Correlation of Rocket Nozzle Gas Injection Data", AIAA Journal, Vol. 1, No. 8, August 1963

13. J. J. Janos, Loads Induced on a Flat Plate Wing by an Air Jet Exhausting Perpendicularly Through the Wing and Normal to a Free Stream Flow, NASA TN D-649, March 1961

14. W. E. Stoney, Collection of Zero-Lift Drag Data on Bodies of Revolution from Free Flight Investigations, NACA TN 42-1, January 1958

15. Nash, Quincey, and Callihan, Experiments on Two-Dimensional Base Flow at Subsonic and Transonic Speeds, ARC 25 070, January 1963

16. F. A. Woodward, A Method of Optimizing Camber Surfaces for Wing-Body Combinations at Supersonic Speeds - Theory and Applications, D6-10741, The Boeing Company, prepared under NASA Contract NASA-2282, October 1965

17. S. Lampert, Some Applications of Conical Flow Methods to Subsonic Lifting Surface Problems, NACA TN 2262, 1950

18. H. Carlson and W. Middleton, A Numerical Method of Estimating and Optimizing the Supersonic Aerodynamic Characteristics of Wings of Arbitrary Planform, AIAA Preprint No. 64-590, August 1964

19. A. L. Courtney, "A Collection of Data on Lift-Dependent Drag of Uncambered Slender Wings at Supersonic Speeds", Aeronautical Research Council Current Paper, C.P. 757, 1964

20. W. P. Henderson, "Studies of Various Factors Affecting Drag Due to Lift at Subsonic Speeds", NASA SP-124, May 1966, pp. 327-339

21. G. B. Whitham, "The Flow Pattern of a Supersonic Projectile", Communications on Pure and Applied Mathematics, Vol. V, pp. 301 to 348, 1952

22. Royal Aeronautical Society Data Sheets, Vol. IV

23. Tentative Airworthiness Standards for Supersonic Transports, Federal Aviation Agency, Flight Standards Service, November 1, 1965

24. Roy V. Harris Jr., "A Numerical Technique for Analysis of Wave Drag at Lifting Conditions", NASA SP-124, May 1966, pp. 399-409

25. John B. Peterson Jr. and William J. Monta, "Considerations Regarding the Evaluation and Reduction of Supersonic Skin Friction", NASA SP-124, May 1966, pp. 437-455

26. Report No. NADC-ED-6282, Proposal for Revised Military Specification, "Flying Qualities of Piloted Airplanes" (MIL-F-8785ASG), with Substantiating Test, Bureau of Naval Weapons

27. "Design Objectives for Flying Qualities of Civil Transport Aircraft," ARP 842, Society of Automotive Engineers

28. USAF Stability and Control Handbook (DATCOM)

29. USAF Stability and Control Handbook (M-03671)

30. B. Etkin, Dynamics of Flight, John Wiley and Sons, 1959

31. Bruce R. Wright and Benjamin J. Averett, Transonic Aerodynamic Damping and Oscillatory Stability in Yaw and Pitch for a Model of a Variable Sweep Supersonic Transport Airplane, NASA TM X-1207, March 1966

32. C. J. W. Meles and K. B. Bridgman, "Measurements of the Direct Pitching Oscillation Derivatives for Three Cropped Delta and Three Arrowhead Planforms at Subsonic and Transonic Speeds," British R & M No. 3397, 1965

33. R. Middleton, R. R. Larson, and J. Waddell, Crosswind Landings, The Boeing Company, D6-11455

34. Lawrence D. Guy, and Hoyt V. Brown, "Effects of an Inset Tab on the Hinge-Moment and Effectiveness Characteristics of an Unswept Trailing-Edge Control on a 60° Delta Wing at Mach Numbers from 0.75 to 1.96," NACA RM L54K16a, February 1955

35. Douglas R. Lord and K. R. Czarnecki, "Hinge-Moment Characteristics for a Series of Controls and Balancing Devices on a 60° Delta Wing at Mach Numbers of 1.61 and 2.01," NACA RM L57B01, April 1957

36. William C. Martz, James D. Church, and John W. Goslee, "Rocket-Model Investigation to Determine the Force and Hinge-Moment Characteristics of a Half-Delta Tip Control on a 56° Sweptback Delta Wing Between Mach Numbers of 0.55 and 1.13," NACA RM L52H06, January 1952

37. David G. Stone, "Recent Data on Controls," NACA RM L52A10, January 1952

# APPENDIX A

## CONFIGURATION DESCRIPTION

The geometric and basic weight data required to determine aerodynamic characteristics of the configuration are presented in this Appendix.

### Geometric Data


| | | |
|---|---|---|
| General Arrangement Drawing | Fig. A-1 | 285 |
| Wing Planform | Fig. A-2 | 287 |
| High Lift Devices | Fig. A-3 | 289 |
| M 1.0 Area Plot, GE | Fig. A-4 | 291 |
| M 1.0 Area Plot, P&WA | Fig. A-5 | 292 |
| Wing Section Definition at Various Leading Edge Sweep Angles | Fig. A-6 | 293 |
| Wing Geometry | Table A-A | 294 |
| Airfoil Ordinates, Leading Edge Sweep, 72 Degrees | Table A-B | 295 |
| Airfoil Ordinates, Leading Edge Sweep, 42 Degrees | Table A-C | 297 |
| Airfoil Ordinates, Leading Edge Sweep, 30 Degrees | Table A-D | 298 |
| High Lift Devices | Table A-E | 299 |
| Lateral Control Surfaces | Table A-F | 301 |
| Horizontal Stabilizer | Table A-G | 302 |
| Vertical Tail and Rudder | Table A-H | 303 |


### Weight Data


| | | |
|---|---|---|
| Design Weights | Table A-I | 304 |
| Moment of Inertia, Pitch and Yaw | Fig. A-7 | 305 |
| Moment of Inertia, Roll and Product | Fig. A-8 | 306 |

# DATA MODEL B-2707

| | G.E. | P&WA |
|---|---|---|
| POWER PLANTS (4) | G.E. 4/J5P | JTF 17A-21B |
| TOTAL ENGINE AIRFLOW | 2480 LBS/SEC | 2748 LBS/SEC |
| MAX. DESIGN TAXI WEIGHT | 675,000 LBS | 675,000 LBS |
| NOMINAL PAYLOAD | 50,000 LBS | 50,000 LBS |
| OPERATIONAL EMPTY WEIGHT | 287,500 LBS | 285,000 LBS |
| FUEL | 374,700 LBS | 374,700 LBS |

| | |
|---|---|
| MAIN GEAR | 16 - 45 x 19.2 TIRES TYPE VIII |
| NOSE GEAR | 2 - 34 x 16 TIRES TYPE VIII |
| MAX. DESIGN TAXI WEIGHT C.G. - LIMITS, GEAR DOWN | |
| MOST FORWARD C.G. | 59.5% REF. LENGTH - WINGS FWD |
| MOST AFT C.G. | 64.0% REF. LENGTH - WINGS AFT |

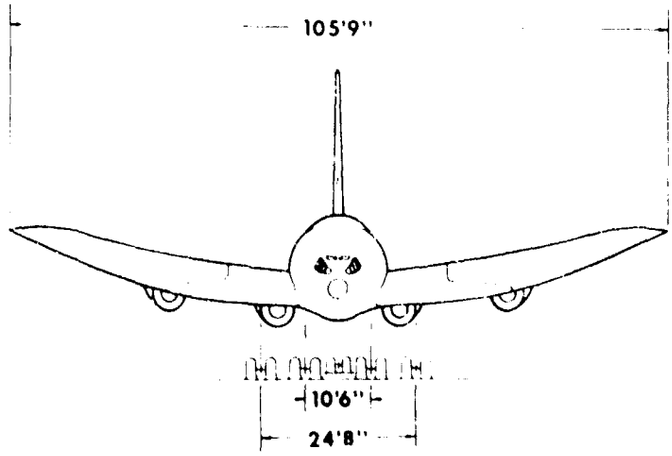


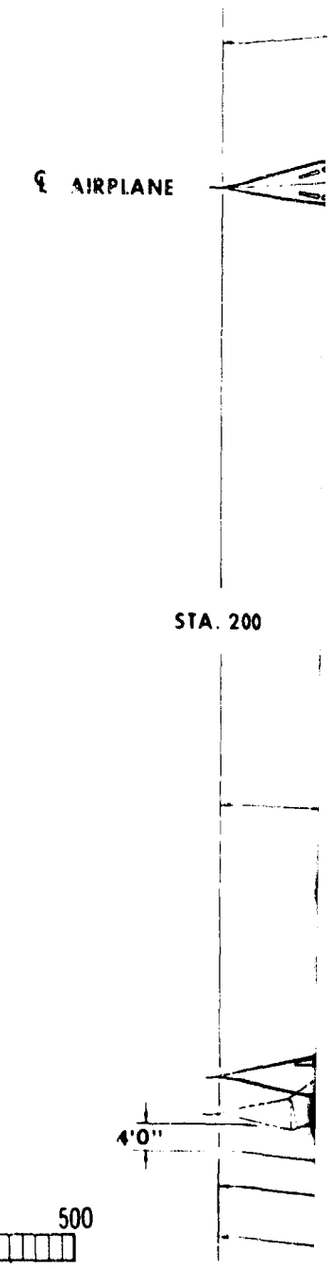


0 250 500

SCALE (INCHES)

&WA

A-21B

S/SEC

00 LBS

00 LBS

00 LBS

00 LBS

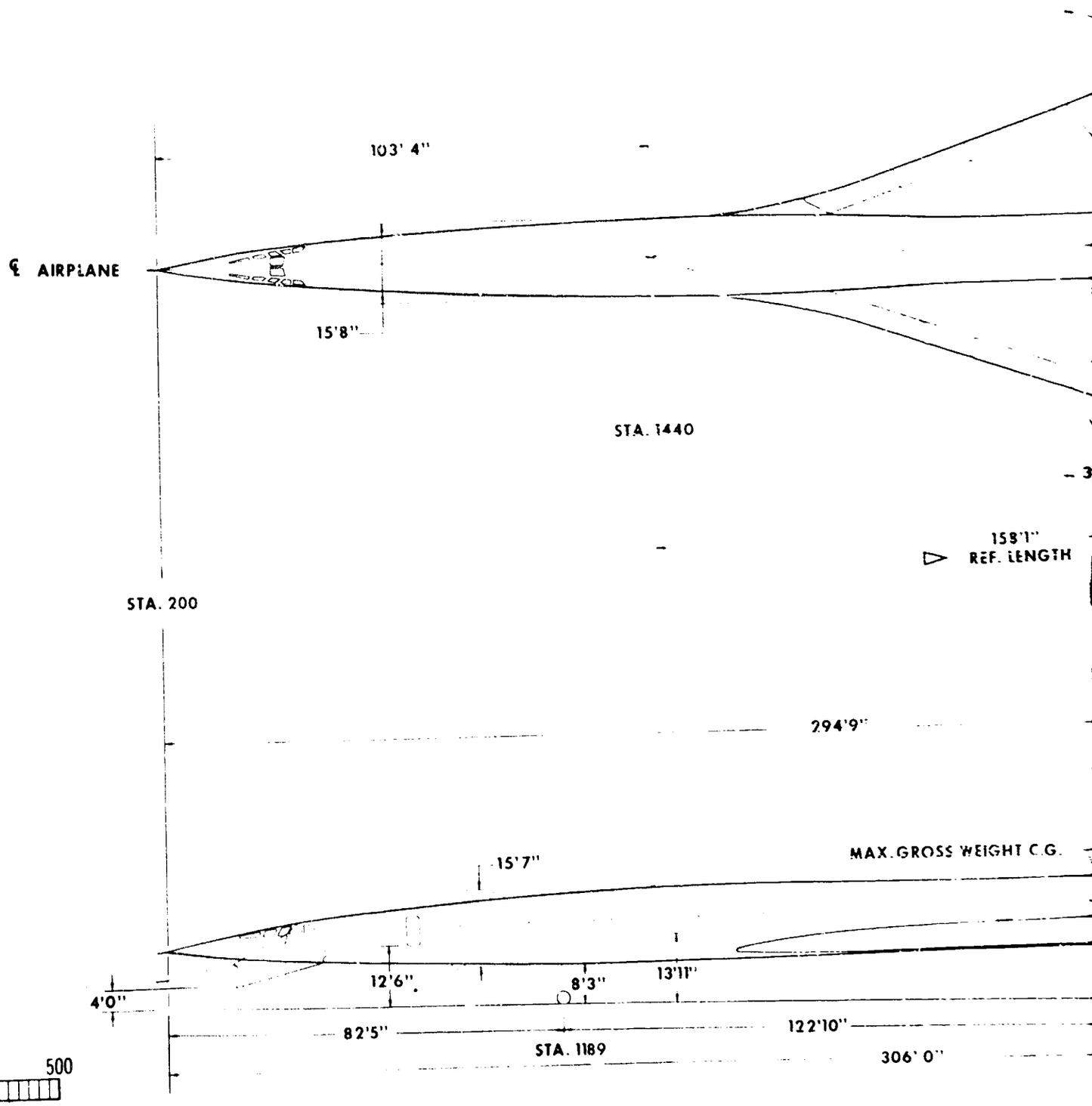


250 500

SCALE (INCHES)

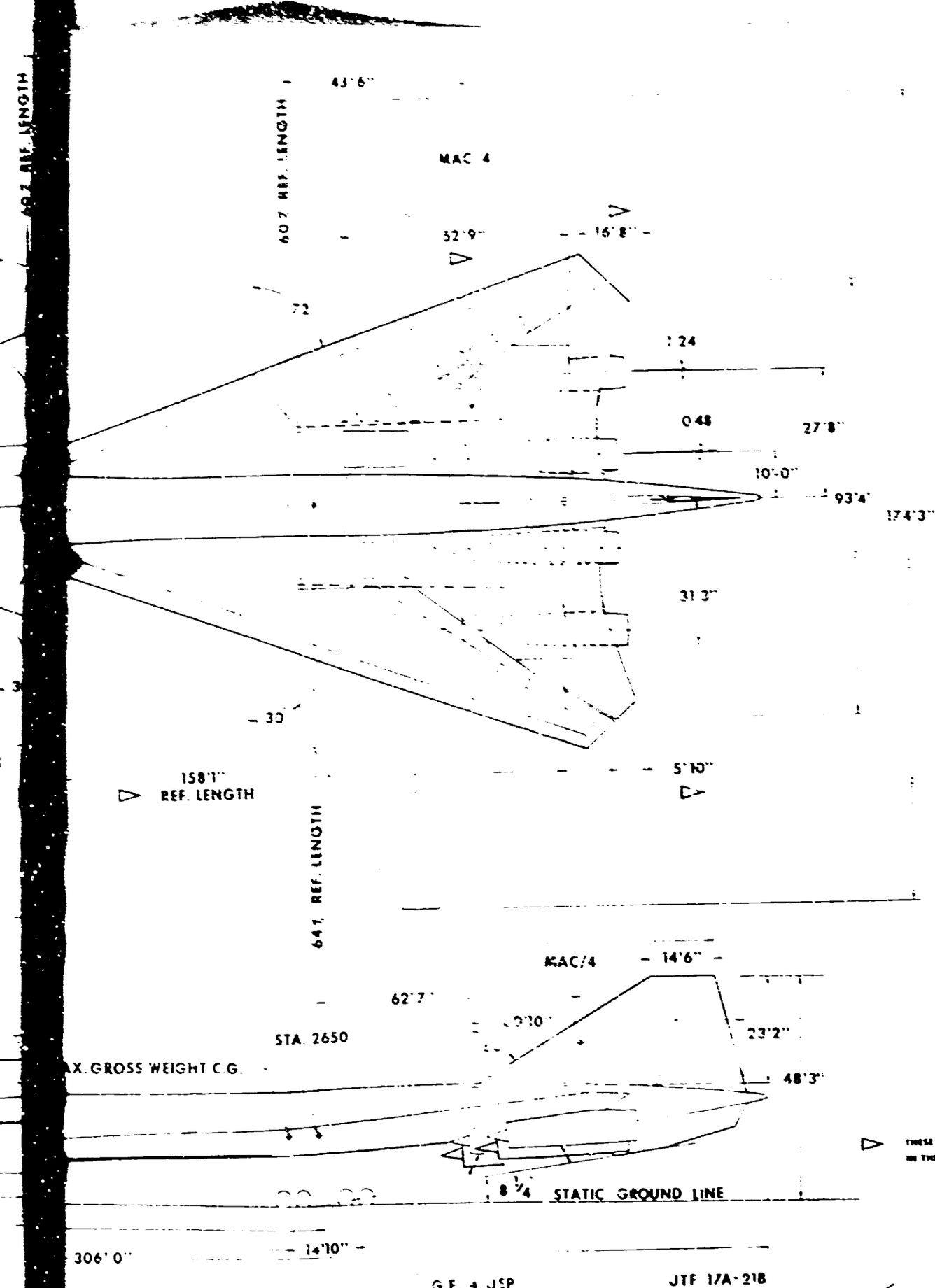


*Figure A-1. General Arrangement Model B-2707*

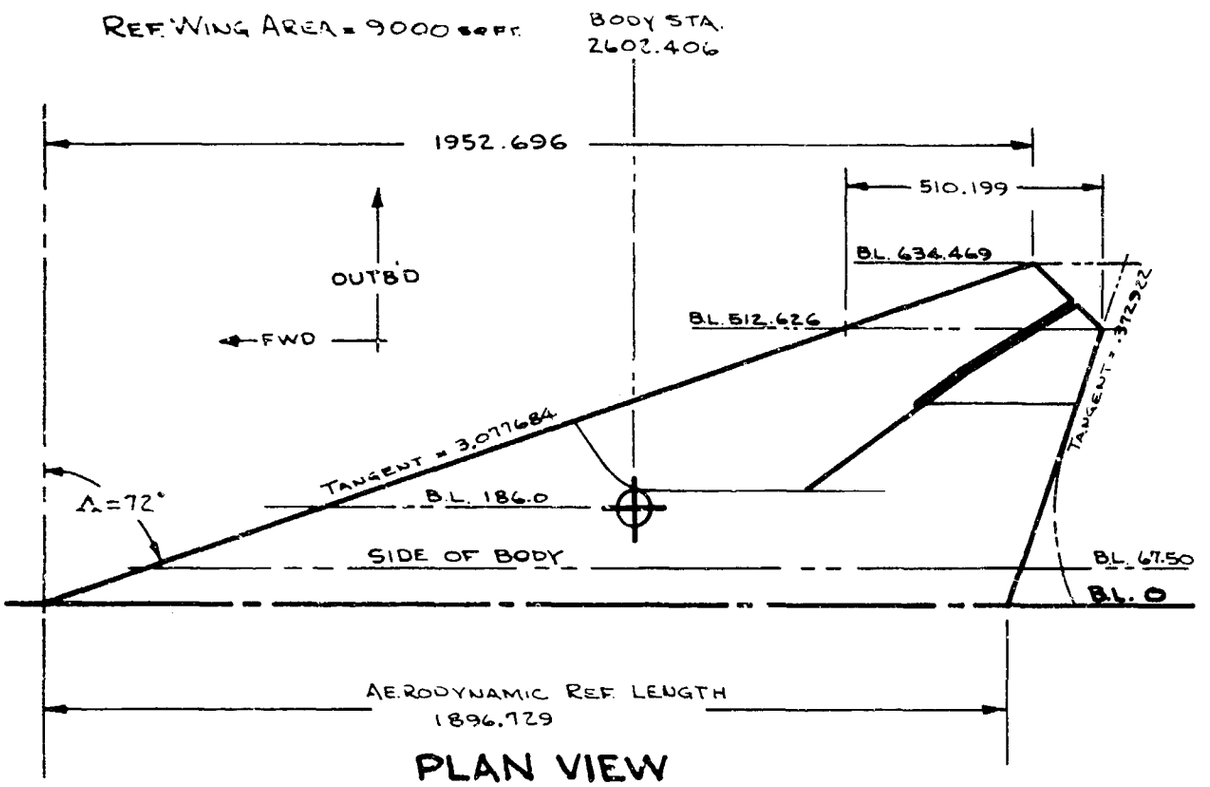


*Figure A-2. Wing Planform*

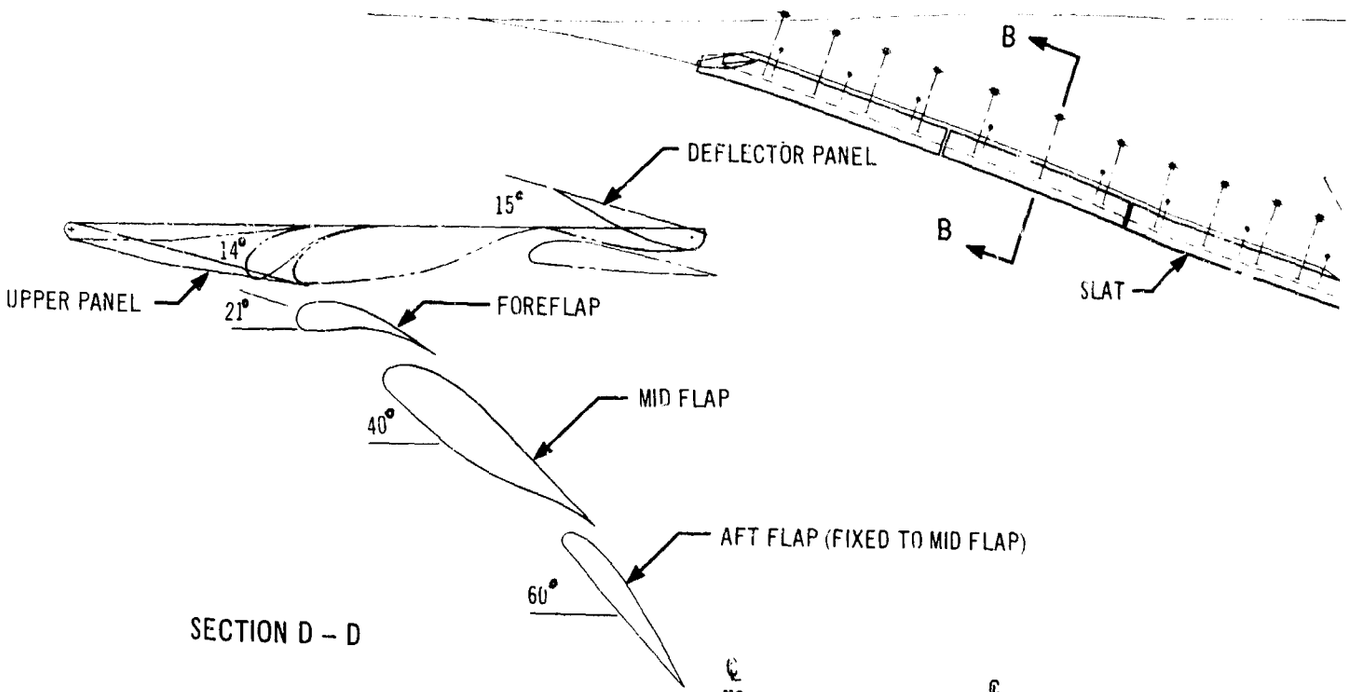


SECTION D – D

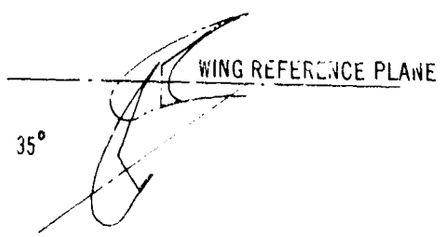


SECTION B – B

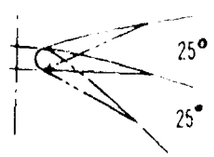


SECTION A – A

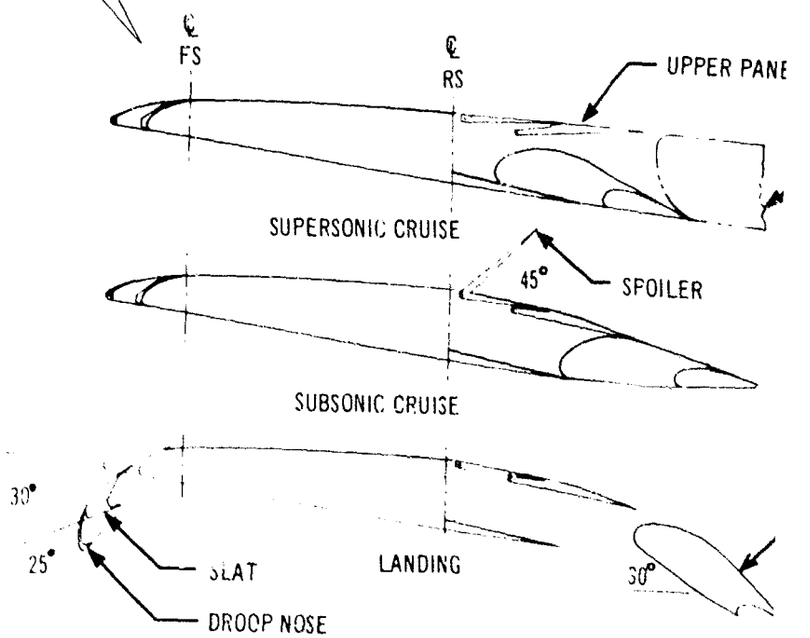


SECTION C – C

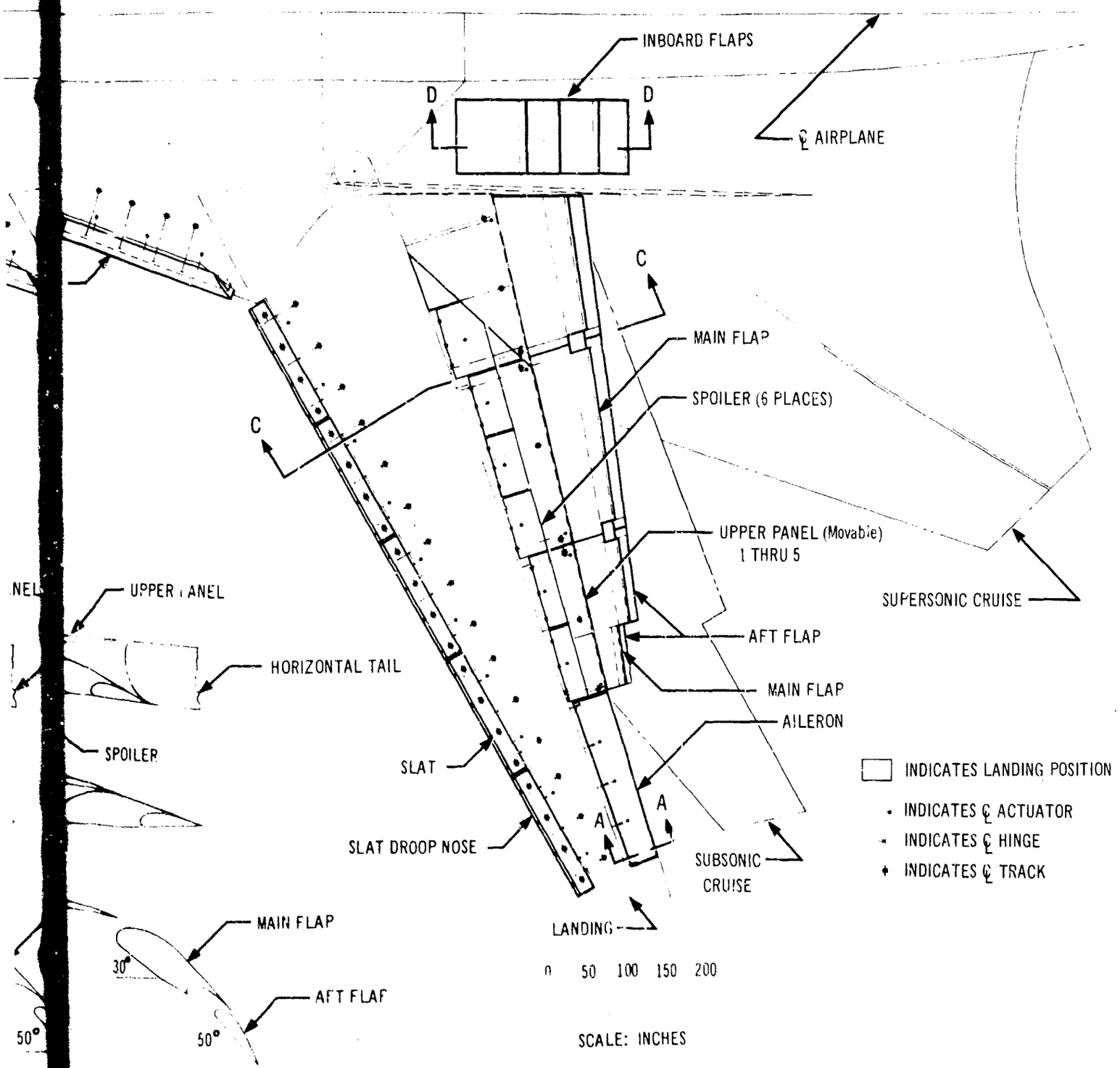


*Figure A–3. High Lift Devices*

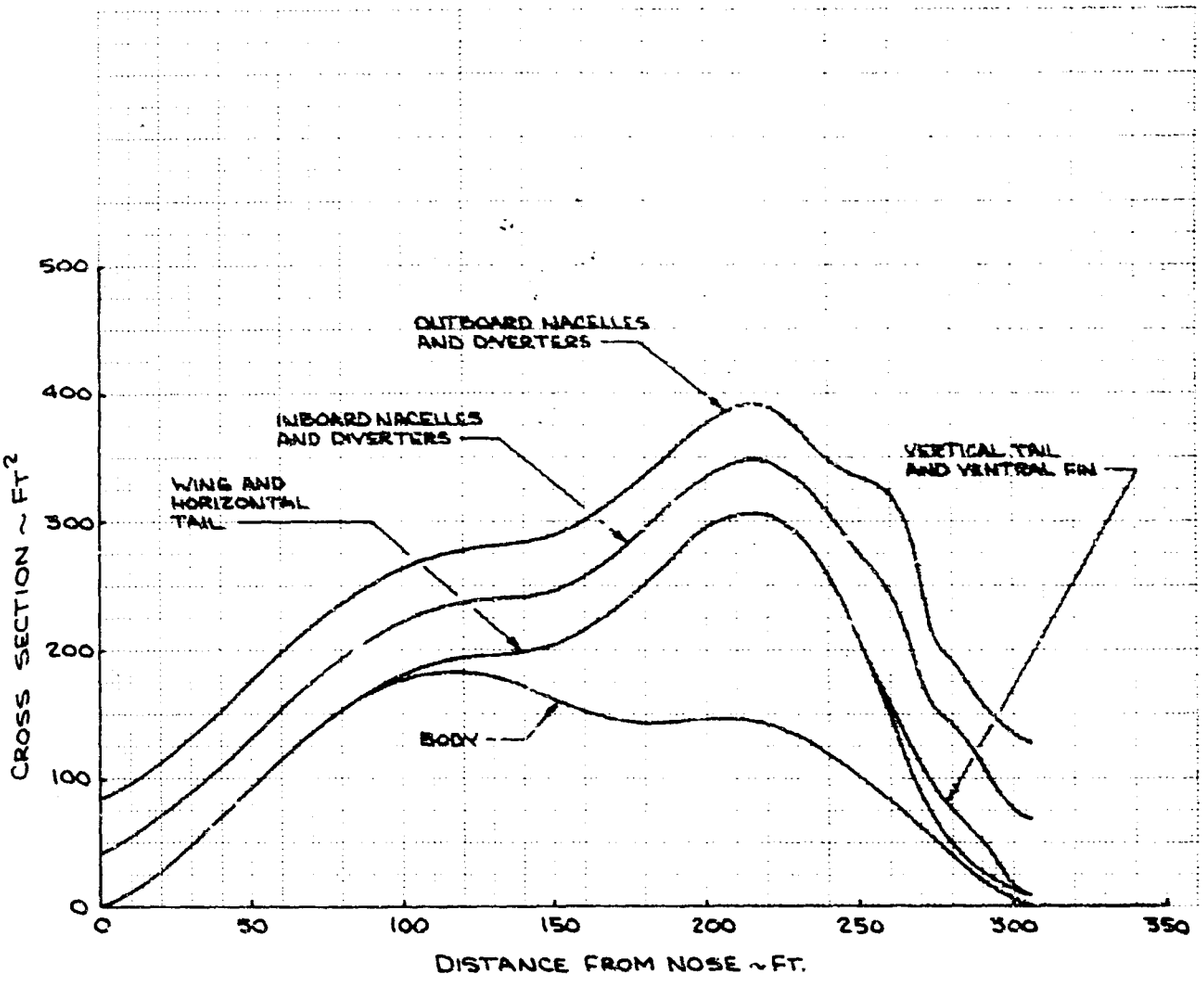


*Figure A-4. M 1.0 Area Plot - G E*

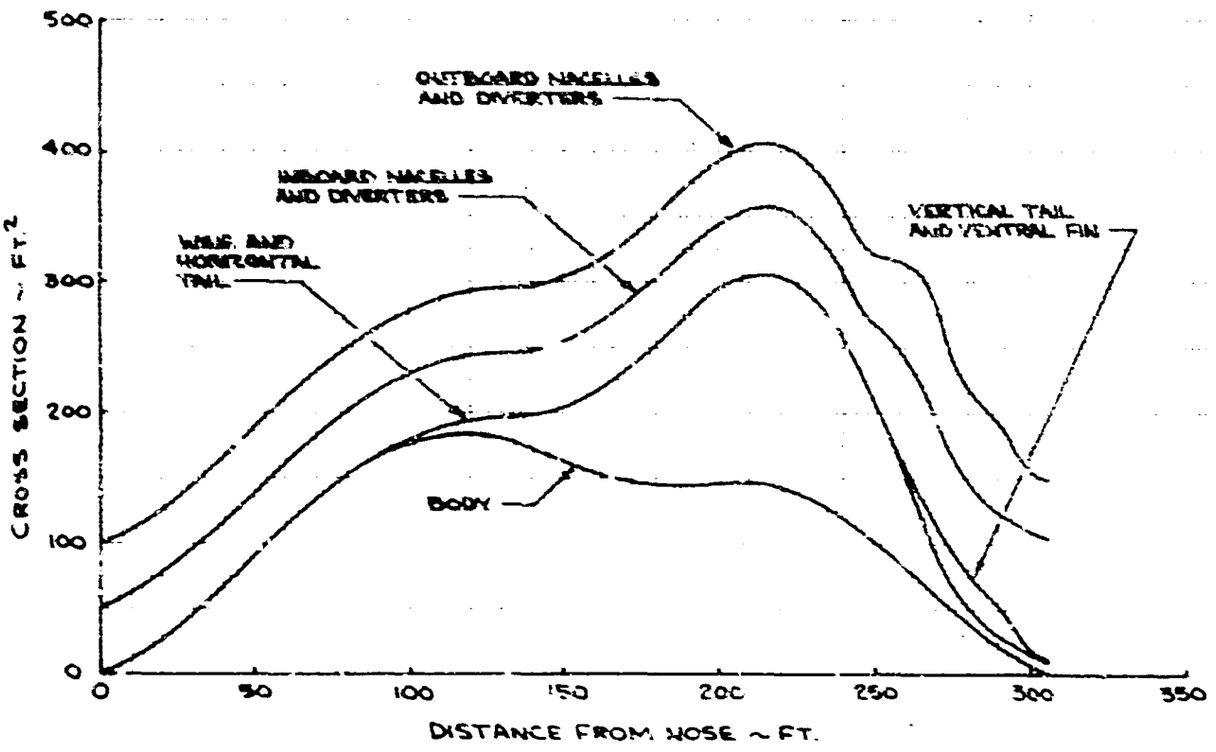


Figure A-5. M 1.0 Area Plot - P3WA

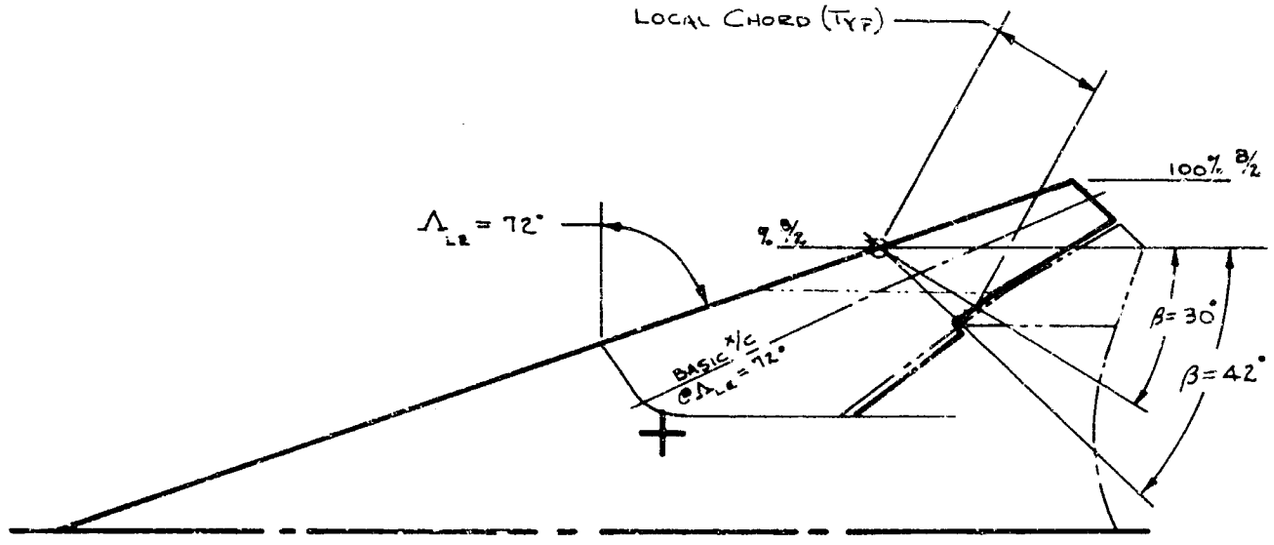


| L.E. Sweep | $\beta$ |
|---|---|
| 72° | 0° |
| 42° | 30° |
| 30° | 42° |

PIVOT AXIS NORMAL TO WING DESIGN PLANE.

*Figure A–6. Wing Section Definition at Various Leading Edge Sweep Angles*

*Table A-A. Wing Geometry*

| | |
|---|---|
| Reference wing area, $ft^2$ | 9000 |
| Aerodynamic reference length, ft (see Fig. A-2) | 158.06 |
| Leading edge sweep, degrees | $72^{o}00'$ |
| Aspect Ratio @ $\Lambda_{LE}$ = 72 degrees | 1.24 |
| Sweep @ 0.25 Chord | |
| Wing aft, degrees | $69^{o}58'$ |
| Dihedral, degrees | 0 |
| Angle of incidence of root chord to fuselage | |
| Ref. line (wing aft), degrees | $-0.718^{o}$ |
| Angle of incidence of chord @ 100% semi-span | |
| to fuselage ref. line (wing aft), degrees | $-4.958^{o}$ |
| Span, ft | |
| Wings aft | 105.74 |
| Wings fwd | 174.28 |

*Table A-B. Airfoil Ordinates – Leading Edge Sweep, 72 Degrees*

| | 10.6388 % B/2 Chord = 1804.8307 | | 18.6460 % B/2 Chord = 1636.8416 | | 29.3159 % B/2 Chord = 1422.9724 | | 47.3680 % B/2 Chord = 1086.4714 | |
|---|---|---|---|---|---|---|---|---|
| X/C % | Z/C % Upper | Z/C % Lower | Z/C % Upper | Z/C % Lower | Z/C % Upper | Z/C % Lower | Z/C % Upper | Z/C % Lower |
| 0 | 1.6095 | 1.6095 | 1.1514 | 1.1514 | 0.4384 | 0.4384 | -0.6233 | -0.6233 |
| 5 | 2.3177 | 0.9657 | 1.9390 | 0.6268 | 1.2752 | -0.0094 | 0.3087 | -0.9493 |
| 10 | 2.5265 | 0.7313 | 2.1771 | 0.3711 | 1.5697 | -0.1915 | 0.7308 | -1.0252 |
| 15 | 2.5902 | 0.4848 | 2.2073 | 0.0751 | 1.6873 | -0.4351 | 0.9775 | -1.1375 |
| 20 | 2.4700 | 0.1374 | 2.1068 | -0.2636 | 1.6646 | -0.7108 | 1.1109 | -1.2673 |
| 30 | 2.0040 | -0.5996 | 1.7482 | -0.8922 | 1.4420 | -1.2312 | 1.1598 | -1.5462 |
| 40 | 1.3862 | -1.3176 | 1.2121 | -1.5247 | 1.0479 | -1.7379 | 0.9940 | -1.8186 |
| 50 | 0.6494 | -2.0322 | 0.5560 | -2.1748 | 0.5439 | -2.2305 | 0.7594 | -2.0386 |
| 60 | -0.1230 | -2.6052 | -0.1179 | -2.6325 | -0.0070 | -2.5510 | 0.4399 | -2.1701 |
| 70 | -0.8632 | -2.9686 | -0.7618 | -2.8512 | -0.5656 | -2.6444 | 0.0422 | -2.1058 |
| 80 | -1.5736 | -3.0140 | -1.4540 | -2.8836 | -1.1441 | -2.5467 | -0.3878 | -1.8598 |
| 90 | -2.1824 | -2.8950 | -2.3887 | -3.0973 | -1.6577 | -2.3605 | -0.8295 | -1.5635 |
| 100 | -2.6999 | -2.6999 | -3.4415 | -3.4415 | -2.1100 | -2.1100 | -1.2469 | -1.2469 |

$\beta = 0^{o}$ (See Fig. A-6)

*Table A–B. (concluded)*

| | 51.6000 % B/2 Chord = 1012.4744 | | 59.1045 % B/2 Chord = 882.4438 | | 68.4204 % B/2 Chord = 468.3027 | | 88.9317 % B/2 Chord = 294.0694 | |
|---|---|---|---|---|---|---|---|---|
| X/C % | Z/C % Upper | Z/C % Lower | Z/C % Upper | Z/C% Lower | Z/C % Upper | Z/C % Lower | Z/C % Upper | Z/C % Lower |
| 0 | -0.6880 | -0.6880 | -0.8128 | -0.8128 | -0.4951 | -0.4951 | 5.5369 | 5.5369 |
| 5 | +0.2463 | -1.0133 | +0.1100 | -1.1469 | +0.5051 | -0.8145 | 6.6078 | 5.3820 |
| 10 | 0.6776 | -1.0784 | 0.5763 | -1.1759 | 1.0382 | -0.7964 | 7.2946 | 5.4594 |
| 15 | 0.9469 | -1.1667 | 0.8952 | -1.2161 | 1.4715 | -0.7342 | 7.7695 | 5.5626 |
| 20 | 1.0997 | -1.2773 | 1.0892 | -1.2815 | 1.7888 | -0.6888 | 8.1361 | 5.6565 |
| 30 | 1.1931 | -1.5065 | 1.2665 | -1.4237 | 2.2017 | -0.6389 | 8.7655 | 5.9228 |
| 40 | 1.0812 | -1.7284 | 1.2729 | -1.5232 | 2.4339 | -0.5517 | 9.2117 | 6.2239 |
| 50 | 0.0961 | -1.8877 | 1.2210 | -1.5549 | 2.5398 | -0.4557 | 9.4695 | 6.4726 |
| 60 | 0.6328 | -1.9694 | 1.0737 | -1.5022 | 2.5385 | -0.3366 | 9.8113 | 6.9355 |
| 70 | 0.2670 | -1.8670 | 0.7849 | -1.3109 | 2.4098 | -0.1060 | 9.9265 | 7.4101 |
| 80 | -0.3783 | -1.8341 | 0.3922 | -1.0215 | 2.1603 | +0.2436 | 9.9024 | 7.9855 |
| 90 | -1.1055 | -1.8317 | 0.0123 | -0.6916 | 1.7720 | 0.6940 | 9.7425 | 8.6643 |
| 100 | -1.8173 | -1.8173 | -0.3559 | -0.3559 | 1.2501 | 1.2501 | 9.4692 | 9.4692 |

$\beta = 0^{o}$ (See Fig.A-6)

*Table A-C. Airfoil Ordinates, Leading Edge Sweep, 42 Degrees*

| 59.2622 % B/2 Local Chord = 417.8800 | | | 68.4037 % B/2 Local Chord = 347.1133 | | | 90.6270 % B/2 Local Chord = 160.7600 | | | 95.3553 % B/2 Local Chord = 137.3333 | | |
|---|---|---|---|---|---|---|---|---|---|---|---|
| Local X/C % | Z/C % Upper | Z/C % Lower | Local X/C % | Z/C % Upper | Z/C % Lower | Local X/C % | Z/C % Upper | Z/C % Lower | Local X/C % | Z/C % Upper | Z/C % Lower |
| 0 | -1.7181 | -1.7181 | 0 | -0.6715 | -0.6715 | 0 | 11.2603 | 11.2603 | 0 | 16.8211 | 16.8211 |
| 4.7944 | +0.4482 | -2.3395 | 4.5523 | +0.9288 | -1.4423 | 5.5352 | 13.3603 | 10.5746 | 5.5353 | 18.8837 | 16.0618 |
| 9.8777 | 1.5504 | -2.4277 | 9.6448 | 1.7246 | -1.7641 | 9.3578 | 14.1108 | 10.4319 | 9.3578 | 19.6920 | 16.0185 |
| 13.4403 | 2.0377 | -2.5914 | 13.3893 | 2.1053 | -2.0412 | 15.3020 | 14.7317 | 10.1609 | 15.3021 | 20.4814 | 15.9141 |
| 21.0223 | 2.6470 | -3.0886 | 21.0223 | 2.8367 | -2.4654 | 19.4127 | 15.0605 | 10.0283 | 19.4126 | 20.8129 | 15.7873 |
| 29.2815 | 3.0549 | -3.5740 | 29.2815 | 3.2841 | -2.7900 | 28.0124 | 15.4930 | 9.8356 | 28.0125 | 21.2185 | 15.5620 |
| 38.3129 | 3.0653 | -4.2292 | 38.3129 | 3.1350 | -3.4280 | 41.9504 | 15.4389 | 9.3914 | 41.9504 | 21.3139 | 15.2664 |
| 48.2302 | 2.7281 | -5.0861 | 48.2302 | 3.0637 | -4.3795 | 52.0153 | 15.1853 | 9.1884 | 52.0151 | 21.2739 | 15.2808 |
| 59.1703 | 2.0569 | -5.9816 | 59.1704 | 2.7974 | -5.1972 | 62.7728 | 14.5165 | 9.0803 | 62.7730 | 20.8139 | 15.3849 |
| 71.3002 | 0.5908 | -6.4979 | 71.3002 | 1.5421 | -5.1828 | 68.4341 | 14.0463 | 9.1074 | 68.4343 | 20.4575 | 15.5245 |
| 77.8736 | -0.4901 | -6.3950 | 77.8736 | 0.5399 | -5.0651 | 80.3733 | 12.7347 | 9.2436 | 80.3734 | 19.3377 | 15.8568 |
| 92.1879 | -3.5099 | -5.9153 | 92.1879 | -2.4747 | -4.6099 | 93.2115 | 10.9394 | 9.5784 | 93.2115 | 17.5930 | 16.2405 |
| 100.000 | -5.4773 | -5.4773 | 100.0000 | -4.2629 | -4.2629 | 100.0000 | 9.8369 | 9.8369 | 100.0000 | 16.4991 | 16.4991 |

$\beta = 30^{0}$ (See Fig. A-6)

## Table A-D. Airfoil Ordinates, Leading Edge Sweep, 30 Degrees

| 59.2622 % B/2 Local Chord = 394.2800 | | | 68.4037 % B/2 Local Chord = 327.5066 | | | 90.6270 % B/2 Local Chord = 146.2800 | | | 100.0000 % B/2 Local Chord = 104.7400 | | |
|---|---|---|---|---|---|---|---|---|---|---|---|
| Local X/C % | Z/C % Upper | Z/C % Lower | Local X/C % | Z/C % Upper | Z/C % Lower | Local X/C % | Z/C % Upper | Z/C % Lower | Local X/C % | Z/C % Upper | Z/C % Lower |
| 0 | -1.8209 | -1.8209 | 0 | -0.7117 | -0.7117 | 0 | 12.3750 | 12.3750 | 0 | 26.9944 | 26.9944 |
| 4.3794 | +0.4680 | -2.5093 | 5.6896 | +1.2297 | -1.7034 | 5.2366 | 14.6153 | 11.5441 | 5.2354 | 29.0113 | 25.8479 |
| 9.0647 | 1.6587 | -2.6202 | 8.9291 | 1.7551 | -1.9865 | 10.7357 | 15.6491 | 11.2157 | 10.7348 | 30.3368 | 25.9040 |
| 15.8454 | 2.5819 | -3.0617 | 15.8454 | 2.5341 | -2.6345 | 14.5578 | 16.0003 | 10.9324 | 14.5565 | 30.9872 | 25.9292 |
| 19.4902 | 2.8751 | -3.3551 | 19.4902 | 2.9237 | -2.8923 | 18.5119 | 16.3137 | 10.7210 | 18.5112 | 31.3044 | 25.7266 |
| 31.6081 | 3.3980 | -4.2632 | 31.6081 | 3.5644 | -3.6447 | 31.2406 | 16.6938 | 10.1525 | 31.2396 | 31.7583 | 25.2175 |
| 40.8420 | 3.2330 | -5.1287 | 40.8421 | 3.3662 | -4.6155 | 40.5299 | 16.4373 | 9.6286 | 40.5287 | 31.7437 | 24.9355 |
| 51.1965 | 2.7354 | -6.2204 | 51.1965 | 3.1545 | -5.6508 | 50.5505 | 15.9763 | 9.1838 | 50.5503 | 31.7486 | 24.9631 |
| 62.8886 | 1.5519 | -7.0751 | 62.8886 | 2.2044 | -6.3985 | 61.3930 | 15.0103 | 8.8129 | 61.3926 | 31.2408 | 25.0581 |
| 69.3200 | 0.5534 | -7.3258 | 69.3201 | 1.3364 | -6.4399 | 67.1542 | 14.3539 | 8.7044 | 67.1537 | 30.8384 | 25.2018 |
| 83.5628 | -2.3868 | -7.3506 | 83.5629 | -1.4726 | -6.3250 | 79.4320 | 12.5847 | 8.5609 | 79.4320 | 29.5072 | 25.5068 |
| 91.4766 | -4.4537 | -7.2823 | 91.4766 | -3.5071 | -6.2060 | 92.8311 | 10.2446 | 8.6618 | 92.8311 | 27.3473 | 25.7847 |
| 100.0000 | -6.8044 | -6.8044 | 100.0000 | -5.9412 | -5.9412 | 100.0000 | 8.8191 | 8.8191 | 100.0000 | 25.9865 | 25.9863 |

$\beta = 42^{\circ}$ (See Fig. A-6)

*Table A-E. High Lift Devices*

| Buttock lines and percent chord are streamwise to 30 degrees, leading edge | | |
|---|---|---|
| Outboard Flaps | Landing & T/O ($30^{o}$ LE) | Subsonic Cruise ($42^{o}$ LE) (Streamlining Only) |
| Distance from centerline airplane (to trailing edge) | | |
| To inboard edge, ft | 18.3 | -- |
| To outboard edge, ft | 68.2 | -- |
| Maximum deflection (main/auxiliary) | $30/50^{o}$ | $0^{o}$ (20% wing chord extend) |
| Takeoff deflection | As required | $0^{o}$ |
| Chord, % wing chord | 30 | 20 |
| Percent wing area affected (2,245 $ft^2$) | 57 | -- |
| Area, $ft^2$ (total) | 684 | -- |
| Strake Flaps | | |
| Distance from ℄ airplane | | |
| To inboard edge, ft | 8.5 | -- |
| To outboard edge, ft | 16.0 | -- |
| Maximum deflection (fore, main/aft) | $20^{o}$, $40^{o}$ & $60^{o}$ | 0 |
| Area, $ft^2$ (total) | 210 | -- |
| Chord, % wing & strake chord | $15^{o}$ | -- |
| Strake & wing area affected | 1200 $ft^2$ | -- |

*Table A-E. ( concluded )*

| Leading Edge Slats | Wing | Strake |
|---|---|---|
| Distance from ℄ airplane (to leading edge) | | |
| To inboard edge, ft | 28.8 | 10.8 |
| To outboard edge, ft | 87.2 | 28.0 |
| Chord, ft | 3.0 | 4.0 |
| Area, $ft^2$ (total) | 393 | 420 |
| Takeoff deflection | $20^o/37.5^o$ | $35^o$ |
| Landing deflection | $20^o/37.5^o$ | $35^o$ |

*Table A-F. Lateral Control Surfaces*

| | |
|---|---|
| Aileron (subsonic only) | |
| Area, ft $^2$ | 120 |
| Span, ft | 17.2 |
| Chord, percent | 34 |
| Deflection | |
| Down | 25$^o$ |
| Up | 25$^o$ |
| Spanwise location from ℄ airplane | |
| Inboard edge - ft | 68.2 |
| Outboard edge - ft | 84.5 |
| Spoilers | |
| Area, ft $^2$ (total) | 236 |
| Chord, ft | 4.3, 3.0, 2.0 |
| Span, ft (along hinge line) | 12.1, 18.8, 15.3 |
| Spanwise loc, from ℄ airplane | 41.3 |
| Inboard edge - ft | 29.1 |
| Outboard edge - ft | 68.2 |
| Deflection | 45$^o$ |
| Elevons (supersonic only) | |
| See horizontal tail for specification. | |

*Table A–G. Horizontal Stabilizer*

| Horizontal tail | Wings out | | | |
|---|---|---|---|---|
| Area (exposed), ft $^2$ | 2478 | | | |
| Span (total), ft | 95.2 | | | |
| Aspect ratio | 3.52 | | | |
| Taper ratio | 0.15 | | | |
| Leading edge sweep angle | 55°/60° | | | |
| MAC ft | 36.4 | | | |
| Location of LEMAC from leading edge root, ft | 21.9 | | | |
| Dihedral angle (effective) | +7.5° | | | |
| **Pitch control** | **Inboard auxiliary** | | **Outboard auxiliary** | |
| | **Stabilizer** | **Stabilizer** | **Stabilizer** | **Elevon** |
| Area, ft $^2$ (893 ft $^2$ total) | 211 | 149 | 111 | 422 |
| Chord, % stabilizer chord (ave) | 23 | 30 | 30 | 100 |
| Dist. from ℄ airplane | | | | |
| To inboard edge, ft | 13.0 | 6.0 | 23.8 | 31.0 |
| To outboard edge, ft | 23.8 | 13.0 | 31.0 | 46.7 |
| Deflection (max) | ±30° | +30°, -0° | +30°, -0° | ±30° |
| Airfoil section | --- | --- | --- | Modified double wedge |

Table A-H. Vertical Tail and Rudder

| | |
|---|---|
| Vertical Tail (exposed) | |
| Area, ft$^2$ | 573 |
| Span, ft | 25.2 |
| Taper ratio | 0.238 |
| Aspect ratio | 0.615 |
| Sweep 0.25c degrees | 39° |
| MAC, ft | 42.75 |
| Location of LEMAC | |
| From leading edge root, ft | 15.8 |
| From thrust line, ft (of outboard engine) | 27.7 |
| Airfoil section | Modified double wedge |
| Tail arm (measured from 0.64 wing ref length to 0.25 MAC Tail), ft | 62.58 |
| Rudder | |
| Area, ft$^2$ (30% total area) | 262.5 |
| Span, ft. | 23.9 |
| Chord, Avg ft (30%) | 11.6 |
| Deflection | ±25° |

*Table A-1. Design Weights*

| | GE (lb) | P & W (lb) |
|---|---|---|
| Maximum design taxi weight | 675,000 | 675,000 |
| Maximum design takeoff weight (flaps down) | 672,000 | 672,000 |
| Maximum design flt weight (flaps down) | 668,000 | 668,000 |
| Maximum design flt weight (flaps up) | 666,000 | 666,000 |
| Maximum design landing weight | 420,000 | 430,000 |
| Maximum zero fuel weight | 360,000 | 362,500 |
| Minimum flying weight | 310,000 | 314,000 |
| Operational empty weight | 285,000 | 287,500 |
| Manufacturer's empty weight | 274,250 | 276,750 |
| Max. usable fuel - pounds | 367,100 | 367,100 |
| Gallons at 6.7 lb/gal | 54,790 | 54,790 |

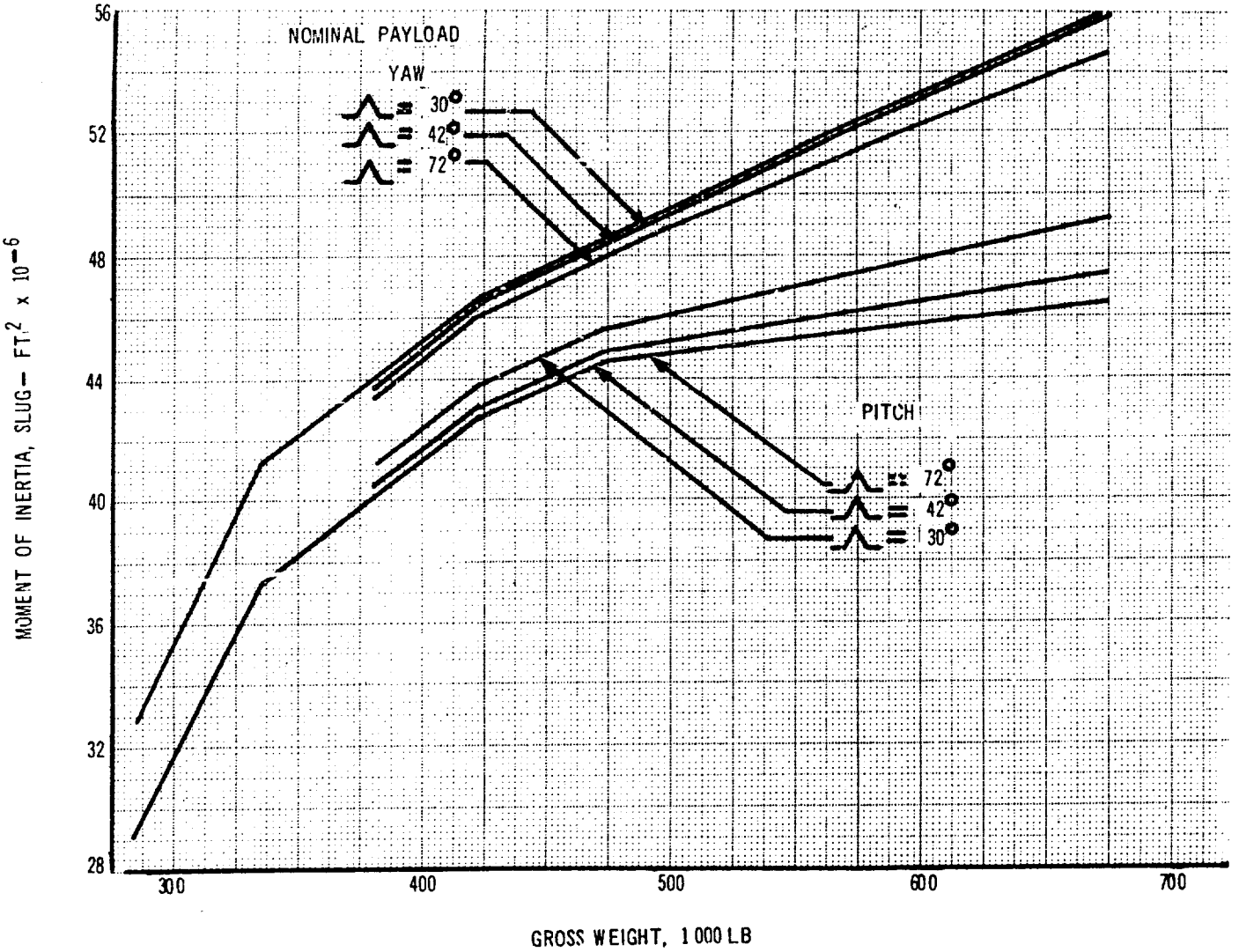


*Figure A–7. Moment of Inertia – Pitch and Yaw*

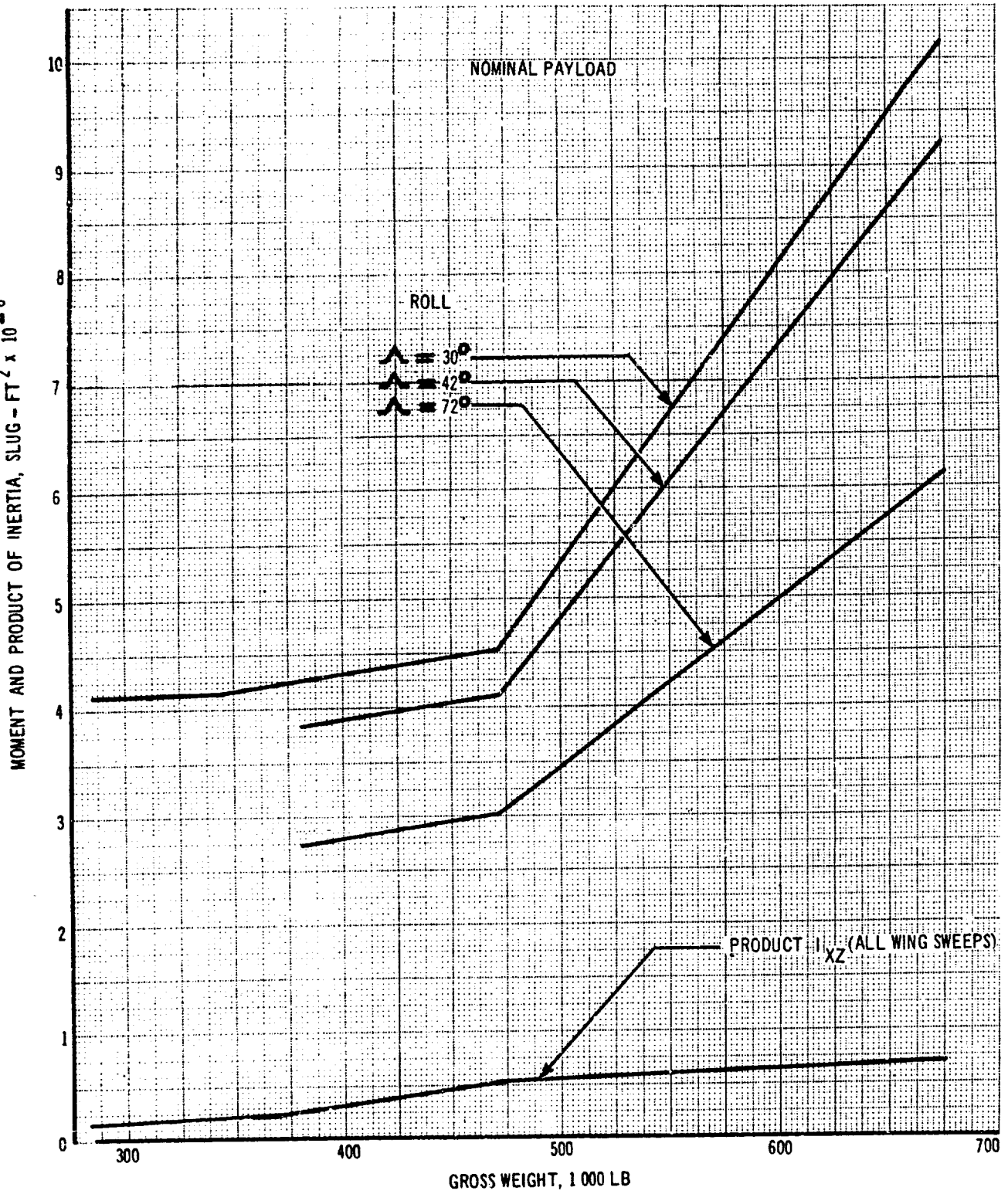


*Figure A-8. Moment of Inertia – Roll and Product*

# ADDENDUM

## SUMMARY REPORT - 8 AUGUST 1966 ENGINE PERFORMANCE DATA

The foregoing document is based upon engine performance data received prior to 15 July 1966.

Because there was insufficient time available to completely revise the B-2707 performance after receiving the 8 August 1966 firm technical engine data, the following summary is provided to show the major effect of the firm data on the airplane performance shown in the Phase III proposal documents. Only the most important figures have been provided herein.

If additional or supplemental data is needed, a request to The Boeing Company, SST Division, will receive immediate attention.

# APPENDIX B

## ADDENDUM

## AERODYNAMIC DESIGN

CONTENTS


| | | Page |
|---|---|---|
| 1.0 | INTRODUCTION AND SUMMARY | 1 |
| | 1.1 ENGINE DIFFERENCES | 1 |
| | 1.2 AIRPLANE PERFORMANCE | 2 |
| 2.0 | ENGINE CHANGES | 5 |
| | 2.1 PERFORMANCE | 5 |
| | 2.2 INSTALLATION | 5 |
| | 2.3 NOISE | 5 |
| 3.0 | AIRPLANE WEIGHT EFFECTS | 13 |
| 4.0 | AIRPLANE PERFORMANCE | 15 |

# SECTION 1.0
# INTRODUCTION AND SUMMARY

The Boeing SST Proposal is prepared on the basis of engine manufacturer technical data received prior to July 15, 1966. On August 8, 1966, firm technical data was received from General Electric and Pratt & Whitney Aircraft which differed in some respects from the data received prior to July 15, 1966. The purpose of this addendum is to describe the significant differences and to summarize effects on performance of the Boeing Model 2707 airplane.

All information in the proposal is based on the July 15, 1966 engine data with the exception of the Phase III Proposal Summary, V1-B2707-1, Propulsion Report - Part C, Engine Evaluation, V2-B2707-14, and this addendum. These documents are based on engine data received from the engine manufacturers as of August 8, 1966.

## 1.1 ENGINE DIFFERENCES

The General Electric GE4/J5P engine data received on August 8, 1966, provided lower airport and community noise levels for all engine operating conditions. These lower noise levels were the result of redesign of the exhaust nozzle and noise suppression data obtained from J-93 engine testing. Acoustic data provided by General Electric also indicated reduced turbine noise from that being predicted by Boeing for the GE4/J5P engine. These changes provide significantly improved takeoff and approach noise for the B-2707 (GE). An improvement in transonic thrust was also provided. Updated installed engine weight, including optional equipment has resulted in a 112-lb weight increase for the GE4/J5P engine installation. Engine changes have not affected the installed pod configuration.

In the case of Pratt & Whitney Aircraft JTF17A-21B engine, a 2-percent reduction in specific fuel consumption (SFC) at essentially all operating conditions was the principal change. This improvement reduces B-2707 (P&WA) fuel consumed over the design mission and lowers the reserve fuel requirements. Updated installed engine weight including optional equipment has resulted in a 190-lb weight increase for the JTF17A-21B engine installation. Engine changes have not affected the installed pod configuration.

## 1.2 AIRPLANE PERFORMANCE

The major effects of these engine changes on airplane performance are summarized in Table 1-A for the international B-2707 with a maximum design taxi weight of 675,000 lb and in Table 1-B for the domestic airplane with a maximum design taxi weight of 575,000 lb. The improved hot day range capability and noise characteristics of the B-2707 (GE) are apparent, as is the improved range capability of the B-2707 (P&WA).

*Table 1-B. Performance Changes, Domestic Mission*

| | | Domestic B-2707 (GE) | | Domestic B-2707 (P&WA) | |
|---|---|---|---|---|---|
| Maximum Taxi Gross Weight = 575,000 lb | | July 15, 1966 Basis | Aug. 8, 1966 Basis | July 15, 1966 Basis | Aug. 8, 1966 Basis |
| Operational Empty Weight lb | | 275,500 | 275,500 | 273,000 | 273,760 |
| Range with 50,000 lb Payload | | | | | |
| $\Delta P_{max}$ = 2.0 psf Climb; 1.5 psf Cruise | | | | | |
| Standard Day, nmi | | 2,450 | 2,465 | 2,442 | 2,493 |
| Standard Day + 10°C, nmi | | 2,295 | 2,368 | 2,268 | **2,307** |
| M = 0.85 Cruise | | | | | |
| Standard Day, nmi | | 2,571 | 2,571 | 3,042 | 3,100 |
| Takeoff Noise, PNdb | | Maximum Dry Thrust | | 80% Maximum Aug. Thrust | |
| Standard Day | Airport Noise | 117 | 115 | 114 | 114 |
| | Community Noise cg at 0.595 $C_R$ | 99 | 93 | 103 | 103 |
| | cg at 0.615 $C_R$ | 98 | 92 | 102 | 102 |
| Standard Day 15°C | Airport Noise | 116 | 114 | 114 | 114 |
| | Community Noise cg at 0.595 $C_R$ | 107 | 99 | 108 | 108 |
| Landing Approach Noise, PNdB Standard Day | | | | | |
| Landing Weight, lb | | 410,000 | 410,000 | 400,000 | 400,000 |
| 20°, 10° Flaps | cg at 0.595 $C_R$ | 112 | 104 | 115 | 115 |
| | cg at 0.615 $C_R$ | 110 | 102 | 114 | 114 |
| 30°, 50° Flaps | cg at 0.615 $C_R$ | 112 | 106 | 116 | 116 |
| Decelerating Approach | | 108 | 98 | 111 | 111 |

*Table 1-B. Performance Changes, Domestic Mission*

| | | Domestic B-2707 (GE) | | Domestic B-2707 (P&WA) | |
|---|---|---|---|---|---|
| Maximum Taxi Gross Weight = 575,000 lb | | July 15, 1966 Basis | Aug. 8, 1966 Basis | July 15, 1966 Basis | Aug. 8, 1966 Basis |
| Operational Empty Weight lb | | 275,500 | 275,500 | 273,000 | 273,760 |
| Range with 50,000 lb Payload | | | | | |
| $\Delta P_{max}$ = 2.0 psf Climb; 1.5 psf Cruise | | | | | |
| Standard Day, nmi | | 2,450 | 2,465 | 2,442 | 2,493 |
| Standard Day + 10°C, nmi | | 2,295 | 2,368 | 2,268 | **2,307** |
| M = 0.85 Cruise | | | | | |
| Standard Day, nmi | | 2,571 | 2,571 | 3,042 | 3,100 |
| Takeoff Noise, PNdb | | Maximum Dry Thrust | | 80% Maximum Aug. Thrust | |
| Standard Day | Airport Noise | 117 | 115 | 114 | 114 |
| | Community Noise cg at 0.595 $C_R$ | 99 | 93 | 103 | 103 |
| | cg at 0.615 $C_R$ | 98 | 92 | 102 | 102 |
| Standard Day 15°C | Airport Noise | 116 | 114 | 114 | 114 |
| | Community Noise cg at 0.595 $C_R$ | 107 | 99 | 108 | 108 |
| Landing Approach Noise, PNdB Standard Day | | | | | |
| Landing Weight, lb | | 410,000 | 410,000 | 400,000 | 400,000 |
| 20° 40° Flaps | cg at 0.595 $C_R$ | 112 | 104 | 115 | 115 |
| | cg at 0.615 $C_R$ | 110 | 102 | 114 | 114 |
| 30° 50° Flaps | cg at 0.615 $C_R$ | 112 | 106 | 116 | 116 |
| Decelerating Approach | | 108 | 98 | 111 | 111 |

# SECTION 2.0
# ENGINE CHANGES

## 2.1 PERFORMANCE

### 2.1.1 General Electric GE4/J5P Engine

A 6-percent improvement in transonic thrust was provided as well as increased transonic hot day thrust by means of higher engine rpm and increased airflow for an incremental 50-lb weight increase. Figure 2-1 shows the change in hot day transonic thrust for a 2.5 PSF sonic boom overpressure climb path. Reduced transonic inlet drag due to lower bypass airflow is also shown.

### 2.1.2 Pratt & Whitney Aircraft JTF17A-21B Engine

The two percent SFC reduction for the JTF17A-21B engine at all power settings except idle power is listed in Table 2-A for important B-2707 operating points. This improvement is provided as a result of increased component efficiencies demonstrated in primary burner, duct burner, and nozzle component development programs.

## 2.2 INSTALLATION

Pod configuration and external contours for both engine installations are unchanged. The final installed pod weights for both engines including added weight for optional equipment are listed in Table 2-B.

## 2.3 NOISE

The noise characteristics of the JTF17A-21B remain unchanged from those data presented in the body of the Boeing SST proposal. The remainder of the discussion concerns the GE4/J5P engine.

### 2.3.1 Engine Noise Characteristics GE4/J5P

The engine noise characteristics of the GE4/J5P engine have been predicted from the engine data and jet noise suppression as supplied by General Electric. Additional engine noise suppression achieved through inlet choking by use of the sonic throat principle as described in the Airport and Community Noise Program report, V4-B2707-4, has also been included. The jet noise suppression values used in the calculation of noise levels for the GE4/J5P engine are shown in Fig. 2-2. These values have been determined by General Electric through acoustic tests that have been conducted on a J-93 engine.

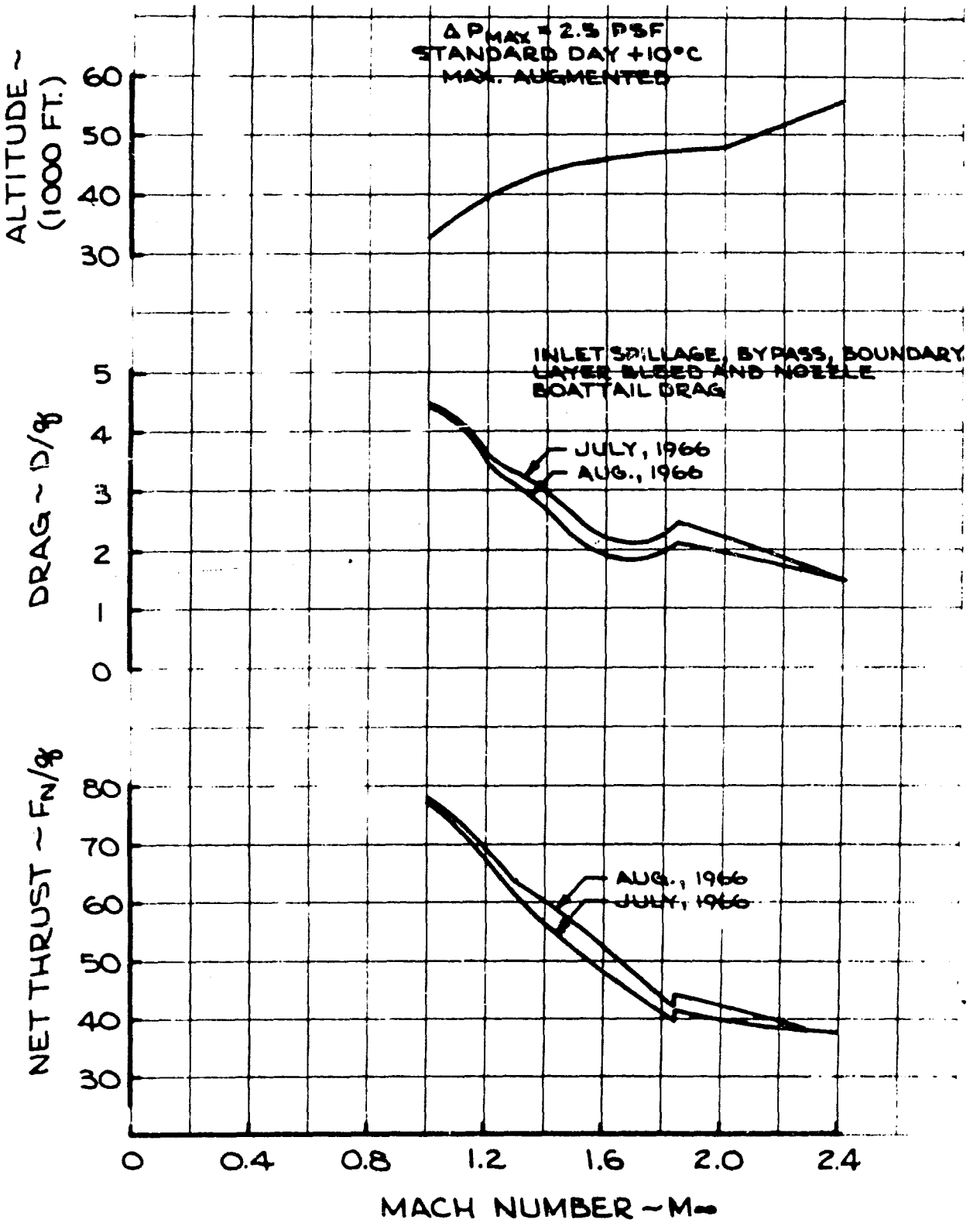


*Figure 2-1. GE4/J5P Climb Performance, Standard Day + 10°C*

*Table 2-A. JTF17A-21B Performance Summary*

| Power Setting | Pressure Altitude ft | Temperature | Mach No | Net Thrust lb | July-1966 SFC lb/hr/lb | August-1966 SFC lb/hr/lb |
|---|---|---|---|---|---|---|
| Max Augmented | 0 | Std | 0 | 56,740 | 1.86 | 1.83 |
| Max Non-Augmented | 0 | Std | 0 | 35,490 | 0.77 | 0.76 |
| Max Augmented | 45,000 | Std | 1.2 | 19,630 | 1.94 | 1.90 |
| Max Augmented | 45,000 | Std + 10°C | 1.2 | 18,140 | 2.00 | 1.96 |
| Partial Augmented | 65,000 | Std | 2.7 | 15,000 | 1.57 | 1.54 |
| Partial Augmented | 65,000 | Std + 10°C | 2.61 | 15,000 | 1.66 | 1.63 |
| Partial Non-Augmented | 36,150 | Std | 0.85 | 5,000 | 1.07 | 1.06 |
| Partial Non-Augmented | 15,000 | Std | 0.5 | 5,000 | 1.10 | 1.08 |

2.3.1 (Continued)

The unsuppressed noise levels for the GE4/J5P engine for ground and flight operations are shown in Figs. 2-3 and 2-4. Also shown in these figures are the predicted noise levels with all suppression included. The effect of the open-nozzle concept wherein the nozzle throat area is maintained on a maximum area schedule is included in the suppressed noise level predictions. The predicted noise spectra for a series of engine operating conditions have also been predicted and are presented in Table 2-C.

Noise levels beneath and to the side of the airplane flight path have been determined from the revised noise data. These levels have been integrated into contours of Perceived Noise Level for takeoff. These contours are shown for the B-2707 (GE) international airplane in Fig. 4-12 and the B-2707 (GE) domestic airplane in Fig. 4-14.

The landing noise characteristics of the B-2707 (GE) have changed significantly due to the noise data presented on August 8, 1966. These data indicated that turbine noise would not contribute significantly to the total noise from the airplane even at landing approach power settings. Boeing had been predicting very significant noise increases due to turbine noise contribution. The predictions were based on the J-75 engine acoustic test results. Since the GE data were obtained on an engine more closely resembling the SST turbojet offering, these data should be more representative of the noise characteristics of the SST engine. Therefore the B-2707 landing noise levels have been revised to conform to the August 8, 1966 data inputs. The results of these revisions are shown in Figs. 4-17 and 4-18.

*Table 2-B. Installed Pod Weight*

| | B-2707 (GE) | B-2707 (P&WA) |
|---|---|---|
| Engine weight | 11,125 | 9,910 |
| Optional equipment | 112 | 730 |
| Total | 11,237 | 10,640 |
| Inlet | 2,070 | 2,485 |
| Cowl panels | | |
| Forward | 325 | 225 |
| Aft | 150 | --- |
| Structure | 495 | 480 |
| Miscellaneous | 35 | 35 |
| Total | 14,312 | 13,865 |

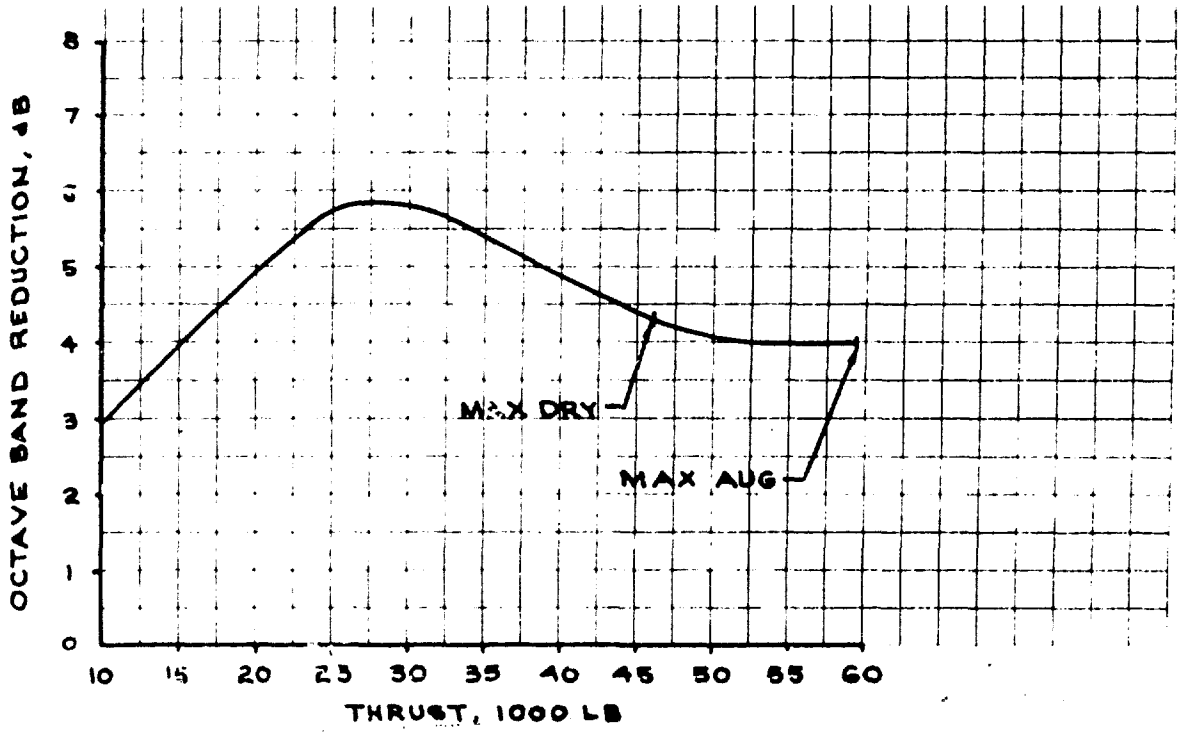


*Figure 2-2. Predicted GE4/J5P Jet Noise Suppression*

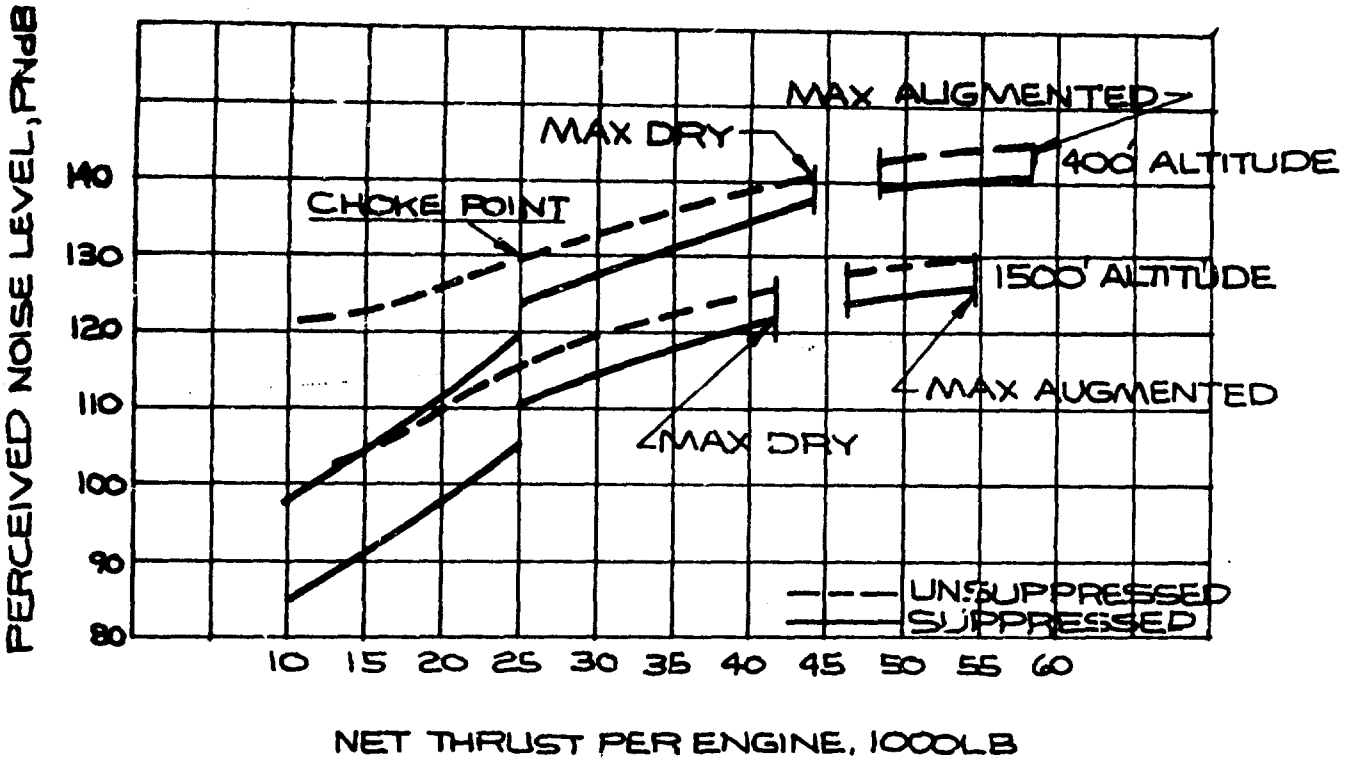


*Figure 2–3. Inflight Noise Characteristics of GE4/J5P Engines*

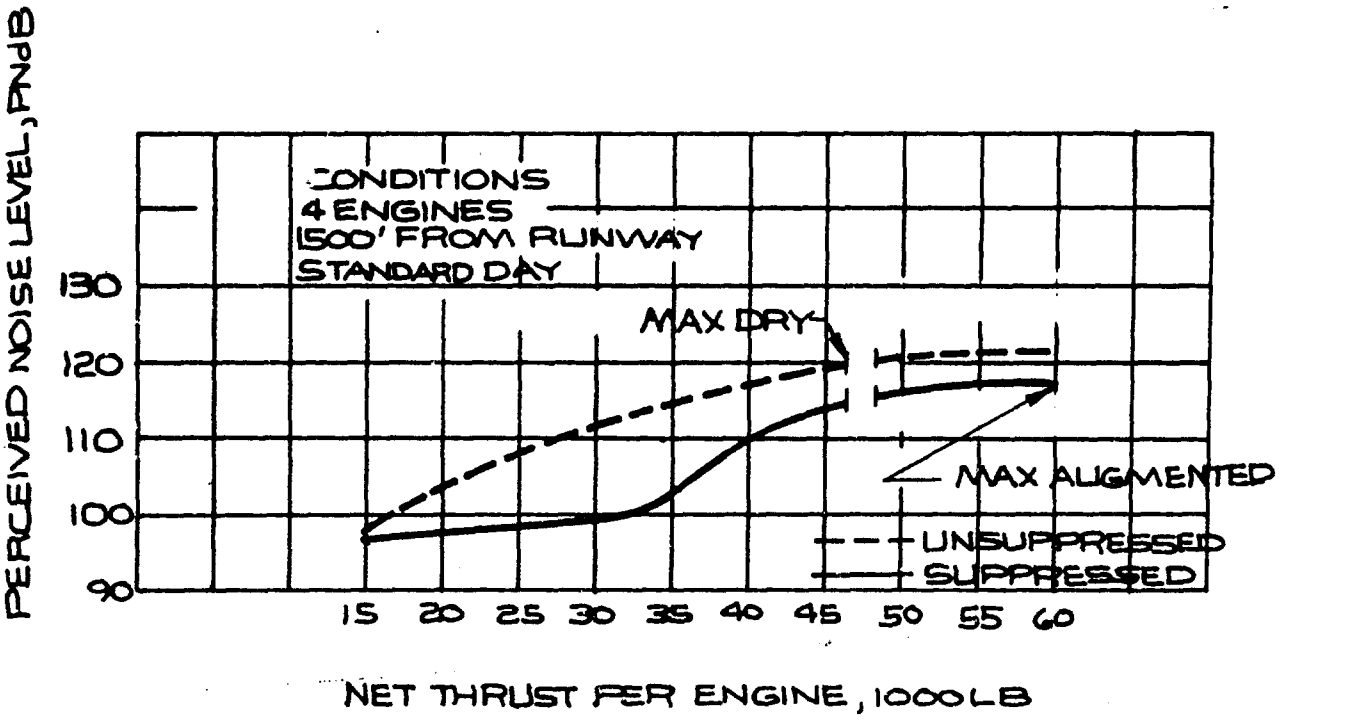


*Figure 2–4. Noise Characteristics of GE4/J5P Engines For Static Ground Operations*

*Table 7-1 Noise Spectra For GE4-15F Engine*

| Operating Conditions (4 Engines) | | Overall SPL (dB) | Octave Band Sound Pressure Level (dB) | | | | | | | | | | | | Perceived Noise (PNdB) |
|---|---|---|---|---|---|---|---|---|---|---|---|---|---|---|---|
| | | | 1 | 2 | 3 | 4 | 5 | 6 | | 7 | | 8 | | | |
| | | | Jet | Jet | Jet | Jet | Jet | Jet | Comp | Jet | Comp | Jet | Comp | | |
| Ground Static 1,500 Ft | | | | | | | | | | | | | | | |
| Max Aug | Unsuppressed | 116.5 | 113 | 116 | 114 | 109 | 102 | 92 | 76 | 78 | 44 | 61 | 62 | | 121.0 |
| | Suppressed | 114.5 | 109 | 111 | 109 | 105 | 98 | 88 | 75 | 74 | 74 | 57 | 62 | | 117.0 |
| Max Dry | Unsuppressed | 117.0 | 111 | 113 | 111 | 107 | 100 | 90 | 76 | 76 | 74 | 60 | 62 | | 119.0 |
| | Suppressed | 113.0 | 107 | 109 | 106 | 103 | 98 | 88 | 75 | 72 | 74 | 56 | 62 | | 114.5 |
| Taxi (5,000 lb/Fn) 200 Ft | | | | | | | | | | | | | | | |
| | Unsuppressed | 106.0 | 85 | 86 | 82 | 80 | 75 | 70 | 101 | 85 | 102 | 60 | 100 | | 119.0 |
| | Suppressed | 97.0 | 85 | 86 | 82 | 80 | 75 | 70 | 91 | 85 | 92 | 60 | 90 | | 111.0 |
| Flight (0.3 M) 1,500 Ft Alt | | | | | | | | | | | | | | | |
| Max Aug | Unsuppressed | 125.5 | 113 | 116 | 121 | 116 | 114 | 108 | 87 | 90 | 86 | 77 | 74 | | 130 |
| | Suppressed | 121.0 | 109 | 114 | 117 | 114 | 110 | 104 | 87 | 91 | 86 | 73 | 74 | | 126 |
| Max Dry | Unsuppressed | 122.0 | 110 | 116 | 117 | 115 | 111 | 104 | 87 | 90 | 86 | 75 | 74 | | 126.5 |
| | Suppressed | 118.0 | 108 | 112 | 112 | 111 | 107 | 100 | 87 | 88 | 86 | 69 | 74 | | 122.0 |
| 18,600 lb/Fn | Unsuppressed | 99.0 | 93 | 94 | 93 | 89 | 83 | 76 | 86 | 81 | 86 | 44 | 76 | | 107 |
| | Suppressed | 95.0 | 89 | 90 | 89 | 84 | 78 | 70 | 81 | 81 | 80 | 43 | 80 | | 97 |
| 15,700 lb/Fn | Unsuppressed | 96.0 | 90 | 91 | 90 | 86 | 80 | 72 | 82 | 88 | 87 | 41 | 88 | | 106 |
| | Suppressed | 92.5 | 86 | 87 | 86 | 81 | 76 | 68 | 87 | 84 | 86 | 37 | 43 | | 94 |
| Landing (0.23 M) 326 Ft Alt | | | | | | | | | | | | | | | |
| | Unsuppressed | 111.5 | 101 | 100 | 98 | 94 | 89 | 84 | 101 | 79 | 107 | 74 | 103 | | 124 |
| | Suppressed | 101.5 | 97 | 96 | 94 | 90 | 86 | 80 | 77 | 76 | 92 | 70 | 78 | | 106 |

## SECTION 3.0
## AIRPLANE WEIGHT EFFECTS

The Airframe Design Report - Part A, Weight and Balance, gives an Operating Empty Weight breakdown of the GE and P&WA powered airplanes. Table 3-A lists these comparative weights as they are modified by the August 8, 1966 engine data and other related airplane changes.

The 760-lb weight change in the P&WA powered airplane increases the Manufacturer's Empty Weight, Operating Empty Weight and Zero Fuel Weight of the following P&WA powered airplanes:

a. 635,000-lb gross weight design point airplane

b. 675,000-lb gross weight production international airplane

c. 635,000-lb gross weight prototype airplane

d. 575,000-lb gross weight production domestic airplane

TABLE 3-A
OPERATING EMPTY WEIGHT

| GROUP | GE | P&WA |
|---|---|---|
| Engines | 44,950 | 42,560 |
| Nacelle | 12,300 | 12,900 |
| Horizontal Tail | 20,400 | 20,460 |
| Engine Accessories - ADS | 1,100 | 1,160 |
| Anti-Icing and Anti-Fogging | 280 | 330 |
| Starting System | 400 | 430 |
| Fuel System | 7,400 | 7,510 |
| Hydraulic System | 3,600(1) | 3,420 |
| Body Structure | 47,300(1) | 47,220 |
| Other | 149,770 | 149,770 |
| Operational Empty Weight (Max. design taxi weight 675,000 lb) | 287,500 | 285,760 |
| Original Operating Empty Weight | 287,500 | 285,000 |
| Weight Change | 0 | +760 lb |

(1) Includes effect of ram air turbine - B-2707 (GE) only

## SECTION 4.0
## AIRPLANE PERFORMANCE

The effect of the changes in engine data on the standard day payload-range capability are illustrated in Fig. 4-1 for the international B-2707 and Fig. 4-2 for the domestic airplane. As noted, there is no significant effect on the standard day range of the B-2707 (GE). The improved specific fuel consumption of the Pratt & Whitney Aircraft engine results in slightly less than 2 percent increase in range. The effect of temperature changes from standard day on range are shown in Fig. 4-3 for the B-2707 (GE) and Fig. 4-4 for the B2707 (P&WA). There is no change for the B-2707 (P&WA) curve since the effect of temperature on the engine data did not change.

Figures 4-5 and 4-6 show the off-loaded supersonic range capability and corresponding transonic thrust margins for the airplanes. The range performance with a mixed subsonic and supersonic mission is shown in Fig. 4-7. Figures 4-8 and 4-9 show fuel, time, and distance breakdowns for a nominal, standard day, intercontinental mission at a maximum sonic-boom overpressure of 2.5 psf for both airplanes.

Summaries of takeoff performance, using maximum augmented thrust, are shown in Figs. 4-10 and 4-11. The significant change in takeoff performance is in the airport and community noise of the B-2707 (GE). The changes in noise characteristics are shown in more detail by the noise contours around the airport in Figs. 4-12 through 4-15.

The noise data shown on the preceding curves are based on the engines as proposed by the engine contractors with the use of a sonic throat in the inlet at reduced powers. With the Boeing noise suppressor, the August 8, 1966 General Electric engine data have resulted in an additional 1 PNdb reduction in the airplane's noise characteristics at maximum augmented thrust. Noise contours with the Boeing jet suppressor are compared in Fig. 4-16 for the B-2707 (GE).

The only change in landing performance for the airplanes caused by the changed engine data is in the approach noise for the B-2707 (GE) as shown in Figs. 4-17 and 4-18. Figure 4-19 shows the B-2707 (P&W) landing performance.

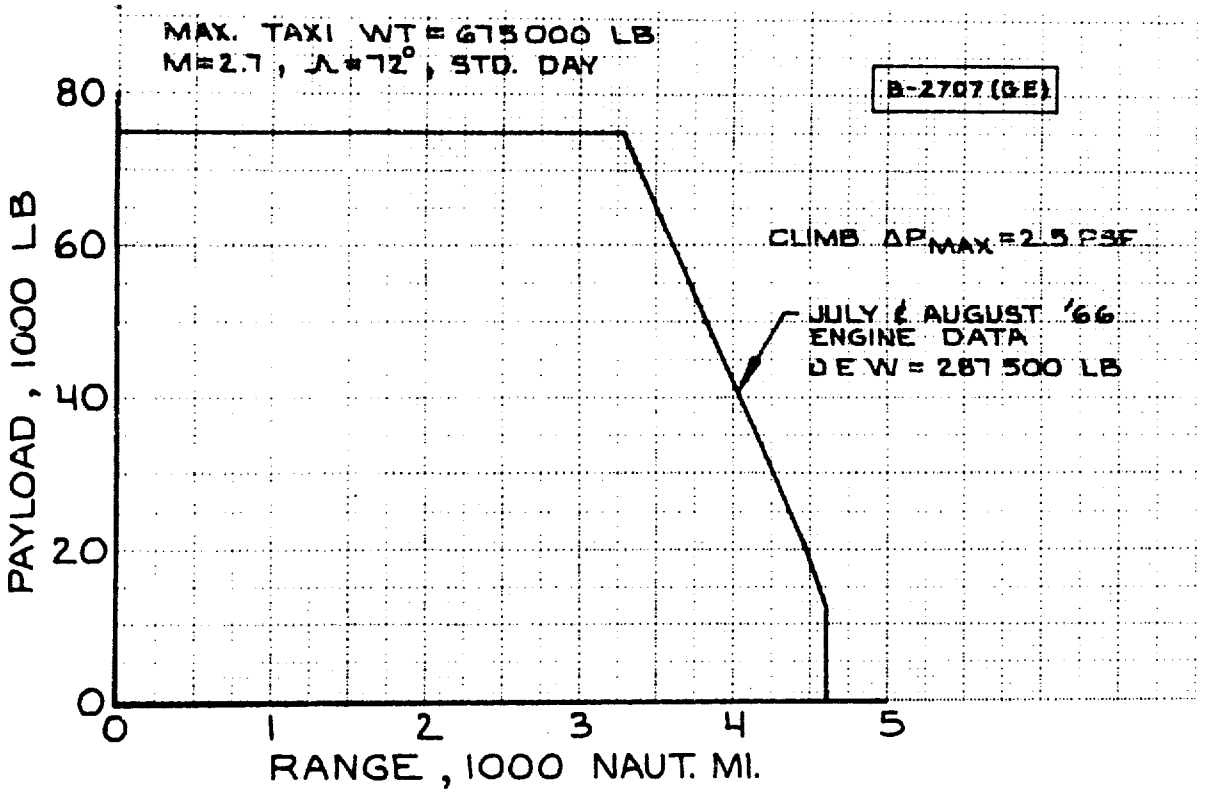


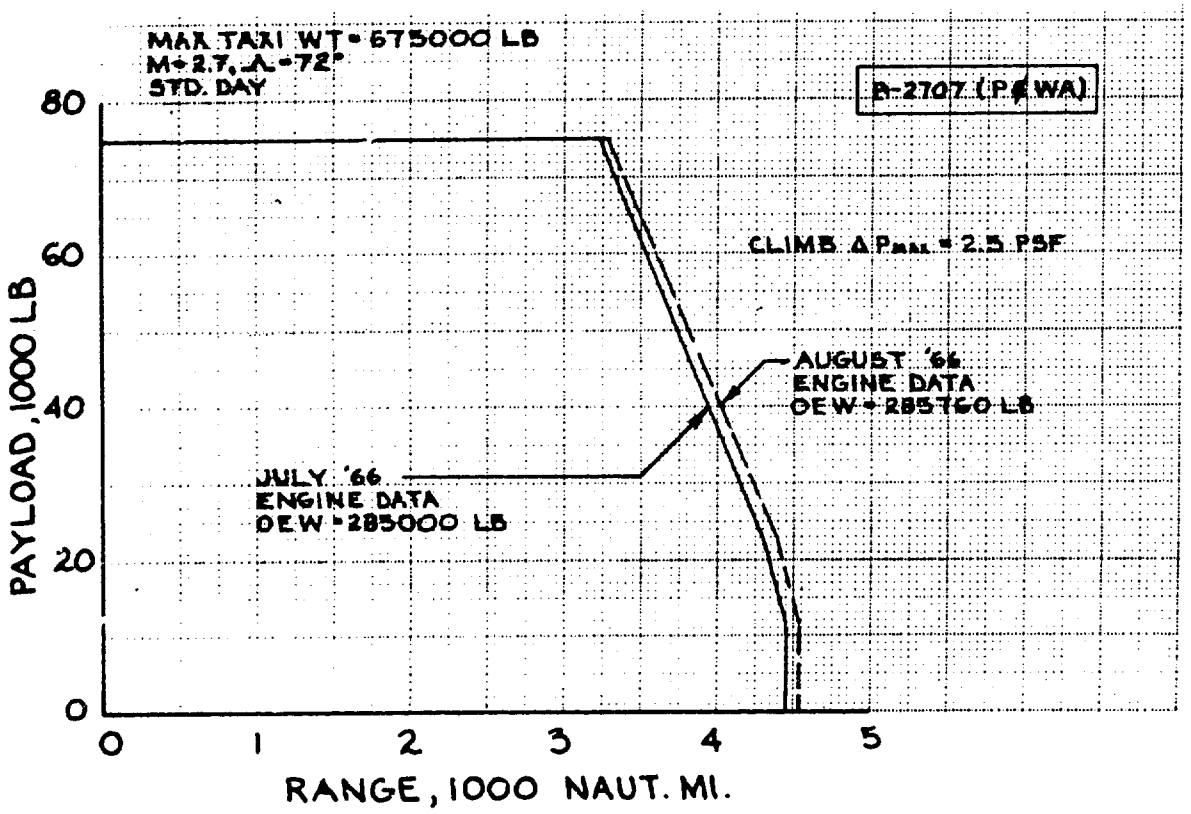


*Figure 4–1. Payload–Range, International Model B–2707*

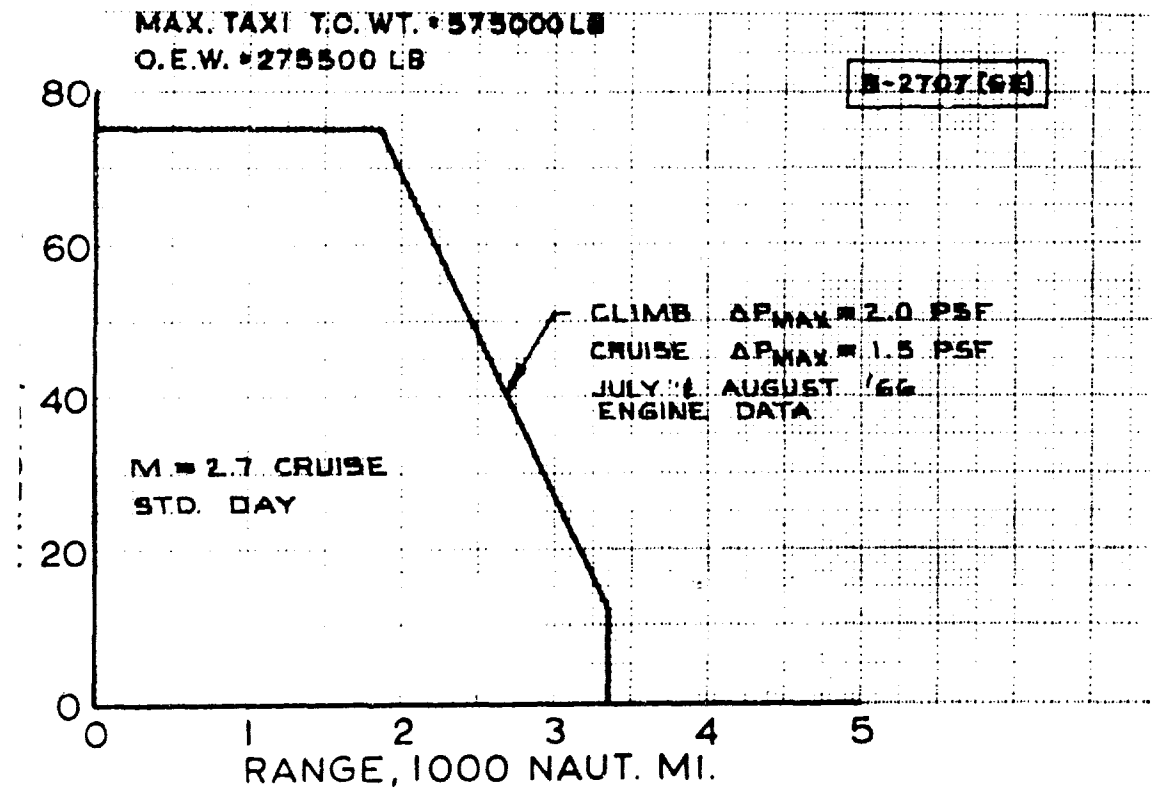


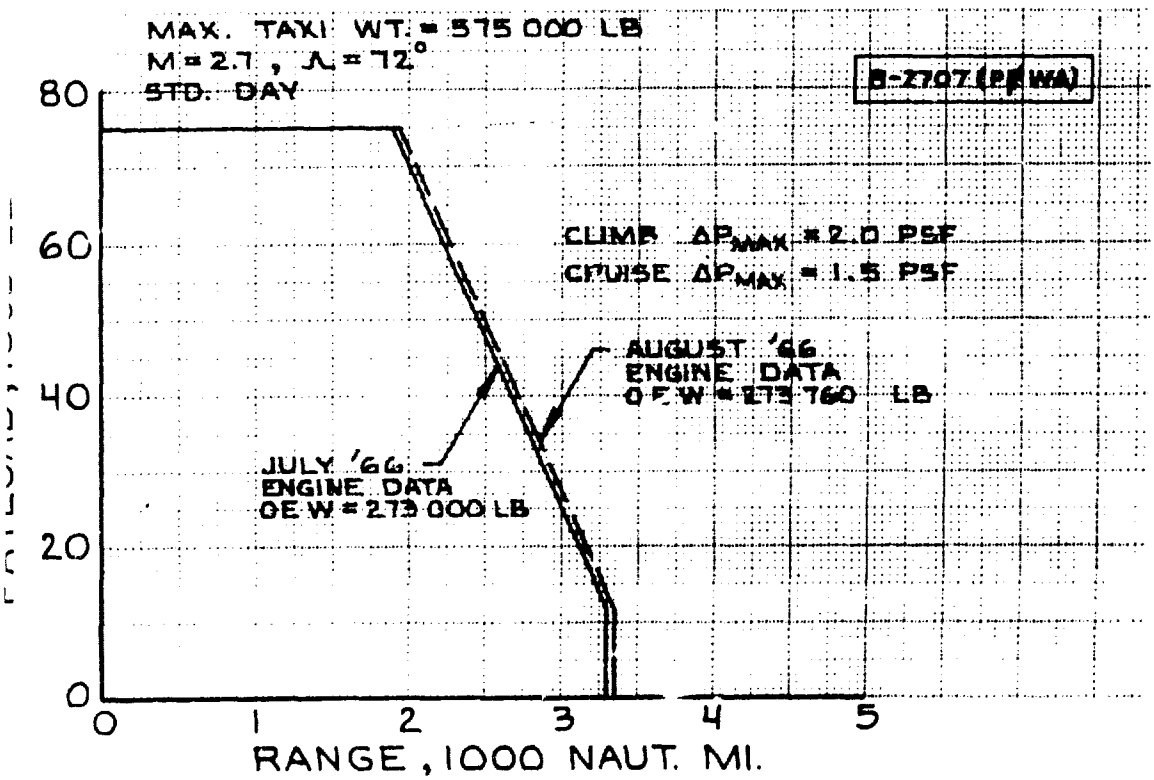


*Figure 4–2. Payload–Range, Domestic Model B–2707*

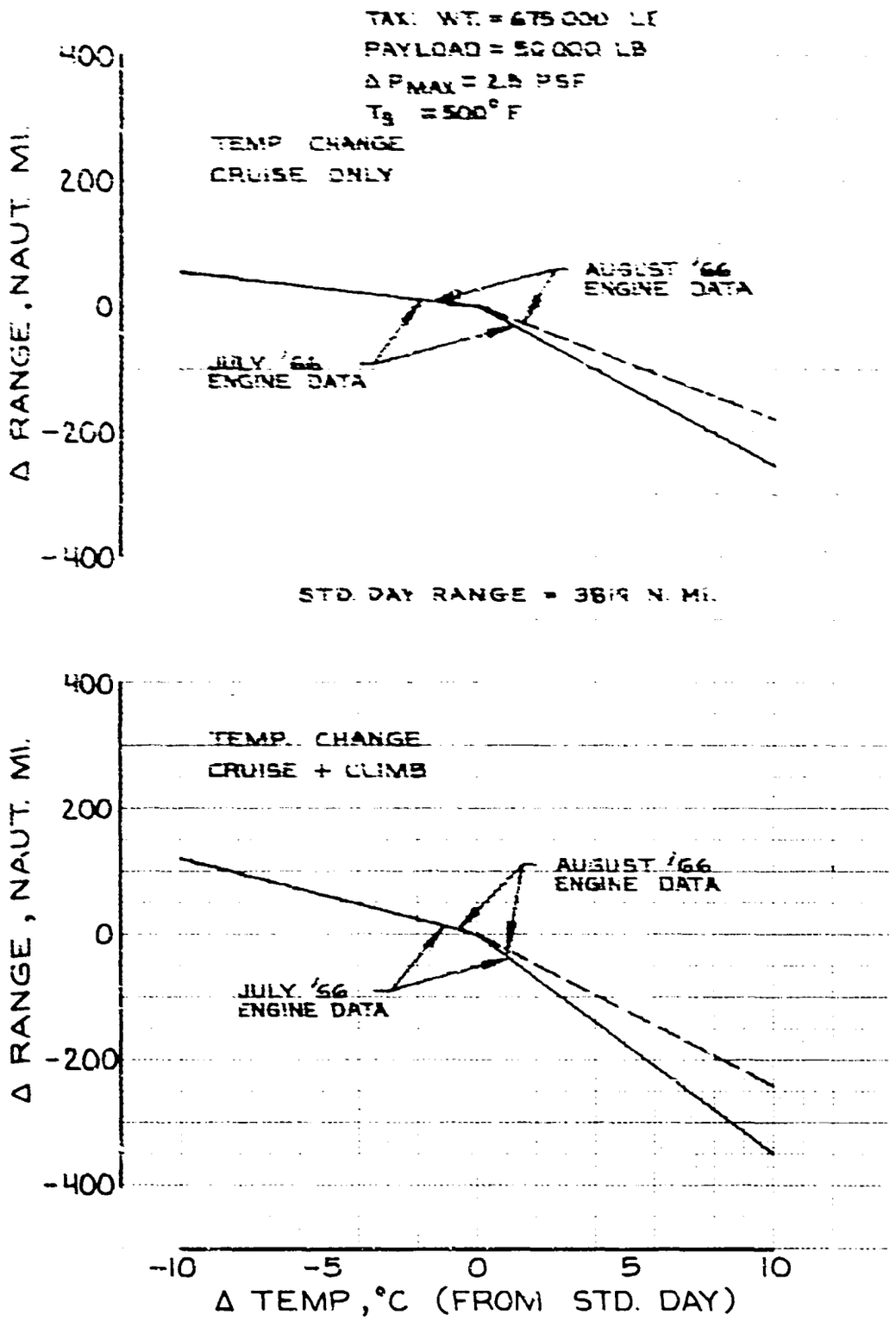


*Figure 4-3. Effect of Temperature Change on Range Model B-2707 (GE)*

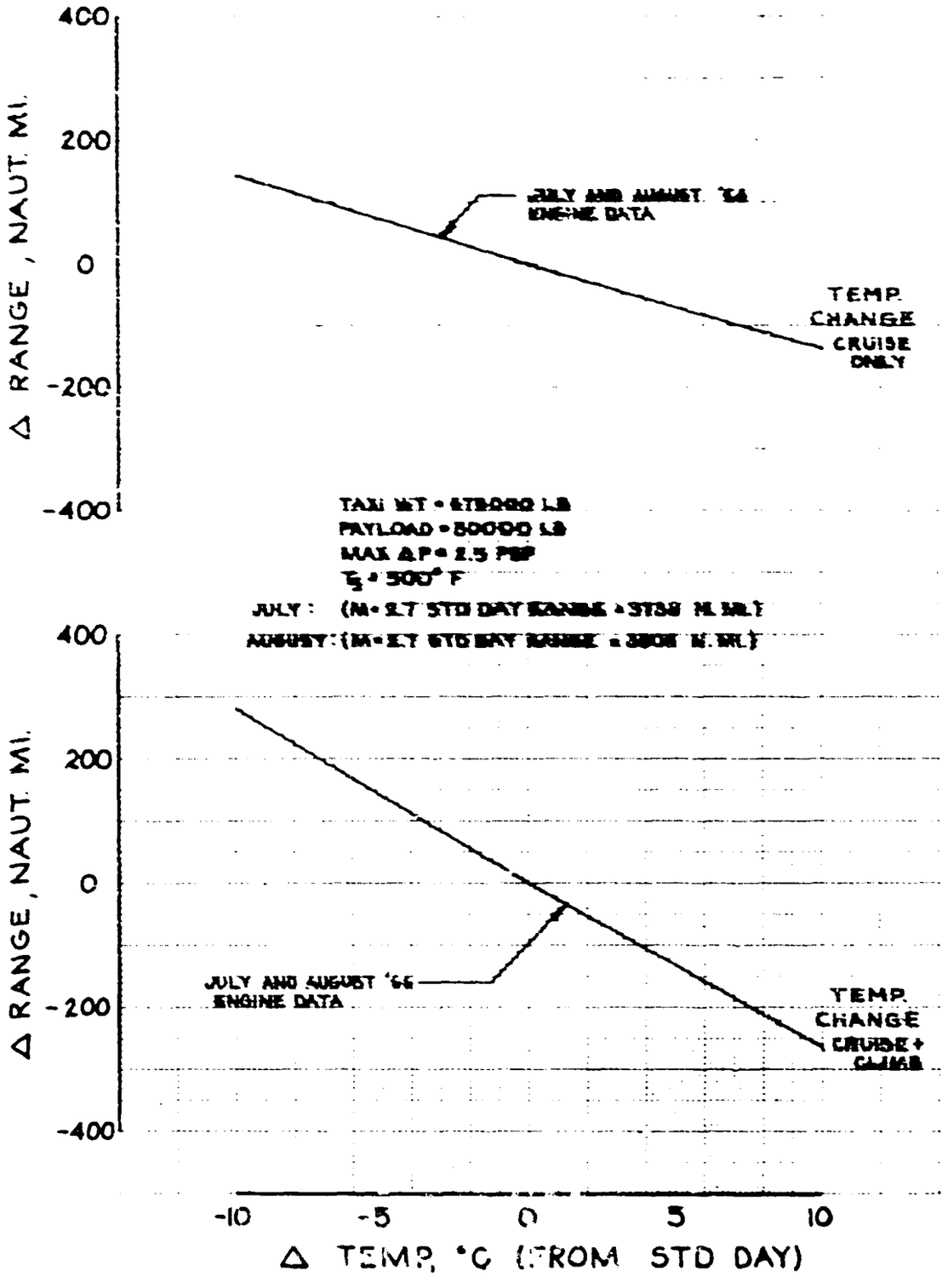


*Figure 4-4. Effect of Temperature Change on Range Model B-2707 (P&WA)*

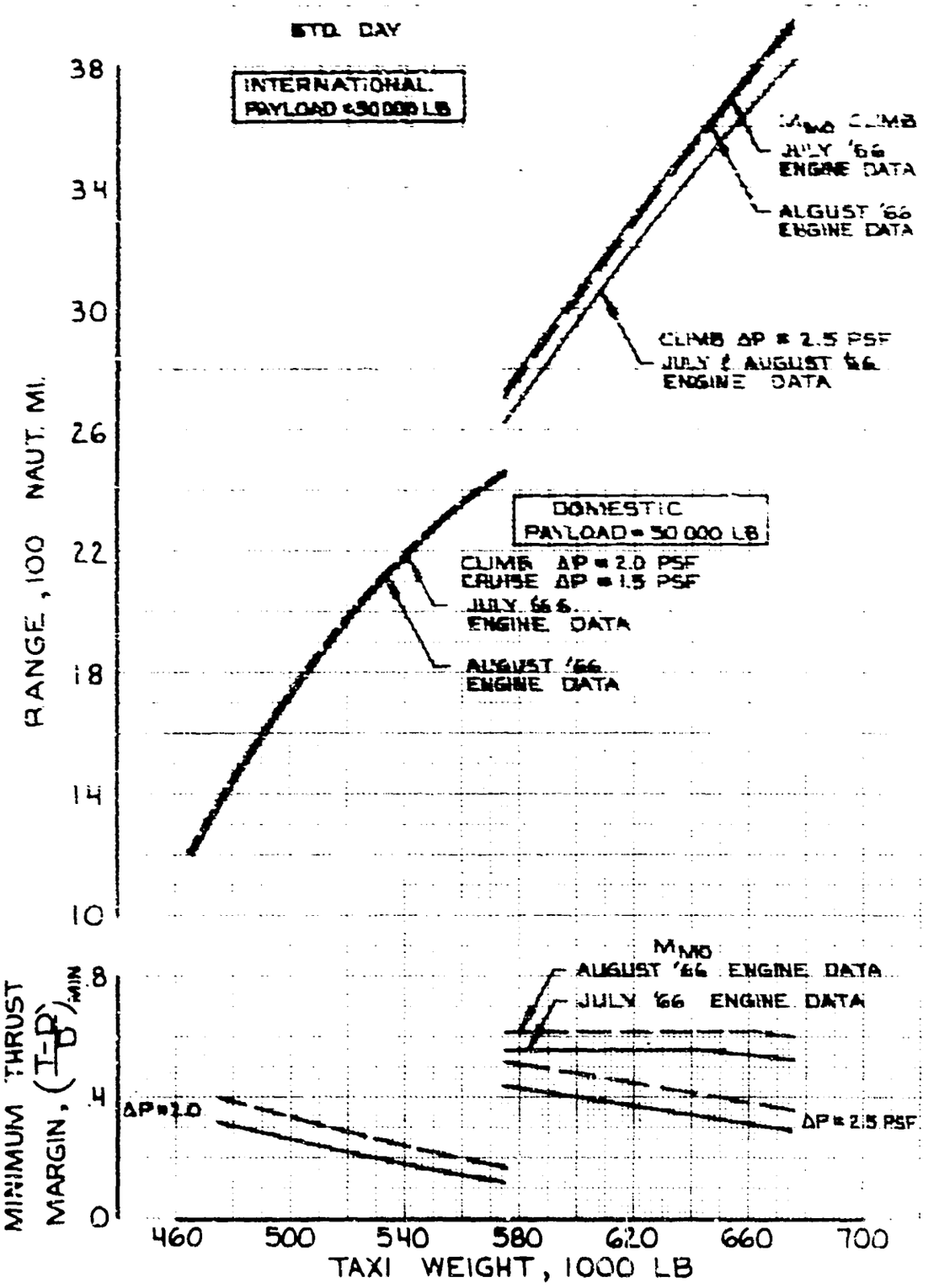


*Figure 4–5. Off–Loaded Airplane Performance Model B–2707 (GE)*

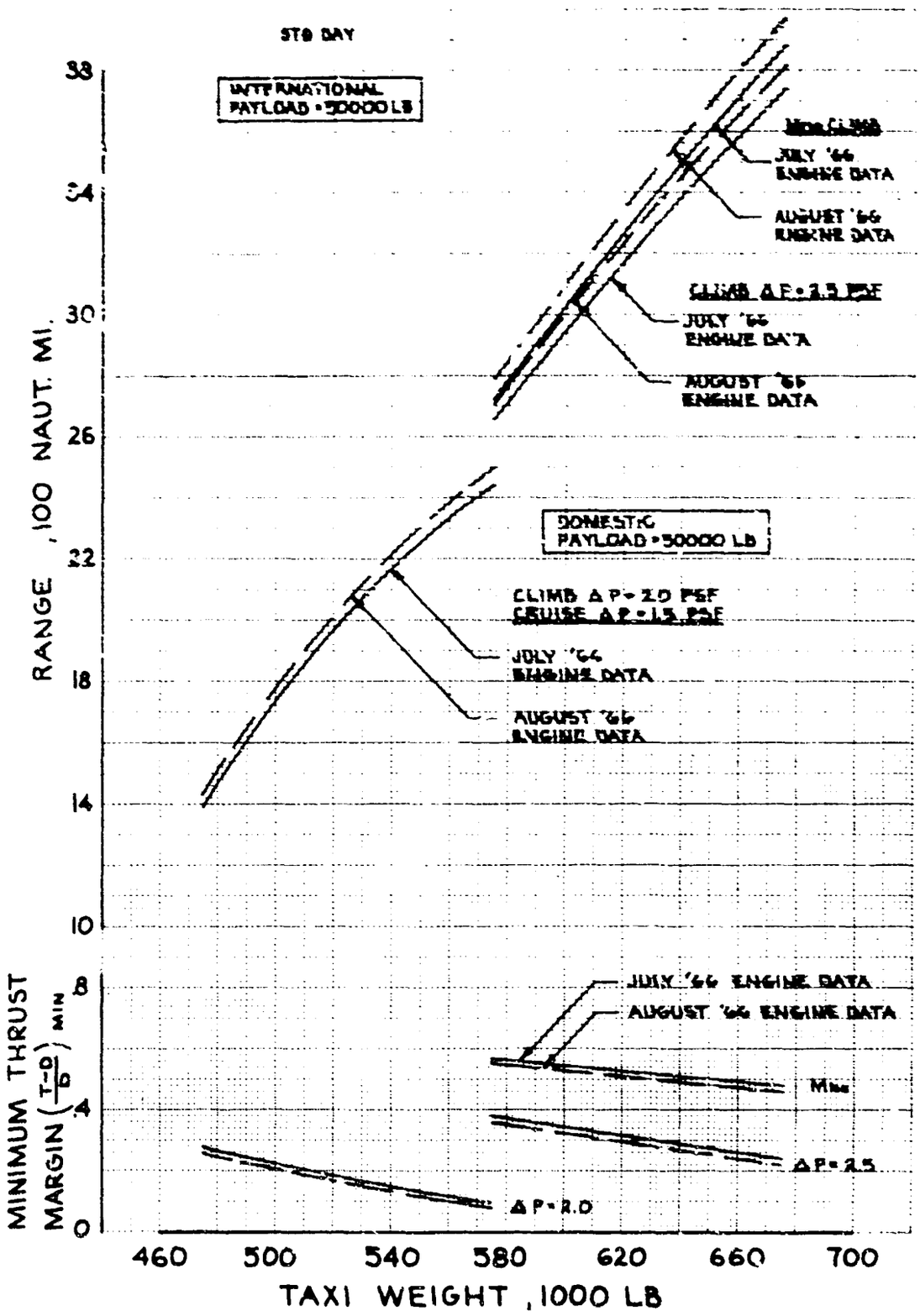


*Figure 4–6. Off–Loaded Airplane Performance Model B–2707 (P&WA)*

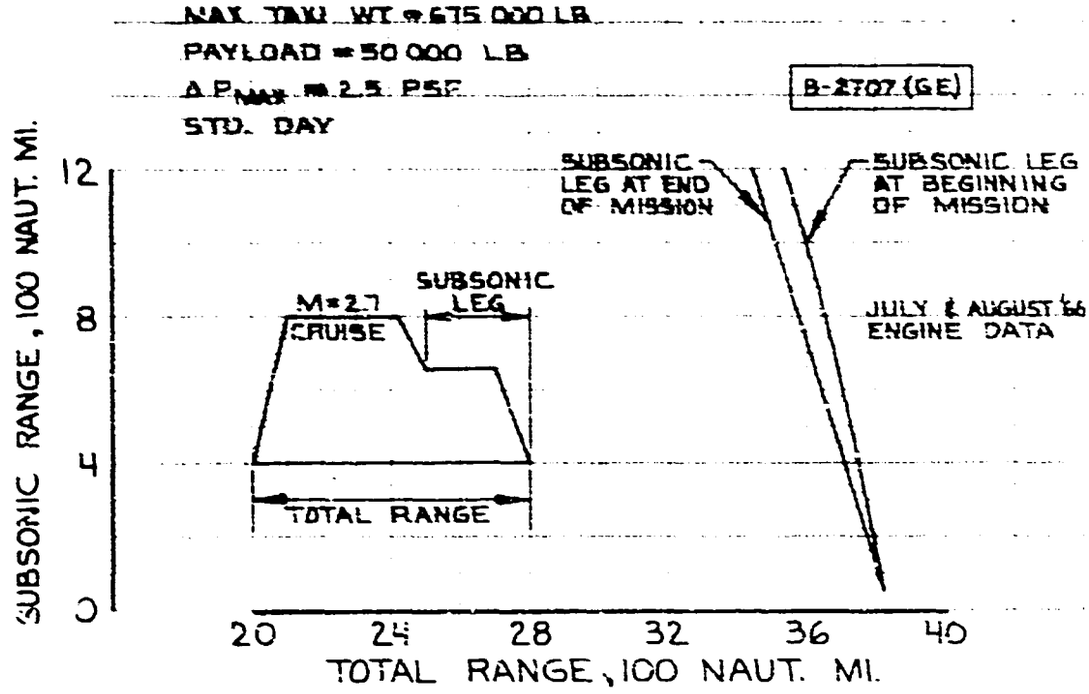


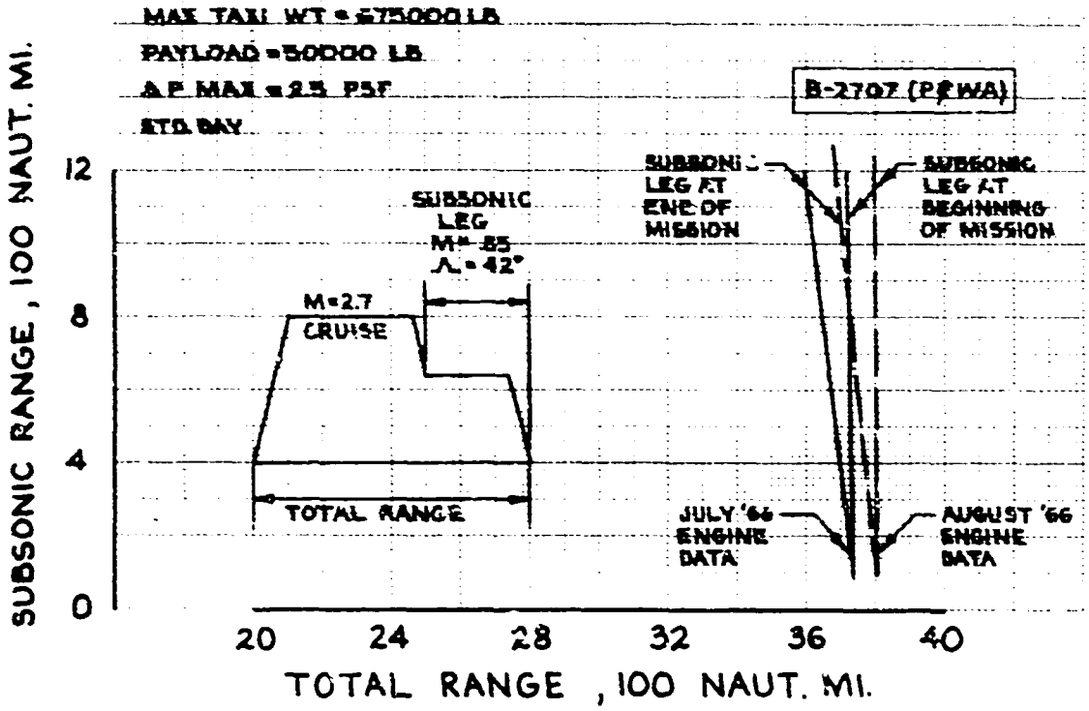


*Figure 4–7. Operational Versatility Model B–2707*

Max. Design

| | |
|---|---|
| Taxi Weight | 675,000 lb |
| OEW | 287,500 lb |
| Payload | 50,000 lb |
| Wing Area | 9,000 ft$^2$ |
| Engine | GE4/J5P |
| Airflow | 620 lb/sec |

Std Day, Zero Wind
Phase III Rules

| | |
|---|---|
| Block Time | 3.290 hr |
| Block Fuel | 292,181 lb |

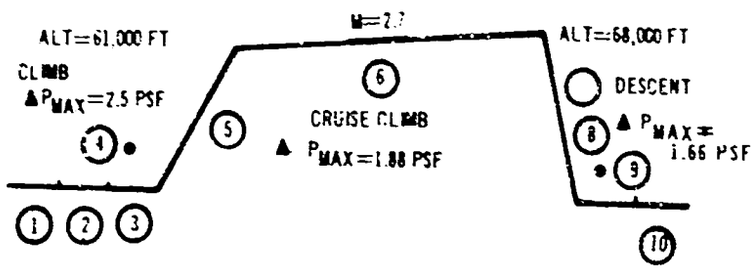


| | | Fuel Burned (lb) | Fuel Remaining (lb) | Weight At End of Operation (lb) | Time (hr) | Distance (nmi) |
|---|---|---|---|---|---|---|
| 1. | Taxi-out | 4,060 | 333,440 | 670,940 | 0.167 | — |
| 2. | Takeoff (Sea level to 35 ft) | 4,150 | 329,290 | 666,790 | 0.010 | — |
| 3. | Acceleration to climb speed | 4,790 | 324,500 | 662,000 | 0.024 | 5.0 |
| 4. | Departure air maneuver allowance (250 kts EAS & 5,000 ft) | 4,000 | 320,500 | 658,000 | 0.0673 | — |
| 5. | Acceleration and climb | 81,400 | 238,800 | 576,600 | 0.411 | 337 |
| 6. | Supersonic cruise climb | 186,791 | 52,309 | 389,809 | 2.112 | 3271 |
| 7. & 8. | Deceleration and descent (cruise altitude to 1,500 ft) | 2,330 | 49,979 | 387,479 | 0.333 | 206 |
| 9. | Destination air maneuver (Approach & Landing Allowance, 250 kts EAS at 5,000 ft) WT = WT at (8) = 5% block fuel | 2,940 | 47,039 | 384,539 | 0.083 | — |
| 10. | Taxi-in | (1,720)* | | | 0.083 | — |
| | TOTAL MISSION | 290,461 | | | 3.290 | 3819 |
| | Reserves | | | | | |
| A. | 5 percent block fuel | 14,609 | | 369,930 | | |
| B. | Missed approach (climb sea level to 1,500 ft) | 2,510 | | 367,420 | | |
| C. | Climb from 1,500 ft subsonic cruise, descent to sea level at altn (300 st mi) | 20,070 | | 347,350 | | |
| D. | 20 min hold at 15,000 ft over alternate | 9,850 | | 337,500 | | |
| | TOTAL RESERVES | 47,039 | | | | |
| | TOTAL FUEL | 337,500 | | | | |

* Fuel burned not included in mission fuel; for D.O.C. only

*Figure 4-8 R-2707 (GE) International Supersonic Cruise Mission*

**Max Design**

| | | |
|---|---|---|
| Taxi Weight | | 675,000 lb |
| OEW | - | 285,760 lb |
| Payload | | 50,000 lb |
| Wing Area | = | 9,000 sq ft |
| Engine | = | PWAJT F17A-21B |
| $W_a$ | = | 687 lb/sec |

Std Day, Zero Wind

**Phase III Rules**

| | |
|---|---|
| Block Time | 3.400 hr |
| Block Fuel | 297 890 lb |

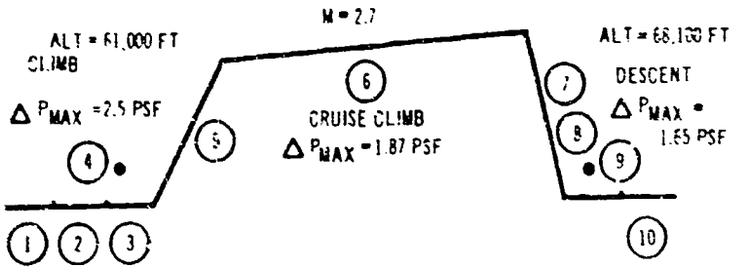


| | Fuel Burned (lb) | Fuel Remaining (lb) | Weight At End of Operation (lb) | Time (hr) | Distance (nmi) |
|---|---|---|---|---|---|
| 1. Taxi-out | 2,880 | 336,360 | 672,120 | 0.167 | — |
| 2. Takeoff (Sea level to 35 ft) | 4,385 | 331,975 | 667,735 | 0.010 | — |
| 3. Acceleration to climb speed | 4,880 | 327,095 | 662,855 | 0.043 | 10 |
| 4. Departure air maneuver allowance (250 kts EAS @ 5,000 ft) | 3,160 | 323,935 | 659,695 | 0.067 | |
| 5. Acceleration and climb | 95,400 | 228,535 | 564,295 | 0.570 | 422 |
| 6. Supersonic cruise climb | 181,626 | 46,909 | 382,669 | 2.051 | 3,180 |
| 7. & 8. Deceleration and descent (cruise altitude to 1,500 ft) | 2,070 | 44,839 | 380,599 | 0.326 | 196 |
| 9. Destination air maneuver (Approach & Landing Allowance, 250 kts EAS at 5,000 ft) WT = WT at (8) = 5% block fuel | 2,234 | 42,605 | 378,365 | 0.083 | — |
| 10. Taxi-in | (1,255)* | | | 0.083 | — |
| TOTAL MISSION | 296,635 | | | 3.400 | 3,808 |
| **Reserves** | | | | | |
| A. 5 percent block fuel | 14,895 | | 363,470 | | |
| B. Missed approach (climb sea level to 1,500 ft) | 2,200 | | 361,270 | | |
| C. Climb from 1,500 ft subsonic cruise, descend to sea level at altn (300 st mi) | 17,670 | | 343,600 | | |
| D. 20 min hold at 15,000 ft over alternate | 7,840 | | 335,760 | | |
| TOTAL RESERVES | 42,605 | | | | |
| TOTAL FUEL | 339,240 | | | | |

* Fuel burned not included in mission fuel; for D.O.C. only

*Figure 4-9 B-2707 (P&WA) International Supersonic Cruise Mission*

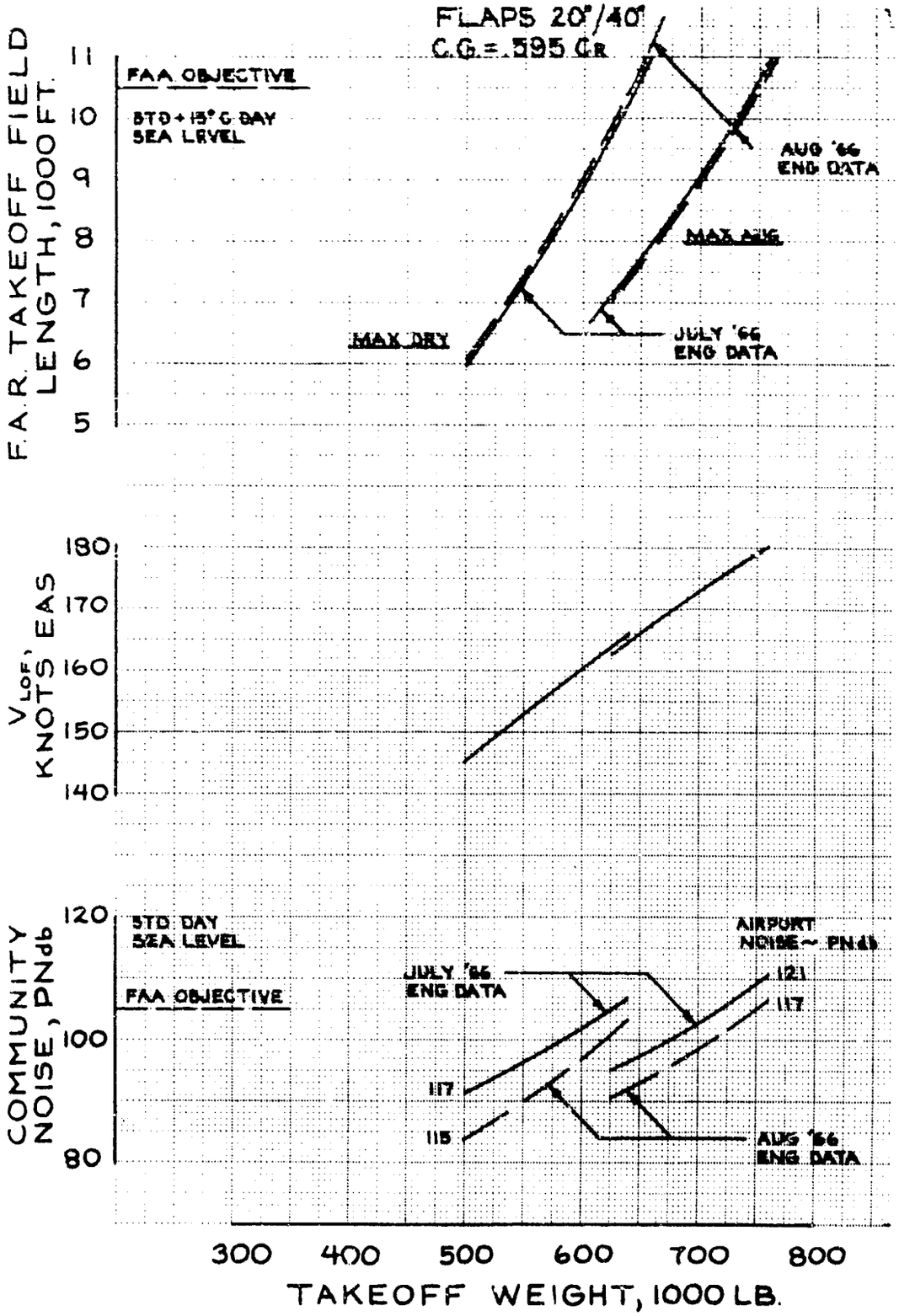


*Figure 4–10. Takeoff Performance Model B–2707 (GE)*

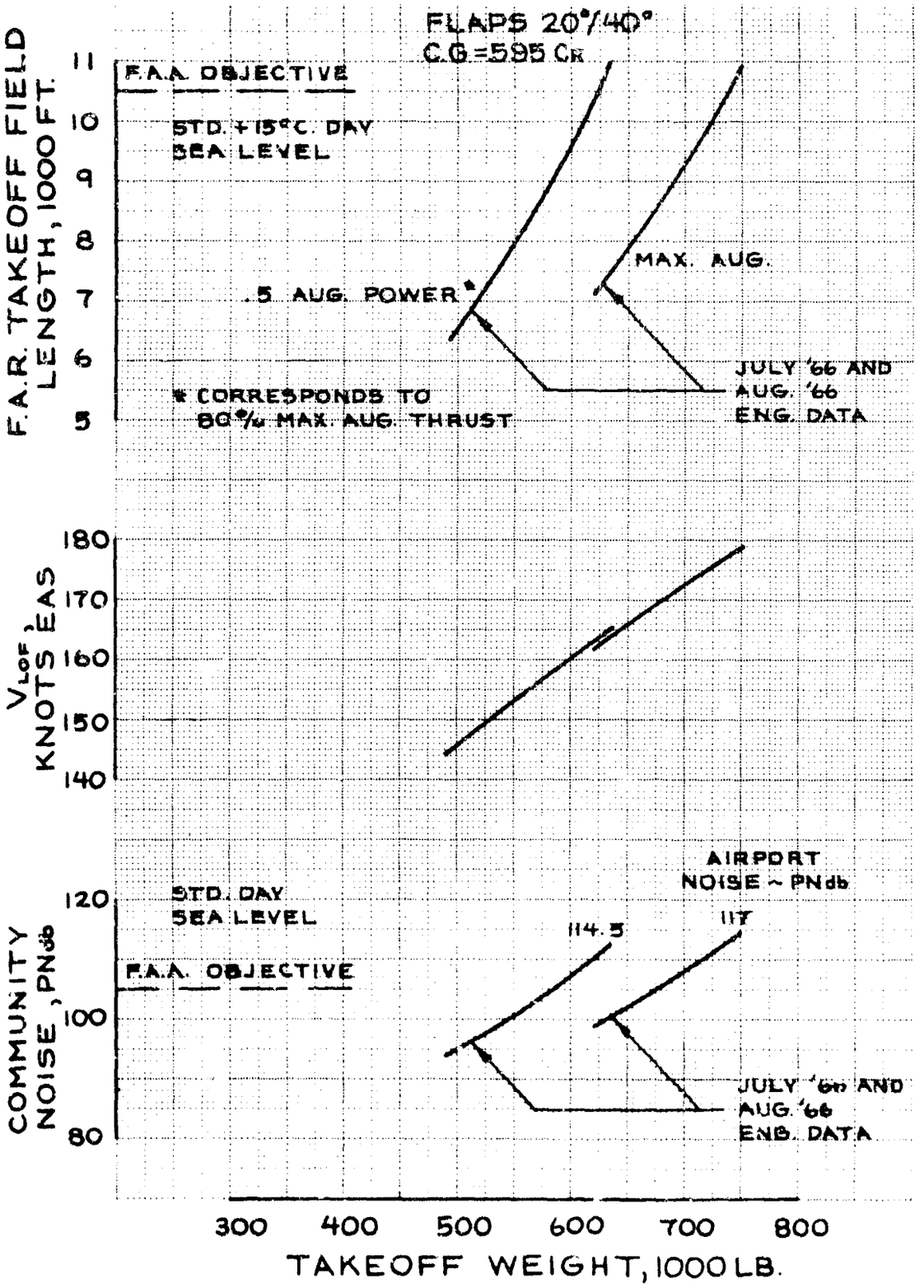


*Figure 4-11. Takeoff Performance Model B-2707(P&WA)*

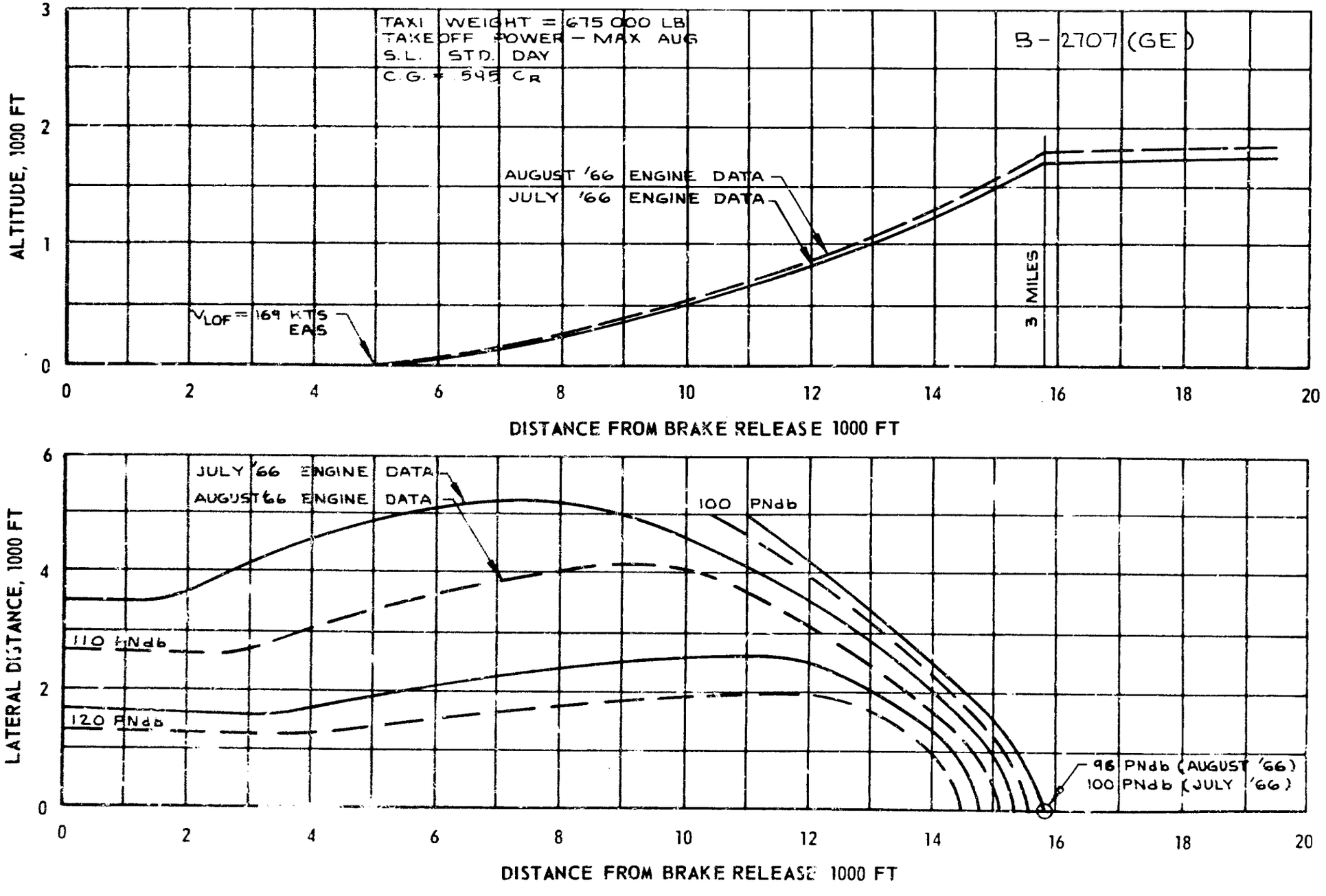


*Figure 4–12. Noise Contours, International Mission, Standard Day Model B–2707 (GE)*

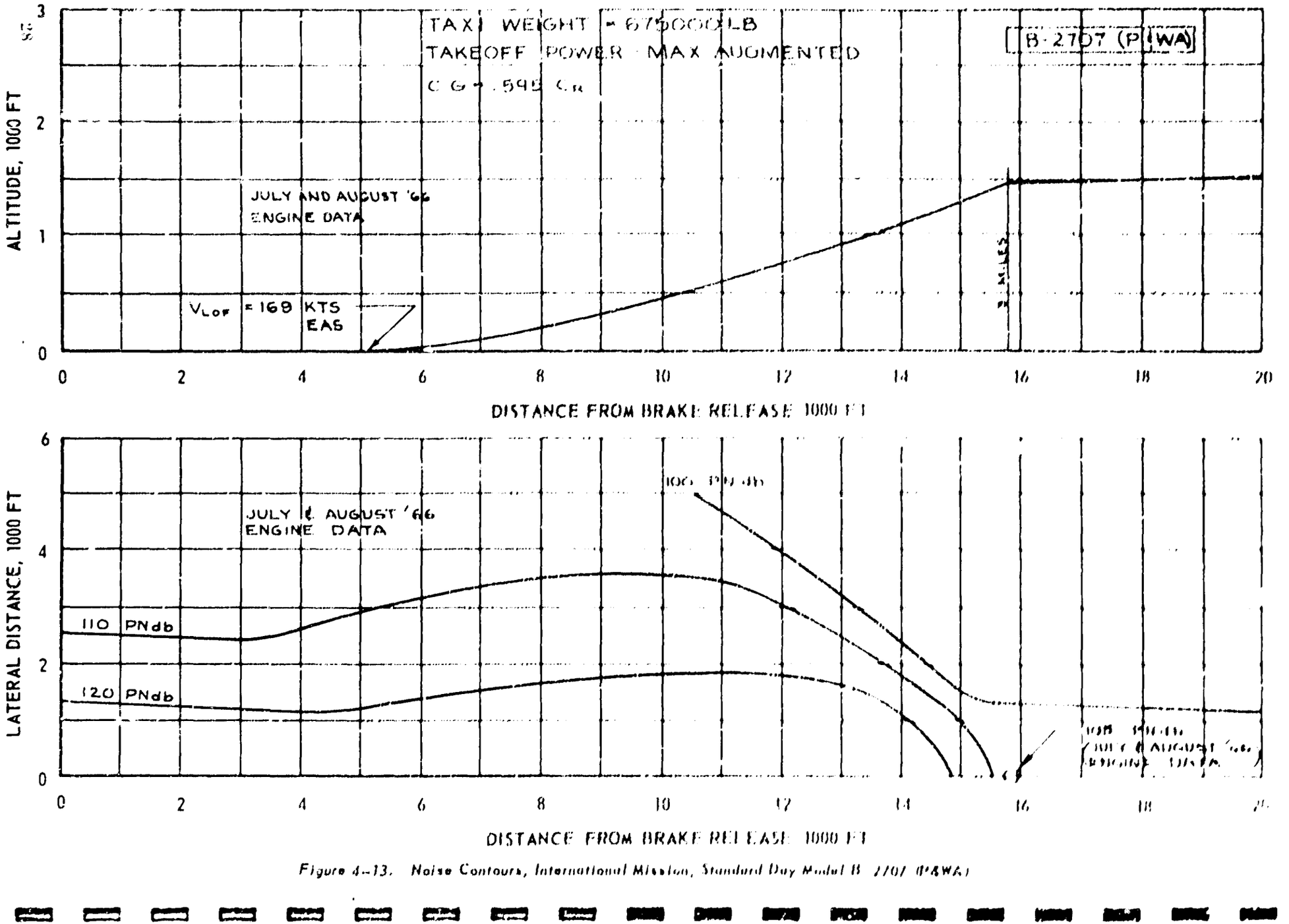


*Figure 4-13. Noise Contours, International Mission, Standard Day Model B-2707 (P&WA)*

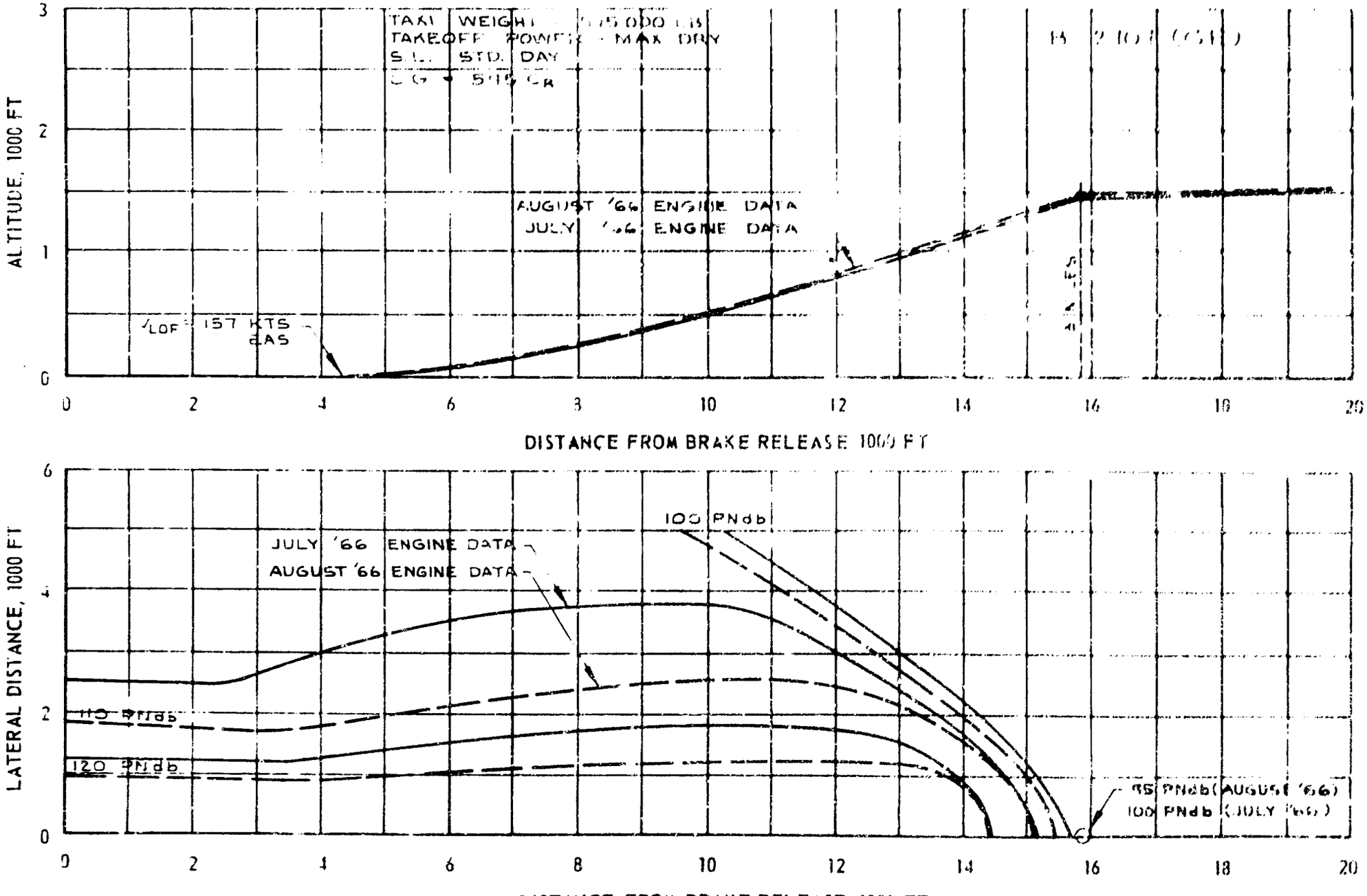


*Figure 1-11. Noise Contours, Domestic Mission, Standard Day Model 8-2707 (GE)*

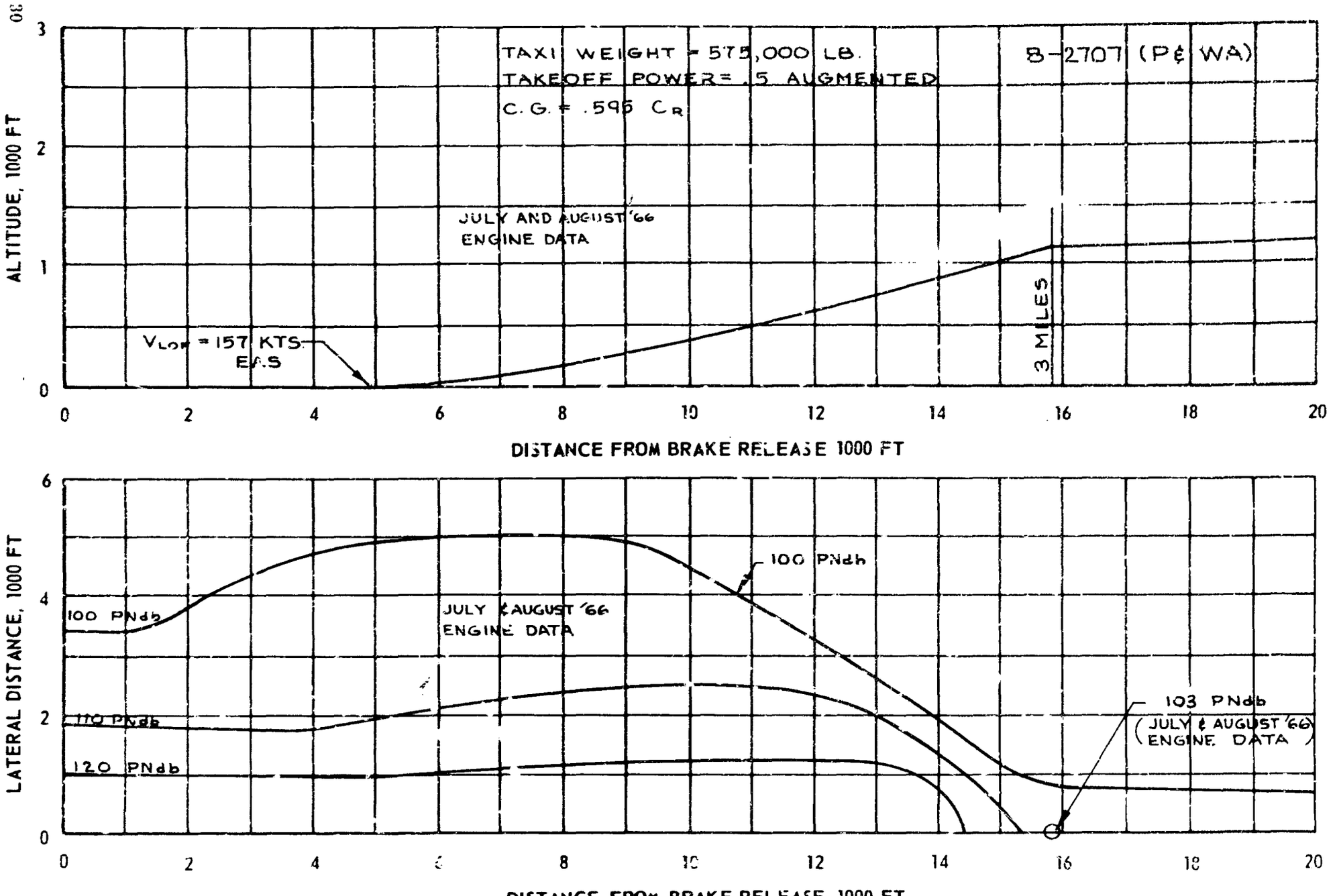


*Figure 4-15. Noise Contours, Domestic Mission Standard Day Model B-2707 (P & WA)*

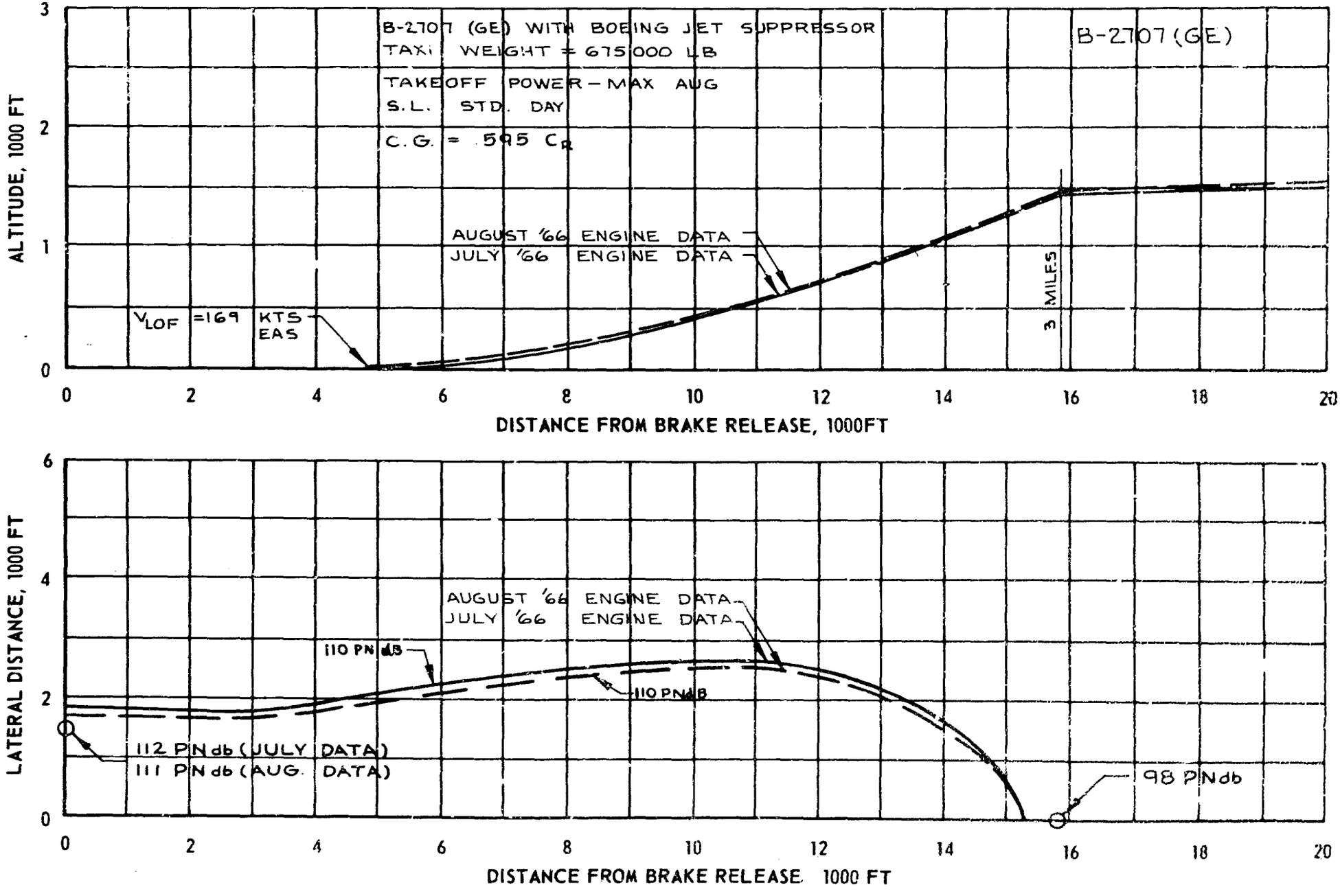


*Figure 4–16. Noise Contours, Boeing Jet Suppressor, Model B–2707 (GE)*

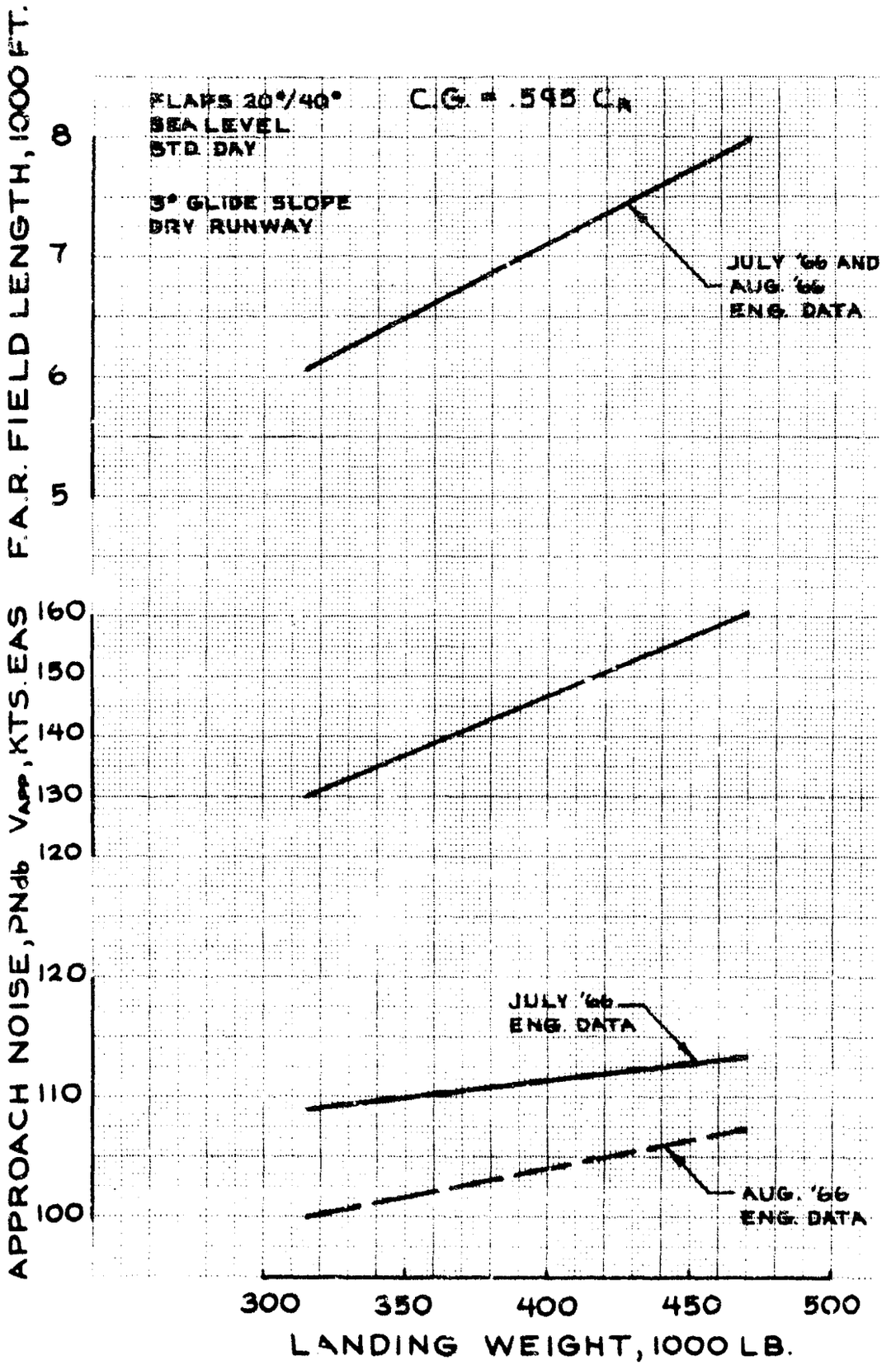


*Figure 4–17. Landing Performance Model B–2707 (GE)*

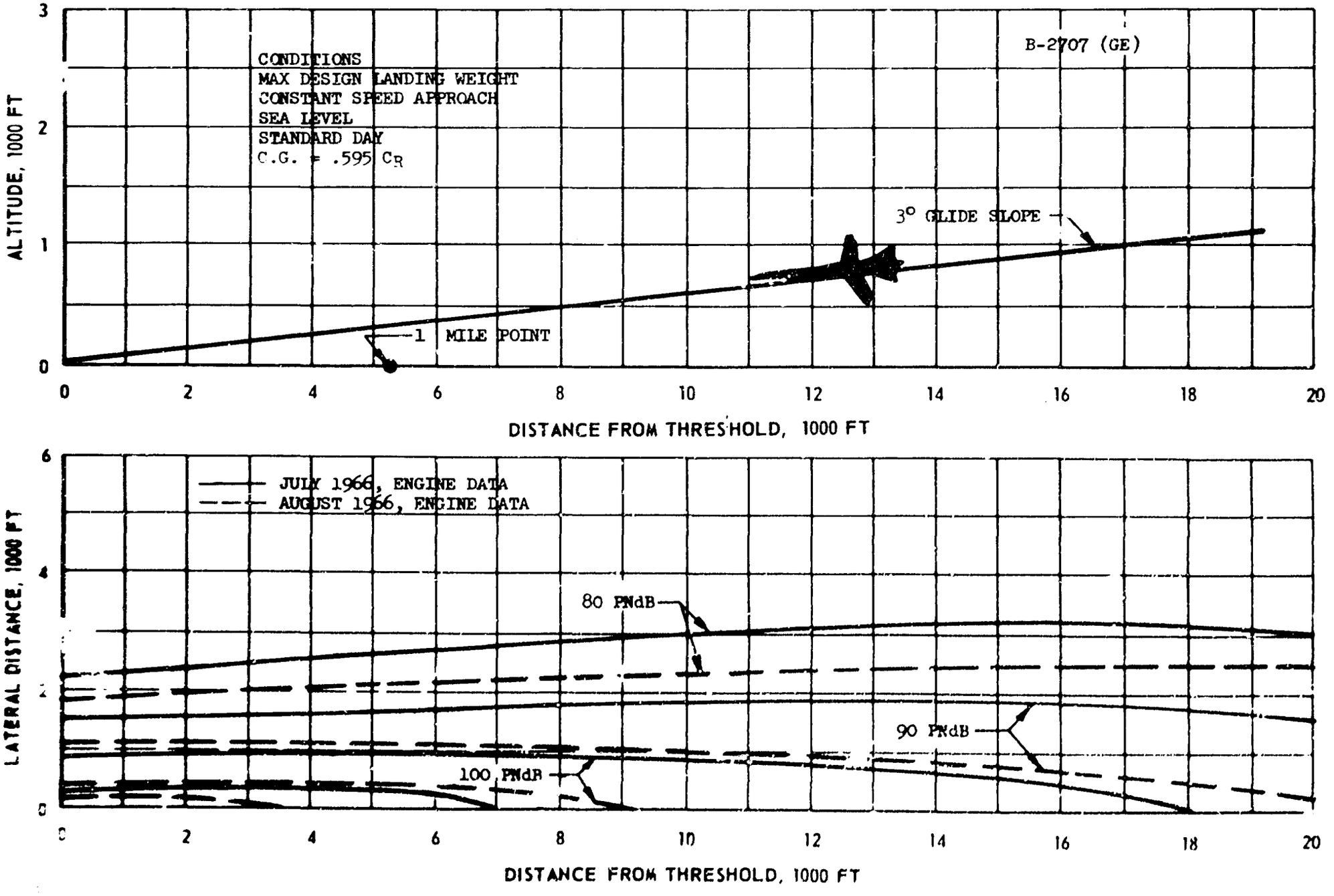


*Figure 4-18. Landing Noise Contours, International Mission B-2707 (GE)*

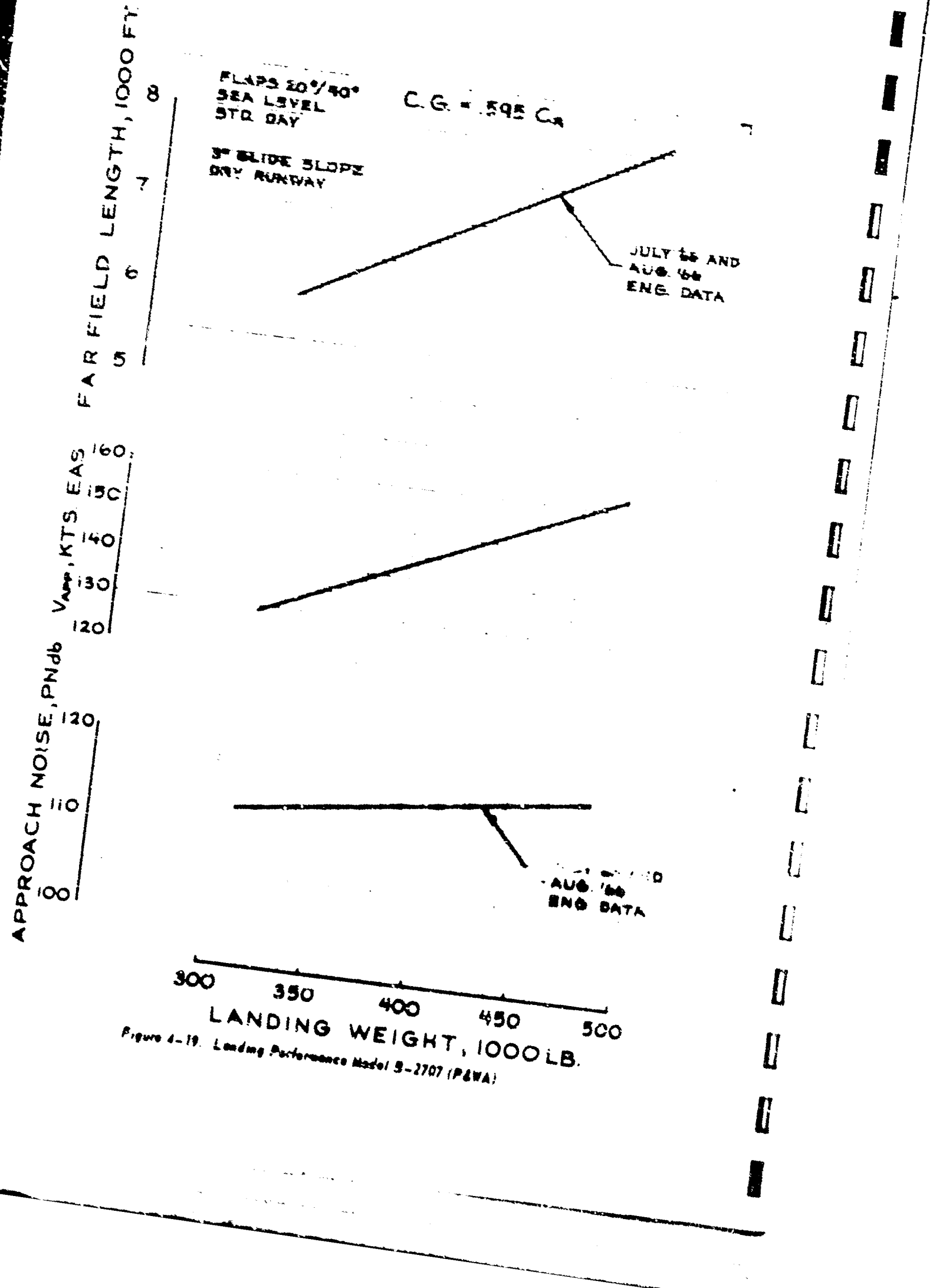


Figure 4-19. Landing Performance Model B-2707 (P&WA)